# ICSAT 2012

Aleksandar Subic
Jörg Wellnitz
Martin Leary
Lucien Koopmans

*Editors*

# Sustainable Automotive Technologies 2012

Proceedings of the
4th International Conference

## Springer

Sustainable Automotive Technologies 2012

Aleksandar Subic, Jörg Wellnitz, Martin Leary,
and Lucien Koopmans (Eds.)

# Sustainable Automotive Technologies 2012

Proceedings of the 4th International
Conference

Springer

*Editors*

Prof. Aleksandar Subic
RMIT University
School of Aerospace Mechanical &
    Manufacturing Engineering
Melbourne
Australia

Dr. Martin Leary
RMIT University
School of Aerospace Mechanical &
    Manufacturing Engineering
Melbourne
Australia

Prof. Dr.-Ing. Jörg Wellnitz
UAS-Ingolstadt
Ingolstadt
Germany

Dr. Lucien Koopmans
RMIT University
School of Aerospace Mechanical &
    Manufacturing Engineering
Melbourne
Australia

# Preface

The total number of vehicles on world roads today has surpassed 1 billion. The impact of this on the environment, our economies and societies is significant. With the predicted growth in population worldwide, increased density and congestion in urban environments, and with greater purchasing ability of individuals in the largest populated countries such as China and India, the impact of personal mobility and road transport in general will reach new heights.

Researchers and vehicle manufacturers have been exploring different technology scenarios and vehicle concepts in order to meet the many challenges we are facing in the domain of personal mobility. While vehicle electrification based on hydrogen fuel cells and new generation battery technologies seems inevitable, there are many transitional technologies that offer immediate solutions for reduction of emissions and fuel consumption. These include alternative fuels such as biofuels and gaseous fuels, new optimised technology solutions for downsizing of internal combustion engines, vehicle lightweighting based on alternative materials and multifunctional structures, new design and manufacturing concepts that utilise digital design and digital manufacturing systems, and others.

This book on Sustainable Automotive Technologies explores the wide range of transitional vehicle technologies that are emerging in response to the challenges and opportunities confronting personal mobility. The research reported in this book aims to provide a deeper insight into the technological solutions that have the capacity to facilitate the transition of the automotive industry and the market from now to the future. The book comprises of the following main chapters: (i) lightweight vehicle structures and materials; (ii) sustainable propulsion systems and fuels; (iii) systems solutions for sustainable mobility; and (iv) vehicle refinement and new technology concepts. Papers selected for publication in this book have been presented at the 4th International Conference on Sustainable Automotive Technologies ICSAT2012 held in Melbourne, Australia in March 2012.

All contributions included in this book have been reviewed independently by international experts with experience in relevant fields and have been edited accordingly prior to publication. We wish to take this opportunity to thank all researchers and reviewers for their respective contributions without which this book would not be possible. Also, we acknowledge in particular the continuing support

of Springer to this research field, which has enabled us to establish and publish an international book series on Sustainable Automotive Technologies that has attracted interest worldwide.

Aleksandar Subic
Joerg Wellnitz
Martin Leary
Lucien Koopmans

*Editors*

# Contents

## Lightweight Vehicle Structures and Materials

## Sustainable Propulsion Systems and Fuels

## Systems Solutions for Sustainable Mobility

## Vehicle Refinement and New Technology Concepts

# Reduction of Nickel-Alloyed Stainless Steels in Automobile Systems by Laser Beam Welding of Austenitic-Ferritic Connections While Maintaining an Adequate Corrosion Resistance

M. Weigl[1] and M. Schmidt[2]

[1] Dipl.-Ing. (FH) Markus Weigl, Bayerisches Laserzentrum, Konrad-Zuse-Str. 2-6, 91052 Erlangen, Germany
phone: +49-(0)9131-97790-16; fax: +49-(0)9131-97790-11
m.weigl@blz.org

[2] Prof. Dr.-Ing. Michael Schmidt, Chair of Photonic Technologies, University of Erlangen-Nuremberg, Paul-Gordan-Str. 3, 91052 Erlangen, Germany
phone: +49-(0)9131-8523456; fax: +49-(0)9131-8523234
michael.schmidt@lpt.uni-erlangen.de

**Abstract.** Nowadays mostly austenitic stainless steels, which are alloyed with the element nickel, are used for applications with demanding requirements concerning the chemical properties and corrosion resistance. Therefore in current automobile systems in the mid-range and premium price segment the exhaust piping is normally made of nickel-alloyed stainless steels, see figure 1. With regard to modern mobile systems, such as automobiles powered by hydrogen fuel cells and alternative liquid propellants nearly all components for the storage, transportation and chemical reactions are made of nickel-alloyed stainless steels. These types of steels typically feature an excellent chemical and thermal performance, which is often not necessary for the whole system. Thus quite a huge amount of nickel is wasted at installation positions and area of operation not requiring that high chemical persistency. For such installations with lower demands on the corrosion resistance also nickel-free ferritic stainless steels could be used. In order enable a reduction of the nickel-alloyed materials by ferritic variants without a decrease of chemical performance in the connection an appropriate joining strategy has to be engineered. In this context the present article presents the latest results of a research project dealing with austenitic-ferritic stainless steel connections performed by laser beam welding. By a reduction of nickel both economic as well as environmental improvements can be reached: On the one hand the high and also fluctuating market price of nickel leads to notably rising prices of nickel-alloyed steels, for which reason nickel-free variants offer cost savings up to 40%. On the other hand there is reasonable suspicion that the element nickel is carcinogen caused serious damage to the health of human beings, hence nickel should also be avoided as far as possible for this reason.

# 1 Introduction

For many automobile applications with higher corrosive loads, such as exhaust pipes in current cars, see Figure 1, or components for the storage, transportation and processing of alternative liquid propellants in modern mobile systems, so-called austenitic stainless steels are used. These materials generally feature excellent forming and welding characteristics [2] and are resistant against diverse chemical substances [3]. In order to realize such an austenitic microstructure, steels are primarily alloyed with the element nickel. Besides the stabilization of the cubic-face-centred austenitic grain structure nickel increases the corrosion resistance of a stainless steel in non-oxidizing acids. In contrast to the advantageous effect on the chemical stability, an alloying with the expensive element nickel leads to a significant price increase of the relevant steel type, see Figure 2.
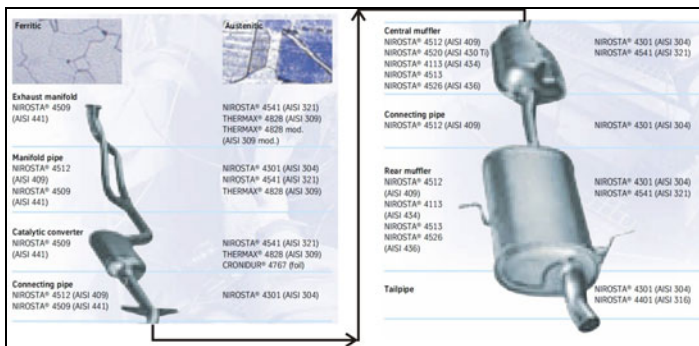


**Fig. 1.** Combinations of ferritic and austenitic stainless steels for exhaust systems of present mid-range and premium price segment automobiles. Left hand side: Ferritic steels, right hand side: austenitic steels [1].
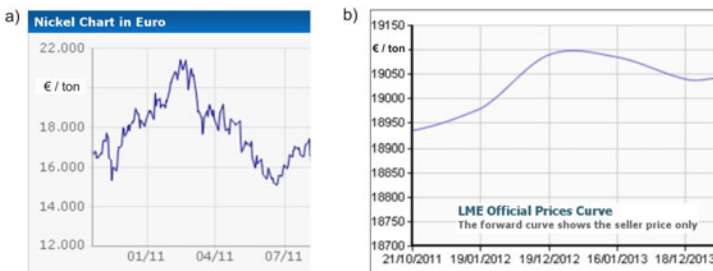


**Fig. 2.** Market price of nickel: a) Current situation [4], b) forecast for the next years [5]

According to Figure 2.a) nickel is on the one hand a comparatively expensive metal with a high average price of more than 18.000 € per ton and on the other hand its market price shows distinctive fluctuations. Both aspects are unfavourable for cost efficient fabrications, cost calculations of corresponding assemblies and

the sale of the final products. In view of the future conditions, figure 2.b) shows a forecast of the price trend for nickel within the next years by the London Metal Exchange (LME). Thus the average market price is supposed to increase furthermore, up to more than 19.000 € per ton at the end of 2012. Consequently a reduction of nickel-alloyed steels is a very promising approach for cost-effective and steady-price constructions in the automotive engineering. In addition to these economic advantages, a downsized use of nickel-alloy steels also prevents the welding and cutting operators from perpetual and excessive exposition by nickel oxides, such as $NiO$, $NiO_2$ and $Ni_2O_3$, which typically occur at laser deep welding of CrNi-steels. New medical studies demonstrate that a long-term contact of human beings with nickel oxides effectuates the generation and growth of tumour, cancer and further remote health damages [6]. Therefore less nickel in the production of current and future automotives is also a sustainable practice to keep the welding personal's health.

For both implied reasons more and more industrial companies endeavour to introduce nickel-free stainless steels in their production, wherever possible. As installations points with very high demands on corrosion resistance can only be realized with austenitic steels, so-called tailored constructions with adapted material properties integrated at the particular assembly-position are designed [7]. For an implementation tailored constructions austenitic and ferritic stainless steels have to bee joint by metallic continuity and especially welding. Laser welding offers fast processing and low heat input, which allows joining thin-walled steel parts at negligible thermal deformation. However laser-welded combinations of austenitic and ferritic stainless steels without any optimization arrangements often results in the formation of local corrosion under demanding chemical loads, compare Figure 3.
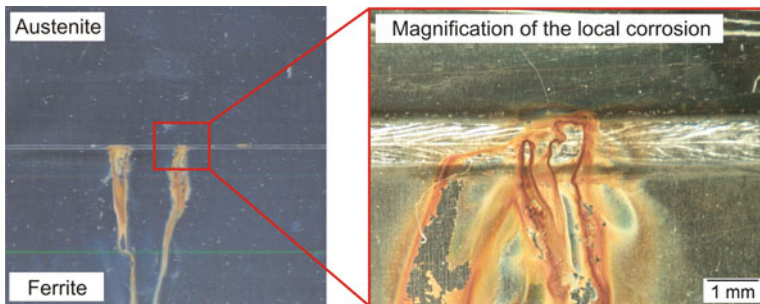


**Fig. 3.** Local corrosion at laser-welded austenitic-ferritic steels after salt spray test of 16 hours [Bavarian Laser Centre].

Local corrosions as seen in figure 3 are usually restricted to small areas of the weld zone, while the bigger part of the connection area is absolutely free of corrosion. However these comparatively small defective areas limit the implementation of such austenitic-ferritic joints up to now.

In order to prevent a local corrosion and enable a reduction of nickel-alloyed stainless steels, the possible causes for such punctual failures under chemical load have been analyzed at the Bavarian Laser Centre. The corresponding investigations highlighted, that local corrosion is particularly effectuated by non-uniform element intermixture in the melt pool, see Figure 4.
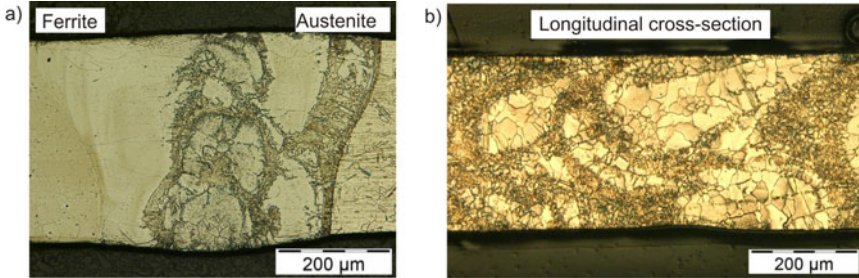


**Fig. 4.** Non-uniform element intermixture in the weld zone of austenitic-ferritic connections [blz]: a) Lateral cross-section, b) Longitudinal cross-section in the middle of the weld zone [blz]

While the external geometry of laser-welded austenitic-ferritic joints appears very constant, the welding process leads to a non-uniform distribution of the alloying elements of the relevant steels. Figure 4.a) shows a lateral cross-section of such a joint and demonstrates the irregular intermixture in the weld zoned. In addition Figure 4.b) reflects a longitudinal cross-section in the middle of a laser-welded connection, evincing a considerable turbulence coming along with highly ferritic zones, that tend to form coarse grain areas. Coarse grains lead to a decrease of the chemical and also mechanical performance of the welds, especially when there are conglomerates extending from the top of the weld to the bottom, compare Figure 4.b).

In order to significantly enhance an intermixture at the molten state and thereby obviate the formation of spaciously coarse grain areas, the present article discusses the use of filler materials and their effect on the chemical performance of welded connections. Although the handling of filler wires complicates laser welding processes and increases the costs for the welding procedure to certain extend, this process variant seems to be adequate to clearly improve the chemical robustness of laser-welded austenitic-ferritic connections at stainless steels. If in this manner a large-scale replacement of nickel-alloyed steels could be realized without decreasing the corrosion performance, overall an economic and environmental benefit is possible.

Hence experimental welding trials have to be set up and performed, dealing with the reproducible production of laser-welded thin-sheet connections with filler wire at high feed rates. After developing a stable joining process, the metallographic, chemical and mechanical characteristics of the welds have to be analyzed. Finally the question, whether a formation of local corrosion can be prevented shall be clarified.

## 2 Experimental Setup

For the experimental welding trials a continuous-wave disc laser from Trumpf is used. This Yb:YAG solid state lasers features a maximum output power of 4,0 kW at a wavelength of 1.030 nm and a focal diameter of 600 µm. Considering the stainless steels, samples with a dimension of 150 mm x 50 mm x 0.5 mm (length x depth x thickness) are cut out of metal sheets by means of laser cutting. The material data of the considered austenitic and ferritic stainless steels is given in Table 1. As austenitic chrome-nickel steel the 1.4301 is used, as this steel is the most prevalent applied austenite in Europe. On the ferritic side two materials, the 1.4016 and the 1.4520 are contemplated. 1.4016 is only alloyed by chrome and features a market price of about 40% less than 1.4301. Because of the extensive formation of coarse grain of 1.4016 during thermal welding also the titanium-stabilized 1.4520 is analysed. By means of stabilization, coarse grain zones within the weld can be prevented.

**Table 1.** Material data for the considered austenitic and ferritic stainless steels.

| Microstructure | Material-Code acc. EN10088-2 | Material-Code acc. ASTM | Chemical composition |
|---|---|---|---|
| Austenitic | 1.4301 | 304 | X5CrNi18-10 |
| Ferritic | 1.4016 | 430 | X6Cr17 |
| | 1.4520 | - | X2CrTi17 |

These types of stainless steels with the implied plate-thickness of 0.5 mm are connected in a butt-weld configuration. For this purpose a clamping device is designed, which allows a reproducible positioning of the samples in a zero-gap constellation. First the austenitic and ferritic sheet metal samples are locked into position by clamping plates, compare Figure 5. Then an adjustable screw can be operated to assure a zero-gap between the samples. The position of the joining area relative to the laser system is given by an appropriate dead stop of the base structure of the clamping device.

For the supply of additional alloying elements and an enhancement of the intermixture in the molten state, a filler wire made of the austenitic steel 1.4576 (ASTM: 318Si, X5CrNiMoNb19-12) is also inserted into the weld zone. Here the wire diameter is set to 0.8 mm, as this is a commonly used and goo available wire, which can be manipulated by all standard wire feeding systems. All the experimental trials are performed under pure Argon shielding gas, which is injected as well from the top as the bottom side of the weld.

1: Adjustable screw and bracket     5:  Ferritic sample
2: Movable support                  6-9: Shielding gas (bottom side)
3: Clamping plates                  10: Rigid support
4: Base structure                   11: Austenitic sample
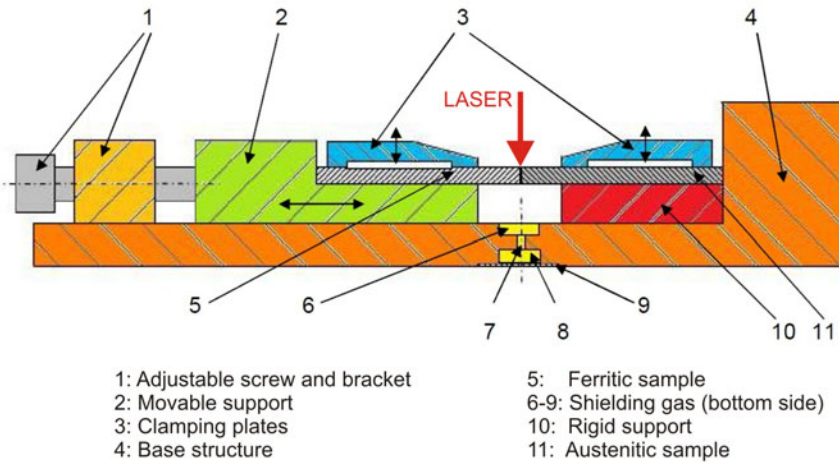
**Fig. 5.** Clamping device for the experimental welding trials [Bavarian Laser Centre].

## 3  Welding Test Results

During the experimental trials it can been seen, that reproducible welds at 0.5 mm sheet metal samples with a 0.8 mm filler wire are achievable with adapted parameters. Too slow process feed rates of less than 3 m/min lead to an immoderate heat input and thereby an excessive formation of coarse grains at both considered ferritic materials. On the contrary, process feed rates of more than 7 m/min require immoderate high laser powers, so that a lot of splatters and melt emissions occur. For all analyzed materials a feed rate of both the process and the filler wire of about 5 m/min lead to the best results and can be recommended. In figure 6 an example of a connection of 1.4016 and 1.4301 demonstrates the feasibility of the implied connections and shows a comparatively balanced element intermixture in the weld zone.

In comparison of welds with the non-stabilized ferritic steel 1.4016 and Ti-stabilized ferritic steel 1.4520, a distinctive formation of coarse grain in the heat affected zone of 1.4016 can be noticed, see Figure 7a). On the contrary an alloying with less than 1 mass-% titanium in case of 1.4520 inhibits an excessive grain growth, compare Figure 7b). As the price difference between materials stabilized and respectively not stabilized with titanium amounts less than 10%, this kind of alloying has to be recommended in order to prevent a mechanical and chemical degradation of the stainless steel connections after laser-welding.
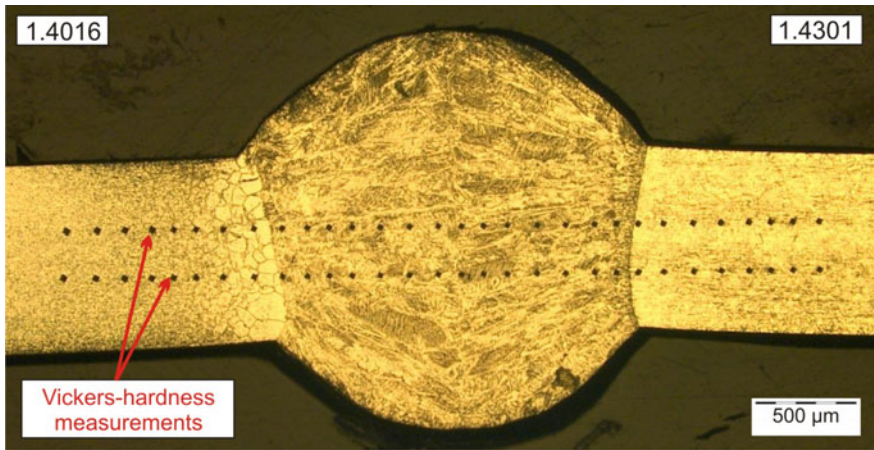
**Fig. 6.** Lateral metallographic cross-section of a austenitic-ferritic weld of 1.4016 und 1.4301, welded with continuous-wave solid-state laser and filler wire 1.4576 (laser power 2.800 W, process feed rate 5 m/min, wire diameter 0,8 mm, wire feed rate 5 m/min).
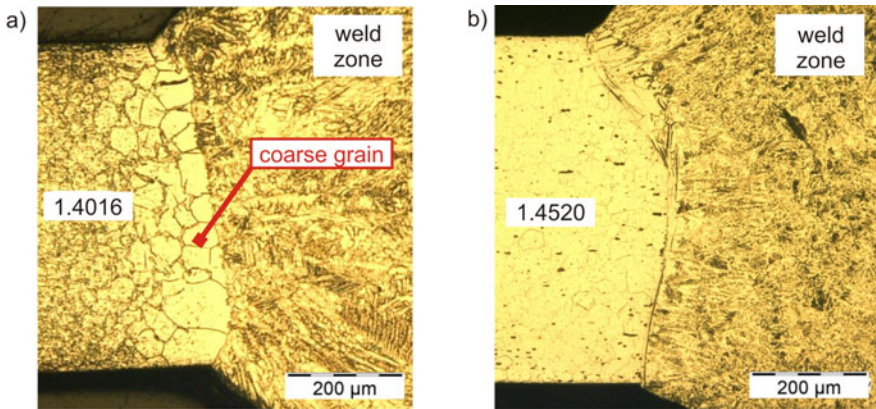


**Fig. 7.** Detailed view on the heat-affected-zones of connections with 1.4016 (a) and 1.4520 (b), welded with continuous-wave solid-state laser and filler wire 1.4576.

## 4  Characterization of the Welded Samples

As assumed, laser-welds without filler material feature a high turbulence of the element intermixture in the weld zone. This can be ascertained by element mappings, which highlight element dispersions within weld in false-colour illustration. For example, Figure 8 shows the nickel intermixture in a laser weld of 1.4301 and 1.4520.
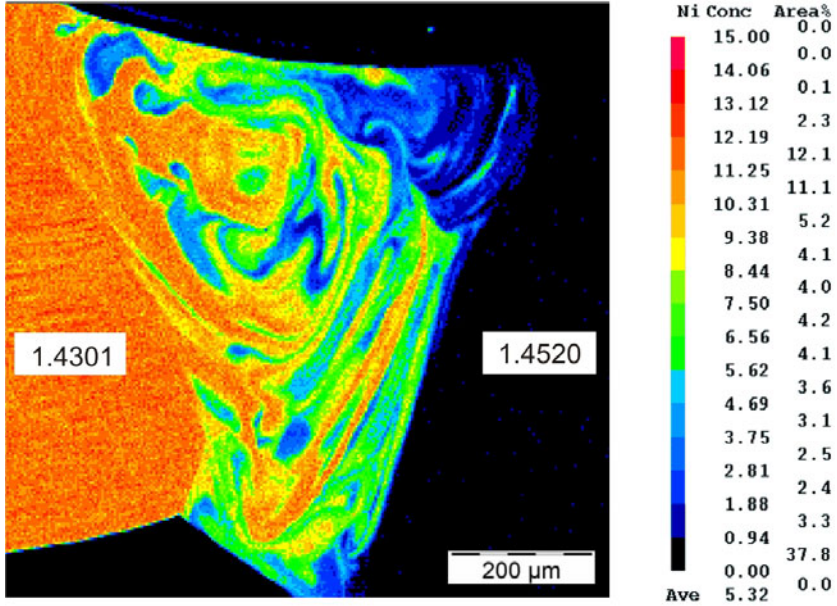
**Fig. 8.** Microprobe mapping for the element nickel in a laser-welded austenitic-ferritic connection: Left-hand side 1.4301, right-hand side 1.4016.
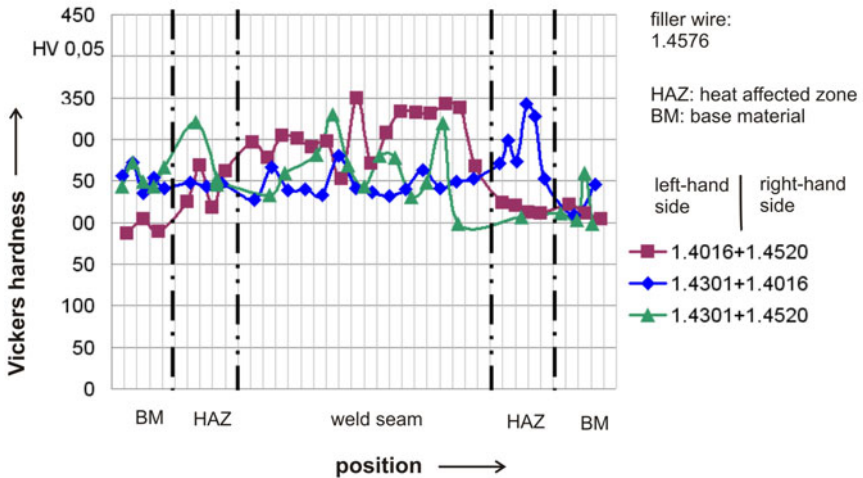


**Fig. 9.** Vickers hardness measurements of laser-welded austenitic-ferritic connections, welded with filler wire 1.4576.

According to Figure 8, the intermixture of alloying elements and particularly of nickel is obviously irregular and leads to a variance of chemical and mechanical characteristics within the weld. In contrast to that, welds with filler wire 1.4576 result in a quite harmonic element distribution. Measuring the hardness of welds with fillers, see Figure 9, it can be seen, that a more uniform element dispersion reduced the hardness fluctuation over the weld zone and limits the hardness traverse to an acceptable band width around the base metal state.
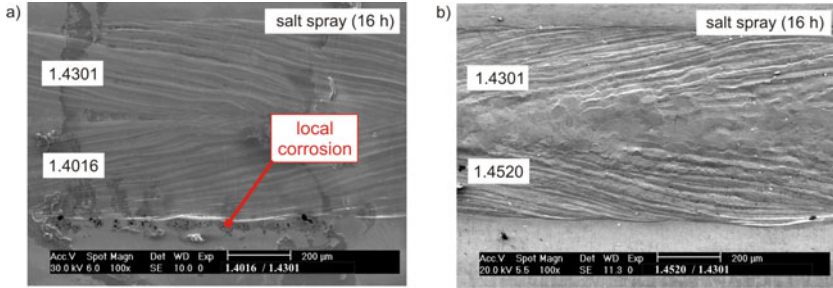


**Fig. 10.** SEM surface analysis of welds 1.4016 / 1.4301 (a) and 1.4520 / 1.4301 (b) with filler material 1.4576 after 16 hours of salt spray testing.

With regard of the chemical characterization of the welded sample salt spray tests with durations of 16 hours are performed. After the chemicals loading SEM analysis are used to examine the surfaces of the welds. As it can be seen in Figure10a) austenitic-ferritic welds with non-stabilized materials, such as 1.4016, feature local corrosion on top of the heat-affected-zone. This is exactly the area, where an excessive formation of coarse grain could be detected according to Figure 7a). At a closer look to Figure 10b) no corrosion can be found at welds with Ti-stabilized stainless steels after the same duration of salt spray testing. Therefore a Ti-stabilization has also to be recommended for chemical aspects and leads to austenitic-ferritic connections with an adequate corrosion resistance. By this way a sustainable replacement of nickel-alloy stainless steels by stabilized nickel-free materials can be realized without decreasing the chemical performance of laser-weld and therewith the whole assembly.

## 5 Conclusions and Outlook

The present article demonstrates the possibility to realized austenitic-ferritic stainless steel connections, by means of titanium-stabilized nickel-free ferritic materials. With appropriate welding process parameters and additional austenitic filler wires a regular intermixture in the molten state can be reached. By this way, adequate mechanical and also chemical characteristics of the laser welded connections are achievable, so that a nickel reduction does not effectuate a degradation of the corrosion resistance and the long-term stability of the relevant assembly. Summarized the present work will help introducing more nickel-free steels for as

well stand of the art as future mobile systems with higher demands for chemical resistance. A limitation of nickel-alloys steels to mandatory installation points allows cost-effective and steady-price constructions in the automotive engineering and prevents welding and cutting operators from perpetual and excessive exposition by nickel oxides.

# References

[1] Nirosta, T.K.: Nirosta and Thermax – Stainless steels for automobile exhaust systems. Krefeld (2010)

[2] DIN EN 10088: Nichtrostende Stähle- Teil 1: Verzeichnis der nichtrostenden Stähle, Teil 2: Technische Lieferbedingungen für Blech und Band aus korrosionsbeständigen Stählen für allgemeine Verwendung. Beuth-Verlag, Berlin (2005)

[3] Nirosta, T.K.: Chemische Beständigkeit der Nirosta-Stähle. Krefeld (2009)

[4] Current market price for nickel (05.08.2011 ), `http://www.finanzen.net`

[5] London Metal Exchange (LME). Forward curve - Seller price of nickel (October 2011), `http://www.lme.com`

[6] Deutsche Gesetzlich Unfallversicherung – Fachausschuss Metall- und Oberflächenbehandlung: Chrom(VI)-Verbindungen bzw. Nickeloxide beim Schweißen und verwandten Verfahren. Informationsblatt Nr. 036, Ausgabe (November 2008)

[7] Pohle, C.: Schweißen von Werkstoffkombinationen – Metallkundliche und fertigungstechnische Grundlagen sowie Ausführungsbeispiele. DVS Fachbuchreihe Schweisstechnik. DVS-Verlag, Düsseldorf (1999)

# Damage Tolerance in Aluminium High Pressure Die-castings and Its Implications on Safety Critical Vehicle Components

R.N. Lumley

CSIRO Future Manufacturing Flagship, Private Bag 33, Clayton South MDC, Victoria, 3169, Australia
Ph:+61395452894, Fax: +61395451128
Roger.Lumley@csiro.au

**Abstract.** High pressure die casting (HPDC) is a widely used production technique for metal components that are required to have close dimensional tolerances and smooth surface finishes. More than 50% of the aluminium castings produced globally are manufactured by HPDC from secondary alloy and these comprise the majority of aluminium components present in each vehicle manufactured. In the current work, the production of high pressure die-castings with superior levels of fracture resistance and damage tolerance is considered. The ability to produce very high levels of damage tolerance may increase the potential applications for high pressure diecast parts. These new alloys allow applications to be realized that have previously not been possible.

## 1  Fracture Resistance and Damage Tolerance

Although heat treatment may improve both the strength and ductility of HPDC's above the as-cast condition [1], it is also well known that tensile ductility is a poor indicator of fracture properties of any material [2]. This is because it is atypical for a part to fail in a tensile mode in service; instead, components usually fail following the initiation and propagation of a crack (e.g. Figure 1).

Fracture resistance is therefore particularly important for HPDC's where a) thinner walls and higher strengths lead to an increased susceptibility to brittle fracture; b) where stressing of the HPDC part involves bending meaning crack initiation and growth is the failure mode; c) fatigue crack growth rate is important; d) for safety critical components with an energy absorption requirement.

The relationship between fracture resistance, design stress and critical flaw size may be represented by the Griffith equation:

$$K_c \cong \sigma d \sqrt{\pi a} \tag{1}$$

Where $K_c$ is the fracture toughness of the material, $\sigma d$ is the design stress and $a$ is the critical flaw size.
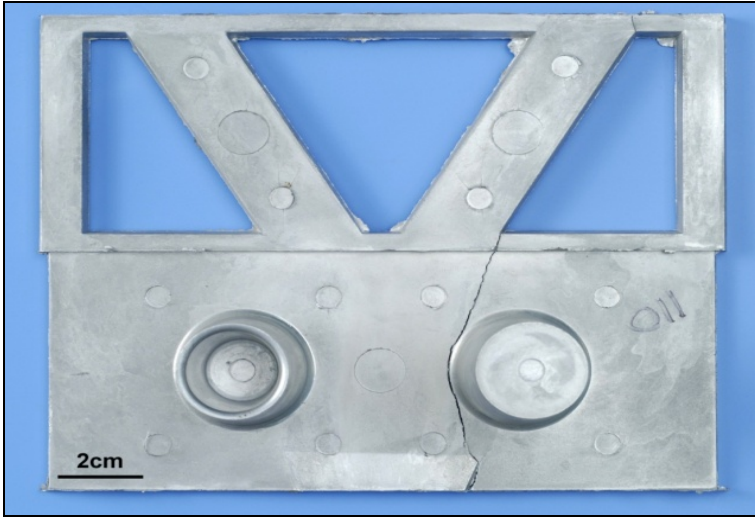
**Fig. 1.** An example of fracture of a HPDC component where tensile properties do not represent the resistance to "real" failures. Here, the crack runs between geometric stress raisers such as notches and changes in section thickness.
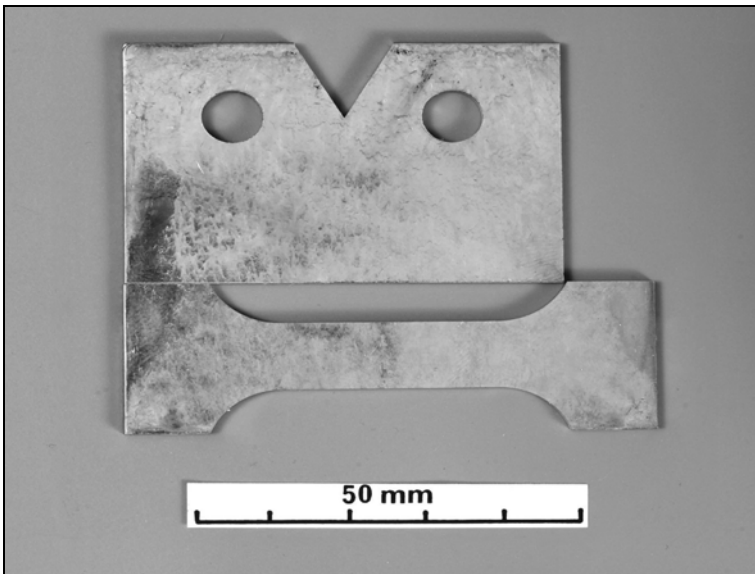


**Fig. 2.** Tear test and tensile sample machined from plates with dimensions 60x70x2 mm.

Equation 1 highlights the important fact that if the critical flaw size is reached at stresses below the design stress, the part may fail rapidly. These considerations are well known for the design of other high strength aluminum parts, such as those used in aerospace, and the microstructural features known to adversely influence fracture resistance in aluminium alloys are discussed elsewhere [3].

It is therefore necessary to consider fracture characteristics as well as tensile properties when assessing the design of new lightweight HPDC components, especially if they are likely to be used in a safety critical application.

The Kahn-type tear test specimen (ASTM B871) machined from a HPDC plate and the corresponding tensile sample (AS1391) are shown in Figure 2. The tear test procedure is highly relevant to HPDC's because it corresponds to typical wall thicknesses. The (tear) specimen geometry is most suitable for sheet or plate of less than 6mm thickness and has an extremely sharp notch (root radius=$25\pm12.7\mu m$), which initiates fracture. Of greatest importance from the results of the tear test procedure is the measure known as the unit propagation energy (UPE), determined from the area under the load-extension curve once cracking has begun. Both the unit propagation energy (UPE) and unit total energy (UTE) are proportional to the critical strain energy release rate $(G_c)$ through UPE $= kG_c$ and UTE $= mG_c$ where k and m are constants [2].

Tear testing therefore provides a limited estimate of the critical stress intensity factor or fracture toughness, $K_c$. In addition to the values of UPE and UTE generated, the tear strength of the material is also derived, which is:

$$\text{Tear Strength} = 4P/bt \tag{2}$$

Where *P* is the maximum load reached, usually at the onset of cracking, *b* is breadth and *t* is thickness.

The tear strength of an alloy is also used to calculate the notch sensitivity ratio, defined as the ratio of tear strength to yield stress (tear-to-yield ratio, TYR). As may be appreciated, when the TYR<1, the material has very high sensitivity to the presence of a crack, notch, or geometric stress raiser. When TYR>1, the material displays low notch sensitivity. A material with TYR ≥1.5 often displays yielding before cracking begins and hence low notch sensitivity. The notch sensitivity ratio also provides important information related to machining of the casting. In particular, a casting with a high value of TYR may tolerate machined in stress raisers far more effectively than one with a low value of TYR.

Detailed studies of the tear test behavior of the alloys A360, A380 and C380 have shown that T4 and underaged (UA) T6 tempers can produce excellent combinations of UPE, UTE, and tear strength [4]. Usually, the fracture properties of UA treated material are between those of the T4 and T6 material, with values depending on the exact heat treatment procedures used.

An experimental program was undertaken directed at developing Al-Si-Cu alloys that showed significantly improved fracture resistance when compared with existing commercial alloys. Eleven experimental compositions were compared against four commercial alloy compositions, (Table 1).

The tensile properties, tear strength, UPE and UTE for the 15 alloys in as-cast, T4 and T6 tempers are provided in Figure 3. Respective values of tensile elongation, tensile strength, tear strength, UPE and UTE are plotted as a function of yield strength in Figures 3(a) to (e) respectively. Each alloy is identified individually by number in Figure 3(a). Figure 3(a) shows the relationship between yield strength and tensile elongation for samples machined from the castings. These trends were similar to those observed for cast test-bar samples, described elsewhere [1].

**Table 1.** Compositions of Alloys Tested [5].

| Alloy type | Number | Composition |
|---|---|---|
| AK9M2 | 1 | Al-8.6Si-0.70Fe-1.36Cu-0.3Mn - 0.56Mg-0.44Zn |
| ADC12 | 2 | Al-10.8Si-0.8Fe-1.74Cu-0.17Mn-0.27Mg-0.51Zn-0.1Ni |
| A380 | 3 | Al-9.0Si-0.86Fe-3.1 Cu-0.16Mn- 0.1Mg - 0.53Zn-0.11Ni |
| C380 | 4 | Al-9.3Si-0.92Fe-3.2 Cu-0.21Mn- 0.26Mg-0.61Zn |
| Experimental | 5 | Al-7.1Si-0.21Fe-1.60Cu-0.5Mn - 0.01Mg |
| Experimental | 6 | Al-8.0Si-0.28Fe-1.84Cu-0.5Mn - 0.12Mg-0.2Zn |
| Experimental | 7 | Al-7.4Si-0.24Fe-1.82Cu-0.45Mn-0.1Mg - 0.25Zn |
| Experimental | 8 | Al-7.8Si-0.29Fe-1.78Cu-0.52Mn-0.18Mg-0.2Zn |
| Experimental | 9 | Al-7.5Si-0.27Fe-1.74Cu-0.48Mn-0.23Mg-0.2Zn |
| Experimental | 10 | Al-7.2Si-0.23Fe-2.0 Cu- 0.45Mn-0.1Mg - 0.26Zn |
| Experimental | 11 | Al-7.4Si-0.24Fe-2.35Cu-0.45Mn-0.11Mg-0.26Zn |
| Experimental | 12 | Al-7.4Si-0.24Fe-2.59Cu-0.45Mn-0.11Mg-0.27Zn |
| Experimental | 13 | Al-7.5Si-0.24Fe-2.82Cu-0.46Mn-0.11Mg-0.26Zn |
| Experimental | 14 | Al-7.2Si-0.24Fe-2.91Cu-0.45Mn-0.1Mg - 0.26Zn |
| Experimental | 15 | Al-7.2Si-0.24Fe-3.21Cu-0.44Mn-0.1Mg - 0.26Zn |

For each of the respective tempers, several experimental compositions displayed the capacity to develop elevated tensile ductility. However, for compositions with similar levels of yield strength, the tensile ductility and tensile strength were generally similar for commercial or experimental compositions (Figure 3 (a&b) respectively).

The tear strength is plotted against the yield strength in Figure 3(c), and it will be seen that the experimental composition now notably outperform the commercial alloys. In Figure 3(c), the notch sensitivity is indicated by lines describing values of TYR=1, 1.5 or 2. For the as-cast conditions, the commercial alloys display TYR values of between 1 and 1.5.
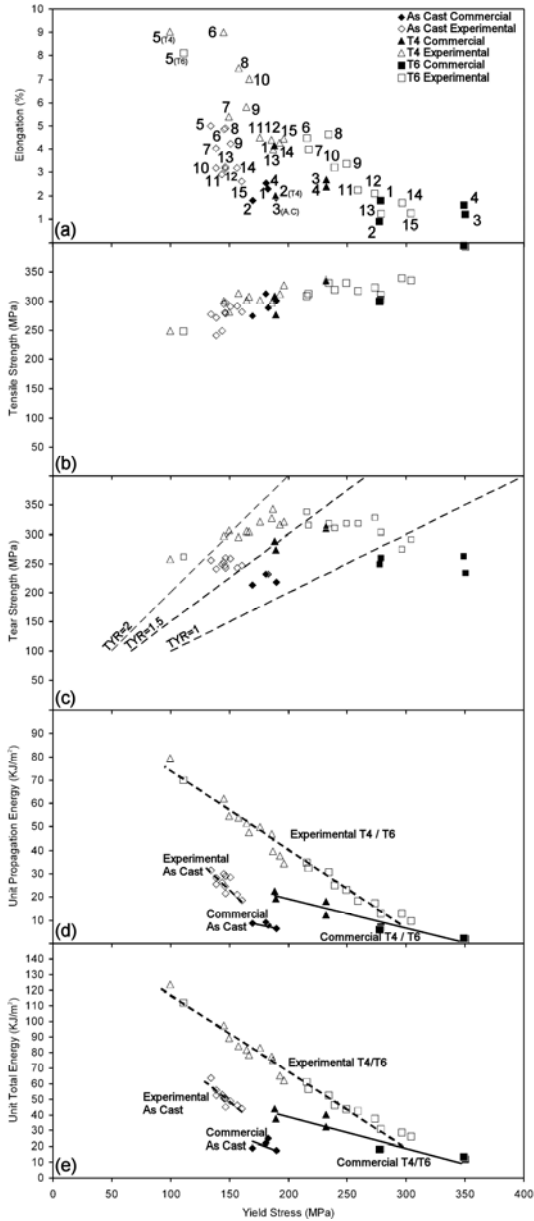
**Fig. 3.** Tensile and tear test results for the 15 alloys examined [5].  See text for details.

The as-cast experimental compositions however display TYR values of between 1.5 and 2. For T4 treated alloys, the commercial compositions display TYR values approaching (but less than) 1.5, whereas the experimental compositions all display TYR values of greater than 1.5. Alloys 5,6&7 all displayed TYR values of greater than 2. For the T6 conditions, the commercial alloys all displayed TYR values of less than 1, whereas the experimental compositions displayed values which mostly ranged between 1 and 1.5. Alloys 5,14&15 were notable exceptions, with Alloys 14 and 15 displaying values less than 1 and alloy 5 displaying TYR> 2. In most cases, at specific levels of yield stress, the tear strength values were higher for the experimental compositions than for the commercial compositions tested.

Figure 3(d) and (e) show the results for UPE and UTE, respectively, for the alloys. In summary, the experimental compositions typically outperform the commercial compositions at yield stress values below 300 MPa. At intermediate yield stress values, (e.g. 190 MPa), the experimental compositions displayed close to double the values of UPE and more than 50% higher UTE. Compared to conventional alloy compositions in the as-cast condition, some experimental compositions when heat treated displayed four times or more greater values of UPE and UTE for the same level of yield stress. Figure 3 therefore shows that the experimental compositions significantly outperformed the existing HPDC compositions in damage tolerance and energy absorption, especially when heat treated [5].

## 2  Summary and Conclusions

In summary, the consequences of improvements to the damage tolerance of automotive components suggested by the current results are significant. It is now possible to specify combinations of high pressure diecast alloy plus heat treatment that offer major improvements to the damage tolerance and fracture resistance of HPDC components. Apart from the potential to significantly reduce mass due to the higher usable design stress, components which are designed around high levels of UPE and UTE also have a much greater capacity to absorb energy and therefore now may be considered viable materials to be used in safety critical applications.

## References

1. Lumley, R.N., O'Donnell, R.G., Gunasegaram, D.R., Givord, M.: Patent Application WO2006/066314. Australian Patent 2005318925 (2005)
2. Kaufman, J.G.: Fracture Resistance of Aluminum Alloys: Notch Toughness, Tear Resistance and Fracture Toughness. The Aluminum Association, ASM International, Ohio, pp. 11–14, 37–74 (2001)
3. Starke, E.A., Staley, J.T.: Application of Modern Aluminium Alloys to Aircraft. In: Lumley, R.N. (ed.) Fundamentals of Aluminium Metallurgy, ch. 24, pp. 747–780. Woodhead Publishing (2010)
4. Lumley, R.N.: Advanced Materials Research, vols. 41-42, pp. 99–104 (2008)
5. Lumley, R.N., Gershenzon, M., Gunasegaram, D.R., Yob, A.C.: International Patent Application, WO 2009/132388 (2009)

# The Application of Magnesium Alloys to the Lightweighting of Automotive Structures

Mark Easton[1], Mark Gibson[2], Aiden Beer[3], Matthew Barnett[3], Chris Davies[1], Yvonne Durandet[4], Stuart Blacket[5], Xiaobo Chen[1], Nick Birbilis[1], and Trevor Abbott[6]

CAST Co-operative Research Centre
[1] Monash University, Department of Materials Engineering, Melbourne, 3800, Australia
[2] CSIRO Process Science and Engineering, Clayton Vic 3169
[3] Centre for Material and Fibre Innovation, Deakin University, Geelong 3217, Australia
[4] Swinburne University of Technology, Hawthorn, Victoria 3122, Australia
[5] Henrob (UK) Pty Ltd, Geebung, Brisbane, Queensland 4034, Australia
[6] Advanced Magnesium Technologies, Sydney, NSW. 2000, Australia

**Abstract.** This paper investigates some of the opportunities for magnesium alloys based on magnesium's attributes, such as excellent die castability and high strength to weight ratio. Barriers to the uptake of magnesium alloys are considered and recent technical advancements outlined including the development of creep resistant alloys, high extrudibility alloys, joining technologies and corrosion performance. Finally issues to do with the life-cycle performance of magnesium alloys are discussed.

## 1 Introduction

Light weighting of transport is a very effective way of improving energy efficiency, with a 5-10% reduction in fuel usage for every 10% decrease in weight [1]. Magnesium alloys have been attracted a lot of attention for such applications because magnesium is the lowest density structural metal (~1.8g/cm$^3$) which suggests that substantial weight reductions can be achieved by the replacement of steel and cast iron (~7.2g/cm$^3$) and aluminium alloys (~2.7g/cm$^3$), which are currently more commonly used in transport applications [1, 2].

The applications of magnesium alloys in automotive applications are limited to a few components, such as steering wheels and instrument panels although there are some engine components, closures, and caps, covers and housings are also made out of magnesium alloys [1]. Whilst the stability of the price of magnesium contributes to this, to realize weight savings a number of technical challenges need to be considered. The properties are important, which requires alloy development. Cost is also particularly important, both the cost of magnesium itself but also the efficiency of the manufacturing process. Longevity in service is also an important consideration. Furthermore, of increasing importance are the life-cycle environmental benefits, which are particularly important for light metals where a high-embodied energy can be off-set by use-phase energy reductions. This paper aims to provide information

on the inherent properties of magnesium alloys, what their advantages are and some of the barriers to use, including technological developments that aim to overcome some of these barriers.

## 2  Strengths of Magnesium Alloys

As already noted, magnesium alloys have a density approximately a quarter of that of steel, but this does not necessarily mean that they will automatically reduce the weight of a car by 75% by replacing steel. It is the combination of material properties, loading configuration and density that are important. A comparison of the modulus to density, as would be the case for stiffness limited applications in uniaxial tension or compression suggests that the lower density is counteracted by its lower elastic modulus. However, for constant rigidity, i.e. under bending loads, where stiffness in bending of a beam or a plate is considered, magnesium becomes more attractive. The optimal material for a beam in bending has a high value of $E^{1/2}/\rho$. For a plate, the relevant index is $E^{1/3}/\rho$. For a constant rigidity of a plate, magnesium is 37% of the weight of steel and 74% of the weight of Al (Table 1). Hence in the best situations, e.g. bending of sheet or plate, substantial weight reductions can be achieved [2, 3].

Other natural advantages that magnesium alloys have are excellent high pressure die castability [4] where the lower heat capacity compared to Al allows for reduced cycle times; the high fluidity of magnesium alloys allows thinner, larger and more detailed components to be cast compared with Al alloys; and the lower soluability of Fe in Mg melts compared with Al alloys decreases soldering and extends die life. Magnesium alloys are therefore excellent candidates for parts consolidation, where a large thin-walled casting can replace parts fabricated from many components such as instrument panels and door inners.

Magnesium alloys are also easily machinable compared to competitor alloys, have high damping resistance when the alloy content remains relatively low and have good electromagnetic shielding properties. These factors, combined with the high castability and low weight, mean that many of the casings and other structural components in electronics are made out of magnesium.

**Table 1.** A comparison of key properties of magnesium, aluminium and iron/steel including performance in uniaxial loading and for constant rigidity of a plate.

|  | Density ($\rho$) (g/cm$^3$) | Modulus (E) (Gpa) | E/$\rho$ | E$^{1/2}$/$\rho$ | E$^{1/3}$/$\rho$ | Weight for constant rigidity in bending | |
|---|---|---|---|---|---|---|---|
|  |  |  |  |  |  | beam | plate |
| Mg | 1.74 | 45 | 26 | 3.86 | 2.04 | 48% | 37% |
| Al | 2.70 | 70 | 26 | 3.10 | 1.53 | 60% | 50% |
| Fe | 7.87 | 211 | 27 | 1.85 | 0.76 | 100% | 100% |

# 3  Challenges for Magnesium

There are a number of technical challenges that have limited the further uptake of magnesium alloys, particularly in automotive applications. This section seeks to highlight recent progress to address these issues.

## 3.1  Creep Resistance–Powertrain Applications

The common magnesium alloys such as AZ91 (Mg-9wt.%Al-1wt.%Zn) and AM60 (Mg-6wt.%Al-0.3wt.%Mn), have limited strength and creep resistance at temperatures above 125°C. Recently, there have been substantial improvements in the creep resistance of high pressure die cast Mg-based alloys. One approach has been to alloy Mg-Al based alloys with elements that improve the creep resistance, such and Sr, Ca, Sn and rare earth based elements [5, 6]. This has lead to the development of AJ62 (6wt.%Al-2wt.%Sr), which has been used in the BMW Al/Mg hybrid engine block, and AE42/4 [7], which contain 4wt.%Al and 2-4wt.% rare earths which has been used as an engine cradle [6]. AE44 combines very good castability, excellent ductility and very good creep resistance. For alloys that require high temperature creep resistance, alloys that do not contain Al are required. AM-HP2plus [8] is a magnesium rare earth based alloy with creep resistance superior to the incumbent Al based alloy, A380 (Fig. 1.).

## 3.2  Extrusion and Joining – Automotive Structures [9]

Since magnesium has a hexagonal close packed crystal structure it has generally been considered to be difficult to form at low temperatures. One of the side effects of this is that wrought alloys have generally had very low productivity compared to Al-based alloys and steels during forming processes. An alloy with high extrudability and good mechanical properties similar to that found in 6000 series aluminium alloys has been developed and called AM-EX1 (Fig. 2.). It is based on the M1 (1wt.%Mn) alloy but contains further micro-alloying additions that refine the grain size without significantly affecting extrudability. The alloy is also less strongly textured than AZ31, which means that as well as being much more extrudable its tension-compression anisotropy is reduced.

A further challenge for magnesium alloy sections is that whilst they absorb a lot of energy during deformation in bending [2, 10] and uniaxial compression, they fracture instead of folding uniformly like aluminium and steel sections during compression [11]. This loss of structural integrity is likely to limit the application of magnesium in applications such as crash boxes and front rails. However, they could be very suitable for bumper beams and other applications where bending is the primary deformation mode.

A further challenge is how to join magnesium to dissimilar metals. There are two important considerations here. One issue is how to join the metals. Welding is not an option as brittle intermetallics form. Hence a mechanical join is required.

One of the most common mechanical joining techniques for aluminium and steel is self-piercing riveting SPR. However, SPR of magnesium leads to extensive cracking due to its relatively low room temperature ductility.
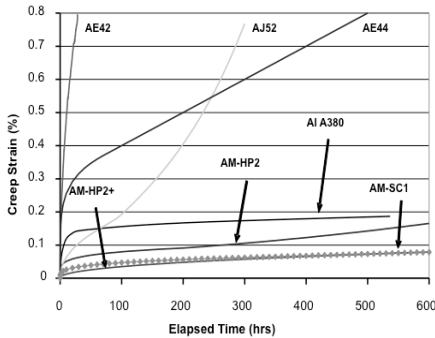


**Fig. 1.** A comparison of a range of creep resistant magnesium alloys at 177°C and 90MPa with the aluminium alloy, A380. Data from Reference [9].
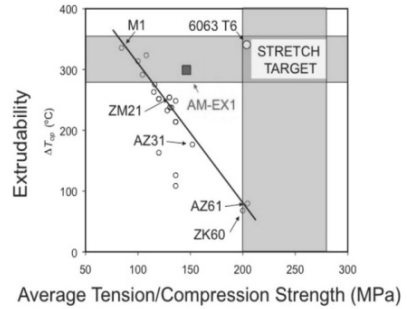
**Fig. 2.** A comparison of the extrudability and strength for a range of magnesium alloys compared with the aluminium alloy 6063 in the T6 heat treated condition.

There have been a number of approaches to heat the magnesium pieces to make them more ductile and allow for self-piercing riveting to be done successfully. However, one of the major issues has been the problem of heating the magnesium fast enough that productivity is retained. CAST has added a laser to the SPR process to locally heat the magnesium ply to temperatures where the magnesium becomes more formable before riveting creating crack-free joints (Fig. 3. ). This technique has demonstrated that satisfactory joining by SPR, with or without adhesive bonding, can be done within a cycle time of less than 5 seconds [9, 12], and the technology has already been implemented up to a pre-production level by CAST CRC and their partner for SPR, Henrob.
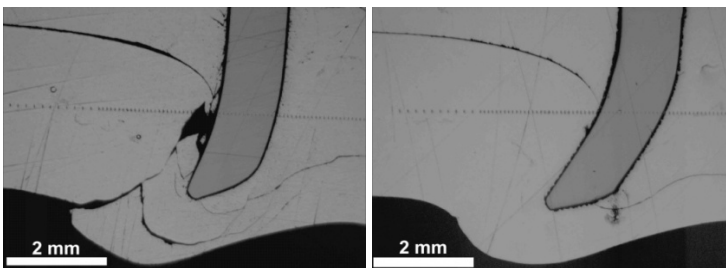


**Fig. 3.** A comparison of a self-piercing rivet in a two-ply magnesium alloy stack (a) without laser pre-heating and (b) with laser pre-heating. After [9].

## 3.3   Corrosion Resistance

Magnesium is one of the most electrochemically active elements. Hence corrosion resistance is a major issue. Cathodic impurity elements such as Fe, Ni and Cu are particularly detrimental [13]. Careful control of these elements has lead to the development of alloys relatively tolerant to general corrosion, with high pressure die cast AZ91D having comparable corrosion resistance to aluminium alloy A380.

More challenging is corrosion related to galvanic couples, especially with steel. Magnesium alloys need to be electrically insulated from steel, which can be done, however, at an expense. Furthermore, for example, in riveting or other mechanical fastening operations, steel is often used which provide a substantial driving force for corrosion. This can restrict magnesium alloys to internal applications.

Coating systems are an important part of the corrosion prevention strategy for magnesium alloys and there are a number of different commercial products. An evaluation of these in a variety of environments has shown that their effectiveness can vary widely. In a ZE41 (4wt.%Zn and 1wt.%REs) alloy, used for helicopter gearbox housings it was found that Tagnite is superior to other new coating developments and a substantial improvement on the incumbent technology. Recently a technology solution for an e-coating a body-in-white containing magnesium components has been proposed [14], which promises to allow magnesium parts to be used in body structures.

Hence whilst magnesium based alloys will always be susceptible to corrosion, a combination of improved alloy compositions, engineered galvanic solutions and protective coatings enable magnesium alloys to be used even in challenging environments.

## 3.4   Life Cycle Analysis

Magnesium alloys, even more so than aluminium alloys, have a very high embodied energy. Typically, the initial higher energy consumption and $CO_2$ emissions are more than saved over the life-cycle of an automobile due to the reduced energy usage during the use-phase [15-17]. The initial environmental cost associated with magnesium usage has been exacerbated by the closing down of state of the art western electrolytic magnesium production facilities often powered by hydroelectricity. Most of the world's magnesium is now produced in China using the Pigeon process leading to a more than doubling of the $CO_2$ emissions required to produce a unit of magnesium. A consequence of this is that whilst significant benefits are still associated with replacing steel with magnesium, there is little benefit in using magnesium over aluminium or even steel in some cases [16-18] or against composites [19]. The use of magnesium in castings is still one of the best choices. It is important to note, however, that the Chinese magnesium industry is working hard to reduce their emissions and it is likely that improvements have already substantially reduced the emissions related to magnesium production. Furthermore, re-entry into the market by an electrolytic magnesium producer would help the situation substantially, particularly if the electricity comes from green sources such as hydropower.

Another challenge for magnesium environmentally is that a cover gas is required during casting as most magnesium alloys burn in the molten state. The most commonly used cover gas has been $SF_6$, which is the worst greenhouse gas known with a greenhouse warming potential 23,900 times that of $CO_2$. AM-Cover, based on HFC-134A is an alternative that saves at least 95% of the greenhouse gas emissions [20]. Recent technology improvements such as eco-Mg may further reduce the need for cover gases that are harmful to the environment.

## 4 Conclusions

Magnesium alloys are an important part of the light-weighting strategy for automotive applications. Many of the technical challenges associated with magnesium usage have been at least partially overcome. There are new alloys with good creep resistance for powertrain applications, new high rate extrusion alloys with good properties and new techniques for joining magnesium to other metals. Controlling the corrosion resistance, particularly in galvanic situations, is still a challenge but with improved engineering solutions and coatings substantial progress has been made. A final challenge for magnesium alloys is that the current dominant magnesium production process has a large environmental footprint. This will reduce as the Chinese magnesium industry improves its practices and hopefully electrolytic production of magnesium will soon return.

## References

[1] Watarai, H.: Science and Technology Trends (2006); Quarterly review No. 18:84
[2] Easton, M.A., Song, W.Q., Abbott, T.: Mater. Design 27, 935 (2006)
[3] Luo, A.: JOM 54, 42 (2002)
[4] Mordike, B.L., Ebert, T.: Mater. Sci. Engng. A A302, 37 (2001)
[5] Luo, A.: Int. Mater. Rev. 49,13 (2004)
[6] Pekguleryuz, M.O., Celikin, M.: Int. Mater. Rev. 55, 197 (2010)
[7] Bakke, P., Westengen, H.: Adv. Engng. Mater. 5, 879 (2003)
[8] Gibson, M.A., Easton, M.A., Tyagi, V., Murray, M.T., Dunlop, G.L.: In: Pekguleryuz, M.O., Neelameggham, N.R., Beals, R., Nyberg, E.A. (eds.) Magnesium Technology 2008, p. 227. The Metals, Minerals and Materials Society, New Orleans (2008)
[9] Easton, M.A., Beer, A., Barnett, M.R., Davies, C., Dunlop, G.L., Durandet, Y., Blacket, S., Hilditch, T., Beggs, P.: JOM 60, 57 (2008)
[10] Hilditch, T., Atwell, D., Easton, M.A., Barnett, M.: Mater. Design 30, 2316 (2009)
[11] Beggs, P., Song, W., Easton, M.A.: International Journal of Mechanical Sciences 52, 1634 (2010)
[12] Durandet, Y., Deam, R., Beer, A., Song, W., Blacket, S.: Mater. Design 31, S13 (2010)
[13] Polmear, I.J.: Mater. Sci. Technol. 10, 1 (1994)

[14] Song, G.L.: Progress in Organic Coatings 70, 252 (2011)

[15] Hakamada, M., Furuta, T., Chino, Y., Chen, Y., Kusuda, H., Mabuchi, M.: Energy 32, 1352 (2007)

[16] Cáceres, C.H.: Metall. Mater. Trans. A 38, 1649 (2007)

[17] Tharumarajah, A., Kultun, P.J.: Clean. Prod. 15, 1007 (2007)

[18] Tharumarajah, A., Koltun, P.: Resources, Conservation and Recycling 54, 1189 (2010)

[19] Witik, R.A., Payet, J., Michaud, V., Ludwig, C., Manson, J.E.: Composites: Part A 42, 1694 (2011)

[20] Ricketts, N.J., Cashion, S.P.: In: Hryn, J. (ed.) Magnesium Technology 2001, p. 31. The Minerals, Metals and Materials Society, Warrendale (2001)

# Performance of Advanced High Strength Steel and Aluminium Alloy Tubes in Three-Point Bending

Gayan Rathnaweera[1,2,*], Yvonne Durandet[1,2], Dong Ruan[2], and Michael Hajj[3]

[1] CAST Cooperative Research Centre, IRIS, Swinburne University of Technology, Hawthorn, VIC 3122, Australia
[2] Faculty of Engineering and Industrial Sciences, Swinburne University of Technology, Hawthorn, VIC 3122, Australia
[3] Henkel Australia Pty Ltd, 135-141 Canterbury Road, Kilsyth VIC 3137, Australia
`grathnaweera@swin.edu.au`

**Abstract.** In this study, quasi-static and dynamic three-point bending tests were carried out to evaluate the performance of tubes made of different materials for their application in side impact protection. The load carrying capacity, total and specific energy absorption, and fracture characteristics were determined for cylindrical welded tubes of an advanced high strength steel (AHSS) and cylindrical extruded tubes of aluminium alloys 6061T6 and 7075T6. The results showed that the peak bending load and energy absorption best correlate to the tube's yield strength and wall thickness. In addition, finite element analysis was performed using the commercial software package LS-DYNA$^{®}$. The simulation outputs showed good agreement with experimental data. The finite element model will be used in the future parametric studies.

## 1 Introduction

Fuel economy, greenhouse gas emissions, carbon regulation and crashworthiness are most important issues being addressed in the research and development of new generation of vehicles. One solution to these issues is by reducing vehicle weight. Active research is being dedicated to innovative designs that involve advanced high strength steels (AHSS), lightweight materials such as aluminium, magnesium and engineering plastics in order to bring down the weight of vehicles while maintaining or improving safety.

Hollow tubes (~ wall thickness of 1-5 mm) are widely used in automotive industry to improve the crashworthiness of vehicle by increasing the specific energy absorption in crash event. In a vehicle crash, vehicle structure is subjected to a variety

---

[*] Corresponding author: +61 (03) 9214 5056.

of loading conditions. The current work focuses on the case of bending especially under side impact loads. There has been considerable research [1-5] into the bending deformation of tubes experimentally and numerically. They found that the bending deformation of tubes runs through three phases: pure crumpling, bending and crimpling and structural collapse. In addition, the bending behavior varies with the tube dimensions and experimental conditions. However, most of these studies have used the tubes made of conventional aluminium alloys and steel, very less work has been published on the behavior of emerging metals AHSS [6, 7] and high strength aluminium alloys [8]. Besides, no comparison study was found between AHSS and high strength aluminium alloys.

The objective of this study was to investigate the performance of cylindrical tubes made of AHSS and high strength aluminium alloys in quasi-static and dynamic three-point bending for their application in vehicle side-impact protection.

## 2   Materials

Welded cylindrical tubes of advanced high strength steel (AHSS) and extruded cylindrical tubes of two aluminium alloys 6061T6 and 7075T6 were used in the current study. Details of the tube's materials and dimensions are given in Table 1.

**Table 1.** Tubes materials and dimensions

| Material | Outer diameter(mm) | Wall thickness(mm) |
|----------|--------------------|--------------------|
| AHSS     | 35.25              | 2.0                |
| 6061T6   | 35                 | 3.0                |
| 7075T6   | 36                 | 4.1                |

## 3   Experimental Procedure

Three-point bending experiments were performed on tubes specimens cut to 340 mm lengths. The support span in the three-point bending rig was set to 260 mm, and the diameter of the indenter and supports was 19.05 mm (3/4') , as shown in Figure 1. The tubes were evaluated through quasi-static and dynamic experiments. Two duplicate tests were conducted for all tubes and conditions to ensure the reproducibility of the results. The energy absorption (EA) of the tubes was determined from the area under the force-displacement curve. The energy absorption was divided by the weight of the tube to calculate the specific energy absorption (SEA).

Quasi-static experiments were carried out using 250 kN mechanical testing machine MTS (Model 819). Testing was executed up to a maximum displacement of 60 mm at a constant speed of 0.35 mm/s. Reaction force and indenter displacement were recorded at 20 Hz sampling rate.
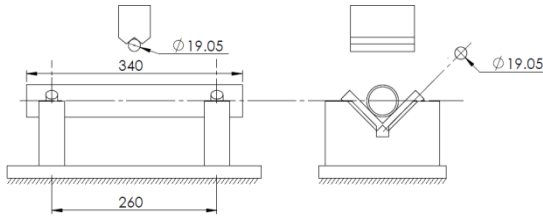
**Fig. 1.** Support rig and indenter used for quasi-static and dynamic three-point bending tests (dimensions are in mm).

Dynamic experiments were carried out using a drop hammer. The combined weight (23.2 kg) of the drop-carriage with the indenter was dropped from 3.5 m height, which gave an impact speed of 29.84 km/h. The indenter's displacement was measured using a laser triangulation displacement sensor LD1627-200 from MICRO-EPSILON. The load at the support base was measured using a Kistler's quartz load cell, model 9081A, with a charge meter type 5015. The data from the charge meter and the laser displacement sensor were acquired on Tektronix's digital oscilloscope (model TDS2024B) at a sampling rate of 50 kHz.

## 4   Finite Element Modeling

Finite element analysis (FEA) of three-point bending was performed using LS-DYNA® [9]. Due to the symmetry of the tube, only a quarter of the tube was modeled. The tubes were modeled with fully integrated solid elements and IHQ=6 in hourglass control. A power law isotropic plasticity material model, MAT_018, was used for the tube material. The indenter and support were modeled as rigid bodies with default Belytschko_tsay shell elements and MAT_020 due to their high modulus of elasticity and negligible elastic deflections compared to the tube. SURFACE_TO_SURFACE contact was utilized for tube-indenter and tube-support contacts. Static friction coefficient FS and dynamic friction coefficient FD were defined as 0.5 for both tube-support and tube-indenter contacts. Quasi-static indenter displacement was modeled using the PRESCRIBED_MOTION_RIGID command in implicit analysis, and dynamic indenter displacement was modeled by introducing INITIAL VELOCITY in explicit analysis.

The material properties of the tubes were derived from inverse finite element analysis of lateral compression tests [10]. The material parameters (density ($\rho$), modulus of elasticity (E), yield stress ($\sigma_y$), work hardening coefficient (k) and exponent (n)) used in the present study are given in Table 2. The analysis was conducted on a HP Z400 workstation with 64-bit Windows 7 operating system.

**Table 2.** The material parameters derived from [10].

| Material | ρ (g/cm³) | E (GPa) | σy (MPa) | k (MPa) | n |
|----------|-----------|---------|----------|---------|------|
| AHSS | 7.8 | 207 | 1460 | 1534.15 | 0.01 |
| 6061T6 | 2.7 | 67.5 | 313 | 410.00 | 0.05 |
| 7075T6 | 2.7 | 70 | 400 | 491.79 | 0.04 |

## 5   Results and Discussion

Lu and Yu [11] have derived an empirical formula to calculate reaction force of a tube in three-point bending (equation 1)

$$P = 3.78 \, \sigma_y \, \delta^{0.47} \, t^{1.6} \, D^{-0.07} \tag{1}$$

The formula was given for L/D=10, where, L is support length and D is tube outer diameter. However, for the current study L/D was 7.2, hence the numerical constant for current study was calculated ((3.78/10) ×7.2).

$$P = 2.72 \, \sigma_y \, \delta^{0.47} \, t^{1.6} \, D^{-0.07} \tag{2}$$

Where, P, $\sigma_y$, $\delta$, t and D are force, yield stress, indenter displacement, wall thickness and outer diameter of the tube respectively. Theoretical peak forces obtained from equation 2 have shown good accuracy for all tubes as shown in Figure 2. Since the tube diameter and indenter displacement at peak force were approximately constant for all tubes, it can be concluded that the peak force of the tubes under quasi-static three-point bending was proportional to the yield stress and tube thickness. Typical force-displacement curves in both quasi-static and dynamic tests for tubes are shown in Figure 2.

AHSS tubes showed the highest total energy absorption in both quasi-static and dynamic test followed by 7075T6 and 6061T6 tubes. However, the specific energy absorption of 7075T6 tube was slightly higher than AHSS and 6061T6 tubes. In addition, AHSS tubes showed the lowest indenter displacement ($\delta$) in dynamic test. Results are summarized in Table 3.
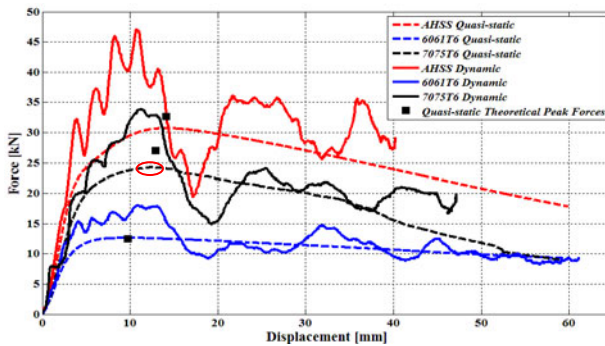


**Fig. 2.** Typical force-displacement curves of tubes in quasi-static and dynamic three-point bending tests.

**Table 3.** Summary of quasi-static and dynamic three-point bending results.

| Material | Quasi-static | | | Dynamic | | | |
|---|---|---|---|---|---|---|---|
| | Peak force (kN) | EA (J) | SEA (J/kg) | Peak force (kN) | EA (J) | SEA (J/kg) | $\delta$ (mm) |
| AHSS | $30.7 \pm 0.5$ | $1444.8 \pm 17$ | $2520.6 \pm 20$ | $47 \pm 0.5$ | $1235.5 \pm 14$ | $2148.7 \pm 15$ | $40.2 \pm 0.3$ |
| 6061T6 | $12.64 \pm 0.1$ | $639.4 \pm 7$ | $2275.4 \pm 30$ | $18 \pm 0.3$ | $704.04 \pm 15$ | $2503.7 \pm 50$ | $61.1 \pm 0.3$ |
| 7075T6 | $24.25 \pm 0.1$ | $1022 \pm 40$ | $2666.3 \pm 50$ | $33.92 \pm 0.4$ | $994.5 \pm 20$ | $2591.9 \pm 50$ | $47.4 \pm 0.3$ |

$\delta$: Indenter displacement in three-point bending tests.

7075T6 tubes fractured (Figure 3) underneath the indenter during both quasi-static and dynamic tests. An instantaneous drop in load was observed immediately after the fracture, which occurred at about 12.9 mm indenter displacement in quasi-static tests (Figure 2). AHSS and 6061T6 tubes did not fracture in any of the tests, which were conducted up to a maximum indenter displacement of 60 mm. However, the rate of load decrease after reaching the peak force was similar for AHSS and 7075T6 tubes, while the 6061T6 tubes showed a much lower rate of load decrease. Higher rate of load decrease in AHSS tube could be due to thinner wall thickness compared to other tubes while fracture was the cause for 7075T6 tube's load decrease.
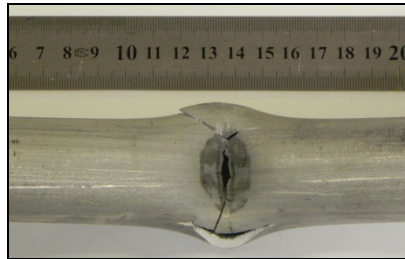


**Fig. 3.** Fracture underneath the indenter for the 7075T6 tube in quasi-static three-point bending test.

A slight increase in energy absorption was observed for dynamic experiments for similar indenter displacements (Figure 4). This could be due to inertia effects since aluminium and high strength steel are not strain rate sensitive materials.

A good correlation between FEA simulations and experimental data was observed (Figure 5 & 6). No failure criterion was applied in the current FEA study. Therefore, the FEA simulation for 7075T6 tubes was not able to predict accurately the load-displacement behavior from the initiation of fracture.

A failure criterion will be used in future studies to improve the FEA model and carry out parametric modeling to optimize the tube dimensions for performance as vehicle side door intrusion beams.
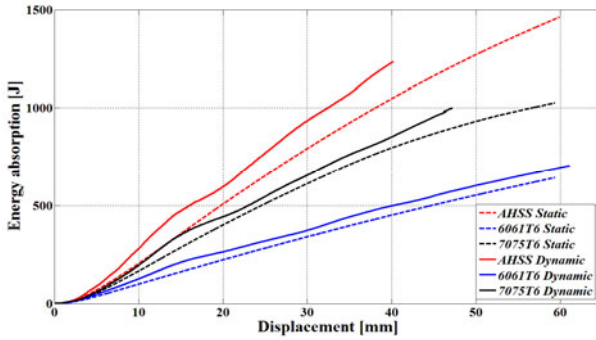
**Fig. 4.** The total energy absorption of tubes in quasi-static and dynamic three-point bending tests.

In addition, material properties of 7075T6 given by Hilditch et al. [8] were used to model quasi-static three-point bending of 7075T6 tubes of current study( Fig. 5). Predicted peak force and energy absorption were considerably higher than all tubes used in current study. This result further explains the proportionality of yield stress to peak force and energy absorption.
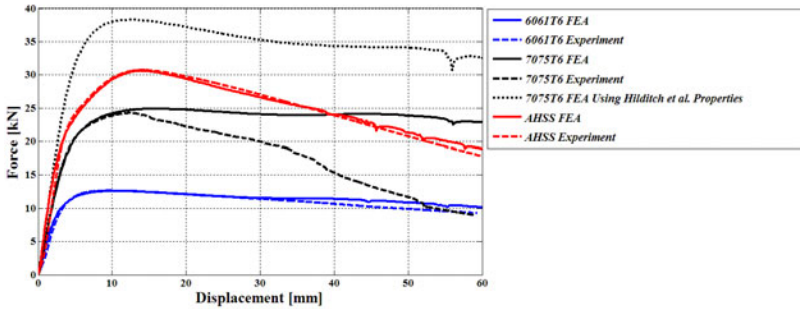


**Fig. 5.** Comparison of FEA and experimental force-displacement curves of tubes in quasi-static three-point bending test.
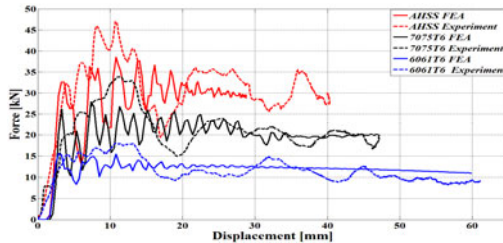


**Fig. 6.** Comparison of FEA and experimental force-displacement curves of tubes in dynamic three-point bending test.

# 6 Summary/Conclusions

The performance of welded AHSS and extruded aluminium alloys 7075T6 and 6061T6 tubes were studied in quasi-static and dynamic three-point bending.

- The peak force of the tubes was proportional to yield stress and tube thickness.
- Among the studied tubes, AHSS showed the highest total energy absorption while 7075T6 showed the highest specific energy absorption in both static and dynamic tests.
- 7075T6 tubes fractured during both quasi-static and dynamic tests and their load carrying capacity and energy absorption decreased, while other tubes did not fracture in either test.
- A slight increase in energy absorption was observed in dynamic tests and it could be due to inertia effects since high strength steel and aluminium are not strain rate sensitive materials.
- A good correlation between FEA and experiments was observed except for 7075T6 tubes after the onset of fracture. A failure criterion needs to be applied to improve the current model and determine the tube dimensions for optimum performance as vehicle side door intrusion beams.
- 7075T6 tubes with higher yield stress and optimized tube dimensions, could obtain considerable weight savings in their application in side impact protection.

# References

1. Thomas, S.G., Reid, S.R., Johnson, W.: Large deformations of thin-walled circular tubes under transverse loading-I. An experimental survey of the bending of simply supported tubes under a central load. International Journal of Mechanical Sciences 18(6), 325–326 (1976); in3-in6, 327–333
2. Watson, A.R., Reid, S.R., Johnson, W.: Large deformations of thin-walled circular tubes under transverse loading-III. Further experiments on the bending of simply supported tubes. International Journal of Mechanical Sciences 18(9-10), 501–502 (1976)
3. Watson, A.R., Reid, S.R., Johnson, W., Thomas, S.G.: Large deformations of thin-walled circular tubes under transverse loading-II. Experimental study of the crushing of circular tubes by centrally applied opposed wedge-shaped indenters. International Journal of Mechanical Sciences 18(7-8), 389–397 (1976); IN11-IN14, 389–397
4. Mamalis, A.G.: Bending of cylindrical steel tubes: Numerical modelling. International Journal of Crashworthiness 11(1), 37–47 (2006)

5. Černiauskas, E., Keršys, A., Lukoševičius, V., Sapragonas, J.: Investigation of anti-intrusion beams in vehicle side doors. Mechanika 86(6), 11–16 (2010)
6. Link, T.M., Jensen, C.M.: Three-Point Bending Crash Performance of Advanced High Strength Steels. SAE Technical Paper No. 2009-01-0797 (2009)
7. Tanabe, H., Miyasaka, A., Yamazaki, K., Iwasaki, T., Akada, H.: High-strength steel tubes for automobile door impact beams. Nippon Steel Technical Report 64, 55–61 (1995)
8. Hilditch, T., Atwell, D., Easton, M., Barnett, M.: Performance of wrought aluminium and magnesium alloy tubes in three-point bending. Materials & Design 30(7), 2316–2322 (2009)
9. Hallquist, J.: LS-DYNA. Keyword User's Manual. Version 971. Livermore Software Technology Corporation (2007)
10. Rathnaweera, G., Durandet, Y., Ruan, D., Kinoshita, S.: Charaterizing the material properties of a tube from lateral compression test. Submitted to International Journal of Protective Structures (2011) (on review)
11. Lu, G., Yu, T.: Energy absorption of structures and materials. Woodhead Publishing Ltd., UK (2003)

# A System Dynamics Approach to Understanding the Influence of Lightweight Materials on the Development of Fuel Efficient Cars

Peter Stasinopoulos, Paul Compston, and Haley M. Jones

Research School of Engineering, College of Engineering and Computer Science
The Australian National University, Canberra, ACT 0200, Australia
peter.stasinopoulos@anu.edu.au

**Abstract.** This paper presents a dynamical model that assists in understanding the influence of lightweight materials on the development trajectory of fuel efficient cars. Preliminary results suggest that car mass and powertrain energy consumption may become significantly non-linear and may generally decrease in the coming decades due to the emergence of new technologies.

## 1   Introduction

In response to consumer demand for economical and fuel efficient cars, many automakers are developing various new powertrain technologies, such as advanced internal combustion engine (ICE) and battery-electric (BE) powertrains. Some automakers are reducing the capacity and capital cost of their BE powertrains by aggressively lightweighting the body-in-white (BIW). Most of these automakers are downsizing their steel BIW, while a few are switching to higher-cost lightweight materials. Estimates of the life-cycle resource (energy and materials) consumption of these new technologies for a single car often show that the high resource costs of production are recovered during use (e.g. Puri et al. 2009). Although the new technologies may be more resource efficient than conventional technologies, they also take a long time come into use due to slow processes such as technology adoption and car fleet turnover. Accounting for these processes requires methods that enable computation parameters to vary dynamically (Stasinopoulos et al. 2011).

The emergence of new options for powertrains and BIW materials will intensify competition amongst automakers and technology producers. Competition is a dynamic process and, in the presence of persistent consumer demand for fuel efficient cars, will likely cause automakers to continually invest in lightweighting and fuel efficiency.

This paper addresses the question: how might the adoption of a lightweight BIW influence (1) car mass and (2) powertrain energy consumption, over time? This investigation takes a System Dynamics approach. Such an approach enables larger investigations, such as Life Cycle Assessments, to account for changes over time in resource flows (e.g. Stasinopoulos et al. 2011).

In this paper, a model is presented, including the dynamic processes, assumptions, and one set of likely input conditions. The model output under those conditions is then analysed, with the significance of the results discussed, leading to suggestions for potential refinements to the model.

## 2   Model

The model considers two cars, a 'steel car' with a steel BIW and a 'lightweight car' with a lightweight-material BIW. The cars may retain their ICE powertrain or adopt a BE powertrain. Each car represents the average large car of its type in the fleet. Figure 1 presents a causal loop diagram of the two hypothetical dynamic processes in the model.

- The upper two loops describe *mass decompounding* using the lightweight car (LW). The same process occurs for the steel car. Since a lightweight BIW requires less energy to move, powertrain and chassis technologies are downsized, leading to further BIW lightweighting. Decompounding is ultimately balanced as producers approach the cost effective limits of downsizing their technologies. Furthermore, BE powertrain technologies with high costs per unit of energy capacity become cost effective sooner.
- The lower three loops describe *market competition* using the ICE and BE powertrains. The same process occurs for the lightweight and steel cars. Producers of steel BIWs invest in lightweighting to protect their market share. In response, producers of lightweight BIWs further invest in lightweighting to expand their market share. Escalating competition is ultimately balanced as producers approach the technological limits of lightweighting. Similarly, when BE powertrains are adopted, producers of ICE powertrains and producers of BE powertrains begin to compete. Escalating competition is balanced either as producers approach the technological limits of conversion efficiency or when automakers abandon ICEs.



**Fig. 1.** A causal loop diagram representing the hypothetical dynamic processes of mass decompounding and market competition. The text elements represent system state variables and the arrows represent influence links. The plus (+) and minus (-) signs on the arrows indicate link polarity. The encircled R indicates a reinforcing feedback loop, and the encircled B indicates a balancing feedback loop.

For the purpose of computation, a stock-and-flow model was constructed using the software STELLA™ (version 9.1.2). It performs dynamical computations by allowing parameters to influence their own values. It consists of two sub-models.

- The *BIW sub-model* simultaneously adjusts the masses of the steel car and the lightweight car. Initially, the lightweight BIW (including exterior panels) is made of aluminium but can switch to a fibre-reinforced polymer composite when the technology becomes cost effective, while the steel BIW is made of conventional steel but can increase its proportion of high-strength steel. The mass of each car decreases over time via mass decompounding in response to competition.
- The *powertrain sub-model* simultaneously adjusts the fuel consumption of ICE powertrains and the electricity consumption of BE powertrains. Initially, each car has a 150kW, ICE powertrain but can switch to a BE powertrain when the technology becomes cost effective for its mass at a range of 300km. The conversion efficiency of each powertrain increases over time in response to competition while both technologies are in use.

The purpose of the stock-and-flow model is to assist in understanding the complex behaviour of the system arising from accumulations, feedback loops, and non-linear relationships between parameters (Sterman 2000). The model is used to understand the influence of key variables on a particular problem, rather than as a purely computational tool. Such a model is typically run under various scenarios with a concurrent sensitivity analysis of its parameters and structure, especially at its boundary, where feedback loops have been broken. In this paper, as a preliminary demonstration, the model is run under one possible scenario, which assumes the following input conditions:

- Prior to any mass decompounding, both cars begin with a 470kg powertrain, 300kg of chassis components, and 600kg of other components (Lovins and Cramer 2004). Steel BIWs have an initial mass of 430kg and a minimum mass of 280kg, aluminium BIWs have an initial mass of 340kg and a minimum mass of 210kg, and composite BIWs have an initial mass of 230kg and a minimum mass of 150kg (FutureSteelVehicle 2011; Kelkar et al. 2001; Lovins & Cramer 2004). BE powertrains do not introduce a mass penalty.
- When the petrol price is high (>$2/L), each iteration of mass decompounding causes, per 1kg of car mass removed, the removal of 0.09kg of powertrain mass, 0.13kg of chassis mass, and 0.09kg of BIW mass (Bjelkengren 2008). When the petrol price is low (<$1/L), no mass decompounding occurs. The rates of mass decompounding vary linearly within this range of petrol price.
- ICE powertrains consume petrol at an initial rate of 2000J/km/kg of car mass (@ 20% conversion efficiency) and at a minimum rate of 1400J/km/kg of car mass (@ 30% conversion efficiency). BE powertrains consume electricity at an initial rate of 470J/km/kg of car mass (@ 70% conversion efficiency) and at a minimum rate of 410J/km/kg of car mass (@ 80% conversion efficiency).

- When the petrol price is high (>$2/L), producers take 15 years to develop their technologies to within 90% of the technological limit under the most competitive conditions. When the petrol price is low (<$1/L), producers take 45 years for the same task. This response time varies linearly within this range of petrol price.
- Compared to the percentage variation in petrol price, steel price varies by 100%, aluminium price varies by 50%, and composite price varies by 100%— roughly the same proportions in which these prices varied around the 2008 oil price peak. Composite price also decreases with increasing production experience. The minimum price of any material is $0.1/kg. Figure 2 shows the assumed prices of petrol and BIW materials.
- The ICE powertrain price is $5000 plus $120/kW; the BE powertrain price is $5000 plus $500-1200/kWh (Mock et al. 2007). Figure 2 shows the assumed energy-dependent component of price of the BE powertrain.
- A car with a steel BIW and an ICE powertrain has a price of $35,000; an aluminum BIW adds a 5% premium, a composite BIW adds 20%, and a BE powertrains adds 10% (Mock et al. 2007). These premiums recover the higher price of the lightweight materials and BE powertrain. All other production costs of the steel car and the lightweight car are equal at any production volume, regardless of the BIW or powertrain.
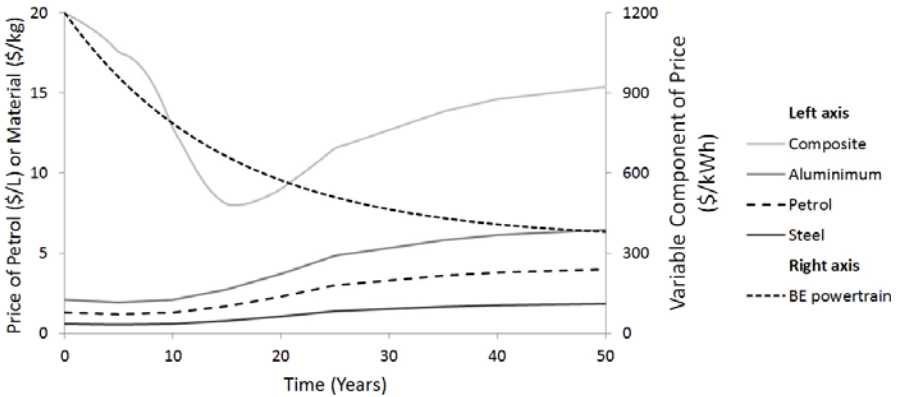


**Fig. 2.** The assumed price of petrol, prices of body-in-white materials, and the energy-dependent component of price of battery electric powertrains. These values are fixed.

## 3 Results and Discussion

Figure 3 presents the outputs of the model under the conditions described above. It shows that car mass and powertrain energy consumption vary nonlinearly over time. Given the purpose of the model, described above, it is the shapes of the outputs in Figure 3, rather than the values on the axes, that are significant. The outputs have the following characteristics:

- *Car mass*: Initially, the lightweight car adopts the aluminium BIW, resulting in a step change in mass (1). Only a small amount of mass decompounding occurs because the petrol price is moderately low (2). The gap between the masses of the cars creates competition, with the steel car aiming to recover the gap and the lightweight car aiming to retain the gap. The mass of the steel car decreases moderately quickly with strong initial competition (large gap to recover) and a moderately low petrol price, and then more slowly as competition weakens (3). Conversely, the mass of the lightweight car decreases very slowly with weak initial competition (large gap as a buffer) and a moderately low petrol price, and then more quickly as competition strengthens (4). Some years later, the composite BIW becomes cost effective for the lightweight car, resulting in another step change in mass (5). A moderate amount of mass decompounding occurs because the petrol price is moderately high (6). The new gap re-establishes strong competition for the steel car (7) and weak competition for the lightweight car (8). Eventually, the masses of both cars decrease very slowly as their BIWs approach the technological limits of lightweighting (9).
- *Powertrain energy consumption*: Initially, both cars have an ICE powertrain, and there is no competition (10). Many years later, the BE powertrain becomes cost effective for the lightweight car, resulting in both powertrains being used. The gap between the energy consumption of the powertrains now creates competition, with the ICE powertrain aiming to recover the gap and the BE powertrain aiming to retain the gap. The energy consumption of the ICE powertrain decreases quickly with strong initial competition and a high petrol price, and then more slowly as competition weakens (11). Conversely, the energy consumption of the BE powertrain decreases slowly with weak initial competition and a high petrol price, and then more quickly as competition strengthens (12). Eventually, the energy consumptions of both powertrains decrease very slowly as they approach the technological limits of conversion efficiency (13). Some years later, the BE powertrain becomes cost effective for the steel car, resulting in both cars having a BE powertrain and competition ceasing.
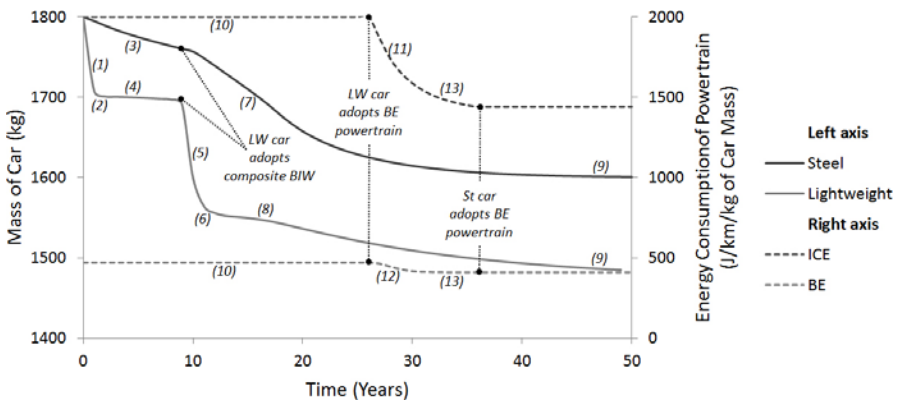


**Fig. 3.** The computed masses of the steel car and lightweight car, and computed energy consumptions of ICE powertrains and BE powertrains.

The first run of the model provides a foundation for simplifying the model without affecting its characteristic behaviour. For example, since the mass decompounding process occurs so quickly, it could be modelled more simply as an instantaneous change in a parameter. By contrast, since the market competition process has a significant influence over the timeframe of the problem, it should be retained (Meadows 2009). A sensitivity analysis would suggest other parameters and structures that should be further investigated. One such parameter is the price premium for cars with composite BIWs. Increasing its value by 40% makes composite BIWs immediately cost effective. Since it is on the system boundary, it could also form new feedback structures with other parameters, such as petrol price.

## 4    Conclusion

This investigation takes a System Dynamics approach to understanding the influence of the adoption of a lightweight BIW on the development of fuel efficient cars. Preliminary results suggest that the values of key computation parameters may become significantly non-linear in the coming decades due to the emergence of new technologies. An understanding of how conditions influence such variables can help to reduce the uncertainty in studies of future scenarios.

## References

Bjelkengren, C.: The impact of mass decompounding on assessing the value of vehicle lightweighting. MSc Thesis, Massachusetts Institute of Technology, p. 37, 38, 61, 66 (2008)

FutureSteelVehicle, FutureSteelVehicle: overview report, World Auto Steel, Middletown, OH, USA (2011)

Kelkar, A., Roth, R., Clark, J.: Automobile bodies: can aluminum be an economical alternative to steel? Journal of the Minerals, Metals and Materials Society 53(8), 28–32 (2001)

Lovins, A.B., Cramer, D.R.: Hypercars, hydrogen, and the automotive transition. International Journal of Vehicle Design 35(1/2), 50–85 (2004)

Meadows, D.H.: Thinking in systems: a primer. Earthscan, London (2009)

Mock, P., Schmid, S.A., Friedrich, H.E.: Market prospects of electric pas-senger vehicles. In: Pistoia, G. (ed.) Electric and Hybrid Vehicles: Power Sources, Models, Sustainability, Infrastructure and the Market. Elsevier (2010)

Puri, P., Compston, P., Pantano, V.: Life cycle assessment of Australian automotive door skins. International Journal of Life Cycle Assessment 14(5), 420–428 (2009)

Stasinopoulos, P., Compston, P., Newell, B., Jones, H.M.: A System Dynamics approach in LCA to account for temporal effects—a consequential energy-LCI of car bodies-in-white. International Journal of Life Cycle Assessment (2011) (in press)

Sterman, J.D.: Business dynamics: systems thinking and modeling for a complex world. McGraw Hill, Boston (2000)

# Functional Fatigue of Shape Memory Alloys

T. Ataalla, M. Leary, and A. Subic

School of Aerospace Mechanical and Manufacturing Engineering, RMIT University, Bundoora Victoria 3083 Australia
martin.leary@rmit.edu.au

**Abstract.** Shape Memory Alloys (SMAs) provide an exceptional opportunity for the design of novel actuators, however their application is limited by the fatigue mode of failure. Fatigue prediction is relatively well defined for traditional materials, however, shape memory alloys display two distinct fatigue failure modes. These are structural fatigue (fracture in traditional materials) and functional fatigue (loss of shape memory effect). Functional fatigue of shape memory alloys are not well defined in literature. This work provides a novel method of analysing SMA functional fatigue data, especially when comparing a large range of potential operating conditions.

## 1  Introduction

Shape Memory Alloys (SMAs) are a unique group of materials which can undergo a solid phase, reversible, phase transformation. This phase transformation is induced by temperature or stress changes during which they can recover "seemingly permanent strains" (Hartl and Lagoudas 2007). Shape memory alloys convert temperature variation (a non-mechanical input) into a mechanical output, such as shape recovery, which can be used to actuate mechanical devices. This shape recovery can occur even under high applied loads, resulting in high actuation energy densities (Kumar and Lagoudas 2008). Due to these and other advantages, SMAs are often preferable to other active materials, and are ideal for applications where high actuation forces and displacements are required in the range of low to medium frequencies. However, much systematic research is still required, especially within the area of fatigue failure (Karhu and Lindroos 2010). The authors have identified opportunities to contribute to this important research field by a novel method of analysing SMA functional fatigue data.

### 1.1  Introduction to Fatigue

The fatigue failure mode is difficult to predict in comparison to the static failure mode. Several methods to predict fatigue failure are presented in literature:

- Stress versus number of cycles ($\sigma$-N)
- Strain versus number of cycles ($\varepsilon$-N)
- Linear Elastic Fracture Mechanics (LEFM)

Traditional fatigue failure involves the accumulation of microstructural damage and progressive crack growth leading to the physical separation of a component (Eggeler, Hornbogen *et al.* 2004). This structural failure mode is relevant to SMA design, and is the typical focus of SMA fatigue testing. However, SMA actuators are also prone to *functional fatigue*, whereby the available SMA actuation force is progressively diminished to the point that an SMA actuator is not able to function as required. This failure mode has not been fully addressed in the literature (Karhu and Lindroos 2010; Mammano and Dragoni 2011). This work presents a novel method of reporting fatigue data that allows insight into the functional fatigue failure mode of relevance to shape memory alloys.

## 1.2   Shape Memory Alloy Fatigue

SMA fatigue data presented in the literature can typically be divided into high cycle and low cycle fatigue performance; a result of cyclic loading with constant stress (McNichols, Brookes *et al.* 1981; Eggeler, Hornbogen *et al.* 2004) or constant strain amplitudes (Miyazaki, Mizukoshi *et al.* 1999). There are also factors of relevance to the fatigue life of SMAs such as stress amplitude (Eggeler, Hornbogen *et al.* 2004), and whether the SMA is subjected to a full or partial transformation.

Although much work has been completed regarding structural fatigue behaviour of SMAs, the available literature lacks much data of importance to functional fatigue. For example, the available fatigue data typically provides either constant stress or constant strain conditions. However, the commercial applicability of SMAs would be greater in many different fields if the available functional fatigue data was more complete.

This work provides novel experimental data to investigate the effect of varying input cyclic loading on fatigue performance using *stress delta* to represent the effect of functional fatigue. The stress delta is the difference between the maximum and the minimum stress observed within a loading cycle. The fatigue life of SMAs is directly related to the stress induced martensitic transformation and its interaction with cyclic strain accumulation. Therefore this investigation of the effect of stress delta is essential to achieve consistent SMA actuation.

## 2   Experimental Setup

The investigations were completed using commercially available shape memory alloy wires. NiTi SMA of 0.254mm (0.01 inch) diameter were purchased from a commercial supplier (Dynalloy 2007), manufactured in lengths of 100mm and pre-crimped to enable connection to other elements on the experimental rig. Integral connection leads were provided to allow connection to a control system and power source.

A custom experimental apparatus was developed to record the following parameters:

- Actuation force of each SMA actuator
- Stroke of each SMA actuator
- SMA fatigue life based on functional and structural fatigue conditions

The SMA wires were cycled under constant voltage and variable current conditions to obtain fatigue endurance data. The cycle duration was 1 second on (heating) and 31 seconds off (cooling). The experimental data enables the optimisation of loading conditions for stable and long life operation of SMA actuators for a range of scenarios of interest. The investigation was conducted for 3.5V, 4.0V, 4.5V, 5.0V, 5.5V, 6.0V and 6.5V. The spring rate was held constant at 1.15N/mm.

## 3   Preliminary Results

In the early stage of this project several experiments were completed to develop an efficient Design Of Experiments (DOE). Physical fatigue endurance tests were carried out to investigate the effect of resistive heating on SMA alloy wires. The maximum and minimum stresses for each loading cycle were recorded and the stress delta was calculated. The stress delta was then graphed against the number of cycles to achieve a realistic representation of the fatigue life of SMA wires.

The preliminary results indicate that increasing the electrical load applied to an SMA wire can dramatically influence fatigue life, for example 6.5V test (Figure 1) compared to 3.5V test (Figure 2).
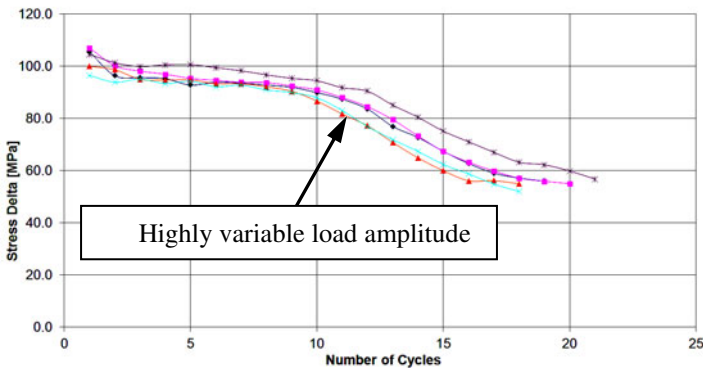


**Fig. 1.**   6.5 Volt S-N curves.
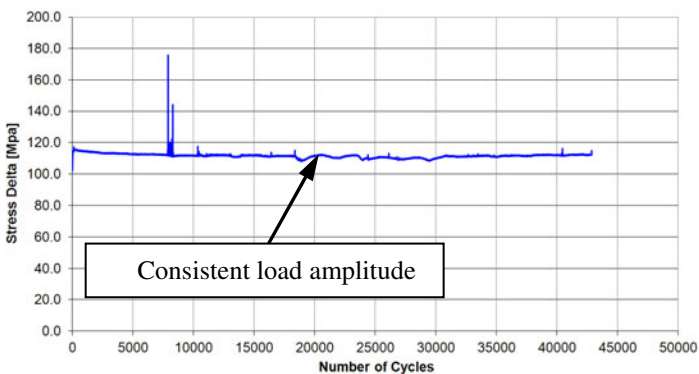


**Fig. 2.** 3.5 Volt S-N curves.

It was found shape memory alloy wire life decreased with increasing voltage. Furthermore, it is evident from the particular combinations of actuation voltage investigated that the stress delta results are highly variable (Figure 3). This experimental observation indicates opportunities to achieve a significant number of cycles while maintaining a consistent stress level. For example, it is evident from Figure 3 that the 3.5V scenario has the highest average stress delta of 106MPa and also the longest life of nearly 45,000 cycles. These outcomes are essential for the design of shape memory alloy actuators, however a close comparison of the behaviour under a range of cyclic loads is very difficult to achieve since the life can range between 20 cycles (6.5V) to 45,000 cycles (3.5V). This limitation provides an opportunity to develop a new analysis method of fatigue data.
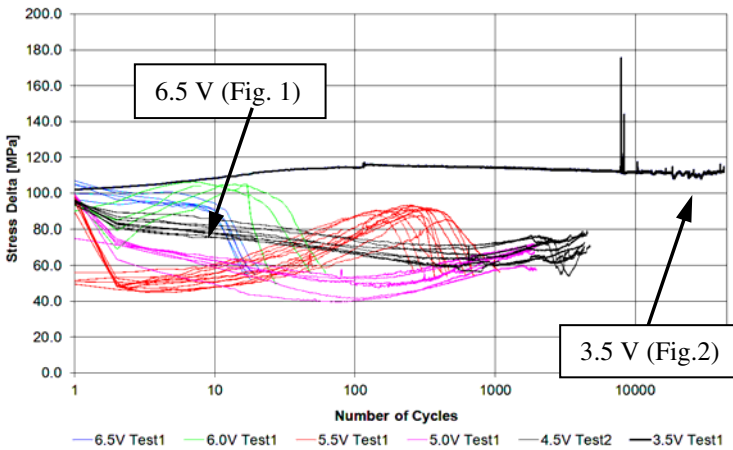
**Fig. 3.** Combined data for all tests.
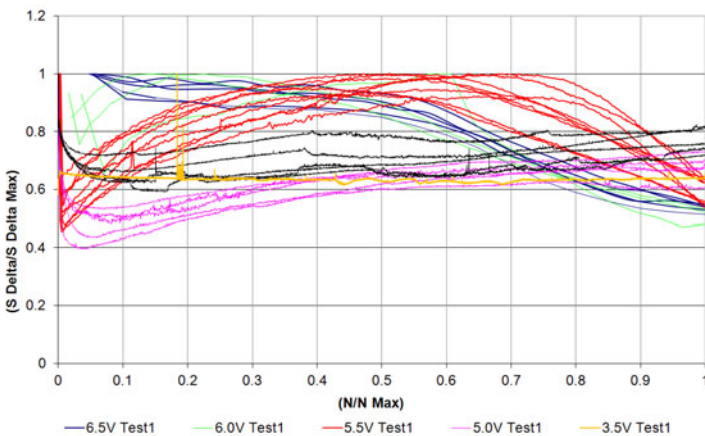
**Fig. 4.** Normalised functional stress curve.

## 4  Normalised Functional Fatigue Curve

The authors present a novel method of analysing fatigue data by normalising the axes of the functional stress chart. By normalising the observed stress delta to the maximum observed stress delta, and the observed number of cycles to the maximum number of cycles, results in a *normalised functional fatigue curve* (Figure 4). It is evident from the normalised functional stress curve (Figure 4) that each set of operating conditions has a distinct trend. These trends are clear and useful representations of shape memory alloy behaviour under different operating conditions.

## 5  Conclusion

A series of commercial SMA were assessed in terms of functional fatigue failure under a range of cyclic loads, 3.5V, 4.0V, 4.5V, 5.0V, 5.5V, 6.0V, 6.5V. The shape memory alloy wires were tested and essential fatigue data was plotted on an S-N curve. It was found that the life of the shape memory alloy wires decreased with increasing voltage. Also at 3.5V the wires seemed to reach an "infinite" lifetime and an apparent endurance limit was observed compared to the other stress levels.

A novel method of normalising the fatigue data was then used to show trends and represent the different operating conditions of interest. Future work can include additional scenarios to cover a larger range of data and obtain a better understanding of the behaviour of shape memory alloys.

## References

Hartl, D., Lagoudas, D.C.: Aerospace Applications of Shape Memory Alloys. Proceedings of the Institution of Mechanical Engineers, Part G: Journal of Aerospace Engineering 221(4), 535–552 (2007)

Kumar, P.K., Lagoudas, D.C.: Introduction to Shape Memory Alloys. Shape Memory Alloys Modeling and Engineering Applications. Springer Science + Business Media, LLC, Lagoudas D.C. (2008)

Karhu, M., Lindroos, T.: Long-term behaviour of binary Ti–49.7Ni (at.%) SMA actuators—the fatigue lives and evolution of strains on thermal cycling. Smart Materials and Structures 19(11), 115019 (2010)

Eggeler, G., Hornbogen, E., et al.: Structural and Functional Fatigue of NiTi Shape Memory Alloys. Materials Science and Engineering A 378, 24–33 (2004)

Mammano, G.S., Dragoni, E.: Functional fatigue of shape memory wires under constant-stress and constant-strain loading conditions. Procedia Engineering 10, 3692–3707 (2011)

Miyazaki, S., Mizukoshi, K., et al.: Fatigue life of Ti-50 at.% Ni and Ti-40Ni-10Cu (at.%) shape memory alloy wires. Materials Science and Engineering A 273-275, 658–663 (1999)

Dynalloy: Technical characteristics of flexinol actuator wires. Dynalloy, Inc., Costa Mesa (2007)

# Fatigue and Damage Tolerance Behavior of Fiber Composites

H. Bansemir

Consulting for Composites, Light Weight Structures and Knowledge Management, Geitnerweg , D-81825 München
e:horst@bansemir.eu

**Abstract.** The outstanding fatigue tolerance features of composite structures were the reason for introducing composite rotor blades in the helicopter design. One goal was to eliminate dynamically loaded metallic hinges. In 1967, the BO 105, a product of the former helicopter division of MBB, now Eurocopter Deutschland GmbH, flew for the first time. Its hingeless rotor was the first serial design with composite blades. Later in 1996, the EC 135 was certified according to the latest damage tolerance and fatigue certification rules. As a consequent design improvement this helicopter has a sophisticated modern rotor without any hinges and bearings. The EC 135 with the "Flexbeam-Rotor" including the bending and torsion element is shown in Fig. 1. More than 1000 helicopters have been produced until today. [Bansemir, Müller: The EC 135…].

The new American and European certification rules concerning fatigue and damage tolerance of composite structure include the establishment of replacement times and inspection intervals ["Damage Tolerance and Fatigue Evaluation…"]:

**<u>Replacement times</u>** must be demonstrated by tests or by analysis supported by tests, to ensure that the structure is able to withstand the repeated loads of variable magnitude expected in service. In establishing replacement times, the following items must be considered: Damage identified by threats, Maximum acceptable manufacturing defects and service damages, Ultimate load strength capability must be shown after application of repeated loads.

**<u>Inspection intervals</u>** must be established to ensure that any damage identified that may occur from fatigue and/or other in-service causes will be detected before it has grown to the extent that the required residual strength capability cannot be achieved. The minimum required residual strength is limit load.

[Emmerling: New Fatigue and Damage Tolerance Evaluation Rules…]. The residual strength capability must include the ability to resist the influence of temperature and moisture as well as impacts. The Wöhler curves (SN curves) of composites are usually relatively flat and the influence of notches on high cycle-fatigue is not important. There is no influence of corrosion fretting.

# 1 Introduction

Outstanding designs are possible with the introduction of fiber composites. The developments of the 60's in the helicopter industry at MBB, now Eurocopter Germany, used composite structures, especially for dynamically high loaded rotor systems, composite structures. In 1967, the BO 105 flew for the first time. This innovative helicopter was equipped with the first serial "hingeless" rotor system. The fibre composite blades were attached to the head with the help of "lug" elements. This allowed the simple design of the rotor having an extremely long lifetime due to the outstanding fatigue strength of the simple design of the rotor having an extremely long lifetime due to the outstanding fatigue strength of composites.



**Fig. 1.** The commercial EC 135 helicopter with the "flexbeam" main rotor blade structure and the cross section of the torsional element

The hingeless BO 105 rotor concept was also used for the design of the helicopters BK 117 and EC 145. The possibility additionally to eliminate bearings resulted in the development of the innovative bearingless and hingeless EC 135 rotor system with the bending and torsion loaded "flexbeam" (Fig. 1). This successful helicopter was certified in 1996 and more than 1000 helicopters have been delivered to the customers until now. Parallel to the development of the helicopter design in the early 60s the methodology of fatigue test and analysis was improved. The material strength was determined in such a way that the data could be used for the establishment of the four-parametric Weibull-curve. Thus the lifetime of a structure can be calculated with test data from fewer specimens (Fig. 2). Using the standard test pyramid the results of small coupon specimens, structural components and structures can be correlated [Och: *"Fatigue.."*]. In the 90s the certification authorities and the helicopter industry developed a new fatigue and damage tolerance approach, including the determination of replacement time and inspection intervals. Both certification possibilities demand a residual strength test (or analysis supported by test results) after applying dynamic loads.

$$\sigma_o = \sigma_\infty + \frac{\sigma_{ult} - \sigma_\infty}{e^{\left[\left(\frac{logN}{\alpha}\right)^\beta\right]}}$$

$\sigma_0$ : Occurring stress

$\sigma_{ult}$ : Ultimate stress value

$\sigma_\infty$ : Endurance limit

$\alpha, \beta$ : Curve parameters

N : Load cycles
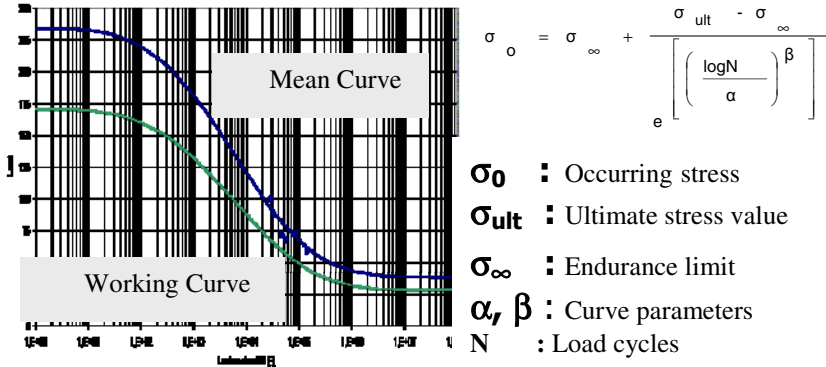
**Fig. 2**. The four parametric Weibull mean (SN curve) and working curve with the relevant parameters

## 2 Fatigue Tests of Glass Fibre Specimens with Shear and Bending Loads at Various Stress Ratios

The design of the "flexbeam" includes several fundamental functions such as the attachment area, the flap bending section and the torsion structure. The flap bending section has the function of a hinge, having a low flapping bending stiffness and high strength. The torsion section was optimized with respect to many parameters, such as high torsion strength and low torsion stiffness. Transverse shear loads, centrifugal loads, bending and torsion moments are transferred by the element. The design certification includes elements of the new rules. The new rule for the helicopter design considering fatigue and damage tolerance (*"Damage Tolerance and Fatigue Evaluation of Composite Rotorcraft Structures"*, FAR 27/29 §573) was introduced in 2010.

After the dynamic test, the residual strength including the influence of higher temperature and moisture was demonstrated. The complicate design of the complete rotor blade is described in [Bansemir H. and Emmerling S.: *Fatigue Substantiation and Damage Tolerance Evaluation of Fibre Composite Helicopter Components*]. Depending on the substantiation possibilities, replacement times or inspection intervals including the respective residual strengths can be used for certification. In Fig. 3 the bended and torsion loaded "flexbeam" of the EC 135 is shown. In both cases a centrifugal force of more than 150 kN is additionally applied. Long beam three point bending specimens are used for the establishment of the bending strength SN curves of the used fibre composite, whereas short beam three point bending specimens are used for the determination of the shear strength.
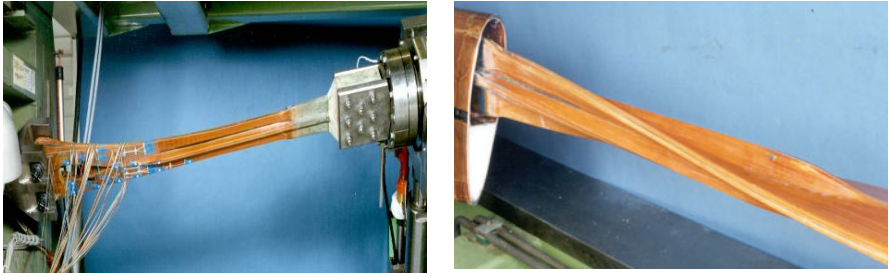
**Fig. 3.** The bended and torsion loaded "flexbeam" including centrifugal force of the EC 135
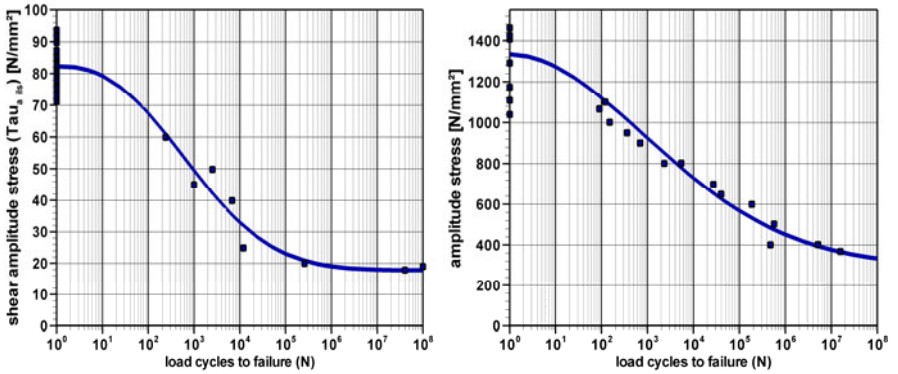


**Fig. 4.** SN curves for shear and bending amplitude strength for E-glass-epoxy unidirectional composites for R=-1 (alternating stresses)
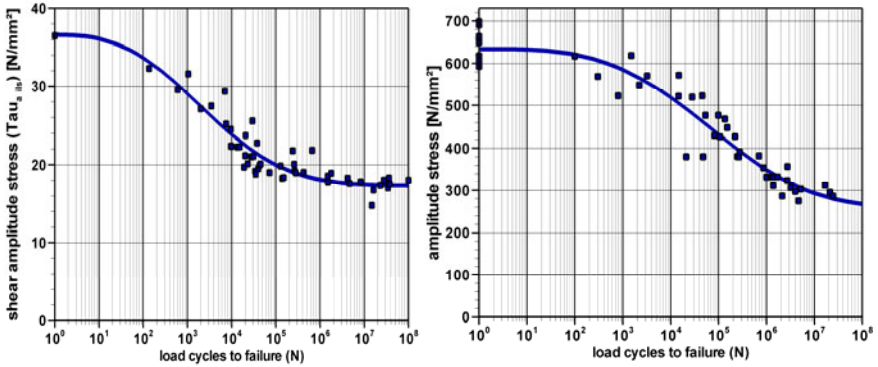


**Fig. 5.** Results for shear- (R=0,111) and bending- (R=0,05) amplitude strength for E-glass epoxy unidirectional composites

Bending and shear strength SN curves of unidirectional glass fibre composites are shown in Fig. 4 and 5 for the different ratios R=0,111, R=0,05 and R=-1, R describes the ratio of lower stress divided by upper stress. The amplitude stresses and the load cycles are given on the axes of the diagrams [Weinert: *"Fatigue Strength Surface."*].

## 3 Fatigue Test Results for Quasiisotropic Glass and Carbon Composites under Shear and Bending Loads Compared to Aluminium and Titanium Results

The fibre composite family with a quasiisotropic lay up has an isotropic stiffness property but marginal anisotropic strength behavior. The interlaminar shear strength is usually lower than for unidirectional lay up (Fig. 4). In Fig. 6 SN curves for transverse shear and bending strength for glass- and carbon composites are shown. The SN curves of carbon composites show higher shear and bending strengths than those of glass composites. In Fig. 6 reduced working SN curves also are given. The reduction of the mean curves corresponds to a survival probability of 99.9%. The diminution due to statistics is higher for carbon composites. The specific weight of carbon composite is about 1.5, for glass it is 1.9, for aluminium 2.7, for titanium 4.5 and for steel 7.8 (kp/dm3). Therefore the specific strength of carbon composites is superior to glass composites. The specific strengths of Alu 2024 T3 and Ti-6Al-4V shown in Fig.7 are low compared to fibre composites.
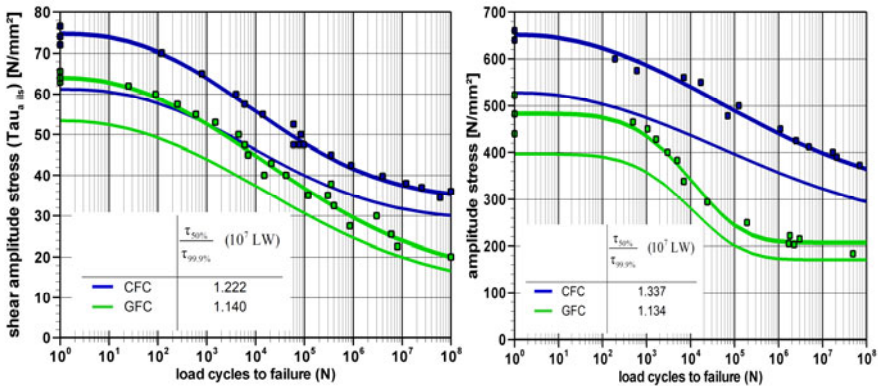


**Fig. 6.** Results for shear- and bending (R=0.111) amplitude strengthfor E-glass- and carbon composites with a quasiisotropic lay up [Properties of Glass- and Carbon Fibre Fabrics…]
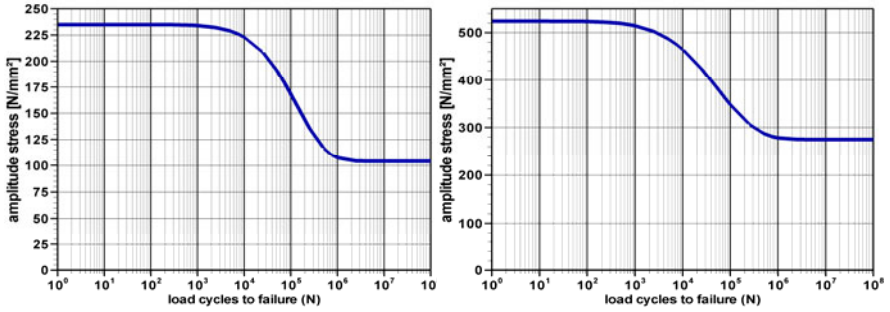
**Fig. 7.** Amplitude SN curves for Aluminium Alu 2024 T3 Kt=1 and Titanium Ti-6Al-4V Kt=1 for R=0 [Handbuch Strukturberechn.]

## 4  The Determination of the Replacement Time and Inspection Interval

The coupon and component test results are used, together with the mission profiles and flight loads, for the calculation of the component life time according to the methodology of Palmgren-Miner (Fig. 8).

The described Weibull curves (SN curves) are mean curves with a survivability of 50%. Often a survivability 99.9% is used for the "working curves", thus a reduction of the mean curve has to be performed. The deviations of the test results to
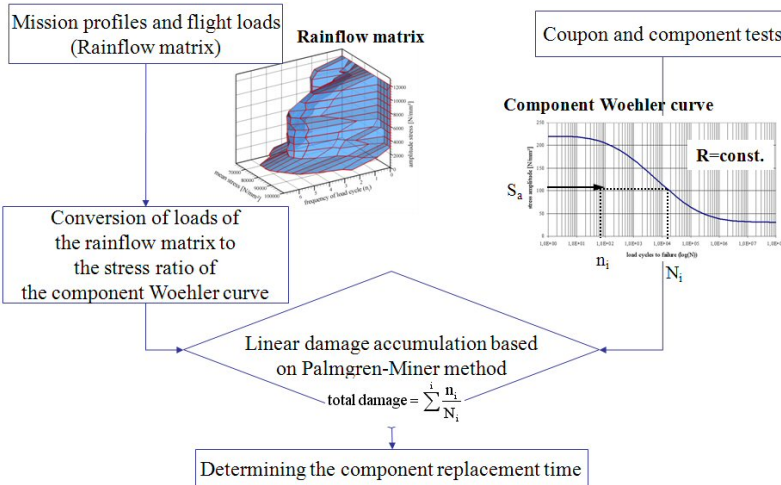


**Fig. 8.** The methodology of Palmgren-Miner for calculating the replacement time.
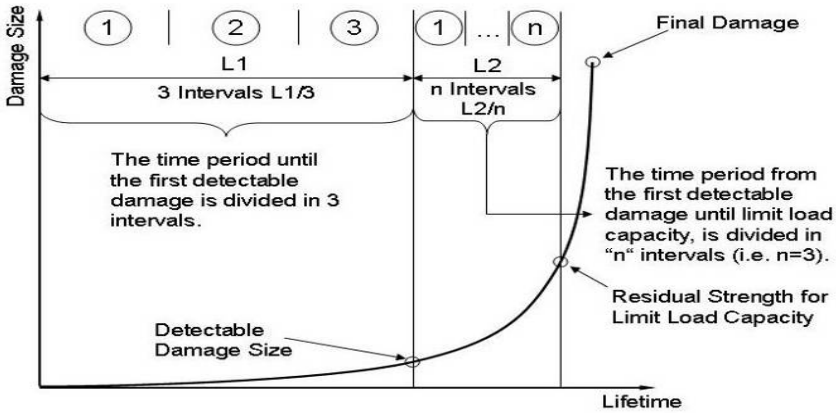
**Fig. 9.** Calculation of the inspection intervals with the help of the "Detectable Damage Size" and the "Residual Strength".

the mean curve are transmitted to the static level of the curve. The static level of the test data can be used in a form of a logarithmic distribution for the establishment of the reduction for the working curve. The constant reduction factor is used for the working curves.

The determination of the inspection intervals can be performed with the methodology described in Fig. 9. The damage size versus lifetime is shown together with the "Detectable Damage Size" and the "Residual Strength for Limit Load Capacity". Two possible inspection intervals can be calculated with the difference between those two points and the difference between "Detectable Damage Size" and begin of life divided by n intervals (i.e. 3). The lower inspection interval has to be taken for the maintenance.

## 5   The Sensitivity to Notches in Multi-directional Composites

As shown in Fig. 10, where the dynamic behaviour of the strain versus load cycles for 3 configurations of Carbon fibre (T300) composites is presented, the static- and low cycle strength is drastically reduced for notched composites. But the high cycle fatigue strength is not reduced due to notches. The slope of curve 1 is very flat compared to curve 3 and therefore the fatigue strength of notched carbon composites is not relevant, having comparable lay ups. Chopped fibre composites recycled from carbon composites have a good ability to resist dynamic loads but are sensitive to static loads. This behavior is different to the attitude of metal structures.
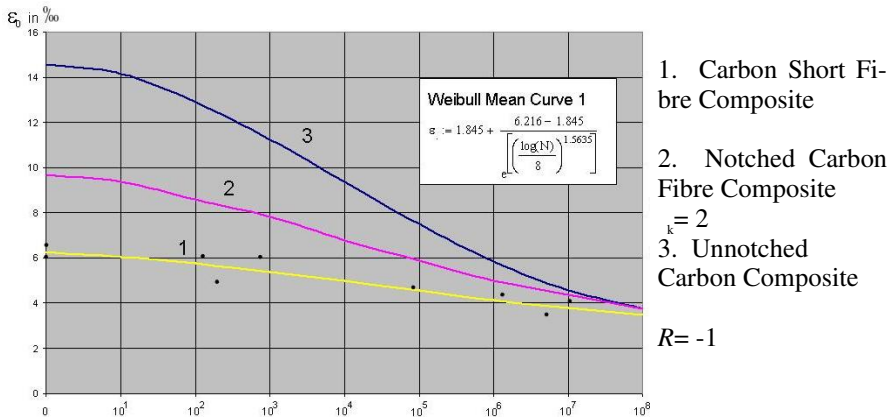
**Fig. 10.** Wöhler curves for alternating strain (R=-1) for a special symmetrical carbon composite lay-up (47,5% 0°; 47,5% ±45°; 5,0% 90°) with and without notches (2 and 3) compared with a carbon short fibre composite.

## 6 Summary

Light weight components are essential for the design of helicopters. In 1967, the BO 105 flew for the first time using composite blades for a "hingeless" rotor design. Later the "hingeless" and additionally "bearingless" rotor of the EC 135 was manufactured. Only the outstanding properties of fibre composites enabled such a progressivedesign. The specific dynamic strength of fibre composites is high compared to metals. Composites are sensitive to static loading but insensitive to dynamic loads. Established rules for fatigue and damage tolerance allow the substantiation and certification of new developments.

## References

Jarosch, E., Stepan, A.: Fatigue Properties and Test Procedures of Glass Reinforced Plastic Rotorblades. American Helicopter Society, 25th Annual National Forum, Paper No. 370 (1969)

Och, F.: Fatigue Strength. AGARDograph No. 292. Helicopter Fatigue Design Guide (November 1983); ISBN: 92-835-0341-4

Weiß, W., Auer, P.: Properties of Glass and Carbon Fibre Fabrics used in Helicopter Rotors. In: 10th European Rotorcraft Forum, The Hague, The Netherlands, August 28-31 (1984)

Bansemir, H., Emmerling, S.: Fatigue Substantiation and Damage Tolerance Evaluation of Fibre Composite Helicopter Components. In: Applied Vehicle Technology Panel: Applications of Damage Tolerance Principles for Improved Airworthiness of Rotorcraft, Corfu, Greece (1999)

Weinert, A., Gergely, P.: Fatigue-Strength Surface – Basis for Structural Analysis under Dynamic Loads. In: DLRK-2011 in Bremen, September 27-29 (2011)

Emmerling, S.: New Fatigue and Damage Tolerance Evaluation Rules – Are we fit for them? In: 37th European Rotorcraft Forum in Vergiate/Callarate, Italy, September 13-15 (2011)

Damage Tolerance and Fatigue Evaluation of Composite Rotorcraft Structures. NPRM No. 09–12 (Notice of Proposed Rulemaking) for FAR 27/29.573 Federal Register, vol. 75(3), (January 6, 2010) Proposed Rule

Damage Tolerance and Fatigue Evaluation of Rotorcraft Structures. NPA No. 2010-04 (Notice of Proposed Amendment) for CS-27/29.573 (April 29, 2010)

Bansemir, H., Mueller, R.: The EC135 – Applied Advanced Technology. In: AHS, 53rd Annual Forum, Virginia Beach, USA, April 29-May 1 (1997)

Handbuch für Strukturberechnung, Ausgabe CIASB (2009)

Schürmann, H.: Konstruieren mit Faser-Kunststoff-Verbunden. Springer, Heidelberg (2004)

# Car Body Design with Polyurethane Composites Produced by an Innovative Pultrusion Process

S.C. Bruckmeier[1] and J. Wellnitz[1,2]

[1] Research-Institute for Technology and Artistic Design GmbH, Marie Curie Straße 6,
85055 Ingolstadt, Germany, Stephanie
bruckmeier@itd-in.de, www.itd-in.de
[2] University of Applied Sciences Ingolstadt, Esplanade 10, 85049 Ingolstadt, Germany
joerg.wellnitz@ haw-ingolstadt.de, www.haw-ingolstadt.de

**Abstract.** An innovative pultrusion process makes it possible to produce fiber rein-forced polyurethane composites with superior mechanical properties compared to most traditional lightweight materials. The outstanding mechanical properties can be achieved, due to a very high fibre volume fraction. Moreover in the highly auto-mated manufacturing process, lineal profiles with highly complex cross-section can be realized with minimal production cost. As a technology demonstrator, in this study, the new pultruded composite will be implemented in a car body of a hydrogen powered vehicle. While the prototype testing's of the materials performance are planned in a DTM (DTM: Deutsche Tourenwagen-Meisterschaft) racing car, the long term vision focuses on an urban car concept, designed completely with this in-novative material. The pultruded composite, as an attractive automotive design ma-terial, reduces weight and consequently cuts emissions and environmental damages. It can be a promising step towards increased sustainability.

## 1 Introduction

The automotive industry is facing a rapidly increasing population with a growing demand on mobility and, at the same time, the problem of declining energy re-sources. In response to this development, the automotive manufacturers are gear-ing towards more sustainable mobility concepts.

This sustainability trend includes the further development and improvement of vehicles powered by alternative energy resources such as environmentally friendly hydrogen production. But also utlising the available energy as efficiently as possi-ble is an important development.

A contribution to the latter aspect can be realized by applying lightweight materi-al technologies. The pultrusion technology presented allows manufacturing lightweight profiles with a very high content of reinforcing fibers. The initial results

of feasibility studies and on-going experimental tests have indicated the great potential of the composited as a structural component in vehicles.

## 2   Manufacturing Process

Pultrusion is a continuous method of manufacturing various reinforced plastic shapes of complex cross sections. The unidirectional roving's are drawn through a liquid specially formulated thermosetting resin bath to thoroughly wet every fiber. A forming-shaping guide assembles the coated fibers. While the fibers are pulled through a die the resin is cured under pressure and heat. Figure 2 shows the classical pultrusion process with two component system of polyol and isocyanate [3, 4].
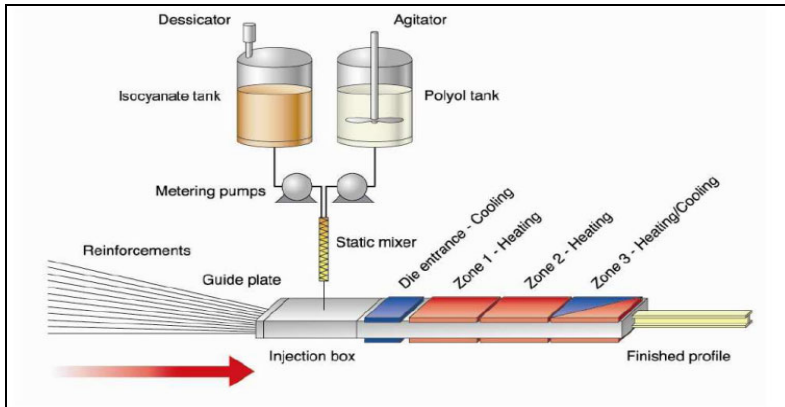


**Fig. 1.** Schematic of a typical polyurethane pultrusion set up [4]

## 3   Core Benefits

The innovative material provides a fiberglass content of up to 72 percent fiber volume fraction. Hence the composite exhibits improved strengths, stiffness and impact resistances. Also specimens of unidirectional E-glass with polyurethane, epoxy, polyester resins have been tested in long term tests. The long term creeping tests, which are usually a critical issue among plastic resins, indicate promising results concerning the polyurethane composite [1]. Besides the glass fiber, other fibres like carbon or basalt can be considered as reinforcement material in the pultrusion process.

   In the Figure below lineal pultruded composites are shown. The variety of cross sections, which can be created, offers a wide range of design flexibility to meet specific engineering requirements.
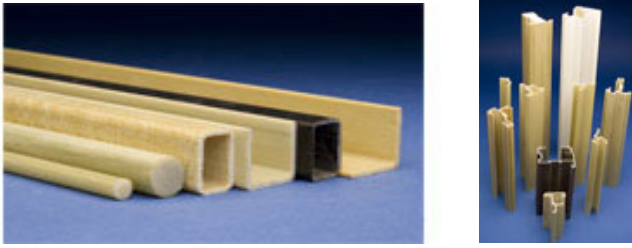
**Fig. 2.** Fiber reinforced beams/bars produced by an innovative pultrusion process [4].

All in all these attractive properties in combination with a low density of 2.0 kg/dm$^3$, qualifies the material for a profile intensive frame design as structural components in car bodies.

So far the greater usage of composites in the automotive section has been mainly restricted by the material and manufacturing cost particular with regard to the automotive mass production. In contrast, the manufacturing process of the pultrusion composites allows high-speed and automated production. The short optimized hardening cycles provide parts in an industrial scale with low labor costs. Moreover the availability of the commercialized polyurethane resin is almost unlimited with a particularly favorable purchase price.

Applying a material to a vehicle, the functionality over time is an important issue. The initial results of environmental expose tests confirmed the chemical and the stability resistance to weathering [4].

Plus excellent resin-to-fiber bonding and transverse properties have been achieved so far. The pultrusion process can be assessed as an environmental friendly process without styrene. [3, 4].

## 4   Application in a Hydrogen Racing Car

In the current study the application of the pultruded composite as a structural part in a racing car powered by hydrogen is investigated. The racing car is used as technology demonstrator and the first prototype for a profile intensive car body design. The long term objective is manufacturing a whole car body of the new composite especially to meet the demands and needs of the increasing urban mass industry.

The car body and its initial material distribution are shown in figure 2. As a first approach the cross member of the alumni space frame vehicle will be replaced by a pultruded bar reinforced with fiberglass in combination with a two component polyurethane resin.
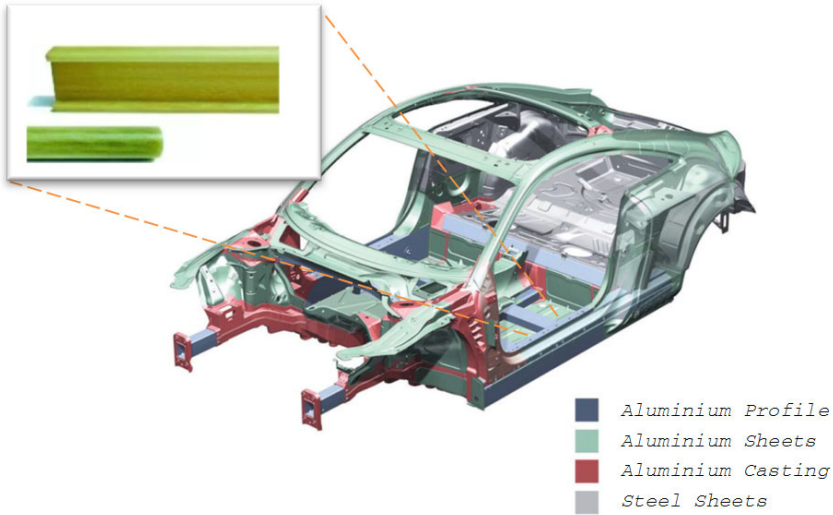
**Fig. 3.** Material distribution of the hydrogen racing car

The lower material stiffness in fibre direction of the pultrusion profile compared the aluminum profile will be compensated by a higher geometrical moment of inertia $I_{GPUR}$ according to (analogous for the torsion stiffness):

$$E_{AI}I_{AI} = E_{GPUR}I_{GPUR} \rightarrow I_{GPUR} = \frac{E_{AI}I_{AI}}{E_{GPUR}} \approx 1{,}4 \; I_{AI}$$

Adjustments regarding the material properties can be obtained by using different fibers like basalt or carbon fibers as reinforcing components alternatively. Note that the availability of the costly carbon fiber is restricted.

The tremendous flexibility regarding the cross section design allows not only an optimized geometrical optimization but provides also huge potential for the connection assembly. Herein the hybrid construction of the car body requires a safe connection of the composite to the aluminum frame structures. This can be realized by installing the composite with positive locking (bolts, special connection assembly or inserts) and conventional adhesive bonding connections in addition.

Besides the elementary bending and torsion stiffness optimization and joining technique other functional requirements will have a major impact on the lightweight part design. This involves the crashworthiness, seat connection solution, noise and vibration, reparability and the robustness in particular with respect to fatigue failure.

## 5   Conclusion

Introducing a new sustainable material and manufacturing process in the automotive industry is a long lasting complex process. For the holistic qualification the

experimental program has to be expanded and numerical models have to be integrated in the design progress.

Basic experiments and on-going feasibility studies have given promise that the pultruded PUR profile can be a competitive substitution or supplement to the aluminum space frame design.

The key benefits of weight saving, wide availability and high performance in combination with a highly automated mass process makes it a promising structural component for sustainable mobility.

## References

[1] Bruckmeier, S., Wellnitz, J.: Kriechen von Pultrudaten, Forschungsbericht, Institut für Technik und Design GmbH, Ingolstadt, Germany (2010)
[2] Cantor, B., Grant, P., Johnston, C.: Automotive Engineering Lightweight. Functional and Novel Materials. Tylor & Francis, New York (2007)
[3] Haberstroh, E., Michaeli, W., Meyer, F., Pauling, A.: PUR – Neue Wege mit innovativem Werkstoff, 24. IKV-Kolloquium Aachen, Germany (2008)
[4] http://www.bayermaterialscience.de

# Modelling the Automated Tape Placement of Thermoplastic Composites with In-Situ Consolidation

C.M. Stokes-Griffin, T.I. Matuszyk, Paul Compston, and M.J. Cardew-Hall

Research School of Engineering, College of Engineering and Computer Science,
The Australian National University, Canberra ACT 0200, Australia
`chris.stokes-griffin@anu.edu.au`

**Abstract.** In situ consolidation of thermoplastic composites opens the possibility of fully automated composite production when coupled with fibre placement technologies such as automated fibre placement (AFP) and automated tape placement (ATP). These approaches show much potential for flexible and efficient manufacture of lightweight and high performance automotive structures, including high pressure storage vessels for gaseous fuels. The placement rate of such systems must be maximised for production, however maintaining composite quality is non-trivial due to the highly dynamic behaviours at the nip point. Bonding is governed by intimate contact, autohesion and degradation processes. The quality is a function of the level of bonding, crystallinity, void dynamics and residual stress generation. The behaviour of these processes is dictated by the temperature and/or pressure distributions at the interface. In order to analyse the welding process it is therefore necessary to have models for each of the processes combined with robust pressure and temperature analysis. Process optimisation is a trade-off between the different aspects of quality. This paper will investigate the limitations of the work to date and identify improvements for future work.

## 1  Introduction

The high specific strength and stiffness of fibre-reinforced polymer composites makes them an attractive choice of material for use in lightweight and high performance automotive structures. Additional benefits include the ability to produce complex geometries which result in lower part counts with fewer assembly and joining operations. One area of particular interest is high pressure gas storage vessels for alternative fuels such as compressed natural gas (CNG), where the cost-benefit of using composite materials is favourable compared to metals.

There are two major hurdles when considering composites for automotive use:

1. *Manufacturing process*
   The manufacturing process for composite materials is normally associated with being slow due to labour intensive layup processes followed by long cure cycles

due to the use of thermoset resins. The additional costs associated with prepreg materials and autoclave cure need to be considered for the processing of high performance composites. Technologies such as filament winding, automated tape or fibre placement (ATP/AFP) have the ability to eliminate most of the labour intensive layup process, however the long cure cycles still remain.

2. *Environmental impact/Recyclability*

   Automotive manufacturers are under pressure to use materials and manufacturing processes with minimal environmental impact. Composites are traditionally made using thermoset resins which produce a significant amount of volatile organic compound emissions during the manufacturing process. Recycling of thermoset composites is difficult and commercially viable solutions are still under development [1].

Thermoplastic composites have the ability to address both of these issues. Thermoplastic materials are processed by fusion bonding: heat and pressure are applied to the interface being joined, and the polymer molecules diffuse across the interface forming a bond. As no solvents are involved, negligible emissions are produced making it a very clean process. Furthermore, when coupled with a placement technology such as ATP or AFP, the composite can be bonded in situ as it is placed. This means that once the placement has finished the component is ready for use- the cure cycle is eliminated making the process time much shorter. Thermoplastic composites are more easily recycled as they can be re-melted.

The in situ thermoplastic ATP process is an attractive manufacturing process for the automotive industry as it is fast, clean, automated and uses sustainable materials. While extensive research has been conducted in the area, the process has not yet reached maturity. A complete understanding of the process and ability to accurately predict material quality in real processes is required in order for industry to adopt the technology. This paper will investigate the limitations of the work to date, identify improvements for future work and discuss the developments required for the commercialisation of the process.

## 2   The In Situ Thermoplastic ATP Process

The in situ thermoplastic ATP process is described by Figure 1. Unidirectional pre-impregnated material is fed into the placement head. As the material approaches the consolidation device it is heated along with the substrate. The melted surfaces of the tape and the substrate and are pushed together as pressure is applied by the consolidation device, resulting in a bond. Parts are made by building up laminates layer-by-layer.
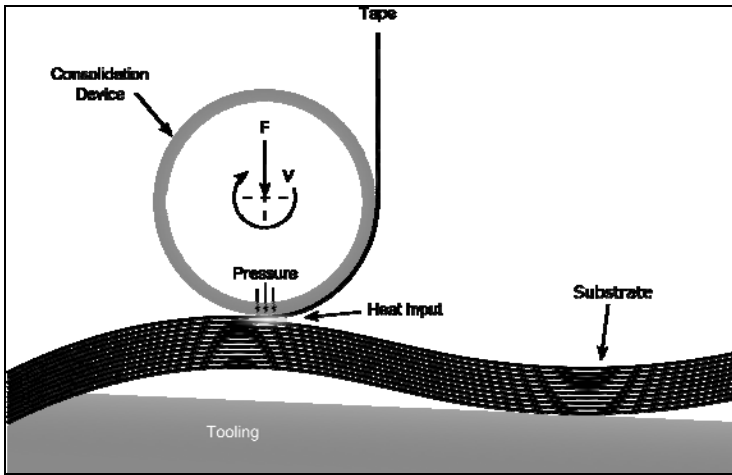
**Fig. 1.** Diagram showing the in situ thermoplastic AFP process

The majority of the literature for in situ thermoplastic placement processes is based around systems using hot gas torches as the heat source due to their low capital cost. Hot gas torches have high ongoing costs as nitrogen must be used to prevent oxidation of the surface at elevated temperatures. Gas torches can only deliver heat at a limited rate due to the convective mode of heat transfer. They are also known to suffer from gas stagnation at the nip point. Process control can be difficult as the torches have a delayed response. In more recent times diode lasers have been used as they are able to deliver more heat, are more efficient and have a near instantaneous response which is ideal for process control [2,3].

The most common consolidation device is a simple roller. Other variations have appeared such as conformable rollers which allows for placement on curved surfaces. One group used a series of conformable line and area compactors which are used to apply pressure, heat and cooling over large curved areas [4].

## 3   Modelling of the Process

The in situ thermoplastic process is highly nonlinear due to the rapid temperature and pressure cycles experienced around the nip point. It involves a number of physical processes that occur simultaneously and each have a substantial effect on the final quality of the composite, therefore robust models for each element of quality are imperative for complete material quality prediction. The modelling work to date for each of these aspects of quality is discussed in the following sections.

### 3.1   Bonding Model

The bonding process is the source of strength development and is based on the diffusion of molecules across the interface, a process known as autohesion. In order for diffusion to occur, the surfaces must first be in intimate contact.

### 3.1.1 Intimate Contact

Intimate contact models are used to determine the degree of physical contact between two surfaces when pushed together. As no surface is perfectly flat, the initial amount of physical contact is limited to asperities. Thermoplastics have viscous behaviour at elevated temperatures, so if pressure is applied, the surfaces will deform over time achieving full contact. The amount of intimate contact is therefore dependent on the initial geometry of the surface, temperature and pressure. Dara and Loos [5] developed a complex an intimate model which used a series of viscoelastic rectangles with varying heights based on statistical distributions. Lee and Springer [6] simplified this model by assuming a series of uniform rectangles. The geometric parameters of the rectangles are determined by adjusting them so as the model fits the experimental data. Mantell and Springer [7] adapted this model to account for time varying temperature, pressure and viscosity. While this model has been shown to predict intimate contact, there is a fundamental problem that the geometric parameters are determined by fitting the model to experimental data. Yang and Pitchumani [8] developed a fractal model for intimate contact development which uses parameters that are determined through surface profile measurements. Extensive experimental validations were performed, confirming the accuracy of the model [8,9].

### 3.1.2 Autohesion

Autohesion is the process of interdiffusion of the polymer molecules across the interface. It is the process that develops the bond strength. The reptation theory developed by de Gennes [10] was extended by Wool and co-workers [11-13] to model the motion of the polymer chains across a polymer-polymer interface. These models have been widely used to describe this strength development process under isothermal conditions. The in situ thermoplastic ATP process is highly non-isothermal therefore a nonisothermal approximation is required. Based on approximate extensions of the reptation theory, Bastien and Gillespie [14] and Sonmez and Hahn [15] presented various nonisothermal models. Yang and Pitchumani [16] formulated a nonisothermal model from first principles of the reptation theory. These models have been compared with results from nonisothermal experiments and it has been found that the Yang and Pitchumani model best correlates with the experimental data [16-18].

## 3.2   Void Growth and Reduction

Thermoplastic composite tapes contain a certain percentage of voids. The void content cannot be zero due to the high viscosity of the polymer melt. As the tape is heated and the matrix softens, the internal pressure of the voids can cause them to grow. When significant pressure is applied at the nip point, the voids will be compressed. If the matrix is cooled sufficiently before the consolidation pressure is released, the voids will remain in this small compressed state. Ranganathan *et al.* [19] developed a void dynamics model. It included a macroscopic void transport

model that was used to determine the pressure distribution within the tape. A microscopic void consolidation model was used to determine the growth and reduction of the voids. This model was subsequently implemented by [20] and [21]. Results confirmed this model to give reliable predictions of void content for a range of processing conditions.

## 3.3 Thermal Degradation

High temperatures are required in order to achieve bonding in situ at a reasonable rate. The temperatures are sufficiently high to cause decomposition and cross linking. Sonmez and Hahn [15,22] adopted a degradation weight loss model. They assumed crosslinking to be negligible due to the short period of time at elevated temperatures. Nicodeau [23] considered degradation due to crosslinking which can be observed by an increase in viscosity. Both of the degradation methods are time and temperature dependent, and a fixed limit of acceptable degradation assumed. These studies have not determined the effect of degradation on material strength.

## 3.4 Residual Stress

Due to the large thermal gradients experienced during in situ thermoplastic ATP and the mismatch of thermal properties between the fibre and the matrix, residual stress will always develop. Residual stress can cause delamination, matrix cracking and distortion of the finished part. Sonmez et al. [24] developed a residual stress model for in situ thermoplastic APT. Due to a lack of available experimental data, the model was confirmed using data from two press moulding experiments. The model was shown to agree with the experimental data.

## 4  Process Studies and Optimisation

Many parametric studies have been performed to analyse the process using various combinations of the models for each aspect of quality. The majority of these studies have used simplified 2D thermal models and consider head a head placing PEEK with a single rigid roller and a hot gas gun. These studies provide a better understanding of the effects of the process parameters on quality, however they do not present a set of optimal process parameters.

   The highly non-linear behaviour and the number of aspects of quality to consider make optimisation of the process difficult. Few studies have appeared in literature. Two optimisation studies [25,26] have been performed using the response surface method, however these are based purely on basic measurements of manufactured samples and do not consider process models. An artificial neural network was implemented for online process optimisation [27] which employed bonding and void dynamics models. Sonmez and Akbulut [28] used a Nelder-Mead zeroth-order approach for optimisation which considered bonding, degradation and residual stress. A simulation tool has been developed [2,29] that simulates a roller and hot gas torch and incorporates models for all but residual stress.

## 5 Conclusions and Future Directions

Although imperative for complete quality prediction, to date there has not been a single study or simulation tool that has encompassed all of the aspects of quality as described in this paper. Appropriate models exist in the literature to create a process model capable of full material quality prediction, however this is yet to be implemented.

In order for the technology to be accepted, the understanding of the process needs to have matured to the point where full quality predictions can be made for real components in real manufacturing processes. Due to the complexity of the process and its strong dependence on thermal history, it is anticipated that process optimisation should be integrated with the path placement planning software. This way the full thermal history of the tape and tooling is captured, and the thermal effects of recently placed tape are taken into consideration.

Future directions include the development of a simulation tool that incorporates all of the models for the different aspects of quality. Ideally this tool would integrate with an FE package where different head designs (heat sources and consolidation devices) could be investigated and optimised for speed and quality. Such a tool could then be used for online process control e.g. use the tool to train an artificial neural network based control system. Demonstration of this level of understanding and predictive capability would bring the confidence in the process to a level that is required for industry acceptance.

## References

1. Pimenta, S., Pinho, S.T.: Recycling carbon fibre reinforced polymers for structural applications: Technology review and market outlook. Waste Management 31(2), 378–392 (2011)
2. Khan, M.A., Mitschang, P., Schledjewski, R.: Identification of some optimal parameters to achieve higher laminate quality through tape placement process. Advances in Polymer Technology 29(2), 98–111 (2010)
3. Grouve, W.J.B., Warnet, L.L., Akkerman, R.: Towards a Process Simulation Tool for the Laser Assisted Tape Placement Process. In: 14th Eurpean Conference on Composite Materials, Budapest (2010)
4. Lamontia, M.A., Gruber, M.B., Funck, S.B., Waibel, B.J., Cope, R.D., Bruce Hulcher, A.: Developing a contoured deposition head for in situ tape laying and fiber placement. In: Cohen, L.J., Ong, C., Arendt, C. (eds.) International SAMPE Symposium and Exhibition (Proceedings), Long Beach, CA, pp. 2062–2076 (2003)
5. Dara, P.H., Loos, A.C.: Thermoplastic matrix composite processing model (trans: Structures CfCMa). Virginia Polytechnic Institute and State University, Blacksburg (1985)

6. Lee, W.I., Springer, G.S.: A Model of the Manufacturing Process of Thermoplastic Matrix Composites. Journal of Composite Materials 21(11), 1017–1055 (1987)
7. Mantell, S.C., Springer, G.S.: Manufacturing Process Models for Thermoplastic Composites. Journal of Composite Materials 26(16), 2348–2377 (1992)
8. Yang, F., Pitchumani, R.: A fractal Cantor set based description of interlaminar contact evolution during thermoplastic composites processing. Journal of Materials Science 36(19), 4661–4671 (2001)
9. Yang, F., Pitchumani, R.: Interlaminar contact development during thermoplastic fusion bonding. Polymer Engineering & Science 42(2), 424–438 (2002)
10. De Gennes, P.G.: Reptation of a polymer chain in the presence of fixed obstacles. The Journal of Chemical Physics 55(2), 572–579 (1971)
11. Wool, R.P., O'Connor, K.M.: A theory of crack healing in polymers. Journal of Applied Physics 52(10), 5953–5963 (1981)
12. Wool, R.P.: Molecular Aspects of Tack. Rubber Chemistry and Technology 57(2), 307–319 (1984)
13. Kim, Y.H., Wool, R.P.: A theory of healing at a polymer-polymer interface. Macromolecules 16(7), 1115–1120 (1983)
14. Bastien, L.J., Gillespie, J.W.: A non-isothermal healing model for strength and toughness of fusion bonded joints of amorphous thermoplastics. Polymer Engineering & Science 31(24), 1720–1730 (1991)
15. Sonmez, F.O., Hahn, H.T.: Analysis of the On-Line Consolidation Process in Thermoplastic Composite Tape Placement. Journal of Thermoplastic Composite Materials 10(6), 543–572 (1997)
16. Yang, F., Pitchumani, R.: Healing of Thermoplastic Polymers at an Interface under Nonisothermal Conditions. Macromolecules 35(8), 3213–3224 (2002)
17. Yang, F., Pitchumani, R.: Nonisothermal healing and interlaminar bond strength evolution during thermoplastic matrix composites processing. Polymer Composites 24(2), 263–278 (2003)
18. Tierney, J.: Modeling of In Situ Strength Development for the Thermoplastic Composite Tow Placement Process. Journal of Composite Materials 40(16), 1487–1506 (2006)
19. Ranganathan, S., Advani, S.G., Lamontia, M.A.: A Non-Isothermal Process Model for Consolidation and Void Reduction during In-Situ Tow Placement of Thermoplastic Composites. Journal of Composite Materials 29(8), 1040–1062 (1995)
20. Tierney, J., Gillespie, J.W.: Modeling of Heat Transfer and Void Dynamics for the Thermoplastic Composite Tow-Placement Process. Journal of Composite Materials 37(19), 1745–1768 (2003)
21. Khan, M.A., Mitschang, P., Schledjewski, R.: Tracing the void content development and identification of its effecting parameters during in situ consolidation of thermoplastic tape material. Polymers and Polymer Composites 18(1), 1–15 (2010)
22. Sonmez, F.O., Hahn, H.T.: Modeling of Heat Transfer and Crystallization in Thermoplastic Composite Tape Placement Process. Journal of Thermoplastic Composite Materials 10(3), 198–240 (1997)
23. Nicodeau, C., Cinquin, J., Regnier, G., Verdu, J.: In-situ consolidation process optimization for thermoplastic matrix composites. In: SAMPE 2006: Creating New Opportunities For The World Economy, Long Beach, CA (2006)
24. Sonmez, F.O., Hahn, H.T., Akbulut, M.: Analysis of Process-Induced Residual Stresses in Tape Placement. Journal of Thermoplastic Composite Materials 15(6), 525–544 (2002)

25. Aized, T., Shirinzadeh, B.: Robotic fiber placement process analysis and optimization using response surface method. The International Journal of Advanced Manufacturing Technology 55(1), 393–404 (2011)
26. Hulcher, A.B., Banks Iii, W.I., Pipes, R.B., Tiwari, S.N., Cano, R.J., Johnston, N.J.: Automated fiber placement of PEEK/IM7 composites with film interleaf layers. In: Repecka, L., Saremi, F.F. (eds.) 46th International SAMPE Symposium and Exhibition -2001 a Materials and Processes Odyssey, Long Beach, CA, pp. 1998–2012 (2001)
27. Heider, D., Piovoso, M.J., Gillespie Jr., J.W.: A neural network model-based open-loop optimization for the automated thermoplastic composite tow-placement system. Composites Part A: Applied Science and Manufacturing 34(8), 791–799 (2003)
28. Sonmez, F., Akbulut, M.: Process optimization of tape placement for thermoplastic composites. Composites Part A: Applied Science and Manufacturing 38(9), 2013–2023 (2007)
29. Schledjewski, R., Latrille, M.: Processing of unidirectional fiber reinforced tapes–fundamentals on the way to a process simulation tool (ProSimFRT). Composites Science and Technology 63(14), 2111–2118 (2003)

# Glass/Carbon Fibre Hybrid Composite Laminates for Structural Applications in Automotive Vehicles

J. Zhang[*], K. Chaisombat, S. He, and C.H. Wang

Sir Lawrence Wackett Aerospace Research Centre, School of Aerospace, Mechanical and Manufacturing Engineering, RMIT University, Bundoora, Victoria 3083, Australia
jin.zhang@rmit.edu.au

**Abstract.** Light-weight structure is one of the keys to improve the fuel efficiency and reduce the environmental burden of transport vehicles (automotive and rail). While fibreglass composites have been increasingly used to replace steel in automotive industry, the adoption rate for carbon fibre composites which are much lighter, stronger and stiffer than glass fibre composites, remains low. The main reason is the high cost of carbon fibres. To further reduce vehicle weight without excessive cost increase, one technique is to incorporate carbon fibre reinforcement into glass fibre composites and innovative design by selectively reinforcing along the main load path. Glass/carbon woven fabrics with epoxy resin matrix were utilised for preparing hybrid composite laminates. The in-plane mechanical properties such as tensile and three-point-bending flexural properties were investigated for laminates with different carbon fibre volume and lay-up scheme. It is shown that hybrid composite laminates with 50 % carbon fibre reinforcement provide the best flexural properties when the carbon layers are at the exterior, while the alternating carbon/glass lay-up provides the highest compressive strength.

## 1 Introduction

Fibre reinforced polymer matrix (FRP) composites offer great advantages in reducing the weight of a vehicle, improving the damage, corrosion resistance and internal damping, consolidating the parts required by traditional manufacture of metal components. However, issues such as high material costs, slow production rates, low recyclability and automotive industry's lack of experience with composite materials limit the wider adoption of composites in primary vehicle structures [1-3]. The most popular reinforcements for polymer matrix composites are carbon and glass fibres. It has been estimated that the use of glass fibre reinforced polymer matrix (GFRP) composites as structural components could yield a 20 - 35 % reduction in vehicle weight; more significantly, the use of carbon fibre reinforced polymer matrix (CFRP) composites could yield a 40 – 60 % weight reduction [4].

---

[*] Corresponding author.

   Cost reduction continuously to be the paramount challenge facing automobile manufacturers while fuel economy and technology transformation are becoming more important [5]. To reduce vehicle weight without excessive cost increase, one technique is to incorporate carbon fibre reinforcement into glass fibre composites and innovatively design by selectively reinforcing along the main load path [6-8]. Hybrid composites are composed of more than one type of reinforcement and they can be classified into interply or laminated hybrid, intraply or tow-by-tow hybrid, intimately mixed hybrid, and other types of mixtures [9]. Glass and carbon fibres are the most popular reinforcements for structural polymer matrix composites; in the current work, E-glass and carbon fibre woven fabrics with epoxy resin matrix have been used for fabricating hybrid composite laminates. Different glass/carbon fibre ratios and stacking sequences were investigated against the tensile, compressive and flexural responses of hybrid composite laminates.

## 2  Experimental

Colan$^{TM}$ E-glass plain weave fabric and Sigmatex$^{TM}$ carbon 2/2 twill weave fabric (T300, 3K Tow, 199 GSM) were used to reinforce the West system epoxy 105 cured with slow hardener 206. Wet lay-up was applied to fabricate laminates with five different lay-up schemes: $[C]_8$, $[C_2G_2]_s$, $[CG_3]_s$, $[CGCG]_s$ and $[G]_8$ where C and G denote carbon fibre and glass fibre respectively. The composite laminates were cured at ambient temperature for 24 hours before cut into specimens for mechanical tests. The overall fibre weight fraction of the composites was approximately 45%. ASTM D3039 and ASTM D970 standards were used for tension and three-point-bending tests; the compression tests were performed using a NASA short block compression fixture. The specimen dimensions were 250 mm × 25 mm for tensile, 100 mm × 25 mm for three-point-bending and 52 mm × 25 mm for compression tests.

## 3  Results and Discussion

### 3.1  *Hybrid Composites under Tensile and Compressive Loading*

The addition of carbon fibre reinforcement lead to reduced density of composites, varying from 1.508 g/cm$^3$ for the plain glass fibre composite $[G]_8$ to 1.460 g/cm$^3$, 1.327 g/cm$^3$, 1.316 g/cm$^3$ and 1.237 g/cm$^3$ for the $[CG_3]_s$, $[C_2G_2]_s$, $[CGCG]_s$ and $[C]_8$ composites, respectively. Fig. 1 shows the tensile and compressive stress-strain curves for all five types of composite laminates. As it can be seen from the graphs, the $[C]_8$ composite had the highest tensile and compressive strength and the $[G]_8$ composite had the lowest tensile and compressive strength, where the average tensile and compressive strength of plain glass fibre composites account for almost 50 % of the plain carbon fibre composites for both tension and compression loading cases. At the same glass/carbon fibre ratio (50:50), $[C_2G_2]_s$ and $[C/G/C/G]_s$ showed similar tensile strength, which accounts for 60 % of the plain

carbon composite; however, higher compressive strength and strain were found for the [C/G/C/G]$_s$ than the [C$_2$G$_2$]$_s$. With the addition of 25 % of carbon fibres in the exterior layers, [CG$_3$]$_s$ exhibited only slight improvement in both tensile and compressive strength than plain glass composite [G]$_8$. The compressive strain resulted from the alternating lay-up scheme ([CGCG]$_s$) showed the highest value above all other composites.
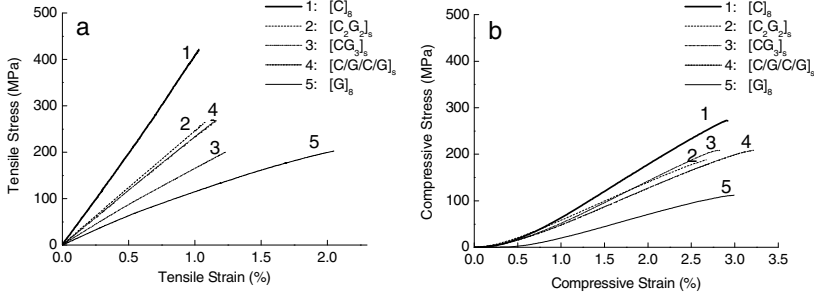


**Fig. 1.** Stress-strain curves for composites under a) tensile and b) compressive loading

The linear rule of mixture (ROM) was used for calculating the tensile and compressive strength. Denoting the carbon fibre ratio of all fibre reinforcement is α, the Young's modulus can be expressed using the simple rule of mixtures as:

$$E = \alpha E_c + (1 - \alpha)E_G \tag{1}$$

Where $E$ denotes the modulus of hybrid composite, $E_c$, denotes the modulus of carbon fibre composite and $E_G$, denotes the modulus of glass fibre composite. So the stress, $\sigma$, of the hybrid composite can be expressed as

$$\sigma = (E_c t_c + E_G t_G)\varepsilon_c /(t_c + t_G) \tag{2}$$

Assuming $\alpha$ equals to the percentage of the thickness of carbon layers ($t_c$) in the whole laminate ($t_c + t_G$) and the composite fails when the elongation of laminates reaches $\varepsilon_c$. However, in real case, the glass fibres can still carry load until the ultimate strain of glass fibre composite is reached. Therefore the maximum stress of hybrid composites is

$$\sigma_{max} = \max[\varepsilon_c (E_c t_c + E_G t_G)/(t_c + t_G), E_G t_G \varepsilon_G /(t_c + t_G)] \tag{3}$$

As it can be seen from Fig. 2, the tensile strength results agreed well with analytical results; however, the compressive strength exhibited a negative hybridization effect, where the hybridization effect is shown by the deviation from the ROM behaviour. The ROM could not demonstrate the difference in the compressive strength of [C$_2$G$_2$]$_s$ and [CGCG]$_s$ composites, due to the same carbon/glass fibre ratio.
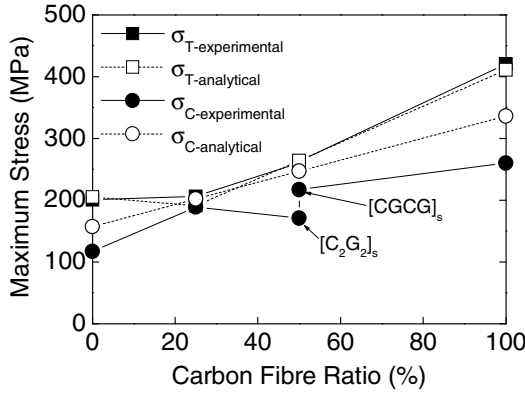
**Fig. 2.** Strength predictions of tensile and compressive composite specimens

## 3.2 Hybrid Composites under Flexural Loading

The flexural stress-strain curves for all five types of composite laminates are shown in Fig. 3. The flexural strength increased significantly by placing two carbon layers at the exterior, which accounts for 89 % of the plain carbon fibre laminate $[C]_8$. Based on the plane section assumption, the strain distribution in the laminate can be expressed in terms of the curvature $\kappa$, with the origin of the coordinate being at the mid plane of the composite laminate

$$\varepsilon(z) = -\kappa z \tag{4}$$

Where $z$ denotes the coordinate along the thickness direction. Different fibre reinforced composite plies can exhibit significantly different failure strains. For a hybrid composite laminate under pure bending load, the maximum bending moment it can carry corresponds to the load when a certain ply in the laminate reaches its failure strain. The maximum curvature at failure of the laminate is

$$\kappa_{max} = \min\left[\frac{\varepsilon_c(z_i)}{z_i}, \frac{\varepsilon_t(z_i)}{z_i}\right], \quad i = 1,2,3...N \tag{5}$$

Where $\varepsilon_c(z_i)$ denotes the strain of the $i$-th ply under compression and $\varepsilon_t(z_i)$ denotes the stress of the $i$-th ply under tension. It is clear that maximum deformation (curvature) occurs when plies with the highest failure strain are placed close to the surface, far removed from the neutral axis. The bending moment of a beam with rectangular section is given by,

$$M = -\int_{-t/2}^{t/2} \sigma_x(z)zBdz = \kappa\int_{-t/2}^{t/2} zE(z)Bdz \tag{6}$$

where $t$ is the thickness of the beam, $B$ is the width of the structure, $\sigma_x(z)$ is the stress either in compression or tension and $E(z)$ denotes the Young's modulus of the material at coordinate $z$. It can be seen from equation 6 that the maximum bending moment of a hybrid laminate depends on through-thickness distribution of the strain-to-failure and lamina stiffness. Considering a symmetric laminate with eight plies, the moment is

$$M = \frac{B}{2} \sum_{i=1}^{N} (t_i^2 - t_{i-1}^2)[E_{(i)T} + E_{(i)C}]\kappa \tag{7}$$

Where $t_i$ denotes the locations of the $i$-th ply of a laminate containing a total of $2N$ plies in a symmetric lay-up. Because for a rectangular section, the maximum flexural stress can be written as

$$\sigma_{max} = M/S = M/(Bt^2/6) = 6M/Bt^2 \tag{8}$$

Where $S$ is the elastic section modulus. The maximum flexural stress can be determined as

$$\sigma_{max} = (3/t^2) \sum_{i=1}^{N} (t_i^2 - t_{i-1}^2)[E_{(i)T} + E_{(i)C}]\kappa \tag{9}$$

If 50% of the reinforcement is carbon fibre, the maximum flexural stress can be obtained when two carbon fibre composite layers are located at the exterior of the laminate. Both the experimental and analytical flexural strength data are shown in Fig. 4. The analytical solutions were able to simulate the experimental trend influenced by hybrid composition and stacking sequence; however, their calculated results were higher than the experimental data due to the shear stresses presented in the specimens which caused additional displacements and led to reduced modulus. For the low span-to-depth ratios and high modulus materials, these shear stresses are more significant [10, 11].
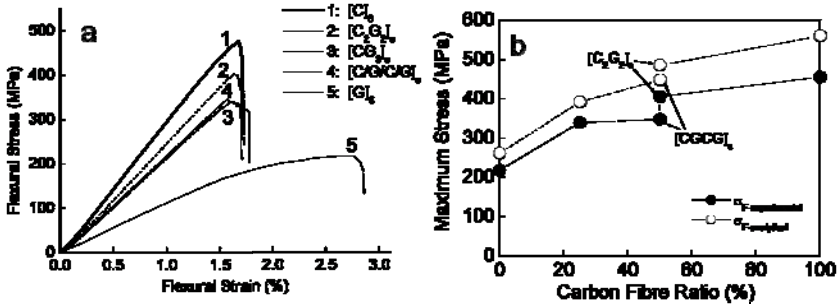


**Fig. 3.** Flexural properties of composites a) stress-strain curves and b) strength predictions of flexural composite specimens

## 4 Conclusions

Five types of composite laminates, i.e. $[C]_8$, $[C_2G_2]_s$, $[CG_3]_s$, $[CGCG]_s$ and $[G]_8$ composites, were investigated under static loading under tension, compression and three-point-bending. To effectively improve the tensile, compressive and flexural strength of the plain glass fibre composite, glass/carbon (50:50) fibre reinforcement was used either by placing the carbon layers at the exterior or by placing different fibre types alternatively. With the same hybrid composition, the stacking sequence did not show noticeable influence on the tensile properties but affected the flexural and compressive properties significantly.

## References

[1] Cramer, D.R., Taggart, D.F.: Design and manufacture of an affordable advanced-composite automotive body structure. In: The 19th International Battery, Hybrid and Fuel Cell Electric Vehicle Symposium & Exhibition (2002)

[2] Beardmore, P., Johnson, C.F.: The potential for composites in structural automotive applications. Composites Science and Technology 26, 251–281 (1986)

[3] Thilagavathi, G., Pradeep, E., Kannaian, T., Sasikala, L.: Development of Natural Fiber Nonwovens for Application as Car Interiors for Noise Control. Journal of Industrial Textiles 39, 267–278 (2010)

[4] Das, S.: The cost of automotive polymer composites: a review and assessment of DOE's lightweight materials composites research, pp. 1–36. Oak Ridge National Laboratory (2001)

[5] Jacob, A.: Automotive composites – the road ahead. Reinforced Plastics 45, 28–32 (2001)

[6] Mahdi, E., Hamouda, A.M.S., Sahari, B.B., Khalid, Y.A.: Effect of hybridisation on crushing behaviour of carbon/glass fibre/epoxy circular-cylindrical shells. Journal of Materials Processing Technology 132, 49–57 (2003)

[7] Hosur, M.V., Adbullah, M., Jeelani, S.: Studies on the low-velocity impact response of woven hybrid composites. Composite Structures 67, 253–262 (2005)

[8] Nordin, H., Täljsten, B.: Testing of hybrid FRP composite beams in bending. Composites Part B: Engineering 35, 27–33 (2004)

[9] Kaw, A.K.: Mechanics of Composite Materials, 2nd edn. CRC Press, Taylor & Francis Group, Tampa (2005)

[10] Kretsis, G.: A review of the tensile, compressive, flexural and shear properties of hybrid fibre-reinforced plastics. Composites 18, 13–23 (1987)

[11] Stevanović, M., Stecenko, T.: Mechanical behaviour of carbon and glass hybrid fibre reinforced polyester composites. Journal of Materials Science 27, 941–946 (1992)

# Lightweight Stiffened Composite Structure with Superior Bending Strength and Stiffness for Automotive Floor Applications

J. Zhang, S. He, I.H. Walton, A. Kajla, and C.H. Wang[*]

Sir Lawrence Wackett Aerospace Research Centre, School of Aerospace,
Mechanical and Manufacturing Engineering, RMIT University,
Bundoora, Victoria 3083, Australia
chun.wang@rmit.edu.au

**Abstract.** The trend towards smaller and lighter, more environmentally friendly vehicles is accelerating, as the petrol price rises and the $CO_2$ reduction target becomes more strict. As a key enabling technology, light-weight but low-cost structure plays an important role in promoting the use of fibre reinforced polymer matrix composites in automotive applications. In this work an experimental investigation is carried out to design, manufacture and analyse a stiffened composite structure, aiming at achieving required bending and torsional strength and stiffness at the minimum weight. One major application of this new lightweight structure is the load-bearing floor component. Some initial results from this work are presented in this paper.

## 1 Introduction

Reduced $CO_2$ emissions and increased vehicle fuel economy is a critical matter for automotive technology development. Automobile manufacturers are now using more composite materials due to their lightweighting benefits, despite of the current higher material cost of carbon fibre composites versus steel and aluminium [1]. Fibre reinforced polymer matrix (FRP) composites are materials that have high specific strength and energy absorption as well as offer other benefits such as part consolidation, styling flexibility, good noise/vibration/harshness characteristics and good corrosion resistance, which are well suited for future lighter, sustainable and more energy-efficient automotive vehicles [2,3]. For example, when advanced composites are used, instead of incremental part-by-part substitutions of metals, they can be applied in a whole-platform approach to solve system-wide issues. The 'Revolution' fuel cell vehicle developed internally by Hypercar had 77% fewer parts in primary structure than in the equivalent portion of a conventional stamped steel BIW [4]. However, there remain great challenges to expand the use of FRP composites from decorative or semi-structural parts to primary

---

[*] Corresponding author.

load-bearing structural components, aiming at taking advantage of these remarkable benefits. Issues such as lack of experience and knowledge in design with composite materials, high material cost of composites, and difficulty with affordable processes for producing composite components in high volume to automotive production standards are main limitations to overcome [4].

Sandwich panels consisting of face sheets and cores are widely used in transportation vehicles and civil infrastructure due to their high flexural and torsional stiffness/strength-to-weight ratio. In particular, sandwich structures are increasingly applied for giving combinational bending and torsional rigidity[5, 6] to components such as body panels, floor pans and aircraft wings [7, 8]. The core keeps the face sheets apart and stabilizes them by resisting vertical deformations and enables the whole structure to act as a single thick plate. Unlike honeycomb cores, a corrugated-core resists bending and twisting in addition to vertical shear [9]. As a result, sandwich structures with corrugated cores have exceptional high flexural stiffness-to-weight ratio and are suitable for constructing structural components which require high level of stiffness characteristics while lightweight is a also an important design consideration.

Electrical and hybrid vehicles are becoming increasingly popular as the petrol price rises. Comparing to other locations, the vehicle floor is the safest place for storing batteries, as it is located outside of the body's impact and deformation zones. In this context, the corrugated sandwich structure provides spaces between the core and face sheets, which is suitable for integrating package of energy resources. When the sandwich structure is used as a vehicle floor, the housed batteries are therefore stored in a safe and secure location [10].

In the current work, composite sandwich panels were fabricated with chopped strand glass reinforcement and polyester resin matrix, due to the low cost of both the reinforcement and matrix resin. The three-point-bending tests were performed both experimentally and numerically on the composite sandwich coupons.

## 2 Experimental

Chopped strand glass fibre mat was used as reinforcement and enydyne dicyclopentadiene modified polyester resin 1735 cured with the methylethyl ketone peroxide (MEKP) catalyst was used as matrix. An aluminium tool was fabricated for making the corrugated core; both the composite core and face sheets were prepared using wet lay-up. Both the composite core and face sheets were cured at room temperature overnight before they were joined together using epoxy adhesive Techniglue CA.

Three-point-bending tests were performed using an Instron 5569 universal tester at a crosshead speed of 2 mm/min. The dimension of the sandwich coupon was 325 mm × 245 mm × 63 mm. The thickness of the face sheet was 4 mm and the core thickness was 3.5 mm. The rollers with diameter of 50 mm were exerted along different directions (Scheme 1 and 2) as shown in Fig. 1a and Fig. 1b,

respectively. The span length was 160 mm for Scheme 1 (roller parallel to the core length direction) and was 220 mm for Scheme 2 (loading in the cross-direction). Finite element models were created with the solid element (C3D8I) in Abaqus 6.10. The sandwich specimen was supported by two rigid bodies at the lower surface; another rigid body was moved down to apply the bending. To establish the contact relationship, an initial displacement was applied to the model. The reaction force and displacement were output to compare with the experiment result.
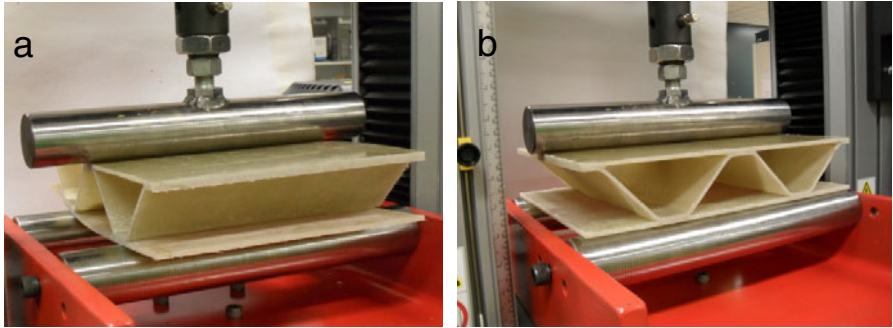


**Fig. 1.** Three-point-bending tests on the corrugated sandwich composite coupon. a) and b) show the set-up for coupons loaded in the machine-direction and the cross-direction, respectively.

## 3 Results and Discussion

Fig. 2 presents the experimental load-displacement curves under loading in the machine- direction and the cross-direction. In the parallel-direction, the downfall load reached 50 kN, which is the limit of the testing machine, after the adhesion between facesheet and core failed. In the case of the cross-direction, the sudden load drop became less significant and the loss of linearity was more progressive. The first load-drop occurred at 41 kN and the second at 33 kN, which correspond to the failure between face sheet and core and the failure in the up facesheet, respectively. The bonding moduli of the corrugated sandwich coupon were calculated by using the following function:

$$E = \Delta \cdot l^3 / 4 \cdot b \cdot H^3$$

Where $\Delta$ denotes the slope of the load-displacement curve, $l$ is the span length, $b$ is the specimen width and $H$ the specimen thickness. The Bending Moduli was calculated to be 232 MPa for the coupon in the parallel-direction and was 333 MPa for the coupon in the cross-direction.
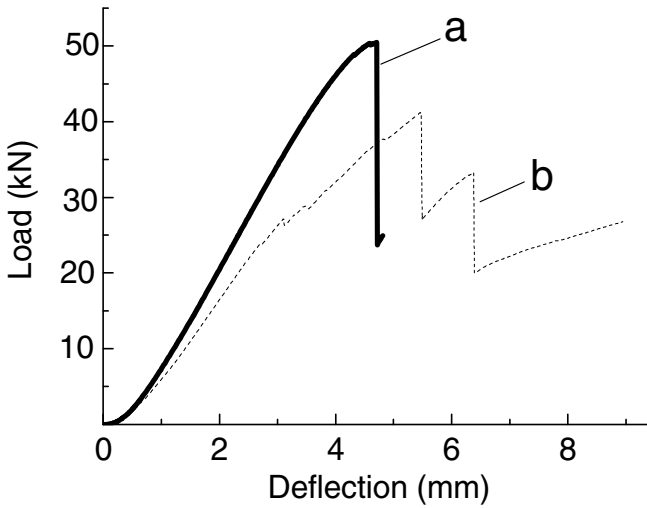
**Fig. 2.** Experimental load-displacement curves of corrugated composite sandwich coupons under bending conditions of: a) Scheme 1 and b) Scheme 2.
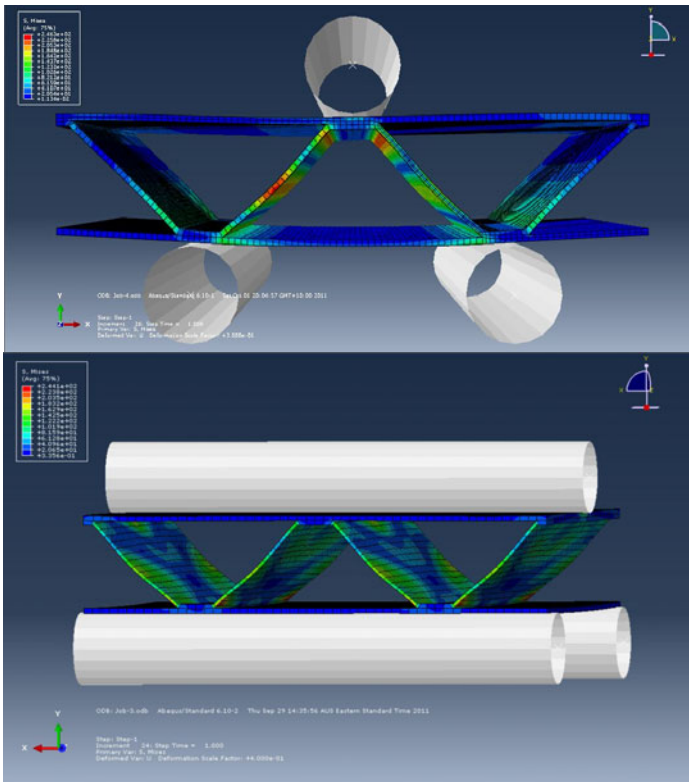


**Fig. 3.** Stress distributions of composite sandwich coupons loaded in both a) the machine-direction and b) the cross-direction
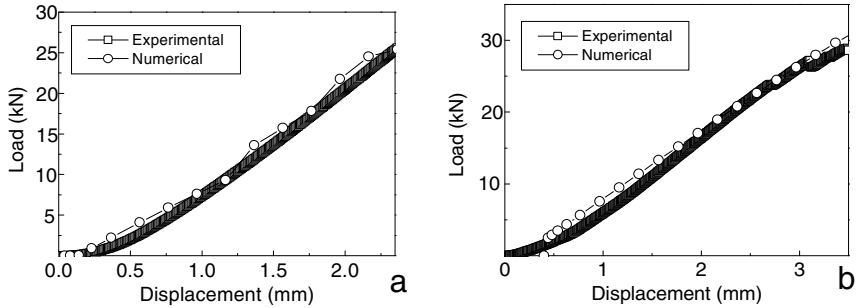
**Fig. 4.** Comparison between experimental and numerical results from load-displacement curves. a). loading in the machine-direction; b) loading in the cross-direction

In order to simulate the mechanical behaviour of corrugated sandwich structure, a FE model was created using Abaqus (Figure 3). The FE simulation will reduce the development costs and accelerate the development of the optimised structure in the early stage of design. At this stage, the adhesion between the core and the face sheets was ignored. As it can be seen from Figure 3 that the stress concentration occured on the corrugation core part and the region where the core and the face sheet meet. The model was able to simulate the load-displacement curves at the initial loading stage. The comparisons between the experimental and the numerical results are shown in Figure 4. It can be seen that at the initial loading stage, the FE models could simulate the experimental results reasonably well.

## 4   Conclusion

A lightweight glass fibre composite structure has been fabricated for applications where high bending strength and stiffness are needed. The sandwich structure with corrugations as core has demonstrated good bending properties. Three-point-bending tests have been performed in both the parallel-direction and the cross-direction of the corrugated sandwich coupons. The FE simulation results simulated the load-displacement curves reasonably well at the initial loading stage. The spaces between core and face sheets provide opportunities for integrating energy resources into the vehicle floor that is a safe and secure location for this purpose.

In the next stage, optimisation of the sandwich structure will be conducted. Factors such as corrugation angle, thickness of core and face sheets, fibre alignment and hybridisation will be considered for maximizing the bending performance with minimum weight.

## References

[1] Stewart, R.: Automotive composites offer lighter solutions. Reinforced Plastics (2010)

[2] Brylawski, M., Lovins, A.: Ultralight hybrid vehicle design: overcoming the barriers to using advanced composites in the automotive industry. Rocky Mountain Institute, RMI (1995)

[3] Beardmore, P., Johnson, C.F.: The potential for composites in structural automotive applications. Composites Science and Technology 26(4), 251–281 (1986)

[4] Cramer, D.R., Taggart, D.F.: Design and manufacture of an affordable advanced-composite automotive body structure. In: The 19th International Battery, Hybrid and Fuel Cell Electric Vehicle Symposium & Exhibition (2002)

[5] Li, X., Li, G., Wang, C.H., You, M.: Minimum-weight sandwich structure optimum design subjected to torsional loading. Applied Composite Materials, 1–10

[6] Li, X., Li, G., Wang, C.H., You, M.: Optimum design of composite sandwich structures subjected to combined torsion and bending loads. Applied Composite Materials, 1–17

[7] Belingardi, G., Cavatorta, M.P., Duella, R.: Material characterization of a composite–foam sandwich for the front structure of a high speed train. Composite Structures 61(1-2), 13–25 (2003)

[8] Gustin, J., Joneson, A., Mahinfalah, M., Stone, J.: Low velocity impact of combination Kevlar/carbon fiber sandwich composites. Composite Structures 69(4), 396–406 (2005)

[9] Chang, W.S., Ventsel, E., Krauthammer, T., John, J.: Bending behavior of corrugated-core sandwich plates. Composite Structures 70(1), 81–89 (2005)

[10] http://www.emercedesbenz.com/autos/mercedes-benz/concept-vehicles/mercedes-benz-at-the-detroit-auto-show-mercedes-benz-concept-bluezero-vehicles/ (accessed on October 1, 2011)

# New Automotive Fabrics with Anti-odour and Antimicrobial Properties

Saniyat Islam, Olga Troynikov, and Rajiv Padhye

School of Fashion and Textiles, RMIT University
25 Dawson Street, Brunswick VIC 3056, Melbourne, Australia
saniyat.islam@rmit.edu.au

**Abstract.** The aim of this research is to explore the application of bio-polysaccharide chitosan for the purpose of incorporating fragrance oil into automotive fabrics and its antimicrobial properties relevant to automotive interior textiles. Chitosan was selected for this study for its film forming ability and inherent antimicrobial attributes. 100% polyester automotive fabrics were used in this study, as 100% polyester is predominant fibre used for automotive interior textiles. The application of microencapsulated strawberry fragrance oil was studied to overcome the low durability issue. The microencapsulated fragrance oil was applied to the finished commercial 100% polyester automotive woven and knitted fabrics, in combination with chitosan. The treated fabrics were then assessed for smell retention. A new qualitative sensorial evaluation method was specifically developed for this study. It was concluded that application of the microencapsulated fragrance oil to the 100% polyester fabrics in combination with chitosan produced durable fragrance finish. The treated fabrics were also assessed for their antimicrobial properties. The assessment of the results indicated that the fabrics treated with microencapsulated fragrance oil in combination with chitosan displayed excellent antimicrobial property. The study concluded that the use of chitosan as a binder for the application of microencapsulated fragrance oil results in high fragrance retention in 100% polyester automotive fabrics and also produces excellent antimicrobial attributes in these fabrics.

## 1 Introduction

Recent years have seen vast evidence of research [1] in the area of finishing of textiles to impart functional properties such as antiodour or fragrance finishing, antimicrobial finishing, cosmeto-textiles for skin care and so on. The finishing process of textiles is one of the main factors which determine the desired effects for the ultimate consumer product. For automotive interiors malodour may be generated from smoking, spillages of food items and many other external reasons along with the microbial growth on textiles. Because automotive interior undergoes minimal cleaning in its life span, malodour and hygiene is of great concern. The application of fragrance in the interior fabrics will not only neutralize these kinds of malodour but also restrict the occurring of microbial growth. It will also

give desired aromatic effects to the finished textiles. Until now limited research has been conducted on automotive interiors for antiodour/antimicrobial or fragrance finishing. The present study investigates the development of 100% polyester automotive fabrics with antiodour and antimicrobial properties. To achieve this chitosan, a biopolymer, was evaluated as a binder and also as an antimicrobial agent. This study also evaluates the gradual or delayed fragrance release properties of the chitosan finished fabrics and their application to automotive textiles. Figure 1 shows the scheme of the proposed finishing of automotive textile substrates.



100% polyester fibre

Chitosan film

Entrapped microcapsules
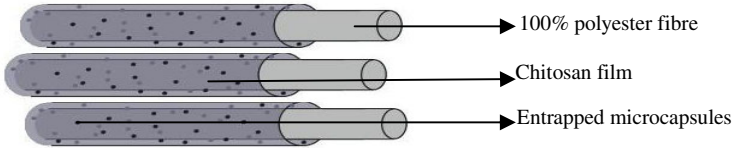
**Fig. 1.** Schematic diagram of the finished fabric

## 1.1  Antiodour and Fragrance Finishing

Antiodour and fragrance finishing is a process where the substrate is subjected to inclusion of fragrance/essential oils which gives effects such as sedation, hypnogenesis, curing hypertension and many more. The term 'Aromachology' [2] was coined in 1982 to denote the science that is dedicated to the study of the interrelationship between psychology and fragrance technology to elicit a variety of specific feelings and emotions such as relaxation, exhilaration, sensuality, happiness and well-being through odours via the stimulation of olfactory pathways in the brain, especially the limbic system [3].A new branch of textiles called "Aromatherapy textiles[2,4]" involves the incorporation of these essential oils onto textile substrate for daily use.

Spraying of perfumes and airing or washing is not a permanent solution for fragrance incorporation, as these are temporary treatments for removal of the malodour. However, incorporation of cyclodextrin or antimicrobial agents to the fabric has been the focus of research in the past decade and is becoming more popular.

The major problem using the cage compounds such as cyclodextrin is when it involves incorporation of fragrance compounds into textiles, because of the volatile nature of the fragrances the smell dissipates after a certain time period. The second option is the enclosure of the fragrances into micro-bubbles and release by bursting the bubbles by external action such as abrasion or rubbing. This method is also referred to as microencapsulation; and this technique is very popular for its versatility in terms of application. The volatile nature of the fragrances is minimized and the durability is increased by a significant margin with the process of microencapsulation. The third possibility as shown in Table 2 involves adsorption in porous metal oxide films, fixed as a polymer network on the fibre surface.

These finishes affect the quality of textiles such as softness and handle and cause problems in downstream processes like sewing.

## 1.2   *Chitosan as an Antimicrobial Agent*

Chitosan is a linear polysaccharide composed of randomly distributed β-(1-4)-linked D-glucosamine (deacetylated unit) and N-acetyl-D-glucosamine (acetylated unit) [5]. Chitosan is formed commercially by deacetylation of chitin, which is the compositional element in the exoskeleton of crustaceans such as crabs, shrimps lobsters etc. Chitosan has three reactive groups namely primary (C-6) and secondary (C-3) hydroxyl (-OH) groups and the amino-NH2 (C-2) group in each repeat of the deacetylated unit of Chitin [6]. Thus it is poly-cationic in nature. The antimicrobial activity of chitosan and its derivatives has been well proven in the previous studies [7, 8, 9] but the mechanism of the antimicrobial action is yet to be discovered. The acceptable interpretation is that the anionic cell surface of the microbes interacts with the cationic chitosan causing extensive cell surface alterations and damage. This leads to inhibition of the metabolism of the cell and results in killing the cell [10]. So far it is considered that chitosan acts as a biocide for some microbes and as biostatic in other cases.

## 2   Materials

100% polyester knitted 4bar warp insert Shelby fabric was used. Courses per inch (CPI) and wales per inch (WPI) were 48 and 26 respectively. Fabric width was 145 cm and weight was 300-320 g/m$^2$.

100% polyester woven fabric consisting yarn of 2/250 Denier in both warp and weft was used. Ends per inch (EPI) were 83-85 and picks per inch (PPI) were 49-51. Weight of the fabric was 280-320 g/m$^2$.Both the knit and woven samples were supplied by Melbatex Pty Ltd. Australia.

High molecular weight (HMW) chitosan supplied by Sigma-Aldrich Pty. Ltd, Australia, were used for the application and used as received. The degree of deacetylation was greater than 90% with a molecular weight of less than 3,75,000 and the viscosity was measured to be approximately 6 at 25 ℃.

RICABOND® SE series fragrance carrier microcapsules supplied by RCA International Pty Ltd. were used in this study. Strawberry range was used for experiments. Fragrance carrier microcapsules have an appearance of a thin white opalescent emulsion with a specific gravity of 1.07 g/m$^3$ and viscosity of 90 cPs at 25 ℃. pH of 10% solution was 4.5-5.5 and had a solid content of 48±2%.

## 3   Testing Method for Evaluating Smell Intensity (Smell Rating Method)

The fragrance microcapsules entrapped by the film formed by chitosan is expected to release the fragrance when it undergoes such instance like abrasion. In the

present study simulation of the same phenomenon was designed to evaluate the release property of fragrance microcapsules by carrying out successive abrasion cycles under controlled circumstances.

**Preparation of Samples**

Freshly prepared solutions containing aromatic microcapsules and chitosan were applied on polyester fabric samples by pad-dry-cure process. Chitosan concentration was varied from 0.1% to 1 %( on the weight of fabric) and fragrance carrier microcapsule concentration was kept constant at 10 g/L. After treating, the fabric samples were then kept in a sealed polyethylene bag. These samples were rated 10(highest smell intensity) on the rating scale. The untreated sample was rated 0(no smell) on the rating scale (Figure 2). Controlled laboratory condition of temperature $(20\pm2)^0$C and relative humidity $(65\pm3)$ % was maintained throughout the study.
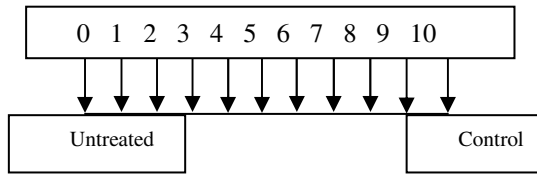


**Fig. 2.** The smell-rating Scale

**Procedure**

The treated controlled fabric samples were subjected to a rubbing action with the standard crock meter for 5 cycles each time for calibration of smell intensity for the observers. The samples which were needed to be tested were also subjected to successive abrasion cycles (10 cycles at a time for each test sample evaluated) till the smell dissipated. After every 10 cycles the observation panel (consisted of three people) was asked to rate and record the rating for each samples using the smell rating scale given in Figure 2. Standard wool cloth was used as abradant and tested sample diameter was 2.5 cm. The weight applied on the abrasion tester was 14 oz.

# 4   Testing Method for Determination of Smell Retention with Abrasion

The treated fabric samples were tested for smell retention on successive abrasion cycles using a Martindale abrasion resistance testing machine. The intensity of smell was evaluated using the same scale described in Figure 2. Successive abrasion cycles were carried out for smell retention until the smell completely disappeared from the samples.

## 4.1 Antimicrobial Activity Test

The antibacterial activity was evaluated quantitatively using the modified AATCC TM 100. *K. pneumoniae* (ATCC 13883), a Gram-negative bacterium commonly found on the human body, was chosen as the test bacterium. A typical procedure involves 1±0.1g of sample fabric, cut into small pieces of approximately 0.5×0.5 cm, was dipped into a flask containing 70 ml of sterile saline with an overnight grown culture solution of 5 ml with a cell concentration of $7.5 \times 10^5 - 1.5 \times 10^6$ CFU/ml. The flask was then shaken on a rotary wrist action shaker at 37°C for 1hour. Before and after shaking, 10μL of the test solution was extracted, serially diluted and spread onto nutrient agar plates. After incubation at 37 C for 24 h, the number of colonies formed on the agar plate was counted. The counting on the nutrient agar plates was done where the bacterial growth of only 30-300 had been found. Percentage bacterial reduction was calculated according to the following equation:

$$R = (B-A) / B \times 100\% \tag{1}$$

Where R is the percentage bacterial reduction, B and A are the number of live bacterial colonies in the flask with control and treated samples after incubation. Commercial knitted and woven were tested with the concentration of 0.3% chitosan and 0.1% of strawberry microcapsules.

## 5 Results and Discussion

The treated samples were tested for film formation and subsequent entrapment of microcapsules. Figure 3 shows Scanning Electron Micrograph (SEM) of treated woven substrate.
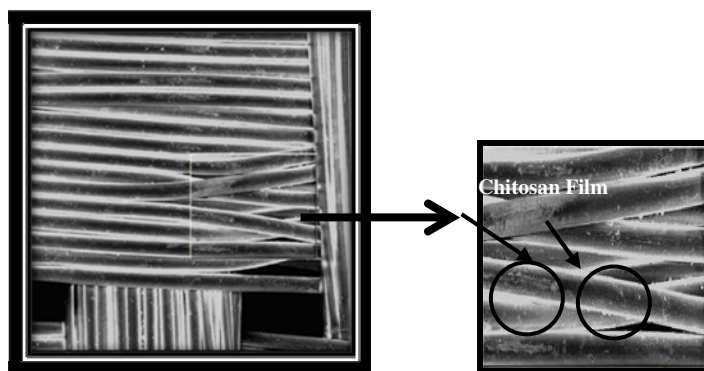


**Fig. 3.** Woven fabric at 800 × magnifications showing the chitosan film entrapping the microcapsules

Figure 4 is plotted based on the number of abrasion cycles the smell lasted as rated by the observer panel for each of the knitted samples to compare each concentration of chitosan varying from 0.1%, 0.3%, 0.5 and 1%.
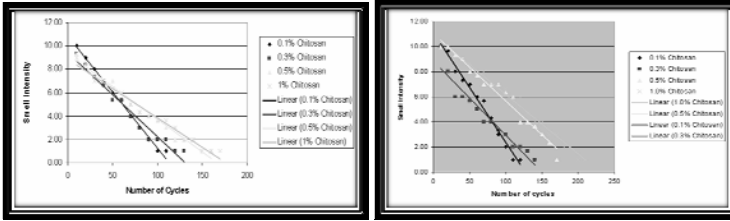


**Fig. 4.** Comparison of concentrations of chitosan treated knitted (left) and woven (right) samples on smell retention

For the knitted fabric samples smell lasted from 110 to 170 cycles (Figure 4). Similar phenomenon was observed when the linear curve was plotted for the four concentrations together. The calculated value of m (smell decay rate) from the equation y = mx+ c were 0.0955, 0.0720, 0.0556 and 0.0515 for chitosan concentration of 0.1%, 0.3%, 0.5% and 1% respectively.

The retention of smell for woven fabric maintained the similar way as for the knitted samples except for the smell lasted from 120 to 210 cycles. This may be attributed to the bulkiness and structure of the woven fabric. The calculated value of m (smell decay rate) from the equation y = mx + c were 0.0871, 0.0591, 0.0539 and 0.0474 for chitosan concentration of 0.1%, 0.3%, 0.5% and 1% respectively. In both fabrics, the trend of decrease in relative rate of decay suggests the chitosan film was stronger with increasing concentration, which increased the durability of smell with successive abrasion cycles. The fabric samples after abrasion experiments were tested again using the SEM. The presence of the chitosan film
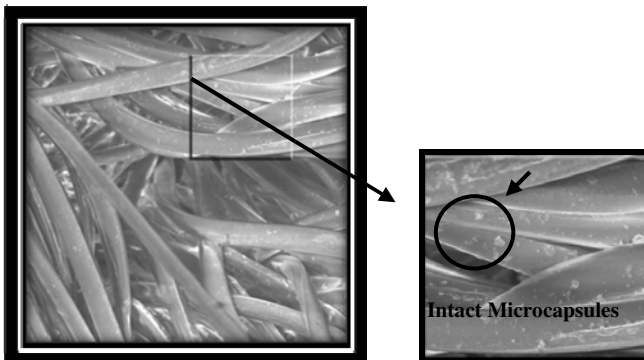


**Fig. 5.** Woven fabric at 400 × magnifications after 180 rubbing cycles

and the microcapsules are much more visible in this picture (Figure 5). This may be attributed to the abrasion cycles as it exposed the inner structure of the fabric more than in the Figure 3. It can be seen that after abrasion there are still a lot of microcapsules intact inside of the fabric structure which may need harsher condition to remove or to release.

The results of the antimicrobial test performed on the knitted and woven samples are tabulated in Table 1 and shown in Figures 6 and 7.

**Table 1.** Antibacterial test results for knitted and woven fabrics against *K. pneumoniae*

| Sample | Experiment number | Bacteria count before shaking | Bacteria count after shaking | Reduction in % |
|--------|-------------------|------------------------------|------------------------------|----------------|
| Knit | 1 | 244 | 0 | 100% |
| | 2 | 298 | 0 | 100% |
| | 3 | 253 | 1 | 99.62% |
| | 1 | 244 | 1 | 99.62% |
| Woven | 2 | 298 | 0 | 100% |
| | 4 | 253 | 0 | 100% |
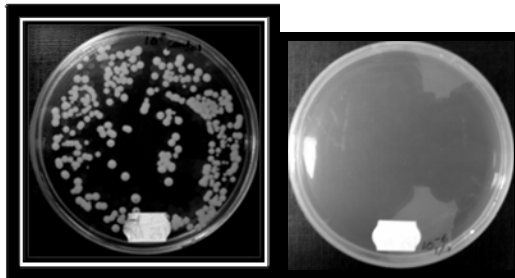


**Fig. 6.** Untreated and Chitosan (0.3%) treated knitted fabric showing respectively showing large and no bacterial growth on agar plate
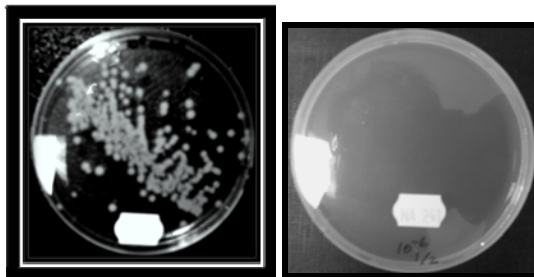


**Fig. 7.** Untreated and Chitosan (0.3%) treated woven fabric showing respectively showing large and no bacterial growth on agar plate

The above results show that chitosan and strawberry microcapsule treated samples were very effective in killing the gram negative bacteria *K. pneumoniae*.

## 6   Discussion

In the present study HMW chitosan with molecular weight greater than 375,000 was used. High molecular weight chitosan was reported previously to have good film forming ability and this is because of its intra and intermolecular hydrogen bonding [11]. The micrographs taken in SEM confirm the morphological aspect of the chitosan film as well as the presence of microcapsules containing fragrance oil. Study[12] on chitosan films reported that the water vapour permeability of chitosan film decreases with increased amount of concentration of chitosan. The concentration of HMW chitosan was varied from 0.1% to 1%, keeping the micro-encapsulated fragrance concentration of 10 gpl, to investigate the effect of different concentration of chitosan on smell retention. The retention of the fragrance smell that was measured by the amount of smell retained after successive abrasion cycles was found to be higher with the increased concentration of chitosan. The resistance to the release of the microencapsulated fragrance during the successive abrasion is attributed to the strength of the film formed by chitosan with increasing concentration. Other studies on chitosan films [13,14] reported that for the HMW chitosan the tensile strength of the film is more and the strength of the film increases with increasing molecular weight of chitosan. This agrees with current study finding that HMW chitosan can form a film to entrap microcapsules onto the fiber surface effectively and the increasing concentration of chitosan slows down the release of the microcapsules with successive abrasion cycles. Although the smells depleted from 100 to 210 abrasion cycles for all the samples the SEM picture (Figure 5) demonstrate that there is still a high amount of microcapsules left inside the interstices of fabric structure. This may be due to the amount and nature of load applied in the abrasion testing machine. The surface abrasion could only remove the film formed on the fabric surface and hence the microcapsules which are loosely held or just adjacent to the substrate surface were removed by abrasion and fragrance was released. But the microcapsules which are entrapped deep inside the structure of the fabric with chitosan film were still intact and need harsher conditions to release the fragrance. The retention of smell increased with increasing concentration of chitosan again, suggesting the film formed by chitosan was stronger with increase in concentration. The antimicrobial activity of the treated samples was evaluated quantitatively. The qualitative test results show that 0.3% HMW chitosan and 10g/L microencapsulated fragrance treated samples showed excellent efficiency against the gram negative bacteria. This also agrees with the previous studies [15] undertaken under similar circumstances but with cotton fabric and without any aromatic microcapsules. Hence it can be seen that the strawberry microcapsules did not inhibit the antibacterial property of chitosan.

## 7 Conclusion

The results demonstrated that the film formed by HMW chitosan can successfully entrap the microencapsulated fragrance oil onto the polyester fabric surface. The slow release property was achieved by external abrasion. For the evaluation of the smell retention a new method was designed, developed and used for the scope of the current study. The current study concluded that natural biopolymer chitosan can be used successfully for the commercially available seat fabrics for fragrance finishing and antimicrobial properties. Further studies can be undertaken to determine the minimal inhibitory concentration (MIC) of chitosan and using the gram positive bacterial strains.

## References

[1] Holme, I.: Innovative technologies for high performance textiles. Coloration Technology 123, 59–73 (2007)
[2] Butcher, D.: Aromatherapy–its Past and Future. DCI 162(3), 22–23 (1998)
[3] Buchbauer, G.: Aromatherapy: Use of fragrance and essential oils as medicaments. Flavour and Fragrance Journal 9, 217–222 (1994)
[4] Jellinnek, J.S.: Aromachology: A Status Review. Perfume & Flavorist 19, 25–49 (1994)
[5] http://en.wikipedia.org/wiki/Chitosan (accessed September 19, 2011)
[6] Tanigawa, T., Tanaka, Y., Sashiwa, H., Saimoto, H., Shigemasa, Y.: Various biological effects of chitin derivatives. In: Brine, C.J., Sand-ford, P.A., Zikakis, J.P. (eds.) Advances in Chitin and Chitosan, pp. 206–215. Elsevier Science Publishers Ltd., London (1992)
[7] Morimoto, M., Shigemasa, Y.: Characterization and bioactivities of chitin and chitosan regulated by their degree of deacetylation. Kobunshi Ronbunshu 54(10), 621–631 (1997)
[8] Sudardshan, N.R., Hoover, D.G., Knorr, D.: Antibacterial action of chitosan. Food Biotechnol. 6(3), 257–272 (1992)
[9] Wang, G.H.: Inhibition and inactivation of five species of foodborne pathogens by chitosan. J. Food Protect. 55(11), 916–919 (1992)
[10] Lim, S.H.: Synthesis of fiber-reactive chitosan derivative and its application to cotton fabric as an Antimicrobial finish and a dyeing-improving agent. Ph.D. Thesis, North Carolina State University (2002)
[11] Muzzarelli, R.A.A., Peter, M.G. (eds.): Chitin Handbook, pp. 437–438. European Chitin Society, Germany (1997)
[12] Sezer, A.D., Hatipoglu, F., Cevher, E., Oğurtan, Z., Bas, A.L., Akbuğa, J.: Chitosan Film Containing Fucoidan as a Wound Dressing for Dermal Burn Healing: Preparation and In Vitro/In Vivo Evaluation. AAPS Pharm. Sci. Tech. 8(2), Article 39 (2007)
[13] Nunthanid, J., Puttipipatkhachorn, S., Yamamoto, K., Peck, E.G.: Physical Properties and Molecular Behavior of Chitosan Films. Drug Development and Industrial Pharmacy 27(2), 143–157 (2001)
[14] Cevera, F.M., et al.: Solid state and mechanical properties of aqueous chitosan-amylose startch films plastysized with polyols. AAPS Pharm. Sci. Tech. 5(1), article 15 (2004)
[15] Momin, N., Padhye, R., Sinnappoo, K.: Chitosan based post treatment for cotton fabric ink jet printed with pigmented inks: Part I. Acta Universitatis Cibiniensis, 43–51 (2007)

# Advanced Concept Modelling Method for Automotive Structural Optimization

Pooja Doke, Mohammad Fard, and Reza Jazar

School of Aerospace, Mechanical and Manufacturing Engineering,
RMIT University, Melbourne, Australia
mohammad.fard@rmit.edu.au

**Abstract.** NVH (Noise Vibration and Harshness) and crashworthiness are highly significant issues related to lightweighting of vehicle bodies. It is recommended to analyse vehicle NVH issues in early design phases in order to optimize vehicle design performance. The early design phase provides functional requirements and specified weight constraints to the designer for geometry optimization. Using available CAD (Computer Aided Design) data, reduced modelling of vehicle structure can be done to achieve NVH performance. The paper demonstrates and verifies an approach to reduced modelling with structural modal and FE (Finite Element) analysis. It focuses on beam selection techniques for reduced modelling and accuracy achieved in NVH performance prediction by appropriate beam cross-section selection.

## 1 Introduction

The industry is focused on sustainable lightweight automotive structural design. Considering reduced product launch time into market it is necessary to develop a faster modelling method. Therefore this method needs to optimize NVH performance in early design phases. Several approaches have been proposed by researches for development of a reduced model. However, they are found to have less applicability due to higher complexity. The presented method is restricted to vehicle development based on a FE predecessor model. However it can be applied to concurrent design method of vehicle development with CAD data, by creating functional library of beam sections in future (which is currently unavailable) [1].

This paper demonstrates an advanced reduced modelling method for optimization of vehicle NVH performance in early design phases. It implements various approaches for column, beam, panels and joint reductions of vehicle components. The analysis is done for global body vibration modes by creation of beam model without implementing joints, which reduces complexity of the method. The focus is given on approach towards property selection of beam and its effect on global vibration mode. In order to validate the proposed approach, a case study is presented. The case study implements reduced modelling using provided method for FE predecessor model redevelopment. The BIW (Body in White) structural modal testing is performed in the lab using modal testing system provided by LMS Company [2].

## 2   Methodology

### 2.1   *Experimental Method*

This method implements Structural modal analysis of Ford Falcon BIW which is available at RMIT. The analysis is done by using LMS measurement system, shaker as force input, the force transducers and accelerometers. LMS measurement system is used for vibration analysis of 133 body node points and prediction of global structure vibration modes at these nodes. The experimental setup and a sample frequency response function of BIW in response to the shaker excitation are shown in Figure 1 and Figure 2.



**Fig. 1.** Laboratory experimental Setup
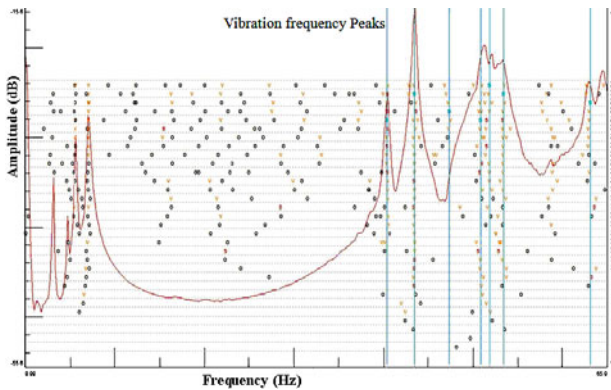


**Fig. 2.** Frequency Response function (FRF) for BIW (Modal Test Result)

The experimental analysis provides FRF (Frequency Response Function) as shown in Fig. 2. The experimental method provides fairly accurate modal analysis to predict global vibration mode frequencies in the form of FRF. Experimental FRF is stabilised for 0-65 Hz to capture significant vibration frequencies. The mode shapes of peak vibration frequency can be observed using LMS system,

which are later compared with the simulated model for validation. The results of experimental modal analysis are discussed in later sections.

## 2.2 Design Method

The reduced beam modelling method includes three different approaches for reduction of primary and secondary members such as columns and beams, panels and joints.

**Beam Modelling Approach for Columns and Beams**
The primary structural members of vehicle chassis such as A, B, C pillar and main roof as well as floor members have beam like appearances (i.e. higher longitudinal dimension and characteristic cross sectional area). Primary members are identified to have strong influence on global natural frequencies of the vehicle body [3]. The modelling method implements component inertia and body centre node reduction approach suggested by Donders *et. Al.* for reduction [4]. This B.C.N (Body Centre Node) is identified as the point of centre of mass along the *x* axis i.e. beam body central axis (not merely the geometrical centre of beam). However, B.C.N is the geometric centre in case of symmetrically cross sectioned beams. All the beams can be reduced to desired beam end-sections with identified mass and stiffness properties as shown in Figure 3.
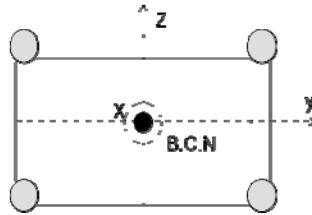


**Fig. 3.** Schematic representation of Beam end-section

The cut section is taken at several node points and a local axis system is defined at each B.C.N. In the later stage, centre of mass of section is identified. The following properties in terms of body inertia are analysed to calculate equivalent properties at body centre node [4]:

- A – Area of cross section
- $I_{xx}$ – Torsional Moment of Inertia
- $I_{yy}$, $I_{zz}$ – Moments of inertia of area; and
- $I_{yz}$ – product of inertia of area

Here *x* represent body centre axis (i.e. beam direction) and *y-z* plane is considered as the intersection plane as shown in Figure 3. An equivalent beam end section and beam section properties can be identified using local principle axis system and then transformed into global system. The global system implements summation of

all shell elements for particular cross section. NASTRAN (super element RBE3) provides a utility to define B.C.N for set of shell elements in FE model [3].

This method provides accurate results for primary members. However, reduction of secondary members (i.e. panels) is identified as a challenging area in beam modelling as it has a significant effect on vehicle body stiffness. The approach for reduction of panels is explained in later section.

**Beam Modelling Approach for Panels**

Though primary members of vehicle chassis effectively impact natural frequencies of vehicle vibration, secondary elements are also significant (as they have larger area of mass distribution). The secondary elements affect mode shapes of vibrations as well as values of body vibration frequencies. The proposed method includes a clamping method of mode shape analysis and an inertia method by Donders *et. al* [4] to reduce panels to a form of a set of beams. The equivalent beams have denoted mass distribution considering centre of mass as well as identified values of mass moment of inertia and stiffness. Virtual analysis of FE model can be done by applying boundary conditions at clamped ends of panels. The end sections of beams are calculated based on mode of vibration, beam centre nodes, centre of mass and inertia method. This method helps successful reduction of panels into effective set of beams inducing same frequencies and modes of vibration in global system.

## 2.3 Beam Cross Section for Joint Stiffness

Guyan reduction [3, 4, and 5] is the most popular and widely used mathematical joint stiffness identification and condensation method. This method is sometimes applied with the wave-based sub structuring theory [6]. The Guyan reduction method is used to reduce the finite element stiffness and mass matrices of structure.
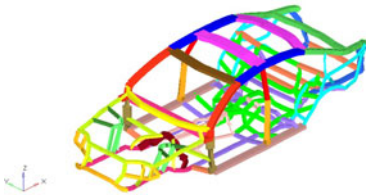


**Fig. 4.** Reduced beam model

This method helps calculating final stiffness value of joints. Using above method of reduction simplified reduced beam model is created as shown in Figure 4. This reduced model is simple, having less elements and complexities compared to conventional detail CAE (Computer Aided Engineering) model and can predict initial NVH behaviours of vehicle body in early design phases with available data.

## 3   Results and Discussion

The results obtained using both the methods are used to validate the vehicle structure NVH performance prediction accuracy of the proposed design method for reduction modelling. Figure 5 and Figure 6 demonstrate similarity in mode shapes for both structures in 1st torsion and bending modes at the mentioned frequencies.

The mode shapes of structure are governed by primary as well as secondary components of chassis as well as few significant joints. Calculation of MAC (Modal assurance criteria) is done using 20 nodes at this stage for all significant and comparable frequencies to identify similarity in mode shapes.
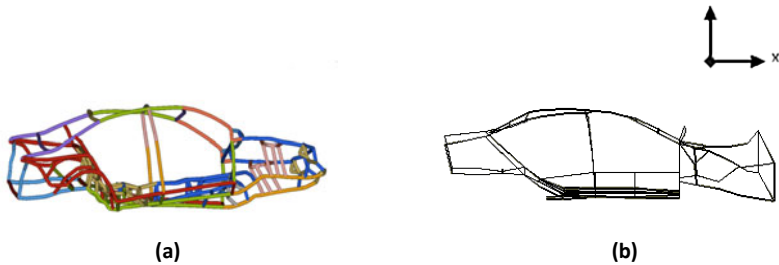


**Fig. 5.** Body torsion (a) Simulated and (b) LMS experimental results for BIW
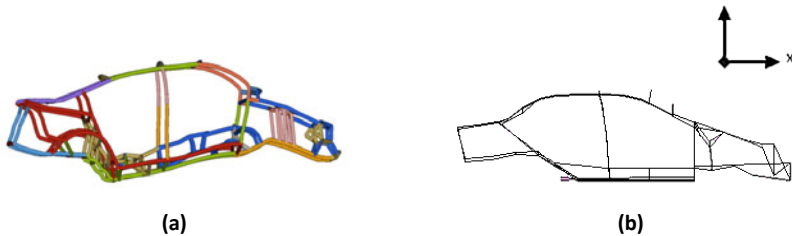


**Fig. 6.** Body bending (a) Simulated and (b) LMS experimental result for BIW

The structural modal analysis results are compared with dynamic CAE reduced beam model results for first five global vibration frequencies. The average value of MAC for the first five global modes were nearly 0.7 indicating a good consistency between the experiment and the developed model.

## 4 Conclusion

The reduced modelling approach for accurate NVH performance prediction and modification is presented in this paper. This approach enables early design lightweighting effect analysis on structural performance of vehicle design. The reduced modelling method implements reduction of vehicle model A pillar, B pillar, roof rails, panels etc. to equivalent beam structures. The four main joints (which connect A and B pillar to the body) are used for joint stiffness calculation by Guyan [7] reduction and stiffness values are implemented in end beam section. The proposed method is validated by structural analysis and dynamic FE analysis using Ford Falcon chassis as test object. This method can be applied to vehicle development which is based on FE predecessor model. A comparison between

structural modal and FE dynamic analysis of model based on first 10 global frequencies is done. The maximum difference of 2.6 Hz and qualitatively better match between mode shapes is identified. The MAC value of difference for first 5 global vibration frequencies is found to be approximately 0.68.

In summary, feasibility of vehicle component reduction and NVH performance optimization is realised. The mass distribution, stiffness consideration and global dynamic frequency comparison enables an accurate approximation of complex CAE model in reduced form. Hence the proposed method provides faster concept optimization of vehicle structure by upgrading individual beam properties and avoids complexities of performance optimization.

# References

[1] Ledermann, C., Hanske, C., Wenzel, J., Ermanni, P., Kelm, R.: Associative parametric CAE methods in the aircraft pre-design. Aerospace Science and Technology 9(7), 641–651 (2005)

[2] LMS International, LMS Virtual, Laboratory Review 6B (November 2006)

[3] Mundoa, D., Hadjit, R., Dondersb, S., Brughmans, M., Mas, P., Desmet, W.: Simplified modelling of joints and beam-like structures for BIW optimization in a concept phase of the vehicle design process. Finite Elem Anal. Des. (2009)

[4] Donders, S., Takahashi, Y., Hadjit, R., Van Langenhove, T., Brughmansa, M., Van Genechten, B., Desmet, W.: A reduced beam and joint concept modeling approach to optimize global vehicle body dynamics. Finite Elem. Anal. Des. (2009)

[5] Panayirci, H.M., Pradlwarter, H.J., Schueller, G.J.: Efficient stochastic structural analysis using Guyan reduction. Adv. in Eng. Softwares (February 2011)

[6] Maressa, A., Mundo, D., Donders, S., Desmet, W.: A wave based substructuring approach for concept modelling of vehicle joints. Computers and Structures (June 2011)

[7] Guyan, R.: Reduction of stiffness and mass matrices. AIAA Journal 3(2), 380–387 (1965)

# Effect of Equivalence Ratio on Combustion Characteristics in a Hydrogen Direct-Injection SI Engine

Roy Mithun Kanti, Nobuyuki Kawahara, Eiji Tomita, and Takashi Fujitani

Okayama University, Japan
`kawahara@mech.okayama-u.ac.jp`

**Abstract.** Gases such as hydrogen are regarded as promising alternative fuels for improving the energy efficiency and reducing the greenhouse gas emissions of conventional internal combustion engines. Hydrogen spark-ignition (SI) engines based on direct injection (DI) promise significant advantages in terms of thermal efficiency and power output, as well as a means of overcoming problems related to knocking, backfiring, and pre-ignition. A better understanding of the effect of the hydrogen jet on the concentration distribution and mixing process in a DISI engine should provide new and useful insights into combustion optimization. The objective of the present work is to gain a deeper comprehension of the characteristics of late-injection hydrogen combustion. An experimental combustion setup is applied to a fired, jet-guided DISI engine operated at 600 rpm in tail ignition (TI) injection mode. A high-speed camera, synchronized with the spark, is focused on a field of view with a diameter of 52 mm through a window at the bottom of the piston crown. A series of single-shot images, captured in different intervals, is used to study the time evolution of the flame distribution. Variations of the equivalence ratio at tail ignition mode combustion are found to impact the development of the early flame, as well as the flame propagation.

## 1 Introduction

The hydrogen internal combustion engine (H2ICE) may be an important step on the road to cleaner and renewable propulsion systems. Advanced hydrogen engine concepts based on direct-injection (DI) fuel systems have shown that the performance potential of H2-DI operation is approximately 17% higher than that of gasoline port injection [1]. DI is particularly attractive in the case of hydrogen engines because it circumvents the air displacement effect in the intake manifold. A major challenge to the use of H2-DI is in-cylinder hydrogen–air mixing. Hydrogen has the highest diffusion coefficient of all gases, and hence the highest driving force for adjusting imbalances in concentration and inhomogeneities in the fuel/air

mixture [2]. Takagi *et al.* proposed plume ignition combustion (PCC) concept for hydrogen DISI engine in order to reduce NOx emissions in high engine load conditions [3]. Planer laser-induced fluorescence (PLIF) techniques have recently been developed to measure mixture formation in a hydrogen DI system; reports favor increased injection pressure and careful nozzle design [1, 4]. Moreover, the interaction of the jet injection event with the intake-induced charge motion was studied using 2D measurements of the velocity and scalar fields by particle image velocimetry (PIV) [5]. Kawahara *et al.* developed a spark-induced breakdown spectroscopy (SIBS) system to measure the influence of the Hα/O intensity ratio on the hydrogen–air mixture concentration during fired engine operation [6]. In direct-injection spark-ignition (DISI) engines, the in-cylinder flow plays an important role, due to the limited amount of time available to achieve optimal fuel–air mixture stratification.

There has been very little research on hydrogen DISI engines in the late stages of the compression stroke, especially under stratified charge operating conditions. Also, there is a need for high-resolution direct-combustion images to measure the fuel distribution and flame propagation under a range of operating conditions. This paper presents experimental results and a discussion of the characteristics of hydrogen stratified combustion in a DISI engine for varying fuel/air equivalence ratios.

## 2  Experimental Setup

A general schematic of the jet-guided DISI engine equipped with a Bowditch piston is shown in Figure 1a). The single cylinder engine with a pancake-type combustion chamber has a bore of 78 mm and a stroke of 65 mm. The engine compression ratio was 9.0. The in-cylinder pressure was recorded using a Kistler piezoelectric transducer. The location of the spark plug and gas injector in the cylinder head, as well as the experimental setup, is shown in Figure 1b). The distance between the injector nozzle tip and the spark plug was approximately 17.4 mm. The inclined injector geometry allows for gas injection towards the spark plug. The engine was driven by an electric motor at a constant speed of 600 rpm. Air was initially introduced into the cylinder through the inlet valve at a pressure of 0.1 MPa and a temperature of 298 K. After a given amount of time, the valve was closed when the piston was located at bottom dead center (BDC). Hydrogen from a high-pressure vessel was supplied directly to the combustion chamber via a solenoid-driven GDI injector. The injection pressure was maintained at 5 MPa. In this experiment, TI injection mode combustion was used (whereby injection is terminated at the instant of spark ignition), resulting in the presence of sufficient hydrogen in the vicinity of the spark plug to create an ignitable mixture. Flame intensity images were acquired from a 45° mirror mounted in the extended piston, using a Photron FASTCAM SA1.1 camera. A 50-mm f/1.2 Nikon lens was employed, and the frame resolution was 384×320 pixels at 40,000 frames per second.
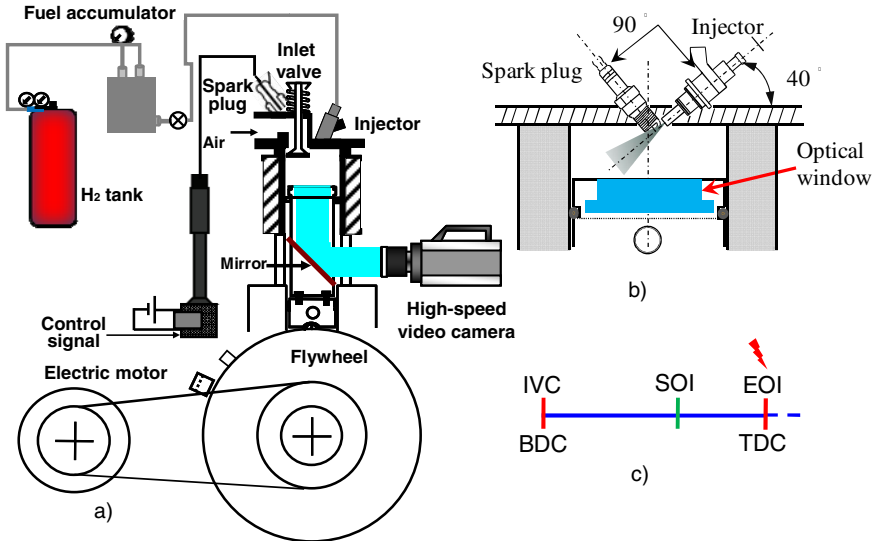
**Fig. 1.** a) Schematic view of the experimental optical engine setup, b) In-cylinder spark plug and injector arrangement, and c) TI Injection timing diagrams.

## 3 Results and Discussion

Photographs combined with thermodynamic data provide an effective tool for combustion analysis. Figures 2a) – e) show time-series combustion images, including in-cylinder pressure histories and pressure-based heat-release analyses for the TI injection mode, for overall equivalence ratios ($\varphi$) of 0.3, 0.5, 0.7, and 0.9. As the overall equivalence ratio increased, the peak pressure also increased, as Figure 2e) indicates. The in-cylinder pressure gradually increases with the increase of overall equivalence ratio due to stratified mixture formed near the spark plug. For an overall equivalence ratio of 0.3, the lean mixture induced a low in-cylinder pressure with a slow-burning heat-release profile.

Figure 2a) shows flame photographs at an overall equivalence ratio of $\varphi = 0.3$. The intensity of the flame was relatively weak at a small overall equivalence ratio. The flame kernel initialized from the center-off of the combustion chamber, and the flame front propagates across the cylinder. Flame photographs at an overall equivalence ratio of $\varphi = 0.5$ are shown in Figure 2b); the flame propagation exhibited a trend similar to that at $\varphi = 0.3$. However, the intensity of the flame was stronger than at $\varphi = 0.3$, suggesting that with the increased equivalence ratio, a higher degree of mixture stratification occurred near the spark electrode gap at ignition. Moreover, the high flame intensity induced by a high gas temperature during the combustion process, which was expected since the amount of fuel increases with the overall equivalence ratio.

Figure 2c) shows flame photographs at an equivalence ratio of $\varphi = 0.7$. Since the intensity of the flame was high, the initial flame development retained a behavior similar to that observed at small overall equivalence ratios (i.e., the flame

a) $\varphi$ =0.3 - SOI = 343 ºCA ; EOI = TDC



b) $\varphi$ =0.5 - SOI = 332 ºCA ; EOI = TDC



c) $\varphi$ =0.7 - SOI = 320.5 ºCA ; EOI = TDC



d) $\varphi$ =0.9 - SOI = 309.5 ºCA ; EOI = TDC
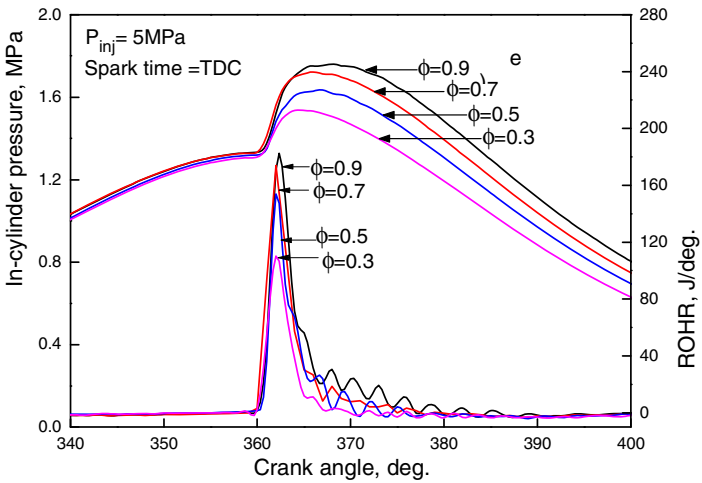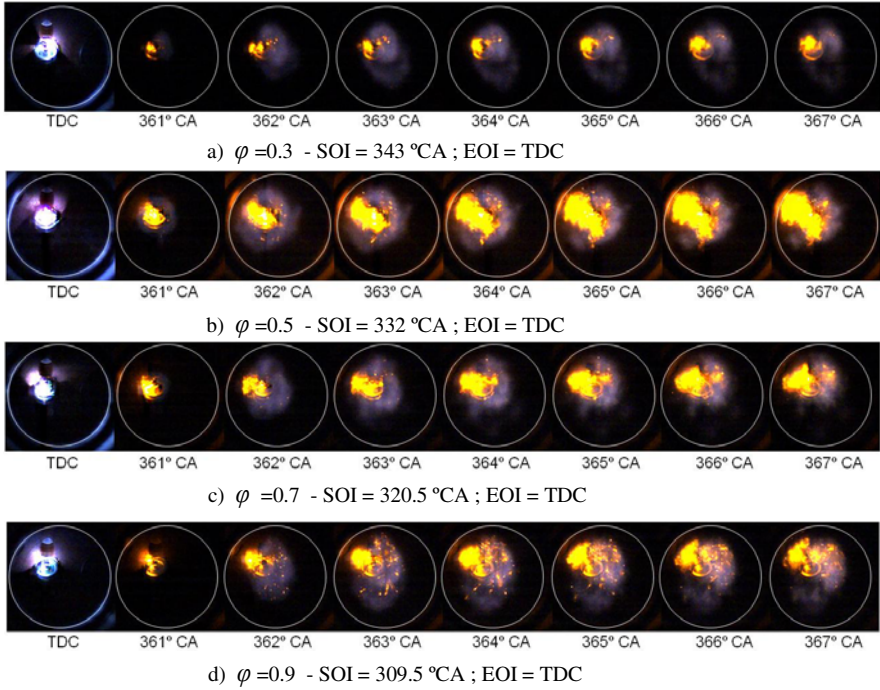


**Fig. 2.** Time-series of high-speed direct images with a) $\varphi$ = 0.3, b) $\varphi$ =0.5, c) $\varphi$ =0.7, d) $\varphi$ =0.9, and e) in-cylinder pressure histories and rate of heat release.

expanded outward from the center-off the combustion chamber). A wrinkled flame front appeared during engine combustion that can effect of gas flow generated by the hydrogen jet as well as piston motion. Figure 2d) shows higher flame intensity at an overall equivalence ratio of $\varphi = 0.9$. This was attributed to the formation of a late-injection rich mixture, so that a stratified charge took place in the combustion chamber.

Digitization of the flame images was carried out to obtain further insight into the combustion process. To determine the flame area per degree of crank angle, images were binarized and the pixel intensities were summed. In this experiment, cycle-averaged flame areas were computed on the basis of pale blue flame intensity. Additional luminous flame intensity produced by lubricating oil combustion was eliminated via image processing while measuring the flame area. Figure 3a) suggests that the longer period of initial flame propagation growth was due to rich fuel exists near the spark-plug at $\varphi = 0.9$. In contrast to the situation at $\varphi = 0.5$ and $0.7$, the initial flame development period were quite faster. Figure 3b) shows the effect of the overall equivalence ratio on the mass fraction burned in TI injection mode combustion. When the overall equivalence ratio decreased, the duration of the initial combustion also decreased, as indicated by comparison of the mass fraction burned. This is consistent with the results observed in the flame visualization, since too rich fuel exists near the spark-plug at large overall equivalence ratios was assumed to increase the duration of the initial combustion. Except for the case $\varphi = 0.5$, the duration of the initial combustion varied slightly that can effect of gas flow.
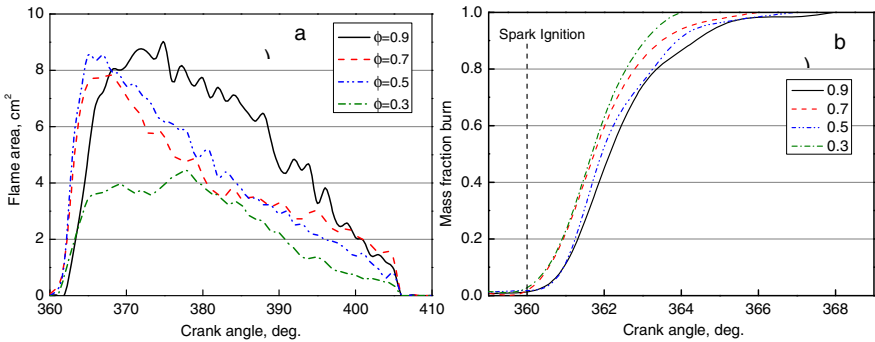


**Fig. 3.** Effect of overall equivalence ratios on a) average flame area and b) mass fraction burn

Figure 4 shows the indicated mean effective pressure (IMEP) at different equivalence ratios in TI injection mode combustion. The IMEP increased gradually with the overall equivalence ratio. The effect of the increased temperature and increased number of moles of burned gas in the cylinder was to increase the IMEP. The present results indicate that a more practical lean limit for combustion is around $\varphi = 0.3$ in engines of this type. The use of lean mixtures in a hydrogen-fueled engine, opens up the possibility of controlling the power output of the engine by changing the fuel flow rate while keeping the air flow unthrottled.
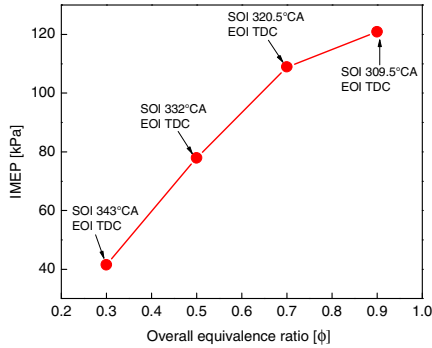
**Fig. 4.** IMEP at different equivalence ratios

## 4   Conclusions

Hydrogen DI combustion was visualized for stratified charge TI combustion at different equivalence ratios in an optical SI engine. The following conclusions can be drawn from this experiment:

1. The flame propagation towards the cylinder wall and a characteristic of turbulent combustion with a wrinkle flame front observed in a Hydrogen DISI engine.
2. The duration of the initial combustion decreased with the overall equivalence ratio. The long duration of the initial combustion at $\varphi = 0.9$ was due to rich fuel exists near the spark-plug.
3. A lean mixture could be realized by exploiting the formation of an ignitable stratified mixture at late injection timing.

## References

[1] Wallner, T., et al.: Investigation of injection parameters in a Hydrogen DI Engine using an endoscopic access to the combustion chamber. SAE 2007-01-1464
[2] Kawanabe, H., et al.: CFD analysis of a high-speed unsteady jet. Heat Transfer Asia Research 36(1), 1–12 (2007)
[3] Takagi, Y., et al.: Optimization of hydrogen jet configuration by single hole nozzle and high speed laser shadowgraphy in high pressure direct injection hydrogen engines. SAE 2011-01-2002
[4] Kaiser, S., et al.: PIV and PLIF to evaluate mixture formation in a direct-injection hydrogen-fuelled engine. SAE 2008-01-1034
[5] Salazar, V., et al.: Interaction of intake-induced flow and injection jet in a direct-injection hydrogen-fueled engine measured by PIV. SAE 2011-01-0673
[6] Kawahara, N., et al.: Fuel concentration measurement of premixed mixture in a spark-ignition engine using spark-induced breakdown spectroscopy. In: 15th International Symposium on Appli. of Laser Tech. to Fluid Mechanics, July 05-08 (2010)

# Effects of Different Port Injection CNG System Configurations on a 3.8L V6 Engine

Jose Herrera, Joshua Toohey, Boxin Jin,
Thomas Rogers, and Lucien Koopmans

School of Aerospace, Mechanical and Manufacturing Engineering
RMIT University, Melbourne, Australia
`lucien.koopmans@rmit.edu.au`

**Abstract.** In light of sustainable mobility and increased fuel prices in Australia, vehicles and engines operated on gaseous fuel are becoming more popular. This paper investigates the effects of different aftermarket compressed natural gas (CNG) fuel delivery system configurations on combustion stability, fuel economy and emissions utilising a commercially available internal combustion engine (ICE). The investigated parameters include the effects of the injector location in relation to the intake manifold as a function of engine speed/load, equivalence ratio as well as injection and ignition timing. Using a combination of computer simulation tools and experiments, effects on the engine and its mechanisms are clarified. A 1D model (Lotus Engine Simulation) of the engine is used to produce realistic pressure fluctuations and flow velocities at the injector nozzle position in the intake manifold, for different engine operating conditions. A computational fluid dynamics code (ANSYS) is used to investigate the fuel distribution in the intake manifold and pulsations in the injection system. The CNG jet was visualized in a spray vessel using Schlieren techniques to increase understanding of the gaseous jet behavior. And finally, the computer simulations and spray visualisations are evaluated together with experimental data to explain the engine's behaviour as a function of different fuel system configurations.

## 1   Introduction

In the current economic and social climate, consumers are looking for cheaper and more environmentally sustainable personal transportation. Rising fuel costs and dependency on oil has prompted research into a number of various alternate fuel sources, one of which being CNG.

In Australia, the transportation sector is the third largest emitter of greenhouse gas emissions ($CO_2$ equivalent) [1] and as such the automotive sector is looking for alternate ways to reduce them. Australia is also burdened with one of the highest per-capita vehicle ownership, globally [2]. Beside the security of vast amounts of fossil CNG fuel available, 1kg of CNG produces approximately 12% less $CO_2$

after stoichiometric combustion ($\lambda$=1) compared to gasoline fuel. Also, Maji *et.al.* [3] suggest that an engine operating stoichometrically on CNG can produce up to 80% less CO and 12% less NOx emissions.

With CNG being a readably available and cheap fuel source, it makes for a realistic option as an alternate fuel source. Currently aftermarket CNG systems are available *off-the-shelf* and can be used to convert a number of different engines to use CNG as the primary fuel source. However, aftermarket fuel systems currently have less stringent regulations with regards to emissions and while a number of researches have focused on engine design specific for one fuel source, very little investigation into adaption onto a factory engine has been done. Moreover, most of the focus has been on engine maximum torque and power. Here a disadvantage of CNG usage becomes apparent when the engine's performance is reduced due to the displacement of air after CNG injection. This investigation however, focuses on part-load and especially mixture preparation since a stable (from cycle-to-cycle) homogeneous mixture of air and fuel, at the end of the compression stroke, is required for high engine efficiency and running smoothness

## 2   Experimental Setup

A GM Holden 3.8lt V6 engine with four different CNG fuel delivery configurations was connected to an engine dynamometer for controlling and measuring engine speed and load, respectively. Equipment for monitoring emissions, cylinder pressure, temperatures, fuel consumption and air-fuel-ratio was used during the measurements.

The engine, see Figure 1, was equipped with an aftermarket CNG fuel delivery system for port fuel injection in addition to the standard port fuel gasoline injection system. The 6 Keihin CNG injectors were used in four different measurement set-ups and supplied with a fuel pressure of 3 bar (relative to the intake manifold pressure). The aftermarket CNG system installation has the injectors mounted on top of the intake manifold and connected to the intake manifold with a rubber hose to a nozzle position approximately 270 mm upstream the intake valve.

Three of the four set-ups involved in these experiments had different length of the hoses that connect the injectors with the nozzles as follows:

- 210 mm: shortest possible length.
- 270 mm: medium length.
- 480 mm: long length.

A fourth setup; six nozzles positioned directly after the throttle valve upstream the plenum, was used to ensure probability of homogenous mixing.

Engine load and engine speed were controlled by a DynoMaster eddy-current dynamometer set-up which also measured the engine torque. An AVL IndiModul 622 with an acquisition rate 800 kHz was used together with the AVL optical crank angle encoder for data acquisition of cylinder pressure data measured with a high sensitivity sparkplug cylinder pressure sensor. The emissions measurement system (Horiba Mexa-8220) included a flame ionization detector for unburned

**Fig. 1.** The GM Holden 3.8lt V6 with the aftermarket CNG fuel system installation

hydrocarbons (including methane), non-dispersive infra-red analysers for CO and $CO_2$ and a chemiluminescence analyser for NOx. The fuel massflow rate was measured real-time with a Siemens Coriolis meter (FC300 DN4). Engine parameters such as injection and ignition timing were controlled using a MoTeC M600 ECU which also measured temperatures and air-fuel-ratio.

## 3  Experimental Methodology

Before each experiment, it was ensured that the engine was fully warm, the emissions measurement equipment calibrated and that the engine had not changed in behaviour compared to the previous test (this was done by operating the engine on a gasoline fuelled reference point). During each test, the engine was operated in steady state conditions at a constant speed of 2000 rpm and a constant load of 2 bar BMEP. During a measurement series, for example varying the air-fuel-ratio (lambda), the engine was operated randomly to eliminate time trends. Selected operating points were repeated at different timing to get an indication of measurement accuracy and spread to ensure that the presented trends are valid.

Optical Schlieren techniques were used for visualisation of a gas jet. Using the Schlieren method, optical inhomogeneities in transparent media not visible to the human eye are measured. These inhomogeneities are localized differences in the optical path length that cause light deviation. This light deviation is converted to a shadow in a Schlieren system. Injecting gas in a steady state environment causes inhomogeneities that are directly related to the gas injected. A high speed camera capable of 30.000 frames per second was used for visualisation.

# 4 Test Results and Discussion

Instability of the combustion process in a firing engine causes cycle to cycle combustion variations and increases the fuel consumption of the engine. These variations can be monitored using a cylinder pressure sensor and after processing expressed as coefficient of variation of the indicated mean effective pressure (COV IMEP) which is the standard deviation of IMEP divided by the mean value of IMEP calculated over 150 engine cycles. The cycle to cycle variations of a spark ignition engine are mainly caused by the variation in flame propagation during the early flame development phase, directly after ignition. These are caused by: inhomogenities in the equivalence ratio, residual mass fraction and turbulent gas velocities in the vicinity of the spark, Heywood [4] and Johansson [5]. Inadequate mixture preparation would therefore result in unacceptable high COV (an acceptable level of COV at part load is approximately 4%). A good method of testing the quality of mixture preparation is operating the engine towards its lean limit. At this limit the $COV_{IMEP}$ is high and occasional misfire might occur. Perfect mixture preparation (completely homogenous distribution of fuel) should allow for a higher air-fuel-ratio (or lambda) since the local lambda in the vicinity of the spark plug is not affected by cycle to cycle variations. On the other hand, the probability of a local deviation towards excessive lean mixture in the vicinity of the spark plug (hence slow burn or misfire) is higher proportional to the degree of bad mixing.

The lambda variation and lean limit of the four CNG fuel system set-ups is shown in Figure 2.
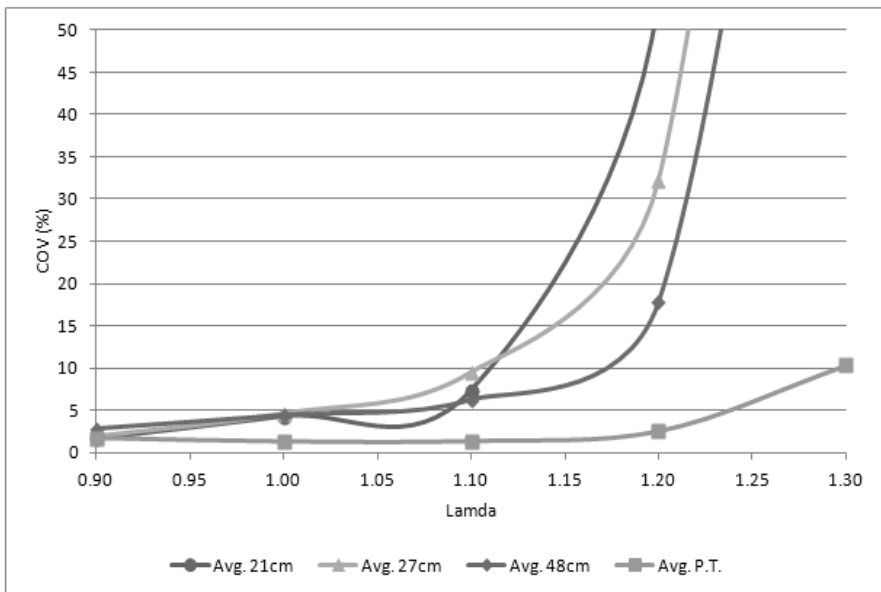


**Fig. 2.** $COV_{IMEP}$ as a function of lambda for four different CNG fuel system set-ups (each line shows the average of the measurement sequence for that particular set-up, hence Avg.)

The lowest $COV_{IMEP}$ and highest tolerance towards mixture enleanment is accomplished by the set-up with CNG nozzles directly positioned after the throttle (P.T.) then the limit decreases inversely  proportional to the rubber hose length (distance of CNG injector from manifold). The discrepancy around $\lambda=1.05$ cannot be explained and needs further investigation.

Figure 3 shows the carbon dioxide, carbon monoxide, unburned hydrocarbon and nitrogen oxides emissions respectively. Normal driving conditions vary between the range of $0.9<\lambda<1.1$, hence the main focus of the analysis was within this range. In general; higher levels of unburned hydrocarbons and carbon monoxide and lower levels of carbon dioxide and nitrogen oxides are produced for the set-ups with a hose. Here the 480 mm hose set-up generates emissions levels closest to the post throttle set-up levels.
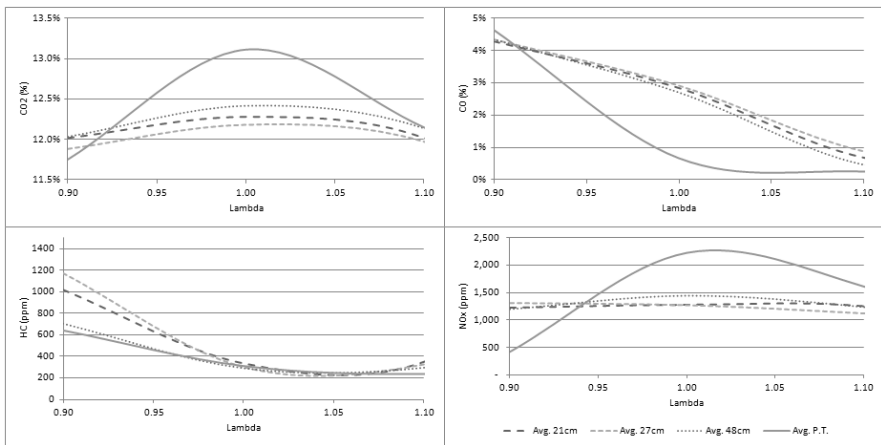


**Fig. 3.** Emissions as a function of lambda for different CNG fuel system set-ups.

The engine dynamometer results indicate a worse mixture preparation for the hose set-up compared to the post-throttle set-up. This is confirmed by the higher lean limit of the post throttle set-up but also by the higher $CO_2$ and corresponding lower CO emissions which indicate incomplete combustion and rich zones in the mixture. Also the lower $NO_x$ emissions level at overall mixture air-fuel-ratio of $\lambda=1$ indicate lean and rich zones which exhibit a lower combustion temperature hence lower $NO_x$ emissions.

To investigate why the mixture preparation is degraded for the hose set-up, spray visualisation and CFD analysis have been used to clarify phenomena and part of that investigation is presented in Figures 4 and 5 respectively. Both results show virtually no mixing with the immediate surrounding air of the spray nozzle. Instead, the gas jet almost collectively hits the opposite wall and forms a fuel rich volume fraction close to the wall. In the engine this would indicate the formation of a fuel rich cloud at the bottom half of the manifold and intake port. After
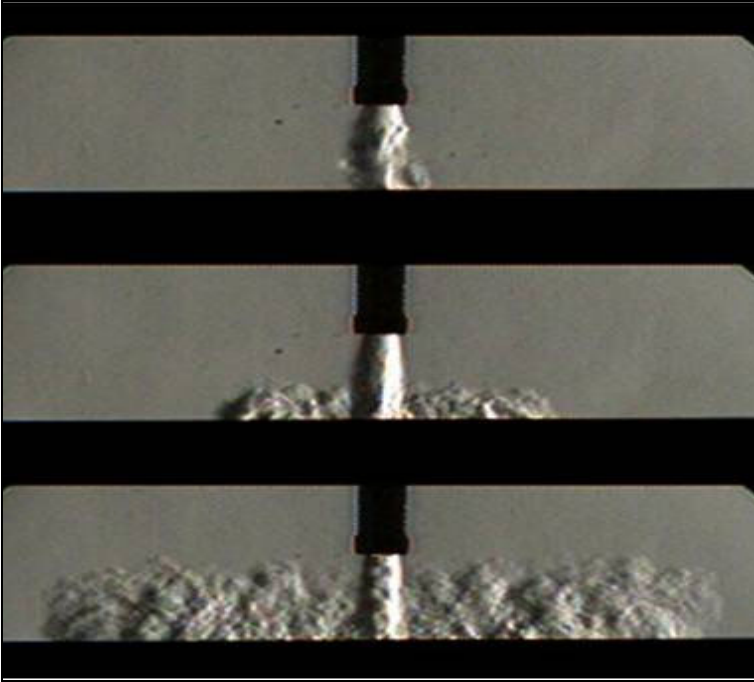
**Fig. 4.** Schlieren images of a developing gaseous jet interacting with a wall at steady state conditions
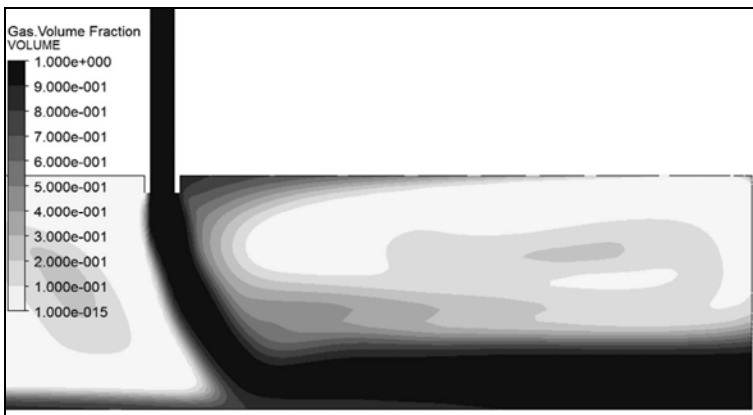


**Fig. 5.** CFD simulation of a gaseous spray interacting with a manifold wall at realistic engine conditions determined by LES (the intake valve is positioned on the right hand side of this simulation).

induction into the cylinder the mixture preparation towards homogeneity relies therefore completely on the large scale fluid motions and turbulence inside the cylinder, which is inadequate for this GM Holden 3.8lt V6 engine (2 valve configuration). An explanation for the better performance of the longer hose can be found in lower gas velocities entering the intake manifold (longer distribution time) and more mixing inside the hose.

Based on the results one would suggest CNG injection directly after the throttle body to ensure lower cycle to cycle variations and therefore better engine efficiency. However, all the experiments were performed under steady state engine conditions. The main reason for multi-point fuel injection close to the intake valves is the control of mixture preparation and fuel delivery to each cylinder during transient conditions.

## 5  Conclusions

The aftermarket CNG system set-up with the injectors positioned away from the intake manifold but with the fuel delivery nozzles close to the intake port generate high combustion instability indicated by high $COV_{IMEP}$. These set-ups also generate high CO emissions, both compared with CNG injection directly after the throttle. The poor performance of these systems was explained by poor mixture preparation. It is recommended that aftermarket CNG injection systems are optimized with respect to installation parameters such as hose length and location of the injection nozzle but also with respect to nozzle geometry and installation angle (future work).

## References

1. DCC, Tracking to the Kyoto Target 2007: Australia's greenhouse emissions trends 1990 to 2008–2012 and 2020, Canberra, DCC (2008d)
2. Barker, T., Bashmakov, I., Bernstein, L., Bogner, J.E., Bosch, P.R., Dave, R., Davidson, O.R., Fisher, B.S., Gupta, S., Halsnæs, K., Heij, G.J., Kahn Ribeiro, S., Kobayashi, S., Levine, M.D., Martino, D.L., Masera, O., Metz, B., Meyer, L.A., Nabuurs, G.-J., Najam, A., Nakicenovic, N., Rogner, H.-H., Roy, J., Sathaye, J., Schock, R., Shukla, P., Sims, R.E.H., Smith, P., Tirpak, D.A., Urge-Vorsatz, D., Zhou, D.: Technical Summary. In: Metz, B., Davidson, O.R., Bosch, P.R., Dave, R., Meyer, L.A. (eds.) Climate Change 2007: Mitigation. Contribution of Working Group III to the Fourth Assessment Report of the Intergovern-mental Panel on Climate Change. Cambridge University Press, Cambridge (2007)

3. Maji, S., Sharma, P.B., Gajendra Babu, M.K.: Experimental Investigations on Performance and Emission Characteristics of CNG in a Spark Ignition Engine. SAE Technical Paper Series (2005-26-344) (2005)
4. Heywood, J.: Internal Combustion Engine Fundamentals. McGraw-Hill (1988)
5. Johansson, B.: Cycle to Cycle Variations in S.I. Engines – The Effects of Fluid Flow and Gas Composition in the Vicinity of the Spark Plug on Early Combustion. SAE Technical Pater Series (962084) (1996)

# On the Application of Compressed Natural Gas for an SI Internal Combustion Engine and Two Different Injector Positions

Christopher Soanes and Lucien Koopmans

School of Aerospace, Mechanical and Manufacturing Engineering
RMIT University, Melbourne, Australia

**Abstract.** The application of compressed natural gas (CNG) as automotive fuel has several advantages over gasoline. Natural gas is more economical, has better knock resistance, a wider range of flammable air fuel ratio, as well as lower carbon monoxide, carbon dioxide and hydrocarbon emissions. It is proving to be a worthy alternative to traditional fossil based fuels. Mixture homogeneity in an internal combustion (IC) engine has a significant effect on performance parameters such as power, torque, fuel consumption, emissions, combustion rate and exhaust temperatures. However, homogenous mixture formation with a gaseous fuel is much harder to achieve than with liquid phase fuel due to the limited shear stress between the CNG jet and air. An experimental study using a 3.8L V6 engine (typical of the popular large Australian sedans) and variations in injector location and injection timing were investigated to gain further understanding of its effects on combustion characteristics, performance and emissions. Beside the standard gasoline fuel delivery system, two different CNG systems with different injector positions were used, targeted and non-targeted. For the targeted injector position, the injectors replaced the gasoline injectors and were placed in the same position and angle pointing towards the intake valves. For the non-targeted position, injection nozzles were equally distributed on an adapter ring which was mounted directly downstream the throttle body. The obtained results showed unexpectedly similar engine stability performance for both CNG systems. Discussions examine different avenues that are likely to explain why there is similar mixing performance for both systems. Also, compared to gasoline operation, lower emissions and higher lean limit were accomplished for the engine operating on CNG.

## 1  Introduction

Global warming, stringent emissions standards and increasing $CO_2$ legislation are helping drive a reduction in emissions, in particular of $CO_2$, in the transport sector. Alternative fuels have the potential to offer: Increased engine efficiencies, lower emissions, reduced costs and increased energy density (by weight).

Compressed Natural Gas (CNG) provides a significant opportunity for future emissions reduction (in particular $CO_2$), as this natural resource is in significant

supply within Australia. Figure 1 below clearly displays the energy density performance of CNG compared to alternative powertrain energies such as batteries. With peak oil, liquid fuels are no longer as viable and the energy density of batteries in weight and volume cannot compare to the performance of conventional fuels. CNG offers high energy densities coupled with low emissions and increased engine performance.
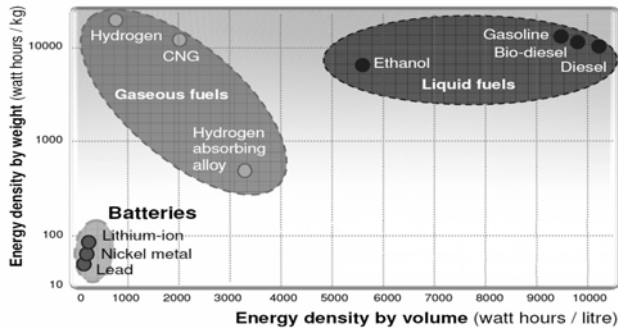


**Fig. 1.** Fuel energy density comparison (adapted from Smith, G., 2010)

Mixture homogeneity hence local mixture composition has a pronounced effect on engine parameters such as peak power, fuel consumption and exhaust emissions composition (Heywood, 1988). Gaseous fuels in general do not mix as well with air as liquid fuels due to the lower shear forces between the fuel jet and surrounding air (Abraham, 1994). Also in engine applications it has been found that obtaining homogenous mixture preparation can be challenging even for port fuel injection systems (Baker et.al., 2009; Herrera et.al., 2012). Both studies show that good mixture homogeneity can be accomplished with gaseous fuel injection at the throttle body but when the injection takes place more downstream closer to the intake valves, mixture homogeneity and engine stability decreases. However, injection at the throttle body is not desired due to inaccurate fuel metering during transients. Therefore this study will investigate if the gaseous mixture preparation hence engine stability can be improved with an injector position, similar to the standard gasoline injector, close to the intake port and a targeted CNG jet towards the intake valve. Also, using similar injector positions, a comparison between gasoline and CNG emissions performance is presented.

## 2   Experimental Setup

Testing was conducted on a standard and modified Holden 3.8L V6 Ecotec engine. The modified engine was fitted with dedicated gas injection system from Prins auto gas system. Using this system two different CNG injector locations (targeted and non-targeted) were investigated towards emissions and engine stability. In the targeted injector position (MPI-G) the injectors replaced the gasoline

injectors and were placed in the same position and angle pointing towards the intake valves. In the non-targeted position (PTI-G), 6 injection nozzles were equally distributed on an adapter ring which was mounted directly downstream the throttle body. The gas injection and injector locations are illustrated in figure 2. Here the position and angle of the gas injector downstream the plenum is similar to the standard gasoline injector.
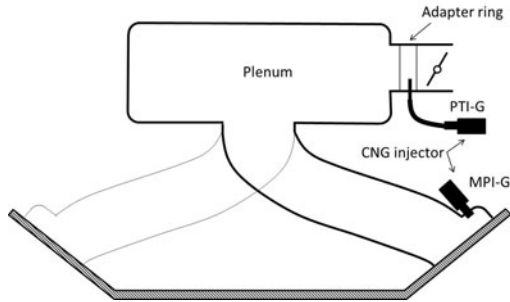


**Fig. 2.** Illustration of CNG injector position and installation (courtesy D. Wallis)

The engine was connected to an engine dynamometer for controlling and measuring engine speed and load, respectively. Equipment for monitoring emissions, cylinder pressure, temperatures, fuel consumption and air-fuel-ratio was used during the measurements.

Engine load and engine speed were controlled by a DynoMaster eddy-current dynamometer set-up which also measured the engine torque. An AVL IndiModul 622 with an acquisition rate 800 kHz was used together with the AVL optical crank angle encoder for data acquisition of cylinder pressure data measured with a high sensitivity sparkplug cylinder pressure sensor. The emissions measurement system (Horiba Mexa-8220) included a flame ionization detector for unburned hydrocarbons (including methane), non-dispersive infra-red analysers for CO and $CO_2$ and a chemiluminescence analyser for NOx. The fuel massflow rate was measured real-time with a Siemens Coriolis meter (FC300 DN4). Engine parameters such as injection and ignition timing were controlled using a MoTeC M600 ECU which also measured temperatures and air-fuel-ratio.

## 3 Experimental Methodology

Experiments were designed to establish and display the mixing performance of the different gas injection strategies and their effect on combustion stability and emissions. The following tests were conducted:

- Start of Injection (SOI) sweeps to determine best injection timing for combustion performance.
- Lambda sweeps to display the effects of mixing performance on emissions composition.

Before each experiment, it was ensured that the engine was fully warm, the emissions measurement equipment calibrated and that the engine had not changed in behaviour compared to the previous test (this was done by operating the engine on a gasoline fuelled reference point). During each test, the engine was operated in steady state conditions at a constant speed of 2000 rpm and a constant load of 2 bar BMEP. During a measurement series, for example varying the air-fuel-ratio (lambda), the engine was operated randomly to eliminate time trends. Selected operating points were repeated at different timing to get an indication of measurement accuracy and spread to ensure that the presented trends are valid.

## 4   Test Results and Discussion

*Start of Injection variation*
Start of injection (SOI) tests were conducted on the MPI-G and the PTI-G systems at 2000 RPM 2 bar BMEP. The purpose of these tests was to find the optimum point for SOI during an engine cycle. This optimum point is defined as that which produces the lowest coefficient of variation of IMEP (CoV IMEP) which is a measure of highest engine stability and therefore represents best gas mixing performance. The engine was operated with SOI at the following crank angle intervals:

- MPI-G: SOI at 60° crank angle intervals, over 720° crank angle.
- PTI-G: SOI at 120° crank angle intervals, over 720° crank angle.

Figure 3 shows the CoV IMEP as a function of SOI. For clarification, also the valve events and injection duration are depicted.

Examination of the data shows two clearly defined drops of CoV of IMEP at 0° CA for the PTI-G system and 0° and 180° CA for the MPI-G system. 0° CA is combustion and thus it can be seen that the lowest values of CoV of IMEP occur during a closed valve (0° and 180° CA). The MPI-G system shows dependence on SOI points compared to PTI-G where there was little variation over the injection points. The following can be concluded:

- PTI-G shows little variation in SOI due to the long mixing length (post throttle to intake valve) and high turbulence after the throttle valve. The long mixing length increases the mixing time before the mixture enters the cylinder.
- MPI-G shows large variation in CoV of IMEP and there is more spread in the measurements. Here the injector is located close to and pointing towards the intake valve. This decreases the mixing length and the mixing becomes a function of intake valve opening and pulsations in the manifold.
- For both MPI-G and PTI-G, SOI timing was chosen to be 0° CA for the remaining experiments.

*Lambda variation*
A good method of testing the quality of mixture preparation is operating the engine towards its lean limit. At this limit the CoV IMEP is high and occasional
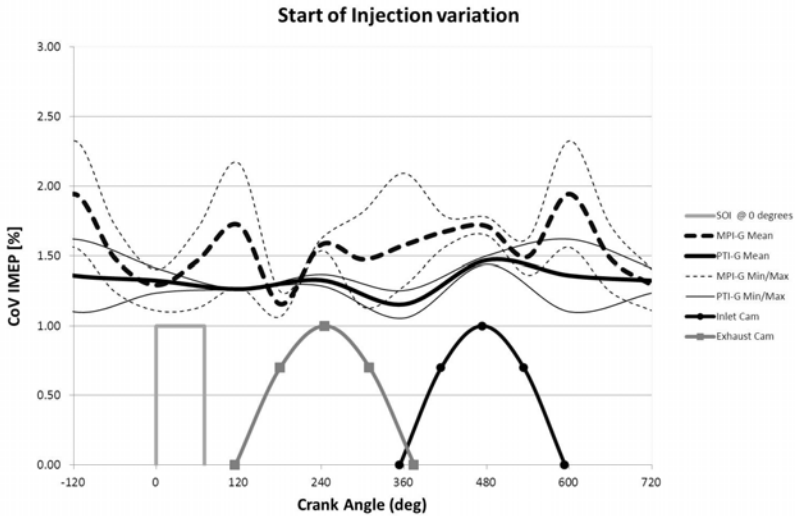
**Fig. 3.** CoV of IMEP as a function of SOI for MPI-G and PTI-G with valve events and in-jection duration at SOI at 0 CAD.

misfire might occur. Perfect mixture preparation (completely homogenous distri-bution of fuel) should allow for a higher air-fuel-ratio (or lambda). Using the cho-sen SOI point, lambda sweep tests were conducted on standard gasoline, MPI-G and PTI-G fuel delivery systems at 2000 rpm and 2 bar BMEP. The lambda sweeps were able to determine the effect of:

- Lambda on mixing performance
- Lambda on engine out emissions
- Injection location on mixing performance
- Injection location on engine out emissions
- Lean misfire limit at the operating point

Figure 4 shows CoV of IMEP as a function of lambda for standard gasoline, MPI-G and PTI-G fuel delivery systems.

The results show that when the mixture becomes leaner (higher lambda) the CoV of IMEP increases exponentially. This demonstrates that the lean limit has been reached (occasional misfire) under these fuelling conditions. An acceptable CoV IMEP for these operating conditions is in the order of 4%. CNG has a higher lean limit than gasoline due to the property of the CNG fuel. This can be utilized when lean engine operation is allowed, it reduces pumping losses hence decreases fuel consumption. The spread in the measurements was in generally lower for CNG fuel.

The experiment also demonstrates that engine stability hence gas mixing per-formance of the MPI-G system exceeds original expectations (poor mixing due to short mixing length). It is believed that due to the targeting of the fuel, the volume
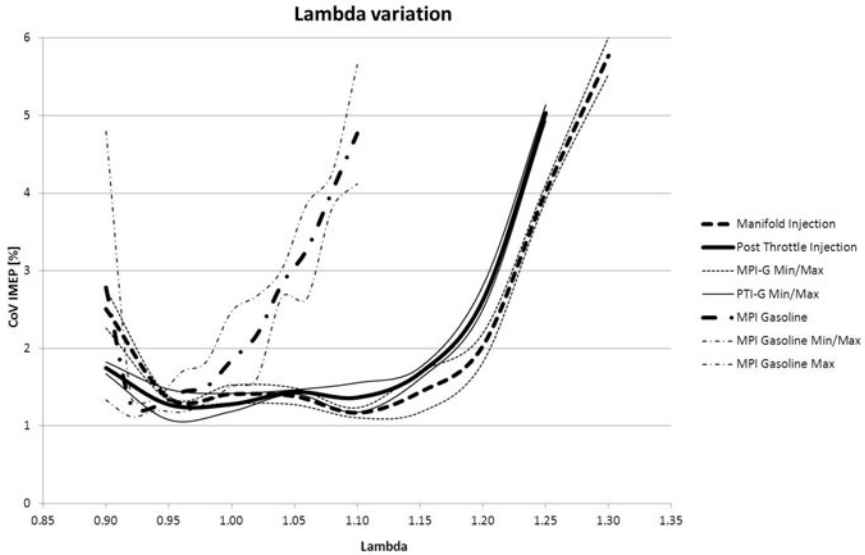
**Fig. 4.** CoV of IMEP as a function of Lambda for MPI-G and PTI-G.

directly upstream the intake valve is filled with gas. When the gas interacts with the port-facing surface of the valve it recirculates and mixes with the air. Therefore, the gas will be more equally distributed upstream the valve as opposed to a non-targeted manifold injection where the gas enters the cylinder only on one side of the valve (Herrera, et.al. 2012). The majority of the mixing of the CNG and intake air occurs from the turbulence created by flow past the intake valve.

*Engine out emissions*
The emissions for MPI-G and MPI gasoline fuel system configurations as a function of lambda are depicted in Figure 5. These two systems have identical injector positions and thus this data shows a direct comparison of CNG and gasoline engine operation.

The results show that compared to gasoline operation, $CO_2$ is reduced when operating on CNG by up to 10%. This can be explained by the lower C:H ratio of CNG and the increased combustion stability of CNG which ultimately increases engine efficiency. Also $NO_x$ emissions are reduced by 4%. This can be explained by the lower maximum temperatures associated with CNG combustion. Higher concentrations of $H_2O$ associated with CNG combustion assist in lowering the maximum in-cylinder temperatures. Peak $NO_x$ emissions of CNG are offset to that of gasoline to the lean side which indicates that the NOx formation mechanisms require more oxygen. This was also reported by Maji et.al. (2005). The large rise in HC emissions is caused by unstable combustion, indicating that the lean misfire
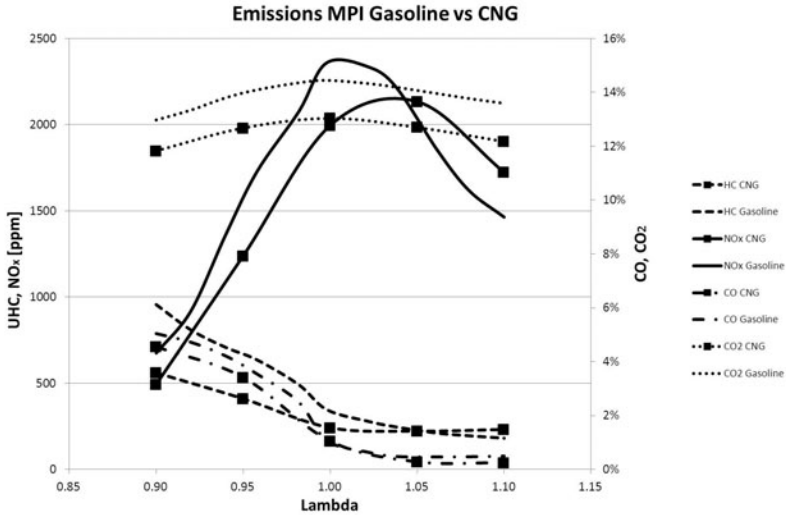
**Fig. 5.** Emissions as a function of lambda, MPI-G and MPI gasoline

limit has been reached. The thicker quench zone conditioned by the lower combustion chamber temperature causes a rise in HC emissions, aggravated by delayed combustion and misfires. Lower unburned hydrocarbons (UHC) and CO indicate more complete combustion hence better mixing during CNG engine operation.

## 5   Conclusions

The mixing of CNG displayed different and better results with respect to engine stability and mixing to what originally was expected from literature reviews.

Both CNG fuel delivery systems with post throttle injection (PTI G) and targeted multi point injection (MPI-G) achieve mixture homogenisation equally well at optimized start of injection. It is believed that due to the targeting of the fuel, the volume directly upstream the intake valve is filled with gas. When the gas interacts with the port-facing surface of the valve it recirculates and mixes with the air where after further mixing will occur through turbulence created by flow past the intake valve at intake valve opening. This hypothesis however needs further investigation.

The engine operating on CNG displays in general lower emissions ($CO_2$, $NO_x$, UHC and CO) compared to gasoline operation. The CNG engine also operates more stable (lower CoV IMEP) and has a leaner operating limit.

# References

Abraham, J., Magi, V., Maclnnes, J., Bracco, F.V.: Gas Versus Spray Injection: Which Mixes Faster? SAE technical paper series, SAE 940985 (1994)

Baker, P., Khan, M., Watson, H.: Mixture Preparation Effects on Gaseous Fuel Combustion in SI Engines. SAE technical paper series, SAE 2009-01-0323 (2009)

Herrera, J., Toohey, J., Jin, B., Rogers, T., Koopmans, L.: Effects of different port injection CNG system configurations on a 3.8l V6 engine. In: Proceedings ICSAT 2012, Springer, Heidelberg (2012)

Heywood, J.B.: Internal combustion engine fundamentals. McGraw-Hill (1988)

Maji, S., Sharma, P.: Experimental Investigations on Performance and Emission Characteristics of CNG in a Spark Ignited Engine. SAE 2005-26-344 (2005)

Smith, G.: Toyota's environmental technologies and approach. In: CUEN Annual Energy Conference on Sustainable Transport (2010)

# Recent Trends in Emerging Transportation Fuels and Energy Consumption

B.G. Bunting

Oak Ridge National Laboratory
buntingbg@ornl.gov

**Abstract.** Several recent trends indicate current developments in energy and transportation fuels. World trade in biofuels is developing in ethanol, wood chips, and vegetable oil / biodiesel with some countries being exporters and some importers. New drilling techniques, including deep-ocean drilling, extended horizontal drilling, and hydraulic fracturing, are bringing new sources of natural gas and crude oil to market. Resulting increases in natural gas availability have also opened new opportunities in gas to liquids and combined gas, coal, and/or biomass to liquids. The energy landscape is currently undergoing unprecedented change, due to world economics and growth, energy prices, local preferences, and concern about regional air pollution and global warming. Most likely, all options will need to be developed to supply future energy needs, and the energy industry will remain in flux for the foreseeable future.

## 1 Introduction

Abundance of energy can be improved both by developing new sources of fuel and by improving efficiency of energy utilization, although we really need to pursue both paths to improve energy accessibility in the future. Currently, 2.7 billion people or 38% of the world's population do not have access to modern cooking fuel and depend on wood or dung and 1.4 billion people or 20% do not have access to electricity. It is estimated that correcting these deficiencies will require an investment of $36 billion dollars annually through 2030 [1]. In growing economies, energy use and economic growth are strongly linked, but energy use generally grows at a lower rate due to increased access to modern fuels and adaptation of modern, more efficient technology [2]. Reducing environmental impacts of increased energy consumption such as global warming or regional emissions will require improved technology, renewable fuels, and CO2 reuse or sequestration. The increase in energy utilization will probably result in increased transportation fuel diversity as fuels are shaped by availability of local resources, world trade, and governmental, environmental, and economic policies. The purpose of this paper is to outline some of the recently emerging trends, but not to suggest winners. This paper will focus on liquid transportation fuels, which provide the highest energy density and best match with existing vehicles and infrastructure. Data is

taken from a variety of US, European, and other sources without an attempt to normalize or combine the various data sources.

Liquid transportation fuels can be derived from conventional hydrocarbon resources (crude oil), unconventional hydrocarbon resources (oil sands or oil shale), and biological feedstocks through a variety of biochemical or thermo chemical processes, or by converting natural gas or coal to liquids. The world currently consumes about 90.5 million barrels of crude oil per day (International Energy Agency).

## 2 Biofuels

The production of biofuels has grown significantly in the last 10 years, driven by environmental concerns, cost incentives, and high oil prices, as shown in Figure 1 [3]. Most of this growth has been in ethanol, mainly in the USA and Brazil. For liquid transportation fuels, biofuels production is only a small percentage of petroleum production, but could grow to 27% of transportation fuels by 2050 [3]. Feedstocks for new biofuels include cane, algae, other cellulosic biomass, energy crops, woody biomass, vegetable oil, animal related waste, and CO2. Conversion processes include biochemical, thermo chemical, esterification, and pyrolysis and related upgrading. This growth is dependent on economically available feedstocks and policies that support investment in the new industries and infrastructure.
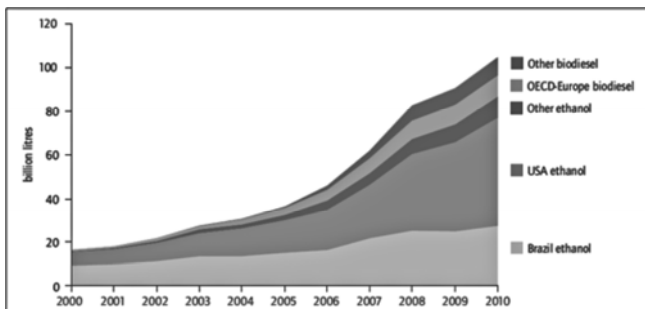


**Fig. 1.** Growth of biofuels in time period 2000 to 2010 [3]

The US EPA has released a Renewable Fuel Standard which requires increasing amounts of biofuels production and consumption each year through 2022, with targets of 9 billion gallons in 2008 and a gradual increase to 36 billion gallons in 2022 with a cap on the contribution of starch based ethanol at 15 billion gallons. Volume requirements for advanced biofuels (non-starch based) can be adjusted yearly based on evaluation of technology and availability [4]. It is expected that the majority of the increase beyond 15 billion gallons will be composed of cellulosic ethanol and cane derived ethanol.

In the US, ethanol can be used as a 10% blend in gasoline (E10), as an intermediate blend (E15, not currently being sold), and as E85, which actually ranges from E68 to E83, per ASTM D5798. Without the use of intermediate blends and a large increase in flex fuel vehicles, ethanol use will reach a limitation commonly known as the 'blend wall' [5]. Currently of the 840 to 880 thousand barrels of ethanol blended per day in the US, only about 5.6 thousand barrels per day are used for E85 and the remainder is blended at up to 10% [6]. As an example of the changes needed to achieve full ethanol utilization in 2022, it has been estimated that the number of flex fuel vehicles will have to increase from about 8 million presently to 100 million, with the number of pumps offering E85 increasing from about 2,000 to 65,000.

Brazil is the second largest producer of ethanol behind the USA, is the world leader in ethanol exports, and is also a large consumer of ethanol. All gasoline in Brazil contains 20 to 25% ethanol and over half of the vehicles are flex fuel and can run on 100% ethanol or any ethanol-gasoline blend. Ethanol production is in the range of 4000 to 4500 thousand barrels per day. Brazil produces and consumes about 2.5 to 3.0 million barrels of crude oil per day, but must export heavy crude and import both light crude and finished fuels in order to match refining capability. Newly discovered deep off-shore oil fields, known as the 'pre-salt zone', contain up to 8.3 billion barrels of oil equivalent and are being developed for 10,000 barrels per day production in 2010 and 4 million barrels per day by 2020. The depth of these reservoirs is about 18,000 feet and presents significant technical hurtles to achieve this production level [7]. Development of these oil reservoirs will make Brazil a net energy exporter and will also allow for future economic growth. These oil deposits are an example of resources which can be developed with improved drilling techniques.

As can be seen in Figure 2, there is existing world trade in biofuels, mainly for ethanol, biodiesel and vegetable oil, and for wood pellets [3].
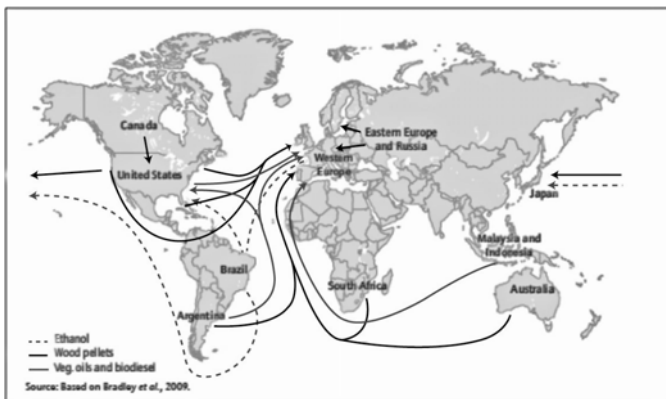


**Fig. 2.** Existing world trade in biofuels [3]

## 3  Natural Gas

Natural gas is not a liquid transportation fuel, but can be used in compressed form to fuel fleets, in liquefied form to fuel large engines or power plants, and can be converted to liquid fuels by thermo chemical processes. The proven reserves of natural gas have increased significantly in recent years due to wider use of hydraulic fracturing or *fracking* to shale based deposits containing tightly bound natural gas. Fracking has actually been practiced since 1947 and in North America over 1,000,000 wells have been hydraulically fractured, representing 95% of all gas wells and 43% of all oil wells [8]. Recent application to tightly bound shale assets, combined with improved horizontal drilling techniques, has resulted in a boom in natural gas production and producible reserves in the United States [8]. Much of the controversy related to fracking has resulted in application of these techniques to areas not accustom to energy production and to a rapid growth in the number of wells being drilled. Natural gas asset estimates have increased by a factor of 2 to 3 times in North America and currently the United States is the largest natural gas producer in the world, followed by Russia and Canada. In the US, development of this energy resource is being driven by promises of energy independence and job creation, although other parts of the world are taking a more cautious approach. Examples of recent news headlines include:

- Oil shale resources could help spur economic growth, 204,500 jobs in Ohio, $12 billion economic benefits by 2015 [9].
- Opening of Alaskan National Wildlife refuge to drilling could create hundreds of thousands of jobs [10].
- Study shows that 45% of NY voters support Marcellus drilling [11].
- France to keep fracking ban to protect environment, Sarkozy says [12].Oil shale resources could help spur economic growth, 204,500 jobs in Ohio, $12 billion economic benefits by 2015 [9].
- Opening of Alaskan National Wildlife refuge to drilling could create hundreds of thousands of jobs [10].

The natural gas boom has resulted in wide global price differences for natural gas, due to lack of infrastructure for transportation from new production areas. For example, in January 2011, natural gas prices varied from $4.50 (USA) to $9.50 (UK) to $11.00 per million BTU (Japan) [13]. Figure 3 indicates areas of North America with significant potential for production of natural gas [8].

The market is still under development and areas of low regional prices may not remain. Prices can be affected by development of export infrastructure, growing use for power generation or natural gas vehicles, colder winters, or shifting of drilling emphasis to reservoirs which can produce both crude oil and natural gas. Examples of recent headlines include:

- Dominion seeks exports of Marcellus Shale gas, 1 billion cubic feet per day as liquefied natural gas, to any country not prohibited [14].
- Drilling shift, power demand could hit gas oversupply: Conoco executive [15].
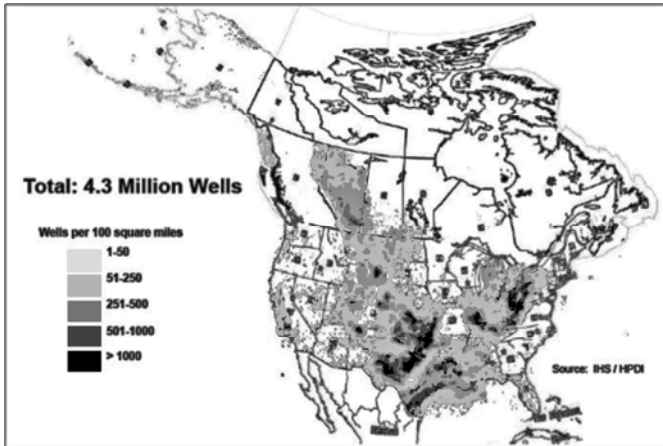
**Fig. 3.** Areas of North America with potential for natural gas production [8]

Low natural gas prices have also created the opportunity for converting natural gas to liquid hydrocarbons. This technology is well known but capital intensive. Abundant, low cost natural gas combined with high petroleum prices could encourage investment in this area. In a recent Hart's Energy seminar [10], three companies developing natural gas conversion processes were featured. The focus of the seminar was development of lower cost conversion technology and the integration of natural gas conversion with biomass and coal gasification with integrated $CO_2$ use or sequestration. An example of such a system is shown in Figure 4 for Accelergy Corporation (16), which can produce syngas from a variety of feeds and convert to liquid hydrocarbons. $CO_2$ is separated before the Fischer Tropsch reactor and used to grow algae, which in turn is used as a bio-fertilizer to
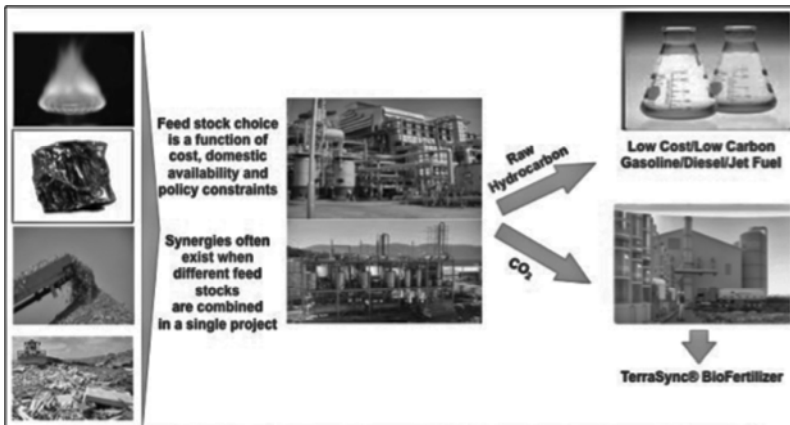


**Fig. 4.** Accelergy Corporation integration of gasification, thermo chemical conversion, and CO2 reuse [10].

enhance crop production. Although it may be unlikely that 100% $CO_2$ reuse will be achieved, the overall process can be made less $CO_2$ intensive by integration of natural gas (a lower carbon fuel), renewable biomass, and $CO_2$ reuse.

## 4   Conclusions

World trade in biofuels is currently centered around ethanol, wood chips, and vegetable oil / biodiesel, with the US, Canada, Brazil, Argentina, South Africa, Malaysia, Indonesia, and Australia being exporters and Europe, Japan, and the US as importers. New drilling techniques, including deep ocean drilling, extended horizontal drilling, and hydraulic fracturing are uncovering new sources of natural gas and crude oil, with the US and Eastern Europe leading development of these resources and many other countries following with their own projects and partnerships. Large increases in natural gas availability have also opened new opportunities in gas to liquids and combined gas, coal, and/or biomass to liquids. Overall, the energy landscape is currently undergoing unprecedented change, due to world economics and growth, energy prices, local preferences, and concern about regional air pollution and global warming. Most likely, all options will need to be developed to supply future energy needs, and the energy industry will remain in flux for the foreseeable future.

## References

[1] International Energy Agency, Energy Poverty, How to Make Modern Energy Access Universal, World Energy Outlook (2010)
[2] Stern, D.: The Role of Energy in Economic growth, The Oil Drum, (October 20, 2011)
[3] International Energy Agency, Technology Road Map, Biofuels for Transport (2011)
[4] US EPA. "RFS2" Federal policy drivers for increased biofuels usage (January 2009), `http://www.epa.gov`
[5] U.S. Energy Information Administration, Growth slows in U.S. ethanol production and consumption, Today in Energy (September 14, 2011), `http://www.eai.gov`
[6] U.S. Energy Information Administration, This week in Petroleum, The Ethanol Blend Wall (July 8, 2010), `http://www.eai.gov`
[7] U.S. Energy Information Administration, Country Analysis Briefs: Brazil (January 2011)
[8] National Petroleum Council, Prudent Development – Realizing the Potential of North America's Abundant Natural Gas and Oil Resources, Final Report (September 15, 2011), `http://www.npc.org`
[9] Cleveland Plain Dealer, as reported by American Petroleum Institute, API SmartBrief (September 21, 2011), `http://www.api.org`
[10] Oil and Gas Journal, as reported by American Petroleum Institute, API SmartBrief (September 21, 2011), `http://www.api.org`
[11] Reuters, as reported by American Petroleum Institute, API SmartBrief (September 21, 2011), `http://www.api.org`

[12] Bloomberg, as reported by American Petroleum Institute, API Smart Brief (October 4, 2011), `http://www.api.org`

[13] U.S. Energy Information Administration, Global Natural gas Prices Vary Considerably, Today in Energy (September 30, 2011)

[14] Fuel Fix, as reported by American Petroleum Institute, API SmartBrief (October 10, 2011), `http://www.api.org`

[15] Platts, as reported by American Petroleum Institute, API SmartBrief (October 12, 2011), `http://www.api.org`

[16] McDaniel, J.: Emerging GTL/BTL Opportunities in North America, Gas-to-Liquids, Biomass-to-Liquids, Hart's Energy Seminar, Hart's Fuel (September 27, 2011)

# Kinetic Modeling of Fuel Effects over a Wide Range of Chemistry, Properties, and Sources

B.G. Bunting[1], M. Bunce[1], K. Puduppakkam[2], and C. Naik[2]

[1] Oak Ridge National Laboratory
 `buntingbg@ornl.gov`
[2] Reaction Design
 `www.reactiondesign.com`

**Abstract.** Kinetic modeling is an important tool for engine design and can also be used for engine tuning and to study response to fuel chemistry and properties before an engine configuration is physically built and tested. Methodologies needed for studying fuel effects include development of fuel kinetic mechanisms for pure compounds, tools for designing surrogate blends of pure compounds that mimic a desired market fuel, and tools for reducing kinetic mechanisms to a size that allows inclusion in complex CFD engine models. In this paper, we demonstrate the use of these tools to reproduce engine results for a series of research diesel fuels using surrogate fuels in an engine and then modeling results with a simple 2 component surrogate blend with physical properties adjusted to vary fuel volatility. Results indicate that we were reasonably successful in mimicking engine performance of real fuels with blends of pure compounds. We were also successful in spanning the range of the experimental data using CFD and kinetic modeling, but further tuning and matching will be needed to exactly match engine performance of the real and surrogate fuels.

## 1 Introduction

In the future, fuel diversity is likely to increase, both from local options related to bio-derived fuels and due to further development of new, more traditional sources of fuels such as heavy crude derived fuels and natural gas. At the same time, there is a growing trend towards world engines and vehicles, manufactured at a single location, and designed to be used anywhere in the world. The ability to accurately model these diverse fuels is important for several reasons. Kinetic modeling provides a deeper, more fundamental understanding of fuel chemistry and property effects and allows CFD based design of engines and evaluation of robustness and control strategies before hardware is made. A better ability to represent fuel variations will allow fuel effects to be more fully factored into engine design and fuel selection early in the design cycle.

Kinetic models of fuels become increasingly large and unwieldy as more fuel components are added and as larger molecules are included to represent the higher boiling point components and as unique chemistries of biofuels or fuels derived

from non-traditional sources such as oil sands, oil shale, pyrolysis, or conversion to liquid fuels (gas, biomass, coal to liquids) are included. Depending on type of combustion system, physical processes can play as large a role as chemical processes of the fuel because physical properties affect spray, mixing, and evaporation.

The field of CFD (computational fluid dynamics) and kinetic modeling of engines is a very broad topic, with many areas of specialty focus. Some of these areas of focus include the surrogate representation of fuels, kinetic behavior of individual compounds, merging of individual chemical mechanisms and reduction of mechanism size, CFD modeling of engine cylinder and port flow and mixing, improved models for sprays and turbulence, and details of heat transfer and boundary layer effects. This paper will provide a very small introduction to this topic.

## 2  Experimental Data

This paper is based on data generated in 2011 on a single cylinder diesel engine located at Oak Ridge National Laboratory and equipped with extensive instrumentation for fuel and air measurement (coreolis and hot wire respectively) , gaseous emissions (California Analytical and AVL smoke meter), and combustion analysis (AVL Indicom). The latter is also equipped with a 1-D engine model and 2-zone combustion model to allow determination of residual fraction, heat transfer losses, and blow-by and for verification of experimental parameters such as TDC, compression ratio, and flows. The engine is a Hatz 1D50Z air cooled diesel engine, naturally aspirated, 2 valve, direct injection, 517 cc displacement, with a mechanical pump-line-nozzle injection system with fixed start of injection and equipped with a mechanical rate shaping nozzle to provide slow initial injection rate. This feature has been particularly difficult to mimic in the modeling. The engine meets Tier 4 EPA certification requirements. Data was taken for 5 of the 9 FACE diesel fuels, which were designed to represent a wide range of properties and chemistry and for 5 surrogate fuels which were designed by Reaction Design to mimic the characteristics of those fuels. The FACE fuels are 'fuels for advanced combustion engines' and were developed in a joint DOE – Coordinating Research Council to mimic the range of commercial diesel fuels available in the USA, as specified by cetane, T90, and % aromatics [1]. Of the 9 fuels available under this program, 5 were selected for the experiments and modeling in this paper. Data was taken at 1800 rpm with 3 fuel rates at ambient temperature intake air and 3 fuel rates with 100°C intake air, to get a wider range of combustion conditions. Data includes combustion analysis, emissions, speciated exhaust emissions by Fourier transform infrared spectroscopy, and particulate characterization by scanning mobility particle size analysis. For this paper only the high load, 100°C is discussed and a more complete summary of the data is included in references 2 and 3. Fuel characteristics are listed in table 1 and details of the surrogate composition are also provided in [2]. The surrogates were blends of 1-methylnaphthalene, n-propylbenzene, decalin, methylcyclohexane, heptamethyl nonane, n-decane, n-dodecane, and n-hexadecane and were designed to match the characteristics listed in table 1 using a Reaction Design surrogate blend optimizer tool.

**Table 1.** Properties of selected FACE fuels and their surrogates

| Fuel | Cetane Number | % Aromatics | % Cyclic paraffins | Smoke point (cm) | H/C molar ratio | Lower Heating Value (MJ/kg) | T50 (K) | Density (g/cm3) |
|------|------|------|------|------|------|------|------|------|
| FACE 1 | 30.3 | 24 | 15 | 21.7 | 1.93 | 42.8 | 463 | 0.81 |
| FACE 3 | 31.3 | 43 | 26 | 14.5 | 1.75 | 42.1 | 467 | 0.84 |
| FACE 5 | 55.0 | 20 | 30 | 25.0 | 1.96 | 42.9 | 488 | 0.81 |
| FACE 8 | 49.0 | 42 | 17 | 15.5 | 1.70 | 42.2 | 537 | 0.87 |
| FACE 9 | 44.0 | 33 | 34 | 14.7 | 1.80 | 42.5 | 521 | 0.85 |
| Surrogate 1 | 30.5 | 20 | 15 | 18.5 | 1.90 | 43.5 | 459 | 0.80 |
| Surrogate 3 | 31.1 | 38 | 25 | 12.7 | 1.71 | 43.0 | 447 | 0.82 |
| Surrogate 5 | 54.8 | 13 | 29 | 22.1 | 1.91 | 43.8 | 442 | 0.79 |
| Surrogate 8 | 50.1 | 37 | 15 | 11.8 | 1.65 | 43.1 | 458 | 0.85 |
| Surrogate 9 | 47.4 | 28 | 37 | 14.4 | 1.73 | 43.3 | 451 | 0.83 |

Figure 1 shows measured cylinder pressure and calculated apparent heat release rate for these fuels and indicate that the fuels and surrogates fall into two discrete groups based on cetane range. It is also apparent that the individual surrogates mimic the combustion behavior of their corresponding fuels. These curves represent a composite of 50 engine cycles.
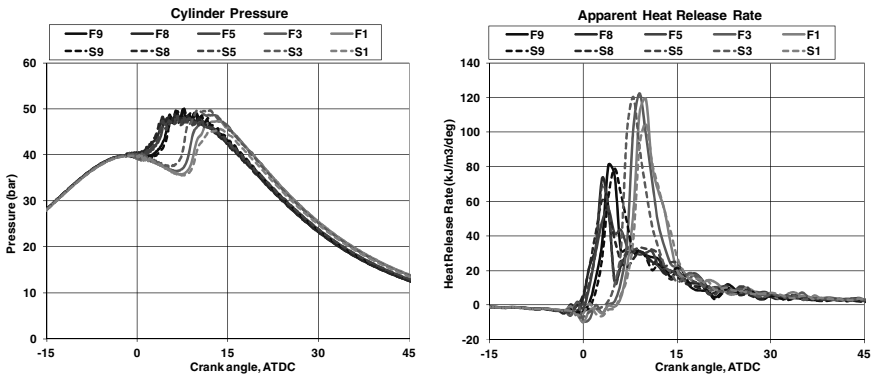


**Fig. 1.** Cylinder pressure and apparent heat release rate for experimental test points

The bar graphs in Figure 2 show how engine performance varies across the fuels and surrogates. First, in the top row, fuel rate and IMEP varies slightly between the fuels, indicating that experimental set-points were not exactly achieved for each fuel. However, indicated specific fuel consumption was very steady across all the fuels. In the second row of graphs, the low octane fuels produced lower soot and higher CO, with the surrogates reproducing the trends of the real fuels. In the lowest row, the low cetane fuels began combustion later due to lack of low temperature heat release, but had very similar MFB50 (point of 50% fuel burn) and dP/dCA (maximum rate of pressure rise, a measure of diesel knock). This data indicates the range of performance to be expected from this engine across a range of fuels and also indicates that this engine is quite robust to fuel

variations, as traditional diesel engines often are. The lower soot and higher CO of the low cetane fuels matches with the later start of combustion, resulting in more fuel / air mixing before combustion begins. The other characteristic preserved between the real fuels and the surrogates was the inability to achieve reliable combustion of the low cetane fuels without intake air heating. This is the reason this paper is based on data with heated intake air, so that all fuels could be included. Small differences in emissions between fuels and fuels vs. surrogates should be examined further for lower level fuel effects.
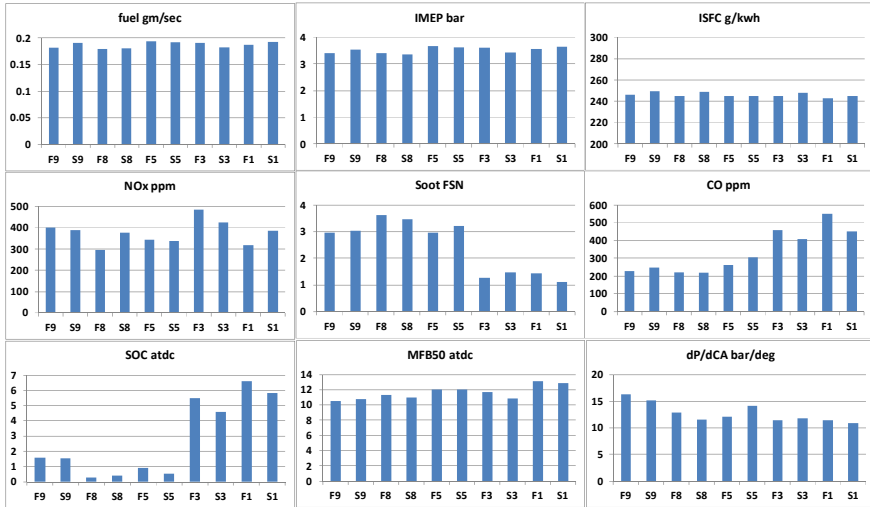


**Fig. 2.** Engine performance data for experimental test points

## 3　CFD Engine Model

A CFD engine model simulates the flow, injection, and combustion processes of an engine. In our model, we used a closed valve simulation starting at intake valve closing (-132 degrees atdc) and engine at exhaust valve opening (140 degrees atdc). Our model was a 1/5 sector mesh, meaning that a pie section of the cylinder was modeled corresponding to one hole of the 5 hole fuel injector. Our model has a grid size of 1 to 2mm per cell and this resulted in 18,000 cells at bottom dead center and 7,700 cells at top dead center. The combustion analysis system and associated instrumentation and models were able to provide values for residual fraction and composition, heat transfer losses. Fuel injection rate and timing were directly measured in a motoring experiment. For this paper, we use tools available from Reaction Design (www.reactiondesign.com) for surrogate fuel development (surrogate blend optimizer), for CFD modeling (Forte CFD), and for reduced kinetic mechanisms. Solution of the problem takes about 12 hours on a 4 processor computer with a reduced mechanism for n-heptane containing 85 species. Figure 3 shows a picture of the CFD sector mesh, location of the fuel spray, and typical

combustion temperature distribution. The model was verified and tuned by simulating actual engine data for n-heptane. This tuning consisted in adjusting starting pressure to match experimental mass and adjusting diesel nozzle characteristics to match combustion characteristics.
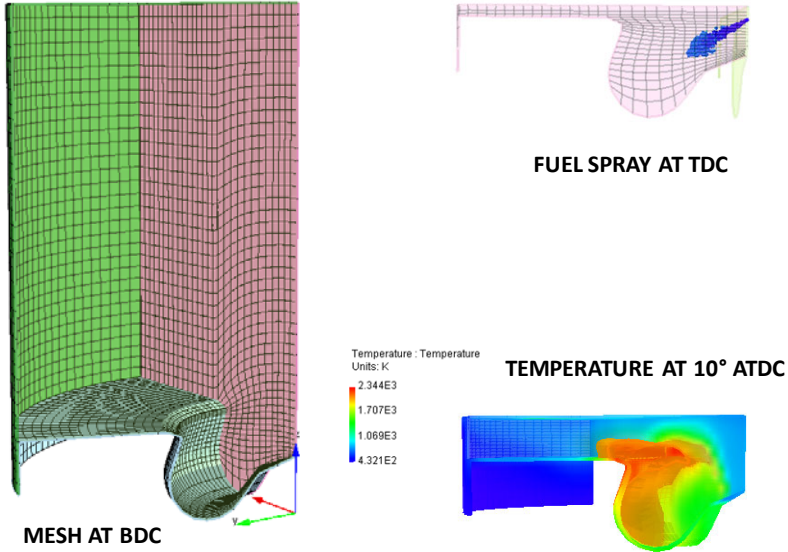


**Fig. 3.** CFD sector mesh showing details of bowl, top ring land, fuel injection location, and temperatures during combustion.

## 4  Surrogate Fuel Options

The simplest representation of diesel fuel for kinetic modeling is generally considered to be n-heptane, which differs from diesel fuel because of its higher cetane (54, per reference 4 average) and high volatility (low boiling point = 372°K). For the kinetic modeling work in this paper, we vary fuel reactivity by adding benzene (cetane = 15, per reference 4 average) to achieve 3 levels of cetane, 54, 44, and 31. This blending is done by molar ratio. The use of benzene to adjust cetane number also mimics the aromatics in the fuel, but does not follow the chemistry trends in the experimental fuels. Fuel volatility will be modified by using different physical properties for these chemical compounds, an option with Forte CFD, and the fuels will be represented physically as n-heptane, n-dodecane, and n-hexadecane, with boiling points of 372, 489, and 560°K respectively. This covers the range of T50 for the experimental fuels, shown in Table 1 but does not reproduce the full boiling range of the fuels. This modeling thus covers the range of fuel reactivity and volatility of the fuels, but in a much more simple way than the actual fuels. The modeling fuels were designed to represent the high, mid, and low

ranges of cetane and volatility of the experimental fuels, but not to exactly represent each specific fuel. Figure 4 is a repeat of Figure 1 with the engine data for the fuels and surrogates shown as gray lines and the modeling runs shown as broader colored lines and labeled by cetane (high, mid, low) and volatility (high, mid, low) per surrogate fuel specifications. Generally, the engine responded to lower cetane with later combustion phasing as expected but showed more sensitivity for modeling results than the experimental data showed.
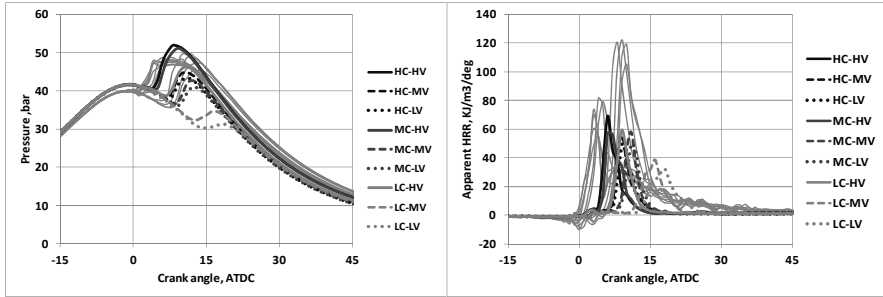


**Fig. 4.** Modeling output plotted over experimental data from Figure 1

Table 2 is a summary of CFD modeling output as related to cetane and fuel volatility represented as discussed in surrogate fuel section above. When these results are compared to Figure 2, it is apparent that the model also responds to lower cetane with later combustion, but that combustion, in general, is more retarded than the experimental data. The other data, NOx, HC, CO2, ISFC, and dP/dCA also show directionally consistent trends, but modeled values are affected by the later combustion when compared to experimental values. Further model tuning is required. This comparison between experimental and modeling data indicates some of the variables which are important to match when developing a CFD and kinetic model and tuning to a set of experimental data. Our combustion analysis capability provides many parameters needed for modeling input, but there are still

**Table 2.** Comparison of CFD modeling runs to experimental variables for key variables of interest

| cetane | HI | HI | HI | MED | MED | MED | LOW | LOW | LOW |
|---|---|---|---|---|---|---|---|---|---|
| volatility | HI | MED | LOW | HI | MED | LOW | HI | MED | LOW |
| fuel gm/sec | 0.1884 | 0.1884 | 0.1884 | 0.1884 | 0.1884 | 0.1884 | 0.1884 | 0.1884 | 0.1884 |
| IMEP bar | 3.42 | 2.54 | 2.30 | 2.62 | 2.41 | 2.21 | 2.82 | 2.36 | 2.37 |
| ISFC gross gm/kwh | 254 | 342 | 356 | 259 | 360 | 393 | 309 | 368 | 367 |
| NOx ppm | 149.0 | 88.4 | 75.4 | 144.0 | 70.7 | 64.5 | 99.8 | 49.9 | 42.5 |
| Soot ppm | 0.032 | 0.044 | 0.045 | 0.030 | 0.038 | 0.041 | 0.027 | 0.029 | 0.028 |
| CO ppm | 2615 | 9445 | 10169 | 2343 | 8770 | 9935 | 4068 | 7226 | 6467 |
| HC ppm | 4206 | 9750 | 11378 | 4898 | 10870 | 12289 | 8924 | 11816 | 11437 |
| MFB02 atdc | 3.04 | 4.04 | 5.01 | 3 | 5.01 | 5.04 | 3.03 | 5.01 | 6.01 |
| MFB50 atdc | 10 | 12.03 | 12.02 | 10.04 | 13.04 | 13.01 | 12 | 17.04 | 20.01 |
| dP/dCA bar/deg | 4.82 | 3.1 | 2.65 | 3.99 | 2.84 | 2.28 | 3.27 | 1.25 | 1.25 |

some variables which must be adjusted to match desired results. It is expected that if this matching is done correctly, that the model will be robust across the fuel variations.

## 5   Conclusions

The modeling of fuel effects on combustion is increasingly important as fuels become more diverse and engine performance becomes more demanding. Tools are becoming available through government laboratories, universities, and commercial companies which make this modeling more adaptable, more accurate, and easier to do. Experimentally, the Hatz diesel engine responds mainly to cetane number in the fuels tested, and the lower cetane fuels required intake heat to combust, produced a later start of combustion, and resulted in lower smoke and higher CO emissions. The current kinetic modeling is able to reproduce the range of experimental data for several key variables, but generally did not provide as close a match to experimental data as desired. This indicates that the modeling inputs or kinetic mechanisms used for this work require further development or tuning. This tuning is most likely to be in the areas of air motion and turbulence, spray characteristics and mixing, definition of surrogate fuel blends, complexity and details of kinetic mechanisms, details of heat release calculation, and heat loss adjustments. This paper also indicates some of the variables which should be compared with experimental data when verifying an CFD and kinetic model.

## References

1. Alnajjar, Cannella, Dettman, Fairbridge, Franz, Gallant, Gieleciak, Hager, Lay, Lewis, Ratcliff, Sluder, Storey, Yin, Zigler: Chemistry and Physical Properties of the Fuels for Advanced Combustion Engines (FACE) Research Diesel Fuels. CRC Report No. FACE-1 (2010), http://www.crcao.org
2. Naik, C.V., Bunting, B.G., Meeks, E.: Experimental Validation of the FACE Fuels Surrogates using a Diesel Engine. Offered for Presentation at 2012 SAE World Congress, 12PFL-0465 (2012)
3. Bunce, M., Bunting, B., Crawford, R., Wang, J.: Experimental and Statistical Comparison of Engine Response as a Function of Fuel Chemistry and Properties in CI and HCCI Engines. Offered for Presentation at 2012 SAE World Congress, 12PFL-0584 (2012)
4. Murphy, M., Taylor, J., McCormick, R.: Compendium of Experimental Cetane Number Data, National Renewable Energy Laboratory Report NREL/SR-540-36805 (September 2004)

# Biofire – Biogenic Fuel Ignition Research

K. Huber and J. Hauber

Ingolstadt University of Applied Sciences
`johann.hauber@haw-ingolstadt.de`

**Abstract.** The increasing use of biofuels is a major challenge for combustion engine manufacturers in terms of performance and CO2 efficiency. The cetane number, as it is one of the most important fuel numbers for Diesel fuels, is derived from the ignition delay which represents the period between the beginning of fuel injection and the start of combustion. This ignition delay is evaluated by using a single cylinder test engine and measuring the time difference between the signal of the needle stroke sensor which is mounted directly at the injection valve and the maximum pressure increase in cylinder.

This conventional test method for fossil fuels, however, determines ignition behavior of biofuels only insufficiently. The pressure increase of biofuels at start of combustion is less steep due to their lower reaction kinetics and spray quality and therefore results in inaccuracies concerning the determination of cetane numbers.

The method suggested by the bioFIRe project starts with a pressure pattern analysis in order to receive parameters that provide important conversion points in the combustion process. Thus, the ignition delay of fuels - as currently understood - is reflected correctly. This can be achieved by the calculation of statistically, thermodynamic and reaction kinetic parameters for the combustion and the pressure pattern. This allows to determine the cetane number for biogenic as well as for fossil diesel fuels.

The final aim for a successful introduction of the new determination method for cetane numbers is to proof its reproducibility and accurateness. Besides, this method has to be licensed by the Standards Committee.

## 1  The Cetane Number as a Quality Standard for Diesel Fuels

Important properties of diesel fuels needed for reliable and efficient operation of diesel engines are described in European standard EN 590. The cetane number describes the ignition behavior of diesel fuel and is of outstanding significance for the combustion process. For this reason the value of the cetane number is demanded to be at least 51 by EN 590. It influences the ignition delay which is the interval between the start of injection (SOI) and the start of combustion (SOC). The interval is the sum of physical and chemical ignition delay. The physical ignition delay consists of the spray breakup of the injected fuel, its vaporization and the mixture with the compressed air. The following chemical ignition delay is

characterized by pre-reactions of fuel and air molecules without considerable energy release.

As the ignition delay influences the burn rate directly, it effects the noise emissions (comfort) as well as pollutant formation and the fuel consumption of an engine.

## 2   Peak Oil and CO2-Limitation: European Law for the Use of Biogenic Fuels and Fuel Diversification

The actual worldwide production (distilling) and conditioning (cracking and blending) of gasoline and diesel fuels is about 1.6 billion tons per year. About the half of the produced amount is diesel fuel. The market share of biogenic and other alternative fuels need to rise due to a decreasing oil output after "Peak Oil" which can no longer satisfy the increasing demand (figure 1).

In addition, the EU aims at reducing the non-regenerative $CO_2$-emissions in order to restrict the greenhouse effect [13,14,15].
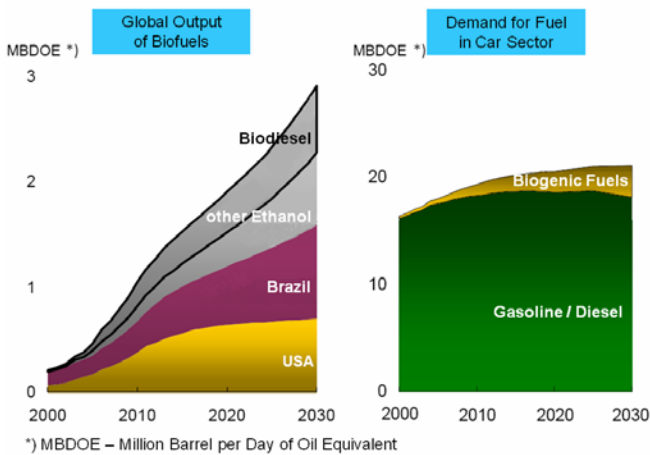


**Fig. 1.** Global fuel market development (fossil and renewable); Source: ExxonMobile

The increasing use of alternative fuels for on-road vehicles – a selection is shown in figure 2 – constitutes an indispensable opportunity to save fossil energy and to reduce the $CO_2$-emissions.

In the scope of alternative fuels, especially biogenic fuels for diesel engines, biodiesel (esterified vegetable oil, e.g. rape oil as well as soy and palm oil and organic fats) has been available on the market for a longer period of time (about 12 to 15 years) [5].

Also vegetable oils, in Europe especially rape oil according to DIN-V 51605, are used as replacement fuels for diesel, whereby its higher viscosity causes

problems at carburetion. Another disadvantage is the shortened shelf life (reduced oxidation stability) because of the partially polyunsaturated fatty acids [11].

Besides esterification, another way to improve the viscosity behavior of vegetable oils is to process them to HVO (Hydrotreated Vegetable Oil), whereby the long-chain unsaturated oil molecules are split up into short-chained paraffines [5,18].

The group of GTL (GasToLiquid consisting of otherwisely burned natural gas or bio methane), CTL (CoalToLiquid produced from coal and water or hydrogen) and BTL (BiomassToLiquid) are regarded as 'premium' replacement fuels for diesel as they distinguish themselves by high pureness and ignition willingness while being free of sulphur [7,10,11,16]. With an increased expend of manufacturing, they also have the potential to process waste products from agriculture and forestry as well as the highest capability to reduce the formation of pollutants.

Furthermore, the possible use of alcohols, which are more commonly known as standard gasoline fuel, is at the experimental stage for the use in diesel engines. This is for example methanol which is processed to DME (dimethylether) or OME (oxymethylenether) [6], and ethanol in form of E85 [8]. These fuels can be produced comparatively easy by fermentation processes.



**Fig. 2.** Selection of different fossil and biogenic diesel fuel samples

These alternative fuels differ much from fossil diesel fuels regarding carburetion, vaporization and combustion. Therefore reference accuracy of engine based test procedures for the measurement of the cetane numbers will not be abandoned in the future. In contrast to previous test methods the new measurement should be characterized by higher accuracy, better handling and universal aptitude for biogenic fuels and fuel blends.

# 3   Overview of Valid Procedures for Cetane Number Measurement

The two engine-based measuring methods for determining cetane numbers are the commonly used Waukesha-CFR-Engine as well as the BASF-Engine test (Figure 3).

Both engines inject fuel into a turbulence chamber and are operated at constant ignition delay [1,2,3]. With the CFR-Engine this is achieved by a variable compression ratio. The BASF-Engine variably restricts the intake air. By bracketing with reference fuels and interpolation of the received values, the cetane number can be determined.
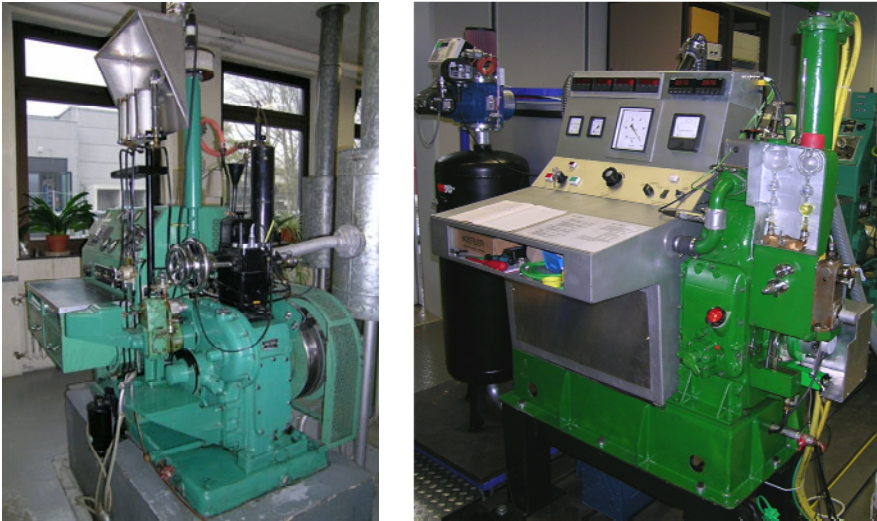


**Fig. 3.** Test engines for Diesel: CFR (left) and BASF (right)

Due to the high maintenance efforts and the moderate reproducibility of the cetane values determined by engine test procedures two non-engine procedures, so called Constant-Volume-Tester, have been developed and approved.

These are the FIT (Fuel Ignition Tester) and the IQT (Ignition Quality Tester) as shown in Figure 4. Both are characterized by low space requirements and mostly automated test procedures and thus they fit the demands of a contemporary laboratory device. The cetane number (DCN – Derived Cetane Number) is derived from the measured ignition delay. Therefore, values from engine based tests are used, which are monitored by round robin tests [3].

With an increasing number of non-engine based test devices the statistic quality of cetane numbers decreases. In addition there would be no possibility to establish an optional fuel number which could be necessary to describe specific properties

**Fig. 4.** Constant volume analyzers: IQT (left) and FIT (right) [3]

of biogenic fuels in engine applications by only using constant volume analyzers. Reason therefore are the missing dynamic process parameters of test engines such as change of pressure, volume, gas temperature, swirl etc.

## 4  Problems and Limits of Cetane Number Measurement

Today's methods for measuring the cetane number are facing, even with fossil fuels, high uncertainties and large scatter ranges. The diagram below shows in exemplary form the results of round robin tests for the determination of the cetane number of different fossil fuel samples with the BASF engine.

The results highlight that there is a comparatively substantial absolute deviation between different engines and users for one and the same fuel, although the BASF is considered as the most reliable method for cetane number evaluation.
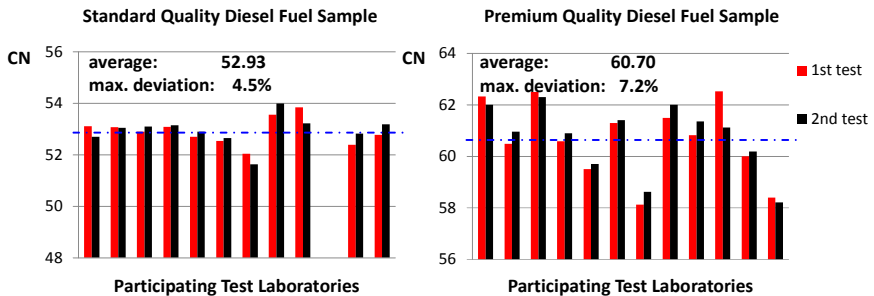


**Fig. 5.** Result of a round robin test (Source: FAM AA643)

The addition of plant oil components to fossil fuel will contribute to increase these deviations further, with the result that evaluating biogenic admixed diesel fuels will no longer be possible with the current standard method. Reasons for this are for example the high viscosity of vegetables oils or the low pressure increase (caused by the combustion) which cannot be detected by the analogue technique.

Further reasons are the operation mode (carburetion and operation point) as well as the measurement and data processing based on analogue technologies.

Biogenic fuels, especially vegetable oils, are characterized by a lower pressure gradient during combustion, regarding the conditions for ignition at the test engine. The reason therefore is the higher viscosity and the boiling range of most bio fuels which affect the spray breakup and carburetion.

As opposed to the described arguments, the molecular configuration of biogenic fuels consists of a long-chained structure with one or more double bonds and contains oxygen which would suggest a shorter chemical ignition delay.

To achieve the in [1] demanded ignition delay of 20° crank angle, biogenic fuels need to be operated at decisively better ignition conditions. This leads to quite low cetane numbers compared to common diesel fuel according to standard EN 590. However these results do not match perceptions from engine test with vegetable oil where they feature a similar combustion behavior.

It is to be assumed that the physical ignition delay of most biofuels is rated too high under the standard-compliant unprofitable ignition conditions in the test engine.

Alternative non engine-based methods for fossil fuels are similarly not an advisable solution for determining cetane numbers of biogenic diesel fuels. One reason is the lack of a standard as there is no reference engine for the determination of the fuel numbers which would allow the composition of fuel components to be changed. Furthermore, the ignition delay and combustion depend on different state variables in the combustion chamber (above all temperature, pressure, volume, swirl and residual gas mass fraction). The measurement in a constant volume combustion chamber (e.g. IQT, FIT) is based on constant state variables. A transfer of the results to an up-to-date combustion engine seems highly improbable.

In conclusion, the common test procedures of cetane number determination of fossil fuels are not advisable or technically not feasible, especially for current and future alternative fuels.

A precise rating of fuels is required for a constant product quality in the context of a larger number of different blends and minimized costs.

## 5   Cetane Number Measurement with a Thermodynamic Approach Including the Evaluation of the Reaction Level by Arrhenius Function

By means of common engine based test methods the start of combustion (SOC) is identified as the point of highest pressure gradient which can vary depending on the used fuel. In the proposed method the SOC is detected by an online pressure pattern analysis as shown in Figure 6 [17,19]. The received thermodynamic values

are, apart from the measured combustion pressure, gas temperature and burn rate including the decisive mass fraction burned values.

The start of injection (SOI), which is usually measured with a needle lift sensor and the calculated SOC then define the actual ignition delay (ID, measured either in milliseconds or °CA) of the fuel.
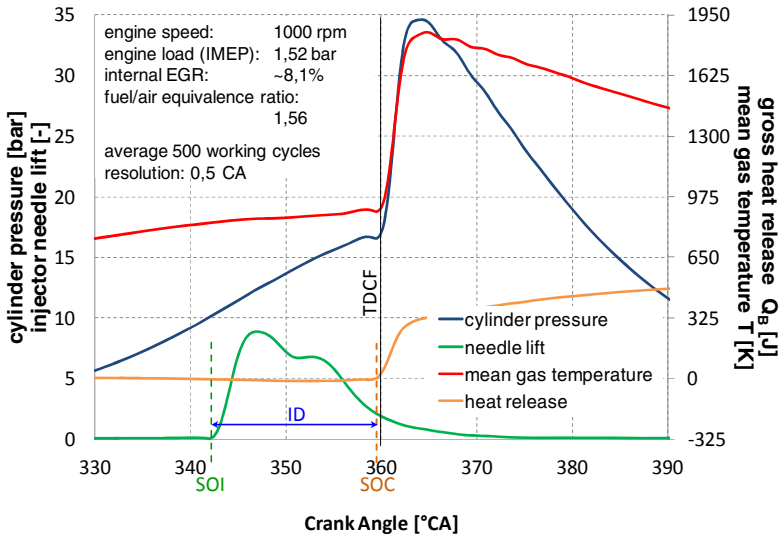


**Fig. 6.** Results of the pressure pattern analysis at the pilot test engine

The available process values (cylinder pressure p, mean gas temperature T) can slip into the calculation of the ignition integral based on an Arrhenius function to evaluate auto ignition of hydrocarbons [17]. Hereby the reciprocal value of the calculated ignition delay $\tau$ defined by the state variables p and T at crank angle $\varphi$ is to be integrated within the actual ignition delay time.

$$critical\ reaction\ level = \int_{SOI}^{SOC} \frac{1}{\tau} \cdot d\varphi$$

with:

$$\tau = A \cdot p^{-n} \cdot e^{\frac{E_A}{\tilde{R} \cdot T}}$$

$E_A$ is the apparent activation energy, $\tilde{R}$ the universal gas constant and A and n are constants which depend on the test device and the charge motion.

The value of the ignition integral at SOC characterizes the required activation energy for auto ignition of a diesel fuel and by the use of a conversion equation it can be transferred into a value for ignition willingness (cetane number). The

higher the calculated critical reaction level for autoignition of an unknown diesel fuel the worse is its ignition behavior and the less its cetane number.

$$Cetane\ Number = f\,(critical\ reaction\ level)$$

Due to the thermodynamic calculation of the burn rate, it is an essential advantage of such a procedure that later SOI (approximately 12°CA before top dead centre firing TDCF instead of 20°CA) in combination with more intake air mass can be chosen which result in shorter ignition delays [17]. Apart from that the test procedure suggested by the bioFIRe project approaches the in-car combustion processes (quality regulation at less ignition delay) better as the operating point of the engine is not changed by variation of the intake air throttle. Thus the fuel/air equivalence ratio is only influenced by the oxygen content of the fuel. Table 1 shows a comparison between standardized and modified BASF test engines.

Further, it is targeted to quit using the common cancer causing and acid calibrating fuels (n-cetane, 1-methylnaphtalene, heptamethylnonane) or to substitute them by more tolerable substances.

**Table 1.** Comparison between standardized and modified BASF test engine

|  | BASF DIN 51773 | BASF modified |
|---|---|---|
| engine speed | 1000+-10 ||
| engine displacement | 850cm³ ||
| compression ratio | ~ 18,6 ||
| cylinder coolant temperature | 100°C (boiling) ||
| fuel injection | indirect diesel injection (IDI) into swirl chamber ||
| fuel injection system | single cylinder in-line-pump | single cylinder in-line-pump, preheating unit for high viscosity fuels |
| SOI | 20°CA before TDCF | ~12°CA before TDCF |
| SOC | controlled, TDCF | depending on ID |
| detection of SOC | by pressure increase at TDCF | by calculating the actual gross heat release using thermodynamics |
| ID | 20°CA | depending on fuel, less than 15°CA |
| fuel/air equivalence ratio | strongly depending on ignition behavior as well as on fuel´s oxygen content; the higher cetane number the fatter (<1 possible) | only depending on fuel´s oxygen content, not less than about 1,4 (or controlled by lambda-sensor) |
| internal EGR | strongly depending on throttle position | constant within narrow tolerances |
| cetane number determination | interpolation of needed air flow between unknown and two known test fuels | derived from the value of the ignition integral without bracketing using test fuels |

In addition, the operating personnels' workload can be reduced; their influence on the results avoided, and the reproducibility of the measurements increased. Also the transparency of the process including the demands of engine developers can be enhanced.

## 6  Conclusion – A View at Further Steps towards Standardization

The disposal of biogenic and fossil fuels is restricted by the relevant standards. The results of the bioFIRe-project will impact the standardization of new fuels as well as the entire global fuel production.

Todays utilized test engines should be equipped or upgraded in accordance to the developed pilot test rig. Precondition for this step is, besides the technical evidence of functionality, the positive resonance after the presentation of the test process to the Standards Committee for Engine Based Test Methods for Liquid Fuels (AA 643) and Engine Based Round Robin Tests for Fuel Measurement (UA 643.1).

Regarding fuel processing concerns, the project allows a reliable determination of fuel numbers for the future and likewise ensures that fuels are produced at a constant quality according to the standards. In contrast to the expectations of higher diversification of fuels, their properties can be kept in a closer range for minimized variation of quality. As a result, combustion engine manufacturers can take advantage by optimizing the engine calibration.

As more detailed information about the combustion process is received from the measurements it would also be possible to define a complementary value besides the cetane number. These could describe further relevant engine parameters such as the combustion duration or the percentage of premixed combustion.

## References

[1] DIN 51773: Bestimmung der Zündwilligkeit (Cetanzahl) von Dieselkraftstoffen mit dem BASF-Prüfmotor
[2] Lauer, W.: Cetanzahlmessung am Prüfdiesel BASF; Betriebsanleitung, Ausgabe C (1966)
[3] Terschek, R., Gorek, W., Feuerhelm, T.: Die Bestimmung der Cetanzahl – Standpunktpapier des Arbeitskreises 643 im Fachausschuss für Mineralölnormung (FAM), Erschienen in Erdöl Erdgas Kohle, Heft 10 (2008)
[4] Attenberger, A., Remmele, E.: Entwicklung einer Prüfmethode zur Bestimmung der Cetanzahl von Rapsölkraftstoff, Berichte aus dem TFZ 6, Straubing (2003)
[5] Picard, K.: Zielkonflikte im Biokraftstoffmarkt – Konsequenzen für den Verbraucher, MTZ 4-2008, pp. S94–S299 (2008)
[6] Lumpp, B., Rothe, D., Pastötter, C., Lämmermann, R., Jacob, E.: Oxymethylenether als Dieselkraftstoffzusätze der Zukunft; MTZ 3-2011, pp. S198–S202 (2011)

 [7] Janssen, A., Jakob, M., Müther, M., Pischinger, S.: Maßgeschneiderte Kraftstoffe aus Biomasse – Potentiale biogener Kraftstoffe zur Emissionsreduktion; MTZ 12-2010, S922–S928 (2010)

 [8] Janssen, A., Jakob, M., Schnorbus, T., Kolbeck, A.: Chancen und Herausforderung der Ethanolbeimischung zum Dieselkraftstoff; MTZ 7/8-2011, pp. S572–S577 (2011)

 [9] Wichmann, V.: Konzepte und Betriebsstrategien für die Nutzung von Rapsölen in Verbrennungsmotoren für den Einsatz in Landmaschinen, Dissertation, Universität Rostock (2008)

[10] Harndorf, H., Schümann, U., Wichmann, V., Fink, C.: Motorprozessverhalten und Abgasemissionen alternativer Kraftstoffe im Vergleich mit Dieselkraftstoff; MTZ 7/8-2008, pp. S640–S646 (2008)

[11] Harndorf, H., Wichmann, V., Schümann, U., Richter, B.: Requirement specification for the use of biofuels in modern high performance engines. FNR Tagung Neue Biokraftstoffe, Berlin, June 24 (2010)

[12] von Hohenthal, M.-Y.: Zwischen Acker und Labor; MTZ 12-2010, pp. S852–S859 (2010)

[13] The Biofuels Research Advisory Council: Biofuels in the European Union – A vision for 2030 and beyond; Final draft report (2006)

[14] Directive 2003/30/EC of the European Parliament and of the Council (May 8, 2003)

[15] Directive 2009/28/EC of the European Parliament and of the Council (April 23, 2009)

[16] Steinbach, N., Harndorf, H., Weberbauer, F., Thiel, M.: Motorisches Potential von synthetischen Dieselkraftstoffen. MTZ 2-2006, pp. S96–S102 (2006)

[17] Heywood, J.B.: Internal Combustion Engine Fundamentals. Mc Graw Hill (1988) ISBN 0-07-100499-8

[18] Aatola, H., Larmi, M., Sarjovaara, T., Mikkonen, S.: Hydrotreated Vegetable Oil (HVO) as a Renewable Diesel Fuel: Trade-off between NOx, Particulate Emission, and Fuel Consumption of a Heavy Duty Engine; SAE 2008-01-2500

[19] Huber, K.; Hauber, J.: PCT/EP2009/054845; Method for Determining the Ignitability of a Fuel (April 22, 2009)

# Ultra-Downsizing of Internal Combustion Engines

V. Gheorghiu

HAW Hamburg University of Applied Sciences, Germany
`victor.gheorghiu@haw-hamburg.de`

**Abstract.** The downsizing of internal combustion engines (**ICE**) is already recognized as a very suitable method for the concurrent enhancement of indicated fuel conversion efficiency (**IFCE**) and the lowering of $CO_2$ and $NO_x$ emissions [1], [2]. In this report, **ultra-downsizing** is introduced as an even higher stage of development of ICE. Ultra-downsizing will be implemented here by means of real Atkinson cycles using asymmetrical crank mechanisms, combined with multi-stage high-pressure turbocharging and very intensive intercooling. This will allow an increase of ICE performance while keeping the thermal and mechanical strain strength of engine components within the current usual limits.

## 1 Introduction

The scarcity of oil and gas reserves and the global warming phenomenon both urge the automotive industry towards a decrease in fuel consumption and thus a reduction in CO2 emissions. These factors will also determine the future R&D trends for ICE.

Downsizing of ICE means simultaneous decreasing the displaced volume (usually by reducing the number of cylinders) and increasing the indicated mean pressure (**IMEP**) by means of turbocharging [1,2]. This allows the preservation of power and torque performance while decreasing the engine size. As a result, a) the mechanical and thermal losses are reduced, b) the engine becomes lighter, leading to a drop in the overall weight of the vehicle, and c) the engine operates more within its optimum fuel consumption zone. The advantages offered by a) and b) hold true even for ICE used in hybrid propulsion systems, while the advantage c) is already a feature of full-hybrid vehicles.

The level of downsizing determines the strength of the thermal and mechanical strains of engine components. In order to avoid exceeding the usual limits, either the boost pressure or the volumetric compression ratio (**VCR**) must be reduced accordingly. As a consequence, the whole potential of downsizing is not achieved and the IFCE and IMEP remain at a low level.

The current ICEs have classical (symmetrical) crank mechanisms (i.e. compression and expansion strokes of equal length) and follow the Seiliger cycles. Real implemented Atkinson cycles require unequal strokes featuring a shorter compression

stroke, which leads to a higher IFCE [3,5]. Atkinson cycles have been used so far mostly with symmetrical crank mechanisms, where the intake valves are closed very late in the cycle [3,4,5]. Thus, a part of the charge sucked into the cylinder is pushed back to the intake pipes, and the effective compression stroke is decreased. This quasi implementation of Atkinson cycles shows no noticeable improvements of the IFCE and, hence, it will not be discussed in the course of this paper (see [3] and [5] for details).

Real Atkinson cycles can be implemented only with the help of asymmetrical crank mechanisms. This allows using concurrently very high boost pressures (to increase the IMEP) and higher VCR (to enhance the IFCE) and to set them much more independently of each other compared to Seiliger cycles [3,5]. As an important part of the fresh charge compression takes place beyond the cylinder, the high compressed fresh charge can be cooled intensively before it is sucked into the cylinder. The following moderate compression in the cylinder (i.e. with relative lower VCR) leads to lower temperature peaks during the combustion process and, consequently, to less NOx emissions.

As previously mentioned, the expansion and compression strokes are identical in the case of the Seiliger cycle. The limitation of the maximum pressure during the cycle determines the pair of parameters VCR - boost pressure. If a relatively high boost pressure is desired, the VCR must be reduced accordingly in order to accomplish the maximum pressure limitation on the cycle. This will also decrease the IFCE since it is determined primarily by the VCR. Furthermore, the expansion in the cylinder occurs largely incomplete and the exhaust gases exit the cylinder with still too high specific enthalpy, which decreases the IFCE even further. However, the expansion of exhaust gases in the turbines with its high specific enthalpy can only be used partly for driving the compressors and, therefore, for enhancing the boost pressure because it exceeds the pressure upper limit during the cycle. This approach has already been proved in several previous theoretical investigations based on ideal Seiliger and Atkinson cycles [3,5].
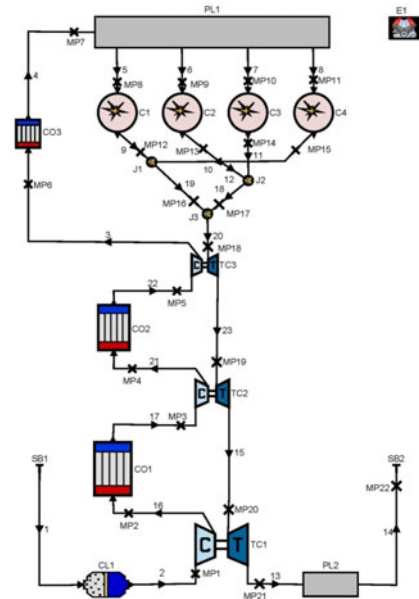


**Fig. 1** BOOST model of a four cylinder TC engine. Simple number denotes pipes, Cx = cylinder, COx = cooler, TCx = turbochargers, PLx = plenum, Jx = junctions, CLx = cleaner, SBx = system boundaries, Ex = engine and MPx = measuring points

These investigations did not take into consideration the effect of heat exchange and frictional losses on the cycle in order to make it easier to check the solution and to draw a comparison between the Seiliger and Atkinson cycles. The performances achieved for IFCE and IMEP using this method are therefore unrealistically high and serve only as a general indication [3, 5].

This Paper expands on the previous investigations from [3, 5] to real Atkinson cycles by using the simulation tool BOOST (AVL Co). This tool allows consideration of the true geometrical dimensions of the engine components (cylinder, valves, channels, pipes, manifolds, turbocharger, intercooler, silencer etc.) and the losses caused by friction and heat transfer along the intake and exhaust gas pipes. In addition, the power balance of turbochargers determines the actual boost pressure level of the engine.

The turbochargers (**TC**) are modeled for these investigations in a simple manner. It describes the expansion process in the turbines (**Tx**) by means of their discharge coefficients while the air compaction in the compressors occurs up to a maximum pressure ratio which depends on the available turbine output. To be able to simulate cycles with very high boost pressures as well, three intercooled TC are placed in line (three-stage turbocharging, see Fig. 1). When the boost pressure required for preserving the pressure limit on the cycle is low, the superfluous TC are kept for simplicity and comparability in use (i.e. are not bypassed). In this case the expansion and compression ratios of the turbines and compressors tend gradually toward 1, i.e. these TC switch off themselves thermodynamically.

The asymmetrical crank mechanism used here can realize classical piston displacements for the Seiliger as well as for the Atkinson cycles with various asymmetries between the compression and expansion strokes (see. Fig. 2A) and enable the variation of the VCR (see Fig. 2B).
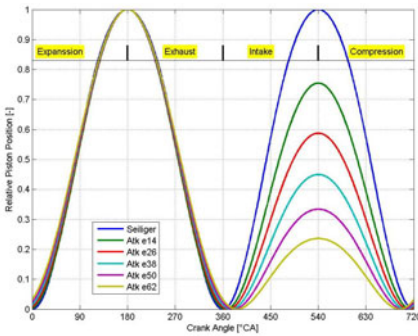


**Fig. 2A** Relative displacements of the asymmetrical crank mechanism used in the **IC A**. The Atkinson (**Atk**) cycles are implemented by means of varying the eccentric radiuses **exx** of the crank mechanism used. The Seiliger cycle is realized with zero eccentric radius.
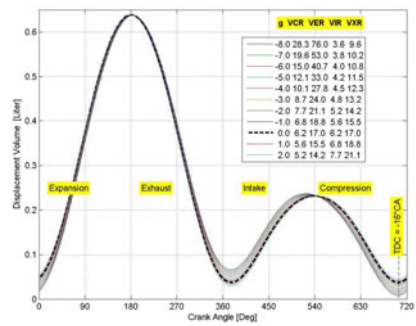
**Fig. 2B** Displacement volume of the asymmetrical crank mechanism used in the **IC B**. The Atkinson (**Atk**) cycles are implemented by means of varying the parameter **g** of the crank mechanism used. The dashed curve represents the null position where a) expansion and exhaust and b) intake and compression strokes are identical.

The following facts can be used to summarize the current situation:

To raise the IFCE, most of the working gas expansion should occur within the cylinder. If, however, the expansion process occurs entirely within the cylinder (ideally, a full expansion occurs up to the ambient pressure), no additional boost pressure can be generated.

In order to increase the expansion part within the cylinder, the crank mechanism must provide a higher VER, which makes a long expansion stroke (and, therefore, an engine with a long piston displacement) necessary. However, that leads to high IFCE but quite low indicated specific power (kW/L) and IMEP of the engine.

For the simultaneously rising of the IFCE and the IMEP, the engine must be turbocharged and the ratio between the expansions within the cylinder and within the turbines (i.e. between internal and external expansion) must be optimized. To be able to optimize this ratio (i.e. between internal and external expansions) regardless of VCR, an asymmetrical crank mechanism is required in order to implement real Atkinson cycles.

## 2  Investigation Cases

The simulations in this Paper are carried out investigation cases, IC A and IC B. In **IC A**, the simulated variants are based on a steady VER and a varied VCR. This means that identical expansion and exhaust strokes are kept unchanged and the identical intake and compression strokes are varied significantly - by means of varying the eccentric radiuses **exx** of the crank mechanism used - to allow the modification of the ratio between internal and external expansion. Some variants of the asymmetrical piston displacement are displayed in Fig. 2A.

In the **IC B**, the simulated variants are based on a steady eccentric radius (**e32**) where VER, VCR, volumetric intake ratio (**VIR**) and volumetric exhaust ratio (**VXR**) are varied simultaneously by means of the parameter **g**. Eleven variants of the asymmetrical piston displacement are displayed in Fig. 2B.

The goal of this Paper is to look for the optimum ratio between internal and external expansion, which leads simultaneously to maximizing the IFCE and enabling sufficiently high values of IMEP.

### 2.1  Setting of the Simulations for Both IC

The simulations of the piston displacements presented in Fig. 2A are carried out using the BOOST model from Fig. 1. The parameters and the performance of seven cycles are shown in Table 1. Many of the parameters from all cycles are kept identical in order to make comparison easier.

Most parameters of the BOOST model are selected for a hypothetical engine and are kept unchanged for all simulations. This includes parameters such as all geometrical dimensions (with the exception of the crank mechanism), valve timing, wall temperatures (300 K) and heat transfer coefficients (Re-analogy) of the pipes, as well as efficiencies and pressure losses of the intercoolers (target efficiency = 0.75, target pressure drop = 5 kPa) and friction coefficients in the pipes

(0.019). Likewise, the efficiency of the turbochargers (compressor efficiency = 0.75, turbocharger overall efficiency = 0.5), as well as the blow by gap size of the cylinder, frictional characteristic curve of the engine and AFR - the combustion parameter (see Table 1A) - are also included.

A simple Vibe function is selected in order to model the combustion process. The different positions of the TDC in the Atkinson and Seiliger cycles (see Fig. 2 and 5) are compensated by choosing a suitable start of combustion (**SOC**), so that combustion begins in all cycles uniformly at 15°CA before TDC.

The various parameters from Table 1A for the IC A and from the Fig. 10B for the IC B are selected for the purpose of obtaining roughly the same maximum cylinder pressure **max(p) ≈ 230 bar** in all cycles. In order to reach this state, the discharge coefficients of the three turbines ($\mu_{T1}$, $\mu_{T2}$ and $\mu_{T3}$) are varied according to a) the influence of the back pressure behind the cylinder (e.g. at the measuring point MP12 for cylinder 1; see Fig. 1) and of b) the boost pressure (e.g. at MP8 for cylinder 1). In order to reach approximately the same expansion rate in all three turbines, their discharge coefficients are set at the same level and compensated with the cross sections ratios of the turbine output pipes. Hence, only the discharge coefficient of the third turbine $\mu_{T3}$ is adapted for each cycle to meet the cylinder peak pressure limit, since this sets the level of the other two discharge coefficients $\mu_{T2}$ and $\mu_{T1}$ (see Table 1A and Fig. 10B).

## 2.2 Simulation Results and Trends for IC A

After analyzing the performance based on the values presented in Table 1A, a host of trends becomes clear. For example:

All Atkinson cycles show better IFCE values than the Seiliger cycles (see also Fig. 5A). However, the Seiliger cycles reach higher IMEP values because of the longer intake stroke and, therefore, larger gas mass sucked in (see Fig. 9A). Furthermore, higher boost pressures $p_{MP8}$ are required in both Atkinson and Seiliger cycles in order to hold the parameter **max(p)** steady when VCR is reduced (see Table 1A).

The comparison of the **Atk e62** (with VCR = 7.1) and **Seiliger** (with VCR = 7) cycles shows that a) the Atkinson cycle has a 30% higher IFCE and reaches 58% less IMEP and b) the Seiliger cycle needs a 30% **higher** boost pressure ($p_{MP8}$ in Table 1A) and must overcome a 50% higher cylinder back pressure - i.e. before T3 ($p_{MP12}$ in Table 1A).

Moreover, the comparison of the **Atk e38 & e26** (with VCR = 12.7 respective = 16.2) and **Seiliger** (with VCR = 15) cycles shows that the Atkinson cycles have a 10% higher IFCE (although the maximum cylinder temperature **max(T)** is ca. 160 K, i.e. 7% lower) and 34% less IMEP.

The highest IFCE value for Atkinson cycles is not reached in the variant with the highest VCR, but in the variant where the VCR is about 50% of VER. Consequently, the optimum variant features an intake stroke equal to approx. 50% of the expansion stroke.

**Table 1A.** Parameter (top) and Performance (bottom) for **IC A**. This table shows **VER** (volumetric expansion ratio), **VCR** (volumetric compression ratio), $\mu_{Tx}$ (turbine discharge coefficients),

**n** (engine speed), **AFR** (air-fuel ratio), **SOC** (start of combustion), **CD** (combustion duration), $m_{Vibe}$ (exponent of Vibe function for cylinder heat release modeling), **IFCE** (indicated fuel conversion efficiency), **IMEP** (indicated mean pressure), **max(p)** and **max(T)** (maximum pressure and temperature during the cycle), $p_{MP8}$ and $T_{MP8}$ (mean boost pressure and temperature; i.e. at the measuring point MP8, see Fig. 1) and $p_{MP12}$ and $T_{MP12}$ (mean exhaust back pressure and temperature; i.e. at MP12, see Fig. 1) for cylinder 1.

| Cycle | VER | VCR | $\mu_{T1}$ | $\mu_{T2}$ | $\mu_{T3}$ | n | AFR | SOC | CD | $m_{Vibe}$ |
|---|---|---|---|---|---|---|---|---|---|---|
| - | - | - | - | - | - | rpm | kg/kg | °CA | °CA | - |
| Atk e14 | 27,0 | 20,6 | 0,480 | 0,258 | 0,161 | 3000 | 14,6 | -21 | 86 | 1,5 |
| Atk e26 | 27,0 | 16,2 | 0,430 | 0,231 | 0,144 | 3000 | 14,6 | -24 | 86 | 1,5 |
| Atk e38 | 27,0 | 12,7 | 0,335 | 0,180 | 0,112 | 3000 | 14,6 | -30 | 86 | 1,5 |
| Atk e50 | 27,0 | 9,7 | 0,256 | 0,138 | 0,086 | 3000 | 14,6 | -36 | 86 | 1,5 |
| Atk e62 | 27,0 | 7,1 | 0,199 | 0,106 | 0,067 | 3000 | 14,6 | -42 | 86 | 1,5 |
| Seiliger | 7,0 | 7,0 | 0,330 | 0,177 | 0,111 | 3000 | 14,6 | -15 | 86 | 1,5 |
| Seiliger | 15,0 | 15,0 | 0,620 | 0,333 | 0,208 | 3000 | 14,6 | -15 | 86 | 1,5 |

| Cycle | VER | VCR | IFCE | IMEP | max(p) | max(T) | $p_{MP8}$ | $T_{MP8}$ | $p_{MP12}$ | $T_{MP12}$ |
|---|---|---|---|---|---|---|---|---|---|---|
| - | - | - | - | bar | bar | K | bar | K | bar | K |
| Atk e14 | 27,0 | 20,6 | 0,419 | 25,7 | 231 | 2209 | 3,02 | 336 | 2,79 | 867 |
| Atk e26 | 27,0 | 16,2 | 0,423 | 28,2 | 234 | 2197 | 4,08 | 343 | 3,78 | 877 |
| Atk e38 | 27,0 | 12,7 | 0,423 | 27,9 | 237 | 2182 | 5,13 | 346 | 4,79 | 877 |
| Atk e50 | 27,0 | 9,7 | 0,413 | 26,7 | 235 | 2167 | 6,55 | 348 | 6,16 | 913 |
| Atk e62 | 27,0 | 7,1 | 0,391 | 24,6 | 229 | 2152 | 8,78 | 356 | 8,07 | 915 |
| Seiliger | 7,0 | 7,0 | 0,301 | 57,9 | 232 | 2292 | 12,48 | 450 | 15,85 | 1396 |
| Seiliger | 15,0 | 15,0 | 0,383 | 42,1 | 232 | 2344 | 4,62 | 361 | 4,62 | 1127 |

Some diagrams are introduced and analyzed below in order to determine the cause of these trends. The pressure-volume (**p,V**) diagrams of all cycles and pressure-specific volume (**p,v**) diagrams of the intake and exhaust gas paths (for cylinder 1) are presented in Fig. 3A and 4A.

It can be inferred from Table 1A, as well as recognized in Fig. 3A and 4A, that the Seiliger cycle with VCR = 7 needs the highest boost pressure to reach the desired **max(p) ≈ 230** bar (because of its low VCR). The consequences are an extremely high back pressure $p_{MP12}$ and falling ISFC because of the very intensive exhaust work required to push the exhaust gases out of the cylinder (see green curves up to **ec** points in Fig. 3A, 4A and 5A). Therefore, this cycle occurs exclusively in the pressure range above 10 bar (see Fig. 3A). For Atkinson cycle **Atk e38**, this situation is reversed (see Table 1A and Fig. 3A, 4A and 5A for comparison). This cycle occurs exclusively in the pressure range above 5 bar (see Fig. 3A). The differences between both cycles can be clearly seen in the intake and exhaust gas paths.

Fig. 4A and 7A show the three-stage compression of the air and all states after passing through each compressor and intercooler (with associated pressure losses). Fig. 4A and 8A show the three-stage expansion of the exhaust gases in the turbines. Fig. 8A shows, the discharge coefficients are properly adapted between the turbines because the expansion occurs almost linearly in all three stages.

The air compression and the exhaust gas expansion for the cycle **Atk e38** occur mostly in **TC3** (see Fig. 4A, 7A and 8A) because the exhaust gas pressure at the MP18 point (i.e. before **T3**, see Fig. 4A and 8A) is too low (see also Table 1A) to be able to adequately drive **T2** and **T1**. Consequently, the exhaust gases compress partly in **T2** and **T1** instead of expanding (see MP19 to MP21 in Fig. 4A).

No modification of the IFCE sequence between variants is obtained by deleting **TC1** from the BOOST model (i.e. there is no need to remove the unnecessary **TC** in these simulations). In all Atkinson cycles, the sucked intake gas mass changes minimally (see the red circle area on the left side of Fig. 9A), i.e. IMEP follows preponderantly IFCE variation and is, for the most part, independent of the boost pressure ($p_{MP8}$) variation.

## 2.3   Simulation Results and Trends for IC B

A number of trends become clear after analyzing the parameter and performances presented in Fig. 10B. For example: This type of crank mechanism – which permits VCR variation (in this case via parameter g) – enables the implementation of Atkinson cycles for part and full-load operating points (**OPs**), where IMEP varies between 8.5 and 42 bar, even with stoichiometric AFR and without throttling. Moreover, IFCE in all these OPs only varies within a 6% wide band (related to its maximum, see also Fig. 11B and 13B).

In all these OPs, the maximum cylinder pressure remains at approx. 230 bar and the maximum cylinder temperature varies between 1800 and 2300 K (see Fig. 12B and 13B). The optimization of the heat release could significantly reduce the maximum cylinder temperature (see [3, 5]). In variant **g+2** (see legend), the maximum boost pressure ($p_{PM8}$) reaches nearly 12 bar, while the boost temperature ($T_{PM8}$) does not exceed 360 K (see Fig. 10B). In this case, the cylinder is filled to maximum (see Fig. 14B). As a result of the extended expansion within the cylinder (see Fig. 10B) the exhaust gas temperatures before turbine **T3** ($T_{MP12}$) only reach a maximum of 1000 K. A benefit is that the turbine wheel must not be protected (e.g. by making the mixture leaner) against a higher gas temperature, while a disadvantage is that a higher exhaust gas pressure is required before **T3** ($p_{MP12}$) in order to achieve the desired boost pressure ($p_{MP8}$).

The required higher exhaust gas pressure before **T3** ($p_{MP12}$) (i.e. the cylinder back pressure) significantly diminishes the level of IFCE (i.e. by approx. 25%, see IFCE variation in Fig. 11B between 540°CA and **ec** position). The load independence of these IFCE losses is quite unexpected, but if the difference between cylinder pressure at **eo** and back pressure ($p_{MP12}$) in Fig. 12B is noted, the positive effect of the exhaust gases released from the cylinder (i.e. of the free exhaust) becomes evident. An additional optimization of valve timing can considerably reduce the back pressure and, therefore, these IFCE losses.

The residual gas concentration decreases, while VXR and boost pressure increase (see Fig. 10B). The increase in VXR makes the cylinder exhaust more complete (see Fig. 12B) and the increase in boost pressure favors the scavenging of residual gases from the cylinder. The IMEP enhancement – from 8.5 to 42 bar, while AFR remains unchanged (stoichiometric) and IFCE only varies within a 6% wide band – is the result of the increase of aspirated gas mass into the cylinder (see Fig. 14B).
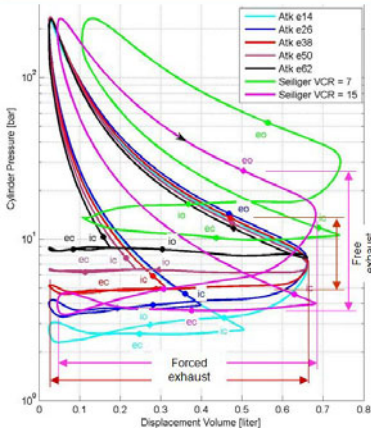
**Fig. 3A.** Cylinder pressure (logarithmic) - displacement volume (**p,V**) diagrams with valves timing for all cycles. Here **eo** denotes exhaust open, **ec** exhaust closed, **io** intake open, **ic** intake closed. The differences between the free and forced exhaust parts can be clearly observed. The forced exhaust diminishes IFCE as shown in Fig. 5A.
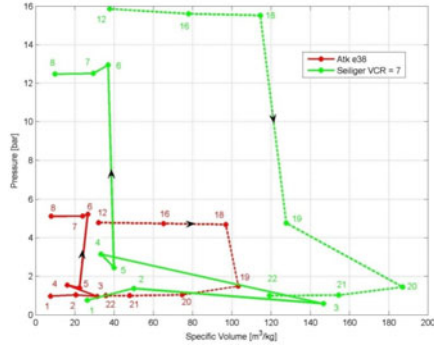


**Fig. 4A.** Pressure - specific volume (p,v) diagrams for some MP from the intake (solid lines) and exhaust (dashed lines) pipes for two selected cycles. The numbers denote the states of measuring points from Fig. 1.
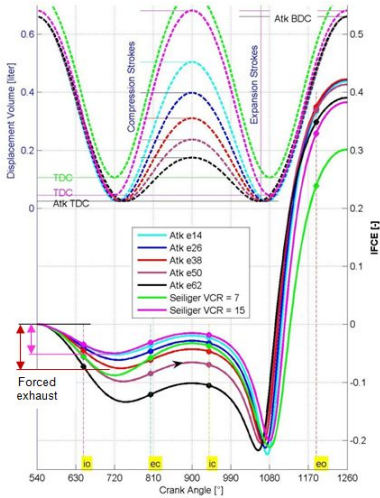


**Fig. 5A.** IFCE - crank angle (**IFCE,CA**) with valves timing (left axis) and displacement volume - crank angle (**V,CA**) diagrams for all cycles. TDC top dead center and BDC bottom dead center are shown here. The forced exhaust diminishes IFCE cycle-dependent
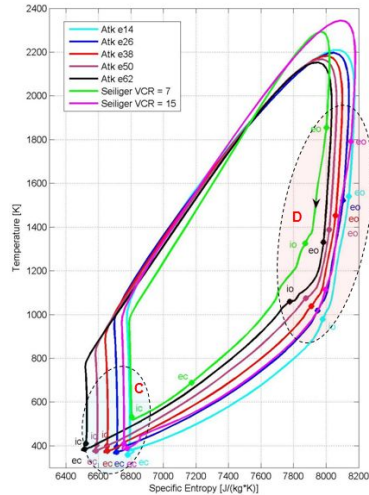


**Fig. 6A.** Temperature - specific entropy (T,s) diagrams with valves timing for all cycles. Details C and D are presented in expanded form in Fig. 7 and 8
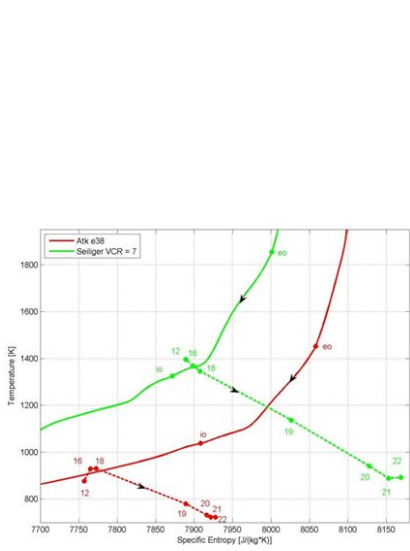
**Fig. 8A.** Temperature - specific entropy (**T,s**) diagrams for some MP (see Fig. 1) from exhaust pipes (dashed lines) superposed on **D** detail of Fig. 6 (solid lines) for two selected cycles
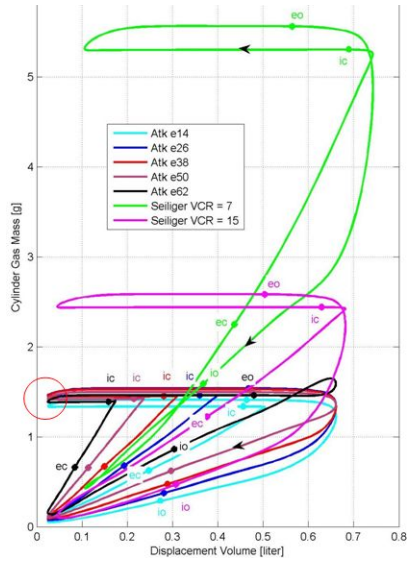
**Fig. 9A.** Gas mass - displacement volume (**m,V**) diagrams with valve timing for all cycles
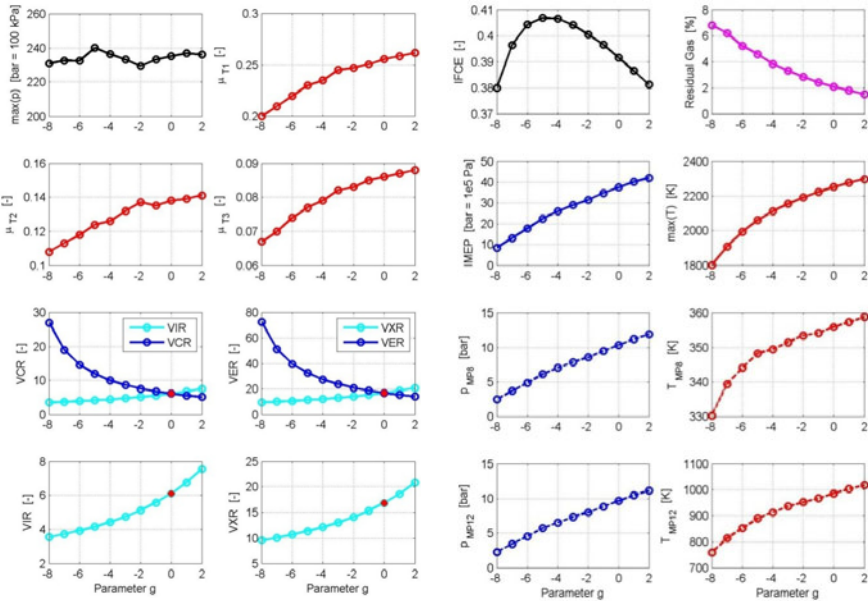


**Fig. 10B.** Parameter (left) and performance (right) for **IC B**. The parameters displayed have the same meaning as shown in Table 1A and Fig. 2B.
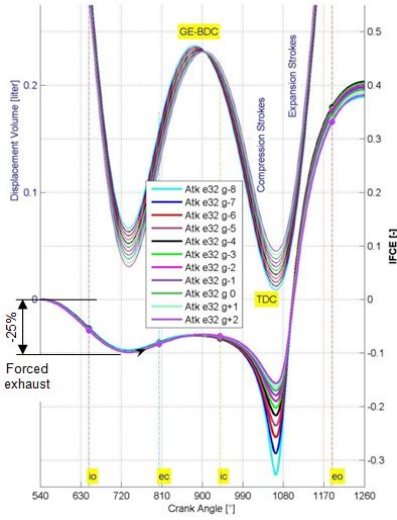
**Fig. 11B.** IFCE - crank angle (**IFCE,CA**) with valve timing (left axis) and displacement volume - crank angle (**V,CA**) diagrams for all cycles. The forced exhaust diminishes IFCE cycle-**in**dependent.
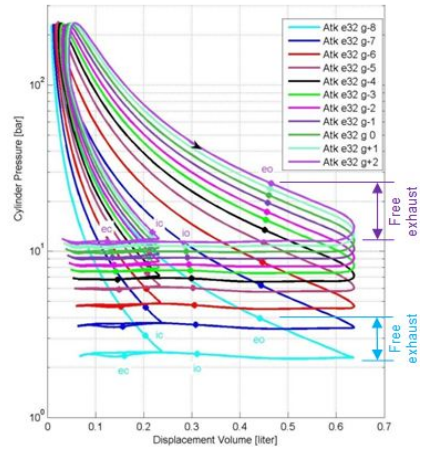


**Fig. 12B.** cylinder pressure (logarithmic) - displacement volume (**p,V**) diagrams with valves timing for all cycles
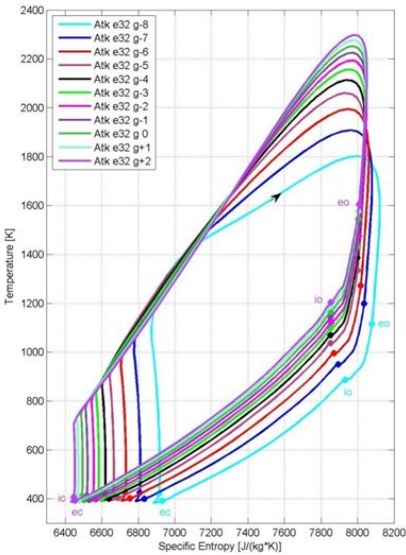


**Fig. 13B.** Temperature - specific entropy (**T,s**) diagrams with valves timing for all cycles
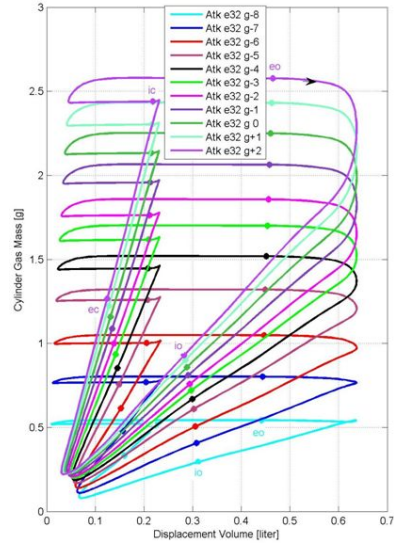


**Fig. 14B.** Gas mass - displacement volume (**m,V**) diagrams with valves timing for all cycles

# 3 Conclusion

The implementation of real Atkinson cycles for turbocharged engines using asymmetrical crank mechanisms offers the following advantages: a) relatively high IMEP, b) higher IFCE leading to few $CO_2$ emissions and c) lower temperatures during the combustion stage leading to few NOx emissions.

In order to achieve these performances, the engine requires the use of turbocharger systems with at least two stages which must be adapted accordingly and controlled with the help of bypasses to maximize their performance.

The optimum ratio between the internal (i.e. within the cylinder) and external (i.e. within turbines) expansion of the exhaust gases which maximize IFCE is reached when the VCR is close to 50% of VER.

An asymmetrical crank mechanism where the VCR may also be varied makes it possible to realize Atkinson cycles for part and full load even with stoichiometric AFR and without throttling.

# References

[1] Weinowski, R., Sehr, A., Wedowski, S., Heuer, S., Hamm, T., Tiemann, C.: Future downsizing of S.I. engines - potentials and limits of 2- and 3-cylinder concepts. In: Vienna Motor Symposium, Austria (2009)

[2] Korte, V., Lumsden, G., Fraser, N., Hall, J.: 30% higher efficiency at 50% less displacement, MTZ 2010 (2010)

[3] Gheorghiu, V.: CO2-Emission Reduction by Means of Enhancing the Thermal Conversion Efficiency of ICE Cycles. In: SAE International Powertrains, Fuels & Lubricants Congress 2010, 10-SFL214-0032, Rio de Janeiro, Brazil (2010)

[4] Schutting, E., Neureiter, A., Fuchs, C., Schwarzenberger, T., Klell, M., Eichlseder, H., Kammerdiener, T.: Miller- and Atkinson-Cycle for Supercharged Diesel Engines, MTZ 06 (2007) (German)

[5] Gheorghiu, V.: Enhancement Potential of the Thermal Conversion Efficiency of ICE Cycles by Using of a real Atkinson Cycle Implementation and (Very) High Pressure Turbocharging. In: ESDA International Automotive Congress, Istanbul, Turkey (July 2010)

# BARM: Bi-Angular Rotation Machine

Boris Schapiro

TPC – Technology & Process Consulting
Kluck Str. 25, D-10785, Berlin, Germany
Tel.: +49172 3008947
`boris@schapiro.org`

**Abstract.** This work is an elaboration of the initial studies presented at the International Conference on Sustainable Technologies, 2011. The BARM machine, originally in the form of a compressor, will be presented here as an internal combustion machine and compared with a classic reciprocating diesel engine. A simplified thermodynamic analysis will also be presented. Power densities of BARM engines should be significantly greater than that of reciprocating engines with the same thermodynamic efficiency.

## 1   Introduction to Trochoidal Rotating Piston Machines (RPM)

The BARM machine was previously presented as a compressor under the name RPK-160 and RPK-300, *Schapiro* 2011-1. These were developed at the Zhukovsky Kharkover Aeronautical Institute and described in *Sukhomlinov (1975)*.

The general advantages of trochoidal rotating piston machines also accrue to BARM machines. Among them are:

- small, light and simple construction requiring little space,
- few moving parts with less wear,
- outstanding power density.
- dynamic balancing provides quiet and smooth operation.

The famous Wankel engine also exhibits these same advantages. But the advantage of its power density could not compensate for its disadvantages in times of energy scarcity.

There are two major reasons for the Wankel motor's less than desired efficiency: first is the geometry selected, with its Reuleaux triangle in the piston's cross section and the epitrochoidal contour of the working chamber with changing algebraic sign of curvature along the chamber contour. The classic Wankel machine's maximum possible compression is wholly defined by its geometry. This geometry limits the machine's compression ratio to a number in the order of magnitude of 10:1. As a result, this machine can be realized as a combustion engine only when employing the Otto and similar processes in a single compression stage.

The much more advantageous diesel process requires a compression ratio no less than the order of magnitude of 20:1. Two-stage diesel Wankel engines exist, in which one stage serves as a pre-compressor and the other as actual motor. This approach has not proved economical as the pre-compressor devours more energy than the efficiency difference between the Otto and diesel processes can yield. Mazda's newly developed diesel Wankel engine with a 14:1 compression ratio cannot compete with a highly developed reciprocating diesel engine.

Second, the problem of sealing the tip of the rotating piston against the chamber wall has not yet been solved very satisfactorily. Compared to reciprocating piston engines or to the RPM machines with jumping instantaneous axes of rotation, *Schapiro 2008*, with their surface-to-surface seal between piston and cylinder wall, the seal between the rotating piston and the chamber wall of the trochoidal machine is normally a line-to-surface seal.

Trochoidal machines can be realized with $n$ orders of rotor symmetry, $n = 2, 3, \ldots$ The piston's spring-loaded sealing lip slides along the chamber wall at a permanently changing angle during piston rotation. This angle's amplitude is defined by the piston's order of symmetry. This amplitude is greatest at $n = 2$ (BARM machine) and is approximately equal to $\pi$ minus the angle between both tangents to the piston's contours at the sealing point. For $n = 2$, this is approximately equal to $\frac{2}{3}\pi$. At $n = 3$ (the classic Wankel machine), the amplitude is approximately $\frac{1}{2}\pi$.

Thus, it is clear why Felix Wankel chose the third order symmetry for his machine's piston – the sealing ability of this machine is roughly 30% better than that of a machine with second order piston symmetry. In the following, attention will be devoted to these trochoidal machines with second order symmetry pistons (previous notation: PPM2, Planetary Piston Machine with 2nd order piston symmetry, now BARM).

## 2  BARM: Symmetry and Compression

Assume that the sealing problem for RPM engines has been solved by means of an independent sealing technology. Assume further that it is possible to disassociate compression from chamber geometry so that compression can be defined by the designer. Which of the almost infinite variety of RPM machines would be most interesting economically as a combustion engine? Given the assumptions above, RPM machine with 2nd order piston symmetry (BARM) should emerge as the clear victor.

The reasons for this are simple. First, the contour of the BARM piston, a trochoidal arc, conforms to one similar arc in the contour of the working chamber. By building a combustion chamber into the arc portion of the chamber wall that conforms to the BARM piston, the machine's compression equals the relation between the maximum volume defined by the BARM geometry and the geometry-independent volume of the combustion chamber. Thus, the compression of

a BARM engine is not defined solely by the trochoidal geometry but, contrary to the Wankel machine, together with the designed size of the combustion chamber. Consequently, the BARM machine can definitely be designed as a one-stage diesel with concomitant, significantly improved efficiency.

Second, the piston's rotation speed and, thereby, the power density of the BARM machine is limited only by its fuel's rate of combustion. That, in turn, means that the BARM engine should be able to achieve the maximum power density possible for any fuel used.
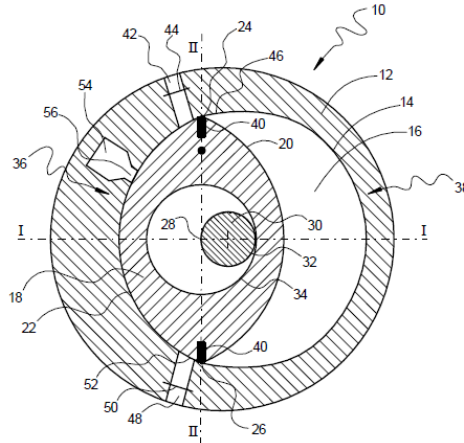


**Fig. 1.** BARM: Basic Configuration as Combustion Machine (Schapiro, 2011-2). Nomenclature: 54 – combustion chamber; 22 – piston arc conforms to chamber arc; 40 – sealing lips; 14 – epitrochoidal chamber contour, 2nd order symmetry; 16 – working chamber; 28-34 – energy transfer mechanism for all trochoidal machines.

There are some known solutions to the problem of maintaining the appropriate position of the piston in respect to the working chamber. One of them involves an eccentric lobe on the power shaft that, during rotation, forces the shaft to keep the piston in its appropriate position (not shown on the Figure 1).

## 3  Desired Seal Qualities

The vision developed in the previous section rests on the assumption that the planetary piston machine's well-known sealing problems can be solved. This problem has been solved – although only theoretically. One solution is based on a newly invented composite material. This material can be used as an elastically deformable element for a seal that adapts to every curvature.

   This material has the following properties decisive for the economic efficiency of BARM machines:

- material design defines its elasticity across an extremely wide parameter range,
- the material can be formed into almost any shape and will conform to every curvature under pressure,
- this material's reaction speed to deformation is at least $4 \times 10^5$ cm/sec. Sealing the piston with this material against the chamber wall of a BARM machine with a chamber diameter of 30 cm theoretically allows rotation speeds of up to 240,000 rpm. However, realistic operating speeds will not exceed 30,000 rpm.
- the wear on this material will be comparable to the wear on currently available sealing materials,
- employing special steels, its elasticity characteristics will remain virtually unchanged up to 1,200° C.

The type of sealing element Figure 2 can automatically adapt to varying curvatures without significant loss of its sealing capabilities. It should function particularly well with a BARM machine because the curvature variations in the chamber's contour are relatively small.

   Another solution is a purely mechanical, self-positioning sealing element simpler than Figure 2. This could suffice for many applications. The fact that the epitrochoidal contour (see Figure 1, 14) does not differ significantly from a circle with constant curvature enables employment as a mechanical sealing element that adapts its position to surface curvatures. Fig. 3 describes such a purely mechanical sealing element suitable for BARM machines.

   The curvature of the sealing element contact surface conforms to the greatest curvature of the chamber contour. In those regions along the chamber contour where curvature is less, the variation in conformation with the sealing element contact surface is so small as to have no effect during high speed and only minimal effect at low speed operation. While travelling over the chamber surface, the sealing element automatically maintains the sealing element neck (Figure 3, 230) in a position normal to the chamber surface.
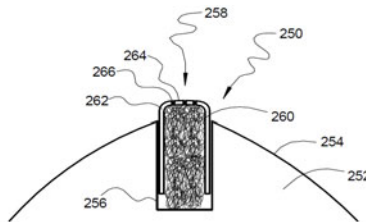


**Fig. 2.** sealing element with steel wool filler. Where: 252 – rotating piston; 258 – sealing element; 262 – flexible steel sheet; 260 – steel wool; 266 – micropores for lubrication; 256 – channel for sealing element (with oil source - not shown);
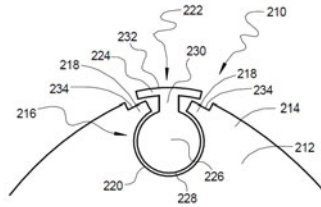
**Fig. 3.** self-positioning mechanical sealing element. Where: 232 – contact surface; 212 – piston; 224 – sealing crown; 234 – arresting notch guarantees continuous piston surface at extreme positions; 226 – rocking element; 230 – neck supporting sealing crown; 216 – channel for rocking element (with lubrication source - not shown); 220 and 228 – contact surfaces; elastic elements required to compensate for thermal expansion not shown.

The current state-of-the-art provides many ways to minimize wear and frictional losses on sliding surfaces. Some of them use lubrication, others employ contactless sealing. This topic will be dealt with when the state of BARM development allows the required research.

## 4   BARM as a Combustion Machine

The sequence of Figure 4 illustrates the function of a BARM machine with the self-positioning sealing element. The magnifying glass shows an enlarged representation of piston end B with the respective position of the sealing element at each stage. This figure displays a 4-cycle diesel configuration with air intake through the combustion chamber. The small table in the upper right of each Figure 4 cell shows the respective states on piston sides A and C. These twelve cells show the piston's positions at the angles indicated during the entire sequence of 4 cycles. The illustrations (Figure 4 and 5) were created by Prof. Sergei Dunin and generated by computer simulation of the thermomechanical function of a BARM machine.

8 intervals on the time axis in the upper right correspond to the full thermodynamic cycle. The diagram in the upper right shows the displaced volume of both machines over time and only near minimum. The two diagrams in the lower right show output power over time. Blue represents the reciprocating machine, red the BARM machine.  In the P-V and T-S diagrams, the blue point displays the state of the reciprocating machine and the two red points display the states of the BARM machine on the A and C sides (Figure 4 and 5) of its piston respectively. The red point near the blue point corresponds to side A.

This simulation was done with somewhat simplified conditions, i.e. the viscosity of the working medium and the intake and exhaust resistances were ignored. The internal frictional losses were assumed to be equal for both machines. For the
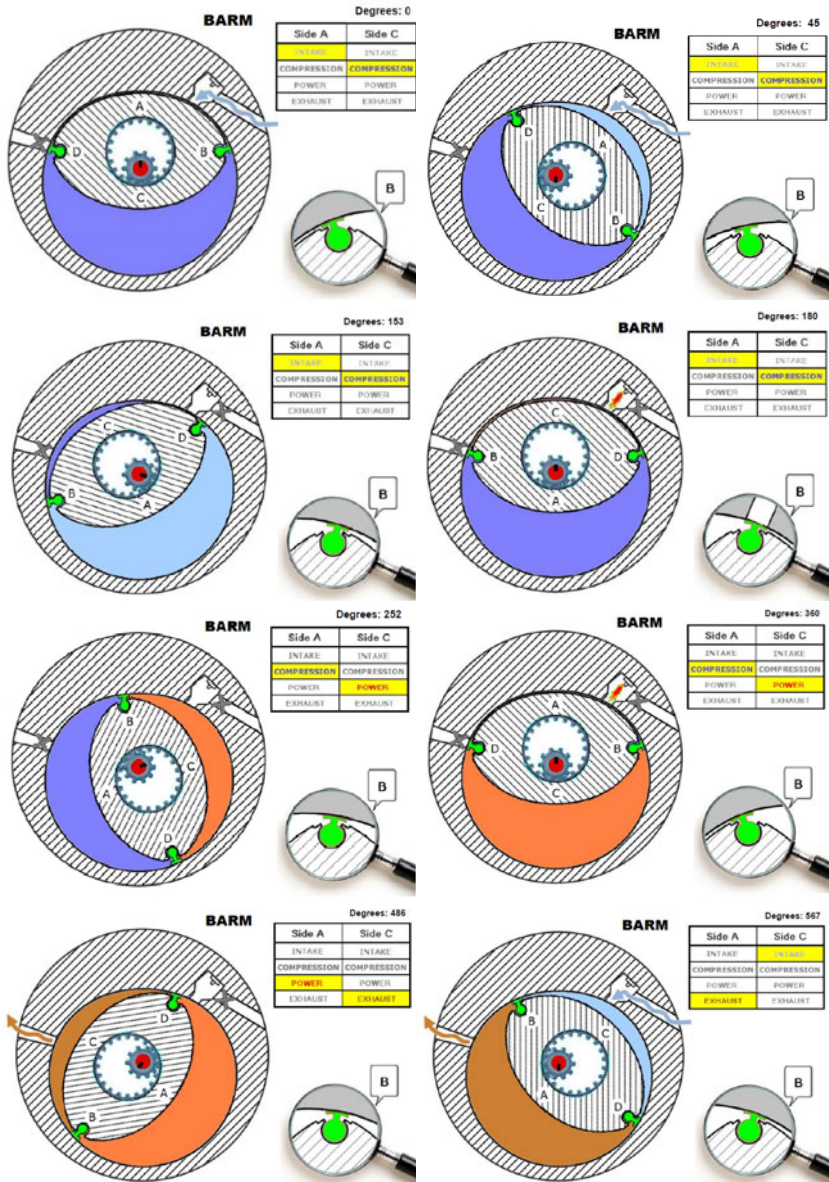
**Fig. 4.** BARM: sequence of piston positions and working strokes. Intake is light blue, compression dark blue; the power cycle is red and exhaust ochre-brown. The self-positioning sealing element is green.
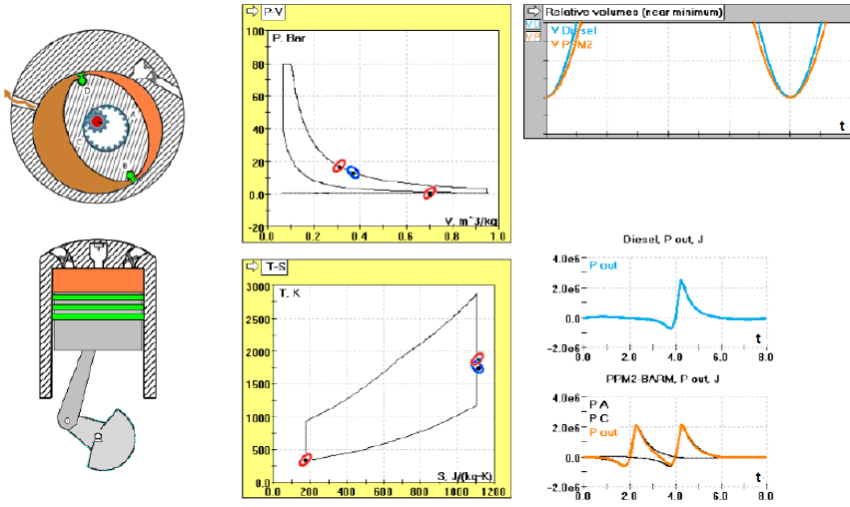
**Fig. 5.** Simulated comparison of thermodynamic function for a 4-cycle Diesel BARM engine with equivalent 4-cycle Diesel reciprocating engine.

thermodynamic comparison of the BARM engine and the reciprocating engine, the following conditions were held equal: displacement, maximum pressure, maximum temperature and fuel. A complete thermodynamic cycle was set at 8 seconds.

It is not surprising that the diagrams of the thermodynamic cycle for both machines look the same under these conditions. The only difference between the two machines is the variation in speed with which they complete the thermodynamic cycle. The thermodynamic state of the BARM engine changes slightly faster during the compression and marginally slower during the work cycle. In the upper right corner of Fig. 5 is the bottom-most section of the graph of both volume displacements over time. The blue curve corresponds to the reciprocating engine, the red to the BARM engine. Both P-V and T-S diagrams display the same thermodynamic cycle for both machines.

All this shows that the thermodynamic efficiency of the diesel versions of the BARM and reciprocating engines are the same. The power densities of both machines are, however, significantly different.

The diagrams in the bottom right of Figure 5 show the relationship between the respective power densities per thermodynamic cycle. The blue curve displays reciprocating engine power output as a function of time. The downward spike corresponds to the power required to complete the compression stroke. The upward spike corresponds to engine power output during the work cycle. The same holds for the red curve showing BARM engine power output.

The power output per thermodynamic cycle of the BARM engine is significantly greater than that of the reciprocating engine because the BARM engine works with both sides of its piston. This is one of the advantages of rotating piston design. The power output of the BARM engine is approximately a factor of 2 greater than that of the reciprocating engine per thermodynamic cycle.

Furthermore, the reciprocating engine's range of thermodynamic cycles per minute is more limited than that of a rotating piston engine. The BARM engine can be expected to complete 3 to 4 times more rotations per minute than the crankshaft of a reciprocating engine with a working chamber of the same volume. As a result, BARM engine power density can be expected to be approximately 6 to 8 times greater than that of a reciprocating engine in total.

The Wankel engine also produces a higher power density than an equivalent reciprocating engine. However, its thermodynamic efficiency is substantially lower. Power densities of BARM engines should be significantly greater than that of reciprocating engines with the same thermodynamic efficiency.

## 5  BARM: Centrally Symmetrical Dual Power Unit Configuration

The Fig. 6 sequence illustrates the function of a BARM engine with dual power units whose centrally symmetric configuration causes all forces, all linear accelerations and all internal tensions in both units to fully compensate each other because the engine's center of gravity lies at the center of the combustion chamber. As a result, the dual centrally symmetric configuration will deliver very low-vibration performance.

But low-vibration performance is not the only advantage of this well balanced dual power unit configuration. The centrally symmetric configuration of dual BARM power units halves volume displacement time, thereby doubling power density.

The small table in the upper left of each Fig. 6 cell shows the respective states on piston sides $A_1$, $C_1$, $A_2$ and $C_2$. The compression cycle is dark blue, the power cycle is red.

The centrally symmetric configuration is the most general form of an existing idea. Peter Hofbauer of Ecomotors International is developing a linear form of the centrally symmetric configuration since 2005, *Hofbauer*. Since 2007, Monty Cleeves of Pinnacle Engines is realizing another, very similar, linear implementation of this idea, *Cleeves*. The time is obviously ripe for a realization of this idea. The centrally symmetrical configuration combined with trochoidal rotation machines, particularly with the BARM technology, provides optimal technical and economic potential.
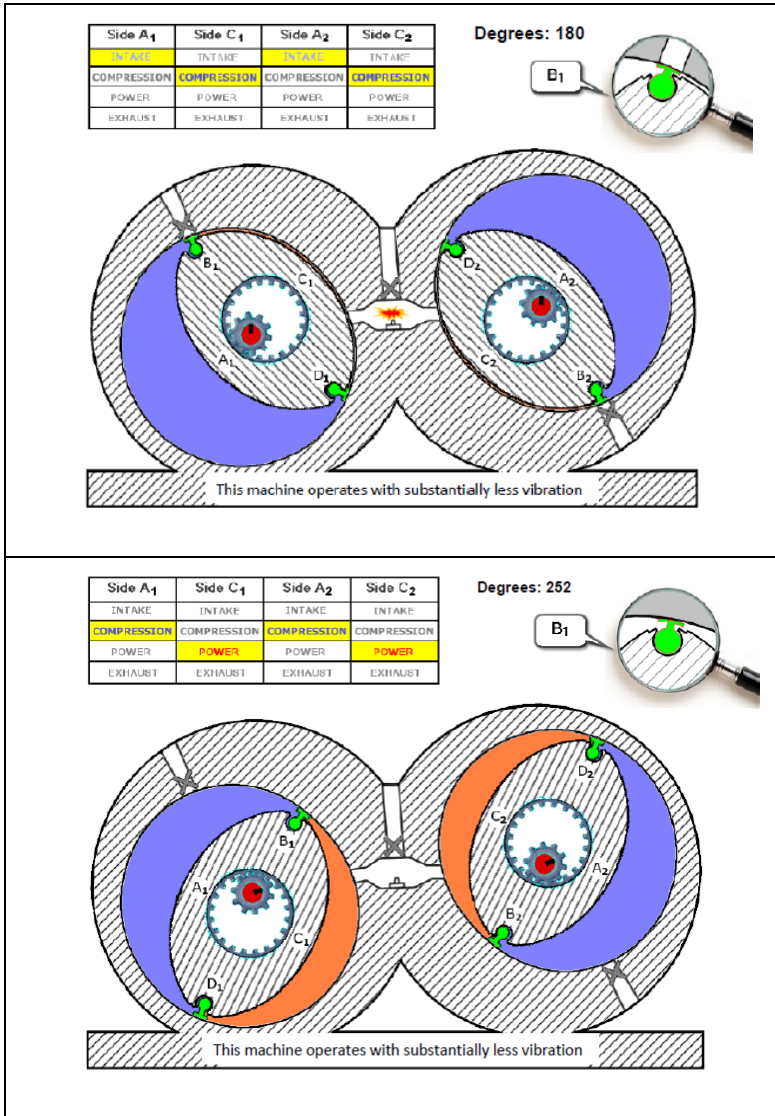
**Fig. 6.** BARM engine with centrally symmetric configuration of power units.

# 5 Conclusion

For political and ecological reasons, the broad public is being led to believe that the era of internal combustion machines has definitely ended and it will be replaced by purely electric mobility before our very eyes.

I welcome electric mobility. Nonetheless, I am convinced that it will be quite a while before it moves out of the subsidized niches. Why? Because, from a purely macroeconomic perspective, it will be several decades at least before the price of an electrically powered kilometer can compete with the price of a kilometer powered by fossil or chemically produced fuels.

This means that internal combustion machines, whether as main power source on the water or in the air or as auxiliary power units and range extenders in combination with electric drives on land, must continue to be developed and optimized.

The basic principles of motor topology have not changed in the last 125 years. Most volume displacing internal combustion machines belong to the topology with the periodically jumping instantaneous axis of rotation, Schapiro 2008, to which the classic reciprocating piston machine also belongs. The 80-year development history of trochoidal machines, including the Wankel engine as its most well-known example, has not come close to realizing its potential.

Trochoidal machines belong to the topology with a smoothly and continuously rotating axis of rotation. It is precisely this topology of trochoidal machines that provides the mathematical underpinnings for their advantageous characteristics listed in Part 1.

This presentation is intended to demonstrate that systematic understanding of trochoidal machines, especially as internal combustion machines, is still in the earliest stages of development. In addition, the barely researched advantages of the bi-angular, trochoidal rotation machine configuration should be brought to professional attention.

# References

Cleeves, M.: Current, `http://pinnacle-engines.com`

Hofbauer, P.: Current, `http://www.ecomotors.com`

Schapiro, B.: The RPM Rotary Piston Machines (in Eng.). In: Plath, P.J., Hass, E.-C. (eds.) Proceedings of Vernetzte Wissenschaften, International Workshop Galtür-Wirl-Zejnisjoch, March 26 - April 2, pp. 61–72. LOGOS Verlag, Berlin (2006/ 2008)

Schapiro, B., Terlitsky, L.: RKMs: New Class of Machines. In: Subic, A., Leary, M., Wellnitz, J. (eds.) Meeting the Challenges to Sustainable Mobility, Proceedings ICSAT 2008, International Conference of Sustainable Technologies, Melbourne, Australia (November 2008)

Schapiro, B.: New Potential of Old Wankel-Type Machines. In: Sustainable Automotive Technologies 2011, Proceedings of the 3rd International Conference, Greenville, NC, USA. Springer, Heidelberg (2011)

Schapiro, B.: Rotationskolben-Verbrennungsmotor, German Patent Application DE 10 2011 001 752.6, 1 (April 2011)

Sukhomlinov, R.: Trochoidale Rotor Compressors. Publishing Houses Union Vishcha Shkola, Kharkov (1975)

# Reducing Emissions Associated with Electric Vehicles

Laurence Sparke OAM

Technical Director, Eday Life Ltd, Melbourne, Australia
lsparke@edaylife.com.au

**Abstract.** A century ago the electric car (now more frequently called electric vehicle or EV) was seen to be the ideal city car, while at the same time addressing the serious transport pollution problems of the time. With the development of lithium ion battery technology, the electric car once again offers to be the ideal city car and at the same time to address transport pollution problems. Concerns have been raised that electric cars merely relocate greenhouse gas emissions from the car exhaust to the exhaust stack of the power generation plant. This paper identifies a range of strategies to ensure that the electric car is truly a zero emissions vehicle, at a time of growing concerns about global warming and the diminishing access to conventional fuels due to peak oil.

## 1 Introduction

There is growing community concern about global warming, and the need to reduce our carbon footprint. The transport sector is the third largest emitter of greenhouse gases in Australia [1]. And we have a simultaneous challenge: when the world recovers from the current economic downturn, oil consumption will outstrip oil supply [2]. Australia will not have access to enough oil in the future. So it's timely to look again at the environmental impact of electric cars.

## 2 The Initial Success of the Electric Car

At the turn of the $20^{th}$ century, the electric car was seen as the environmental saviour of the industrialised world. At the time, London and New York, the two major cities of the western world, were served by 100,000 horse-drawn cabs, buses and delivery carts [3].

The horses deposited 1,000 tonnes of manure onto the city streets each day. The cities had no way of clearing away the mess. It stank, attracted hordes of flies and was a health hazard. When it dried, it blew into the air and caused breathing discomfort and respiratory disease [4].
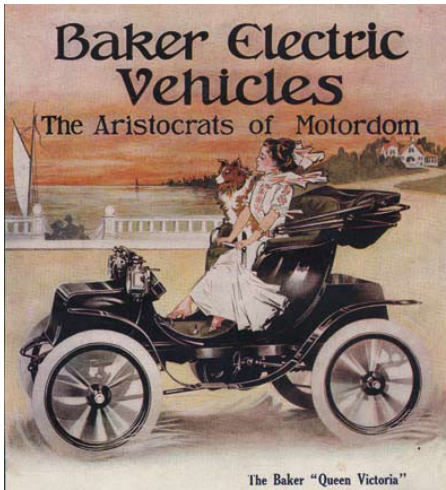
**Fig. 1.** The Baker Electric Car 1906, Thomas Edison's first car [5]



**Fig. 2.** Thomas Edison, Battery Inventor [6]

At this time, electric vehicles, emitting neither exhaust fumes nor noise pollution, were seen as the saviours of the city environments. They started instantly, accelerated away quickly and smoothly, were quiet, non polluting and easy to drive.

By comparison, petrol engine cars were difficult to start, with poor fuel mixture and required hand cranking, considered too difficult and dangerous for women drivers. They were hard to drive without synchromesh gearboxes, and a professional chauffeur was often employed to deal with these difficulties.

The petrol and oil fumes were smelly and polluting, and the exhausts were so noisy that they frightened the horses pulling the many wagons around the city. The American inventor Thomas Edison, seen here admiring the lead acid battery pack of an electric car, was a devotee of all things electric. His friend Henry Ford consulted him about whether he should build the T-model with apetrol or an electric motor. Unfortunately their discussions at this time were not documented, but Henry's decision to utilise petrol engines in his mass produced cars was to decide the future of the auto industry.

## 3   The Dominance of the Petrol Car

With the invention of the muffler, the carburettor by Maybach and Daimler, the fuel pump, and the electric starter by Kettering, these shortcomings were overcome. These new technologies transformed the petrol powered car, and when added to the dramatic cost reduction of Henry Ford's mass produced T-model, the public accepted the petrol powered car and abandoned the electric car.

There were a number of reasons for the electric car to fall from favour. The lead acid battery is heavy, expensive, with an energy density of less than 1% of that of petrol (one kilogram of petrol contains 12 kWh of energy, while a battery stores about 40Wh/kg) [7]. Petrol became cheap and readily available with the discovery of Texas crude oil.



**Fig. 3.** Henry Ford's 1910 T-model [8]

Petrol cars could now travel further than electric cars, just as roads were developed to connect cities and cars ceased to be used just for city transportation. The petrol powered car quickly became the exclusive technology to be used throughout the world for the next 100 years. Electric vehicles continued to find limited application; they hung on in England, where they were use as milk floats, and in Germany as postal delivery vans, but the numbers were negligible compared to the millions of petrol engine cars produced.

## 4   The Revival of the Electric Car

It was not until the invention of the Lithium-ion battery in 1996, and the utilisation of integrated circuits in the power control system that the electric car began once again to compete with the petrol powered car as a suitable form of city transportation.



**Fig. 4. Tesla Electric Car [9]**

The resurrection of the electric vehicle came at the same time as the emergence of community concern about peak oil and global warming. Interestingly, the first of the new generation of electric cars were developed, not by the established global automobile manufacturers, but by new start-ups such as Tesla Motors, founded by IT specialists from Silicon Valley in California.

Predictions of the uptake of electric cars vary. O'Connell of Tesla Motors suggests that by the year 2020, 30% of the cars driving on the road will be battery electric or plug-in hybrid. Carlos Ghosn of Nissan predicts that 10% of cars globally will be EVs by 2020. CSIRO estimates that less than 10% of Australian cars will be EVs by 2020 [10], while JD Power estimates a 7.3% take-up [11].
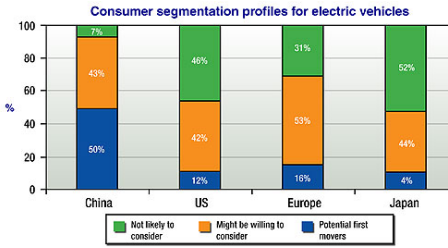
**Fig. 5.** Global Interest in Vs [13]

In a recent study [12] Deloitte found that Chinese consumers were more likely to see themselves as 'potential first movers' in the adoption of EVs – that is, people who are very interested in an EV and likely to purchase or lease one within the next 12 months – compared to people in more developed automotive markets.

In an Australian-specific survey the study found that petrol prices need to reach $2.60 a litre before the vast majority of consumers would be more willing to consider an EV over a regular car.

Analysis of carbon use in Melbourne suburbs [14] shows that low income outer suburbs will be worst affected by increased fuel prices. People living in these areas will benefit most from the lower running costs of EVs, as they frequently must rely on private transport to commute to work.
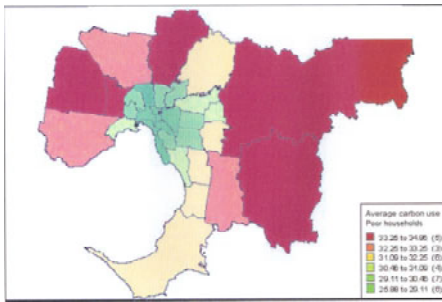


**Fig. 6.** Average carbon use in low income households around Melbourne [14]

After a century of domination by petrol powered vehicles, the time of the electric car has returned. 85% of Sydney and Melbourne residents drive less than 40 km per day [15], so electric cars currently have the range to satisfy this need, and this typical commute can be recharged in 3 hours from a standard power outlet.

Both China ($9 billion) and USA ($3 billion) have invested heavily in battery research, and significant development in battery performance can be expected over the next decade. The range and flexibility of electric powered vehicles will extend as battery mass and cost reduces, and energy density increases.

## 5   The Availability of Electric Energy

At a time when Australia's electrical generation capacity is falling short of peak demand, as experienced by Adelaide last summer when power failures occurred, there is concern that power demand for recharging EVs will exacerbate the situation. As shown in the chart of Daily Power Consumption, there is large off-peak generation capacity, and potentially millions of EVs could be charged overnight without any increase in generating capacity.

Critics of EVs point at the emissions from coal-fired power generation, and argue that efficiency losses in electricity distribution and in EV charging offset the gains in EV powertrain efficiency. Some critics of electric vehicles are concerned that there are significant environmental impacts associated with charging electric vehicle batteries from brown coal power generation, exacerbating power station emissions and grid peak loading.



**Fig. 7.** Daily Power Consumption [16]
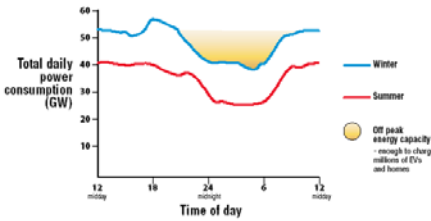
Home Energy Management, controlling the charging of the EV and home storage batteries, and utilising stored energy and solar energy to run the home during the day addresses these issues. Utilising an electronic energy manager ensures that peak energy demand is reduced, that renewable energy sources are utilised to reduce demand, and off-peak energy is utilised to smooth power station loading. Home energy requirements during peak tariff periods will be drawn from the home storage battery, replenished partially during the day by solar panels and topped up overnight from the grid during off-peak power station loading. This power will be supplied as Green Energy. This demand load redistribution enables power stations to run more efficiently, reducing power station emissions and delaying infrastructure upgrades.
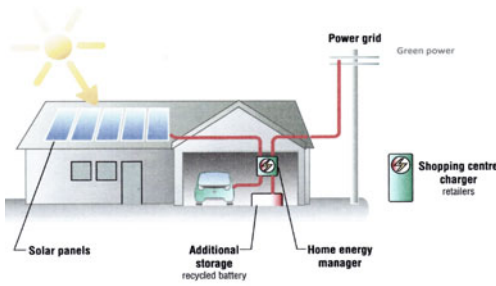


**Fig. 8.** Home Energy Management [17]

The Home Energy Management system utilises solar panels to provide as much of the EV recharging energy as possible, and supplements this by utilising Green Power from the grid. This encourages the power industry to grow the contribution of zero-emissions power sources.
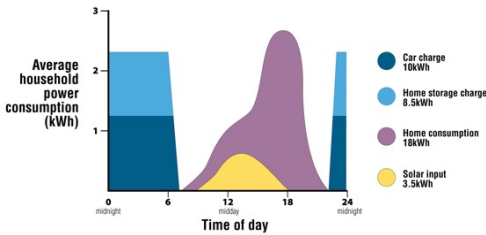


**Fig. 9.** Average Household Power Consumption [18]

A network of storage batteries can become a powerful resource for the electric utilities, allowing better utilisation of existing base load generation capacity, plus overnight utilisation of intermittent wind generator output. The electrical energy

consumed, even with very large EV fleet turns out to be minimal, and will not require additional based load generation capacity to be constructed.

In discussions about transport greenhouse emissions, the emissions associated with the manufacture of the vehicle are frequently overlooked. These emissions are of the same magnitude as those caused by vehicle operation.

This aspect is of critical importance when evaluating the emissions of hybrid vehicles, as the extra manufacturing emissions associated with the additional electric, battery and power control system can equate to 15 years of operation of an equivalent conventional car before the hybrid vehicle achieves an equivalent life-cycle emissions.

In order to reduce the impact of the emissions associated with vehicle manufacture, EDay will recycle their electric cars. The cars will be replaced every 2 years.



**Fig. 10.** EDay Electric Car [19]

A new car will be provided with the next generation of battery and control system technology. The 2 year-old battery will be recycled as home energy storage, part of the Home Energy Management system.

The used cars will be refurbished and fitted with next technology battery and control systems, and leased to new customers. By recycling the cars up to 4 times, the imbedded energy and associated emissions in new car manufacture will be reduced to a fraction of the conventional car ownership model.

The car batteries will also be recycled. At the end of their 2 years of operation in the car, the battery will be utilised for a further 20 years as home energy storage. EDay will then recycle the battery materials in the most environmentally sensitive way, utilising the best technology available by this time.

Eco Driving has the potential to reduce emissions by 15% [20]. Energy use can be minimised and recharging emissions can be reduced by smart driving techniques, informed by electric car feedback technology. An iPad-like portable device located in a docking station on the instrument panel, provides the driver with vehicle system analysis and allows remote management of the car. The EPad also provides information to facilitate more efficient driving. This information allows the driver to select less congested or less hilly routes, and provides real time feedback to the driver of the efficiency of driving, and consequently encourages lower energy use. EPad analysis of the driver's daily energy usage and carbon footprint encourages more economical use of the vehicle, and the selection of public transport, cycling or walking options where appropriate.

# 6 Conclusions

A century after the electric car was first recognised as a desirable technology for convenient city transport and for reducing city transport pollution, it is once again promising the same advantages. Concerns have been expressed that the electric car will not deliver the promised environmental benefits, because of the emissions associated with coal power station electricity generation. Strategies have been described, including Home Energy Management, car and battery recycling and Eco Driving, to address these concerns and provide further environmental benefits, to ensure the electric car is truly zero emissions transportation.

## References

1. Australian Government Department of Climate Change. National Greenhouse Gas Inventory (May 2009)
2. Sparke, L.: Gas for a Sustainable Transport System, Reduced Greenhouse Emissions&Energy Security. In: SSEE International Conference (June 2009)
3. Morris, E.: From Horse Power to Horsepower (access 2007)
4. Davies, S.: The Great Horse-Manure Crisis of 1894. The Freeman (2004)
5. Georgano, N.: Beaulieu Encyclopedia of the Automobile, London (2000)
6. Baker, J.: Thomas A. Edison's Latest Invention. Scientific American (1911)
7. Samarin, A.: Does an electric vehicle fleet hold the key to urban transport? Science Alert (2008)
8. Photograph 1910Ford-T.jpg from Wikimedia
9. Photograph tesla-model s concept 01.jpg from Google Images
10. Higgins, A., Paevere, P.: Diffusion Modelling of Electric Vehicle Uptake: Methodology and Case Study for Victoria (2011)
11. Drive green 2020: More Hope than Reality, JD Power (2011)
12. Rezek, D.: Gaining traction: Will consumers ride the electric vehicle wave? Deloitte (2011)
13. Unkles, B., Stanley, J.: Carbon use in poor Victorian households by local government area (April 2008)
14. Simpson, A.: Proceedings of EV Conference 2009 (November 11, 2009)
15. Chart generated by Eday Life utilising CSIRO data
16. Diagram generated by Eday Life
17. Chart generated by Eday Life utilising CSIRO data
18. Photograph supplied by Eday Life
19. King, J.: Driving the Transition to Electric Vehicles (July 2011)

# Direct Torque Control for Electronic Differential in an Electric Racing Car

C. Fu, R. Hoseinnezhad[*], Simon Watkins, and Reza Jazar

School of Aerospace, Mechanical and Manufacturing Engineering, RMIT University, Victoria 3083, Australia
rezah@rmit.edu.au

**Abstract.** This paper presents a new method for development of electronic differentials for electric racing vehicles. Most electronic differential solutions focus on maintaining the vehicle stability as the first and dominant priority, and are designed to keep some stability-related quantity (e.g. wheel slip) in a "safe region". With racing cars however, the main focus is on the responsiveness of the vehicle and its capability to cope with extreme steering and accelerating demands from the driver. Our focus is on designing a controller to achieve neutral-steer (avoiding over- or under-steer) in race car driving conditions. We show a direct relationship between the steering condition and the difference of the longitudinal tire-road friction forces for the driven wheels. We mathematically derive the desired difference in the tire-road frictions that would achieve neutral-steer and show that it is directly related to the difference in the driving torques provided by motors. A closed-loop-control system is proposed for direct control of the motor torques. The simulation results show a close-to-neutral steering performance of the car (while maintaining its stability) in challenging steering scenarios.

## 1 Introduction

The two major problems caused by internal combustion engine vehicles, energy scarcity and environment contamination, have become public concerns already. Measures are being taken to address these problems, and one of the main focuses of current research and development trends in sustainable automotive technologies is on developing fully electric vehicles.

In electric cars, each driven wheel is individually actuated by an electric motor, which makes it possible to employ an electronic differential instead of the heavy mechanical differential and to benefit from the swift response time of the electric motors. An electronic differential is a torque and wheel speed controller for managing multiple drives. It supervises the distribution of torques and speeds between driven wheels in accordance with the state of the vehicle and the driver's commands. Therefore, the stability and dynamic performance of the car can be

---

[*] Corresponding author, Tel: +61-3-9925-6135.

enhanced by fine tuning of the difference between the torques applied on driven wheels. With a conventional mechanical differential, the stability and performance merits of such a differential torque are implausible.

Most electronic differential solutions, reported so far in the vehicular technology literature, focus on maintaining the vehicle stability as the first and dominant priority, and design to keep some stability-related quantity (e.g. wheel slip) in a "safe region". With racing cars however, the priorities are different. Here, the main focus is on the responsiveness of the vehicle and its capability to cope with extreme steering and accelerating demands from the driver. Vehicle stability can be pushed to its margins (yet maintained) and slips can go beyond the "safe region" levels usually applied with passenger car design.

The easiest method to design an electronic differential is the "equal torque strategy" proposed by Guillermo A. Magallan [1]. The principle of this method is to emulate the behavior of a mechanical differential. Thus, this method always applies even torque to both driven wheels for all vehicle maneuvers. To achieve a better design, many reported electronic differential strategies utilize Ackerman condition to calculate the desired angular speed for each driven wheel. Ackerman condition is a kinematic relation between the inner and outer wheels, allowing them to turn slip free [2]. The "zero slip" condition that is presumed necessary by Ackerman condition is not always the optimal choice in terms of achieving the best vehicle maneuverability. In high performance vehicle dynamic arrangements, some level of wheel slip is allowed to achieve maximum traction while maintaining vehicle stability. For example, in the strategy proposed by Jeongmin Kim and Hyunsoo Kim [3], control commands are generated to produce a desired yaw rate and a desired lateral acceleration which are computed from a vehicle planar dynamic model. In their method, wheel slip explicitly contributes to the control commands generated. Other examples of control methods include an independent motor control strategy using fuzzy logic [4], and an independent motor control method using sliding mode control and a vehicle state observer [5].

In this paper, a closed-loop control system is proposed for direct control of the motor torques. The loop is closed using observers that estimate the tire-road friction and the error signal is the distance between the desired and actual (estimated) values of the difference between the tire-road frictions for the driven wheels. The simulation results show a close-to-neutral steering performance of the car (while maintaining its stability) in challenging steering scenarios.

## 2   Electronic Differential via Direct Torque Control

Consider a rear-driven electric car with a local coordinate frame attached to the vehicle at its center of mass, as shown in Fig. 1. We will show that the reaction forces exerted on the two rear driven wheels, $F_{x3}$ and $F_{x4}$, are directly related to the steering performance of the vehicle, and can be tuned to achieve neutral-steering. Our method is based on tuning $F_{x3}$ and $F_{x4}$ to attain their desired values via controlling the driving torques produced by the two motors.
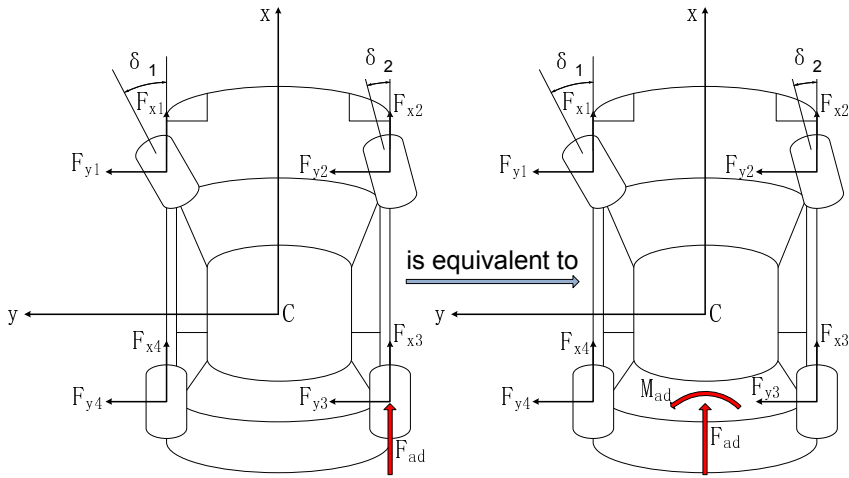
**Fig. 1.** Top view of the local coordinate frame and the force system acting on the vehicle

Let us assume that, in the first place, both reaction forces $F_{x3}$ and $F_{x4}$ are equal. Then we have the following set of equations of motion:

$$\sum F_x = m\dot{v}_x - mrv_y \; ; \; \sum F_y = m\dot{v}_y + mrv_x; \; \sum M_z = I_z \dot{r} \; ; \; \sum M_x = I_x \dot{p} \quad (1)$$

where $m$, $v_x$, $v_y$, $I_z$ and $I_x$ denote the vehicle mass, the longitudinal velocity, the lateral velocity, the yaw moment of inertia and the roll moment of inertia respectively. Expanding the left-hand side of the last three equations, we get the complete version of the equations of motion that govern the lateral, the yaw and the roll motion of the car.

$$C_r r + C_p p + C_\beta \beta + C_\varphi \varphi + C_\delta \delta = m\dot{v}_y + mrv_x$$
$$E_r r + E_p p + E_\beta \beta + E_\varphi \varphi + E_\delta \delta = I_z \dot{r} \quad (2)$$
$$D_r r + D_p p + D_\beta \beta + D_\varphi \varphi + D_\delta \delta = I_x \dot{p}$$

where $r$, $p$, $\beta$, $\varphi$ and $\delta$ represent the yaw rate, the roll rate, the vehicle sideslip angle, the roll angle and the cot-average steering angle of the front wheels (cot $\delta$ = (cot $\delta_1$ + cot $\delta_2$)/2) respectively. The coefficients are explicitly expressed in [2].

When we have electronic differential on-board, we are able to send different torque commands to the two driving motors, so the reaction forces $F_{x3}$ and $F_{x4}$ can be different. Let's define $F_{ad} = F_{x3} - F_{x4}$, then an additional moment $M_{ad} = F_{ad} \times w/2$ ($w$ is the rear track) is applied on the rear axle, as indicated in Fig. 1. Therefore, the equations of motion governing the lateral, the yaw and the roll motion – equation (2) – can be modified as follows:

$$C_r r + C_p p + C_\beta \beta + C_\varphi \varphi + C_\delta \delta = m\dot{v}_y + mr v_x$$
$$E_r r + E_p p + E_\beta \beta + E_\varphi \varphi + E_\delta \delta = I_z \dot{r} \qquad (3)$$
$$D_r r + D_p p + D_\beta \beta + D_\varphi \varphi + D_\delta \delta + \frac{w}{2} \cdot F_{ad} = I_x \dot{p}$$

In order to evaluate the cornering performance of the vehicle, we analyze its steady-state response to steering commands $\delta$ and the extra tire forces $F_{ad}$ induced by an electronic differential. This will simplify equations (3) via replacing all time-derivatives with zero which leads to:

$$
\begin{bmatrix} C_\beta & C_r - mv_x & C_\varphi \\ E_\beta & E_r & E_\varphi \\ D_\beta & D_r & D_\varphi \end{bmatrix}
\begin{bmatrix} \beta \\ r \\ \varphi \end{bmatrix}
=
\begin{bmatrix} -C_\delta & 0 \\ -E_\delta & 0 \\ -D_\delta & -\frac{w}{2} \end{bmatrix}
\begin{bmatrix} \delta \\ F_{ad} \end{bmatrix}
\qquad (4)
$$

Solving the above system of equations, the following yaw rate response is derived in terms of the control inputs $\delta$ and $F_{ad}$:

$$r = \frac{Z_{\delta r}}{Z_0} \delta + \frac{Z_{Fr}}{Z_0} F_{ad} \qquad (5)$$

$$Z_{Fr} = \frac{w}{2}(E_\beta C_\phi - E_\phi C_\beta)$$

$$Z_0 = E_\beta(D_\phi C_r - D_r C_\phi - mv_x D_\phi) + E_\phi(D_r C_\beta - D_\beta C_r + mv_x D_\beta) + E_r(D_\beta C_\phi - D_\phi C_\beta) \qquad (6)$$

$$Z_{\delta r} = E_\beta(D_\delta C_\phi - D_\phi C_\delta) + E_\phi(D_\beta C_\delta - D_\delta C_\beta) + E_\delta(D_\phi C_\beta - D_\beta C_\phi)$$

Equation (5) shows that the yaw rate is directly related to the difference between the two reaction forces on the rear wheels, $F_{ad}$. By controlling the driving torques generated by the two motors, we can tune $F_{x3}$ and $F_{x4}$ to attain the desired difference between their values.

In racing conditions, responsiveness and accuracy become the dominant requirements on the steering performance of the electric car. Hence, it is sensible to maintain the car always in the neutral-steer condition so that it follows the driver's steering command accurately and swiftly. With a neutral-steer vehicle, the yaw rate is expressed as follows:

$$r^* = \frac{v_x}{l} \delta \qquad (7)$$

From equations (5) and (7), the desired reaction force difference $F_{ad}$, needed to achieve neutral-steer, is derived as follows:

$$F_{ad} = F_{x3} - F_{x4} = \frac{\delta}{Z_{Fr}}(\frac{v_x}{l} Z_0 - Z_{\delta r}) \qquad (8)$$

Equation (8) is the control goal of our control system design. Figure 3 shows a block diagram of the structure of the proposed control system. The actual reaction

force difference $F_{ad}$ is obtained by the wheel dynamics block, with torque commands and vehicle roll angle being its inputs. Then, this actual $F_{ad}$ is compared to the desired reaction force difference $F_{ad}^*$ which is calculated based on vehicle longitudinal velocity, steering angle command and vehicle parameters. The error between the desired value and actual value goes to a PID controller which generates the difference between the two motor torques and feeds it back to the torque command generation block.
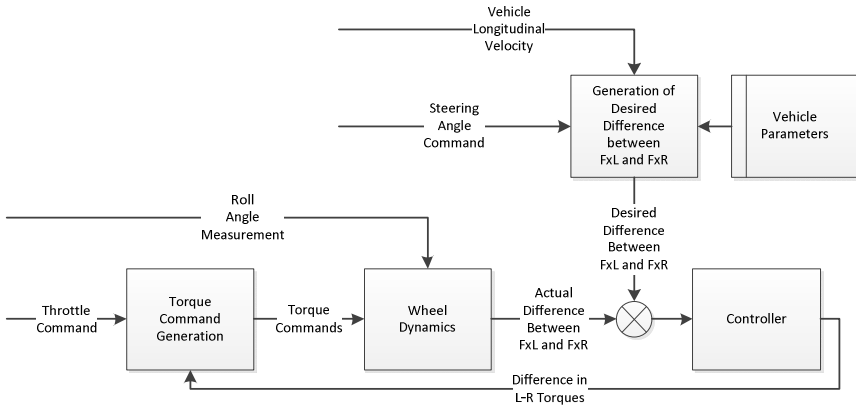


**Fig. 2.** A block diagram of our proposed direct torque control method for electronic differential.

## 3   Simulation Results

The electronic differential control system is constructed, based on the structure shown in Fig. 2, in MATLAB Simulink environment. In our Simulink model shown in Fig. 3, SimMechanics blocks are used to simulate the behavior of wheels, and a vehicle dynamics block (a State-Space block) is employed to calculate the vehicle states in the simulation environment. The vehicle state (roll angle) from the vehicle dynamics block is fed back to the tire dynamics blocks in which the wheel slips and the reaction forces $F_{x3}$ and $F_{x4}$ are calculated. A PID controller is used to track the desired value of the difference between $F_{x3}$ and $F_{x4}$.

Using the Simulink model shown in Fig. 3, we have conducted two simulation studies to verify the effectiveness of the proposed control system. In the first simulation, a fixed steering angle value (0.1 rad) is sent to the model, and the actual yaw rate is observed to be maintained by the closed loop control system at the desired value.
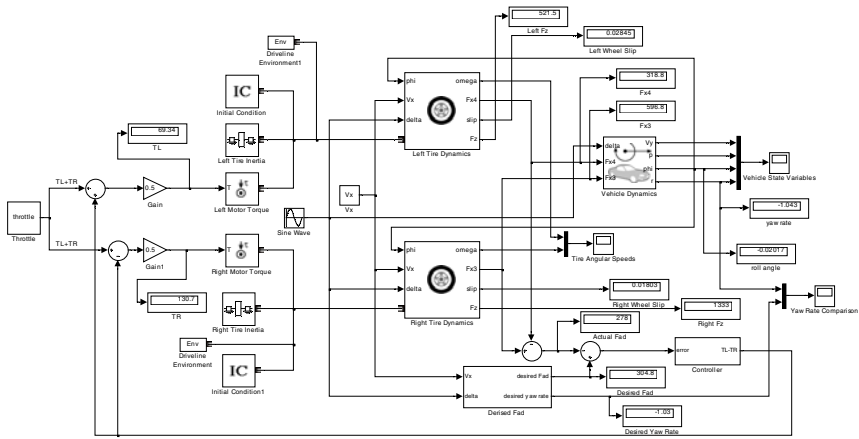
**Fig. 3.** The Simulink model of our proposed direct torque control method for electronic differential.

In the second simulation, a sinusoidal-type steering angle is input to the model. The result shown in Fig. 4 manifests that with a slight lag, the actual yaw rate (shown in blue) is very close to the desired yaw rate (shown in red). Also, as indicated by the wheel slip scopes, the wheel slips of both tires are contained in a reasonable range. Therefore, the proposed control system provides the electric racing car with a close-to-neutral steering performance, while maintaining its stability and keeping slip ratios in a reasonable range in challenging steering scenarios.
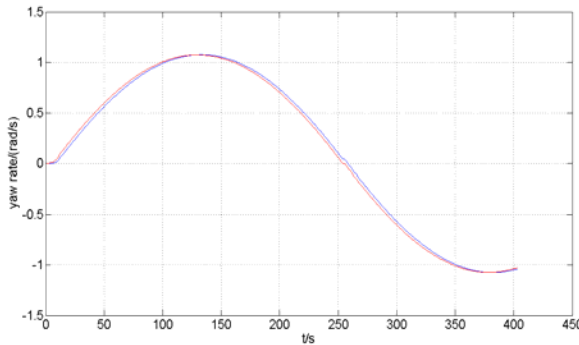


**Fig. 4.** The actual and desired yaw rate response with sinusoidal-steering input

## 4   Conclusions

In this paper, a closed-loop-control system is proposed for direct control of the motor torques, in order to achieve enhanced handling (namely neutral-steer) of an

electric racing car. By individually controlling the driving torques produced by the two motors, the reaction forces exerted on the two rear driven wheels, $F_{x3}$ and $F_{x4}$, can be tuned to attain their desired values. As can be seen from the simulations results, the proposed control system provides the electric racing car with a close-to-neutral steering performance, while maintaining its stability and keeping slip ratios in a reasonable range in challenging steering scenarios.

# References

[1] Magallan, G.A., et al.: A neighborhood electric vehicle with electronic differential traction control. In: 34th Annual Conference of the IEEE Industrial Electronics Society, IECON 2008, Orlando, FL, United states, pp. 2757–2763 (2008)

[2] Jazar, R.N.: Vehicle Dynamics: Theory and Application. Springer, New York (2008)

[3] Kim, J., Kim, H.: Electric vehicle yaw rate control using independent in-wheel motor. In: 4th Power Conversion Conference-NAGOYA, PCC-NAGOYA 2007, Nagoya, Japan, pp. 705–710 (2007)

[4] Yan-e, Z., Jianwu, Z.: Modelling and simulation of the electronic differential system for an electric vehicle with two-motor-wheel drive. International Journal of Vehicle Systems Modelling and Testing 4, 117–131 (2009)

[5] Li, J., et al.: Electronic differential control with vehicle state observer based on Extended Kalman Filter. In: 2011 International Conference on Computer Distributed Control and Intelligent Environmental Monitoring, CDCIEM 2011, Changsha, Hunan, China, pp. 172–175 (2011)

# Ultra High Efficiency Electric Motor Generator

Jeff Brown

Marand Precision Engineering Pty. Ltd, 153 Keys Road, Moorabbin, 3189, Melbourne, Victoria, Australia
Phone: + 61 (0) 3 8552 0600, Fax: + 61 (0) 3 8552 0605
`www.marand.com.au`

**Abstract.** The Ultra High Efficiency Electric Motor Generator is an exciting opportunity to leverage proven technology and apply this technology in new areas, creating new business opportunities in green technology. Marand currently produces this motor/generator at our Moorabbin facility for application in solar race cars. The potential of this motor/generator is far greater than this single application. We are seeking investment partners to develop, not the core technology, but its application potential. We believe we can achieve through economies of scale further cost reduction of the motor/generator and hence open new markets for this great piece of Australian technology.

## 1 Introduction

Awareness of the energy consumed and the impact on the environment is developing at an increasing pace. There is increasing demand for energy efficiency and better use of resources. Energy is not always available in the form we require to be able to use it. To power a machine we usually require electricity, but the available energy source may be in the form of hydro, wind, solar or a non-renewable. Transforming energy from an available form to useable form is an ongoing need. The ability to transform that energy at the highest efficiency is the challenge.

Marand has licensed proven high efficiency motor technology from the Commonwealth Scientific and Industrial Research Organisation (CSIRO), and further developed products originally designed for low volume laboratory construction to products that can be produced using traditional volume manufacturing techniques. These motors are also equally impressive as generators. In 2009 Marand entered in to a licensing agreement with CSIRO to develop and market the CSIRO designed axial flux permanent magnet motor/generator that had been developed for the highly competitive area of solar car racing. This motor, the ultra-high-efficiency-electric-motor-generator (UHEEMG) has a proven track record of race wins, and exceeds the published performance of competitors motors used in that highly competitive application.

However, the potential application of this motor/generator is expected to be far greater than its original intended function. The efficiency of this unit is significant when compared to traditional motor/generators, and it is through the efficiency that new market opportunities arise for this product.

## 2   Why Concentrate on Motor/Generator Efficiency?

A machine that requires an electric motor to perform its task requires a certain amount of input energy, in the form of electricity to operate. If the electric motor is more efficient in converting the electricity to useful mechanical work, then the amount of electricity, and hence the amount of energy required to make that electricity is reduced. In simple terms you need less power from your supply and hence reduce, both cost and emissions. As the cost of electricity increases, the demand for more efficient utilisation will only increase.

For power generation the same principle applies. The amount of electricity produced for a given amount of input power is increased. If the energy comes from a non-renewable source then the consumption and emissions will be lower per kilowatt hour (kWh) produced. In some cases there may only be limited energy available, such as in the case of hydro-electric generation, where the energy available is restricted due to the location or tidal movement. A turbine may also be located in a free flowing river, or irrigation channel, where flow rates are not ideal. When placing a wind turbine (Figure 1), it may not be possible to locate the turbine in an ideal location. In all of these cases the efficiency of the generator may determine if the energy source is viable or not.



**Fig. 1.** Windturbines.

The UHEEMG has a rated efficiency of 98% (CSIRO published efficiency for Halbach variant [1]). This compares favourably with commercial motors such as brushed or induction type motors that may offer efficiencies in the 75-85%.

Specialised motors with similar power ratings that have been developed for solar unmanned aerial vehicles (UAV), see Figure 2, and solar race vehicles have efficiencies up to 93-95%; to date no competitor has claimed a motor to match the CSIRO design.



**Fig. 2.** Unmanned areal vehicle.

A typical industrial machine (see Figure 3) would use an induction motor, and there may be multiple motors per machine; these have efficiencies in the order of 75-85%. An induction motor that has a mechanical output of 10kW at 75% efficiency requires 13.33kW of electricity to operate. The Marand motor at 98.4% requires only 10.16kW, potentially saving in excess of 25kWh over an 8 hour shift. This would save the operator $3100 per year per motor (see equation 1).

$$25kWh*2 \text{ shifts}*6 \text{ days}*52 \text{ weeks}*\$0.20/kWh=\$3120 \text{ per year} \qquad (1)$$



**Fig. 3.** Typical industrial machines.

Electricity is predicted to double in price by as early as 2015. This will provide greater emphasis on more efficient methods of power utilisation. The projected savings as shown above could easily double with the projected increase in energy prices, in only a few short years. This would represent a payback of less than 12 months, demonstrating a great business case.

Higher energy costs from traditional suppliers will drive an increase in the demand for extraction of energy from alternate sources including the need to utilise low grade energy sources.

These low grade energy sources will only be viable with highly efficient energy transformation solutions. Here the high efficiency of the Marand motor/generator will have significant advantage.

Having generated power from these low grade energy sources there will be a need to use this energy in the most efficient manner, here again there will be demand for electric motors that can provide the maximum work from the smallest energy input.

## 3   The Motor/Generator

The ultra-high efficiency electric motor/generator is based on the highly successful CSIRO solar car motor designed in 1997 for the world solar car challenge [2]. This motor has been a proven race winner, due to its robust design and its high efficiency. In solar car racing the amount of solar panels is restricted as are the types of cells. This has the effect of limiting the maximum power available to run the vehicle, a more efficient motor maximises the use of this available power.

The unit is an axial flux permanent magnet motor/generator; the major elements can be seen in Figure 4.

The motor/generator utilises a fixed stator and a rotating magnet array. This removes the need for slip rings or a commutator, increasing reliability and efficiency. The magnet rings have been designed to operate with a rotating housing such as wheel or rotating axle as required by the application. The compact motor design allows configurations with stacked elements giving a wide range of performance options. Every part of the 40 pole motor has been designed with high efficiency and low mass in mind, minimising all sources of electrical, aerodynamic, and mechanical loss in the system. The motor is precision manufactured from high performance Neodymium magnets and high temperature Litz wire to maximise efficiency. Its low mass can be attributed to eliminating any material which is not absolutely required to maintain the performance of the motor, the stator windings have no iron core, and extensive weight reduction is carried out on the steel backing plate in areas of low magnetic flux.
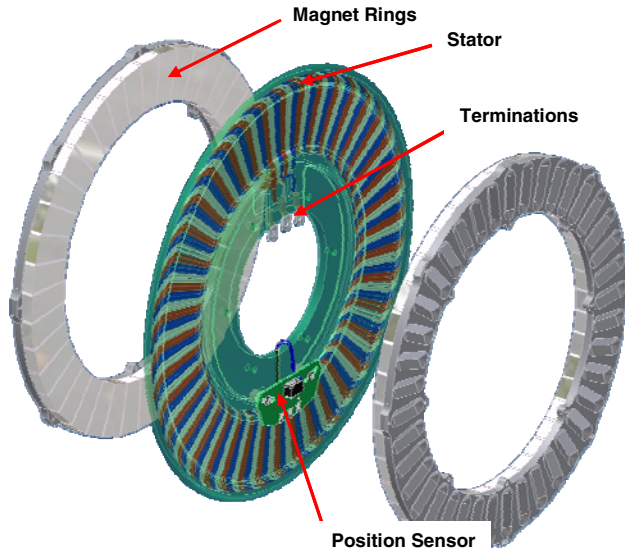
**Fig. 4.** Components of the steel back.

There are two variants of the motor, a surface magnet type as shown in Figure 4, and a Halbach type. The Halbach magnet array provides a more efficient magnet path and improves all areas of motor performance including motor efficiency. A comparison of performance characteristics for both motors can be seen in Table 1.

**Table 1.** Motor performance characteristics.

|  | **Surface Magnet** | **Halbach** |
|---|---|---|
| **Rated Power** | 1.8kW | 1.8kW |
| **Continuous Power** | 4 kW | 5kW |
| **Peak Power** | 10 kW for 72s | 12kW for 72s |
| **Nominal Speed** | 1060 RPM | 1060RPM |
| **Efficiency** | 97.3% | 98.4% |
| **Mass** | 10 kg | 7kg |
| **Torque to Weight ratio** | 3.00 Nm/kg | 3.61 Nm/kg |
| **Torque to Volume ratio** | 10135 Nm/m$^3$ | 10135 Nm/m$^3$ |

The motor/generator allows for design flexibility, it can be configured with either a rotating housing as used in a wheel such as shown in Figure 5 or a rotating shaft as typically used in plant and equipment. Combining multiple motor elements such as shown in Figure 6, allows scaling of the motor/generator to suit multiple applications.
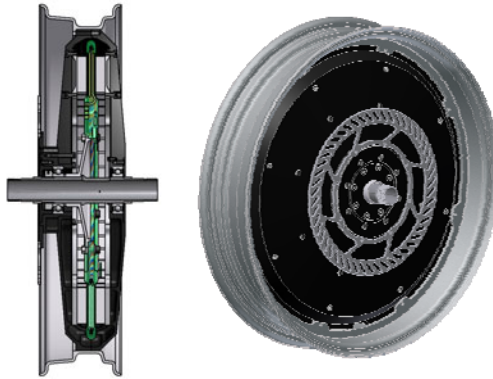
**Fig. 5.** Rotating housing.
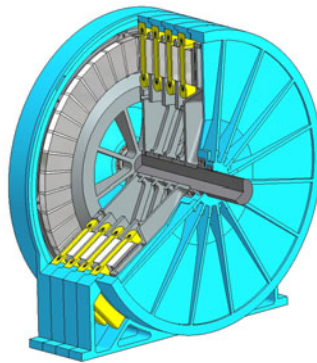


**Fig. 6.** Rotating axle multi stack.

Ideal applications are those where energy is constrained, or there is a desire to reduce the operating cost or emissions. For transport, such as electric cars, bikes and scooters, the range and performance of the vehicle is a balance between the amount of energy stored, usually batteries and the efficiency of the motor. For solar aircraft such as UAVs, the high efficiency and low mass result in greater endurance or greater payload compared to alternate motors.

When harnessing energy such as through water or wind turbines the energy gathered can be maximised, and in applications with marginal available energy the motor/generator can make an unviable energy source viable.

The UHEMG is proven technology; this is not a product that is waiting for the next technological breakthrough to achieve its demonstrated performance. The design is from the CSIRO, Australia's leading research and development institution. Now this proven design is adapted to commercial manufacturing techniques, and

further developed to give the design greater flexibility in its application to areas that can benefit from such an efficient motor/generator such as battery electrical vehicles (BEV), see Figure 7. Marand is in the process of taking this product from current low volumes to the point where economies of scale can be realised.
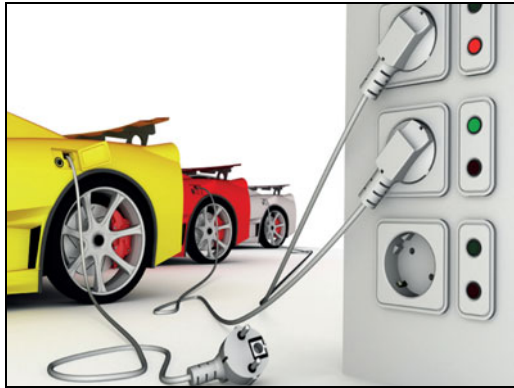


**Fig. 7.** Plug in BEV.

## 4   Conclusions

An ultra high efficiency electric motor/generator has been designed by the CSIRO and now manufactured by Marand.

The motor has a proven track record over a 12 year period and has the potential for application outside of its original purpose in areas that either need or want to leverage the exceptional efficiency that this device offers.

This motor has the fundamentals to be utilised in a variety of applications where the benefits of using an ultra high efficient motor/generator can be leveraged.

## References

1. http://www.csiro.au/Outcomes/Climate/Reducing-GHG/
   Solar-cars-use-CSIRO-motor.aspx (assessed December 15, 2011)
2. Lovatt, H.C., Ramsden, V.S., Mecrow, B.: Design of an in-wheel motor for a solar-powered electric vehicle. In: Eighth International Conference on Electrical Machines and Drives, Cambridge, UK, September 1-3, pp. 234–238 (1997) Conf. Publ. No. 444

# Modelling and Simulation of a Two Speed Electric Vehicle

P.D. Walker[1], S. Abdul Rahman[2], N. Zhang[1], W. Zhan[3], Y. Lin[3], and B. Zhu[3]

[1] University of Technology, Sydney, Ultimo, New South Wales, 2007, Australia
[2] Universiti Malaysia Terengganu, Kuala Terengganu, 21030, Malaysia
[3] Beijing Electic Vehicles, Chao Yang District, Beijing, 100021, China
  Paul.Walker@uts.edu.au

**Abstract.** Electric vehicles offer an alternative to hybrid and conventional vehicles through the use of electric drive without fossil fuel consumption. This shifts green house gas production from the vehicle to power stations, but if power is supplied from renewable sources, such as wind power, zero emissions are generated. Practical vehicle design requires the consideration of competing demands of vehicle acceleration and performance against range and vehicle efficiency. Thus, considering requirements such as grade climbing and acceleration against vehicle range and power consumption, a two speed transmission is suggested for this vehicle study to increase motor operation at high torque and efficiency regions. To evaluate the application of such a transmission, a two speed electric vehicle powertrain is developed in Simulink® for a full sized sedan. Simulations are conducted to demonstrate the performance of the two speed electric vehicle. Results demonstrate the capability of the two speed vehicle to meet various performance criteria and provide an indication of effective range under different drive cycles.

## 1  Introduction

Pure electric vehicles (EV) have become an alternative to hybrid electric vehicles and conventional passenger vehicles as they produce zero emissions on the road. Such vehicles rely on significantly higher energy in battery cells compared to the hybrid equivalent to produce reasonable vehicle range. For example the 1100kg iMIEV compact EV has arrange of 130km on 16kWh (Kamachi, Miyamoto, & Sano 2010), whereas the all electric range of the Chervrolet Volt, weighing in at 1715kg is less than half that at 60km (Brooke 2011), though the overall range is closer to 500km. To therefore provide a reasonable range capability for a full sized EV sedan, evaluation of performance capabilities against design range is required to ensure correct size of batteries, motor and reduction ratio in the vehicle.

Vehicle drive cycles are frequently used to evaluate vehicle range under "normal" driving conditions, generally defined as either highway or urban drive cycles. Examples include Abdul Rahman, Zhang, & Zhu (2008), studying energy management for series-parallel HEVs with a planetary transmission. Driving simulations are then used to evaluate energy management, storage, and fuel consumption.

For EVs energy management is reduced to acceleration and braking requirements, reducing complexity, however the energy storage system becomes critical to the vehicle. While there is a push to super-capacitors, electric vehicles rely on large battery modules to achieve range (Jinnui, Zhifu, & Qinglian 2006).

The application of multispeed transmissions for EVs has the potential to improve average motor efficiency and hence range, or even reduce the required motor size. There is a range of transmissions available for application to EVs for multispeed drives, in Rudolph, et al, (2007) it is suggested that DCTs have higher efficiency than other automatic drives, making them particularly suitable.

This paper presents a systematic model of a two speed EV for evaluation of vehicle range and performance with an integrated two speed transmission. In the following sections are divided into EV powertrain model development in Section 2, including electric machine, battery, transmission, vehicle, and driver models. This is followed by vehicle performance evaluation and range simulations using two drive cycles. Finally, conclusions are drawn and project direction identified.

## 2   EV Powertrain Modelling

The main components of the electric vehicle power train that are considered for modeling are as follows:

- electric machine
- battery pack
- transmission and vehicle
- Driver model.

### 2.1   Electric Machine Model

Electric machines (EM) in electric vehicles have a dual role, providing driving torque to the vehicle and recovering energy during braking events. However, EM are frequently designed to provide higher efficiency as either a motor or generator. This leads to limitations in implementing the EM as a generator. It is modelled using look up tables to define motor efficiency as a function of speed and input power, while the actual output torque is defined from the input power and motor speed, limited by the rated motor torque. When acting as a generator it is assumed that only 30% of the generated power can be used to charge the battery, and for a vehicle speed under 15kph the generator is ineffective and disabled, friction brakes are then only used for braking. From energy conservation, electric machine torque is:

$$T_{EM} = \eta_{EM} \eta_{PC} \frac{P_B}{\omega_{EM}}$$

## 2.2   Battery Model

The battery model is based on lithium-ion batteries using interpolation to evaluate battery characteristics, similar to the model described in Abdul Rahman, Zhang, & Zhu (2008). Requirements are to determine cell characteristics ($R_{INT}$ and $V_{OC}$) as a function of temperature and SOC, and calculate the output voltage, battery temperature and change of SOC, all based on the input current to the battery. The output voltage of the battery during charge or discharge is:

$$V_{OUT} = V_{OC} - R_{INT} \times I$$

Maximum capacity is determined from the battery temperature ($CAP_{MAX}$), and used capacity ($CAP_{USED}$) from the initial conditions and supply/demand from the motor/generator. The absolute state of charge ($SOC_{ABS}$)is defined as:

$$SOC_{ABS} = \frac{CAP_{MAX} - CAP_{USED}}{CAP_{MAX}}$$

## 2.3   Transmission and Vehicle Models

The purpose of vehicle transmissions is to provide maximum vehicle performance and efficiency using many ratios. For an EV the transmission is based on a DCT with only two gears, with shifting controlled using a shift map designed to promote the operation of the EM in the higher efficiency region. Detailed ratio design is available in Lechner & Naunheimer (1999) for grade and speed requirements. Here maximum grade climbing is used to evaluate lowest possible ratio, while top speed and driving torque are used to limit the top gear ratio.

The vehicle model takes all the input torques, calculates vehicle acceleration and performs numerical integration to determine vehicle speed. Inputs are supplied motor torque, $T_{EM}$, brake torque, $T_B$, and vehicle resistance torque, $T_V$, and the output is vehicle acceleration. Equation of motion for the vehicle is:

$$m_V r_t^2 \alpha = \eta_{PT} \gamma T_{EM} - T_V - T_B$$

The vehicle resistance torque is the combination of rolling resistance force, incline load and air drag. It is defined as:

$$T_v = \left( C_R m_V g \cos \phi + m_V g \sin \phi + 0.5 C_D \rho A_V \omega_V^2 r_r^2 \right)$$

## 2.4   Driver Model

The vehicle driver is modeled using a PID controller, where the difference between demanded drive cycle speed and actual vehicle speed is the input error. The PID output is demand power to drive the vehicle, where a positive signal is considered the power demand required for vehicle acceleration, and a negative demand is the power required for braking.

## 3   Simulations and Analysis

The purpose of performing simulations is to provide a demonstration of the performance capabilities of the proposed vehicle. Simulations are conducted to evaluate the driving criteria of range under one highway and one urban style drive cycle, acceleration, overtaking acceleration, and grade climbing. The vehicle specifications are summarized in Table 1.

**Table 1.** Vehicle parameters

| Parameter | | Parameter | |
|---|---:|---|---:|
| **Mass** | 1760 kg | **Battery Layout** | 1P120S |
| **Wheel radius** | 0.266 m | **Battery Voltage** | 384 V |
| **Frontal area** | 2.2 m$^2$ | **Battery Capacity** | 66 Ah |
| **Rolling resistance** | 0.016 | **Gear ratios** | 8.68, 5.7 |
| **Motor torque** | 255 Nm @ 3000 RPM (peak) 127 Nm @ 9000 RPM | | |

The first cycle is a highway style drive, known as Highway Fuel Economy Test (HWFET), with repeated long high speed cycles to simulate highway driving. The second cycle is Urban Dynamometer Driving Schedule (UDDS), designed to simulate city driving with repeated stop starts.

The modeled vehicle is capable of 0-100kph in 13.7s, overtaking acceleration of 50-80 kph in 4.7s, and grade climbing of over 30%. Figure 1 below shows vehicle response to HWFET drive cycle, while Figure 2 shows the vehicle response to a UDDS cycle. A single cycle vehicle speed is shown in (a), while (b) shows the gear ratio changes for both figures. The vehicle range with the HWFET drive cycle is 141.2 km, equivalent to approximately 1.8 hours running time, a short but reasonable distance for an EV. By comparison the vehicle range under the UDDS cycle, Figure 2, is 128.2 km, a total drive time of about 4 hours. The longer range using HWFET is realized by the vehicle running continuously at a relatively stable speed with low torque demand. The UDDS cycle range is extended by frequent application of regenerative braking.
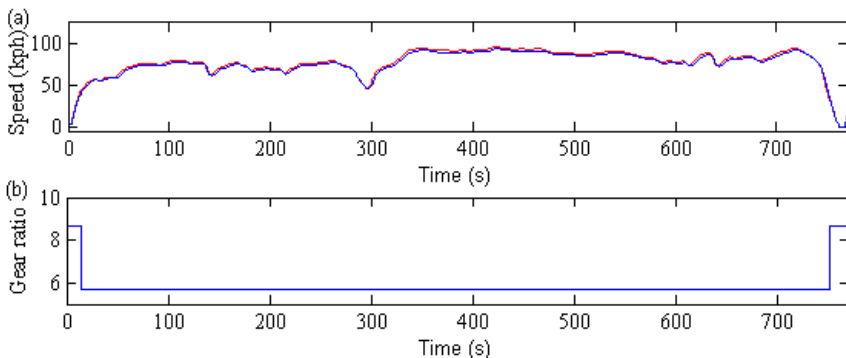


**Fig. 1.**   Simulation results for HWFET cycle (a) drive cycle and (b) gear ratio.
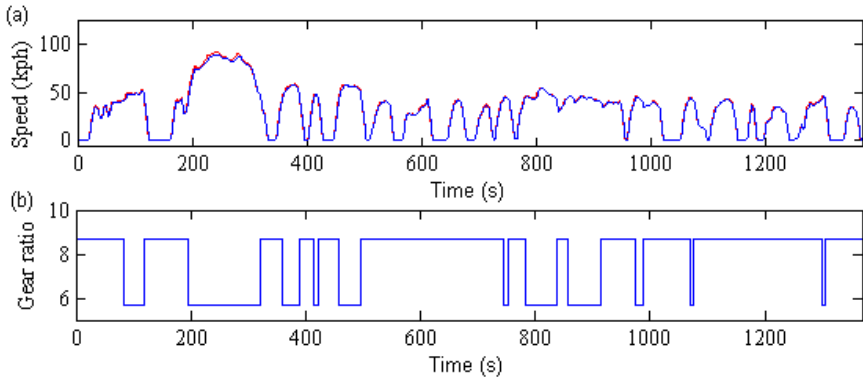
**Fig. 2.** Simulation results for UDDS cycle (a) drive cycle and (b) gear ratio.

Results in Figure 3 demonstrate the operating locus of the electric machine for both drive cycles. The results using only first gear demonstrate operation at higher speeds, with low efficiency. However, the employment of a two speed transmission shows improved efficiency by reducing operation in low efficiency zones.
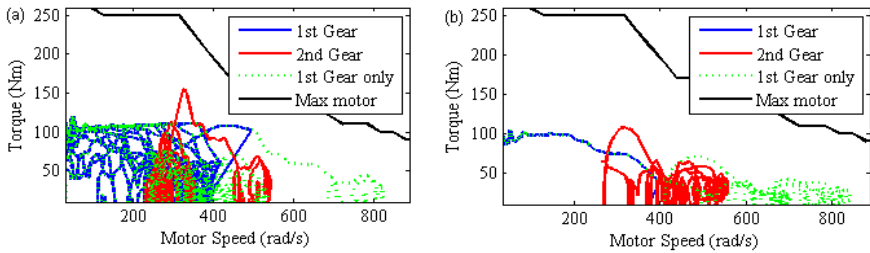


**Fig. 3.** Motor torque-speed traces for (a) UDDS cycle and (b) HWFET cycle.

## 4  Conclusion

This paper presented a compact model of a two speed electric vehicle to be used for performance evaluation in the Matlab/Simulink® environment. Simulations were conducted to evaluate performance specifications and range simulations. The results demonstrate that the larger vehicle is capable of meeting several performance criteria for acceleration and grade climbing, and provides a reasonable range for a large EV. Continued research for this project will focus on component optimization, shift dynamics, and significant experimental validation.

# References

Kamachi, M., Miyomoto, H., Sano, Y.: Development of Power Management System for Electric Vehicle 'iMIEV'. In: 2010 International Power Electronics Conference, pp. 2949–2955 (2010)

Brooke, L.: Chevrolet Volt: AEI Best Engineered Vehicle AEI-Online.Org, pp. 22–25 (2011)

Abdul Rahman, S., Zhang, N., Zhu, J.: Optimal Energy Management for Plug-in Hybrid Electric Vehicles. In: 3rd International Conference on Mechatronics, pp. 1–6 (2008)

Jinrui, N., Zhifu, W., Qinglian, R.: Simulation and Analysis o Perofrmance of a Pure Electric Vehicle with a Super-capacitor. In: Vehicle Power & Propulsion Conference, pp. 1–6 (2006)

Rudolph, F., Schafer, M., Damm, A., Metzner, F.T., Steinberg, I.: The Innovative Seven Speed Dual Clutch Gearbox for Volkswagen's Compact Cars. In: 28th Internationales Wiener Motorensymposium (2007)

Lechner, G., Haunheimer, H.: Automotive Transmissions: Fundamentals, Selection, Design, and Application. Springer, Germany (1999)

# Electric Vehicle Propulsion System Design

Ambarish Kulkarni[1,*], Ajay Kapoor[1], Mehran Ektesabi[1], and Howard Lovatt[2]

[1] Faculty of Engineering and Industrial Sciences, Swinburne University of Technology, Hawthorn, VIC 3122, Australia
[2] CSIRO Future Manufacturing Flagship, Australia CSIRO, Bradfield Rd, West Lindfield, NSW 2070, Australia
`ambarishkulkarni@swin.edu.au`

**Abstract.** Today's global community strives for a greener and cleaner environment, car manufacturers are given with the enormous task of coming out with more sustainable cars with lower carbon emissions. One of the more sustainable alternative fuel vehicles chosen by automotive manufactures is electric vehicle (EV). Currently emphasis by auto manufacturers is on development of propulsion which is low cost, light weight with optimal power outputs. In this research, major modifications will be conducted on a GM Holden Barina Spark CDX 2010 in order to convert it from a regular internal combustion vehicle into full EV propulsion. In this particular study, more specifically the modifications made on the components within the rear wheel hub and propulsion system will be analysed and looked upon in detail. This is to ensure with all the changes made to the car, the possibilities of failure of any of the drive train components are either minimized or diminished entirely to avoid any compromise on the safety of road users.

## 1 Introduction

Environmental awareness worldwide has influenced development of variety of technologies; EV is one of the commercially successful technologies. In comparison with ICEV's (Internal combustion engine vehicle) has intrinsic advantage such as zero-emission when used with sustainable resource. Many automotive companies have launched EV's in Australia and overseas including Chevrolet Volt in 2010, Nissan Leaf in 2010, Mitsubishi i-MiEV in 2009 and the Smart ED in 2011. EV industry is chosen as an alternative fuel technology by many automotive manufacturers. Many new players have come up to utilise this opportunity, such examples are Blade electric vehicle and EDAY in Australia. However many automotive manufacturers have adopted Permanent magnet propulsions (PM), which produces a very good torque, however is not very cost effective in general. These PMs also have disadvantage of using magnets which are rear earth fossils. The Switch reluctance motors (SR motors) have advantage of cost effectiveness and optimal solution to EV propulsion system. At present three factors are seen as main barriers to widespread adoption of EV technology; limited range costs and infrastructure. The objective of

---

* Corresponding author: +61 (03) 9214 8097.

this research was to evaluate EV propulsion system which is low cost low weight. The regular internal combustion engine powered 2010 GM Holden Barina Spark CDX is converted into a fully electrical powered vehicle by adding in wheel motors within the rear wheel of the car. Starting with technology mapping, several design systems including hub, shaft and motor designs will be investigated.

## 2 Electric Vehicle Propulsions

EV's date back 1890's when first ever EV was built and by early 1900 first ever in wheel motor was designed by Smith Motor Company. Environmental pollution, global warming and depletion of fossil fuels have led manufacturers and governments to choose EV as alternative technology. EV's are zero emitters when used with sustainable power source (Islam 1999; Chan 2002; Van Mierlo and Maggetto 2007; Lixin 2009). This creates an opportunity to develop and align new technologies in automotive environment. The future of EV is predicated in a higher scale though very small number of cars are seen on the roads today (Chan 2002).

EV motors are different to industrial motors since they use frequent start stop phases (Nanda and Kar 2006). Among four general types of motors, brushed DC motor, induction motor (IM), Permanent Magnet (PM) and switched reluctance motor (SRM) are typically used (Xue 2008), the SRM is used in this research. Brushed DC motor has the advantage of producing high torque at low speed, but are heavy, high cost and high maintenance, making them unsuitable (Lee 2001). IM though simple in construction and highly reliable, the shape and bulkiness makes it disadvantageous (Chan 2002; Xue 2008). Advantages with PM are weight to power ratio, since they are made up of permanent magnets. This produces a high coercive force which provides a high residual magnetic flux density. Heat deception is simple and advantageous over other motors, hence many auto manufacturers prefer this architecture (M. Ehsani; K. 1997; Zeraoulia, Benbouzid et al. 2006). Thus PM's are more efficient, compact construction and reliable than DC, induction and switched reluctance motors as well. For motor capacity and efficiency PM drives are a good choice (Jack, Mecrow *et al.* 1996). Conversely, permanent magnet motors are very expensive and permanent magnets rear earth and would depict in years to come. SR motors have potential for EV propulsions since they are simple in construction, low manufacturing cost and reasonable weight ratio. The torque-load characteristics of SRM are favorable for required EV load characteristics (Vikas, Dr. G. Tulsiram et al. 2005). Among some of challenges using SRM are space requirement and effective weight ratios. High torque ripples at low speed and acoustic noises are other associated issues in SRM technology (Ehsani 1996; R. 2001; Zeraoulia, Benbouzid et al. 2006; Xue 2008). However when designed compact and light weight these can be viable alternative in long term. When SR motor is used as in-wheel propulsion it can generate maximum torque. This increase higher efficiency and reduces losses during power transmission since packaging of gearboxes, differentials, drive shafts and axles can be removed (King 1997; Cakir 2006). This archives low weight, simple construction and low cost motor. Recently EV has gained lot of momentum in automotive industry and it becomes vital to develop a low carbon sustainable architecture in near future. As a matter of fact today many leading auto

manufacturers including GM, Mitsubishi, Testla Nissan and Toyota have launched series production of EV at early 2011. Additionally new players like Siemens, Michelin, E traction and XTi are developing in wheel drive train technology. Following are the few findings from the literature review:

- Despite potential benefits, widespread adoption of EV's faces several barriers and limitations. As of 2011, EV's are significantly more expensive as compared to conventional internal combustion engine vehicles. Other factors effecting adoption of EV's are limited range, lack of infrastructure and costs associated. From literature review and industry survey it is evident that today many automotive OEM's including GM, Mitsubishi, Ford, Nissan and Toyota are conducting research on series of production models and some examples of launched vehicles are Tesla Roadster, Mitsubishi MiEV, and Nissan Leaf.
- Literature review indicates using in wheel direct drive technology power loss is minimal since it eliminates gear and transmission components from vehicle. In wheel design simplifies with minimum parts, resulting in reduced weight, space utilisation and cost.
- The concept of the SRM was around for long time in many industrial electrical applications. Predominantly permanent magnet motors are used in EV technology as they are more efficient, compact and hence more suitable for EV. But this literature review indicates the appropriateness of SRM technology as compared to permanent magnet in context of cost and weight, though there is still a compromise with the efficiency of the motor.
- According to the industry survey in this study, Michelin displays an ingenious arrangement of a geared motor within the inside of a drive wheel. E-traction offers a self-propelled electrically powered wheel with optional electric or mechanical steering including suspension and shock dampening, delivers up to 15000 Nm of direct drive traction at the only place where it requires. XTi Hub Motors uses in-wheel technology with brush permanent magnet bi-directional DC motor and pneumatic integrated solid rubber tire.

## 3   Propulsion Design

The research objective was to develop EV by replacing propulsion of existing vehicle designs with low cost, in wheel, direct drive electric motors, whilst retaining much of the existing vehicle design, engineering, and supply chain. Replacement drivetrain, control and support systems are intended to be scalable to enable fitment to a range of vehicle types, thus spreading the research and development investment over a product range. The replacement drivetrain system currently in development uses low cost, direct drive, switched reluctance, in wheel motors which occupy the space normally occupied by the braking system, thus requiring its relocation. The drivetrain and suspension packaging requirements dictate mounting the brake disc to the motor housing rim.
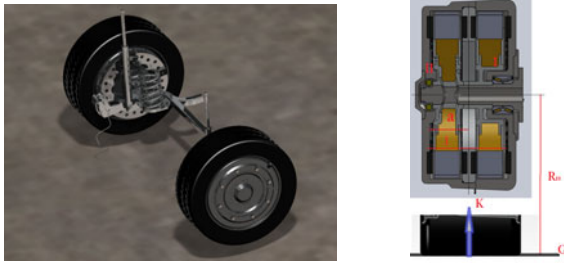
**Fig. 1.** Left: EV architecture with in-wheel SR motors (on right side is Motor tyre model for calculating bearing loads)

The SR motor is a type of electric motor run by energizing and de-energising the phases operated by reluctance torque. It consists of wound coils for the stator however none of the coils or magnets are present in the rotors. This particular type of motor has the ability to run in very high speeds and produce high efficiencies which makes it the ideal motor to be used in the EV. In this case, two bearings were required for each hub providing two supports for different purposes on different ends of the shaft while the SR motor rotates around it. The first bearing which slides inside of the hub, acts as the main load carrier, takes up high radial loads. The second bearing located on other end of hub which is also known as the outer bearing will act as a support bearing to the more dynamic end of the shaft. Unlike the previous bearing, the outer bearing is designed to allow deflection in shaft; this makes it feasible to forces both radially and axially. The shaft plays a substantially critical role as part of the hub member providing as the backbone to the system. As shown in figure 1, SR motor is planted within the rear rims of the vehicle which requires a new hub to accommodate each SR motor. Each hub consists of a bearing, shaft and the motor itself. Unlike other motors, shaft is not rotating which is completely stationary and instead, acts as the main hub support in which the SR motor will rotate around and hence rotating the wheels. Shaft role is vital as it supports the stator packs, without compromising the structural ability of the motor. The design was ensured that at no point safety was compromised or tolerated by diminishing the possibilities of failure of the shaft.

## 4   Evaluations of Design

Each and every component in the hub design was needed to be analysed, so that safety is not compromised. Each electric motor contains two bearings one for the inner section of the shaft and another one for the outer section of the shaft. Analysis has been carried out to determine whether the bearings can withstand the radial and axial loading exerted on each the outer and inner section of the shaft. From the design following dimensions are taken as reference to calculate the bearing loads

(refer Figure 1 right side view and Figure 2): $l$ = 195.2mm, RH = 241.3mm, $a$ = 98.5mm. Load acting on each wheel is taken as 4kN. However under rough operating conditions, it is increased by 20% making it K = 4.8kN, thus calculating radial loads:

FR inner = $\varepsilon_1.K + \varepsilon_2 Fk$ and FR outer = $(1- \varepsilon_1)K \pm \varepsilon_2 fK$ (1&2)

Whereby $(\varepsilon_1 = a/l)$ and $(\varepsilon_2 = R_H/l)$ (3&4)

For a commercial vehicle, $f$ is taken as 0.05 therefore, $\varepsilon_1$= 0.5046 and $\varepsilon_2$= 1.236 FR inner = 2.71kN and FR outer = 2.08kN and 2.67kN. Taking a larger value as reference centrifugal force, $K_d$ is calculated. Scenario is created considering worst case of the car taking its maximum wheel base right turn of 9.9m at a velocity of 60 km/hr. Whereby G: Weight of the car= (962kg)   ,v: Velocity = 16.67m/s, and r: Turning radius= 9.9m. Therefore, $K_d$ = 212.54. From the vehicle dimensions, wheel dia h= 482.6mm and wheel base b= 1414mm. Calculating forces acting on inner and outer bearing during the turn formula to calculate $K_d$ is:

$(K_d/ G)= (1/127) * (v/r)$ (5)

$K_{outer} = [1+ 2(h/b) (K_d/G)](4800)$ and $K_{inner} = [1- 2(h/b) (K_d/G)](4800)$ (6&7)

Thus Forces on $K_{outer} = 5.52$kN   and   $K_{inner} = 4.07$kN

$K_{a,outer} = (K_d/G) [1+ 2(h/b) (K_d/G)]K$ (8)

$K_{a, inner} = (K_d/G) [1- 2(h/b) (K_d/G)]K$ (9)
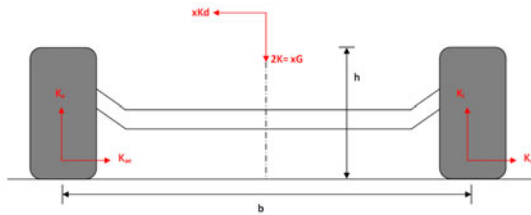


**Fig. 2.** Wheelbase model for bearing calculations.

Calculating the axial loads which will act on bearings by calculating $K_{a,outer}$ =1.22kN and $K_a$ inner = 0.98kN. The life of bearing is determined by calculating the dynamic load rating, $C_r$. Where $f_h$ = life factor. For this scenario general passenger vehicle wheel bearing life expectancy is considered 21,700 hours. From suppliers data, for the life of 21,700 hours, the life factor $f_h$ = 3.1. $f_n$ is the speed factor and is calculated using following formula:

$C_r = (fh/fn) X (Fr)$ (10)

$f_n = (33.3/rpm) 0.3$ (11)

| | Radial Load, Fr (KN) | Axial Load, Ka (KN) | Dynamic Load Rating, Cr (KN) |
|---|---|---|---|
| ■ Inner Bearing | 2.71 | 1.22 | 24.06 |
| ■ Outer Bearing | 2.67 | 0.98 | 23.68 |
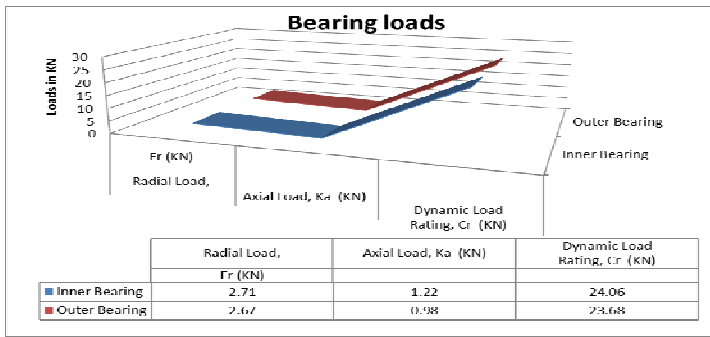
**Fig. 3.** Bearing loads for hub of EV propulsion

Where maximum velocity is 1666.67m.min$^{-1}$ and wheel diameter (Rim and Tyre) is 0.4826m therefore wheel circumference is 1.516m. Wheel RPM is 1100rpm, hence, $f_n$= 0.3502. Therefore the dynamic load rating, $C_r$ outer = 24.06kN and $C_r$ inner = 23.68 kN. This loading analysis ensures that hub designs are safe at the roughest operating conditions. Based on specifications given by supplier, the recommended inner bearing (paired tapered roller bearing) can withstand $C_r$ of up to 105 kN thus the previous calculation of 24.06kN proves it is robustly designed. For the recommended outer bearing (deep groove ball bearing), the specifications indicate that it can withstand up to 27kN which also makes it robustly designed for our calculated value of 23.68kN. Figure 3 above is a summary of loads in which both bearings perform under worst case scenarios.

## 5　Summary and Conclusions

The performance study of propulsion hub design is performed using dynamic load bearing analysis. These designs have two bearings for SR motor hub and this is due to its rugged nature of operation. One is located in the inner vicinity of the shaft and designed to withstand high load characteristics. This inner bearing is very rigid and sturdy with extremely high reliability. The other bearing, located at the outer section of the shaft and unlike the other is light weight and dynamically controlled allow radial and axial loads. This bearing allows any deflections in the shafts due to varying loads on the other end of the shaft. This is due to the close proximity of the wheel to this outer bearing. Therefore calculations were done in order to determine the maximum axial and radial loads acting on both bearings and later on the optimum bearings are selected from SKF Bearings. The dynamic load ratings of the bearing were also retrieved to further validate bearing selection.

- This research outlines development of packaging for motor which uses switch reluctance technology and can be made at substantial lower prices compared to permanent magnets. It is also understood that at this point in time there is no vehicle available which claims to have fully defined in wheel designs. For these reasons this research can be viewed as significant original contributor to the EV

technology market. SR motor is an alternative to PM motors and offers cost effective propulsion system. When designed in modular, low weight performance of SR motors are effective.

- Other advantages of the SR motor include low cost, higher heat withstanding capabilities and the robustness of the construction. Apart from that it is also learned that the existence of gears may be unconsidered hence minimising transmission loss and therefore maximizing efficiency. The SR motor is also known to be very flexible in terms of its shape and construction and allows better fitting range within an in wheel motor system whereby space is a very precious commodity.

- This not only achieves easy assembly structures but also make it modular to scale it to suite different vehicle architectures. Modularity of SR motors makes it sizable to any vehicle architectures including small, medium and mid-level sports utility vehicles. Each of the rotors, stators are packed to form assembly.

Tapered roller paired face to face for inner wheel hub bearing and single row deep groove ball bearing for outer hub to allow proper load bearing on hub bearing with allowable deflection on the deep grove ball bearing makes it feasible to allow shaft deflections. The bearing dynamic tests and their load carrying capacity during rough road rides proved to be safer. A good correlation between bearings was observed to ensure that bearings will not fail under worst case scenarios.

# References

Cakir, K., Sabanovic, A.: In-wheel motor design for electric vehicles. In: 9th IEEE International Workshop on Advanced Motion Control, Istanbul, p. 613 (2006)

Chan, C.C.: The state of the art of electric and hybrid vehicles. IEEE (2002)

Ehsani, K.M.R.M.: Performance Analysis of Electric Motor Drives for Electric and Hy-brid Electric Vehicle Applications. IEEE Power Electronics in Transportation (1996)

Islam, I.H.M.S.: Design, Modelling and Simulation of an Electric Vehicle System. Advance in Electric Vehicle Technology, SP-1417, pp. 9–16. Society of Automotive Engineers USA (1999)

Jack, A.G., Mecrow, B.C., et al.: A Comparative Study of Permanent Magnet and Switched Reluctance Motors for High-Performance Fault-Tolerant Applications. In: IEEE Transactions on Industry Applications, Lake Buena Vista, FL., vol. 32, pp. 889–895 (1996)

King, J.T.G., Chen, H.: Computer-Aided Design and Analysis of Direct-Driven Wheel Motor Drive. IEEE on Power Electronics 12, 517–527 (1997)

Lee, B.K., Ehsani, M.: Adv. BLDC motor drive for low cost and high performance propulsion system in electric and hybrid vehicles. In: IEEE International Electric Machines and Drives Conference, IEMDC 2001, Cambridge, MA (2001)

Lixin, S.: Electric vehicle development: The past, present & future. In: 3rd International Conference on Power Electronics Systems and Applications, PESA (2009)

Ehsani, M., Rahman, K.M., Toliyat, H.A.: Propulsion System Design of Electric and Hybrid Vehicles. IEEE Transactions on Industrial Electronics 44, 19–27 (1997)

Nanda, G., Kar, N.C.: A survey and comparison of characteristics of motor drives used in electric vehicles. In: 2006 Canadian Conference on Electrical and Computer Engineering, vol. 1-5, pp. 796–799 (2006)

Krishnan, R.: Switched Reluctance Motor Drives. C. Press (2001)

Van Mierlo, J., Maggetto, G.: Fuel cell or battery: Electric cars are the future. Fuel Cells 7(2), 165–173 (2007)

Vikas, S.W., Tulsiram, D.G., et al.: Performance Analysis of Switched Reluctance Motor; Design, Modeling and Simulation of 8/6 Switched Reluctance Motor. Journal of Theoretical and Applied Information Technology 4(13), 1118–1124 (2005)

Xue, X.D.C.K., Cheung, N.C.: Selection of Electric Motor Drives for electric vehicles. In: Power Engineering Conference, AUPEC 2008. Australasian Universities Sydney, NSW (2008)

Zeraoulia, M., Benbouzid, M.E.H., et al.: Electric motor drive selection issues for HEV propulsion systems: A comparative study. IEEE Transactions on Vehicular Technology 55(6), 1756–1764 (2006)

# The Low Speed Electric Vehicle – China's Unique Sustainable Automotive Technology?

Hua Wang[1,*] and Chris Kimble[2]

[1] Associate Professor in Innovation Management and Managerial Economics,
Euromed Management, École de Marseille
`william-hua.wang@euromed-management.com`
[2] Associate Professor in Strategy and Technology Management,
Euromed Management, École de Marseille
`chris.kimble@euromed-management.com`

**Abstract.** This paper discusses the emerging market for Low-Speed Electric Vehicles (LSEVs) in China and examines the various constraints and challenges it faces. It looks at some of the problems faced by those developing LSEVs and highlights the role that institutional factors play. The paper concludes with three scenarios for how the market for LSEVs in China might develop over the coming years and speculates on the wider impact this might have.

## 1 Introduction

Thanks, in part, to its national strategy of building a base of industrial competitiveness founded on "*new-energy vehicles*" (a classification that includes pure electric, electric hybrid and other forms of alternative energy vehicles), China is currently a huge laboratory for the development of alternatives to vehicles powered by the internal combustion engine. Many examples of such vehicles are now being tested by China's central and regional governments. However, the high profile new-energy vehicles are not the only market for electric vehicles in China. In parallel to this, a new market segment has emerged beyond the boundaries of the mainstream automobile industry, based around Low-Speed Electric Vehicles (LSEVs), a form of vehicle that is largely indigenous to China. In our previous work, we have focused on China's capacity for technological and business model innovation (Wang and Kimble, 2010b, 2011) that has lead to the growth of the industries that surround new-energy vehicles. In this chapter, we examine the potential impact of this lesser known aspect China's attempt to develop more sustainable forms of automotive technology.

---

[*] Corresponding author.

## 2　Low-Speed and Electric Vehicles in China

China is already a major manufacturer of low-speed light vehicles powered by internal combustion engines. Together with low-speed e-solutions for transport, such as two and three wheel e-bikes, e-scooters and e-motorcycles, these industries form the foundation for the emerging market for LSEVs. We will first examine e-mobility in China and the low-speed light vehicle industry before going on to look at LSEVs themselves.

### E-Mobility in China

The e-mobility industry, which includes e-bikes, e-scooters, e-motorcycles and other forms of electric vehicle, began in China in the early 1990s. E-bikes are bicycles with a small electric motor, an average speed of 20 km/h and cost between 1000 and 2500 ¥ ($200 and $400). E-scooters and e-motorcycles are equipped with heavier motors, have speeds between 40-80 km/h and are priced between 2000 and 20,000 ¥ ($310 and $3,100).
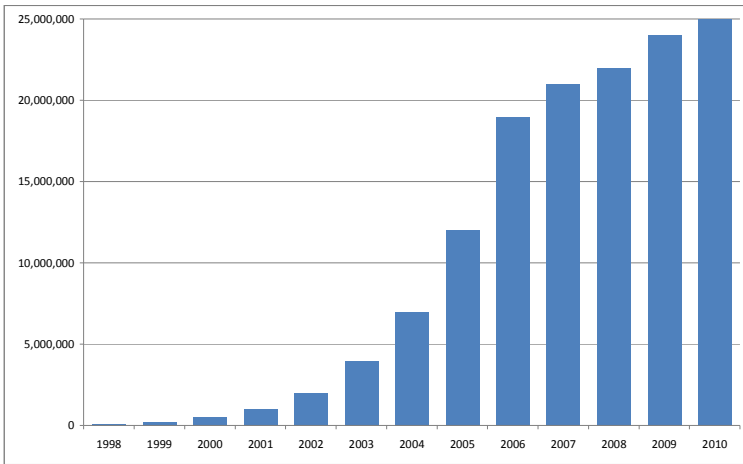


**Fig. 1.** Production of two wheel electric vehicles in China (Sun, 2010)

The production of 2-wheeled e-vehicles has grown to 25 million units in 2010, with more than 400 thousand units being built for export and is expected to reach 35 million units in 2015 (Figure 1). However, despite the high volume of production, the industry is still at an early stage. Currently the sector consists of around 2,700 licensed producers with the market share of the top 50 companies being around 50% (Sun, 2010), much lower than a mature industry.

For the Chinese consumer, e-bikes, e-scooters and e-motorcycles are now widely accepted. Ninety percent of the total production of e-bikes is for the domestic market. In 2009, there were 140 million users of e-bicycles, e-scooters and

e-motorcycles and 500 million users of standard bicycles. Over time, it is expected that a significant proportion of the users of bicycles will move to e-bicycles, e-scooters or e-motorcycles as income levels increase. It is also expected that some of these users, together with the 80 million motorcycle users, will switch to the low-speed electric vehicles that we describe in the following sections.

### Low-Speed Vehicles in China

The low-speed light vehicle industry first emerged in China in the 1980s and found a ready market in rural areas. The Chinese authorities initially used the term "farm vehicle" and later "low-speed vehicle" to describe them; they are designed to carry both people and loads for short distances along farm roads (Wang, 2002). Three-wheel models are priced between 6,000 and 12,000 ¥ ($1,000 to $1,900), and four-wheel models between 15,000 and 40,000 ¥ ($2,400 and $6,200).

The low-speed light vehicle industry is now beginning to show signs of maturity, both in terms of its sales and structure. In 1998, there were 218 companies producing low-speed vehicles, with the four leading companies accounting for 55% of the output. By 2009, there were still 207 producers, but the four leading companies now accounted for 81% of the output. Currently the market leader, the Shifeng Group, accounts for 44.7% of the total sales. Similarly, sales reached 3.2 million units in 1999 but have now stabilized at around 2 million units / year (Figure 2).
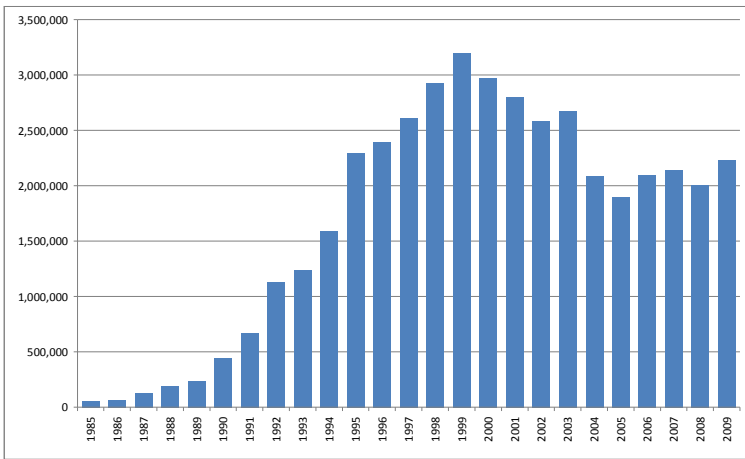


**Fig. 2.** Production of low-speed vehicles in China (CAIY)

### Low-Speed Electric Vehicles in China

The production of low-speed electric vehicles began in 2007. The market was created by the efforts of companies from a range of different industries (Wang &

Kimble, 2010a). Some, like the Shifeng Group, produced low-speed diesel and gasoline powered light vehicles; others produced golf carts, sports vehicles or special purpose vehicles like post office vehicles or ambulances. Few however came from the traditional motor vehicle industry.

The typical LSEV is composed of an accelerator, brakes, steering wheel and a lead acid battery pack. Gearshifts, air-conditioning and safety equipment are omitted to reduce the total costs. The electric motor is connected directly to the speed controller and most models do not have a sophisticated battery management or motor control system. A typical LSEV has a top speed of between 40 and 70 km/h, the dimensions of a compact car and weighs less than 1,100 kg. Depending on the number of battery packs, it has a cruising distance of 80 km, 100 km or 150 km, and costs between 20,000 and 40,000 ¥ ($3,100 and $6,200).

There are two main variants. The first is based on a golf cart, which has the advantage of low cost and a simple product platform. The only change that is needed is the addition of a car body, which is often based on some popular model of small car and is handmade using glass-fibre. For the second type, the product architecture is copied from a small, traditional internal combustion engine powered car, such as the QQ from Cherry. Here the main change needed to produce a LSEV is the replacement of a traditional engine and transmission system by an electric motor assembly and battery.

In the second type of LSEV, the car body is often purchased directly and is identical to that used in small cars; however, due to costs associated with the more complex product architecture of traditional cars, this does not significantly reduce the price. Consequently, some companies are trying to redesign the chassis and suspension to benefit from the simplicity of electric vehicles. If successful, this would significantly lower the cost of this type of LSEV.

## 3   The Market for LSEVs in China

Before discussing the market for LSEVs, it is important to note that the Chinese economy has a dual-structure, with significant differences in income between rural and urban areas. According to the China Statistical Yearbook (2010), the per capita annual income of rural households was 5153 ¥ ($790) in 2009, compared to 17,175 ¥ ($2,650) for urban households, giving rural consumers an income of less than a third of those who live in urban areas (Figure 3).

### The Value Proposition of LSEVs
Currently, the main market for LSEVs is in the rural areas of China. More than 70% of the population, around 900 million people, live in the rural areas. The first point to make about the value proposition of LSEVs is that, at 25,000 ¥ ($3,900), the purchase price of a LSEV is much more affordable that a small traditionally powered car, which is priced at around 40,000 ¥ ($6,200).
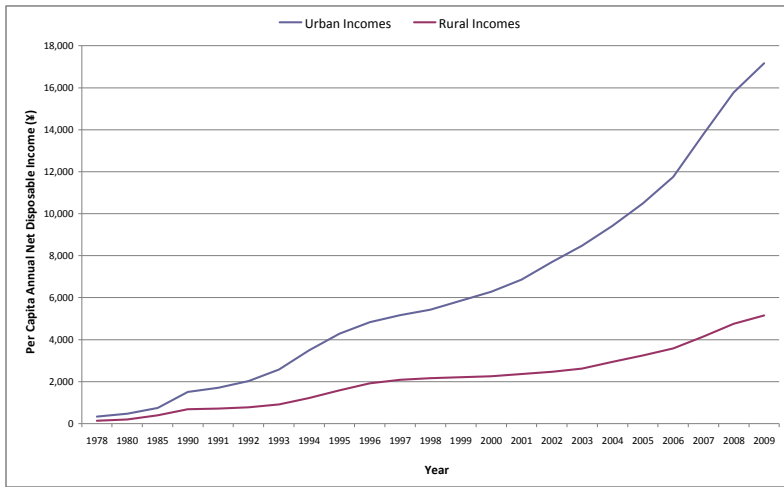
**Fig. 3.** The growing gap between rural and urban incomes (CSY, 2010)

However, the attraction of a LSEV lies not only in its low price, but also in its low running costs. The cost of the electricity needed to travel 100 km is around 6 ¥ ($0.9) whereas for a small gasoline powered car the cost for the same distance would be 49 ¥ ($7.5), or 8 times higher. In addition, the battery can be charged from an ordinary 220-volt outlet at home. In rural areas, where households have private parking spaces, this way of charging is more convenient than gasoline po-wered vehicles, as petrol station networks are not well developed in rural areas.

Thus, the LSEV has a clear value proposition to (low-income) consumers who live in rural areas; however, it may also offer certain advantages to a segment of the more affluent urban market. The top speed of a LSEV corresponds to the standard downtown speed limit of 60 km/h and offers urban consumers a good compromise between price and practicality. In addition, as most urban commut-ing distances are less than 20 km, LSEVs have the potential to meet the basic transportation needs of urban as well as rural consumers.

### Chinese Institutions and LSEVs

China is what is termed a transition economy and is still in the throes of changing from a monolithic, centrally planned economy on the Soviet model to one based on international trade with the free market economies of the West (Lukas, Tan, and Hult, 2001). Such economies are characterized by complex and often con-flicting institutional requirements that are seen by some as obstacles to developing competitive capabilities (Peng, 2003).

Perhaps the most obvious sense in which the decisions of various Chinese insti-tutions might shape the future of the LSEV market in China is the simple fact that, in most of China, LSEVs cannot be used on the road. The companies that produce LSEVs are not listed in the "*Announcement of Vehicle Producers and Vehicle Products*", an official document published by the *Ministry of Industry and*

*Telecommunication* and the "*Law of Road and Transportation Security*", which applies to the whole of China, does not have policy or regulations to cover the use of LSEVs; consequently, LSEVs have no right to use the roads.

When there is a lack of laws or regulations that clearly define the boundaries of a new industry, provincial governments often step in to develop the industry in the interests of local economy, a situation termed "*Chinese federalism*" by Qian & Roland (1998). Thus, although modifications to national laws by local authorities are not (strictly) permitted, provincial governments in areas where LSEVs are produced have created "temporary" local policies to stimulate production of LSEVs. These include, tax rebates, funding for R&D, permission to use LSEVs on roads, and tax and road charge waivers for LSEV owners.

## 4   The Implications of LSEVs for Mainstream Carmakers

Because of its low price, low running costs and the ease of charging from a 220-volt home electric outlet, the LSEV offers a clear value proposition to low-income consumers living in rural areas in China. In addition, most Chinese consumers do not have a fixed notion of what a passenger car or an electric vehicle is, which may make this type of technology more acceptable outside of rural areas.

However, for most western consumers, a passenger car is thought of as a long distance cruising vehicle that has the capacity of reaching relatively high speeds. The size of fuel tank, the power of engine and a long history of use have led us to expect our cars to carry us for long distances at speeds in excess of 100 km/h. Notwithstanding this, the reality is that most people who live in urban areas are subject to the speed limits of 50 km/h or less and travel under 50 km/day. Could the LSEV offer a new value proposition to people outside of China?

Chinese LSEVs have already begun to find markets outside of China; foreign institutional buyers (e.g. governments, police departments, hospitals, post offices and airports) have bought LSEVs as a "green solution" whilst also cutting costs. Private consumers in the US, for example, have also bought LSEVs as a second or third car. The sales of LSEVs to the US have increased from 5,000 vehicles in 2008 to around 20,000 in 2010. Will LSEVs prove to be the breakthrough that some (Wang and Kimble, 2010c) have forecast? The final section of this chapter examines some possible scenarios for the future growth of the market for LSEVs.

## 5   Scenarios for the Development of LSEVs in China

The market in China is large enough to experiment with many different types of technology and to incorporate those technologies into many different types of product. Currently these include e-bicycles, e-scooters and e-motorcycles, low-speed light-duty vehicles powered by internal combustion engines and low-speed electric vehicles. We have seen that the future development of such vehicles in China is complex, difficult to predict and involves interactions in both the

economic and the political arena. Based on a number of factors, we see three possible scenarios for the future development of the LSEV market in China.

In the first, central government does not encourage the development of LSEVs but waits for the market to overcome existing legal and institutional barriers. If this trajectory is followed then, due to the low entry cost, we predict that the industry will remain fragmented for perhaps another 10 years after which industrial restructuring, mainly driven by competition, will reduce the number of companies. Depending on developments elsewhere, this may, or may not be to the disadvantage of the Chinese LSEV manufacturers.

The second scenario offers a more pessimistic forecast. Here the central government deliberately limits the development of LSEVs, preferring instead to favour the development of electric vehicles based on designs that try to recreate the key features of western passenger vehicles. This will hinder the development of LSEV and place Chinese manufacturers in direct competition with European and American car giants.

The final scenario sees the LSEV industry flourishing thanks to appropriate interventions by central government. In this scenario, expansion into international markets and the growing commercialization of LSEVs elsewhere acts as a boost to LSEV production in China. However, while the outlook the Chinese LSEV industry is good it will almost certainly have a negative impact in Europe, America and elsewhere.

These, of course, are only possibilities. Western consumers may come to recognize the value proposition of the LSEV for short distance urban commuting and western manufacturers may begin to develop their own LSEVs, which would pose a significant challenge to the existing producers of LSEVs in China.

# References

CSY: China statistical yearbook. National Bureau of Statistics of China, Beijing (2010)

Lukas, B.A., Tan, J.J., Hult, G.T.M.: Strategic fit in transitional economies: The case of China's electronics industry. Journal of Management 27(4), 409–429 (2001)

Peng, M.W.: Institutional transitions and strategic choices. Academy of Management Review 28(2), 275–296 (2003)

Qian, Y.Y., Roland, G.: Federalism and the Soft Budget Constraint. American Economic Review 88(5), 1143–1162 (1998)

Sun, L.: The light EV in China. Paper Presented at the World Electric Vehicle Symposium and Exposition Shenzhen, China (2010)

Wang, H.: The Coexistence of Two Automotive Systems in China. Paper Presented at the 10th GERPISA International Colloquium: Co-ordinating Competencies and Knowledge in the Auto Industry, Paris (2002)

Wang, H., Kimble, C.: Betting on Chinese electric cars? – analysing BYD's capacity for innovation. International Journal of Automotive Technology and Management 10(1), 77–92 (2010a)

Wang, H., Kimble, C.: Low-cost strategy through product architecture: lessons from China. Journal of Business Strategy 31(3), 12–20 (2010b)

Wang, H., Kimble, C.: Product Architecture as a Driver of Breakthrough Strategy: The Case of Chinese Carmakers. In: Reynolds, J.V. (ed.) Emerging Markets: Identification, New Developments and Investments. Nova Science Publishers, Inc., New York (2010c)

Wang, H., Kimble, C.: Leapfrogging to Electric Vehicles: Patterns and Scenarios for China's Automobile Industry. International Journal of Automotive Technology and Management 11(4), 312–325 (2011)

# Sustainable Racing Utilising Solar Power

Simon Watkins[1] and Andris Samson[2]

[1] RMIT University, Australia
  `simon@rmit.edu.au`
[2] Aurora Vehicle Association Chairman, Australia

**Abstract.** Sustainable technologies are described for two racing types; solar racing, focussing on the World Solar Challenge (WSC), and Formula SAE-E (Society of Automotive Engineers-Electric). The former uses solar arrays on the body surface whilst the latter uses solar electricity generated in a renewable energy park and stored onboard in lithium polymer cells. The Aurora team (which has broken many records, including winning the WSC across Australia) is used to illustrate the importance of having low aerodynamic drag and frontal area, a highly efficient powertrain and low rolling resistance for "long circuit" racing. For short circuits such as FSAE Electric the R10E car from RMIT is described. The challenges of kinetic energy recovery systems (KERS) for racing are considered in order to emphasize the relative importance of different drive cycles.

## 1  Introduction

The majority of racing cars are powered by internal combustion engines utilising fossil-based fuel. However an increasing number of racing vehicles utilise electricy or hydrogen as energy carriers. This offers the possibility of renewable energy generation. Such vehicles include low energy density electric vehicles, such as the ones competing under regulations set by Greenpower in the UK [1] to higher energy density vehicles including those in the recently started EV Cup, [2]. A significant advantage of electric-powered vehicles is that they can utilise the kinetic energy that is normally "lost" whilst braking (in the form of heat) to charge batteries or supercapacitors. This can be later expended in acceleration or overcoming the non-conservative forces (aerodynamic drag and rolling resistance). This has been exploited in hybrid road cars as well as the KERS used in Formula One.   In this paper two different forms of electric racing vehicles are described that can utilise electricity generated from solar energy; solar-powered racing vehicles such as the *Aurora 101*and a new all-electric version of FSAE (Formula Society of Automotive Engineers) focussing on experiences at RMIT University.

## 2  Sustainable Racing

**Solar Racing** - For more than 25 years, futurists and adventurers have staged competitive events for solar-powered vehicles. Of them all, the World Solar

Challenge is the most significant and longest running.  Held every two years, it re-
quires competitors to cross the Australian continent using only the power of the
sun.The World Solar Challenge is currently the pinnacle of solar car competition
and ideal venue to demonstrate creative thinking and new transport technology.



**Fig. 1.** Route for the World Solar Challenge

The route comprises of approximately 2000 miles (3200 km) of sealed road, is
relatively flat and has low levels of traffic and no traffic lights. Competitors must
obey public road rules, travel during a set time period each day, and recharge their
energy storage systems using only sunlight.  The fastest cars have completed the
trans-continental course in four days at an average speed of 100 km/h.



**Fig. 2.** *The Aurora 101* Solar Racing Car in WSC.

The *Aurora 101* vehicle represents a high end entrant.  Great attention is paid to
mass minimisation with much of the body structure being carbon fibre and the

motor housing cast from magnesium.  To minimise rolling resistance Michelin developed 16-inch, 185/60 dedicated tyres with low rolling resistance coefficients.

The design of a solar powered racer is a balance between maximizing the projected surface area exposed to the sun, yet minimizing the aerodynamic drag. Over the history of the competition the shapes have changed; initially it was thought that a tiltable solar panel would offer optimum overall performance since this permits the panel to be kept at an angle that would optimise the solar input (i.e. solar tracking).   However as speeds have increased, the shapes used by the leading cars, including *Aurora 101*, have integrated the solar collection surfaces into the main body, leading to a lower aerodynamic drag but providing less solar collection.  In contrast with conventional passenger cars the shape is far more streamlined since a solar car "package" only has to house one (usually small) driver.  This shape results in negligible flow separations and a small projected frontal area, thus minimal pressure drag, see Figure 3.  Despite these challenges a road-going solar concept passenger vehicle is being designed, see Figure 4.
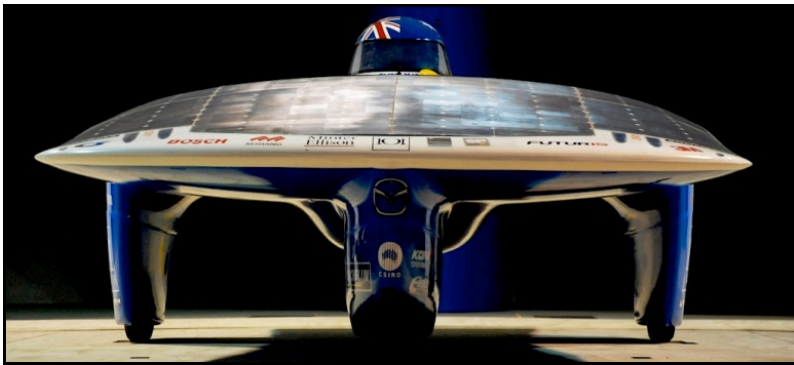


**Fig. 3.** *Aurora 101* Solar Racing Car



**Fig. 4.** Aurora Solaris Concept

The requirement to have a surface area exposed to the sun (for the solar array) results in considerable "wetted" area, which generates skin friction drag. In order to minimize this drag component the profile of the Aurora 101 is shaped to keep the state of the boundary layer laminar for as long as possible. (Note that this philosophy is also employed on some aircraft; such aerofoil shapes are often termed "laminar flow" sections. For the World Solar Challenge the average solar density is~1000 W/m$^2$ which varies during the day. The rules stipulate a maximum allowable array size that depends upon cell type. For silicon solar cells this is 6 m$^2$ with ~23% maximum efficiency. Most teams will have < 1.5 kW solar array output and energy management is extremely important as the leading cars may finish the event within minutes of each other. Solar racing cars are examples of very high operational efficiency, requiring less than 10% of the energy used by a conventional passenger car to travel at highway speed. This performance is possible in part through low aerodynamic drag and rolling resistance but also high power-train efficiency. The *Aurora 101* specifications are:

- Top speed > 150 km/h
- Daily range > 700 km at highway speed
- Power consumption @ 100 km/h < 1400 W
- Power consumption @ 150 km/h < 5500 W
- Weight < 140 kg including batteries
- 4.1 m length, 1.8 m width and 1.1 m height
- 6 m2 of monocrystalline silicon solar cells
- 22 kg of Lithium polymer batteries
- Drag coefficient x area, 0.106 m2
- Electric wheel motor efficiency @ 100 km/h > 97%
- Total drive train efficiency @ 100 km/h > 90%

Batteries are used since the rules permit storing energy from the solar panel before and after the daily racing times on the WSC. This results in teams tilting entire cars such that the solar panel is held orthogonal to the sun to maximise energy capture in the early morning and evening. The *Aurora 101* in-hub motor was designed specifically for this application and can develop a peak power of 15.0 kW for a short time but is rated to operate continuously at 1.8Kw, with an input operating range of 100-170 volts and can draw up to 100 amps. Regenerative braking is generally not used in the WSC since braking is relatively infrequent.

**FSAE Electric Racing** This class of racing arose out of the FSAE competition which traditionally used 600cc four stroke IC engines. Small four-wheeled cars are designed and built every year by tertiary level students. It is the largest student-based competition in the world with teams competing at events in America, UK, Brazil, Italy, Germany, Australia and Japan, with more events planned. Since the cars are designed for short, twisty circuits (see later) the design considerations differ markedly from solar racing cars. The rules can be found at [3].

A FSAE circuit is normally about 0.8 to 1 km long and is designed to restrict the top speeds of the cars and dynamically challenge the car and driver. This is

achieved by having many small radius bends, including hairpins typically at the end of the short (45 to <60m) straight(s) and several chicanes and slalom parts of the course. This leads to average speeds of 40 t0 50 km/hr and maximum speeds of the order of 100 km/hr, which leads to the car being in an almost continual state of either accelerating or braking. Thus a car that performs well dynamically will have an advantage over one that does less well in this regard but may have significantly greater power. The highest scoring event – the Endurance Event - comprises sufficient number of laps to give a total distance of approximately 20 km and usually 2 runs are made whereas the second highest driving event - Autocross Event - is a single lap of the circuit. Environmental concerns led to the adoption of a hybrid competition, the encouragement of ethanol fuel (with minor revisions to the rules, including reducing restrictor size) and a new event for all electric cars, which was first held in Germany in August 2010.

The first all-electric FSAE car was built by RMIT University in 2009. Denoted RO9E, it was a demonstration car, as then were no official rules for an electric competition, and utilized a relatively simple electrical system. R09E was a modified version of an earlier carbon-fibre IC FSAE race car, with the rear Yamaha 450cc engine replaced with a single, commercially available, brushed DC motor driving the solid (no differential) rear axle via a chain drive. Side-mounted battery boxes housed Lithium Thundersky cells, with extra strengthening added to the CF tub to withstand the loads imposed by the mass of the batteries.

This vehicle was followed by R10E which was intended to be "mildly" regenerative and to obtain sustainably generated electricity from solar (fixed) panels at the RMIT renewable energy park[4]. The car used a purpose-designed steel space frame with twin brushless motors(total power 40kW) controlled by two Kelly BLDC Inverter / Controllers. Each motor drives a integral 4.6:1 planetary gear boxes independently driving the rear wheels. In the intervening time between R09E and R10E battery technology had improved and this car used Dow Kokam Lithium Polymer batteries. Details are given below.

- Max charged capacity = 13.4kWh (80Ah)
- Nominal voltage = 155.4V, peak power = 150kW
- Number of cells = 84 (2x42), total mass = 82kg
- Charge time = 5-6 hours
- Advanced Elithion BMS (monitors temp and voltage during charge/discharge) and cell balancing

The most recent vehicle R11E (see Figure 7) featured further refinement utilising a ¾ carbon- fibre "tub" with a small steel space-frame chassis. These changes reduced the overall weight of the car to 246 Kg – less than some IC FSAE cars.

As with solar racing, energy management is crucial. A starting point for sizing motors, batteries and supercapacitors was a simulator to help understand the sensitivities in design parameters and energy and power tradeoffs. Note that a traditional (IC racing) lap simulator focuses on the simulation of vehicle parameters for minimum lap times – this is usually achieved by maximizing the longitudinal and lateral accelerations and decelerations around a circuit, utilizing concepts such as G-G diagrams, where the lateral and longitudinal accelerations are plotted as the

vehicle travels around race circuits.    In all-electric vehicles there is far greater sensitivity of mass to energy carrying capacity (battery energy density is orders of magnitude less than fossil fuels).  Planned regenerative braking and an electronic differential were not implemented due to the unexpected complexity (see later).



**Fig. 5.** RMIT R10E All-electric FSAE Race Car
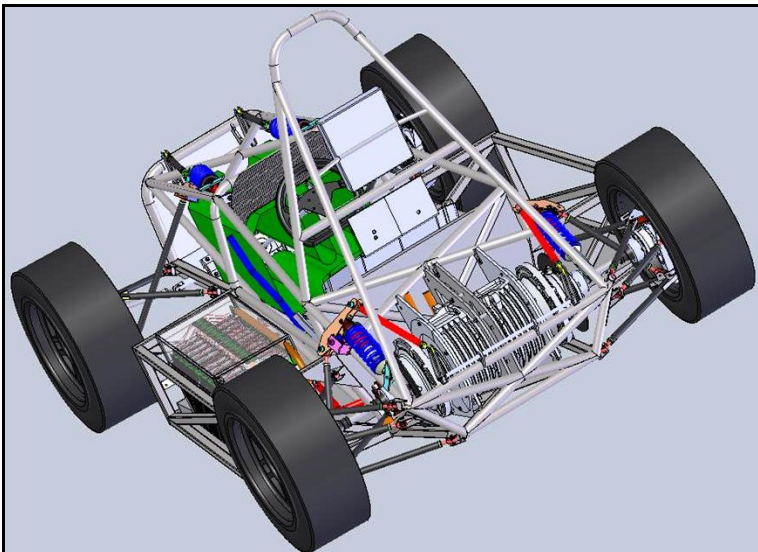


**Fig. 6.** RMIT R10E showing twin rear drive motors (the heavily finned items between the mounting plates), outboard of which are the planetary gearboxes.

**Fig. 7.** RMIT R11E All-electric FSAE Race Car

For a rear wheel drive race car, the fact that relatively little braking takes place on the rear (driven) wheels under high deceleration also makes the use of regeneration and the associated system complicated and the added mass makes it use questionable. Part of the design philosophy for a race car is for unsprung mass to be minimised. This has advantages in handling; particularly during rapid dynamic manoeuvres. In an electric car it is desirable (from a packaging viewpoint) for a hub-mounted motor/generator to be utilised. Since the mass of the motors and gearboxes is considerable this conflicts with the desire to minimising unsprung mass – thus the twin motors are mounted in-board, as can be seen in Figure 5.

To permit the relative motion of left and right rear wheel during cornering a rear differential is required. In IC racing vehicles (when a single rear drive from the IC engine is used) a variety of differentials are employed. With twin rear wheel- drive (or all wheel drive) in electric vehicles there is the possibility of varying the velocity and torque to each wheel. Whilst this provides considerable flexibility it provides new challenges in control systems. It is planned to have an electronic differential based on steering angle, yaw rate and velocity sensors.

## 3 Concluding Remarks

The driving cycle has a major influence on a cars regenerative energy requirement. For the WSC the "circuit" is long and straight thus there is no need for regenerative braking. In stark contrast is a FSAE circuit; short and tortuously twisty, resulting in cars being in a continual state of acceleration and deceleration. Road driving cycles fall between these two extremes and for typical road driving the braking and acceleration is far less demanding than road racing, lending road vehicles to more easily benefit from regenerative brakes. Despite the great benefits

to be gained in racing from regenerative braking in short circuit racing, it poses formidable challenges; the energy transfer has to be done in very short times (of the order of a second), thus systems have to cope with high power densities that are rapidly reversing. Due to mass transfer under the heavy braking most energy has to be scavenged from the front wheels thus brakes/generators should be positioned here. This brings additional mass, complexity and lack of reliability. These are challenging requirements, but if efficient solutions can be found the mass of batteries needed may be reduced and the breed will improve.

## References

[1] `http://www.greenpower.co.uk`
[2] `http://www.evcup.com/`
[3] `http://www.formulastudent.de/uploads/media/ FSE_Rules_2010_v1.1.pdf`
[4] `http://rmit.net.au/browse;ID=2su62rct92on#_ RMIT_Energy_Care`

# Solar Vehicle for South Pole Exploration

Nicholas Lambert[1], Milan Simic[1], and Byron Kennedy[2]

[1] RMIT University, Bundoora, Victoria 3083, Australia
[2] Fasco Asia Pacific, 1/14 Monterey Rd, Dandenong South, VIC 3175, Australia

**Abstract.** This is a report on the feasibility study performed to find solar energy solution for Antarctic explorations. Antarctica is one of the world's last frontiers characterized by extreme environmental conditions. Travel is expensive and difficult due to the high cost of fuel and vehicle maintenance. Given the right conditions, a solar vehicle could be a viable form of transport during the summer months. Based on the study of previous investigations shown in the articles [2], [4], and [5], we have conducted comprehensive research on the feasibility of the solar car project. A working prototype of the solar car was used for testing. We have conducted various measurements before the car departure to the South Pole.

## 1 Introduction

Antarctica explorations have many challenges. Use of fossil fuels for transportation, comes at a great cost, both financially and environmentally. A considerable amount of planning and control must be used to ensure efficient usage in order to minimize pollution to the environment [1]. We are looking for alternative solutions. Development of photovoltaic cells (PV) will allow applications of this renewable energy source everywhere and also in Antarctica. Simultaneously, there is fast progression of electric vehicle's research. This project aims to present a solution which harbors both concepts in a vehicle which could be used in Antarctica.

## 2 Solar Power

An Antarctic based solar vehicle operating in December, could receive approximately 800 - 1300 $W/m^2$ of solar irradiance, acting on the surface of the PV panels [6]. Experimental data has been collected for two 185W panels, vertically mounted to the Antartica horizon [9]. Graphical representation of the measurements is shown in Figure 1. We generated more power than expected.

The addition was contributed by Antarctica environmental characteristics as: high solar irradiance with clear air visability, low temperature, and high reflection off snow surface. Further additional power can be achieved by angling the PV panel perpendicular to the sun. More power can be gained due the reflectivity of Antarcticas suface. This allows cells that are not facing the sun to receive a portion of power. Results from the projects presented in [9] and [2] prove this.
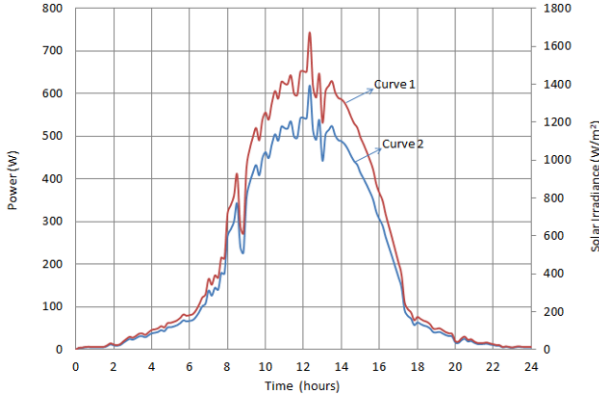
**Fig. 1.** Solar Power measure from 2 x 185 W PV within Antarctica, information is provided by team member Prof. John Storey [9]. (Curve 2: Power produced by 2 x 185 W vertical PV panels, Curve 1: Solar Irradiance)

## 3 Traction

The next step is to investigate energy requirements and losses. Resistance to the vehicle motion can be expressed by 3 components:

$$R = Ri + Rc + Ra \qquad (1)$$

Where $Ri$ represents total internal resistances, such as losses from the tires and road friction, and internal losses in the bearings and motors; $Ra$ refers to the aerodynamic drag and $Rc$ is a compaction resistance. Due to the low average speeds expected, power consumption will be mainly dominated by rolling resistance. Components $Ri$, and $Ra$ can be defined from the results of the model vehicle physical testing. Because of the sinking, the vehicle needs to overcome the obstruction caused by the portion of snow in front of the leading wheels, as shown in Figure 2. Bekker [8], Wong [7], Richmond [5], and Lever *et al.* [2] formulated the following equations to calculate $Rc$:

Flexible tire:
$$Rc / W \approx 0.5 \left( \frac{p_0^2 b}{Wk} \right) \qquad (2)$$

Sinkage for flexible tire:
$$z_0 = \left( \frac{p_0}{k} \right)^{1/n} \qquad (3)$$

where $p_0$ represents contact pressure, $b$ is wheel width, $W$ is the weight of the vehicle, $D$ is the diameter of wheel, and finally as Lever *et al.* assume $n=1$, and $k \approx 1$ MPa.m$^{-1}$ [2].
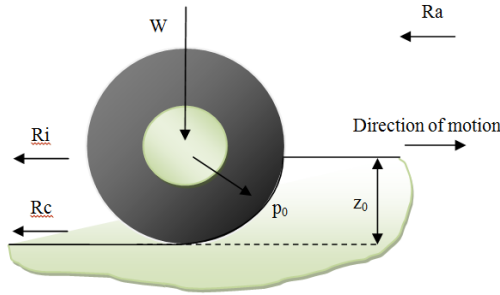
**Fig. 2.** Free body diagram of a wheel moving through a compressible medium.

## 4 Prototype Description and Physical Testing

A prototype vehicle has been built and used for testing. Main characteristics and subsystems are: Light weight with strong chassis; Large surface area of PV cells used to produce more energy; Battery subsystem for energy storage; Multiple wheels application, six in our case, in order to reduce sinkage; Large floatation tires to have low contact pressure to minimize sinkage.

The vehicle has a bespoke frame made from chromoly steel, covered in aluminum sheet and 6 wheels with the 4 rear wheels driven, each independently suspended with a single a-arm setup as shown in Figure 3. Permanent magnet (PM) electric motors with inbuilt 1:8 reduction gear boxes are used to propel the vehicle. The tires are low pressure ATV, used to help reduce sinkage. Overall vehicle weight is 270 kg, which includes battery pack and solar panel. With the floatation tires, a single a-arm suspension setup was used to ensure even tire contact independent of terrain.



**Fig. 3.** The Solar Dog, a prototype solar vehicle for an expedition in Antarctica

The prototype vehicle has an 8 m$^2$ PV panel made from 2 sets of 5 panels in series, coupled with a maximum power point tracker for each set. A 5 kWh lithium battery pack is used for energy storage and power buffering, and a dataTaker DT600 for data logging auxiliary sensors and driver controls. It is anticipated that

the 'Solar Dog' will be installed with an additional 8 m$^2$ of PV cells before the expidition. These cells will be placed on the opposite side of the main panel. Additional cells will collect reflected sun power, during operation, but will be reoriented when the vehicle is not moving to collect direct sunlight. Figure 4 shows the expected solar power that could be generated by PV panel.
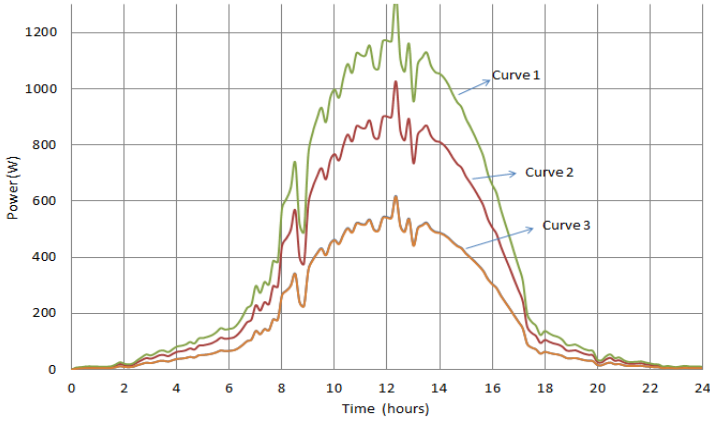


**Fig. 4.** Projected solar power over the course of a day for an 8m$^2$ panel. (Curve 1 refers to the Perpendicular panel to sun, Curve 2 refers to the Vertical panel, and Curve 3 refers to the Opposing to sun panel).
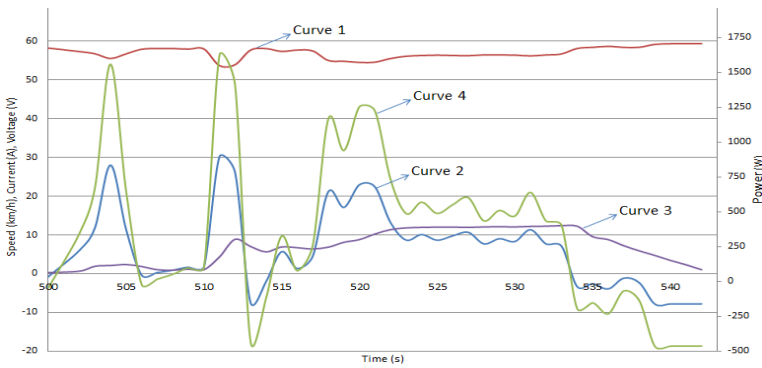


**Fig. 5.** Initial test data from datalogger for Solar Dog (Curve 1:Voltage, Curve 2: Current, Curve 3: Speed, Curve 4: Power)

Figure 5 shows the power as Solar Dog was in motion. The graph shows a simple run across asphalt and gravel. The maximum speed reached by the vehicle was 12 km/h. In that case the consumed power was only around 500 W while at

constant speed. The negative power sections within figure 5 are due to input power ether from the PV panel or, power regeneration within the motors during braking.

## 5 Power Budget

The following graph was created by applying equations (2) and (3) in order to determine the resistance to motion, for our prototype vehicle.
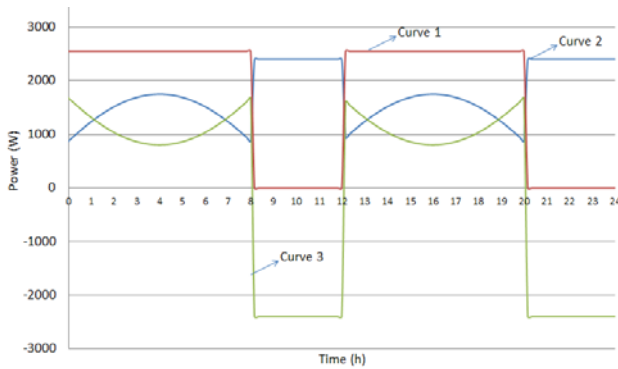


**Fig. 6.** Power requirements for "Solar Dog" over the course of 24 hours (Curve 1: Motor Power, Curve 2: Solar Power, Curve 3: Battery Power)

Figure 6 shows both the input and output power requirements for "Solar Dog" over the course of 24 hours within Antarctica. The assumptions made are: clear sky, smooth terrain with roughly about 2-3 cm of new snow, vehicle speed 15 km/h. A good strategy should be based on 8 hours of driving with 4 hours pause for battery system recharging. By defining speed and finding terrian characteristics, we can determine the required battery capacity and solar panel size which would enable solar vehicle to achieve desired performances.

## 6 Conclusion

After verification of the theoretical model with a purposely built prototype, we found that it is technically feasible for a solar power vehicle to be used for exploration within Antarctica. The next step is a trip to Antarctica.

# References

[1] Environmental Impact Assessment, ANNEX I to the Protocol on Environmental Protection to The Antarctic Treaty, The Madrid Protocol (viewed July 2011),
http://www.ats.aq/documents/recatt/Att008_e.pdf
[2] Lever, J.H., Ray, L.R., Streeter, A., Price, A.: Solar power for an Antarctic rover. Hydrological Processes 20, 629–644 (2006)
[3] Grenfell, T.C., Warren, S.G., Mullen, P.C.: Reflection of solar radiation by the Antarctic snow surface at ultraviolet, visible, and near-infrared wavelengths. Journal of Geophysical Research 99(D9), 18668–18684 (1994)
[4] Luong-Van, D.M., Ashley, M.C.B., Cui, X., Everett, J.R., Feng, I., Gong, X., Hengst, S., Lawrence, J.S., Storey, J.W.V., Wang, L., Yang, H.J., Zhou, X., Zhu, Z.: Performance of the autonomous PLATO Antarctica Observatory, over two full years
[5] Richmond, P.W.: Motion Resistance of Wheeled Vehicle in Snow, CRREL Report 95-7 (1995)
[6] CMDL. Archive of the climate monitoring and diagnostics laboratory, meteorological data measured at Amundsen–Scott South Pole station (viewed April 2011),
http://www.cmdl.noaa.gov/obop/SPO/
[7] Wong, J.Y.: Theory of Ground Vehicles, 3rd edn. Wiley-Interscience, New York (1993)
[8] Bekker, M.G.: Theory of Land Locomotion. University of Michigan Press, Ann Arbor (1956)
[9] PLATO dome A Robotic Observatory (viewed July 2011),
http://mcba11.phys.unsw.edu.au/~plato/plato.html

# Battery-to-Wheel Efficiency of an Induction Motor Battery Electric Vehicle with CVT and Adaptive Control

Stefan Smolenaers and Mehran Ektesabi

Faculty of Engineering and Industrial Sciences,
Swinburne University of Technology, Australia
Stefan.skos@gmail.com

**Abstract.** This paper addresses inefficiencies in the power-train of an Induction Motor (IM) driven battery electric vehicle. The paper provides a new drive-train and strategy solution, and a comparative study, to demonstrate an overall battery-to-wheel efficiency gain. A continuously variable transmission is coupled with an IM drive and is simulated using an adaptive control algorithm. Battery DC-Watt hours per km driven is used to test the overall battery-to-wheel efficiency. A comparative study of battery-to-wheel efficiency is then preformed. Results of this paper show an overall increase in battery-to-wheel efficiency in the FTP-75 drive cycle when using a CVT in the two vehicles modelled.

## 1 Introduction

This paper seeks to increase the overall battery-to-wheel efficiency of a Battery Electric Vehicle (BEV), by coupling a relatively inexpensive Induction Motor (IM), with a Continuously Variable Transmission (CVT). IMs have reasonable peak efficiency at full load, but efficiencies at loads of a fraction of full load torque (FLT) are significantly lower [1]. The addition of a CVT would complement the IM by allowing slight adjustments of the drive ratio, providing the required traction effort at the most efficient motor RPM and torque. When low power is needed, reducing the RPM of the motor will increase the torque requirement, utilising more of the motors available torque (FLT); thus increasing efficiency. The CVT can also increase the regenerative braking potential by spinning the motor at its optimum RPM. Due to a larger final reduction ratio, an induction motor coupled with a CVT can also generate higher negative torque, increasing braking capacity.

Models of two induction motor driven BEVs are presented with and without a CVT. The simulation will identify battery-to-wheel efficiencies across different cruise speeds as well as in the North American FTP-75 drive cycle.

## 2   Experimental Details

A model BEV is created, with customizable specifications, including: vehicle size, weight, drag, transmission and efficiency, tyre and rim data, motor parameters, VSD settings, battery power, battery energy and gross weight. This virtual vehicle can perform in a range of scenarios depending on throttle input and drive cycle.

A IM per-phase equivalent mathematical model [2] is coupled with an adaptive control loop, which uses feedback, and an iteration loop to determine the most efficient voltage, frequency and CVT value (within limits) for the requested traction effort. This powertrain model is part of a larger physics generator which then determines the behaviour of the virtual vehicle. This setup provides a robust simulation platform, which can provide the most efficient control of any vehicle, regardless of the chosen parameters. Once all parameters have been optimised and finalised, patterns in the control can be extracted to provide a less CPU intensive control algorithm to be used in a real world application. The simulations are then run with and without a CVT, and compared by the total Battery DC-Watt hours per km driven (Wh/km) as a measure of the total battery-to-wheel efficiency.

The master control unit (MCU) is responsible for controlling the motor and CVT to provide the requested torque as set by the driver or cruise control. The MCU (Figure 1)  is controlled by limits, such as how fast the CVT can change ratio's, losses involved in changing CVT ratio's, motor RPM, and the battery state of charge (SoC).

All vehicles will be assumed to be using 31Ah Dow-Kokam batteries with discharge and charge characteristics [3]. Effects of temperature are neglected and all tests are assumed to be at 20deg C. The batteries have been programmed to not accept regenerative braking above 90% SoC.

Both vehicles are also simulated with 93% inverter and HV line efficiency, and 420A RMS power capabilities. No reactance in the HV lines is accounted for except from those stated in the IM mathematical model.
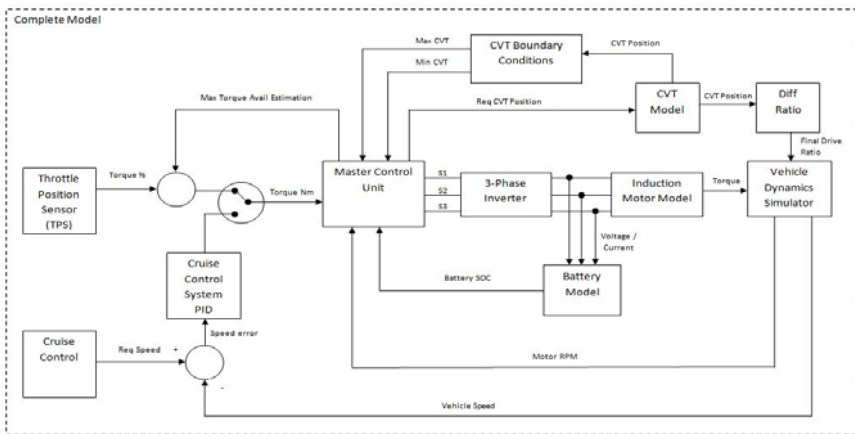


**Fig. 1.** Master Control Unit Control Diagram

The motor used in both cases has 4 poles, and is delta wound. The rotational losses of the motor have been estimated in Watts as equal to a third of the RPM.

Inertias of the drive-train and rotating bodies have been modelled. The inertias of the drive-train components are 0.388kg.m$^2$ per wheel, 0.0288kg.m$^2$ for the rear axle, and 0.1kg.m$^2$ for each pulley of the CVT and the single-speed transmission.

The equipped CVT is modelled on the JATCO CVT with a ratio spread of 7.3 [4]. The author of [5] suggests the average efficiency of a modern CVT to be between 88%-93%, therefore, in the following simulations the average efficiency of the CVT is assumed to be 88%. By contrast, the efficiency of the single-speed transmission is assumed to be 98%. The CVT and mounting is estimated to weigh 100kg more than a single-speed transmission.

## 3   Simulation Vehicle Details

Two types of vehicles were compared with and without the proposed CVT drive-train. The first vehicle was designed as a compact city car with specifications based on BMW's Mini E. Parameters used were modelled on specifications released by BMW [6] and validated against the U.S. Department of Energy Advanced Vehicle Testing Activity [7]. The second vehicle was designed as a sports car that resembles the Tesla Roadster, and the vehicles performance was based on specifications released by Tesla [8].

As per the Mini E specifications [6], the motor was modelled at 220N.m and 150kW, and the Tesla's motor was modelled at 215kW motor with 380Nm [8].

Road grade is assumed to be level, and both cars are equipped with low rolling resistance tyres with $C_{rr}$=0.01. The steady-state cruise velocity power requirement in Watts at 20deg C is estimated using the following equation:

$$P_{Req} = \frac{\frac{3}{5} * V_{MS^{-1}}^3 * C_d * A + C_{rr} * N * V_{MS^{-1}}}{1000}$$

For each vehicle, the CVT equipped model has a higher power requirement due to the assumption of much lower transmission efficiency. The increased weight of the CVT equipped vehicle also slightly increases its rolling resistance. Both vehicles were simulated for three scenarios: steady-state velocity, 100kph to 0kph deceleration, and FTP-75 drive cycle simulation.

## 4   Results and Discussion

*Steady-State Velocity*
Both vehicles were simulated with and without a CVT equipped at a steady-state velocity on a flat road. All tests were performed at 100% battery SoC, and are an instantaneous snapshot of the power requirements in ideal conditions.

EVAmerica tested the Mini E to have an efficiency rating of 147 Wh/km at 88kph, and 177 Wh/km at 105kph [7]. A comparative graph can be formed using the most efficient battery-to-wheel Wh/km value for each velocity of the single-speed transmission and CVT as seen in Figure 2.
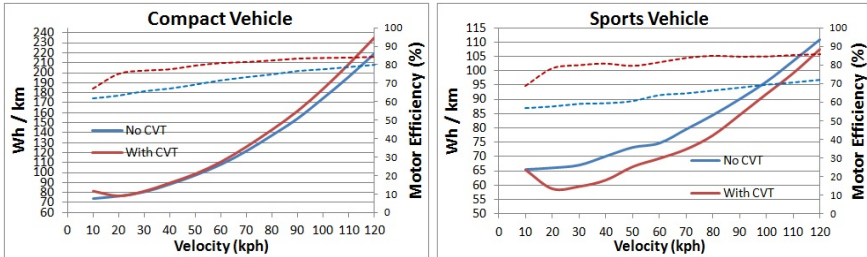


**Fig. 2.** Compact vehicle (left) and sports vehicle (right) Wh/km (solid) and efficiency (dashed) with and without a CVT.

### 100kph to 0kph Deceleration
In this test the vehicle was decelerated from 100kph to a complete stop at different deceleration rates. Here the CVT equipped vehicles extra weight plays an important factor, creating a higher kinetic energy and allowing for more regenerative braking to take place. The results of the regenerative capabilities are shown in Figure 3 for the compact and sports vehicles respectively.
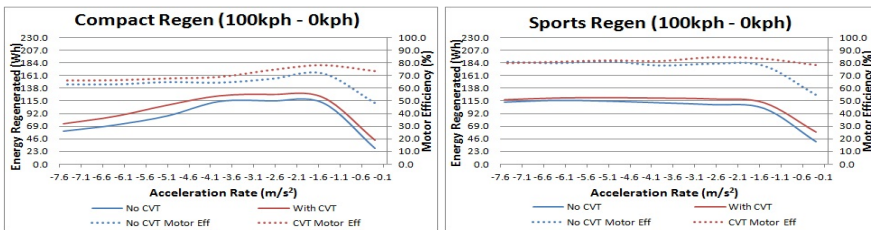


**Fig. 3.** Compact Vehicle (left) and sports vehicle (right) 100kph – 0kph regenerative braking energy with and without a CVT.

### FTP-75 Drive Cycle Simulation
The vehicles were simulated according to the North American Federal Test Procedure (FTP-75) [9]. The results of the simulation for the compact and sports vehicles are shown in Table 1 and Table 2 respectively.

The CVT equipped compact vehicle was less efficient during the FTP-75 drive cycle at full charge. This is due to the vehicle being 2.6% less efficient on average during the acceleration and cruise speed elements of the cycle. No regenerative braking charge was accepted during this cycle as the vehicle stayed above the 90%

**Table 1.** Compact FTP-75 drive-cycle results at 75% and 100% SoC, with and without a CVT.

|  | 75% SoC | | 100% SoC | |
|---|---|---|---|---|
| **Transmission** | **Single** | **CVT** | **Single** | **CVT** |
| **Energy consumed (Wh)** | 3,127 | 3,212 | 3,127 | 3,212 |
| **Energy regeneration (Wh)** | 610 | 728 | 0 | 0 |
| **Net energy used (Wh)** | 2,517 | 2,484 | 3,127 | 3,212 |
| **Watt hours per km (Wh/km)** | 141.6 | 139.8 | 176.0 | 180.7 |

SoC threshold. The CVT equipped vehicle was however more efficient overall in the drive cycle at 75% SoC when regeneration was possible. While the CVT vehicle was still less efficient during the acceleration and cruise elements, the 19% extra regenerative braking capabilities yielded a net increase in efficiency of 1.3%.

**Table 2.** Sports FTP-75 drive-cycle results at 75% and 100% SoC, with and without a CVT

|  | 75% SoC | | 100% SoC | |
|---|---|---|---|---|
| **Transmission** | **Single** | **CVT** | **Single** | **CVT** |
| **Energy consumed (Wh)** | 2,324 | 2,297 | 2,324 | 2,297 |
| **Energy regeneration (Wh)** | 565 | 686 | 0 | 0 |
| **Net energy used (Wh)** | 1,759 | 1,611 | 2,324 | 2,297 |
| **Watt hours per km (Wh/km)** | 99.0 | 90.7 | 130.8 | 129.3 |

The CVT equipped sports vehicle was more efficient during the FTP-75 drive cycle at full and 75% SoC. The CVT provided a 1.2% increase in efficiency during accelerating and cruise, and a 21% increase of regenerative braking. At 75% SoC, this yielded a significant net increase in efficiency of 9.15%.

## 4  Conclusions

From the results it can be shown that a CVT would benefit an IM driven, light and aerodynamic BEV, especially one fitted with a powerful motor. This is due to the light power requirements on the motor in most driving scenarios, causing the motor to inherently run inefficiently. The CVT however is a much less efficient means of transferring power and therefore any increase in motor performance must outweigh this decrease in efficiency. In both cases modelled, the CVT and adaptive control actively addressed inefficiencies in the operation of the vehicle. The CVT equipped compact vehicle was 1.3% overall more efficient, whereas the CVT sports vehicle gained 9.15% overall efficiency. The CVT sports vehicle regenerated 30% of the power used during the drive cycle.

The CVT's benefit could be further enhanced if the motor and vehicle were optimised for the use of the CVT.

# References

[1] Srivastava, Agarwal, P., Thanga Raj, C.: Energy Efficiency Control of Three-Phase Induction Motor - A Review. International Journal of Computer and Electrical Engineering 1(1), 1793–8198 (2009)

[2] Chapman, S.J.: Electric Machinery Fundamentals, 4th edn. McGraw-Hill (2005)

[3] Kokam Co. Ltd., Superior Lithium Polymer Battery Technical Specification (2009)

[4] Nissan. Nissan Technological Development Activities (2010),
    `http://www.nissan-global.com/EN/TECHNOLOGY/`
    `OVERVIEW/cvt.html`

[5] Heath, R.P.G.: Seamless AMT offers efficient alternative to CVT (2009),
    `http://www.zeroshift.com/pdf/Seamless%20AMT%20Offers%20Eff`
    `icient%20Alternative%20To%20CVT.pdf`

[6] BMW, Mini E Specifications, Specifications (2011)

[7] U.S Department of Energy Advanced Vehicle Testing Activity, BMW 2009 Mini E Vehicle Specifications. Electric Transportation Applications, DE-FC26-05NT42486 (2009)

[8] Tesla Motors. The Electric Tesla Roadster (2010),
    `http://www.teslamotors.com/roadster`,
    `http://www.teslamotors.com/roadster`

[9] United States Environmental Protection Agency. Testing & Measuring Emissions,
    `http://www.epa.gov/nvfel/testing/dynamometer.htm`

# Use of GSM Technology as the Support to Manage the Modal Distribution in the Cities

Grzegorz Sierpiński and Ireneusz Celiński

Silesian Technical University, Faculty of Transport,
Department of Traffic Engineering Krasinskiego 8 Str,
40-019Katowice, Poland
`grzegorz.sierpinski@polsl.pl, ireneusz.celinski@polsl.pl`

**Abstract.** The concept of use of GSM technology to manage the congestion in the agglomerations and metropolitan areas is described in the paper. The topic is reviewed from two different angles. Firstly, by the acquisition of dynamic information about relocations (with the accuracy of up to a single user and vehicle type) it becomes possible to better adapt the offer of the urban public transportation to the needs of the passengers. Secondly, the data on the identification of movements of the urban public transportation vehicles may, due to the application of GSM technology, be made available to the passengers in real time allowing them to make rational decisions on the choice of the mode of travel. The presented problem discussion is aimed at supporting the solutions reducing the congestion in the cities (in this case by changing the modal split of the traffic) and at reducing the negative influence of the transportation on the environment (the increase of the share of environmentally friendly means of transportation in the overall traffic).

## 1  Background

A transportation system is an integral part of every city's structure. Extension capabilities of such a system in a situation of the area being densely built up are largely limited. With the constant growth of a number of vehicles entering the city and high mobility an effect of a strong congestion is observed still more frequently. Such a situation is typical for a morning and afternoon rush hours but in the strict city centre area the congestion may sustain for more than ten hours during a day (especially in agglomerations). The congestion effect means not only time losses and extensive travel times. One of its effects is increased negative influence on the environment due to excessive noise, emissions ($CO_2$ and $NO_x$), increased fuel consumption and high maintenance cost of the transportation infrastructure. In addition, the increased travel time effect has influence on all the travel purposes and destinations. Public transportation buses and cargo vans travelling on the same lanes alongside passenger cars experience the same delays. In case of the public urban transportation the congestion may cause irregularities in operation leading to the reluctance of the passengers to use this form of transportation. As the number of passengers drops, the

service frequency is being reduced as well, causing further drop in the number of travellers and consequently leading even to the extreme cases of a line being not profitable and finally being shut down.

The significant growth in the number of relocations, in particular by passenger cars, causes road transportation to be the dominant energy consumer among all the branches of transportation. This implies a need to seek solutions which improve the general statistics of fuel consumption. Road transportation sector is by magnitude the second largest source of greenhouse gas emissions in the EU, responsible for ca. 12% of the total carbon dioxide emissions into the atmosphere. It is estimated that 40% of $CO_2$ emissions and 70% of all other emissions generated by transportation sector come from urban transportation [17].

One of possible solutions to the above problems is a change of the modal split towards the environmentally friendly vehicles. Switching from a car to a bus or a tram decreases the number of vehicles on the roads. One bus can replace from 30 (when only seats are taken into consideration) up to 70 cars depending on the adopted ratio of people to cars. At the same time in the subsequent years an effect of reduction of average vehicle occupancy (payload per vehicle) has been noted with the value dropping from 1.4 to 1.3 or even 1.2 passengers per vehicle.

Increasing mobility brings about not only the increase of the number of relocations but also an increase of the amount of information sent electronically and the growth in the number of telephone calls made. In a number of countries of the world the number of mobile phones used considerably exceeds the number of citizens. The users of mobile phones represent therefore the whole of the population as far as the studies of the relocations of people in towns and cities are concerned. The availability of the GSM technologies stimulates the use of the data already gathered and stored by the mobile telephony operators.

Can the use of GSM technology based solutions facilitate and speed up the introduction of changes resulting in the increase of the share of public transportation in the overall traffic? This question is approached in the current paper from two different angles:

- the area of the acquisition of data on moves and relocations of travelling persons (regardless the means of transportation used)
- the domain of real time passenger information both in the public transportation vehicles and as a support in congestion management in the cities

## 2   GSM Network as a Source of Relocation Data

In recent years a number of research and development as well as scientific institutions carry out an intensive research on data acquisition enabling calculation of the journey parameters using GSM networks. The main assumption is that the operating specifications of the GSM system allow the determination (or estimation) or moves (relocations) of the users of mobile phones/terminals (MS – mobile stations). In fact, a GSM network is not only a telecommunications network but also a specific transportation network, mapping the concrete transportation network as to its operating area. In GSM system (GSM stands for Global System for Mobile

Communications) the structure mapping by coverage of the city areas is as high as 100%.

One of the possibilities of the identification of the trip parameters based on the features of the GSM network is provided by the procedure of updating the position of a mobile terminal in the GSM network. Every GSM network is subdivided into cells, the total of which constitutes the area covered by the network. GSM network subscriber logs into the network to a base station (BSS) with the strongest signal at the point the subscriber is located. In reality, logging takes place to the nearest BTS (base transceiver station), i.e. the nearest transmitting aerial. When the subscriber moves with his terminal, also the BTS with the strongest signal changes (Figure 1). In this way the moves of the subscriber within a transportation network (and also within the GSM network) are mapped by means of the data of BTS login procedures. The described process is related to the procedure of updating the subscriber's location in the GSM network (LUP – Location Update Procedure).
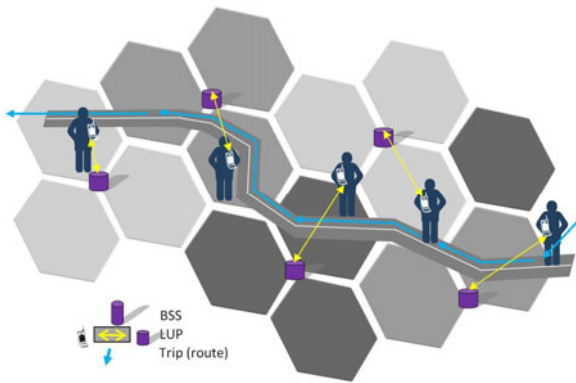


**Fig. 1.** Location Update Procedure based on GSM architecture and transportation network.

Another means of identification of a position of a user in a mobile telephony network are the procedures related to the determination of an accurate location basing on the geographic position of the mobile terminal MS in GSM network. Different methods of locating the MS terminal in a mobile telephony network structure have been described in [2,6,7,13,14,15,16].

The procedure of identification of the moves of a subscriber outlined above (and utilising the GSM network) is superior to other methods (based on questionnaires, measurements or investigations) due to the following advantages (Caceres, Wideberg and Benitez, 2007):

- data sample is large, proportional to the index of mobile phone use
- any area may be monitored, given the extent of mobile phone coverage
- no installation of additional devices is required either in vehicles or in the network for them to be monitored
- the data may be generated almost in real time

The identification of moves of a user within a GSM network structure allows also trip identification within a transportation network associated with the mobile telephony network. Main goal problem is the data correlation between the structures so that the data can be transferred across. In addition, the aggregation of GSM data allows performing interesting additional analyses as to the nature of the relocations of GSM network users as related to the transportation network [1].

In practice, the identification of the MS location is not technically complicated. Based on the location update procedure, information on the transportation-related needs can be gathered for the purposes of environmentally friendly public transportation. An important issue remains the split of the actual relocation data into the specific categories related to the means of transportation. Due to the regular situations of congestion in the city centres the allocation of a relocation data to a specific means of transportation may not be unambiguous (as noted by, among others, Gómez-Torres and Valdés-Díaz, 2011). In such a case the algorithm of identification of the means of transportation requires a combination of reasoning based on the overall route, stops (e.g. at bus stops) and the speed. Figure 2a illustrates the image of the distribution of the mobile telephony users. In a micro scale, after the relocations are superimposed on the existing road system, a dynamic picture of relocations at selected routes was obtained (cf. Figure 2b). Higher values on the graph mean higher numbers of users over a small area and hence can be identified as a trip by bus and micro-bus (mode with the capacity of >4, 5 persons).

Correct identification of the moves allows better structuring of the traffic in a city and hence allows protection against congestion and further optimisation of the offer of the public transportation (which may be executed by means of environmentally friendly means of transportation). As a further step, this leads to the change in modal split.

A key aspect issue related to such use of the GSM network is the privacy of the network users. The key data are stored on the servers of mobile network operators allowing (as described previously) precise identification of trip routes of specific persons. Thus the access to such data must be controlled and must not allow reaching a specific person personally.

## 3   Real-Time Passenger Information

Sophisticated ITS allow, besides the enhancement of the utilisation of the existing transportation infrastructure, also the accomplishment of other objectives, such as:

- improvement of traffic safety for all traffic participants
- reduction of pollution due to transportation
- reduction of transportation costs by limiting the power and fuel consumption by the means of transportation
- increase of the transportation mobility and improvement of travel comfort
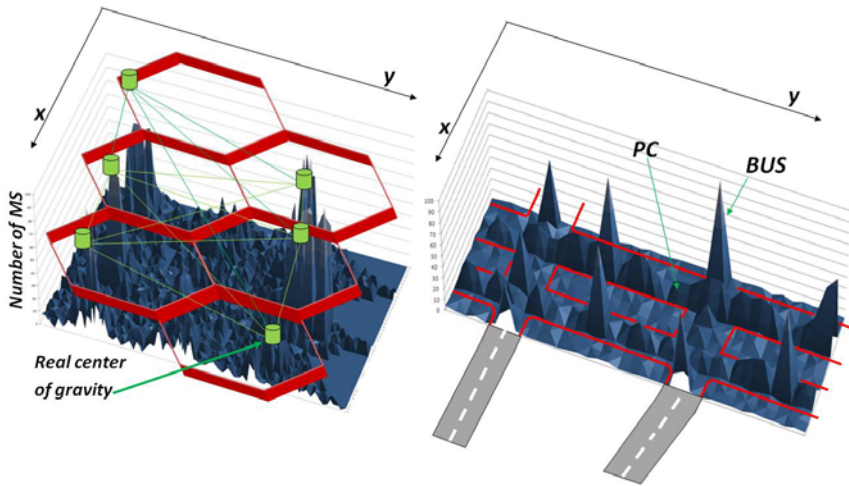
**Fig. 2.** An example image of the distribution of the locations of mobile subscribers (MS users) a) mapped o the GSM network with the reflection of the relocations, b) after mapping onto the road network.

One of the important elements of the ITS is a travel information system (other key elements are the intelligent vehicles, intelligent transportation infrastructure as well as the traffic management and control centres). The information system on the roads is most widely implemented in the form of VMS (Variable Message Signs). In some countries special radio bands (frequency allocations) are created providing current information on the traffic obstructions in specific areas. A number of other solutions exist as well.

## 3.1   The Goal: Mobility Management

The information provided to the travellers using modern technologies should influence the perception of the means of transportation alternative to passenger cars. The passengers should have the opportunity of familiarising themselves with the transportation system of the city and of the region (with the goal of reducing the congestion). Thus, the information system should, with the destination selected, provide the knowledge about (among others):

- current options of the choice of the model of transportation
- timetables of urban public transportation with actual information on the delays
- alternative routes, taking into account the real traffic obstructions
- costs and travel times in a comparative view
- current fees and charges and the ticket purchase points

In the way described above the GSM technology (often also supported by GPS technology) allows locating the individual vehicles of the urban public transportation

currently being on the route. The information on locations is transferred to the command centre by the GSM system and then is being transferred to the right sites together with the electronic passenger information. In this way a passenger receives information not only in the scheduled departure ties but also about the currently forecasted time as well as on the delays. An example of an electronic passenger information display is shown in Figure 3.
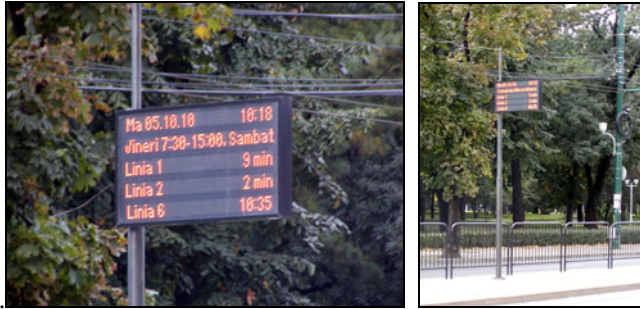


**Fig. 3.** Example electronic passenger information display for public urban transportation (City of Timisoara, Romania).

## 3.2   Integrated Traffic Congestion Management Systems versus Intelligent Navigation

Also the possibilities of using the on-board GPS/GSM devices installed in private passenger cars are worth paying attention to. Such devices may, due to the capability of defining the current location of the vehicle in the city and of communicating with the command centre, support the decision making processes in congestion management. The operating principle of the system would be as follows (cf. Figure 4a):

1.   The vehicles transmit the information about the current location and on the destination
2.   Integrated congestion management system analyses the data and distributes the traffic streams in an optimal way (so as to limit the congestion)
3.   The devices located in the vehicles receive feedback information on the route, as suggested by the system

The term 'intelligent navigation' refers to the situations when the route is indicated not directly by a device but by the urban traffic management system.

From the driver's level the situation looks as in Figure 4b). Naturally, the final decision on the route stays with the driver yet the system receives continuously full information about the traffic (assuming both the transmitters and receivers are located in every vehicle). Such a solution is related to the research work on Intelligent-car.
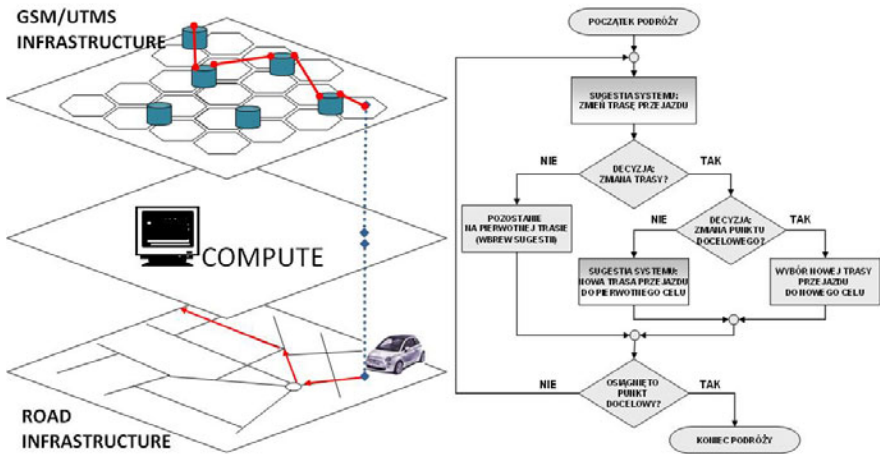
**Fig. 4.** The stages of congestion management utilising the intelligent navigation a) general diagram at the level of integrated traffic management system, b) general scheme of driver activity.

The process which is simple by assumption requires that unified GSM/GPS transponders are installed in the vehicles. At the same time, all the elements of the integrated system need to be standardized so that smooth run is possible across the areas with traffic management in the neighbouring cities or agglomerations.

## 4   Final Remarks

The paper presents the selected applications of the GSM technology supporting the activities aimed at changing the modal split in the city traffic. Such changes, favouring the increase of the share of alternative means of transportation (e.g. green cars, car-sharing systems, clean buses, trams and bicycles) are becoming necessary. The reduction of congestion in the cities (as it generates most transportation losses in the form of time losses, harmful emissions, noise pollution and fuel consumption) is possible by changing the modal split of the traffic. It requires the physical activities from the traffic engineering domain, implementing a right transportation policy, media information, business activities and informing the society about the changes undertaken. Only full integration will bring proper result - the sustainable transportation.

Modern technologies, such as GSM create new opportunities of reaching the ultimate goal of sustainable transportation. This is achieved, among others, by provision of the information on the relocations and moves. The described method allows, among other:

- to determine the main traffic flows in the city (from the perspective of relocations); it can therefore support the urban public transportation at selected routes, for example by increasing the frequency of operation,
- to identify the routes in the network which have not been considered so far as appropriate to open new public transportation lines,
- to estimate the particularly high intensity of relocations on specific routes (source-destination relations) at specific times; this allows to make the operation of the urban public transportation more efficient.

The above listed activities form a basis for a change of habits of the travellers, which may result in the change of the mode of transportation from a passenger car to a urban public transportation.

## References

1. Caceres, N., Wideberg, J.P., Benitez, F.G.: Deriving origin-destination data from a mobile phone network. IET Intelligent Transport Systems 1, 15–26 (2007)
2. Celiński, I., Sierpiński, G.: The Study of Modal Distribution of the Travel Based on Mobile Phone Networks Data. In: IIIrd International Scientific Conference Transport Problems. Katowice - Tarnowskie Góry (June 20-22, 2011); International Scientific Journal Transport Problems (in press)
3. Fontaine, M.D., Yakkala, A.P., Smith, B.L.: Probe Sampling Strategies for Traffic Monitoring Systems Based on Wireless Location Technology. Final Contract Report FHWA/VTRC 07-CR12
4. Gómez-Torres, N.R., Valdés-Díaz, D.M.: GPS Capable Mobile Phones to Gather Traffic Data. In: Ninth LACCEI Latin American and Caribbean Conference (LACCEI 2011), Engineering for a Smart Planet, Innovation, Information Technology and Computational Tools for Sustainable Development, Medellín, Colombia, August 3-5 (2011)
5. Green Paper. Towards a new culture for urban mobility. COM, 551 (2007)
6. Privat, L.: Orange to Provide Road Traffic Data Based on GSM Signal, http://www.gpsbusinessnews.com/
7. Rutten, B., van der Vlist, M., de Wolff, P.: GSM as the Source for Traffic Information. In: European Transport Conference (2004)
8. Sierpiński, G.: Cars Navigation and Drivers Behavior in Roads Disturb Situation. vol. 6, Logistyka – Nauka (2009)
9. Sierpiński, G.: Modeling of City Traffic and Sustainable Development. In: 14th International Conference TRANSCOMP, Computer Systems Aided Science, Industry and Transport, Zakopane, December 6-9, vol. 6, pp. 3027–3034, Logistyka – Nauka, (2010)
10. Sierpiński, G.: Travel Behaviour and Alternative Modes of Transportation. In: Mikulski, J. (ed.) TST 2011. CCIS, vol. 239, pp. 86–93. Springer, Heidelberg (2011a)
11. Sierpiński, G.: Integration of activities as a method to the sustainable mobility. In: Janecki, R., Sierpiński, G. (eds.) Contemporary Transportation Systems. Selected Theoretical and Practical Problems. New Culture of Mobility, Monography, nr. 324, pp. 93–102. Publishing House of Silesian University of Technology, Gliwice (2011b)

12. Sobh, T., Elleithy, K., Mahmood, A., Karim, M.: Innovative Algorithms and Techniques in Automation, Industrial Electronics and Telecommunications. Springer, Netherlands (2007)
13. Ule, A., Boucherie, R.J.: Adaptive dynamic channel borrowing in road-covering mobile networks. Faculty of Mathematical Sciences, University of Twente, University for Technical and Social Sciences (2001)
14. Valerio, D.: Road Traffic Monitoring from Cellular Network Signaling. FTW-TR-2009-003, No. of Pages: 48 (2009)
15. Valerio, D., D'Alconzo, A., Ricciato, F., Wiedermann, W.: Exploiting Cellular Networks for Road Traffic Estimation: A Survey and a Research Roadmap. In: IEEE 69th Vehicular Technology Conference (IEEE VTC 2009-Spring), Barcelona, Spain, April 26-29 (2009)
16. Valerio, D., Witek, T., Ricciato, F., Pilz, R., Wiedermann, W.: Road Traffic Estimation from Cellular Network Monitoring: a Hands-on Investigation. In: IEEE 20th Personal Indoor Mobile Radio Communication Simposium 2009 (IEEE PIMRC 2009), Tokyo, Japan, September 13-16 (2009)
17. Keep Europe moving - Sustainable mobility for our continent. Mid-term review of the European Commission's 2001 Transport White Paper, 314 (2006)

# Future Mobility in Tropical Megacities

R. Kochhan and D. Gleyzes

TUM CREATE Centre for Electromobility, Singapore. Research Office. 62 Nanyang Drive, Block 1.2, #01-28/29, Singapore 637459
Tel.: +65.6592.1612
`robert.kochhan@tum-create.edu.sg`

**Abstract.** Based in Singapore, TUM CREATE focuses on a holistic approach towards electric mobility in tropical megacities. One field of research within TUM CREATE deals with the development of transportation concepts for tropical megacities like Singapore. Urban mobility in tropical megacities can be expected to change dramatically in the future. Understanding how tropical urban mobility can look like in the next ten or 20 years would be advantageous for car manufacturers as well as for researchers. This article provides an overview of a possible approach to analyse future mobility in tropical megacities. It mainly aims towards the opportunities of defining and using future scenarios to derive feasible and suitable vehicle concepts for megacities like Singapore. It also shows the possibilities of a breakthrough in battery technology which can have an impact on future scenarios.

## 1 Introduction

Different definitions of megacities can be found. According to the UNO, megacities have more than ten million inhabitants [6, 13]. Other definitions say that urban areas with a minimum population of five million people can be considered as egacities [9]. Regardless the definition, megacities worldwide are very different concerning climate, cultural background, density and several other factors. This is why it makes sense to focus on some cities which have certain similarities.

With TUM CREATE being based in Singapore, this research is supposed to focus on tropical megacities. This constraint makes it possible to develop vehicle concepts which fit into a tropical urban environment. In this case, "vehicle concepts" means vehicle type (2-wheeler, 4-wheeler, taxi, bus etc.) including usage models like buying, leasing, renting, car-sharing or public transportation. Moreover, some problems of megacities seem to be more evident in emerging markets where many tropical megacities are located: air pollution due to feeble emission regulations, noise pollution due to high numbers of scooters and motorbikes or traffic jams due to inefficient transportation planning. Over 70 million people live in major South-East Asian metropolitan regions with more than ten million residents (calculation based on [13]), which is a large potential market. Hence, megacities in this region could be a first reasonable selection of cities being a basis for this research.

## 2  Scenario Planning

In general, the future is not predictable. According to [5], scenarios are conceptions of the future which are justifiable. A scenario can be considered as a description of a possible future situation, including the way to get to this situation. It is possible to make and justify assumptions about the development of factors influencing a future situation.

Scenarios should be clearly distinguishable and consistent [5]. Hence, it often makes sense to develop and analyse a small number of two or three scenarios only. Following this, three different scenarios to analyse mobility in tropical megacities could be set up:

- One *trend* scenario of influences on future mobility in tropical megacities reflecting one highly probable development. This scenario will certainly be based on facts and figures about current and past developments which allow making justified projections into the future. Hence, the main work will be to gather the necessary data.
- Two *alternative* scenarios which can contain trend-breaking developments of selected factors influencing future mobility in tropical megacities. These scenarios could be derived from the trend scenario by varying the development of some of the influences which make up a scenario.

As many tropical megacities are situated in emerging markets, mobility in these cities in ten, fifteen or 20 years may look completely different than today. This future development of mobility certainly depends on many factors of different nature.

A basic assumption of the Scenario Technique is that the topic to analyse is influenced by external factors [5]. These influencing factors may vary between the cities. In order to analyse these influences, scenarios can be set up. Therefore, several approaches exist [10, pp. 230-232; 2, pp. 807-808]. Hence, in order to develop the scenarios, external influences having an impact on the mobility situation in megacities need to be defined.

A description of process steps of scenario planning to develop and analyse scenarios can be found in [5]. One of the first steps is to clearly define the impact factors. The following mindmap shows a first overview of fields of impact on mobility in megacities, including possible main impact factors of each field. In [7], some comparable groups of factors can be found to analyse the German mobility market.

So far, the work progress showed that there are many sub-categories of the different impact factors in figure 1. Moreover, interdependencies between them exist. This is why it is important to group them to a small number of key factors. Then, in order to determine the interdependencies, these factors can be structured in a matrix [5]. It helps to identify how the factors depend on each other. Some factors can have a strong impact on others and some are mainly influenced by others, but do not have much impact.
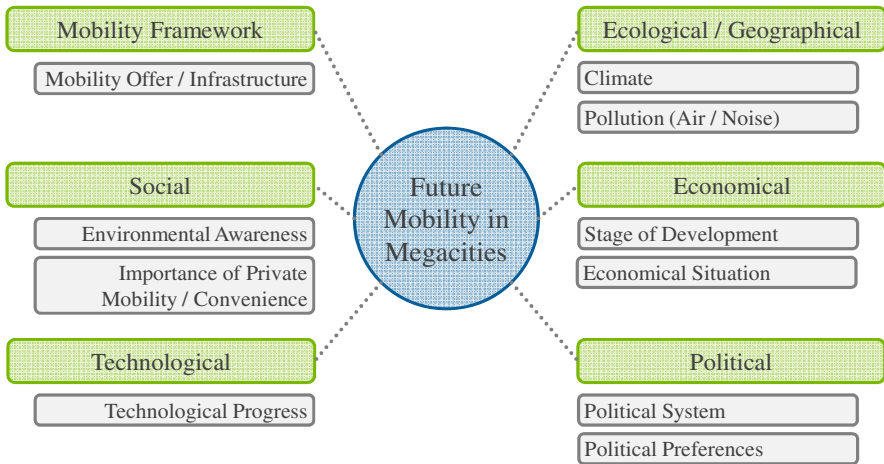
**Fig. 1.** Fields of impact [referring to 4] and possible impact factors influencing mobility in megacities

Based on the key factors, the scenarios can be set up. Therefore, their development needs to be predicted. Experts can be involved into this procedure in order to make plausible statements about the future development of the influencing factors, and also to make assumptions about how probable it is that they develop this way [7]. In this case, it seems to be reasonable to involve experts related to each of the fields shown in figure 1. It also makes sense to involve locals who can describe the situation in their cities from their point of view. Additionally, existing studies about future mobility scenarios in megacities certainly can provide a good basis for this research. However, it can be misleading to attach probabilities to the scenarios. As the future cannot be predicted, a scenario should simply be considered as one possible evolution among others.

At the end, a small number of scenarios are supposed to give an overview of the development of important influences on future mobility in selected tropical megacities. They also should be a basis providing hints for new ideas about vehicle concepts and usage models in these cities. Consequently, the scenarios cannot be considered as complete mobility scenarios, but rather as scenarios of factors which have an impact on future mobility in tropical megacities.

Studies for the German market have shown that it is possible to make plausible statements about future mobility using the scenario technique. Several developments which were predicted in earlier studies (2002 and 2005) could be confirmed later [8]. The further we look into the future, however, the more uncertain these predictions become, because the number of possibilities of evolutions of the impact factors increases [5]. This effect is symbolised by the funnel in figure 2.
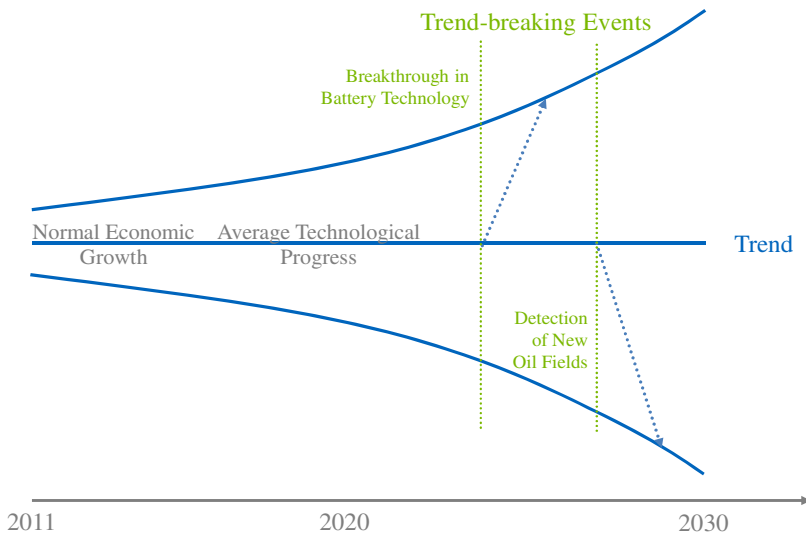
**Fig. 2.** Example of a *Scenario Funnel*: a scenario for 2030 is more uncertain than a scenario for 2020

Figure 2 also shows the effect of trend-breaking events. These events are sudden happenings that cannot be predicted and that break the normal development of some impact factors [5]. They can change future scenarios and let research continue on a different level. The "trend" scenario could be considered as one probable evolution of the factors influencing future mobility in tropical megacities. For example, the scenario could contain steady technological progress and average economic growth.

## 3  Next Steps

Scenario planning and analysis can be used for a wide range of topics, with mobility being only one of them. Certainly, many research results about future mobility in megacities exist already. Regarding this, the main work on the scenarios will consist in assembling relevant pieces of information to build up a basis for further steps.

Thus, a key question of this research is how the scenarios can provide a basis to derive vehicle concepts and related usage models which are suitable for tropical megacities of 2020 or 2030.

One possibility could be to use the scenarios in order to get an idea of future customer behaviour. This behaviour can be considered as a consequence of the external influences which change the customer's environment. Therefore, techniques or methodologies need to be found that help to clearly define a relationship between the external influences and (individual) customer behaviour. Then, this behaviour would be a basis to derive vehicle concepts which are feasible and which make sense regarding the future situation described by the scenario.

For example, progress in electric vehicle technology and a high oil price could make battery electric vehicles (BEVs) more affordable than conventional ones with internal combustion engines (ICE). Additionally, political regulations could discourage people from using private vehicles, for example by high taxes, as it is already done in Singapore. Assuming a certain price sensitivity of the customers, electrified public means of transportation like electric buses would be a suitable solution. A detection of new oil fields would probably have the opposite consequence due to deceasing fuel prices (see figure 2).

Consequently, the intermediate step of a stereotype customer's behaviour regarding external influences is supposed to facilitate the further work. It can be difficult to define this link between scenarios and vehicle concepts because this requires clustering individual customer's behaviours in different megacities. Hence, methods which allow concluding directly from the scenarios onto vehicle or mobility concepts could be more promising. It remains to become apparent how far the procedure described above can lead. Figure 3 contains a summary of this approach.

Despite the focus on tropical megacities, it can be challenging to define vehicle concepts which meet the requirements of all these cities in the same way. Some of the possible impact factors like cultural background, political system or stage of development are still too different so that there might not be one single vehicle concept for all tropical megacities. It could make more sense to group megacities with certain similarities and, on that basis, define vehicle concepts. The advantage of this approach is that the result would be valid for a certain number of places. This means that the target market could be large enough to economically develop and produce specific and adapted types of vehicles.
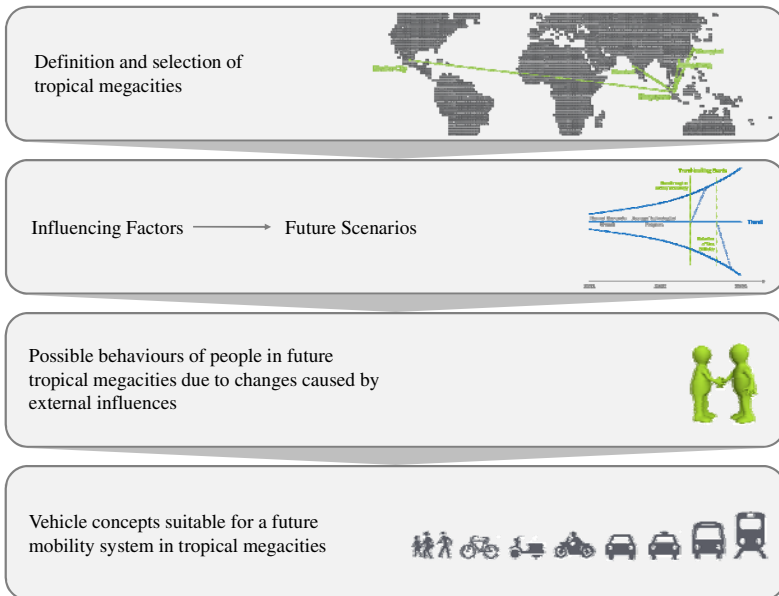


**Fig. 3.** Possible workflow towards vehicle concepts for future tropical megacities

**Comments on trend-breaking events: breakthroughs in battery technology**

As explained above, a progress in battery technology and a high oil price can support the introduction of BEVs. Compared to cities in Europe or Northern America, more efforts could be necessary to set up electric vehicle infrastructure in tropical megacities located in emerging markets. Trend-breaking events concerning electric vehicle technologies, however, are most likely not specific for tropical megacities. Variations of the oil price would be a worldwide phenomenon. A breakthrough in battery technology, which is hereafter outlined more in detail, would also have a global impact.

State-of-the-art automotive batteries face several challenges:

Firstly, batteries are very costly. According to [3], battery systems cost about 1,000 US$/kWh at low production volumes for OEMs today, including the battery management and cooling systems. The Nissan Leaf, a mid-sized private car, has a battery capacity of 24 kWh [11], which implies battery costs of 24,000 US$ for the OEM. Considering the OEM and dealer margins, the end customer needs to pay even 40 to 45 % more [3].

Secondly, the energy density of today's batteries is still relatively low. State-of-the-art battery systems for use in BEVs have a specific energy of 80 to 120 Wh/kg [3], which is less than one percent of that of gasoline (13 kWh/kg). This low energy storage capacity limits the range of the vehicles. Based upon the Environmental Protection Agency (EPA) five-cycle test, the Nissan Leaf has a driving range of 73 miles ($\approx$ 117 km) [11], which is very low compared to similar ICE driven cars.

Thirdly, the time to recharge the battery takes much longer than refuelling gasoline. For example, charging the 24 kWh battery of the Nissan Leaf to 80 % by means of the 3.3 kW on-board charger takes roughly six hours.

Finally, further challenges to overcome are increasing the battery safety [12], extending the lifetime and improving the performance for use under different climate conditions.

Currently, OEMs try to *solve* some of these challenges by using bigger battery packs [3]. They allow storing more energy for a longer range of the vehicle, they provide sufficient power even at adverse temperatures and they still have a sufficient energy storage capacity after a large number of charging cycles and years of usage. However, larger batteries increase the price and weight of the vehicle. Thus, a breakthrough in battery technology means to achieve a progress concerning one or more of the challenges mentioned above: higher energy density, shorter charging times, longer battery lifetime, safer batteries and high performance at all temperatures without significantly increasing battery costs.

Considering these challenges, breakthroughs in battery technology could be:

Firstly, 70 to 75 % of the battery costs are volume dependent [3]. Hence, battery production technology allowing cheap (automated) mass production of battery cells and packs could significantly reduce the costs for BEVs. In order to reduce the battery price of the Nissan Leaf to under 5,000 US$, costs of around 200 US$/kWh need to be achieved. According to [3], this is not likely to happen within the next 10 years.

Secondly, concerning the energy storage capacity, increasing today's average energy density in battery cells by the factor five would result in a range of the Nissan Leaf of 365 miles ($\approx$ 587 km). This would make it more comparable to nowadays ICE cars.

Thirdly, the charging time could be reduced using technologies such as fast charging or battery swapping. With a 200 kW fast charging station [1] and improved cell chemistry, the Nissan Leaf could be recharged within only 8 minutes. An alternative could be a redox-flow battery containing an exchangeable (semi)fluid electrolyte. This opens new possibilities of on-board electrical storage such as rapid refuelling of vehicles by fuel or tank exchange [4].

The probability of a breakthrough in battery technology is high. Between 1999 and 2008, patent filings on battery topics increase by 17 percent which is twice as much as in the previous ten years, and above-average in comparison to the overall patent growth in the same period of time [3]. With the on-going interest of the public in electric mobility one can expect an even increasing R&D effort and – similar to the mobile communications industry in the last decades – regular breakthroughs in the future.

# References

[1] ABB: Electric Vehicle Infrastructure, DC Fast Charge Station; product information sheet (2011)

[2] Bradfield, et al.: The origins and evolution of scenario techniques in long range business planning. Futures 37(8), 795–812 (2005)

[3] Dinger, et al.: Batteries for Electric Cars. Challenges, Opportunities, and the Out-look to 2020. The Boston Consulting Group (2010)

[4] Dudata, et al.: Semi-Solid Lithium Rechargeable Flow Battery. Advanced Energy Materials Journal 1(4), 511–516 (2011)

[5] Geschka, H., Schwarz-Geschka, M.: Einführung in die Szenariotechnik. Geschka & Partner Unternehmensbetratung, Darmstadt (2011); document for information

[6] GlobeScan, MRC McLean Hazel: Megacity Challenges, A stakeholder perspective. Siemens AG, Munich, Germany

[7] IFMO: The Future of Mobility, Scenarios for the Year 2020; Institute for Mobility Research, Berlin, Germany (2002)

[8] IFMO: Zukunft der Mobilität, Zenarien für das Jahr 2030. Institute for Mobility Research, München, Germany (2010)

[9] International Year of Planet Earth: Megacities – our global urban future. Earth Sciences for Society Foundation, Leiden, The Netherlands (2005)

[10] Mietzner, Reger: Advantages and disadvantages of scenario approaches for strategic foresight. Int. J. Technology Intelligence and Planning 1(2), 220–239 (2005)

[11] Nissan USA: Nissan LEAF, features + specifications; product data sheet (2011)

[12] NTHSA: Statement of National Highway Traffic Safety Administration On Possible Fires in Lithium-Ion Vehicles Involved in a Crash (November 11, 2011) (press release)

[13] UN: World Urbanization Prospects, The 2009 Revision. United Nations Population Division, New York, USA (2010)

# Energy Efficiency Development of Urban Passenger Transport in China

Li Zhenyu[*], Zhang Min, and Chen Xumei

Associate Professor in CUSTReC, China Academy of Transportation Sciences (CATS),
Ministry Of Transport, P.R. China
`lizhenyu_sxcz@163.com`

**Abstract.** Considering the global energy shortage, the improvement of energy efficiency is one of the most important tasks in China's urban passenger transport. But what is the potential improvement and what policies are needed in the next two decades for it. Based on the current situation in China, this paper introduces a methodology and a simple model based on it to calculate the future energy demand in the urban passenger transport. The energy demand scenario analysis is used to analyse the different energy demand and the efficiency changes. Finally, this paper gives some policy options for the improvement of energy efficiency in the urban passenger transport in China.

## 1   Introduction

Energy consumption from transport has been increasing at a faster speed than any other sectors in China, now the transport sector is the one of the largest emitters of greenhouse gases in China. Urban transport is a major part in the overall energy consumption in the transportation. The growing focus on global warming places big pressure on urban transport to reduce its $CO_2$ emission. The most powerful driver of the fast growth in transport energy consumption is rapid urbanization and motorization, particularly in cities. Rapid economic growth, urbanization and motorization contribute directly to the growth in energy consumption in China cities, notably through: (i) increased trip-making; (ii) increased trip distances; (iii) lower fuel economy; (iv) shift towards motorized, low-capacity modes (Zhou, 2005). Rapid motorization is also causing severe urban traffic congestion, traffic injures and urban air pollution.

For the international energy consumption and energy demand of urban transport, some researchers calculate the transport energy demand by running the models such as AIM/Technology, LEAP, and others (Jiang, 2008). Based on the GEF project, the World Bank calculates the energy use of urban transport from 2002 to 2006 in China, and gives the energy intensity by trips (Darido, 2009). Wright and Fulton (2005) calculate the transport energy use and $CO_2$ emissions patterns by considering different factors including behaviour, design and technology.

---

[*] Corresponding author.

## 2    Methodology

A number of factors in urban transport contribute directly and indirectly to the potential growth in energy consumption, including the number of vehicles, travel demand, model split, vehicle kilometre travelled (VKT), land-use patterns and fuel efficiency of different transport modes.

For the future energy demand growth, considering the factors above, based on the actual statistic system in China, a methodology is given and a simple model is made in this paper according the new methodology. In the methodology, the energy consumption of private transport can be calculated by the equation (1), while the energy consumption of public transport can be calculated by the equation (2). In the both two equations, $E$ is defined by the energy use, $i$ is defined by the transport modes. VKT is defined by the number of vehicle kilometre travelled per year. Occupancy is defined by the number of persons in each vehicle. In equation (3), PKM is defined by passenger turnover per year.

$$E(i) = \text{Vehicles}(i) * \text{VKT}(i) * (E/\text{VKT})(i) \tag{1}$$

$$E(i) = \text{Trips}(i) * \text{Trip distance}(i) * (E/\text{PKM})(i) \tag{2}$$

$$\text{Energy Intensity}(i) = E(i)/\text{PKM}(i) \tag{3}$$

For the indicators of energy efficiency of urban transport, without any national or international normalization until now, different indicators are used to evaluate the energy efficiency of urban passenger transport. Although in the China's statistic system, the trip is the only indicator to monitor the transport efficiency. From my point of view, the energy consumption per PKM is a better and more scientific indictor than indicator of energy consumption per trip.

## 3    Scenario Analysis and Evaluation

Scenario analysis of energy consumption growth in the period from 2005 to 2030 is developed. It includes the future travel demand forecast and the energy consumption in different scenarios. An evaluation of the improvement potential because of shift from private car to public transport and new energy application is conducted in the analysis. Two scenarios are defined:

1. Business as Usual (BAU): with rapid car growth and no obvious technological improvement, the existed energy saving policy will continue to be executed, and public transport will be improved steadily.
2. Energy saving scenario: Reduce transport demands by different measures such as compact city, improve public transport greatly (+20%), rational use of private cars, on-line service, encourage Non-motorized-Transport (NMT).

The main characteristics impacting on energy efficiency of urban passenger transport are identified. According to the report of Policy for Energy Saving of Urban Transport in China (Jiang, 2009), the Annual Report on Sustainable Transport Development in Chinese Cities (CUSTReC, 2007) and the different middle and long term plans, the future development tendency is forecasted as follows.

## 3.1    Population and Urbanization

In the next few decades, the "One family, one child" policy will continue to be executed in China. According to the Plan from National Population and Family Planning Commission of China, the prediction of population growth by using the IPAC-Population Model, the population will increase and the summit will be between 2030 and 2040. In 2009, the urbanization rate is 46.6% in 2009, and it will be 60%, 70% in 2020, 2030 respectively in Figure 1 (ERI, 2009).
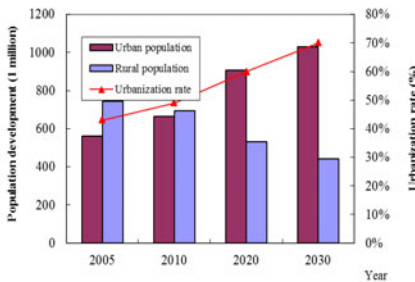


**Fig. 1.** Population and urbanization          **Fig. 2.** Urban passenger trip growth in China
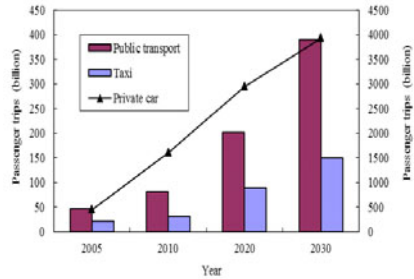
## 3.2    City Size Distribution

The city size will become larger with the urbanization and urban sprawl. During the next few decades, the number of cities which have over 1 million inhabitants will be 100 in 2020. The number of cities witch have over 2 million inhabitants will be 132 in 2030, and the total population will be over 350 million (Jiang, 2009).

## 3.3    Urban Passenger Trip Growth

With the economic development, the travel demand in urban area will increase significantly. And the travel characteristics such as trips, trip distance, model split will be changed. Private cars will compete with public transport each other in the long time in China. So the improvement of public transport becomes more obviously important in this key period. In 2030, the total trips will be over 10 000 billion trips, which is 25 times of in 2005. And the trips from public transport will also have a rapid growth, with an annual growth rate 15% in Fig. 2.

## 3.4　Daily Trips and Trip Distance

From the survey, in 2005, averagely, there are only 2.1-2.8 trips for each urban inhabitant in China. And the international experience shows the trips will increase to 3.5-4.0 and it will keep rather stable. Based on this, in 2030, we assumed the average trips will increase to 3.2 in China in Figure 3.

From the research report from World Business Council for Sustainable Development, the trip distance per year of private transport will increase in most countries, but China has the highest growth rate 3% from 2000 to 2030 in the world.



| | 2005 | 2010 | 2020 | 2030 |
|---|---|---|---|---|
| ■Mega city | 2.1 | 2.4 | 2.9 | 3.2 |
| □Super city | 2.1 | 2.4 | 2.9 | 3.2 |
| ■Big city | 2.4 | 2.7 | 3 | 3.2 |
| □Middle & small city | 2.8 | 3.1 | 3.2 | 3.3 |
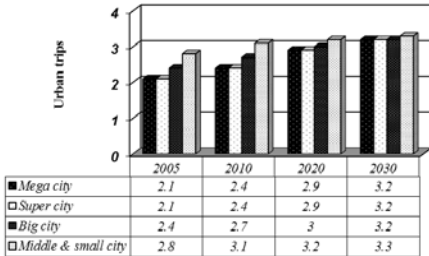
**Fig. 3.** Urban passenger daily trips　　　　**Fig. 4.** Urban rail development in China.
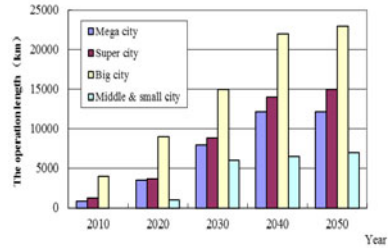
## 3.5　Improvement of Public Transport

After the public transport priority strategy has been implemented since 2004, public transport made a big progress in China. In the next twenty years, mass transit (urban rail and BRT) will have a huge growth, and the model split will be improved greatly. In recent years, some big sites (Beijing, Shanghai, Guangzhou and Tianjin) have a good urban rail system in China. The rail operation length is more than 900 km in 2009. By the end of 2009, urban rail plan in another 22 cities was got approved with a total 882 billion investment. In 2016, China will have 89 new lines, with the total construction length 2500 km. The total operation length will be 17 thousand km and 37 thousand km in 2020 and 2030 in Figure 4. In the meantime, the operation length of BRT will be 2500 km in China (Urban rail construction plan, 2009).

## 3.6　Civil Vehicle Stock

In 2009, the civil vehicle stock was 76.2 million, with an annual growth rate 18.8% from 2000 to 2009. In the next two decades, the civil vehicle stock will increase fast. The average vehicle stock per 1000 inhabitants will increase to 100 and 150 in 2020 and 2030. In 2030, the vehicle stock will be over 390 million, which is 12.5 times of that in 2005, with an annual growth rate 10.7%. And private car has the highest growth rate, it will go up to 300 million, which is 28 times of that in 2005, with an higher annual growth rate 14.6% in Figure 5 (ERI, 2009).
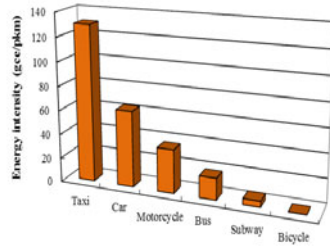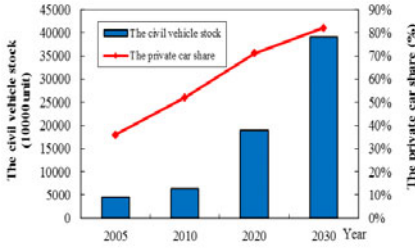
**Fig. 5.** Civil vehicle stock forecast in China.



**Fig. 6.** The energy efficiency characteristics of different transport modes

## 3.7 Energy Efficiency of Different Transport Modes

Different motorized transport modes show different energy efficiency characteristics. The most energy efficient mode is subway, prior to BRT and Bus. And the lowest energy efficient mode is Taxi. Because of empty running, so the energy efficiency of Taxi is lower than private car in Figure 6. These data shows the improvement of public transport is the important approach to reduce transport energy consumption and improve energy efficiency in urban transport system (Jiang, 2009).
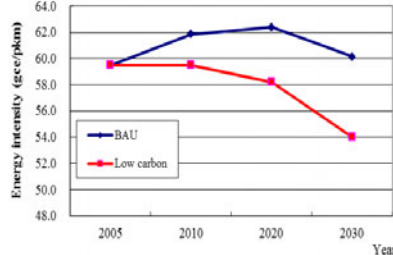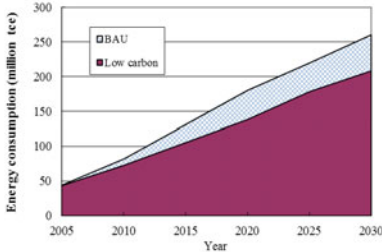


**Fig. 7.** The energy consumption of urban passenger transport



**Fig. 8.** The energy intensity of urban passenger transport

Based on the possible future travel characteristics change, the energy consumption and energy efficiency of urban passenger transport can be obtained from the model.

## 3.8 Energy Consumption

In the BAU, the energy consumption of urban passenger transport in China will be around 1.8 million ton in 2020, with an annual growth rate 9.8%. Then it will continue to increase to 2.6 million ton in 2030, with an annual growth rate 4.4%. The growth rate from 2010 to 2030 is higher than that from 2005 to 2010 because of the rapid economic development and urbanization, huge growth of private car ownership.

But in the energy saving scenario, the energy consumption of urban passenger transport in China will be around 1.3 million ton in 2020, with an annual growth rate 7.9%, which is reduced 23.5% than BAU. Then it will continue to increase to 2.1 million ton in 2030, with an annual growth rate 4.4%, which is reduced 22.2% than in BAU in Figure 7.

### 3.9    Energy Intensity

In the BAU, the energy intensity of urban passenger transport will be 23.6 gce/pkm in 2020, with an annual growth rate 2.6%. In 2020, the energy efficiency will reach the summit. After 2020, the energy efficiency will decrease to 23.3 gce/pkm in 2030, with an annual reduction rate 0.4%.

While in the energy saving scenario, because of the modal split of public transport will increase 20% than BAU and compact city development. The energy intensity will decrease to 21.5 gce/pkm in 2030, with an annual reduction rate 0.3%. In the years of 2010, 2020, 2030, the energy intensity in the energy saving scenario will be reduced 0.8%, 2.3% and 5.2%, the energy efficiency will be improved steadily in Figure 8.

## 4    Conclusions and Policy Implications

This paper identifies and analyses the main travel characteristics in China, then gives a methodology and a simple excel-based model to calculate the energy consumption. In China, the energy consumption growth of urban passenger transport is inevitable because of urbanization and motorization in the next two decades. And rapid private car ownership growth will lead to the energy intensity growth of urban passenger transport in the next ten years. But if the energy saving policies are used, and the public transport (Bus, BRT, Urban Rail) will be improved greatly, the energy intensity growth of urban passenger transport will be reduced steadily from now on.

In order to improve the energy efficiency of urban passenger transport in Chinese cities, based on the results from the scenario analysis, the overall policy options should be adopted as following:

1. Urban form should be compact and mixed land use, try to avoid cities with the high energy intensity transport modes. And urban planning is the important approach to reduce the rigid travel demand from the source. The trips and trips distance is closely linked with urban planning.
2. To improve the public transport, especially build the mass and rapid rail transport in large cities. For the large cities with the population more than 200 million, establish a public transport oriented urban transport system is the only option. Currently, China has launched its strategy for the urban transportation development. Due to the rapid development of urban construction, to reduce the huge cost, improve the public transportation system as soon as possible, particularly the urban rail transport, is necessary.

3. Integration of environment-friendly transport modes in planning processes for urban development (incl. routes for Suburban Railways, Metros, BRT, tram, bike). Currently, the vehicle travel is the major approach in all cities' transportation system. The non-motorized travel has been ignored in the urban planning and construction, as well as in the urban transport planning in the metropolis, and in the large, middle, & small scale cities; whiles, more than 50% among the all approaches of traveling is non-motorized travel. It is crucial and urgent to make the non-motorized travel as the core in the comprehensive urban transportation system, maintain a high level of non-motorized passenger transport with bicycles and walking in urban areas, especially for short distances.

4. Use the advanced high efficient, low carbon emission vehicles. It is not only able to reduce the emission, but also reduce the energy consumption by using certain kind of vehicles with the mature energy-saving technologies, like the low energy consumption diesel cars, hybrid vehicles. Using the low energy consumption vehicles can reduce the cost for vehicle fuel. For the usage of the vehicles with the new technologies, such as fuel cell vehicles, it is necessary to first design the roadmap, and involve it into the urban planning and the construction of the gas station in advance.

5. Take various measures and approaches to reduce travel demand. For instance, the traffic demand can be reduced around 5% by using the Information and Communications Technology (ICT) to realize the nearby-payments, conference calls, online shopping.

## References

1. China Urban Sustainable Transport Research Center (CUSTReC), Annual report on Sustainable Transport Development in Chinese Cities. China Communications Press. Beijing (2007)
2. Darido, G., Torres-Montoya, M., Mehndiratta, S.: Urban Transport and $CO_2$ Emissions: Some Evidence from Chinese Cities. The World Bank (2009)
3. Eads, G.C.: Presentation of World Outlook for Transport-Related GHG Emissions. WBCSD's Sustainable Mobility Project (2005)
4. Kejun, J., Songli, Z.: The research report of the medium and long term energy analysis of urban transport in China (2008) (unpublished)
5. Jiang, Y., Jiang, K.: Policy for energy saving of urban transport in China. China Communications Press (2008)
6. Wright, L., Fulton, L.: Climate Change Mitigation and Transport in Developing Nations. Transport Reviews 25 (November 2005)
7. Fei, M.: The thesis of the Impact of Urban Transportation Modes on Energy Consumption and the Environment. Tsinghua University (2008) (unpublished)
8. Dhakal, S.: Urban Transportation and the Environment in Kathmandu Valley, Nepal, Integrating global carbon concerns, into local air pollution management (2006)
9. The task force of Energy Research Institute, NDRC. Scenario Analysis of Energy Demand and Carbon Emissions. China's Low Carbon Development Pathways by 2050. China Science Press (2009)
10. Wei, Z., Szyliowicz, J.S.: Policy research on China's energy and environment of transport sector. China Communications Press (2005)
11. (Online Sources style) Urban rail construction plan, 0821 (2009),
    `http://cn.chinagate.cn/economics/200908/21/`
    `content_18377596.htm`

# Sustainability Assessment of Cooperative Vehicle Intersection Control at Urban Intersections with Low Volume Condition

Byungkyu Brain Park[1,2,*], Kristin Malakorn[3], Joyoung Lee[1],
and Jaehyun Jason So[1]

[1] Center for Transportation Studies, University of Virginia, Charlottesville,
  VA 22904-4742, USA
[2] Information and Communication Engineering, Daegu Gyeongbuk
  Institute of Science and Technology, Daegu, South Korea
[3] Vanasse Hangen Brustlin (VHB) Inc., Watertown, MA 02472, USA
  bpark@virginia.edu

**Abstract.** In this study, sustainability of the cooperative vehicle intersection control (CVIC) algorithm realizing wireless communications between vehicles, and between vehicles and infrastructure at urban signalized intersections was assessed. In addition, its performance was compared with an actuated control (AC) developed by the state of the practice program, Synchro, based on a microscopic traffic simulation model, VISSIM, at a low volume condition scenario. The simulation results indicated that the CVIC algorithm significantly improved vehicular delay, fuel consumption and emissions, when compared to those of Synchro.

## 1 Introduction

Transportation has been one of the largest sectors consuming fossil fuel and emitting greenhouse gas emissions in the US. In addition, travellers have done little to change their transportation habits and curb their fuel usage, furthering national dependency on foreign oil. As such, sustainability has emerged as one of the key focus areas in transportation. In fact, technology has improved vehicular performance in terms of better gas mileage. A recent initiative of US Department of Transportation in connected vehicle technology is one of the promising technologies that would lead to significant improvements in mobility as well as sustainability measures such as greenhouse gas emissions and fuel consumption. The research plan of the connected vehicle initiative will be focusing on mobility (i.e., dynamic mobility applications) and sustainability (i.e., applications for the environment: real-time information synthesis, AERIS). An example of the dynamic

---

[*] Corresponding author: +1 (434) 924-6347,

mobility application research would be a cooperative vehicle intersection control (CVIC) algorithm developed by Lee and Park [1]. The CVIC algorithm allows vehicles move through the intersections without traffic lights – the key element is cooperatively adjusting vehicles' accelerations and speeds to avoid crashes among the conflicting vehicles. The purpose of this paper was to investigate the performances of the CVIC algorithm in terms of sustainability (i.e., fuel consumption and emissions) by comparing its performances with those from the best existing traffic control method.

## 2   Methodology

In order to assess the sustainability impacts of the CVIC algorithm along the urban intersections, this paper incorporated two software programs: i) a CVIC simulation test-bed utilizing VISSIM, a commercial microscopic traffic simulator [2] and ii) the VT-Micro model [3] estimating fuel consumption and emissions based on individual vehicular speeds and accelerations. Furthermore, to develop the best existing traffic control setting along the urban intersections the state of the practice software, Synchro [4], was utilized. In this section, CVIC algorithm, VT-Micro model [3], and Synchro are briefly presented.

### 2.1   CVIC Algorithm

This algorithm assumes 100% market penetration of connected vehicle technology (i.e., every vehicle and infrastructure – traffic controller – are seamless connected via wireless communications such as dedicated short range communication). The algorithm can be best explained with an example shown in Figure 1, where
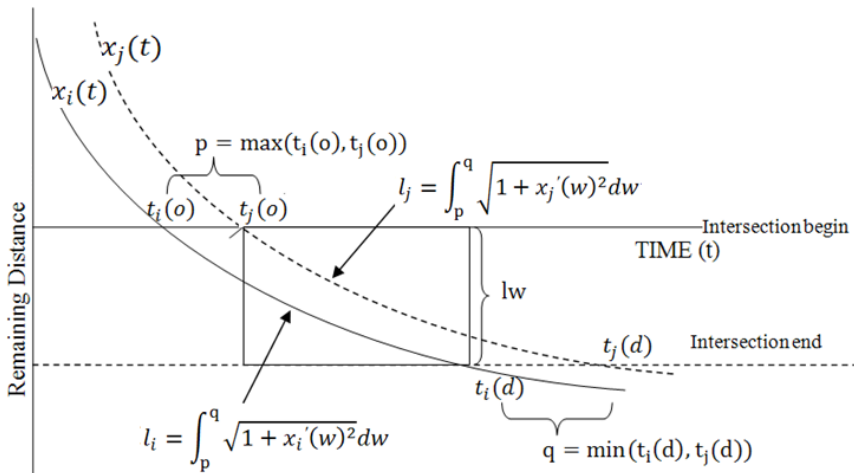


Fig. 1. Illustration of Vehicle Trajectory Overlap at an intersection [1].

trajectories of two conflicting vehicles to the intersection area are displayed. Depending on the speeds and accelerations of these two vehicles, they might run into crash. The algorithm adjusts their accelerations such that any potential conflicts among vehicles at the intersection area would be avoided – in real world, vehicles would cooperatively change their accelerations. The implementation could be realized by a road-side equipment (RSE) determining every vehicular acceleration as they come into conflicting area, or simply cooperative adjustments among conflicting vehicles via vehicle-to-vehicle communications.

## 2.2 VT-Micro Model

Sustainability measures such as fuel consumption and emissions can be estimated by utilizing a macroscopic model such as MOVES [5] or a microscopic model such as VT-Micro [3]. This paper uses microscopic emissions and fuel consumption model developed by the Virginia Tech researchers. This is because it is generally believed that macroscopic models utilizing average link speed with driving cycle do not properly capture individual vehicular driving variations. It is noted that the VT-Micro model, which has a two-regime regression model form as in equation (1), was developed by intensive experiments consisting of numerous speed-acceleration combinations.

$$\ln(MOE_e) = \begin{cases} \sum_{i=0}^{3}\sum_{j=0}^{3}\left(L_{i,j}^{e} \times S^{i} \times a^{j}\right) & for\, a \geq 0 \\ \sum_{i=0}^{3}\sum_{j=0}^{3}\left(M_{i,j}^{e} \times S^{i} \times a^{j}\right) & for\, a < 0 \end{cases} \tag{1}$$

Where,
  MOE: CO, $CO_2$, $NO_x$, HC, and Fuel
  $L_{i,j}^{e}$ and $M_{i,j}^{e}$: Model coefficients for each MOE
  S: speed in kilometer in hour
  a: acceleration rate in meter per second per second

## 2.3 Synchro Program

The state of the practice in the traffic signal timing optimization programs uses macroscopic flow model for quick estimation of delay at a given traffic signal control setting during the optimization. Synchro program [4] has been widely accepted by many State Department of Transportation, localities and academia due to its easy to use and the quality of control settings that are based on percentile delay measure. It is noted that the percentile delay measure uniquely considers stochastic variability within the macroscopic flow model. The traffic control setting developed by Synchro represents a typical control method used in real world.

# 3 Case Study

## 3.1 Experiments Set-Up

In order to assess sustainability impacts of the CVIC algorithm along urban intersections, a hypothetical arterial network consisted of four intersections was developed using a VISSIM simulation program. It is noted that the VISSIM model represents real-world allowing individual vehicular movements with explicit consideration of drivers' aggressiveness. The network is a 2.7-kilometer long and each intersection along the corridor is spaced at about 400 meters with each other. Figure 2 shows the hypothetical network modeled in VISSIM.
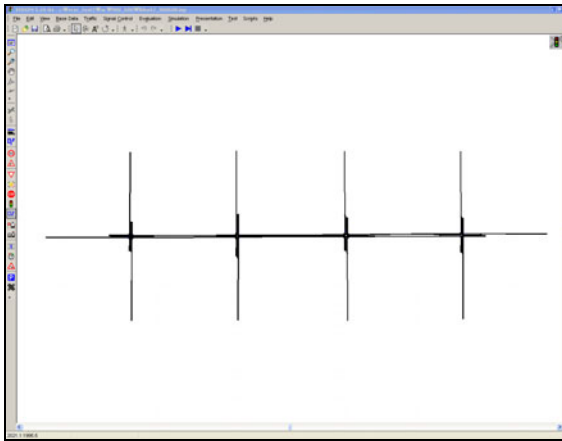


**Fig. 2.** A hypothetical test network in VISSIM.

In the experiment, this study only used a low volume condition: 400 vehicles per hour per lane per direction on major corridor movements and 300 vehicles per hour per lane per direction on cross streets. As noted, Synchro was used to develop the coordinated actuated traffic signal control setting for the given volume condition and the network shown in the VISSIM model.

# 4 Results and Discussion

Both CVIC algorithm and the actuated control (AC) traffic signal setting were implemented five times each with varying random seeds using the VISSIM simulations. In the assessments, mobility measures including average speed, number of stops, and total travel time, and sustainability measures including $CO_2$ emissions, fuel consumption and fuel economy are used. The summary results are shown in Table 1.

**Table 1.** Summary of CVIC and AC simulation results.

| Measures | CVIC | | Actuated Control (AC) | | CVIC Improvements over AC |
|---|---|---|---|---|---|
| | Mean | Std. Dev | Mean | Std. Dev | |
| Average speed [km/h] | 51.6 | 0.3 | 42.2 | 0.3 | 22% |
| Number of Stops | 7.0 | 6.9 | 1927.4 | 31.8 | 100% |
| Total travel time [h] | 29.9 | 0.7 | 37.5 | 0.6 | 20% |
| Emissions $CO_2$ [kg] | 333.1 | 8.0 | 516.9 | 9.4 | 36% |
| Fuel Consumption [kg] | 150.0 | 3.7 | 239.0 | 4.3 | 37% |
| Fuel Economy [mpg] | 24.1 | 0.3 | 15.5 | 0.1 | 36% |

It is clear that the CVIC algorithm improved both mobility and sustainability measures. It is noted that the different between CVIC and AC measures are statistically significant at 99th percentile confidence level. While the average speeds and total travel times were reduced by 20-22%, the emissions and fuel consumptions were improved by 36-37%. Interestingly, the number of stops was reduced by 100% under the CVIC. It is noted that the CVIC algorithm produced a small number of stops (i.e. 7.0) due to the implementation of recovery algorithm in which implements possible complete stops of vehicles on one approach when cooperative adjustments are not feasible.

## 5 Conclusions and Recommendations

Based on the VISSIM microscopic traffic simulations, the sustainability performance measures including fuel consumption and emissions of the cooperative vehicle intersection control (CVIC) algorithm outperformed those from the state of the practice Synchro traffic signal control setting. While the CVIC algorithm requires 100% market penetration and cooperative control among the vehicles and infrastructure, the results indicate that significant improvements in fuel consumption and emissions can be expected through the CVIC algorithm and the connected vehicle technology.

This paper only considered a low volume condition (i.e., 400 vehicles per hour per lane on major approaches and 300 vehicles per hour per lane on minor approaches). Without a doubt, the CVIC algorithm would work well under this kind of low volume conditions. However, it might not work very well when traffic volumes increase to congested conditions. Additional research by the authors is currently being conducted to assess the impacts under high volume conditions.

The CVIC algorithm evaluated in this paper assumed 100% market penetration. Future research should enhance the algorithm for imperfect market penetration

conditions as well. In addition, future research should explore assessments of surrogate safety using safety headway distance measure [6] or crash triggers [7]. Finally, given the assessments were made by sustainability measures, the CVIC algorithm should be compared with the traffic control settings designed for sustainable transportation [8].

# References

[1] Lee, J., Park, B.: Development and Evaluation of a Cooperative Vehicle Intersection Control Algorithm under the Connected Vehicles Environment. IEEE Transactions on Intelligent Transportation Systems (in press)

[2] PTV America. VISSIM Traffic Simulation, Version 5.10 (2009)

[3] Rakha, H., Ahn, K., Trani, A.: The VT-Micro Framework for Modeling of Hot Stabilized Light Duty Vehicle and Truck Emissions. Transportation Research, Part D: Transport & Environment 9(1), 49–74

[4] Husch, D., Albeck, J.: SYNCHRO 6 User Guide. Trafficware (2004)

[5] US EPA, Motor Vehicle Emission Simulator (MOVES) , http://www.epa.gov/otaq/models/moves/index.htm (last accessed on November 24, 2011)

[6] Son, H., Kweon, Y., Park, B.: Development of Crash Prediction Models with Individual Vehicular Data. Journal of Transportation Research, Part C 19, 1353–1363 (2011)

[7] Park, B., Chen, Y., Hourdos, J.: Opportunities for Preventing Rear-End Crashes: Findings from the Analysis of Actual Freeway Crash Data. Journal of Transportation Safety & Security 3(2), 95–107 (2011)

[8] Park, B., Yun, I., Ahn, K.: Stochastic Optimization for Sustainable Traffic Signal Control. International Journal of Sustainable Transportation 3, 263–284 (2009)

# Software for Management of Maintenance System for Truck, Passenger Car, Coach and Work Machines

Gradimir Ivanovich[1], Radivoje Mitrovich[1], and Dragan Jovanovich[2]

[1] Faculty of Mechanical Engineering, University of Belgrade, Kraljice Marije 16,
  11000 Belgrade, Serbia
  {givanovic,rmitrovic}@mas.bg.ac.rs
[2] Economic Assosiattion Thermal Power Plants and Mins Kostolac,
  Nikole Tesle 12080 Kostolac, Serbia
  dragan.jovanovic@te.ko.rs

**Abstract.** Software has been designed and implemented for the exploitation and maintenance of truck, passenger car, coaches and work machines in a transportation company. Without specialized software, adequate planning, quality control, maintenance of vehicles and work machines cannot be achieved. Software has been designed with the aim of following up, monitoring, analyzing and managing maintenance vehicles (i.e. planning, organizing, managing and controlling). This paper presents the developed and implemented software, as part of information system, used to manage the maintenance system of vehicle and spare parts in a company which transports good (coal, sand, old steel, and other) and passengers in inter-city and international and tourist travel with a high-degree of reliability, readiness and availability and with the aim to minimize costs.

## 1  Introduction

Integration of the core business processes in an enterprise becomes the key success factor in modern business environment. Process oriented enterprise is a highlighted characteristic of a modern enterprise that ensures greater flexibility, comparing to functional organizational structure recognized by management and administration hierarchy. Process modeling of Quality Management System (QMS) defined by ISO 9001:2000 contributed to a strict definition of end-to-end processes of product or service realization (from customer demand to the delivery of product/service to a customer) and strict definition of performance measurement of processes and enterprises as such. Information system/ information and communication technologies (IS/ICT) are inevitable component of modern enterprises and a foundation of completely new enterprise business concepts.

Organizationally, Vehicle fleet and Vehicle maintenance comprise the logistics support. Logistics support's task is to ensure high reliability, availability and readiness of truck, passenger car, coaches and work machines (referred to as the vehicles).

The vehicle database (category, type, purpose of a vehicle, registrations, drivers in charge, technical check, tachograph (odometer) check and other common and specific data on a vehicle) contains persistent data on vehicles and it is the main component of integration of all business processes of an auto-transportation enterprise.

Features of Software of maintenance management system for vehicles are presented in this paper (referred to as: Maintenance system for vehicles). This software is integrated into vehicle maintenance business process. Using modern software architecture and information technologies, data, maintained by Maintenance system for vehicles, are available to other business processes as well (e.g. Transport service realization, Planning and managing, Calculation of income and costs per vehicle etc.). This shows how immediate integration of business processes was realized through the development and implementation of modern IT solution. To support the decision making at operational and top management levels of an enterprise, managing data became available in real time.

## 2   Business Process

Maintenance system for vehicles includes support to the process of Vehicle maintenance with sub-processes [1]: preventive (daily, weekly, monthly and quarterly controls and services) and corrective (after a failure) maintenance. Activities included in this process are: from registration, through maintenance to delivery of technically aptitude vehicle from the maintenance, with exploitation of necessary resources (workshop, qualified staff, spare parts, devices for motor and vehicle check, technical documentation, information system for maintenance management system) to support realization of goals: increase readiness and availability of vehicles and maintenance cost reduction, etc., Fig. 1.  For maintenance process, an activity flow was defined on corrective and preventive vehicle maintenance within and out of Autotransport. Behavior of all participants in the process of vehicle maintenance was defined as well. The result of such approach is a defined flow algorithm on vehicles and actors in the vehicle maintenance process.

**Registration for maintenance.** Vehicle fleet sends vehicles to corrective/preventive maintenance, with the document Registration Q.VF.0, in electronic form. **Vehicle maintenance and Check out.** Maintenance refers to a period from vehicle check in (sent by Vehicle fleet) to vehicle check out and handing it back to Vehicle fleet. It includes following activities: Check in the workshop (Q.MV.01), Diagnostics, defining Work order (Q.MV.02) and Work lists (Q.MV.04) for worker in charge of maintaining, Correction of Work order and Work lists and Closing work lists and Work order. Once, vehicle maintenance is complete, the Workshop "checks out a vehicle from the service", informs Vehicle fleet that initiated activity of vehicle maintenance is completed. If the maintenance is performed in **(external) service outside Autotransport**, instead of Work order Q.MV.02, a Way bill Q.MV.03 is being created.
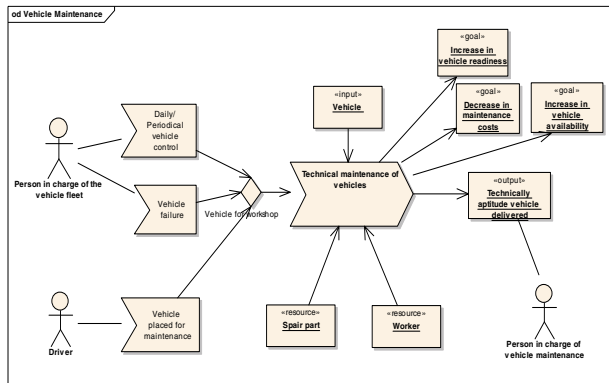
**Fig. 1.** Business process "Vehicle maintenance"

## 3 Software

Autotransport's "Maintenance system for vehicles" [1] is aligned with defined maintenance process. It can be accessed from any workstation within the network, according to assigned rights and authorization to each user of IS, based on its tasks and responsibility within the business process.

*Vehicle fleet: Registration.* As previously stated in the business process Vehicle maintenance, **Vehicle fleet** is responsible for the initiation of this process. Through appropriate application, the role "Vehicle fleet" realizes tasks for which it is in charge of. Functionalities of this application (main menu options) are: Check in; Check out; Report on vehicles (Status of a vehicle, Vehicle for corrective maintenance, Current availability of vehicle fleet); Service (workshop) capacity; Help and Exit. Vehicle fleet generates electronic document.

*Registration of vehicle for maintenance* (within the Vehicle fleet) (Fig. 2). Information on "Date and time of registration" are system date and time, thus recording the time of vehicle failure (when vehicle stopped being available) and it is stored in the database.

*Maintenance workshop* is responsible for: Check in of Vehicle in Autotransport's workshop (service), Diagnostics, Issuing and closing work orders and work lists, Check out from maintenance, Sending vehicle for a service outside of Autotransport**.** When activating appropriate option of *Maintenance workshop* application ("Register vehicle in the service"), one receives adequate electronic form for Registration, which can be printed into corresponding paper document "Registration No." (Fig. 2).

*Check in vehicle in the workshop* begins with the search for a vehicle: "Selection based on the number of Registration", "Selection based on the plate number" or "Selection based on the internal Autotransport's (AK) number". It enables automatic

move of Registration, with already inserted data in Vehicle fleet to the Workshop. The Workshop inserts other data regarding the vehicle check in the maintenance Workshop (e.g. data regarding vehicle check-in/check-out – Date, Time, Name). The Workshop can review and print Registrations of vehicles in queue for maintenance.



**Fig. 2.** "Registration No."form          **Fig. 3.** Diagnostics - Failure database updating

*Diagnostics.* Based on performed diagnostics, the diagnostician opens software application "Diagnostics" in order to verify/update related Registration, i.e. diagnostics for the vehicle.

*Failure input.* After performed diagnostics, the diagnostician *enters information on vehicle failure*. For information input to "Corrective maintenance", "Failure database" (Fig.3) is being used and continuously updated The diagnostician selects the Group of a vehicle, then the Part that failed and the Type of failure (e.g. motor, muffler pipe, deformation etc.). The diagnostician, with administrator's rights, for "Diagnostics" application, can use administrator's function "diagnostics update" to add new failure to the "Failure database". For data entry in "Preventive maintenance", one selects a preventive maintenance service from "Service database".

*Work order.* After it has performed diagnostics, worker in charge, within Maintenance service, activates the appropriate functionality from the application menu of Work order, Work list and Way bill for a maintaining service outside Autotransport: Creating a New work order ("New work order"); Correction of existing work order; Diagnostics update; Closing work lists and work orders; Opening new Way bill, Closing the (existing) Way bill and Vehicle test. By activating "*New work order*" option, a Work order is being opened. By choosing a vehicle, data from "Diagnostics No." are being obtained automatically. Based on diagnostics, operation maintenance ("*Operation maintenance*") is being selected with defined "Hour-norm". Selection of worker who will work on repairing a failure and/or preventive maintenance is being made based on maintaining operation and worker qualifications "work position" and "Worker/Load". Previously defined data are

being inserted in worktable by a click on "*Insert operations in the table*". Operation of saving work order ("*Save work order*"). **Way bill.** When a vehicle is maintained outside Autotransport's Workshop, a Way bill for maintenance in external service workshop is created, based on Registration and Diagnostics (data on external service workshop are stored in "Partner database").

***Vehicle fleet: Check out***. After completion of the work in the Workshop, a worker in charge closes Work lists and Work order for maintenance, where the system (automatically) initiates operation "Check out a vehicle from the service". System time of the check out is the time of maintenance completion (the vehicle becomes available again) and it is stored in the database. With initiation of application software Vehicle fleet (option "Check out").

***Workshop (Service)–Vehicle fleet: Taking over.*** After maintenance of a vehicle is done, Vehicle fleet takes over the vehicle from the maintenance Workshop Fig. 4.

***Views and reports***. In order to provide data and information for Vehicle maintenance management system in Autotransport, Views and Reports are defined with all the data that support operational processes and/or with the data on Vehicle maintenance process performance. These reports can be initiated and reviewed from the applications of Vehicle maintenance system, but from other applications as well (e.g. General Manager's  - GM's application).
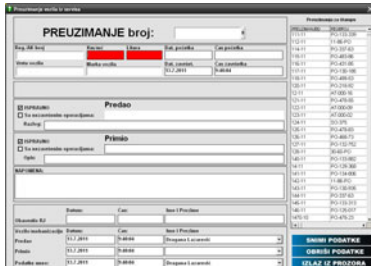


**Fig. 4.** Taking over a vehicle from maintenance          **Fig. 5.** Views and Reporting
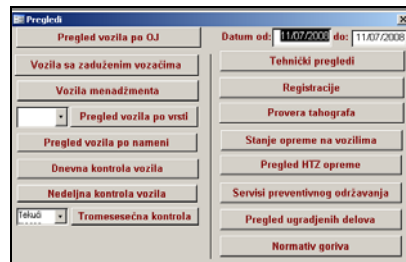
By activating an option "Views and Reporting", Fig. 5, following reports can be reviewed and printed: List of vehicles sorted by organizational units; Vehicles and work machines with drivers in charge; Vehicles for Autotransport's management;   List of vehicles with data on drivers' in charge sorted by the brand and the type of vehicle; List of vehicles with data on drivers' in charge sorted by the purpose of a vehicle; (for) Daily and Weekly vehicle control; (for) Quarterly vehicle control; (for) Technical control (period for performing technical control); (for) License Registration (period for registration renewal), (for) tachograph (odometer) check; Vehicle equipment condition control; Control of Chemical and technical protection equipment (assortment and quantity); Preventive maintenance services; Review of parts built in a vehicle; Fuel norms.

***Integration within ISAT*** (IS Autotransport's)***.*** Previously elaborated characteristic Views and Reports show that ISAT applications are integrated at data level they reflect, but at the level of business processes they support too. To that effect, the correlation within application software for business processes Transport service realization, Vehicle maintenance and Vehicle fleet should be pointed out. Key performance indicators of Maintenance process – availability of a single vehicle and vehicle fleet as a whole, are available to the "owners" of stated process and to the top management of the enterprise.

## 4  Conclusion

Information system for maintenance management of vehicles and work machines in Autotransport in Kostolac is an R&D project of Faculty of Mechanical Engineering, University of Belgrade, which is being realized in cooperation with the Autotransport's project team. Maintenance management system includes business processes with integrated operational activities supported by application software through which the business documents are generated. This approach provides data on realized events (activities) regarding vehicle maintenance operations to be stored in databases. From that point data become available in real time to the Autotransport's management (e.g. Vehicle fleet availability as an indicator of Vehicle maintenance process performance indicator, availability of a certain vehicle for transport services).

Some of, already achieved, effects of data analysis obtained from IS for maintenance management system relate to cost reduction of maintenance, indicating vehicles and spare parts for vehicles with failures. Besides, owing to the established ranking of drivers according to the number of vehicle failures, the drivers have become more "careful" in driving their vehicle.

Presented maintenance management system for vehicles (trucks, passenger cars & coaches, construction machines/ vehicles), i.e. conceptual solution of the system, can be applied in other transport companies because it is based on business process management approach.

## References

[1] Ivanović, G., Pantelić, S., Mojović, P., Nenadić, S., Stefanović, B., et al.: Establishing enterprise business process model, development and implementation of Information System/Information Technology of Autotransport: Vehicle fleet, Maintenance system for vehicles, Warehouse business activities, Transport service system, Calculation of income and costs per vehicle, GM's application. Faculty of Mechanical Engineering, Belgrade (2005- 2011) (in Serbian)

[2] Pantelić, S.: Information Technology in RMS Business Engineering Processes (Workshop). In: 16th International MIRCE Symposium, Woodbury Park Exeter, United Kingdom, December 6-8 (2006)

[3] Ivanović, G., Djordjević, S., Radulović, Z., Janković, Z.: The "Fix-it" Subsystem of Motor Vehicle Maintenance Information System. SAE Technical Papers, Number: 2001-01-3196, Book Number P-371 (2001)

[4] Pantelić, S., Ivanović, G., Bojanić, M.: Integration of the Transportation Services Application within Transportation Realization Business Process. In: Proceedings IS, YUINFO 2007 Symposium, Kopaonik (March 2007) (in Serbian)

# E-Mobility Generates New Services and Business Models, Increasing Sustainability

M. Knoppe

International Retail Management, Strategic Marketing & Innovation Management
Faculty of Business Administration
Ingolstadt University of Applied Sciences
P.O. Box 21 04 54, D-85019 Ingolstadt, Germany
marc.knoppe@haw-ingolstadt.de

**Abstract.** High-tech cars are driving the automotive industry success. Technical features, emotions and branding are important elements of the automotive success story and value chain. The present customer is still interested in cars delivering speed, power, status symbols, individual comfort, daily convenience or a better personal image. All well-known brands like Audi, BMW, Mercedes Benz, General Motors, Toyota and all others are working hard to improve their fleet`s sustainability. E-mobility is a welcome technology improving manufacturer`s sustainability. Investment banks, consulting companies and research institutes predicted market penetration rates from 2% to 25% until 2020. E-mobility might be driven and commercialized by regulations and governmental sponsoring, but in the moment the customer`s ease of use is low compared to traditional cars. Does a green e-car deliver real customer value? Is the automotive value chain transferable? Who is the real target group? Little information is available on customer experiences, specific needs and personal use. How to reach the market penetration of 25%? Thinking about the Unique Selling Proposition (USP) of E-mobility will help to solve the issue. Large cities are concerned about the future of traffic and its impact on the people. The highways are crowed and driving a car is expensive. Many young people cannot afford driver permission, an own car or a downtown garage. There is no real infrastructure for e-vehicles. Automotive retailers are selling and distributing cars, a customer-oriented service is very often missing. There is a strong brand loyalty and a low automotive retailer loyalty. The automotive industry should face the situation and not wait for customers or retailers pushing the market. After identifying target groups and their needs, new business models will appear like car sharing solutions, mobility shops, e-mobility provider services or e-infrastructure services. The service-oriented e-value chain will generate the new services and increase sustainability, customer comfort and customer binding at the same time.

## 1 Green Trend versus Old Economy

The IAA 2011 shows the radical change of the automotive industry. New markets, new rules, and new concepts: the automotive future will be different. Dieter Zetsche,

CEO Daimler, postulated the second invention of the automobile. The futuristic car has to be light, eco- and energy friendly (Handelsblatt, 2011). At the same time the consumer is expecting an integration of his entertainment and personal IT-world. Wolfgang Müller-Pietralla, Volkswagen Head of Future Research and Trend Transfer, is convinced that a car will be a personal lounge (Handelsblatt, 2011). In the United States over 90 percent of new cars have already an option for iPod connectivity. Moreover customers would like to have fun while driving a car. Rupert Stadler, CEO Audi, is convinced that the car as status symbol is still key for the emerging markets like China or Russia, but also for traditional markets like the USA (Handelsblatt, 2011). Norbert Reithofer, CEO BMW, knows the time for traditional cars is limited in China. Big towns like Beijing or Shanghai will prefer green-cars to avoid a collapse of their infrastructure. The present trend is towards the green-car fulfilling all these requirements. However, while the automotive industry is investing big amounts in green-cars, a clear competitive advantage is missing.

## 2   Traditional and Green-Car Concepts

In analysing e-mobility generating new services and business models, increasing sustainability and understanding the market chances of green cars, it is necessary to mention the different engine concepts (Figure 1) (Elektromobilität, 2011).
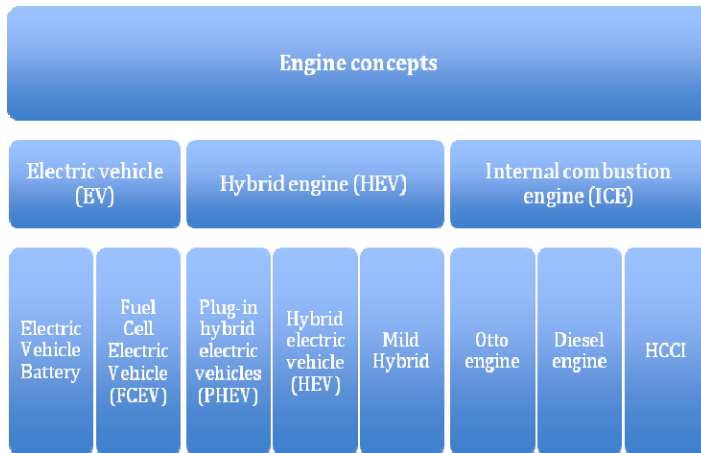


**Fig. 1.** HCCI: Homogeneous Charge Compression Ignition.

Every engine concept is associated with different variables influencing the consumer willingness to accept new technologies, different types of vehicles and linked mobility concepts. These variables are:

- Product value
- Service value

- Personal value
- Image value
- Monetary cost
- Time cost
- Energy cost
- Psychic cost.

## 3   Means-End-Chain Model

The variables will have a strong impact on buying patterns, driving patterns and consumer behaviour. The comprehension of consumer-decision making processes is key to the evaluation of consumer value and the acceptance of each engine concept. The general consumer value depends on the total of *personal* values of all customers. In other words every engine concept offers a different personal value. A sporty driver would prefer a powerful car, great design and high-end technical features. A family would prefer a comfortable SUV, a lot of space and comfort. Functional, conditional, social and emotional values of the product or related services are forming the consumer-decision-making process and the personal value. The means-end-chain model is a scientific and operative concept, which allows understanding how consumers perceive the use of the different engine concepts (Reynolds and Gutmann, 1988).



**Fig. 2.** Means-end-chain model.



**Fig. 3.** Details of the means-end-chain model.

## 4   A Scenario ICE versus EV

Renault`s car portfolio 2011 delivers e-car facts (Renault, 2011) to compare a new Renault Kangoo Generation 2011 (ICE) with a Renault Kangoo Z.E. 2011 (EV). The scenario illustrates the scientific and operative value of the means-end-chain model creating new e-mobility services and business models. The scenario assumes there is a salesman for sporting goods. The salesman is visiting his retailers in a greater area of 200 kilometres. During the weekend he is traveling by car and testing the sporting goods. Figure 4 shows how the salesman (consumer) perceives the value of ICE and EV Kangoo. The analysis considers different attributes (e.g. prices), consequences (e.g. long or short range) and the personal values (flexibility, freedom, green image, no debts…). The means-end-chain model is an important tool to analyse the customer needs to identify the customer value, to develop a clear USP and to cluster the customer segments. In this scenario the personal value of the salesman is flexibility and freedom. To reach his personal values he would prefer to buy a traditional Renault Kangoo Generation 2011 (ICE).
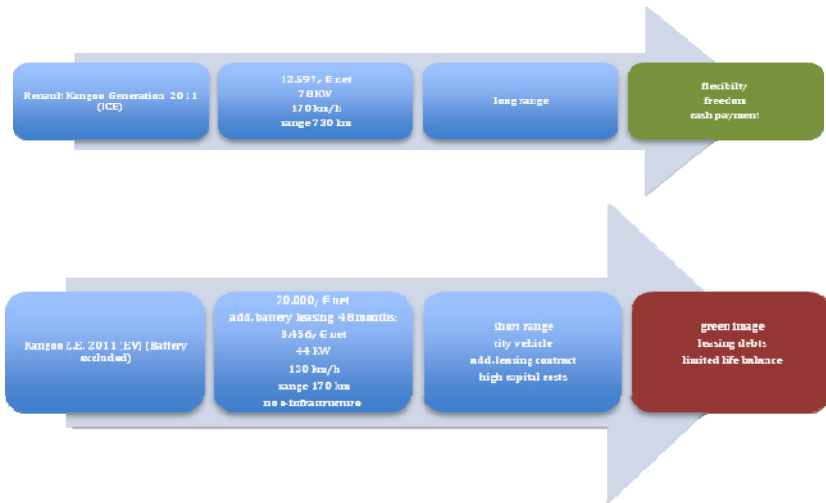


**Fig. 4.** A means-end-chain scenario Renault Kangoo.

## 5   Green-Car Ease-of-Use Is Low

Green-cars are the future of the individual mobility: independent of oil, no emission, eco-friendly – daily headlines of the automotive industry and governments. Analysing the determinants of the customer value the consumer does not share the green-car euphoria (Price Waterhouse Coopers, 2010):

- Product value: low battery performance, no real technical innovation
- Service value:  no charging infrastructure

- Personal value: no guarantee of green electricity (solar or wind energy)
- Image value: no status symbol
- Monetary cost: high capital costs and costs of maintenance
- Time cost: delivery time, cost of acquisition
- Energy cost: unclear development of oil and energy costs
- Psychic cost: unhappiness and doubts.

Different studies underline the low green-car customer value (Price Waterhouse Coopers, 2010). In addition OEMs realise the highest margins in the luxury and SUV segments. Reducing these segments would harm the OEMs profit margin and innovation power. This scenario is unlikely. Furthermore OEMs are used to implement technology-push-strategies: innovations will be presented to the market (e.g. I-Drive-System BMW). There is a change towards a pull-strategy. This means OEMs have to integrate the consumer requirements into their processes (Heiss, 2009). To respond to the requirements the automotive industry needs a clear positioning along the e-mobility value chain. OEMs have to think about their business models. "How can OEMs segment the market?" and "What is the USP of green-cars?" and "Who are my target groups?" Answering these questions OEMs will learn much more about their potential customers and emerging competitors beyond the traditional automotive value chain. Figure 5 shows a strategic approach to segment the e-mobility market and to identify the customer-related USPs.



**Fig. 5.** Green-car market segmentation

## 6 E-mobility Offers New Services and Business Models

*E-mobility shops, classical car sharing, e-mobility provider and e-infrastructure*

Large cities worldwide are crowed. New traffic systems and intelligent solutions are needed. E-mobility and classical car sharing offer the chance to reduce the negative impact of city traffic. Projects like Car2go by Daimler or DriveNow by BMW and Sixt offer a new approach to city mobility. The USP of mobility shops is a flexible car-sharing system for registered users: No membership, no basic fee and no deposit. Mobility shops organise pick-up and return points within walking distance. The registered customer can use the car anywhere and at any time. Different business models are possible: billing by minutes, billing by kilometres and time or billing by fixed rates. New target groups will be opened like young people who can not afford a car or a down-town garage, people who use very seldom a car or tourists who use park and e-ride systems. The classical car sharing is a comparable service. In general the customer pays a basic fee and a deposit. Therefore the minute or kilometre price should be cheaper (Lippautz and Winterhoff, 2010).

Car rental services are classical mobility providers. Their target groups are business people and travellers. Rental services like Europcar, Hertz, Avis or Sixt have worldwide hubs at airports and railway stations. Their infrastructure and direct contact to the customer allow them to implement an e-infrastructure and to identify new trends. Lifestyle is changing. Young and urban drivers would like to use a car according to their mobility needs. The consumer is interested in using a city car during the week, a SUV for vacations and a sports car at the weekend. According to existing full-service leasing concepts the customer would prefer to pay a flat rate (Lippautz and Winterhoff, 2010). OEMs should face the situation: new competitors are emerging. OEMs started the trend towards complete solutions offering financial services and fleet management (Lippautz and Winterhoff, 2010). E-mobility provider is a good example of the change towards the pull-strategy. OEMs have to adapt their classical business model. The new trends of strong branding, driving fun, sustainability, service providing, or urbanization will improve the automotive value chain.

## 7 A New Automotive Value Chain Approach

The customer value will push the automotive industry. A new generation, a different lifestyle and urbanization require solutions. Apple produced computers and moved towards services. Apple`s focus is to improve the life of their customers. The automotive industry needs a comparable vision to bind the customers. "How can OEMs improve the life of their customers?" To succeed in the e-mobility market OEMs should adapt their value chain towards full service broadening the portfolio: from car technology to service technology.
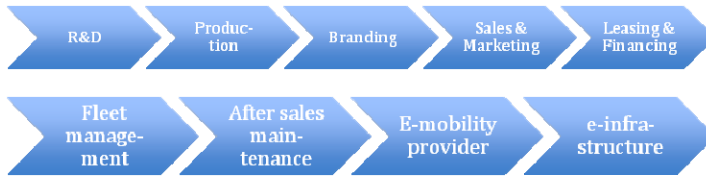
**Fig. 6.** A new automotive value chain approach

# References

AECOM / Department of Transport: Forecast uptake and economic evaluation of electric vehicles in Victoria, final report (May 06, 2011)

Elektromobilität: Herausforderungen für Industrie und Handel, Fraunhofer Studie, Frankfurt am Main 2010, p. 36 (2010); AECOM, pp. 13–14 (2011)

Becker, D.: (KPMG): Value chain crash – new business models for the automotive industry (2010)

Burger, F.: Mobilization for millions in Automotive now, vol. (1) ( Spring 2011)

Grunert, K.G., Grunert, S.C.: Measuring subjective meaning structures by the laddering method: theoretical considerations and methodological problems. International Journal of Research in Marketing 12, 209–225 (1995)

Handelsblatt Nr. 175 (September 9, 2011)

Heiss, S.F.: Kundenwissen für Forschung und Entwicklung in der Automobilindustrie: Fallstudie und Modellentwicklung zum Wissen von und über Kunden, Munich (2009)

KPMG: Mobility for a global life: Concepts for the future (2009)

Lippautz, S., Winterhoff, M., Little, A.D.: Winning on the E-mobility playing field (2010)

Peter, J.P., Olson, J.C., Grunert, K.: Consumer Behaviour and marketing strategy, European Edition, London (1999)

PriceWaterhouseCoopers / Fraunhofer Institut: Elektromobilität: Herausforderungen für Industrie und Handel, Frankfurt , Main (2010)

Reynolds, T., Gutmann, J.: Laddering Theory, Method, Analysis and Interpretation. Journal of Advertising Research 28(1), 11–31 (1988)

Vallette-Florence, P., Rapacchi, B.: Improvements in means-end chain analysing: using graph theory and correspondence analysis. Journal of Advertising Research, 30–45 (February/March 1991)

Renault: Price list (September 30, 2011), `http://www.renault.de/renault-modellpalette/renault-pkw/kangoo/kangoo/preise-und-technische-daten`

Renault: Price list (September 30, 2011), `http://www.renault-ze.com/de-de/modelle-z.e./kangoo-z.e./vorstellung-642.html`

# E-Mobility Will Change Automotive Retailing – A Strategic Approach

M. Knoppe

International Retail Management, Strategic Marketing & Innovation Management
Faculty of Business Administration
Ingolstadt University of Applied Sciences
P.O. Box 21 04 54, D-85019 Ingolstadt, Germany
`marc.knoppe@haw-ingolstadt.de`

**Abstract.** Retailing is the last step of the automotive value chain. Automotive retailers complete all transactions with customers: product presentation, closing, after sales, maintenance and repair. OEMs focus on developing new car technology, manufacturing and branding. Branding is one core competence of OEMs. Brands like Audi, BMW or Mercedes Benz invest a lot of money in advertising, sponsoring, events or public relations to cultivate the market for new customers or to increase brand loyalty of existing customers. E-mobility is a new business. Most consumers cannot identify the Unique Selling Proposition (USP) and customer value of a green car. To succeed in the e-mobility market, OEMs have to create new customer services. To make e-mobility shopping and service easier or to accommodate costumer desires, OEMs have to engage in new distribution systems. They need a closer customer contact, several points of contact and a strong branding to implement e-mobility concepts.

## 1 Market Penetration 2020

A new study of Bain predicts that 50 % of the new cars in 2020 will have an electric engine concept (electric vehicle or hybrid electric vehicle concept). Bain`s research estimates 100.000 e-cars in Europe in 2020. Worldwide Bain forecasts 350.000 e-cars. According to Bain`s market study typical e-mobility customers are premium car clients, who spend in average 60.000 Euro for a premium car in 2011. The e-car might be used as additional city vehicle (Stricker et al. 2011). E-cars offer new business models and services like e-mobility shops, car-sharing, e-cars on demand or e-infrastructure services (Becker, 2010). Does this impact on the traditional car dealer system?

## 2 The Traditional Dealer System

The traditional car dealer system is a typical retail business. Also in the automotive industry retailing is the last arena in a complicated process of manufacturing

and distribution. Automotive retailing is the physical movement and transfer of ownership of cars, after sales products and services like car repair and maintenance (Berman and Evans, 2007). Car dealers (retailers) are the interface between automotive manufacturers, automotive importers (wholesalers), automotive brands and consumers. Figure 1 and 2 show the dealer`s role in the traditional automotive sales process (Capgemini 2009):

- single brand dealer: sale of one brand: e.g. Audi
- multi-brand dealer: sale of several brands e.g.: Jaguar, Ferrari
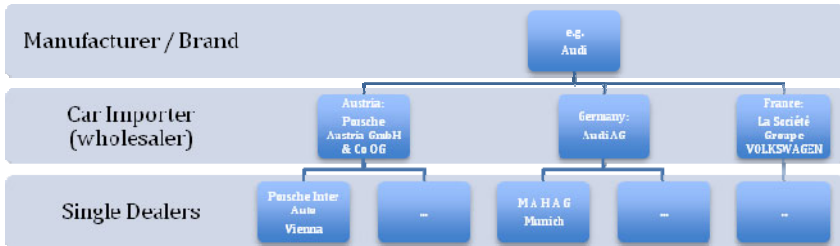


**Fig. 1.** Single brand dealer.
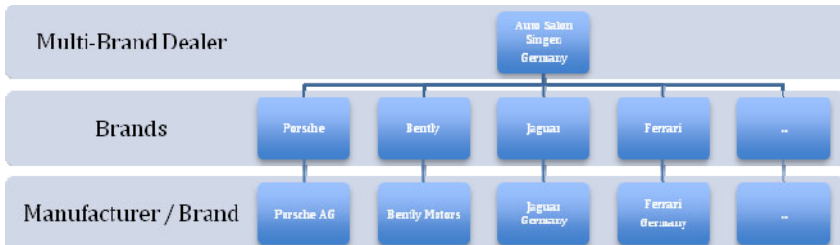


**Fig. 2.** Multi-brand dealer.

In general dealers have to handle consumers. Dealers take care of convenient locations, product presentation, local marketing, contract closing and customer service. OEMs focus on developing new car technology, manufacturing and branding. The OEM`s job is to increase customer`s loyalty and attracting new customer groups. In addition OEMs are directly involved in the B2B sales, will mean a direct key account management for industrial customers and public customers like police, military or fire service.

To make the brand even more attractive and to accelerate the margin development, most branded manufacturers like Volkswagen, Audi, Porsche, Mercedes Benz, Ford, Opel, are also engaged in direct sales to consumers like VIP or journalist sales. E-mobility will change the automotive value chain towards full

service: from car technology and branding to branding and service technology (Becker 2010, Burger 2011, Lippautz and Winterhoff, 2010, Stricker et al., 2011).

## 3  Multi-Channel-Retailing: Key to E-Mobility Success

A diversity of retail formats exists for the non-food business (Zentes *et al.* 2007). Benchmarking of different luxury industries can help to understand the competitive advantages of multi-channel retailing. Best practices in multi-channel-retailing are the fashion brands and retailers like H&M (Hennes & Mauritz), Esprit, Zara or Adidas. These fashion brands are using very smartly retail formats diversity combining distribution channels of traditional retailers, own outlets, flagship stores and own e-commerce channels improving market presence, customer binding, brand loyalty and profit margin.

OEMs are still missing the chance to use a variety of different retail formats to push the consumer business. A combination of retail formats including the traditional dealer system would support the OEMs to strengthen their brand awareness and sales power (Capgemini 2009). Especially multi-channel-retailing offers the automotive industry the option to sell green-cars and related e-mobility services to customers through multiple retail formats (KPMG, 2009a). A strategic multi-channel approach would also support the dealers to bind and serve the new e-customers. In the most cases dealers will not have the financial funds and human resources to build an own e-infrastructure-, e-maintenance- or e-service-system (KPMG, 2009a). – It is the job of the OEMs.

Combining different retail formats OEMs can exploit the unique benefit of each channel (Zentes *et al.*, 2007):

- Speciality stores (subsidiary or dealer's shop)
- Flagship or Event stores
- Internet (financial services, rental services, e-mobility service provider)
- Direct selling (VIP sales, Fleet sales).

Using a multi-channel-approach OEMs can expand their market presence and overcome limitations of traditional sales and services structures. Multi-channel retailing is a strategy and tool to enter the e-mobility market, to reach new target groups and to implement new services (Zentes *et al.*, 2007). Mercedes Benz, BMW, Audi, Ford, Porsche, for example, have strong and well-known brands, which support a consistent image across all sales channels and accelerates the e-mobility market entry through (Aberdeen Group, 2005; AT Kearney, 2008; Heinemann 2008).

- Common brand and corporate design
- Coordinated communication along the value chain
- Cross corporate culture
- Corporate pricing
- Central customer relationship management for all channels

- Complexity and cycle time reduction
- Central channel controlling
- Corporate legal concept.

The multi-channel concept increases the customer's perception of the brand and establish new sales system, product and services.

## 4 E-Mobility Dealership Management 2020

OEMs are struggling with increasing competition, new players, demographic change, new lifestyle trends, new communication or entertainment technologies, urbanization and climate related regulations. Figure 3 shows a strategic concept of automotive retailing 2020.
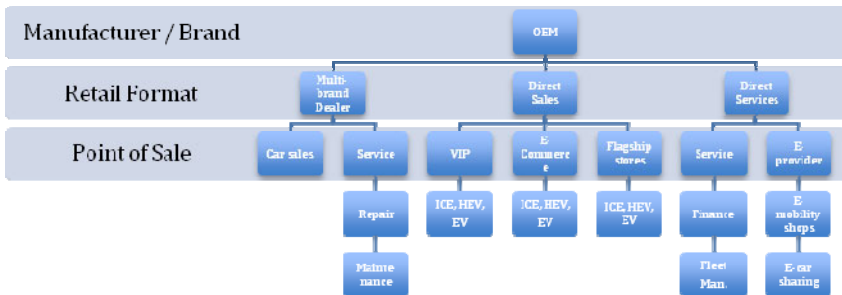


**Fig. 3.** Strategic concept of automotive retailing 2020

The clear approach will allow the OEMs to manage the diversity of their sales channels. A clear structure offers the chance to segment the traditional and e-mobility target groups according to their lifestyle and requirements. The strategic integration of e-mobility and related services creates a wide range of new business units and direct customer services. To succeed in e-mobility OEMs have to define clear sales and service responsibilities between OEMs and dealers. OEMs are forced to develop solutions according to the customer trends. These solutions allow OEMs increasing benefits (Stricker *et al*. 2011). The concept of automotive retailing 2020 is an approach to reach the predicted forecasts of e-mobility, to co-operate intensively with the dealers and to enter new e-service markets directly.

## References

Aberdeen Group: The Multi-Channel Retail Benchmark Report, Boston (2005)

Kearney, A.T.: Multi-Channel Retailing, Düsseldorf (2008)

Becker, D.: (KPMG): Value chain crash – new business models for the automotive industry (2010)

Berman, B., Evans, J.R.: Retail Management: A Strategic Approach. New Jersey (2007)

Burger, F.: Mobilization for millions in Automotive now, vol. (1) (Spring 2011)

Capgemini: Dealership of the Future – The Emergence of New Dealer Formats and New Busi-ness Realities (2009)

Heinemann, G.: Multi-Channel-Handel: Erfolgsfaktoren und Best Practices. Wiesbaden (2008)

KPMG: Multi-channel sales approach for premium autos: raising cost effectiveness in mar-keting and sales (2009a)

KPMG: Mobility for a global life: Concepts for the future (2009b)

Lippautz, S., Winterhoff, M., Little, A.D.: Winning on the E-mobility playing field (2010)

Stricker, K., Matthies, G., Tsang, R.: (Bain & Company): Vom Automobilbauer zum Mobi-litätsdienstleister, München (2011)

Zentes, J., Morschett, D., Schramm-Klein, H.: Strategic Retail Management, Wiesbaden (2007)

# Sustainability in the Automotive Supply Chain

M. Mesterharm[1] and P. Tropschuh[2]

[1] Volkswagen AG, AutoUni, Letter Box 1231, 38436 Wolfsburg, Germany
 michael.mesterharm@volkswagen.de
[2] AUDI AG, Corporate Responsibility, 85045 Ingolstadt, Germany
 peter-felix.tropschuh@audi.de

**Abstract.** The globalisation of supply chains is posing challenges to multinational corporations in terms of the conformance of suppliers to environmental and social standards. A responsible corporate policy responds to those challenges by integrating sustainability standards and by implementing appropriate measures in the procurement and supplier development processes. The article demonstrates the elements of a sustainability management system in the automotive industry based on Volkswagen AG.

## 1  Introduction

The automotive industry is characterised by a broad division of labour within the value creation process and by a highly complex network of global component suppliers. This is demonstrated by the large number of suppliers with which an automobile manufacturer has direct contact (horizontal supplier structure) and by the fact that the suppliers in turn frequently operate in conjunction with a multi-level supply chain (vertical supplier structure) (Arnold, 1997).  Caused by the trend towards global sourcing of input components and materials, automobile manufacturers involve suppliers in their networks who are based not only in the traditional industrial nations but also in emerging economies and developing countries. Automobile production is rising especially in emerging markets such as China, India and Brazil, and the percentage of components sourced from local production is continuously increasing. Although they have made substantial progress in recent years, these countries usually apply lower ecological and social standards than the automobile manufacturer's home country. Differences in the respective environmental and social conditions arise due to the lack of legal framework in the country concerned, or due to enforcement problems (Scherer et. al., 2002).  Since interest groups – and especially in this context non-governmental organisations (NGOs) – generally assign responsibility for the behaviour of suppliers to their respective customers, major risks may be entailed for the automobile manufacturer in terms of public reputation and customer appeal. It is therefore important for companies to identify, minimise and – as far as possible – eliminate risks arising from potential non-conformance by suppliers. Globalisation has not only expanded the economic activity of multinational companies in a geographic sense, it has also meant that they are now expected to take on a more

active role in social and political matters. By acting in a responsible, forward-thinking manner, companies can set their own agendas and areas of focus, show a sense of social responsibility, open up potential to influence policy-making, and enhance their credibility among relevant interest groups.

## 2  Sustainability Management in the Supply Chain

Supply chain management is a key element of corporate activity aimed at delivering the maximum possible customer satisfaction in terms of quality and price. It involves questions of market transparency, global access to the latest technologies and top suppliers, and maximising economies of scale by consolidating Group purchasing volumes. The Volkswagen Group spent some 90 billion Euro on production components in 2010.

With its "Sustainability in supplier relationships" concept launched in 2006, the Volkswagen Group has introduced standards, structures and processes aimed at integrating environmental and social requirements more closely into its procurement processes (Koplin/Seuring/Mesterharm, 2007). The concept comprises four elements: (1) requirements in relation to supplier sustainability; (2) early detection of risks; (3) integration into procurement processes; and (4) supplier improvement and development processes.

The integration of sustainability aspects into procurement processes pursues two key goals: Firstly, potential risks and problem areas can be identified at an early stage. Secondly, an additional competitive edge can be developed through the company's relations with its suppliers over the medium to long term. This approach is based on the idea that an environmentally aware and socially committed supplier will also be an outstandingly good, reliable partner in a commercial sense too, delivering performance from which the company can profit as a customer over the long term. Simply safeguarding the company against external criticism is not enough to ensure long-term future-oriented sustainability of supply chain management. Rather, policies must be focused on the development capability of the supply chain based on reciprocal learning processes from "win-win situations," both for the supplier and for the customer. For example, improvements to a supplier's environmental management system can lead to increases in productivity thanks to the elimination of defects and mistakes, thereby enhancing delivery performance.

A fundamental aspect of sustainable supply chain management is risk management, and in particular the early detection of risks. The early-detection phase can be used to gain advance knowledge in order to identify and assess risks and problems before they arise. In this context the know-how of both external experts and internal staff working in close contact with suppliers (such as purchasers and quality assurance specialists) can be useful. In terms of external early-detection measures, it is useful to observe the global agenda of industry-specific sustainability issues in order to identify social and ecological problems. The findings from the early-detection phase are then analysed in-house in conjunction with the relevant departments, including Procurement, Quality, Environment and HR, and rated against the background of local conditions.

In terms of sustainability requirements in the procurement process, a distinction can be made between two levels: (1) product/component-related requirements; and (2) production/location-related requirements. A major difference between product and production-related requirements is the extent to which the automobile manufacturer is able to verify conformance to them. Whereas component requirements can be continuously monitored by the in-house quality assurance function, production requirements apply to the specific supplier location. Consequently, it is only possible to verify conformance to such production-related requirements on-site at the supplier's facility.

At the product standards level, environmental and quality requirements are closely interlinked in the automotive industry. Environmental aspects such as recommended or prohibited materials frequently form part of the quality standards for purchased components. Indeed, within the Volkswagen Group "Environmental Protection and Recycling" is part of the "Formel Q Specifics" in the quality management system. Further Group-wide and industry-specific environmental standards and regulations are also imposed on suppliers as part of the process of procuring component assemblies and modules. Examples of this include the VW and Audi environmental policy, the so-called "General Environmental Specification" setting out cross-model requirements for environmental protection and recycling, and the VDA rules governing hazardous materials subject to mandatory declaration (VDA 232-101) and relating to the marking of materials (VDA 260). These requirements seek to ensure that the environmental compatibility of the vehicles produced is continuously improved in the course of the product development process. As such, they are an integral element of invitations to bid, and are circulated to suppliers in the course of the tendering process.

Alongside these product-related requirements, production- and location-related environmental and social standards are also important. Suppliers' production processes and working conditions should adhere to global minimum norms. International standards such as the ILO Core Labour Standards, the OECD Guidelines for Multinational Corporations and the UN Global Compact provide a suitable framework for these requirements. In 2006 the Volkswagen Group established its "Supplier Sustainability Requirements" which include, for example, stipulations relating to the creation and implementation of environmental management systems; employee training; anti-corruption policies; social rights, including the right to constitute trade unions; pay; and working hours. The requirements are based on the same principles to which Volkswagen adheres in its own policies and practices.

The integration of environmental and social aspects into the procurement structures and processes of a company is dependent on the specific circumstances of the company concerned. The procurement process extends from the material requisition by the line department through to the final decision on award of contract and thus selection of the supplier. It is important that each step in the procurement process be checked for weaknesses in terms of the embedding of environmental and social standards and appropriate additions be made as necessary. It must first be ensured that suppliers are informed of all requirements

and selection criteria laid down internally by the procurement process, so that they can incorporate them as appropriate into their bids. Basic and specific requirements relating to environmental and social matters must be specified as soon as a material requisition is drawn up. This is done on the basis of the aforementioned environmental specifications, for example, or by specifying detailed requirements in the invitation to tender. Volkswagen informs its suppliers of sustainability requirements through its Group procurement platform VWGroupSupply.com as well as through an office set up specifically to deal with sustainability questions. Suppliers must acknowledge and affirm their consent to Volkswagen's requirements in a binding manner. If needed, an ad-hoc team of experts can be convened from representatives of the Environment, HR, Health and Safety, Procurement, Quality and External Relations departments to assist in supplier development.

Suppliers who are unable to meet environmental and social requirements should not be immediately delisted from the supplier pool. Experience shows that delisting results in a further deterioration in environmental and social conditions at suppliers, as a lack of orders poses a risk to their commercial position. It is more useful to instigate a supplier improvement and development process, with mandatory verification of the individual steps taken, a fixed timetable, and submission of interim results. Information on the improvement process or current developments must be submitted to the customer promptly by the suppliers themselves. The customer should monitor and supervise this process, and in turn provide support and assistance in the form of information and advice. This improves cooperation and enhances mutual trust between the two parties.

## 3  Summary

Against the background of globalisation of businesses and procurement processes, the implementation of global environmental and social standards in the supply chain is becoming increasingly important. Multinational corporations should therefore introduce instruments for the early detection of risks in their supply chains, specify required environmental and social standards, and measure the success of their suppliers in attaining the set goals. Based on these measures, a collaborative development partnership with suppliers in relation to sustainability can be initiated and continuously implemented.

## References

Arnold, U.: Beschaffungsmanagement [Procurement management], 2nd revised and expanded edition, Stuttgart (1997)

Dietzelfelbinger, D., Hütter, G. (eds.): Globalisierung und Sozialstandards [Globalisation and social standards], Munich, Mering, pp. 11–21 (2002)

Dyllick, T.: Management der Umweltbeziehungen: öffentliche Auseinandersetzungen als Herausforderung [Management of environmental relations: Public debate as a challenge], Wiesbaden (1992)

Koplin, J., Mesterharm, M., Seuring, S.: Umwelt- und Sozialstandards als Steuerungsinstrumente ökologischer und sozialer Verantwortung in Lieferantenketten der Automobilindustrie [Environmental and social standards as instrument for managing ecological and social responsibility in supply chains in the automotive industry]. In: Gad, G., Hiß, S., Wienhardt, T. (eds.) Wirtschaft, Ethik und Entwicklung – Wie Passt das Zusammen? [Business, Ethics and Development – how does it All Fit Together?]. Wissenschaftlicher Verlag, Berlin (2005)

Koplin, J., Seuring, S., Mesterharm, M.: Incorporating Sustainability into Supply Management in the Automotive Industry: The Case of the Volkswagen AG. Journal of Cleaner Production (15), 1052–1063 (2007)

Scherer, A., Blicke, K.-H., Dietzelfelbinger, D., Hütter, G.: Globalisierung und Sozialstandards: Problemtatbestände, Positionen und Lösungsansätze [Globalisation and social standards: Problem areas, positions and potential solutions]. In: Scherer, A., Blicke, K.-H., Dietzelfelbinger, D., Hütter, G. (eds.) Globalisierung und Sozialstandards [Globalisation and Social Standards], Munich, Mering, pp. 11–21 (2002)

# A Sustainability Approach in Road Project Evaluation, Case-Study: Pollutant Emission and Accident Costs in Cost Benefit Analysis

Saeed Asadi Bagloee[1,*], Mohsen Asadi[2], and Claire Bozic[3]

[1] Parsons, P.O. Box 9123 Dubai, UAE
  Fax: +971-4-336-7920; Phone: +971-50-945-3192
  Saeed.Asadi@parsons.com
[2] Tarbiat Moallem University
[3] Chicago Metropolitan Agency for Planning (CMAP)

**Abstract.** Sustainability issues are often viewed as fancy topics that are interesting only to academia. It is necessary to bring such ideas into daily engineering practice through easy and straightforward methodologies. In this study we dealt with two aspects of sustainability in road project evaluation practices: pollutant emissions and losses associated with traffic accidents. In addition to the traditional costs and benefits associated with such projects, we propose a methodology to convert such sustainability impacts into currency units. This would enable conducting an apples-to-apples comparison when analyzing different projects. This was made possible by localizing some international research findings to reflect conditions where this case-study was undertaken.

## 1 Introduction

The Emirate of Abu Dhabi has recently witnessed, and will continue to witness, unprecedented traffic growth due to expansion of the economy and the population. Accordingly, infrastructure improvements are needed to keep pace with traffic growth and to support future development. The authorities have therefore undertaken a massive transportation construction program which includes expansion of existing Road E-75 in the peripheral area, mainly to serve freight mobility. This road is currently constructed with one lane in each direction, and is proposed to be expanded to two lanes in each direction. Another proposal would improve operations within the study area by extending a bypass road known as the Dubai Bypass Road. Ongoing engineering practices are lagging behind sustainability debates, so we would expect standard evaluation measures to include traffic volumes, travel time savings, congestion, and changes in accessibility. Due to the complexity of sustainability measures adopted in the academic environment, such measures are unlikely to be used for project evaluation. However, the gateway to promoting

---

[*] Corresponding author.

sustainability in transportation infrastructure is to enforce sustainability considerations when the projects are analyzed and evaluated. By doing so, the projects weak in sustainability characteristics can be discarded. If sustainability will continue to be a desired outcome of infrastructure investment, it is critical to develop easy and straight-forward methodologies to take sustainability features into consideration in the project evaluation process. This research proposes a straightforward approach to carry out a cost-benefit analysis (COBA) which takes pollutant emissions and traffic accident costs into consideration as two sustainability measures.

Three scenarios have been defined. These are:

- Do-Nothing Scenario: Keep the existing E-75 Road as 1x1 road.
- Scenario 1: Widening the E-75 Road from 1x1 road to 2x2 road over a distance of 79 km.
- Scenario 2: Extending the Dubai Bypass as a 3x3 road from the Dubai border to the Abu Dhabi-Al Ain Road, a length of about 68 km.

The above proposed scenarios are shown in Figure 1. A traffic model is employed to quantify the traffic impact of the above scenarios (Section 2). On the basis of the results of traffic model, benefit and costs of the scenarios including sustainability measures are monetized (Section 3). In Section 4 a Benefit-Cost analysis is conducted on the monetized measures to identify best scenario. The paper is concluded in Section 5.

## 2   Traffic Model

A traffic model was developed using EMME3 software to study the impacts of the projects in the horizon year of 2030. Figure 2 depicts the extent of the model beyond the city of Abu Dhabi limits, and the defined traffic analysis zone system with respect to the upcoming developments according to the city's master plan [1]. The analyses are carried out assuming the existence of recently planned developments expected for the year 2030, as reported in previous studies [2].

According to the traffic model, the 2030 truck traffic is 118,808 vehicle trips per day without the planned developments, while such massive developments would add an additional 343,604 truck-trips.

In summary in the year 2030 the following is the traffic outlook of Abu Dhabi, excluding the mainland:

Car = 1,406,006 vehicle trips /day and
Truck = 462,412 vehicle trips/day

It is an accepted practice to convert daily traffic volumes to peak hour traffic using a conservative factor 10% [3]. The impact of the proposed alternatives on traffic patterns indicates the attractiveness of the roads. To measure this, traffic assignments were carried out and the results were compared on a plot showing the volume differences between the widened E-75 and the no-build scenario see Figure 3. Figure 4 shows a comparison between the Dubai Bypass extension road

volumes and the no-build scenario volumes. Figure 3 and 4 clearly suggest the profound impacts of the both E-75-widening and Dubai Bypass extension. From a transportation point of view, the Dubai Bypass attracts much more traffic than the additional lanes on the E-75, regardless of the investment involved. Next section makes a through comparison and analysis.

## 3   Monetary Value of Benefits

The traffic assignment results allow us to calculate evaluation measures which can be used to compare the alternatives. The measures in Table 1 were calculated based on those results with respect to three established scenarios. The economic evaluation of the various alternatives can be carried out using the results as described in the following sections.

### 3.1   Vehicle-Hour of Travel

Total Vehicle Hours Traveled (VHT) provides a proxy measure of the overall pressure on the highway network due to the congestion impacts of regional travel. Based on the results of the traffic assignment, a comparative analysis was done for the VHT for the various scenarios. Table 1 below presents the results of the daily VHT and annual cost converted to currency for the three scenarios.  Based on the
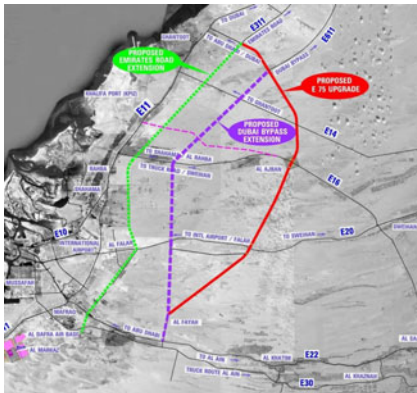


**Fig. 1.** UAE, Abu Dhabi, Proposed Alternative Routes
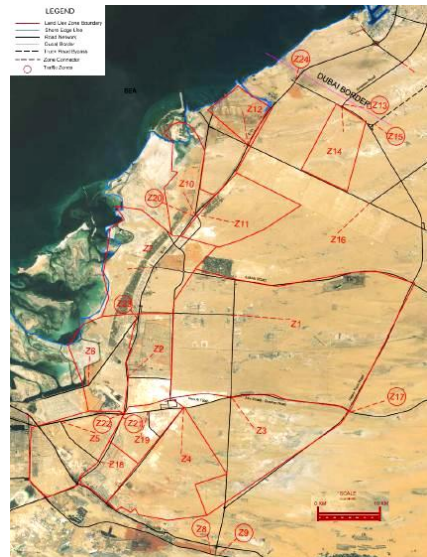
**Fig. 2.** Traffic Analysis Zone System in the Periphery Area of City of Abu Dhabi

**Fig. 3.** Comparison Plot E-75 Widening Vs Existing E-75

**Fig. 4.** Comparison Plot Dubai Bypass Extension Vs Existing E-75

UAE's per capita GDP [4] (22 working days per month and 8 working hours per working days), the value of time for an average UAE resident is AED 31 per hour (AED 3.7 = $ 1).

From Table 1, we infer that widening E-75 will improve the overall network performance by reducing vehicle hours traveled. The Dubai Bypass Extension will also improve the traffic circulation within the sector by reducing the overall vehicle hours traveled. By far the Dubai Bypass Extension does better job to lower VHT compared to widening E-75.

## 3.2   Environmental Assessment

Road traffic is one of the major contributors to air pollution [5]. The unit cost value of the various pollutants found in some literatures is summarized in Table 2 [6,7,8]. The emissions calculations were carried out based on the German 2000 MLuS-92 manual, (Randbebauung gemaess MLuS-92) using outputs of the traffic assignments [9]. Hourly emissions   generated for each scenario were developed and are detailed in Table 3. Using the cost values obtained from the references, it is possible to evaluate the total annual emission cost caused by road traffic for each of the three scenarios, shown in Table 4.

## 3.3   Savings in Accident Costs

Measuring the safety impacts of projects is an emerging issue in alternatives analysis. Subjective ratings for the safety assessment were assigned to each of the

three alternatives based on various factors such as the expected number of accidents and road lengths [12]. The subjective ratings vary from 1 to 4, wherein 1 is the safest condition, 2 and 3 are the mild and medium condition, and 4 is the worst condition. The Do Nothing Scenario was assigned a rating of "4", the E-75 widening was assigned a rating of "3" and the Dubai Bypass Extension was assigned a rating of "2."

**Table 1**. Vehicle Hours Traveled (VHT) Comparison for Various Scenarios

| No | Alternative | Daily Cars (VHT) | Daily Trucks (VHT) | Total Daily (VHT) | Equivalent Annual Value of time Travelled (AED) | Equivalent Net Annual Gaining of Saved Travel Time (AED) |
|---|---|---|---|---|---|---|
| 1 | Do Nothing Existing E75 | 5,737 | 1,985 | 7,721 | 718,098,105 | - |
| 2 | Widening E75 | 5,271 | 1,836 | 7,107 | 660,964,950 | 57,133,155 |
| 3 | Dubai Bypass Extension | 2,305 | 1,004 | 3,309 | 307,766,760 | 410,331,345 |

**Table 2.** Unit Cost Value of Pollutants

| Pollutants | Unit Cost Value (AED per kg) |
|---|---|
| CO | 1.1 |
| HC | 8.7 |
| NOx | 29.4 |
| SO2 | 49.7 |
| PM10 | 39.7 |

**Table 3.** Hourly emissions generated

| | Emission Generated (kg) | | |
|---|---|---|---|
| Pollutants | Do Nothing Existing E-75 | Widening E-75 | Dubai Bypass Extension |
| CO | 3,441 | 3,248 | 2,939 |
| HC | 2,892 | 2,720 | 2,453 |
| NOx | 1,273 | 1,207 | 1,097 |
| SO2 | 169 | 160 | 145 |
| PM10 | 75 | 71 | 63 |

Accidents impose costs due to the loss of life and property. For the existing E-75, studies reveal that a significant number of accidents occur. The crash data analysis from the 2010 data shows 80 injuries, including 13 deaths, 4 serious injuries, 35 minor injuries and 28 light injuries (over a distance of 79 km) [10]. Based on the current insurance policy, costs incurred due to loss of life and property can be calculated as follows: Assuming the cost for one fatality is AED 250,000 and considering 2 serious injuries as equivalent to one fatality with a cost of 125,000 AED each, 4 minor injuries as equivalent to one fatality resulting in a cost of AED 62,500 each, and 8 light injuries as equivalent to one fatality with a cost of AED 31,250 each, the safety cost for the existing E-75 can be calculated as AED 6,812,500 for the year 2010.

The safety costs must be calculated for each scenario. In order to do this, accident rates for the various accident severities must be calculated. The following procedure was developed in which the frequency of accidents was calculated based on the latest state of the practice methodology specifically for the Emirate of Abu Dhabi and then converted to the equivalent costs:

The following formula was used to determine the accident frequency (AF) for the study. The formula was derived by developing multivariate regression models

using accident frequency as the dependant variable and a set of explanatory variables such as mean speed, traffic flow, and link length as independent variables. The multiple regression method used was Generalized Linear Modeling (GLM). The effect of the explanatory variables and of the road type factor were estimated using a Multiplicative Poisson model fitted to the personal injury accident counts for the 5 year period.

$$AF = (3.281*10\text{-}7).Q^{0.727}.L^{1.000}.V^{2.479}.G_i \qquad (1)$$

*Where: Q = AADT flow (per day), L = Link length (km), V = Mean speed (miles/hour). Gi = 1.000 for Group 1; 0.539 for Group 2; 0.364 for Group 3 and 0.253 for Group 4*

Based on the descriptions given in the Table 5 and considering the type of independent variables such as mean speed, traffic flow and link length of corresponding scenarios, Group 1 is assumed for the Do Nothing Scenario, Group 2 is assumed for widening E-75 and Group 3 is assumed for the Dubai Bypass Extension.

**Table 4.** Annual Emissions Costs

| | Emission Cost (AED) | | |
|---|---|---|---|
| Pollutants (hourly) | Do Nothing Existing E-75 | Widening E-75 | Dubai Bypass Extension |
| CO | 3,768 | 3,557 | 3,218 |
| HC | 25,249 | 23,748 | 21,417 |
| NOx | 37,446 | 35,504 | 32,269 |
| SO2 | 8,404 | 7,956 | 7,211 |
| PM10 | 2,975 | 2,816 | 2,499 |
| Total | 77,842 | 73,582 | 66,613 |
| Total Annual Cost | 233,526,000 | 220,743,000 | 199,842,000 |
| Cost Savings based on Pollution Reduction (AED) | - | 12,783,000 | 33,684,000 |

*In respect to transportation activities we assume: 1 years = 300 days and 1 day = 10 hours*

**Table 5.** Description of the road groups

| | Group 1 | Group 2 | Group 3 | Group 4 |
|---|---|---|---|---|
| Mean speed | Low* | Below Average* | Above Average* | High* |
| Accident rate | High* | Average | Below Average* | Low* |
| Junction density | Average | Average | High | Low* |
| Bend density | High* | Above Average | Below Average* | Low* |
| Access density | Below Average | High | Average | Low* |
| Hilliness | High | Average | Below Average | Above Average |

*\*Indicates statistically significant different from Average (at 5% level at least)*

In order to obtain the costs resulting from the accidents, the international formula must be adjusted for local conditions based on the previously calculated AF. The following formula including a *k* factor was adopted.

$$\text{Cost of the Accident} = (3.281\text{x}10^{-7}).Q^{0.727}.L^{1.000}.V^{2.479}.G_i.k \qquad (2)$$

Where $k$ is a localizing and converting factor which is calibrated based on the existing accident rates and costs of the existing E-75.

Simply by applying the above formula to the available accident data of the existing E-75 (Cost of the Accident: AED 6,812,500) and extracting the other terms (Q, L and V) from the traffic estimation module the $k$ was computed as 40632.110. The calculated $k$ based on the current data is then applied to the other two alternatives:

Either of the alternatives would ease the longitude traffic movements along themselves (longitudes implies movement from one end in Dubai border to the other end Abu Dhabi-Al Ain road in Figure 2). Thus it can be inferred that any enhancement would lower the traffic cost along the longitude roads which are the E-75 and Dubai Bypass. Therefore the accident costs in the year 2030 for both alternative scenarios are compared to the corresponding costs in the Do Nothing scenario in the year 2030.

*Scenario 0 (E-75 existing):* The calculated $k$ value, the value of $G_i$ belonging to group 2, and the independent variables of scenario 0 (length, mean speed, and volume) obtained from the traffic assignment were applied in the formulas to estimate the accident cost for this scenario. The cost of accidents for this scenario was computed as AED 42,661,183.

*Scenario 1 (E-75 widening):* The calculated $k$ value, the value of Gi belonging to group 2 and the independent variables of scenario 1 (length, mean speed and volume) obtained from the traffic assignment were applied in the formula to get the corresponding accident cost for this scenario. The cost of the accidents for this scenario was computed as AED 32,993,261.

*Scenario 2 (Dubai Bypass Extension):* The same procedure was carried out for Dubai bypass Extension. Since this project is a combination of widening in one section and new construction in the other section, the computation was done accordingly. The cost of accidents in this alternative was calculated as AED 10,641,749.

## 4 Benefit Cost Ratio

The above preparations have made the final economic appraisal possible. Now both the monetized costs and benefits are known. Table 6 depicts the economic performance of the three scenarios with respect to all evaluation measures. The benefit cost ratio can be calculated as presented in Table 6 [13].

On comparing the two alternative scenarios, it is clear that the Dubai Bypass Extension provides the highest total benefits in comparison to its costs and can be considered the best project. This is unsurprising since the Dubai Bypass serves the center of the large planned 2030 developments while E-75 serves only the margins of the developments. From a safety point of view, a comparison of accident costs indicates that the Dubai Bypass Extension is far ahead of the E-75 widening (32 million AED versus 9.6 million AED in Table 6). Note that the modeling suggests that even more capacity or alternatives should be added in either scenario to serve the large volumes of traffic generated by the planned developments.

**Table 6.** Benefit-Cost Analysis

| | | | Widening of   E-75 | Dubai Bypass Extension |
|---|---|---|---|---|
| | | Estimated Construction Cost (AED) | 900,000,000 | 2,000,000,000 |
| First Year of Operation | Benefits | Savings in Accident Cost (AED) | 9,667,922 | 32,019,434 |
| | | Savings in Time (AED) | 57,133,155 | 410,331,345 |
| | | Savings in Emission Cost (AED) | 12,783,000 | 33,684,000 |
| | | Total Benefit (AED) | 79,584,077 | 476,034,779 |
| 50 Year of Operation | Fixed Cost (Construction Cost) + Maintenance cost* | | 1,350,000,000 | 3,000,000,000 |
| | Benefit | | 3,979,203,850 | 23,801,738,950 |
| | Benefit / Cost | | 2.9475 | 7.9339 |

\* Assuming that:
• the useful life of the transportation projects is 50 years,
• the annual maintenance cost is 1% of the construction cost, and
• the interest rate is zero, (due to low inflation rates and natural resource in the emirate of Abu Dhabi),

## 5   Summary

A practical methodology was developed to measure pollutant emissions and the cost of traffic accidents using the results of conventional engineering practices generally used for road project evaluations. In addition to construction costs and traffic improvement advantages, the amount of pollutants emitted is calculated using documented methods and codes and the pollutants are monetized by converting to equivalent costs. The expected fatality and injuries resulting from the road improvement and forecasted traffic volumes were calculated by localizing an international formula. Fatalities and injuries were also monetized using information on insurance compensation for such losses. Finally all these costs can be viewed as a single currency unit such that the comparison is more comprehensive. By monetizing all roadway impacts (as much as possible), sustainability variables can be considered when identifying the best alternative.

## References

[1] U.A.E., Abu Dhabi, DoT, Surface Transport Master Plan (STMP), http://dot.abudhabi.ae/en/stmp/ (accessed by 2011)
[2] U.A.E., Abu Dhabi, Urban Planning Council, http://www.upc.gov.ae/ (accessed by 2011)
[3] U.S. Department of Transportation, Federal Highway Administration, http://knowledge.fhwa.dot.gov (accessed by 2011)
[4] Encyclopedia of the Nations, Asia and Oceania, United Arab Emirates, Income
[5] http://www.nationsencyclopedia.com/Asia-and-Oceania/United-Arab-Emirates-INCOME.html (accessed 2011)
[6] Avec Sommer, H., Künzli, N., Seethaler, R., Chanel, O., Herry, M., Masson, S., Filliger, P., Horak, F., Kaiser, R., Medina, S., Puybonnieux-Texier, V., Quénel, P., Schneider, J., Studnicka, M.: Economic evaluation of health impacts due to road traffic-related air pollution: an impact assessment project of Austria, France, Switzerland. In: Dans Rapport de l'OCDE, Ancillary Benefits and Costs of Greenhouse Gas Mitigation, pp. 451–480 (2000)

[7] AEAT, Methodology for the Cost-Benefit Analysis for CAFE. Reports Prepared for the Clean Air for Europe Programme 1, 2, 3 (2005)

[8] RWDI, South Fraser Perimeter Road Regional Air Quality Assessment: Technical Volume 16 of the Environmental Assessment Application. BC Ministry of Transportation (2006)

[9] Wang, M.Q., Santini, D.J., Warinner, S.A.: Monetary Values of Air Pollutants in Various U.S. Regions. Transportation Research Record 1475, 33–41 (1995)

[10] Spiess, H.: Implementation of German air pollution model MLuS-92, EMME/2 Support (2000)

[11] U.A.E., Abu Dhabi, DoT, Traffic Impact Study, Al Faya Truck road, Jacob consultant (2010)

[12] Taylor, M.C., Baruya, A., Kennedy, J.V.: The relationship between speed and accidents on rural single-carriageway roads, TRL Reports, TRL511. Transport Research Laboratory, Crowthorne (2002)

[13] Boardman, E., Anthony, H., David, G., Vining, A.R., Weimer, D.L.: Cost-Benefit Analysis: Concepts and Practice, 2nd edn. Prentice Hall, Upper Saddle River (2001)

# Improving Life Cycle Assessment by Considering Worker Health and Comparing Alternatives Based on Relative Efficiency

S. Lloyd, K. Scanlon, and D. Lengacher

Concurrent Technologies Corporation, 100 CTC Drive, Johnstown,
Pennsylvania, 15904, USA
Tel.: +1.814.248.7599
lloyds@ctc.com

**Abstract.** Designing automobiles to support sustainability requires assessment of life cycle economic, environmental, and social impacts. Environmental and economic performance is increasingly evaluated with life cycle assessment and life cycle cost analysis. Analytical methods are needed to assess the associated life cycle social impacts. Additional sustainability criteria will make it more difficult to compare alternatives and select the "best" option. To enhance the evaluation of social impacts, a method for considering life cycle worker health impacts is proposed. To reduce reliance on subjective weighting, an approach using data envelopment analysis is proposed for comparing alternatives across multiple sustainability criteria. Conceptual approaches for both are presented as part of a case study focused on lightweighting vehicles through material selection.

## 1 Introduction

Automobile manufacturers are increasingly using sustainability assessment to evaluate the cradle-to-grave implications of vehicle design choices. Life cycle assessment (LCA) is often used in conjunction with life cycle cost analysis (LCCA) to evaluate the environmental impacts and costs incurred over a product's life cycle. Ongoing efforts to include other important dimensions of sustainability in life-cycle-based assessments are important for improving the sustainability of products; however, comparing alternatives becomes increasingly more challenging as more sustainability criteria are considered.

This study focuses on two specific areas for improving LCA. First is the inclusion of social impact categories in LCA. Efforts toward sustainable production require consideration of economic, environmental, and social impacts. Decision-making lacking comprehensive information in any of these domains may result in false optimization and problem-shifting. New methods, as well as case studies and practical application, for assessing life cycle impacts to society, consumers, and workers are needed. This research proposes a work environment-LCA (WE-LCA) method, a type of social LCA, to assess occupational health impacts.

Secondly, this study addresses the challenge of comparing alternatives as more sustainability criteria are introduced. Decision-makers often want to know which alternative is best. In LCA, this is typically accomplished through weighting – each criterion is assigned a weighting factor based on its relative importance to decision-makers and results are aggregated into a single score. While an optional step in LCA, this value-based approach is a contentious issue with many LCA practitioners (Bare and Gloria, 2006). This research proposes the use of data envelopment analysis (DEA), a method that is free of subjective weighting factors, to compare the life cycle performance of alternatives.

## 2   Case Study

Numerous studies explore the potential life cycle environmental and economic implications from vehicle lightweighting through material substitution with the goal of improving fuel economy. For example, Kim *et al.* (2010) summarize the results of studies on weight reduction from using aluminum and high strength steel. The scopes of existing studies vary considerably. In addition, various methods are used to estimate the potential weight and fuel savings, as well as the resulting impacts, from material substitution.

The appropriate modeling approach depends on the intended purpose of the study. The purpose of this study is to demonstrate novel methods for considering worker health in LCA and comparing alternatives across many design objectives. Therefore, existing literature is used to obtain realistic parameter estimates and engineering estimates are used to estimate material requirements and fuel consumption associated with the panels, as shown in Figure 1.
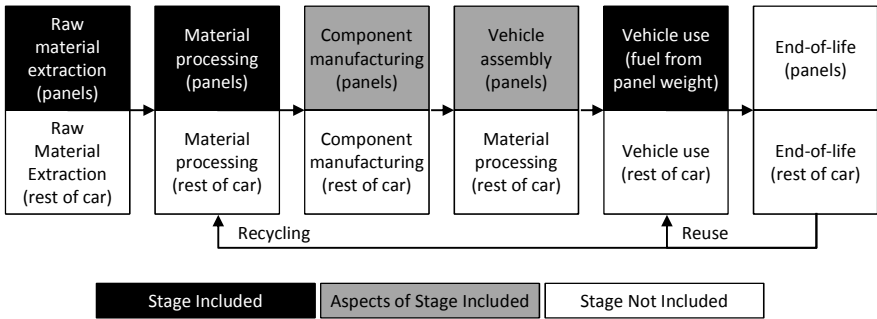


**Fig. 1.** Life Cycle stages considered

Table 1 summarizes key parameter estimates and performance for each alternative. Mild steel is used as a baseline, HSS is high strength steel, CFRP and GFRP are carbon and glass fiber reinforced polymers. Material substitution and cost factors relate the mass and cost of alternative material required to that of the baseline material. Values were estimated based on existing studies. Production scrap is

assumed to be 40% for metals and 20% for composites. The baseline vehicle is assumed to have a curb weight of 7,500 kg, including 750 kg of steel body panels that $0.80/kg to produce, and a fuel efficiency of 11.0 km/l. The fuel economy of each alternative is estimated using the sedan equivalent equation used by Lloyd and Lave (2003). A vehicle lifetime of 150,000 km and fuel cost of $1/liter are assumed. Vehicle fuel use associated with panels is estimated based on the ratio of closure panel mass to the curb weight. This analysis represents rough approximations for the purpose of demonstrating the WE-LCA and DEA methods.

**Table 1.** Characterizations and approximate performance for material scenarios considered

| Material | Material Substitution Factor | Panel Mass (kg) | Cost Factor | Material Cost ($) | Panel Fuel Use (l) | Fuel Cost ($) |
|---|---|---|---|---|---|---|
| Mild steel | 1.00 | 750 | 1.00 | $600 | 1,364 | $1,364 |
| HSS | 0.81 | 609 | 1.25 | $609 | 1,134 | $1,134 |
| Aluminum | 0.58 | 432 | 1.65 | $571 | 799 | $799 |
| CFRP | 0.40 | 300 | 6.00 | $1,440 | 552 | $552 |
| GFRP | 0.65 | 484 | 6.00 | $2,323 | 896 | $896 |

## 3 Life Cycle Sustainability Assessment

### 3.1 Traditional Life Cycle Assessment

Environmental peformance for material alternatives were estimated using traditional LCA. Life Cycle Inventory (LCI) data for material production and fuel production and combustion were estimated using the most relevant datasets from the ecoinvent database. Several mehtods for converting LCI data into potential environmental impact are available. The ReCiPe life cycle impact assessment (LCIA), cumulative energy demand (CED), and Intergovernmental Panel on Climate Change (IPCC) 100-year timeframe methods were used to derive the environmental peformance results presented in Figure 2.

### 3.2 Work Environment – Life Cycle Assessment

The health status of the workforce is a particularly relevant gauge of sustainability; if indicators of health status reveal adverse outcomes, then it can be assumed that basic needs are not being met (Pfeffer, 2010). Indicators of occupational health status include the incidence of nonfatal and fatal occupational injuries and illnesses. The Bureau of Labor Statistics (BLS) within the U.S. Department of Labor provides annual information on the rate and number of work-related incidents resulting in morbidity or mortality. The WE-LCA considers these statistics, in addition to industry specific data, in the quantification of occupational health impacts.

The WE-LCA inventory was constructed by identifying processes that compose the product system (from the traditional LCA) and aligning those processes with work-related activities to industry sector descriptions. Here, the U.S. Census Bureau's North American Industrial Classification System (NAICS) codes are used. In this study, raw material extraction and processing of the materials were considered. For example, for a steel panel, the raw material extraction was matched with the industry sector responsible for iron ore mining and the processing stage is matched with the industry sector encompassing iron and steel mill activities.

The WE-LCA impact assessment translates inventory impacts (damage) to worker health as measured in disability-adjusted life years (DALY). Several LCIA methods assess damage to human health using the DALY, a measure developed by the World Health Organization to measure the burden of disease representing a reduction in human health and well-being. The DALY combines years of life lost due to premature mortality with years of life lived with morbidity. In the case of worker health, one WE-DALY is the equivalent of one lost year of healthy life from premature mortality due to work-related injuries and years lived with a work-related injury and illness. Using publicly available data, each industry sector was assinged a WE characterization factor equal to the ratio of the WE-DALY per year for the sector and the physical quantity produced per year by the sector.

## 3.3   Results

Figure 2 uses a radar diagram to illustrate the normalized results of the life cycle sustainability assessment. The diagram compares the results of the life cycle
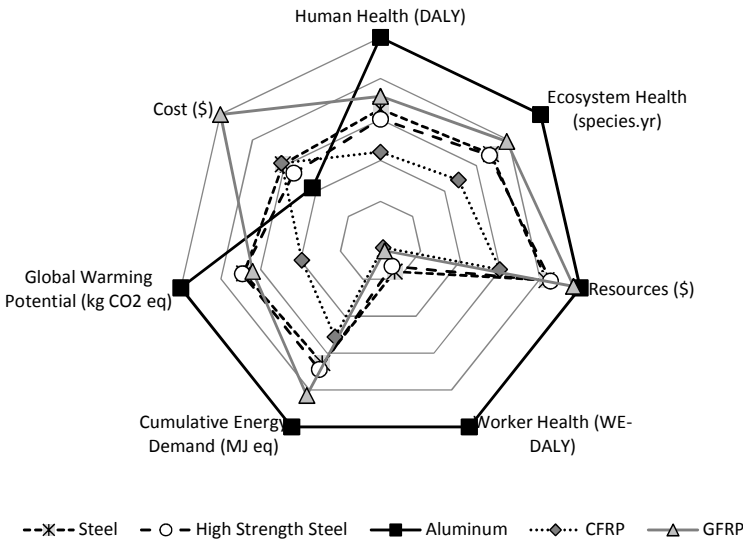


**Fig. 2.** Results of the life cycle sustainability assessment

model for each of the five lightweighting material options for each of the seven impact categories: five from the LCA, one from an LCCA, and one social LCA category (i.e. the WE-LCA). These results can be used to inform decision-making activities. However, determining the best alternative would require subjective weighting.

## 3.4 Comparison of Alternatives Using Dynamic DEA

DEA is a linear programming-based methodology used to measure the relative efficiency of decision making units (DMUs) which consume various levels of inputs and produce various levels of outputs (Charnes *et al*., 1978). DEA measures the efficiency of a DMU relative to an empirical production possibility frontier determined by all DMUs under appropriate assumptions regarding returns to scale and orientation (input-oriented or output-oriented).

DEA is a unique decision support tool because it allows analysts and scientists to introduce externalities into the economical analysis and make these impacts part of the decision making process (Luhmann, 1990). Because DEA measures efficiency, and places no limit on the types of the inputs and output variables, diferse sustainabilty factors can be easily integrated into the same efficiency measurement process.

One of the strengths of DEA is its generality; DEA makes no assumptions regarding the internal operations of a DMU. Instead, DEA treats each DMU as a "black box"; a perspective that is sufficient in many cases. However, this approach provides no insight regarding the specific sources of inefficiency. To help solve this problem and to allow DEA models to capture inefficiencies in more complex operations, Sexton and Lewis (2003) considered a two-stage DEA Model to evaluate the relative efficiencies of each DMU and Sub-DMU. Although this approach suits some sustainability assessment needs, the system considered here contains less intermediate products and more shared inputs and outputs between sub-processes. More fitting for this system, which has an intricate internal design of the production process, is the Network DEA Model formulated by Sexton and Lewis (2004) (see Figure 3).

The model structure proposed here assumes each DMU is composed of a set of Sub-DMUs. Each input to a Sub-DMU is either exogenous to the DMU or is the output of another Sub-DMU (an intermediate product). Correspondingly, each output from a Sub-DMU either leaves the DMU or is an input to another Sub-DMU (see Figure 4). Following Sexton and Lewis (2004), a Network DEA model is proposed to measure the efficiency of alternative material production and consumption approaches by using sub-DMUs to represent both processes. This approach captures both comprehensive and component efficiencies of each DMU. The first Sub-DMU consumes inputs and produces outputs, one of which is consumed by the second Sub-DMU. The second Sub-DMU also consumes the same inputs as the first Sub-DMU. Both Sub-DMUs produce the same outputs, with the second Sub-DMU producing one additional output. The advantage of this network model is that it can evaluate the relative efficiencies of each DMU and each of its sub-DMUs in a value/impact chain.
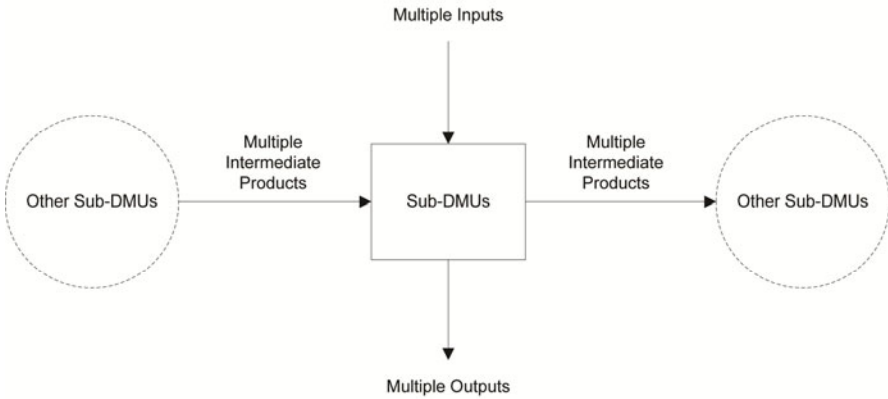
**Fig. 3.** Network DEA structure
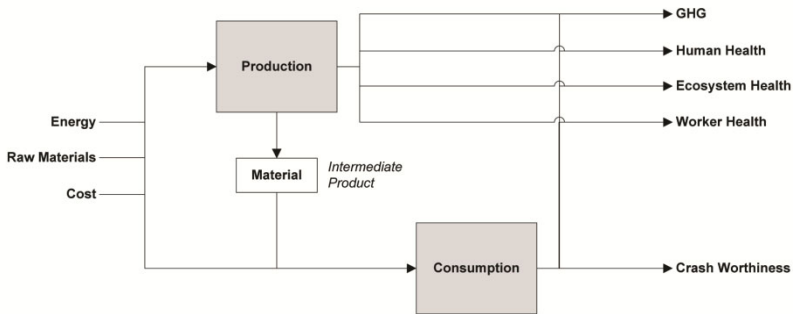


**Fig. 4.** Material substitution network DEA model structure

## 4   Conclusion

This paper presented a life cycle sustainability assessment method for evaluating lightweighting material alternatives. Two new concepts were explored: the WE-LCA model and the Network DEA model -- both aim to enhance evaluation of economic, environmental, and social impacts. Unlike previous life cycle studies comparing alternatives for lightweighting materials, this study could produce results that better capture and promote sustainable products.

## References

Bare, J.C., Gloria, T.P.: Critical Analysis of the Mathematical Relationships and Comprehensiveness of Life Cycle Impact Assessment Approaches. Environmental Science & Technology 40(4), 1104–1113 (2006)

Charnes, A., Cooper, W.W., Rhodes, E.: Measuring the Efficiency of Decision Making Units. European Journal of Operational Research 2(6), 429–444 (1978)

Kim, H.J., McMillan, C., Keolian, G.A., Skerlos, S.J.: Greenhouse Gas Emissions Payback for Lightweighted Vehicles Using Aluminum and High-Strength Steel. Journal of Industrial Ecology 14(6), 929–946 (2010)

Lewis, H., Sexton, T.: Network DEA: efficiency analysis of organizations with complex internal structure. Computers & Operations Research 31(9), 1365–1410 (2004)

Lloyd, S.M., Lave, L.B.: Life Cycle Economic and Environmental Implications of Using Nanocomposites in Automobiles. Environmental Science & Technology 37(15), 3458–3466 (2003)

Luhmann, N.: Ökologische Kommunikation, 3rd edn. Auflage, Westdeutscher Verlag, Opladen/Wiesbaden (1990)

Pfeffer, J.: Building Sustainable Organizations: The Human Factor. Academy of Management Perspectives 24(1), 34–45 (2010)

Sexton, T.R., Lewis, H.F.: Two-stage DEA: an application to major league baseball. Journal of Productivity Analysis 19(2/3), 227–249 (2003)

# Platinum Group Element Emissions from Automobile Catalysts

M. Paraskevas and M. Ochsenkühn-Petropoulou

National Technical University of Athens, School of Chemical Engineering,
Laboratory of Inorganic and Analytical Chemistry,
Iroon Politechniou 9, 15773, Athens, Greece
Tel.: +302107724022
msparaskevas@gmail.com

**Abstract.** In the last 19 years the use of automotive catalytic converters in the European union has been mandatory in order to control exhaust gas emissions. A new sampling system was developed in order to be applied directly at the exhaust pipe of vehicles combined with an exhaust gas analyzer in order to achieve total sampling of Pt, Pd, Rh (Platinum Group Elements, PGEs) on filters in particle form and simultaneous gas monitoring. This work aimed to examine the catalyst emissions according to the age, the thermal state and the capacity of the automobile engine. The main analytical methods used were ICP-MS and GF-AAS, while the exhaust gas emissions were analyzed with an automotive test system. The data collected were in good agreement with the recent technological advancement in catalyst technology and led to important observations and conclusions.

## 1   Introduction

Catalysts for automotive traction implemented in all new cars registered in the EU since 1993 contain Pt, Pd and Rh (platinum-group elements, PGEs) for conversion of the gaseous pollutants such as carbon monoxide, nitrogen oxide and hydrocarbons (CO, $NO_x$, HC) into the more innocuous gases $CO_2$, $H_2O$ and $N_2$. In the last 10-15 years the most dominant catalyst for gasoline vehicles has been the monolith or honeycomb structure catalyst. This catalyst consists of a cordierite skeleton coated with a highly porous washcoat of about 90% $\gamma$-$Al_2O_3$ and a mixture of alkaline-earth metals, oxides etc and last the noble metals (Pt, Pd and Rh) which are fixed in the washcoat surface (Twigg 2007).

   Great progress has been made in creating ultra low level emission vehicles, because of the increased use of Pt, Pd and Rh in vehicle exhaust catalysts, which led to observations of higher concentrations of PGEs in environmental matrices. A rough estimation shows that the annual Pt emission from automotive converters is as high as 0.5-1.4 tons per year. PGE contamination initially occurs in environmental samples until it results in bioaccumulation in living organisms and finally humans. These metals emitted in their metallic form are considered to be inert in

biological reactions, but some of their salts have been associated with serious health problems (Heck 2001).

This research consists in analyzing the quantity of PGE (Pt, Pd and Rh) spread in the environment through particles emitted from "real" gasoline cars of different engine capacity, catalyst age and thermal state that have not undergone any artificial aging in order to give a realistic image of the catalyst behaviour. One of the main goals of this study was to use automobiles that represent the average everyday vehicle without taking into consideration factors like fuel quality or frequent car service as the average driver does not either.

The sampling was done on filters because the PGE contamination initially occurs in airborne particulate matter (PM). In metal analysis, most of the techniques require decomposition of the solid sample and its transformation into a homogeneous liquid phase. Acid digestion in an autoclave bomb was used with success because high temperature and pressure allow the required decomposition to occur. Generally such techniques allow total metal recovery. As regards quantification techniques for metals, inductively coupled plasma mass spectrometry (ICP-MS) has proved to be advantageous because of characteristics such as low detection limits, simultaneity and wide dynamic concentration range.

## 2 Experimental

### 2.1 Reagents and Instrumentation

Single-element standard solutions (1000 ppm) of Platinum, Palladium and Rhodium by Fluka were used. High-purity deionized for dilution of samples and standards was used together with suprapur 65% $HNO_3$ (Merck) and suprapur 30% HCl (Merck) which were used also for digestions. The filters used for sampling were Whatman QMA $PM_{10}$ quartz filters of 47mm diameter fitted in a THERMO Model 6186 FRM Exhaust Dual Filter Holder. For the acid digestion of the filter, a Parr 4744 General Purpose Bomb was used. All measurements of the samples were done with an Agilent 7700x ICP-MS instrument.

### 2.2 Sampling

Each vehicle was placed on a dynamometer in order to execute the standard New European Driving Cycle (NEDC) that covers a distance of 11.2 km, which consists of 4 urban driving cycles (ECE) that last 800 seconds and one extra-urban driving cycle (EUDC) that lasts another 400 seconds, in total 20 min (DieselNet). The sampling of the emitted particles from automobile catalysts was performed directly at the exhaust pipe of the vehicle. The sampling procedure involved a separating aerocyclon at the end of the exhaust pipe, with the THERMO 6186 FRM Exhaust Filter Holder System containing a quartz filter, attached underneath. The aerocyclon then was followed by a Leybold D4A Trivac A Dual Stage vacuum pump, employed at a flow rate of 5.4 $m^3$/h, in order to boost particle retention on

the filter. The exit of the aerocyclon led to the Horiba Mexa 8420 Motor Exhaust Gas Analyzer. The filters used for sampling were Whatman QMA $PM_{10}$ quartz filters of 47mm diameter, because they have the ability to collect particles of size >10 μm to 0.3 μm with a 99.95% success, which contain ~100% of the PGE concentration (Paraskevas et. al. 2011)

## 2.3 Sample Treatment

After the sampling the filters were kept in a drier to dispose of the humidity caused by exhaust water vapors. The filters were processed by the use of an acid digestion technique with aqua regia in a small autoclave bomb, together with a small teflon covered magnetic stirer at about 150 Celsius in order to dissolve the metals collected on the filter. Next a filtration of the solution occurred to separate any filter or other solid residues and then the solution was evaporated to dryness in order to dispose of the aqua regia. The final residue from filters that were sampled was dissolved in HCl (0.5M) and brought into a 25ml volumetric flask in order to be analyzed by ICP-MS.

## 3 Results and Discussion

In order to check the effect of the thermal state on catalyst emissions, 3 random vehicles of 2979cc, 1781cc and 1598cc were put into the test of repeating 3 consecutive NED Cycles each.

In the Tables 1, 2 and 3 the emission results of the 3 vehicles are presented and it can be observed that as the catalyst passes from the colder stage (1st NEDC) to the hotter stages (2nd and 3rd NEDC), there is a decrease of both the PGEs and exhaust gas emissions. These results show that at a colder stage there is a more violent thermal strain on the catalyst which leads to higher PGE emissions. On the other hand the catalytic conversion of the gaseous pollutants into more innocuous gases seems to be more efficient when the catalyst is hot.

In order to study the age as a factor of the catalyst emissions, more than 36 vehicles tested were categorized according to their engine capacity. As seen in Figure 1 in the 2000cc vehicle category we observe that the fresher a catalyst is, the higher the PGE emissions are due to the fact that at the beginning it takes some time for the normalization of the catalyst. The same observations were made also in other vehicle categories of lower or bigger engine capacities.

Furthermore the average values of the measured exhaust gases of the vehicles were 0.619±0.522 g/km for CO, 0.035±0.033 g/km for HC and 0.031±0.024 g/km for $NO_x$ which are below the exhaust gas emission standards of 1.0 g/km for CO, 0.10 g/km for HC and 0.08 g/km for $NO_x$ according to the directive "Euro 4 (2005) for any vehicle - 98/69/EC (& 2002/80/EC)" (DieselNet) and indicates that the PGE loss during a catalysts life does not affect the gas emissions. Although recommended replacement for a catalyst is at 80000 km, even catalysts with ages of almost double that age, emit ultra low exhaust gases (Paraskevas and Ochsenkühn – Petropoulou 2010).

**Table 1.** Emission results of 2979cc vehicle

| NEDC | Pt µg/l | Pd µg/l | Rh µg/l | CO g/km | HC g/km | NOx g/km | CO2 g/km |
|------|---------|---------|---------|---------|---------|----------|----------|
| 1st  | 2.1     | 10.05   | 1.3     | 0.173   | 0.025   | 0.020    | 235.552  |
| 2nd  | 1.2     | 8.03    | 0.3     | 0.110   | 0.002   | 0.003    | 195.359  |
| 3rd  | 0.9     | 5.2     | 0.1     | 0.144   | 0.004   | 0.003    | 199.119  |

**Table 2.** Emission results of 1781cc vehicle

| NEDC | Pt µg/l | Pd µg/l | Rh µg/l | CO g/km | HC g/km | NOx g/km | CO2 g/km |
|------|---------|---------|---------|---------|---------|----------|----------|
| 1st  | 2.6     | 17.5    | 1.7     | 0.969   | 0.030   | 0.069    | 268.614  |
| 2nd  | 1.2     | 10.01   | 0.6     | 0.426   | 0.005   | 0.046    | 238.383  |
| 3rd  | 0.8     | 6       | 0.4     | 0.131   | 0.007   | 0.007    | 107.019  |

**Table 3.** Emission results of 1598cc vehicle

| NEDC | Pt µg/l | Pd µg/l | Rh µg/l | CO g/km | HC g/km | NOx g/km | CO2 g/km |
|------|---------|---------|---------|---------|---------|----------|----------|
| 1st  | 0.5     | 5.02    | 0.5     | 0.280   | 0.012   | 0.013    | 161.873  |
| 2nd  | 0.3     | 0.91    | 0.1     | 0.036   | 0.001   | 0.005    | 146.860  |
| 3rd  | 0.1     | 0.43    | 0.1     | 0.022   | 0.001   | 0.003    | 145.157  |
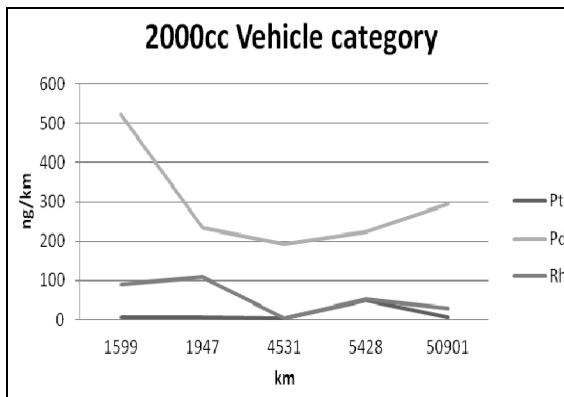


**Fig. 1.** PGE emissions in the 2000cc vehicle category, according to the age in driven km

# 4  Conclusion

According to the findings of this project it emerges that in most cases platinum has been substituted with palladium in newer generation catalysts in order to comply with the new standards which demand palladium use as a low toxicity metal and because of its lower price. Fresh catalysts emit higher concentrations than aged ones because of the normalization that needs to occur during the first kilometres of a new automobile. The fact that all vehicles independently from age or engine capacity remain within the Euro 4 limits, shows that even new catalyst technology focuses more towards ultra low gas emissions, than PGE emissions.

# References

Twigg, M.V.: Progress and future challenges in controlling automotive exhauts gas emissions. Appl. Catal B-Environ. 70, 2–15 (2007)

Heck, R.M., Farrauto, J.R.: Automobile exhaust catalysts. Appl. Catal. A-Gen. 221, 443–457 (2001)

DieselNet, Emission Test Cycles-Summary of worldwide engine and vehicle test cycles, http://www.dieselnet.com/standards/cycles/ece_eudc.php

Paraskevas, M., Papoutsi, K., Ochsenkühn-Petropoulou, M.: A novel way of sampling particles containing platinum group elements from automobile catalysts. Anal. Let. (2011) (in print)

Paraskevas, M., Ochsenkuehn–Petropoulou, M.: A new way of sampling particles containing Platinum Group Elements from automobile catalyst. In: 7th Aegean Analytical Chemistry Days, p. 74 (2010)

# A Comparative Study of Vehicle Drive Performance and Energy Efficiency

S. Abdul Rahman[1], P.D. Walker[2], N. Zhang[2], J.G. Zhu[2], and H. Du[3]

[1] Department of Physical Science, Faculty of Science and Technology,
  Universiti Malaysia Terengganu, 21030 Kuala Terengganu, Terengganu, Malaysia
[2] School of Electrical, Mechanical and Mechatronic Systems,
  Faculty of Engineering and Information Technology,
  University of Technology, Sydney, P. O. Box 123, Broadway,
  NSW 2007, Australia
[3] School of Electrical, Computer and Telecommunications Engineering,
  Faculty of Informatics, University of Wollongong, NSW 2522, Australia
  salisa@umt.edu.my

**Abstract.** In this paper, two types of increasingly more efficient and greener vehicles are analyzed and compared. These vehicles are: a proposed conceptual series-parallel powertrain, the University of Technology, Sydney plug-in hybrid electric vehicle (UTS PHEV); and, a conventional series-parallel hybrid electric vehicle with an internal combustion engine.. The UTS PHEV requires only a single electric machine to function as an electric motor or generator in different time intervals controlled by a special energy management strategy. The UTS PHEV uses two energy storage devices, the battery and the ultracapacitor, which can work together effectively to maintain the state of charge at a high level in order to improve the vehicle drive performance and energy efficiency. With the assistance of a novel automatic transmission, the UTS PHEV can operate under multiple modes to suit the needs of various driving cycles including those in an emergency. A special power and energy management strategy was developed to control the power flows within the vehicle according to the desired operating mode. The overall structure of UTS PHEV, known as UTS PHEV code are derived and implemented numerically in the MATLAB/SIMULINK environment for further analysis. Through simulations, the performance of the UTS PHEV has been evaluated in terms of the fuel economy, all electric range (AER), electrical consumption and operation cost for low and high density traffic patterns drive cycles. The comparison between the performance and efficiency of the UTS PHEV and those obtained results using existing powertrains are also presented. The obtained results demonstrate that the UTS PHEV outperforms most existing powertrains and has great potential in applications to passenger cars for city and urban transportations.

## 1  Introduction

Society's concern with oil depletion, global warming, fuel economy and emissions standard have led many automotive manufacturers to produce alternative vehicles, which are more fuel efficient and environmentally friendly, without sacrificing the comfort and drive performance of internal combustion engine (ICE) powered vehicles. New types of clean and energy efficient vehicles are needed in order to boost the fuel economy and all electric range (AER), and at the same time can reduce emissions, electrical consumption and operation cost.

Pure electric vehicles (EVs) are most energy efficient and zero emissions if the energy storage system (ESS) is recharged by electricity generated from clean energy sources, such as wind and solar. However, the travel distance is limited by the energy density of the ESS, which is mainly battery for the time being. On the other hand, the hybrid electric vehicles (HEVs) can cover a drive range much larger than that of the pure EVs with lower emissions and fuel consumption compared to the ICE powered vehicles. With the recent breakthrough in battery technology, high energy density battery pack can become the major energy source for HEVs to have much larger degree of electrical drive and be charged from the power grid (Abdul Rahman, Zhang and Zhu 2008). This new HEV is known as PHEV. Compared to the HEVs, the plug-in hybrid electric vehicles (PHEVs) use a large electric machine (EM) to function as primary driving force, which is more efficient than an ICE and hence can reduce fuel consumption, emissions and operation cost.

Most of the existing PHEVs contain two separate EMs functioning as an electric motor and generator, respectively. A new conceptual series-parallel PHEV, is proposed, known as University of Technology, Sydney (UTS) PHEV. The UTS PHEV contains only one EM, operated as either an electric motor or generator in different time intervals, controlled by a special energy management strategy (EMS). The main strategy of energy management is to optimize the energy and power demands throughout the system (Yoo, Sul, Park and Jeong 2008). To operate the UTS PHEV in multiple modes ranging from EV to all types of HEVs, which suits the needs of various driving cycles, a novel 4-speed automatic transmission (AT) without torque converter is introduced. To improve the drive performance and energy efficiency, high power density ultracapacitor is incorporated effectively with the battery.

This paper presents a comparative study on the fuel economy, AER, electrical consumption and operation cost between the UTS PHEV, a conventional series-parallel HEV and an ICE powered vehicle for low and high density traffic patterns drive cycles.

To perform a quantitative comparison, the overall structure of UTS PHEV, known as UTS PHEV code as demonstrated in Figure 1 is derived and simulated numerically in MATLAB/SIMULINK environment for further analysis (Abdul Rahman, Zhang and Zhu 2010).
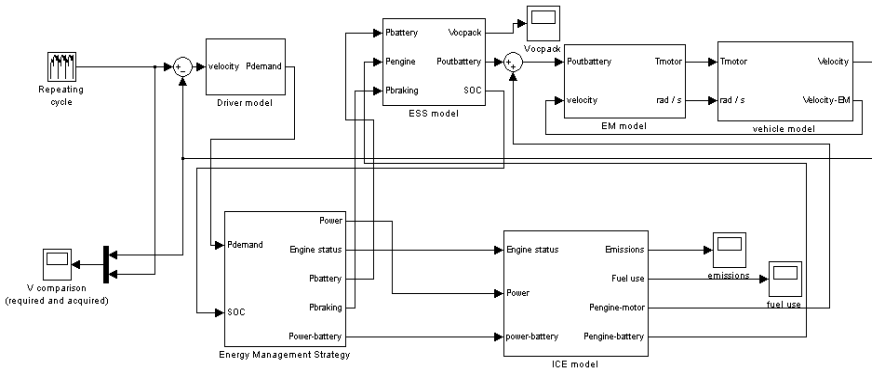
**Fig. 1.** Schematic illustration of the UTS PHEV code in MATLAB/SIMULINK environment

## 2 Vehicle Parameters, Specifications and Modelling

Table 1 listed the vehicle parameters and specifications for the UTS PHEV, a HEV and an ICE powered vehicle used in this study (Markel and Wipke 2001).

**Table 1.** Vehicle parameters and specifications

| Powertrain / Item | UTS PHEV | HEV | ICE powered vehicle |
|---|---|---|---|
| ICE | 1.5 L, 43 kW @ 4000 rpm | 1.5 L, 57 kW @ 5000 rpm | 1.8 L, 100 kW @ 6000 rpm |
| EM: | | | |
| Motor | 75 kW AC induction motor | 50 kW synchronous AC | - |
| Generator | - | 25 kW synchronous AC | - |
| ESS: | | | |
| Battery | NiMH, 10.08 kWh, 28 Ah | NiMH, 1.3 kWh, 6.5 Ah | - |
| Ultracapacitor | Maxwell, 122 Wh, 2.1 Ah | - | - |
| Transmission | 4-speed AT without torque converter | CVT | 4-speed AT |
| Aerodynamic drag coefficient | 0.335 | 0.3 | 0.335 |
| Coefficient of rolling resistance | 0.009 | 0.009 | 0.009 |
| Frontal area | 2.00 m$^2$ | 1.746 m$^2$ | 2.00 m$^2$ |
| Wheel radius | 0.282 m | 0.287 m | 0.282 m |
| Vehicle mass | 1379 kg | 1332 kg | 1295 kg |

To meet operational needs, apart from the control systems for the EM and ESS, the UTS PHEV requires a 4-speed AT to provide various power propulsion modes, varying the gear ratio between the ICE and the wheels and charging the battery pack. As illustrated in Figure 2, a 4-speed AT has dual desired inputs, which are from the electric motor and the ICE, and dual outputs, which are to the wheels and the electric generator. With the assistance of a 4-speed AT, a special EMS was developed to control the power flows within the vehicle according to the desired operating modes including those in emergency, which are EM only, EM and ICE combined, ICE only, ICE recharge, regenerative braking and mechanical braking as in Figure 3 (Gonder and Markel 2007).
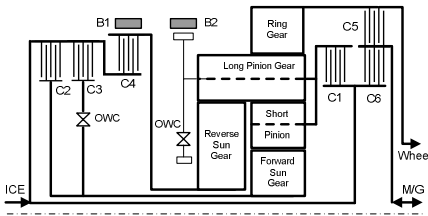


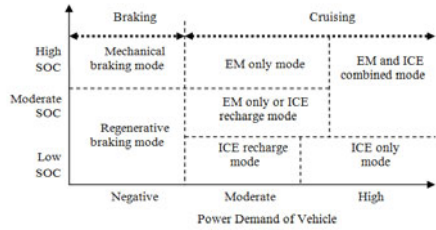**Fig. 2.** Power flow schematic of the 4-speed AT



**Fig. 3.** The EMS modes of operations.

# 3  Simulation Results

For this analysis, a low and high density traffic patterns drive cycles as shown in Figure 4 were used in order to experience the different level of aggressiveness or driving style for different traffic patterns.
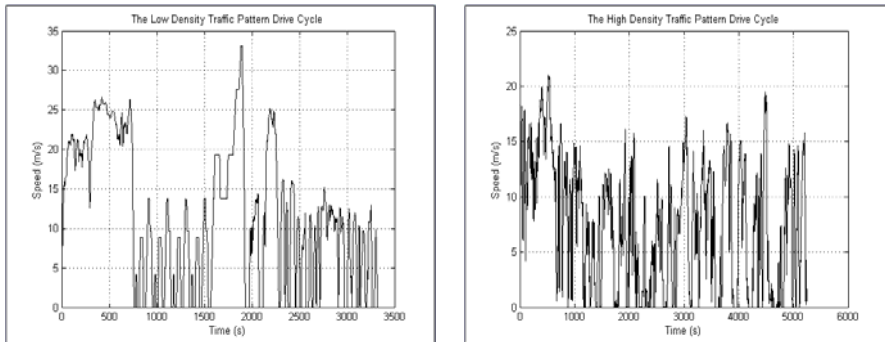


**Fig. 4.** Low and high density traffic patterns drive cycles.

A comparative study on a daily and annual operation cost was conducted during 40 miles distance travelled under the low and high density traffic patterns drive cycles. The reasonable daily trip is assumed as 40 miles distance covered from house to workplace and back to the house. The assumptions used to generate the annual energy cost estimates were fuel and electricity costs of \$2.50/gallon and \$0.09/kWh, respectively, and an annual driving distance of 15,000 miles.

Table 2 listed the fuel economy, AER and electrical consumption of the UTS PHEV, HEV and ICE powered vehicle during the low and high density traffic patterns drive cycles. As expected, specifically for the UTS PHEV, the high density traffic pattern requires lower electrical consumption and has a longer AER compared to the aggressive driving style. Based on the fuel economy results during the aggressive driving style, UTS PHEV has lower fuel economy because of more energy is required to repeatedly accelerate the vehicle. While the fuel economy of a HEV and an ICE powered vehicle are higher during low density traffic pattern. This is because the primary source for both powertrains is an ICE, which is more efficient at high and constant speed.

**Table 2.** Fuel economy, AER and electrical consumption

| Powertrain | UTS PHEV | | HEV | | ICE powered vehicle | |
|---|---|---|---|---|---|---|
| Item | Low | High | Low | High | Low | High |
| **Fuel economy (mpg)** | 84 | 105 | 55 | 46 | 37 | 25 |
| **AER (miles)** | 31 | 36 | 8 | 5 | - | - |
| **Battery usable energy (kWh)** | 8.064 | 8.064 | 1.04 | 1.04 | - | - |
| **Electrical consumption (Wh/mile)** | 260 | 224 | 130 | 208 | - | - |

Based on the daily and annual operation cost listed in Table 3, since the UTS PHEV uses less fuel to travel the same distance, it can save about 33% and 53% annually for the low and high density traffic patterns drive cycles, respectively, compared to a HEV. During the low and high density traffic patterns, the annual operational cost saving of the UTS PHEV is around 56% and 75% compared to the ICE powered vehicle. Based on this analysis, it can be concluded that the UTS PHEV is more suitable for city driving cycle, where the traffic is moving slow and there are more opportunities to recover the regenerative braking energy during the stop-and-start events and most of the energy used to move the vehicle comes from the grid, which is a lot cheaper compared to the fuel price.

## 4 Conclusions

Comparing the simulation results of fuel economy, AER and electrical consumption of the UTS PHEV subject drive cycles of low and high density traffic patterns, one can readily conclude that the AER of high density traffic pattern is significantly better than that for low density traffic pattern. With more effective regenerative braking, the UTS PHEV uses less energy than the HEV and ICE powered vehicle, especially for the high density traffic pattern, which leads to reduce the vehicle operation cost.

It also can be concluded that the UTS PHEV can improve the drive performance and energy efficiency with only one EM and ultracapacitor pack through the implementation of a sophisticated EMS and 4-speed AT without torque converter.

**Table 3.** Daily and annual operation cost under same distance of 40 miles

| Powertrain/Density traffic pattern / Item | UTS PHEV | | HEV | | ICE powered vehicle | |
|---|---|---|---|---|---|---|
| | Low | High | Low | High | Low | High |
| **Fuel consumed (gallon)** | 0.19 | 0.11 | 0.72 | 0.85 | 1.08 | 1.60 |
| **Energy consumed (kWh)** | 8.064 | 8.064 | 0.780 | 0.780 | - | - |
| **Daily fuel cost ($)** | 0.48 | 0.28 | 1.80 | 2.13 | 2.70 | 4.00 |
| **Daily electricity cost ($)** | 0.73 | 0.73 | - | - | - | - |
| **Daily operation cost ($)** | 1.20 | 1.01 | 1.80 | 2.13 | 2.70 | 4.00 |
| **Annual fuel cost ($)** | 176.25 | 105.00 | 675.00 | 798.75 | 1012.50 | 1500.00 |
| **Annual electricity cost ($)** | 273.75 | 273.75 | - | - | - | - |
| **Annual operation cost ($)** | 450.00 | 378.75 | 675.00 | 798.75 | 1012.50 | 1500.00 |

# References

Abdul Rahman, S., Zhang, N., Zhu, J.G.: A Comparative Analysis of Fuel Economy and Emissions between a Conventional HEV and the UTS PHEV. IEEE Transactions on Vehicular Technology for Special Issue on Vehicle Power and Propulsion 60, 44–54 (2010)

Abdul Rahman, S., Zhang, N., Zhu, J.G.: Recent Advancements in Management of Hybrid Vehicle Powertrains. In: International Conference on Sustainable Automotive Technologies 2008, Australia, pp. 1–4 (November 2008)

Yoo, H., Sul, S.K., Park, Y., Jeong, J.: System Integration and Power Flow Managements for a Series Hybrid Electric Vehicle using Supercapacitors and Batteries. IEEE Transactions on Industry Applications 44(1), 108–114 (2008)

Gonder, J., Markel, T.: Energy Management Strategies for Plug-in Hybrid Electric Vehicles. Presented at the 2007 SAE World Congress, Detroit, Michigan (April 2007)

Markel, T., Wipke, K.: Modeling Grid-Connected Hybrid Electric Vehicles Using ADVISOR. In: Proceedings of the Sixteenth Annual Battery Conference on Applications and Advance, Long Beach, California (January 2001)

# New Insights into the Australian Automotive Recycling Business

E. El Halabi and M. Doolan

The Australian National University, Canberra, ACT 0200, Australia
`ezzat.elhalabi@anu.edu.au`

**Abstract.** Eight automotive dismantlers/parts recyclers across News South Wales, South Australia and Victoria were interviewed to obtain an understanding of material flows and influences within the Australian automotive recycling system. This paper gives new insights into the current automotive recycling business and its operations by presenting and analysing some key quantitative and qualitative data that was collected through these interviews.

## 1 Introduction and Background

Automotive parts recyclers[1] or dismantlers are an important link in the reverse supply chain of cars. They seek to purchase End of Life Vehicles (ELVs) that are then dismantled and sold as parts or materials for profit. With 793 firms all over Australia, 3410 employees and a turnover of $1.1 Billion Australian Dollars (IBISWorld, 2011); this niche industry plays an essential role in the recycling of vehicles. Over the past five years, it handled 610,000 ELVs annually, which is about 4% of the Australian automotive fleet (Australian Bureau of Statistics, 2011).

In recent years environmental awareness has brought attention to the industry practice when dealing with pollutants contained in the ELVs such as hazardous fluids and chlorofluorocarbons etc. (Department of Environment and Heritage, 2002). The issues of car theft and car rebirthing[2] also became of concern. The industry in Australia remains largely unregulated. In other parts of the world like Europe and Japan, laws were adopted to help tackle the environmental issues through industry regulations - albeit with mixed results (El Halabi *et al.*, 2008).

This project attempts to create a policy decision tool that helps stakeholders discuss policy options and their implications on the Australian automotive

---

[1] Vehicle dismantling and parts recycling are two different but closely related activities. The first one is the process of taking a vehicle apart. The latter refers to the trade of used parts. Some parts recyclers do not completely dismantle vehicles themselves, like the U-Pull-It wrecking yards where customers do it. Both terms are used interchangeably in this paper.

[2] Car rebirthing is an activity which involves re-registering a stolen vehicle by using another vehicle's identity (Crimes Act, 1900).

recycling sector. We are using System Dynamics (SD) as a systems thinking method to model the ELV processing system in Australia. We are adapting the Modeling Process from (Sterman, 2000) in engaging with the stakeholders.

To date very limited information about the Australian automotive dismantling business is available. This paper attempts to address this gap, by providing a quantitative and qualitative snapshot of the average Australian automotive recycling business and its operations.

## 2  Interview Design and Questions

When designing the semi-structured interviews we loosely followed the interview design recommendations of (Vennix, 1996). We then interviewed thirteen stakeholders to get an understanding of the flows of products and materials in the system as well as the factors that influence these flows.

The interviewed stakeholders include: eight automotive recycling business owners/managers, two representatives from state industry associations, two managers of salvaged cars auction houses and officers of a law enforcement agency. In this paper we focus on the business characteristics and operations of the eight dismantlers in New South Wales (1), South Australia (3), and Victoria (4).

In trying to understand the operators' business characteristics, we specifically asked them about how long they've been in business for, their affiliation with industry associations, premises area, workforce size, working hours, specialisation (if any), and annual turnover.

For each of these points we prompted interviewees for trends and changes. Most of these factors vary over time and we wanted to gather an understanding on how their businesses evolved. To cover aspects of business processes we asked about stock control (handling of incoming cars, use of labelling), the use of Information and Communications Technologies (ICT), and the handling of hazardous waste.

## 3  Results and Analysis

In this section we present the aggregated results and analysis for each focus point with a brief description.

### 3.1  Business Characteristics

Years in business: On average, the interviewed operators have been in business for 20 years (3 of them have been operating for almost 30 years). They have well-established businesses with strong commercial presence and links with suppliers and customers. They are generally proud of their line of work and are constantly on the lookout for ways to improve their business. Most view role as doing something good to both the environment and the public (extraction of hazardous materials and recovery of reusable parts).

*Affiliation with industry association:* 7 out of the 8 interviewed operators are members of their state's automotive/motor trade association. An interviewee expressed his dissatisfaction with the industry association he is member of, in terms of lack of campaigning against illegitimate operators. Another one sees the association meetings as an opportunity to voice concerns or to propose ideas that could be beneficial to all. Membership of an industry association is not compulsory (by law). Those who are members link non-members to illegitimate in the industry practice.

*Premises area size:* On average, the area size of a dismantling business is 18,800sqm. This figure is based on operators having more than just a single site. Half of those interviewed had two or more sites. Dismantlers in general need large premises. This is due to the stocking system they use and the physical dimensions of cars.

*Workforce Size:* On average, size of workforce is 13 employees. Most of the operators indicated that they decide to grow or shrink their workforce size depending on how well their business is doing. We found that labour cost varies depending on the function of the employee. Skilled mechanics and salespeople are well paid and represent a major cost factor as well as an asset/investment for the business.

*Working Hours:* 6 out of the 8 interviewed operators are open 9 to 5, Monday to Friday. They recognise that overtime labour is costly and generally try to avoid it. Operators that engage in mechanical repairs activity are the ones more likely to have overtime. 2 of the interviewed operators operate 7 days a week to cater for the Do-It-Yourself market. Dismantlers that rely on another revenue stream such as mechanical repairs recognise its profit potential and hence are able to afford the costs of overtime work. Revenue from parts/materials trade alone cannot justify the added costs.

*Specialisation:* 5 out of the 8 interviewees have some form of ELV-type specialization that allows them to operate within specific market niches. Some, for example, specialise in a specific make and/or model like Holden Commodore. Others may specialise in vehicles older than 10 years or 4WD/commercial vans, or even in a group of makes like all Japanese or all German. In addition to used parts trade, all interviewed dismantlers were found to engage in mechanical repairs and used car trade. In a couple of cases we noted that mechanical repairs were the core business activity, while the used parts trade being only supplemental.

*Annual Turnover:* In terms of fiscal turnover and based on information given from 2 interviewees who agreed to share their figures, we have an average of 2.5 Million Australian Dollars. In terms of number of vehicles processed and based on the 8 interviews: 1530 ELVs per year. Though when taking into account the maximum capacity that some operators are capable of, the number can go up to 1910 ELVs. It is worth noting that the combined total of ELVs turnovers from these interviews is 12,258 (2% of the total ELVs in Australia).

We found that the operators could be grouped according to the number of ELVs they handle each year. Small scale (less than 300 ELVs), mid-range (300-2000 ELVs), and large scale (more than 2000 ELVs). The interviewed auto recyclers are spread across these groups (three small, three mid-scale, and two large).

## 3.2 Business Operations

*Handling of incoming cars:* All interviewed dismantlers have well-established systems to manage incoming ELVs. The process includes the labelling of vehicles (creating a file for every ELV), testing (if driveable), depollution (draining engine fluids, removal of batteries, tyres), and stocking the vehicle in the yard. A small scale operator that we interviewed pointed that they sometimes do not 'depollute' a vehicle if they see a potential in it being sold as a cheap old car.

*Labelling:* All interviewed operators engage in some form of labelling (incoming ELVs stock, parts) to help manage their stock. U-Pull-It type operators only label vehicles while parts stay on the vehicles until they are removed by the customers.

*Use of ICT:* 7 out of the 8 interviewees make use of ICT to help find potential stock in the market, manage incoming ELV stock (labelling, sorting), and manage dismantled parts stock and sales.

*Hazardous waste:* All interviewees were aware of their local EPA requirements concerning the handling of hazardous materials. Batteries, drained fluids, and even air conditioning gas are collected then sold to their respective markets. Tyres were the only component that operators had to pay for to dispose of. Two dismantlers have certified systems to capture left over petrol and liquid petroleum gas (LPG) from ELVs then use them to power their business vehicles.

## 4 Discussion

One of the early challenges that we faced when we first attempted to create an SD model of the ELV processing system in Australia was to find relevant and concrete data about the automotive recycling business. Reports like (Accenture & VACC, 2006) provide a good high level perspective about the industry but lack the data about businesses. We needed to know how long these businesses have been in operation for, workforce, annual turnover, sources of revenue, etc. along with their historic trends as well as the norms and processes being followed.

The results presented in this paper serve both as reference point and as a part of the bases of a SD model being developed to study policy options and their implications on the industry.

## 5 Conclusion

Prior to these interviews, little information was available about the automotive recycling business in Australia. Through this paper, we presented relevant business characteristics data. We identified three different groups of operators based on the volume of ELVs they handle per year. We also shed light on key aspects of their business operations that included a major environmental concern (the handling of hazardous waste).

# References

Accenture & Victorian Automobile Chamber of Commerce, HORIZON, - Changes and Challenges for the Australian Retail Automotive Industry, Victorian Automobile Chamber of Commerce, Melbourne (2006)

Australian Bureau of Statistics, Motor Vehicle Census, cat. no. 9309.0, ABS, Canberra (2011)

Crimes Act 1900 (NSW) s. 154G (Austl.).

Department of Environment and Heritage, Environmental Impact of End-of-Life (2002)

Vehicles: An Information Paper, Canberra

El Halabi, E., Doolan, M., Newell, B.: A Global Comparison of End-of-Life Vehicles Policies. In: International Conference on Sustainable Automotive Technologies, Melbourne (2008)

IBISWorld, Motor Vehicle Dismantling and Used Part Dealing in Australia Industry Report, F4624 (2011) (retrieved from IBISWorld database)

Sterman, J.D.: Business Dynamics: Systems Thinking and Modeling for a Complex World. McGraw-Hill, Boston (2000)

Vennix, J.A.M.: Group Model Building: Facilitating Team Learning Using System Dynamics. Wiley, Chichester (1996)

# An Analytical Method for Acoustic Characterisation of EV Interior Trims

Vipil Varghese[1], Laith Egab[1], Vignesh Rajan[1], Mohammad Fard[1], Reza Jazar[1], and Jason Miller[2]

[1] School of Aerospace, Mechanical and Manufacturing Engineering,
  RMIT University, Melbourne, Australia
 `mohammad.fard@rmit.edu.au`
[2] Futuris Automotive Interiors (Australia) Pty Ltd

**Abstract.** The growing concern for the environment and advancement in technology has led the automotive industries to develop green vehicles. The development of EV among alternative power-train has attained popularity. Replacing conventional power-train with an electric powertrain does not resolve the acoustic issues of vehicles. However, acoustic tests performed on EV shows that noise levels in the cabin are significant in high sensitivity region of human hearing. At present, limited research has been carried out in the acoustics of EV interiors due to the complexities involved in predicting noise level. This paper aims at developing an efficient method to optimize vehicle interior acoustics by characterizing interior trims. Alpha cabin and impedance tube experiments were conducted on porous materials to obtain acoustic and non-acoustic properties. The non-acoustic properties thus obtained were used as input parameters for a Statistical Energy Analysis (SEA) tool to obtain simulation results. Experiment and simulation results showed good correlation which would assist in creating a database of interior trims. The proposed method can therefore be used as an effective and efficient means to predict and optimize EV interior acoustic performance in the early design phase. The assistance of the developed analytical method in optimizing NVH performance has a significant impact on saving time and the cost of design.

## 1 Introduction

In the automotive industry, current research is focused on the design of fuel efficient vehicles such as an electric vehicle (EV) made of lightweight and cost effective materials. However, the design and manufacturing sectors are not taking acoustic performance into account, resulting in interior cabin noise that effect human sensitivity at the higher end of the scale.

There are existing materials that can improve acoustic performance such as fibre, foams, etc. Characterization of these materials requires the evaluation of their acoustic and non-acoustic properties. Non- acoustic properties were evaluated

using classical methods. Porosity and air flow resistivity were measured directly while tortuosity, viscous and thermal characteristic lengths were measured by an inverse method [1].

Acoustic properties such as sound absorption coefficients and transmission loss of acoustical materials have been studied for many years. For example, Cherng et al. performed a comparative study on sound absorption coefficients and transmission loss of various porous acoustical materials [2]. The study investigated several fibrous and foam materials including needled shoddy and resinated shoddy. The results showed that the acoustic properties such as sound absorption and transmission loss are not only related to the type of the material but also the material structure. In addition, the resinated cotton fibre acoustically outperformed the absorption of needled cotton fibre. Duval *et al.* [3] investigated a simulation approach using finite transfer matrix method (FTMM) to analyse two types of materials for acoustic absorption in the cabin with limited validity. Claudio *et al.* [4] then extended the analysis to more test cases and substantially improved the correlation between simulations and testing results.

However, each cabin is likely to perform acoustically in different ways. Designers have difficulty characterizing the noise in term of sound absorption and transmission loss. Current technologies such as Finite Element Method (FEM) and Boundary Element Method (BEM) are applicable only for low frequency range. In this study, numerical investigation based on Statistical Energy Analysis (SEA) is presented which is suitable in the mid-high frequency range (>400 Hz). The obtained results are then correlated with results obtained by experimental testing in order to limit the amount of practical tests .The proposed method can therefore be used as an effective and efficient method to predict and estimate EV interior acoustic performance in the early design phase. The assistance of the developed analytical method in optimizing NVH performance has made a significant contribution to saving time and reducing the cost of design.

## 2   Methodology

Sound absorption coefficients of the test materials were measured using the Alpha Cabin and the Impedance Tube. Further, acoustic modelling (simulation) also produced the sound absorption coefficients to correlate with the experimental results. Figure 1 below shows a systematic flow chart that outlines the validation process between the experimental and simulation tests.

The Alpha cabin is a small reverberation chamber with non-parallel walls, which is used to measure the random sound absorption coefficient (RSAC) of the test sample. The acoustic absorption of the alpha cabin is very low and this design ensures a high level of sound insulation so as to maintain the low levels of background noises at that particular frequency. Following the ASTM C423 standard,
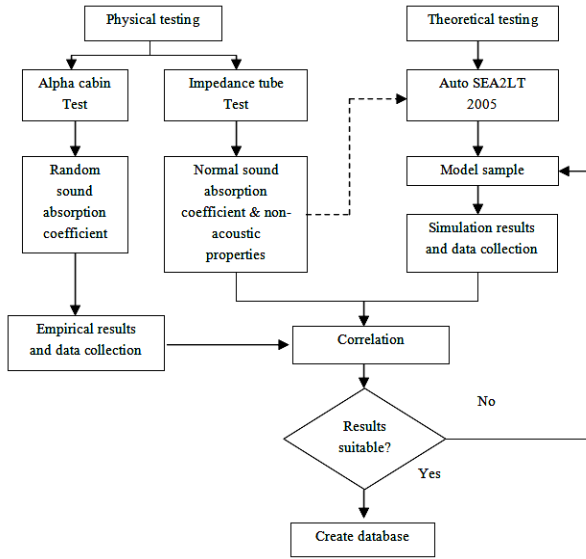
**Fig. 1.** Process validation cycle

the reverberation time in the Alpha Cabin is measured in order to determine the RSAC, according to Sabine's formula given below:

*Total Sound Absorption: Sα = (55.3\*V/c)\*(1/T$_2$-1/T$_1$)*

Where c is the speed of sound, V is the volume of cabin, S is the surface area, α is the absorption coefficient, T$_2$ and T$_1$ are the reverberation time with and without a sample respectively.

The Impedance tube is an acoustic duct used to measure the normal sound absorption coefficient (NSAC) of the test sample. It works on the principle of standing wave interference patterns, where the transfer function method is used to measure the pressure difference between two adjacent microphones.

Following the ASTM E1050 standards, the NSAC of the test sample is determined. Table 1 shows the non-acoustic properties of the test sample which is required as the input parameters for acoustic modelling. Porosity and flow resistivity are found using the direct measurement technique. The inverse method was used to determine tortuosity, and characteristic thermal and viscous length [2].
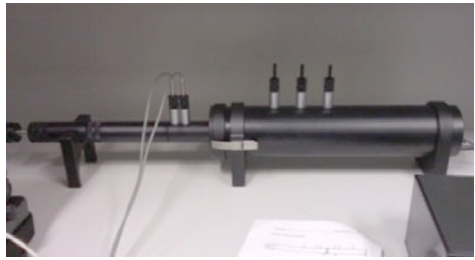
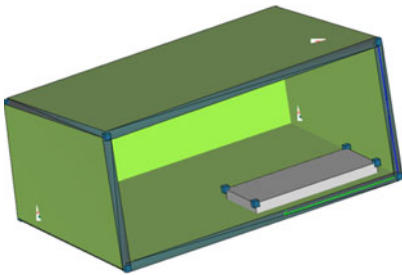**Fig. 2.** Alpha Cabin



**Fig. 3.** Impedance Tube



**Fig. 4.** Simulation of Alpha Cabin and Foam using SEA

Statistical Energy Analysis (SEA) is used for acoustic modeling of the test samples as the previous methods such as Finite Element Method (FEM) and Boundary Element Method (BEM) become less reliable at mid-high frequency (<400 Hz). Basically, SEA is the power flow between sub-systems within a given system and dissipation of power within the sub-system [6]. AutoSEA2 LT was the simulation package used to perform the analysis.

## 3 Result and Discussion

Sound absorption of porous material is one of the important factors in quantifying the quality of interior cabin noise. The test was carried out on materials SM200L and SM300L. These materials are a combination of polypropylene and polyester with a black scrim. They are used in many automotive applications such as instrument panels and inside door panels.

**Table 1.** Physical Parameters of Porous Materials ( + Direct method , # Indirect method)

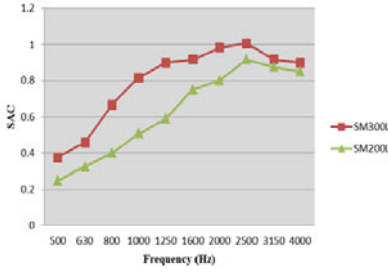|                                       | SM200L | SM300L |
|---------------------------------------|--------|--------|
| Density (Kg/m$^3$) [+]                | 18.1   | 16.2   |
| Porosity (-) [+]                      | 0.99   | 0.99   |
| Flow resistivity (Ns/m$^4$) [+]       | 36000  | 31288  |
| Tortuosity (-) [#]                    | 1.1    | 1.1    |
| Viscous char. Length (µm) [#]         | 196    | 196    |
| Thermal char. length (µm) [#]         | 384    | 384    |
| Thickness (mm)                        | 13     | 21     |

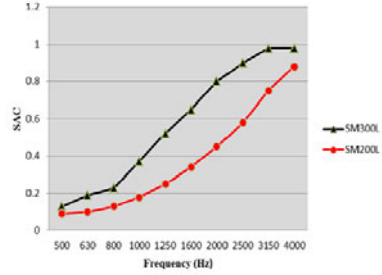**Fig. 5.** Random sound absorption coefficients of SM200L and SM300L

**Fig. 6.** Normal sound absorption coefficients of SM200L and SM300L

These two materials were tested in the Alpha Cabin and Impedance Tube to determine the RSAC and NSAC respectively. Figures 5 and 6 reveal that SM300L has better absorption across the whole frequency range. Although SM200L has higher flow resistivity than SM300L, the latter has a better sound absorption coefficient. This is due to the greater thickness of SM300L.

As expected, it should also be noted that the RSAC measured in the Alpha Cabin is much higher than the NSAC measured by the Impedance Tube. This is due to the Alpha Cabin's ability to take random incidence sound absorption into account.

Figure 7 shows that the correlation of the NSAC between the simulation and the experimental test for both materials is relatively close. It is clear that the physical parameters of porous materials can be used to predict the sound absorption of porous sound absorbing materials.

Figure 8 show a significant difference between the simulated and the measured acoustic absorption coefficients. These differences are known to be due to non-perfect diffusivity of the measurement environment, as well as to a diffraction of sound at the "edge effect" [4, 7].
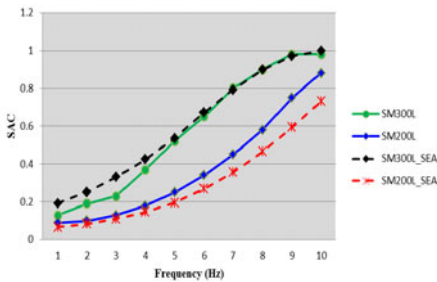


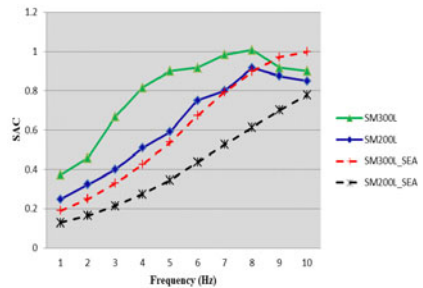**Fig. 7.** Normal Sound Absorption coefficients Correlation of SM200L and SM300L

**Fig. 8.** Random Sound Absorption Coefficients Correlation of SM200L and SM300L

## 4 Conclusion

The potential usefulness of the Statistical Energy Analysis (SEA) for characterizing interior trim noise has been demonstrated in term of sound absorption of materials. The acoustical Simulated and measured results of material sound absorptions show the similar trends for normal and random sound absorption coefficients. However correlation for random absorption is yet to be achieved. The physical properties and micro structure of these two materials (SM200L, SM300L), helps conclude that material with higher thickness; larger airflow resistivity will have higher noise absorption than material with lower thickness, smaller airflow resistivity. Non- acoustic properties such as flow resistivity and porosity are identified to have significant impact on characterizing the sound absorptions of the acoustical materials.Further study on Investigation of different materials is to be done in order to validate the methodology for acoustic characterisation of interior trim.

## References

[1] ASTM C423: Standard Test Method for Sound Absorption and Sound Absorption Coefficients by the Reverberation Room Method

[2] Doutres, O., Salissou, Y., Atalla, N., Panneton, R.: Evaluation of the acoustic and non-Acoustic properties of sound absorbing materials using a three-microphone impedance tube. J. Applied Acoustics 71, 506–509 (2010)

[3] Cherng, J., Xi, Q., Mohanty, P., Ebbitt, G.: A comparative study on sound transmission loss and absorption coefficient of acoustical materials SAE Technical paper 2011-01-1625; doi:10.4271/2011-01-1625

[4] Duval, A., Roundeau, F., Dejaeger, L., Sgard, F., Atalla, N.: Diffuse field absorption Coefficient simulation of porous materials in small reverberation rooms: finite size and Diffusivity issues. In: 0th French Congress on Acoustics, Lyon (2010)

[5] Bertolini, C., Guj, L.: Numerical Simulation of the measurement of the diffuse field absorption coefficient in small reverberation rooms. SAE Technical paper 2011-01-1641; doi:10.4271/2011-01-1641

[6] Lyon, R.H., Dejong, R.G.: The Theory and Application of Statistical Energy Analysis, 2nd edn. Butterworth-Heinemann (1995)

[7] Saha, P., Pan, J., Veen, J.: Thoughts behind Developing SAE Standard J2883 - Random Incidence Sound Absorption Tests Using a Small Reverberation Room. SAE Technical Paper 2009-01-2141 (2009); doi: 10.4271/2009-01-2141

# Noise Evaluation of a Control Valve in a Variable Compressor

Yong-Joo Lee[1], Geon-Ho Lee[2], and Byeong-Eun Lim[3]

[1]. Doowon Technical University,An-sung City, Kyoung-ki do, Korea Republic
 yjlee@doowon.ac.kr
[2]. Doowon Technical University,An-sung City, Kyoung-ki do, Korea Republic
[3]. Doowon Electronic Company, A-san City, Chungcheongnam-do, Korea Republic
 trylim98@doowonhi.com

**Abstract.** In an automobile air conditioning system with variable compressor, there was a noise from a control valve at special range. An experimental study was conducted on elimination of noise and improving performance and quality. First, the cause of noise was analyzed through NVH tests of a control valve and a vehicle. Second, two methods were selected to improve the NVH; frequency change and inserting grease in control valve. Finally, the effect was verified.

## 1    Introduction

Due to the increase in oil prices, the demand on high efficiency vehicles and fuel efficient engines has increased recently. Therefore, high efficiency compressors will be applied gradually on in-vehicle air conditioning systems because the air conditioning compressor consumes a lot of engine power.

   In this paper, the causes of noise from control valve in variable compressor and methods to reduce the noise were investigated. Through evaluating the NVH tests of control valve, compressor and vehicle, it was found out that noise had been made by the external control valve in variable compressor. Based on the results of experiments a way to reduce the noise was presented.

## 2    Noise investigation

### 2.1    Cause of Noise – Working Principle of Control Valve

First, the cause of noise through the structure and working principle of control valve was investigated. The external control valve is composed of connector pins, plunger, solenoid, valve, and bellows. The connector pins supply input current to solenoid. The plunger is a part actuated by current and the solenoid creates the magnetic forces. Bellows is a sensor detecting suction pressure.

The air conditioning controller in vehicle supplies a 400Hz PWM signal to the control valve. When the input current supplied to the connector pin is increased above a set value, the plunger is magnetized and moves to the core, decreasing an air gap. This will close the valve. After the valve is closed, pressure of the swash plate chamber is decreased since the refrigerants are kept from flowing into this chamber. Then, the swash plate is tilted up to the maximum angle causing the compressor to discharge with maximum capacity. Conversely, when the input current is decreased under a set value, pressure of the swash plate chamber is increased due to the increment of refrigerant flow. The plunger is returned to the original position by the spring force and the valve is opened. Then, the swash plate is tilted down to the minimum angle causing the compressor to discharge with minimum capacity. When the input current is between maximum- and minimum value, the valve is moved to a position proportional to input current. The refrigerant flow into the swash plate chamber is controlled. Then, the swash plate is tilted to the controlled angle and the compressor discharges with the controlled capacity.

Magnified illustrations of the valve that controls refrigerant flow including the cause of noise, are shown in Figure 1.
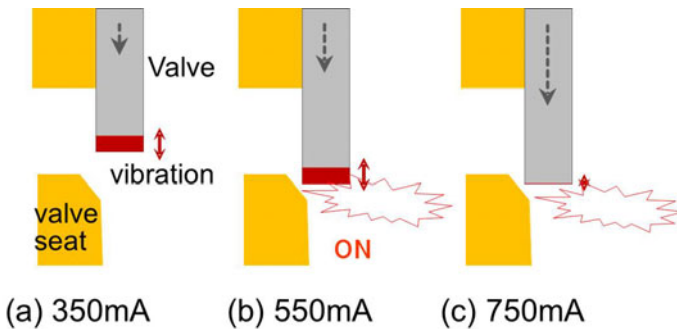


**Fig. 1.** Vibration of valve and valve seat according to currents

When the valve is initially assembled, it is in open state. When the PWM signal of 400Hz voltage is exerted, the valve begins to vibrate. When the current is 350mA, noise is not produced since the valve is not in contact with valve seat. But at near 550mA, the valve is very close to the valve seat and vibration of valve cause noise. At current levels over 750mA, the valve pushes on the valve seat by the magnetic force and vibration decreases.

## 2.2    Noise Evaluation – Measurement of Control Valve Sound

### Measurement of Control Valve Sound

Noise and vibration of the control valve were measured. The valve was inserted into a test jig on which a vibration sensor was mounted. A microphone was

positioned horizontally at 100mm from the valve. Setting values for measurement of noise and vibration were as follows: supply pressure Pd was fixed at 8kgf/cm$^2$g; current was swept from 200mA to 800mA.

A colour map of noise and vibration in vertical direction at 350mA is shown in Fig.2. Noise was not found in the whole frequency domain and vibration insignificant. Therefore, it was concluded that noise did not occurr in the low current range such as 350mA.
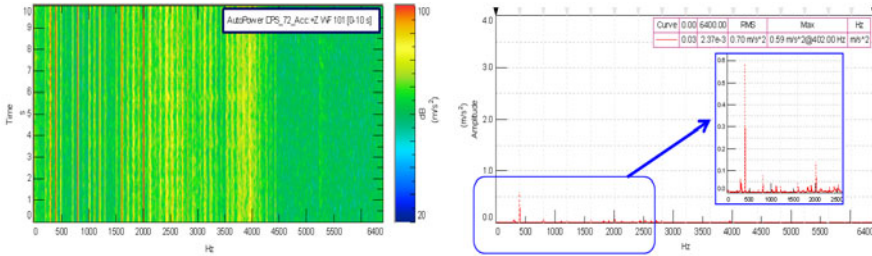


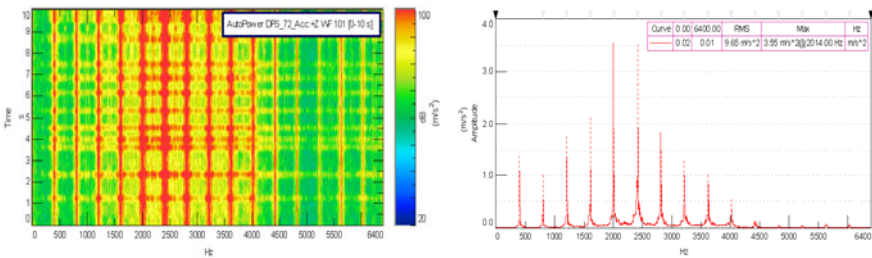**Fig. 2.** Noise colour map and vertical vibration for 350mA input current



**Fig. 3.** Noise colour map and vertical vibration for 550mA input current

The colour map of noise and vibration in the z axis direction at 550mA is shown in Fig.3. It was found that the noise level was higher than for the case of 350mA, and the noise occurred in multiples of the 400Hz input current. Therefore, it was concluded that the level of noise was affected by the input current. The noise current range has been known through the experiments at Pd 8kgf/cm$^2$g to be in the range of 500mA~600mA.

The characteristic change of vibration as a function of the discharge pressure was tested. The discharge pressure, Pd was changed to 8kgf/cm$^2$g, 15 kgf/cm$^2$g and 25 kgf/cm$^2$g when noise occurred. The characteristic of vibration changed as a function of discharge pressure. It was concluded that discharge pressure was one of the factors affecting noise and vibration of the control valve.

*Measurement of Variable Compressor Sound*
The noise test of variable compressors, in mass production, equipped with the control valve was carried out. External variable compressor samples of companies A

and B were checked whether noise would occur or not under changing current conditions. In the case of compressor A-1 (first compressor of company A); the noise occurred in the 250mA~450mA range. The A-2 compressor had noise occurring in the 550mA~800mA range and the A-3 compressor in the 250mA~350mA range. Summarized, the A-1 and A-3 compressors sounded in the low current range and the A-2 (and B) compressors sounded also in the high current range.

### Measurement of Vehicle Sound

The noise evaluation was also performed in vehicle. This time it was tested by human feeling in engine-off conditions, changing the current level from 250mA to 750mA. The test vehicles; A, B, C, and D were of different type and all experienced noise. Therefore, it can be concluded that noise occurs to some extent in almost all vehicles equipped with external variable compressor.

## 3    Reduction of Noise

Noise occurs inevitably on vehicles equipped with an external variable compressor. In order to reduce this noise, 2 different methods were suggested. The first method is to make the frequency higher and the second was to insert grease into plunger chamber. These two methods were evaluated.

### 3.1    Making the Frequency Higher

The force equation of the damped vibration system is as follows:

$$m\ddot{x} + c\dot{x} + kx = F_0 \cos\omega_d \tag{1}$$

The steady state response equation is as follows:

$$X_P = A_0 \cos(\omega_d t - \emptyset) \tag{2}$$

Deriving the amplitude of $A_0$:

$$A_0 = \frac{F_0/m}{\sqrt{(\omega^2 - \omega_d{}^2)^2 + (2\varsigma\omega\omega_d)^2}} \tag{3}$$

From eq. (3), the system amplitude $A_0$ decreases with increasing supply frequency $\omega_d$. The standard applied frequency to the control valve is 400Hz. Noise reduction was measured when the applied frequency was changed to 500Hz and 600Hz. First only the control valve was measured. After that, it was measured in a vehicle equipped with the control valve at engine-off conditions. It was concluded that vibration of valve decreased proportional to higher frequency (from 400Hz to 600Hz). This was also experienced in the vehicle.

## 3.2 Insert Grease

For the second noise reduction method, the plunger was daubed with grease. The high viscosity of grease increases the damping coefficient in eq. (1). The vibration of valve decreased during the test. With approximately 0.1g ~ 0.2g grease an improvement of 8 dB in maximum noise level and 2.1 m/s$^2$ in vibration was accomplished. However, the weakness of this method is the difficulty to control the amount of grease in production.

## 4 Conclusion

The external control valve of a variable compressor made a sound actuated by a PWM frequency in a distinct range. The noise of the external control valve was affected by the discharge pressure. In almost all external variable compressors a noise occurred to some extent.

Two methods are suggested for improvement: high frequency and grease. These methods were verified by experimental results. It was effective to decrease the noise approximately 3dB when applying a high PWM frequency of 600Hz and about 8dB when inserting grease.

## References

Charel, M.: Analysis of fuel consumption reduction potential through the use of an electrically air conditioning compressor, Theses for Master's Degree Nelson Mandela Metropolitan University (2007)

Lee, G.H., Lee, T.J.: A Study of dynamic analysis of variable displacement swash plate type compressor with internal control valve. In: Summer Season Conference The SAREK (2005)

Kim, K.B.: An Experimental Study on Power Consumption of Vehicle Air Conditioning Compressor, Theses for Master's Degree in Ajou university, pp. 9–12 (2009)

# Design for Improving the Performance
# of a Control Valve in a Variable Compressor

Yong-Joo Lee[1], Geon-Ho Lee[2], and Byeong-Eun Lim[3]

[1]. Doowon Technical University,An-sung City, Kyoung-ki do, Korea Republic
 yjlee@doowon.ac.kr
[2]. Doowon Technical University,An-sung City, Kyoung-ki do, Korea Republic
[3]. Doowon Electronic Company, A-san City, Chungcheongnam-do, Korea Republic
 trylim98@doowonhi.com

**Abstract.** This is the study on design of a control valve for the control of the variable capacity compressor. The theoretical and numerical analysis was performed for solenoid interpretation and compared with experimental results. Maxwell program was used for numerical analysis of the solenoid. The air flow in the control valve was analysed as a mathematical model and verified through experiments. Through the interpretation of the correlation of input current and suction pressure, major factors affecting the compressor have been identified. To improve the performance of the compressor in main parameters; bellows, diameter of the sleeve, and electromagnetic forces can be changed in the control valve.

## 1    Introduction

Compressors used for vehicle air-conditioning systems are one of the highest efficiency requiring parts since it consumes a lot of engine power. Recently in the automotive industry, transitions are being made from fixed capacity compressors, (which are high energy consuming types) to variable capacity compressor (which are low energy wasting and high efficient). Variable compressors can be classified into two general categories namely: internal variable compressor and external variable compressors. The discharge capacity of the former is controlled by a mechanical valve as a function of the suction pressure in air conditioning systems. The discharge capacity of the external variable compressor is controlled by external electrical signals. Variable compressors are connected to the engine and use a pulley and a belt driven by engine power. Reciprocating pistons riding on the face of a rotating swash plate make the refrigerant to discharge or suctioned.

When cabin temperature is high or load of the engine is low, the angle of the swash plate can be increased, which also causes the piston stroke to increase. When doing so, the discharge flow rate and the amount of refrigerant circulating in air conditioning system increase, resulting in a quick drop of cabin temperature. When cabin temperature becomes properly lowered, the angle of the swash plate can be decreased, shortening the piston stroke, and minimizing the discharge flow

volume. In this case, engine's power consumption decreases as well. As per the above explanation, an external control valve is used for control of the angle of swash plate in compressor. "The plunger" installed in the external control valve is driven by electromagnetic force, which is proportional to the input current. The plunger's movements directly influence the amount of refrigerant flow.

In this study, we would like to find out how to interpret the flow in the control valve using a mathematical mode. The model will be verified with experiments. The main parameters to improve the performance of a variable compressor were discovered.

## 2 The Analysis of Electromagnetic Force

### 2.1 Modelling of Solenoid

The solenoid was modelled in order to analyse the magnetic force. Only one side of the solenoid was modelled since it is axial symmetric. The modelled solenoid consists of a disk, housing, housing body, plunger, core, and coil. Magnetic flux can pass through these parts of which the material was chosen to be SUM24L or free cutting steel. In addition, the material of the tube which supports the plunger was SUS303 and bobbin & mold surrounding the coil was modelled as air because of its permeability being equivalent to nylon 66. The analysis result of electromagnetic force was shown using Maxwell V.12 software.

### 2.2 Measuring Electromagnetic Force

Electromagnetic force was measured in order to verify modelling results. The force could be measured using a load cell, attached to the electromagnetic force tester. While the plunger's air gap was maintained to 0.2mm by turning the handle, the required amount of current was supplied to the pulse width modulated (PWM) controller. The measuring range is 250mA to 750mA which is the practical limit of the driving current of the valve.

Similar to a vehicles' ECU module, the PWM controller generates a PWM signal which is proportional to the input current and feeds into the control valve at 400Hz. Then eventually, a magnetic force proportional to the PWM signal is generated in the control valve.

A comparison between experimental and numerical results is shown in Figure 1 for an air gap of 0.2mm and 0.6mm, changing current from 0mA to 750mA. In both cases, numerical results from Maxwell agree for over 90% with the experimental ones. It was found that electromagnetic forces for different air gaps change varying the current from 102mA to 712mA. Despite of air gap increment, electromagnetic force was not significantly lowered. It shows that the control valve was designed to make the electromagnetic force more depend on input current instead of air gap.
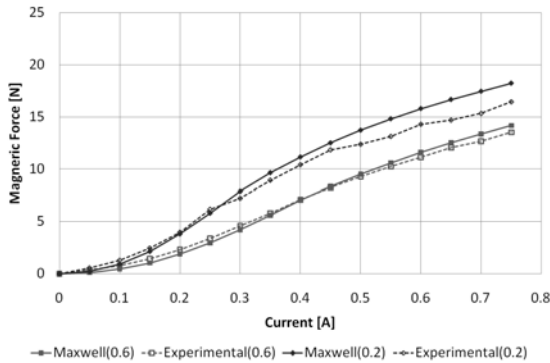
**Fig. 1.** Comparison of experimental and simulation results

## 3    Equations

### 3.1    *Equation of Motion*

Characteristic of the valve in the steady state conditions provides an important base for deciding the volume when designing valve. The balanced forces in steady state condition can be expressed as:

$$\sum F = -P_S A_S + P_C A_C + F_A + F_{km} + F_{bel} - F_{mag}$$

(1)

Where: $A_s$ is the area applied by suction pressure; $A_c$ the area applied by control pressure; $P_s$ the suction pressure; $P_c$ the crank room pressure; $F_A$ the aerodynamic force; $F_{km}$ the plunger spring force; $F_{bel}$ the bellows assay spring force and $F_{mag}$ the solenoid magnetic force.

The compressible fluid flow rate is classified as sonic or subsonic according to the critical factor as shown in Eq. (2)

$$F_C = \left(\frac{2}{k+1}\right)^{\frac{k}{k-1}}$$

(2)

If $\frac{P_1}{P_2} < F_C$, the flow is sonic and the mass flow rate is obtained as:

$$\dot{m} = CAC1\frac{P_1}{\sqrt{T_1}}$$

(3)

Where: $A$ is the effective valve area, $C1 = \sqrt{\frac{k}{R}\left(\frac{2}{k+1}\right)^{\frac{k+1}{k-1}}}$ , and $T$ the temperature at the valve seat.

If $\dfrac{P_1}{P_2} > F_C$, the flow is subsonic and the mass flow rate is obtained via:

$$\dot{m} = CAC2 \frac{P_1}{\sqrt{T_1}} \left(\frac{P_2}{P_1}\right)^{\frac{1}{k}} \sqrt{1 - \left(\frac{P_2}{P_1}\right)^{\frac{k-1}{k}}}$$

(4)

Where: $C2 = \sqrt{\dfrac{2k}{R(k-1)}}$, $F_c$ is calculated from the specific heat of air,

$\kappa$=1.4, coefficient of gas $R$=287.05 [Nm/KgK], and converting to MKS unit as $F_c$=0.528. The mass flow rate is obtained as:

$$\dot{m} = 0.03816A \frac{P_1}{\sqrt{T_1}}$$
(sonic)

(5)

$$\dot{m} = 0.149A \frac{P_1}{\sqrt{T_1}} \left(\frac{P_2}{P_1}\right)^{\frac{1}{k}} \sqrt{1 - \left(\frac{P_2}{P_1}\right)^{\frac{k-1}{k}}}$$
(subsonic)

(6)

The effective valve area $A$ is expressed as follows considering geometrical relations:

$$A = \frac{\Pi(D+d)}{2} \cdot L = \frac{\Pi(D+d)}{2} \cdot X\cos\alpha$$

(7)

Where, $D=d+2X\cos\alpha \cdot \sin\alpha$.

Therefore, pressure differential rate is obtained from:

$$\dot{P}_2 = \frac{R \cdot T_C}{V_C}(\dot{m}_{IN} - \dot{m}_{OUT})$$

(8)

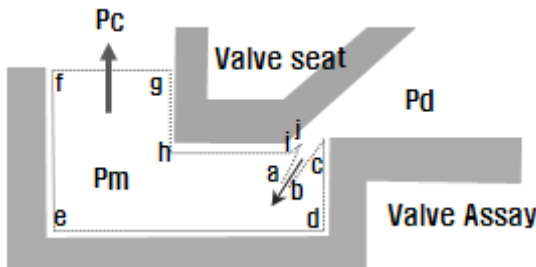Where, $\dot{m}_{IN}$ is inlet mass flow and $\dot{m}_{OUT}$ is outlet mass flow.



**Fig. 2.** Construction detail of valve and valve seat

Flow-force is a momentum change on the control surface when a fluid passes a valve space and orifice. The reaction force of the flow-force acts on the valve assay. The Axial force on valve is the same as the sum of axial ingredients in influx and out-fluxes through a boundary as shown in Fig.2. The a-b is a contraction in the jet. In a real valve, the flow velocity is very much faster in a-b because the a-b area is smaller than area f-g. Because the out-flux momentum in f-g is very much smaller than the influx in a-b, it can be ignored. The pressure in i-j and c-d regions has become lower than other regions because the inflow speed is greatly increased around the input orifice.

Pressure ingredient in k-i region is to ingredient of $(PP_{de}-P_{ki}) \cdot A_{de}$, the force is left direction and valve is closed. Flow force $F_A$ acting on valve is in Eq. (9).

$$F_A = \left(1 - E1 \frac{A_{12}}{A_S}\right) \cdot (P_1 - P_2) \cdot A_S$$

(9)

Where: $A_{12}$ is the flow rate, $A_S$ the seat area and $E1 = 0.97$ for a 45° poppet valve angle.

It was assumed that the pressure before the valve is uniformly equal to $P_1$ and the pressure after the valve is uniformly equal to $P_2$.

## 2    Flow Test

$N_2$ gas at a pressure of 7 kgf/cm²g was supplied to the control valve for flow testing. The volume pressure $P_c$ and suction pressure $P_s$ were measured as a function of input current, changing, from 0.01A to 0.75A. Data logging occurred when $P_s$ conditions were steady state. A comparison of simulated- and experimental results is shown in Figure 3. A good match between the results is observed in the operating region hence the mathematical model is verified. The characteristic graph shows a decreasing suction pressure $P_s$ when the input current increases. This is because the opening-length of valve decreases when the magnetic force increases.
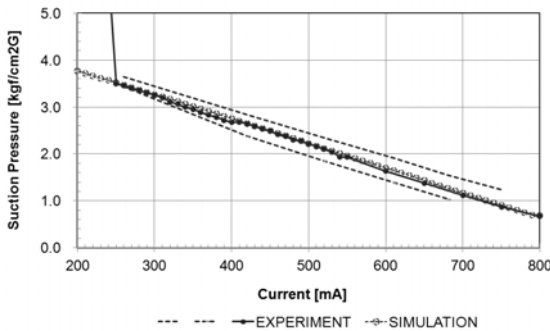


**Fig. 3.** Comparison between simulated- and experimental results of Ps versus current

## 3.    Design Parameters Study

Firstly, an investigation was conducted on the change of suction pressure as a function of the bellows spring constant. The spring constant was adjusted to: 14N/mm, 18.14N/mm, 22N/mm, and 26N/mm. It was found that suction pressure performance increased with an increasing bellows spring constant. However, in the low current region, it did not increase any more for constants higher than 26N/mm. Here the magnetic force was smaller than the bellows spring force.

Secondly, an investigation was conducted on the change of suction pressure as a function of the bellows compression length. The compression length was adjusted to: 1.25mm, 1.45mm, 1.65mm, and 1.85mm. It was found that suction pressure performance increased with an increasing compression length.

Thirdly, an investigation was conducted on the change of suction pressure as a function of the sleeve diameter. The sleeve diameter was adjusted to: 5.5mm, 6.5mm, 7.5mm, and 8.5mm. It was found that suction pressure performance decreased with increasing sleeve diameter.

Fourthly, an investigation was conducted on the change of suction pressure as a function the maximum magnetic force. The magnetic force was adjusted to: 14.8N, 16.8N, 18.8N, and 20.8N. It was found that suction pressure performance increased with increasing magnetic force.

## 4    Conclusion

The following conclusions were obtained through analysis of a control valve in a variable compressor.

The solenoid in the control valve was analysed and the magnetic force calculated. Also the flow in the control valve was interpreted using a mathematical model and verified with experiments.

Changing main design parameters such as: increasing the bellows spring constant; increasing the bellows compression length; decreasing the sleeve diameter and increasing the magnetic force were found to improve the performance of the variable compressor.

## References

Blaine, W.: The Analysis and Design of Pneumatic Systems, pp. 77–88. Wiley, New York (1967)

Han, J.H.: A Study on the Cartridge Type Pressure Compensated Proportional Flow Control Valve. HanYang Univ. Master. Thesis, pp. 13–18 (1992)

Song, C.S.: A Study of Static and Dynamic Characteristics for an Electro-Hydraulic Proportional Compound Valve. KAIST Doctor. Thesis, pp.1–21 (1980)

# New Mobile Air Conditioning Fluid HFO-1234YF – In Car Performance

M. Bryson[1], C. Dixon[1], and S. St Hill[2]

[1] RMIT University, Bundoora, Victoria 3083, Australia
[2] Formally Air International Thermal Systems, Port Melbourne,
  Victoria 3207, Australia
  Matthew.Bryson@rmit.edu.au

**Abstract.** The dominant mobile air conditioning refrigerant has come under scrutiny recently due to its high global warming potential. Legislated regulations have dictated that an alternative must be found at least for the European automotive market. Leading contenders in the synthetic sphere appear to be the drop-in replacements R152a and the more recently developed HFO-1234yf. Both of these potential R134a replacements have some flammability concerns but cause no ozone depletion (neither does R134a) and a significantly reduced global warming potential in comparison to R134a. This paper examines the in-vehicle testing of the refrigerants as confirmation for the extensive laboratory testing of the cooling performance and the coefficient of performance.

## 1  Introduction

Evidence is being continually amassed on the causes of the greenhouse effect and global warming. A recent report produced by the United Nations Environment Program estimates that the average global warming potential (GWP) of the mixture of hydrofluorocarbons in the atmospheric is 1600 times that of the datum gas carbon dioxide ($CO_2$) (UNEP 2011). It states that the hydrofluorocarbon (HFC) refrigerant R134a, which was initially assessed as having a GWP of 1300 (IPCC 2001) and later assessed to have a GWP of 1430 (IPCC 2007), has become the most abundant HFC in the atmosphere. Figure 1 shows three possible scenarios that were developed  for modelling the contribution of HFCs to the greenhouse gases present in the atmosphere if no restrictive action is taken in regard to these gases. It can be seen that the predicted contribution is between 18% and 45% of the contribution of $CO_2$ itself by 2050.

 Figure 2 displays the historical consumption of HFCs in various applications. It shows that in 2010, over half of all HFCs consumed are used in stationary refrigeration and air conditioning systems. While this is a majority, the next greatest user is mobile air conditioning (MAC) and accounts for approximately 24% of consumption when measured in $CO_2$ equivalent tonnes. Another notable feature of Figure 2 is the rapid increase in the use of HFCs between 2002 and 2010 with

the global consumption rate more than doubling during this period. The increase from 1990 to 2002 can significantly be attributed to the effect of the Montreal Protocol phasing out the use of ozone depleting chlorofluorocarbons and hydrochlorofluorocarbons in favour of using HFCs.
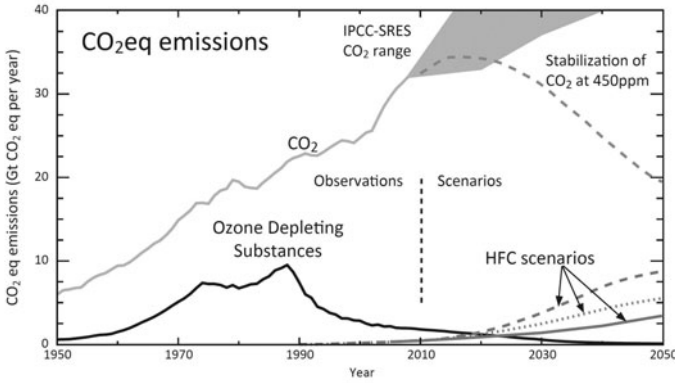


**Fig. 1.** Comparison of the projected contribution of $CO_2$ to global emissions (uppermost broken line) with the projections for the $CO_2$ equivalent emissions of HFCs which are shown by the three scenarios depicted in the lower portion. Velders et al. (2009) produced the two upper HFC projection lines (shown in broken and dotted lines), while Gschrey et al. (2011) produced that shown by the solid line. The figures showing the global $CO_2$ emissions were taken from the IPCC-SRES scenarios (IPCC 2000; 2001) (grey shaded area), and for a 450 ppm $CO_2$ stabilization scenario (IPCC 2007) (grey broken line). The figure is sourced from UNEP 2011.
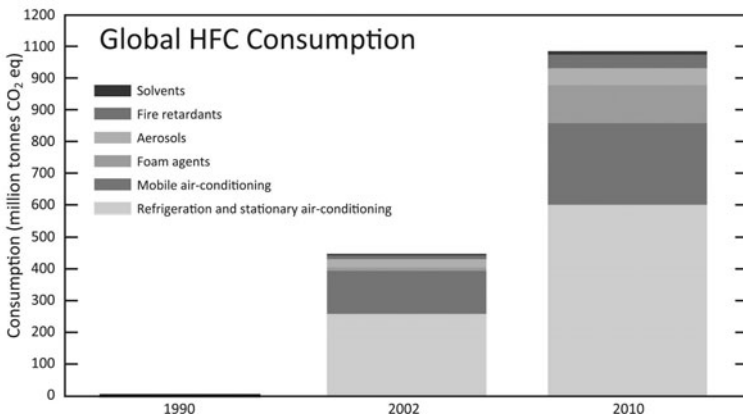


**Fig. 2.** Calculated estimate of HFC consumption shown by application (TEAP 2005, EPA 2010). Figure sourced from UNEP 2011.

   Various laws and regulations have been put in place around the world in an attempt to limit the amount synthetic gasses contribute to the greenhouse effect and consequently to global climate change. With a view to protecting the environment by limiting the future contribution to the problem by MAC systems, the European Union Parliament passed in 2006 a directive that all new vehicle types from January 1st 2011, and all new vehicles from January 1st 2017, must not contain fluorinated air conditioning refrigerants with a global warming potential of greater than 150 as defined under the IPCC's third assessment report (EU 2006; IPCC 2001). Under the legislation, existing R134a systems will be able to be recharged with their original substance for the life of those systems. Fluorinated R134a (1,1,1,2-Tetrafluoroethane) holds a dominant position as the mobile air conditioning refrigerant used in nearly all applications and as its GWP is approximately an order of magnitude greater that the law allows it is consequently banned under this parliamentary directive. This has led automotive industry manufacturers and chemical companies alike on a quest for an alternative refrigerant that not only can be used under the directive but is also comparable in performance and not prohibitive in cost.

   Several possible replacement contenders have been put forward. Naturally occurring refrigerants have had strong support for taking the place of R134a in mobile air conditioning (MAC). Carbon dioxide ($CO_2$), well established in the stationary refrigeration industry, has had a flurry of activity behind a push for its use in MAC systems with a large degree of the interest and development coming from Germany. For a time, it appeared as though the powerful German Association for the Automotive Industry (VDA) was to exclusively throw its weight behind the use of $CO_2$ based systems. It became apparent, close to the 2011 deadline, that this was not to be the case. It is true that the cost for a $CO_2$ based system performing to the same standard is higher but the performance and cost of such system is improving as time progresses. In 2006, it was suggested that a $CO_2$ system comparable to a current R134a system would cost between €100 and €300 in addition to the current cost of an R134a system[4]. While this data is somewhat historical now in light of the more recent developments in $CO_2$ MAC, it is none the less indicative of the increased cost of such a system.

   Another factor bearing on the search for a new refrigerant also comes from the cost imperative of the auto manufacturers. As producing lower volume local variants is more expensive than producing a global platform where economies of scale can be employed and systems do not have to be re-engineered, the car companies are keen to find a standardised refrigerant system that can be deployed across their range in all markets. Optimally the new refrigerant would require minimal or no redesign of the system and therefore be a "drop-in" solution.

   Hydrocarbon refrigerants, which can pass under the GWP limit, have mainly been dismissed by the large automotive manufacturers for use in their cars due to concerns of high flammability. 1,1-Difluoroethane, the long established refrigerant designated R152a, has similar concerns due to its flammability but has been put up in recent times for use in direct use systems as well as "secondary loop" type cooling circuits where the refrigerant itself is kept out of the passenger cabin altogether. After several failed attempts, the chemical industry seems to have

produced a refrigerant that is possible to use in MAC, although it is not the perfect candidate. A joint venture between Honeywell and DuPont has seen the development of HFO-1234yf (2,3,3,3-Tetrafluoroprop-1-ene) for use in MAC and, although flammable, it is less flammable than R152a and is passing the regulatory hurdles set by various authorities to be able to be used in vehicles. It is set to come, however, with a high price when compared to other refrigerants.

Much of the information disseminated throughout the industry comes from participants that have an interest in seeing the MAC refrigerant tussle go one way or another and so that information must be viewed in the light of possible bias. It was speculated by an organisation promoting the use of natural refrigerants that the European vehicle manufacturers may be intentionally evading compliance with the EU MAC directive by using a stock of approvals submitted under the previous regulations (Beyond HFCs, 2011). The article goes on to say that only two vehicles have been type approved for sale in Europe after the new regulations came into effect and these have both been from Japanese manufacturers using systems based on HFO-1234yf.

## 2 R152a and HFO-1234yf as Possible R134a Replacements

As previously stated, R134a systems are being phased out in Europe for MAC systems due to the requirement that new systems have to use a refrigerant with a GWP of less than 150, a criterion that R134a does not meet. The natural occurring refrigerant $CO_2$ can be used in systems that have been redesigned to meet the very different operating pressures of greater than ten times those in found in R134a. The lower cost option is to retain the majority of the current systems without requiring a significant redesign and to use a drop-in synthetic replacement for R134a. The front runners for being a drop-in replacement are R152a and HFO-1234yf. R152a has a GWP of 120 (IPCC 2001) which allows its use in European vehicles. R152 has the benefit of being well documented in terms of its thermophysical properties (ASHRAE 2009) and safety properties (Thundiyil 2008). R152a has the significant barrier to its introduction being its moderate flammability. In the US, R152a has Environmental Protection Agency (EPA) approval for use in motor vehicles but only for new systems that are "designed to avoid occupant exposure to concentrations of R–152a above 3.7% in the passenger cabin free space for more than 15 seconds, even in the event of a leak" (EPA 2008).

HFO-1234yf can be seen to be the current top candidate as a synthetic replacement for R134a. It has a GWP of 4 (Nielsen et al. 2007), which allows its use in European markets but does have the drawback of being mildly flammable. A media release from Honeywell stated in 2009 that HFO-1234yf has been approved for use in Japanese markets by the appropriate authorities (Honeywell 2009). The US EPA have also approved the use of HFO-1234yf in MAC applications under the conditions that the systems comply with SAE International safety standard J639_201102 and the manufacturers conduct failure mode effect and analysis studies on the HFO-1234yf systems to SAE International standard J1739 (EPA 2011). In mid 2010 General Motors announced that they will be introducing

HFO-1234yf in their 2013 Chevrolet, Buick, GMC and Cadillac models in the U.S. (General Motors 2010).

## 3   In-Car Testing of HFO-1234yf, R152a

While laboratory style testing is a useful method for investigating the performance of any refrigerant, it is logical that no testing regime for MAC systems is complete without performing in-vehicle testing.  For the set of trials conducted during this project, a current production vehicle was sourced and instrumented for use in a climatically controlled wind tunnel of the mobile air conditioning manufacturer Air International Thermal (Australia). The air conditioning system used for the baseline R134a tests and the two alternative refrigerants was identical except for employing altered settings on the production thermostatic expansion valves which were set to the superheat requirements of the individual refrigerants.  The other components of the production system were a variable displacement compressor, a tube and fin evaporator as well as a tube and fin subcooled condenser.
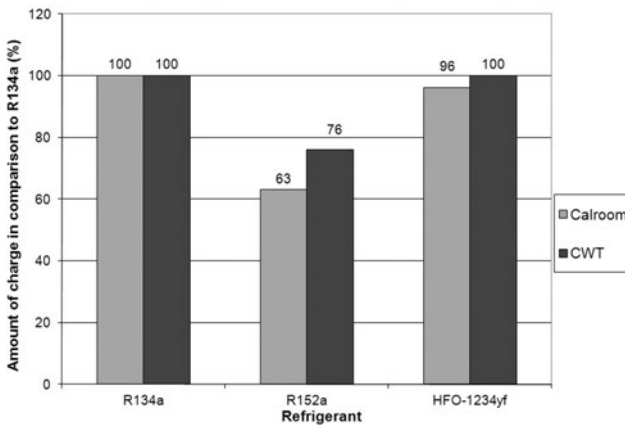


**Fig. 3.** Charge determination results comparing R152a and HFO-1234yf normalised against the baseline for R134a.  Calroom figures denote those found during laboratory style testing while (Climatic Wind Tunnel) denote those found during in-car testing.

   The first test performed was to optimise the quantity of refrigerant required to achieve a desired AC performance over a broad range of conditions.  Using the in-house procedure generated by the air conditioning system manufacturer (Air International Thermal) the following charge levels were determined and are shown in Figure 3 normalised by mass against the charge amount for R134a.  Note charge levels are also provided for the laboratory style "calroom" tests for comparison to those found for the in-vehicle climatic wind tunnel (CWT) testing.  It can be noted that there is a 24% reduction in the amount of R152a used and an

equal amount of HFO-1234yf when compared to the R134a charge. Much of the published literature on charge levels for HFO-1234yf denote a reduction in charge of between 5% and 10%, but while this was borne out in the calroom testing, the charge determination test performed in the vehicle does not have this result.

The most important information coming from any MAC test is that of the unit's performance in relation to providing passenger comfort. A standardised performance test, developed and used by one of the multinational vehicle manufacturers, was conducted and the data recorded and analysed. In order to gain information on the performance of the drop-in refrigerants in relation to passenger comfort, 12 of the 93 thermocouples placed throughout the vehicle were analysed for Figure 4. A mean reading of the 12 probes, installed in the positions for the four main occupants at mouth level, lap position and in the foot wells was calculated to give an average cabin temperature for comparison. This is the information provided in Figure 4. It can be seen that HFO-1234yf does not quite achieve the performance of R134a with the time-average cabin temperature being 1.2°C above that recorded during the R134a tests. The plot also illustrates that the performance of R152a is slightly better than that of R134a with a time-averaged cabin temperature of 0.5°C below that of the R134a tests.
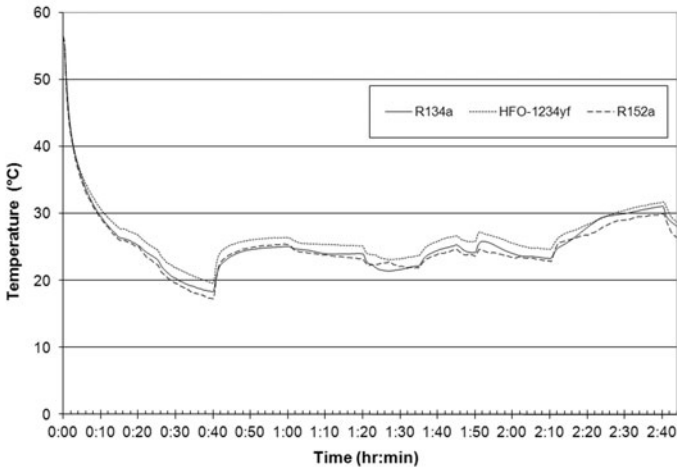


**Fig. 4.** Average cabin temperatures of vehicle during performance testing for R134a, HFO-1234yf and R152a

## 4   Conclusion

In the race to find a drop-in synthetic replacement for R134a, HFO-1234yf has become the leader over other candidates due to its low level of flammability. Early testing of HFO-1234yf saw the manufacturers concede that there is approximately a 5% reduction in both the cooling capacity and the coefficient of performance of

HFO-1234yf in comparison to R134a (Minor 2008). This level of performance degradation is supported by independent laboratory studies (Bryson et al. 2011) and the in-vehicle tests performed during this study. Honeywell, is more recently claiming that the cooling performance of HFO-1234yf is 'just as effective' as R134a (Honeywell 2011), which is not supported by the findings of these trials where it was used as a drop-in replacement. It is acknowledged however that if appropriate component sizing is carried out the cooling capacity can be increased.

# References

ASHRAE: Handbook Fundamentals, American Society of Heating, Refrigerating and Air-Conditioning Engineers, Atlanta, Georgia (2009)

Bryson, M., Dixon, C., StHill, S.: Testing of HFO-1234yf and R152a as mobile air conditioning refrigerant replacements. Ecolibrium, 30–38 (May 2011)

EPA: 40 CFR Part 82 Protection of the Stratospheric Ozone: Alternatives for the Motor Vehicle Air Conditioning Sector Under the Significant New Alternatives Policy (SNAP) Program (2008),
`http://www.gpo.gov/fdsys/pkg/FR-2008-06-12/pdf/E8-13086.pdf`
(viewed February 4, 2009)

EPA: Transitioning to low-GWP alternatives in domestic refrigeration; and other sectors. Environmental Protection Agency, Washington DC (2010),
`http://www.epa.gov/ozone/intpol/mpagreement.html`
(viewed February 6, 2011)

EPA: 40 CFR Part 82 Protection of Stratospheric Ozone: New Substitute in the Motor Vehicle Air Conditioning Sector Under the Significant New Alternatives Policy (SNAP) Program; Final Rule (2011),
`http://edocket.access.gpo.gov/2011/pdf/2011-6268.pdf`
(viewed May 5, 2011)

EU: Directive 2006/40/EC of the European Parliament and of the Council. Official Journal of the European Union, May 17 (2006),
`http://eur-lex.europa.eu/LexUriServ/LexUriServ.do?`
`uri=OJ:L:2006:161:0012:0018:en:PDF` (viewed September 23, 2008)

General Motors: GM First to Market Greenhouse Gas-Friendly Air Conditioning Refrigerant in U.S., GM Media Release (2010),
`http://media.gm.com/content/media/us/en/news/`
`news_detail.brand_gm.html/content/Pages/news/us/en/2010/Jul`
`y/0723_refrigerant` (viewed September 24, 2010)

Gourdon, S.: MAC Summit: Are we ready for 2011? In: MAC Summit 2006, Saalfelden, Austria, February 17 (2006)

Gschrey, B., Schwarz, W., Elsner, C., Engelhardt, R.: High increase of global F-gas emissions until 2050. Greenhouse Gas Measurement & Management 1, 85–92 (2011)

Honeywell: Honeywell's Low-Global-Warming Refrigerant for Vehicles Approved For Import, Use by Japan Regulators. Honeywell (2009),
`http://www.1234facts.com/pdf/1234yf%20Japan%20Approval%`
`20Press%20Release%208-4-09%20Final.pdf` (viewed September 23, 2009)

Honeywell: Solstice yf Refrigerant - The Next-Generation Refrigerant for Automotive Air Conditioning (2011),
`http://www.1234facts.com/pdf/Solstice_yf_MAC_`
`EN_BR_11_lo.pdf` (viewed December 5, 2011)

IPCC: Climate change 2001: The scientific basis, in contribution of working group I to the IPCC third assessment report of the international panel on climate change of the WMO and UNEP. Cambridge University Press, Cambridge (2001)

IPCC: Climate change 2007: The scientific basis, in contribution of working group I to the IPCC fourth assessment report of the international panel on climate change, p. 212. Cambridge University Press, Cambridge (2007)

IPCC: Special report on emissions scenarios. Cambridge University Press, Cambridge (2000)

Minor, B.: HFO-1234yf Low GWP for MAC Applications, Mobile Air Conditioning Climate Protection Partnership Meeting, Washington DC, USA, December 9 (2008)

Nielsen, O.J., Javadi, M.S., Sulbaek Andersen, M.P., Hurley, M.D., Wallington, T.J., Singh, R.: Atmospheric chemistry of $CF_3CF=CH_2$: Kinetics and mechanisms of gas-phase reactions with CI atoms, OH radicals, and $O_3$. Chemical Physics Letters 439, 18–22 (2007)

TEAP: Supplement to the IPCC/TEAP report, UNEP, Nairobi (2005)

Thundiyil, K.: U.S. Environmental Protection Agency, Update on EPA SNAP Regulations. In: 2008 SAE Alternate Refrigerant Systems Symposium, Scottsdale, Arizona (2008)

UNEP: HFCs: A Critical Link in Protecting Climate and the Ozone Layer. UNEP (2011) ,
`http://www.unep.org/dewa/Portals/67/pdf/HFC_report.pdf`
(viewed Novebmer 30, 2011)

Velders, G.J.M., Fahey, D.W., Daniel, J.S., McFarland, M., Andersen, S.O.: The large contribution of projected HFC emissions to future climate forcing. Proceedings of the National Accedemy of Science 106, 10949–10954 (2009)

Vainio, M.: European regulation of mobile air conditioning and global implications. In: VDA Winter Meeting 2006, Saalfelden, Austria (2006)

# Solid-State Automotive Lighting: Implications for Sustainability and Safety

John D. Bullough

Lighting Research Center, Rensselaer Polytechnic Institute,
21 Union St., Troy, NY 12180 USA
Tel.: +1.518.687.7100
bulloj@rpi.edu

**Abstract.** Solid-state technologies using light-emitting diodes are increasing in acceptance for use in automotive lighting. For signalling systems they have already achieved widespread use; for forward lighting systems they have been introduced and there are substantial ongoing efforts to introduce them for illumination. In the present paper, a brief overview of solid-state lighting technology for automotive applications is given. This overview first focuses on the implications of solid-state lighting for energy utilization and environmental impacts compared to incumbent lighting technologies. Secondly, the unique photometric, colorimetric and temporal characteristics of solid-state lighting systems are described with emphasis on the safety-related implications for driver vision and visual comfort.

## 1 Introduction

The use of solid-state lighting systems for many lighting applications is an area of growing interest. Light-emitting diodes (LEDs) for indicator lights and other low-light applications have been available for several decades, but only within the past 25 years or so have LEDs produced sufficient luminous flux to make them practical for exterior lighting on vehicles. Among the first LED lighting systems used on automobiles were center high-mounted stop lamps (CHMSLs), which arrived during the late 1980s (Teshima et al. 1987) and used aluminum gallium arsenide (AlGaAs) red LEDs, which could achieve intensities that were visible outdoors. Subsequently, even brighter aluminum gallium indium phosphide (AlGaInP) red and yellow LEDs became commonplace (Conway and Bullough 1999) and these made exterior signal lighting even more practical. With the introduction of indium gallium nitride (InGaN) LEDs that could generate short-wavelength (blue) light, white LEDs were made practical by combining the LEDs with a cerium-doped yttrium aluminum garnet (YAG:Ce) phosphor. The phosphor down-converts some of the blue light into yellow light; the resulting combination appears white. The availability of white LEDs had made automotive headlamps, running lamps, reverse lamps, and license plate lamps possible. LEDs differ from the primary incumbent automotive lighting technology, filament lamps, in several ways:

- Their narrowband spectral output results in saturated color appearance without optical filters needed by broadband sources like filament lamps

- White LEDs can be produced with substantially higher correlated color temperatures (CCTs) than filament sources, resulting in cooler (more "bluish") color appearance
- They presently exceed the luminous efficacy of filament lamps (80-100 lm/W, compared to 10-20 lm/W for filament lamps and even lower values for color-filtered lamps)
- They have very rapid onset and offset times (10-20 ns, compared to 80-250 ms for filament sources)
- With proper thermal management (Bullough 2003) they have substantially longer expected operating lives than filament sources (30,000-100,000 h, compared to 100-2000 h for filament lamps)

In addition, unlike many light sources that have been used as alternatives to filament sources for automotive and other applications such as fluorescent and high-intensity discharge lamps, LEDs do not contain mercury, a known neurotoxin. They are not without the potential for other hazardous materials, however (Lim *et al.* 2011), and their environmental impacts are presently being studied. The characteristics of LEDs have important implications for automotive lighting in terms of energy and environmental impacts, and in terms of potential safety-related impacts such as visual effectiveness.

## 2  Energy and Environmental Implications

Because of their higher luminous efficacies compared to filament sources, solid-state automotive lighting systems using LEDs can have substantially reduced

**Table 1.** Power, annual hours of use and estimated annual energy use for filament and LED vehicle lighting systems.

| Function | Power per vehicle (W/vehicle) | | Annual use (h/year) | Annual energy use (kWh/year) | |
|---|---|---|---|---|---|
| | Filament source | LED source | | Filament source | LED source |
| Low beam headlamp | 124 | 87 | 97 | 12.08 | 8.47 |
| High beam headlamp | 132 | 64 | 10 | 1.29 | 0.63 |
| Daytime running lamp | 48 | 18 | 382 | 18.30 | 7.03 |
| Position lamp | 14 | 3 | 107 | 1.54 | 0.29 |
| Front turn signal | 52 | 14 | 22 | 1.15 | 0.31 |
| Rear turn signal | 52 | 10 | 22 | 1.15 | 0.22 |
| License plate lamp | 17 | 2 | 107 | 1.80 | 0.16 |
| Reverse lamp | 43 | 7 | 4 | 0.16 | 0.03 |
| CHMSL | 34 | 4 | 81 | 2.73 | 0.28 |
| Brake signal | 52 | 11 | 81 | 4.16 | 0.86 |
| Tail lamp | 14 | 2 | 107 | 1.52 | 0.26 |
| *Total annual energy use (kWh/year):* | | | | *45.9* | *18.5* |

power requirements. Hamm (2009) and Schoettle *et al.* (2009) have estimated wattages for conventional filament source-based systems and for LED lighting systems for different lighting/signaling functions; the average of these estimates are presented in Table 1. Table 1 also includes estimates for the annual hours of use for these systems based on driving patterns in the U.S. (Buonarosa et al. 2008), with the resulting total annual lighting energy use for filament- and LED-based systems. Assuming each kWh on a gasoline-powered vehicle corresponds to 1.29 kg of $CO_2$ emissions (Schoettle et al. 2009), the 27.4 kWh/year energy reduction associated with a transition from filament to LED sources for automotive lighting corresponds to an annual $CO_2$ emissions reduction potential of about 35 kg/year per vehicle.

## 3   Safety and Human Factors

The photometric, colorimetric and temporal properties of LED sources can also influence drivers' ability to see and respond to potential hazards in and along the roadway.

With respect to the detection of vehicle signal lighting, the shorter onset time of LEDs compared to filament lamps can be of particular advantage, especially for brake lamps. Bullough (2005) reported that visual response times to the onset of a light signal were predicted by the amount of light-energy received at the eyes of drivers. The thermal mass of an energized tungsten filament results in a relatively gradual illumination of the filament that can take up to 250 ms. LEDs, with their nearly instantaneous onset times, can produce the necessary light-energy threshold more rapidly and therefore produce shorter response times (Bullough *et al.* 2002). Since the deceleration of a vehicle is linked to the same action that initiates the brake signal light (namely, pressing the brake pedal), shorter onset times can provide up to 7 m of additional stopping distance for a following driver (Sivak *et al.* 1994), a modest but occasionally meaningful increase.

For forward illumination systems, the spectral power distribution of most phosphor-converted white LEDs, based on blue InGaN devices, has a relatively greater proportion of short-wavelength light than that of typical filament sources (Figure 1). This is relevant to visual performance while driving, because at typical nighttime driving light levels with roadway pavement luminances on the order of 0.1-1 cd/m$^2$ (He *et al.* 1997), visual function is provided by a combination of rod and cone photoreceptors in the human eye, but photometric quantities such as lux, cd/m$^2$ and lumens are based solely on the response of the eye's cone photoreceptors, which are used exclusively for vision at typical daytime light levels experienced outdoors and indoors (i.e., 10-1000 cd/m$^2$). This mismatch between photometry and vision is important because collectively, rods are relatively more sensitive to shorter visible wavelengths (i.e., blue and green colors) than cones. As a result, conventional photometric quantities may underestimate the visual effectiveness of LED light sources at low light levels compared to filament sources. A unified photometric system has recently been recommended by the Commission Internationale de l'Éclairage (CIE) to account for the combined role of rods and cones (Rea *et al.* 2004; CIE 2010) in vision at low, nighttime light levels.

Consequently, it might be possible to justify conventional photometric light levels from LED sources that are 20%-30% lower than from filament sources (Van Der-lofske and Bullough 2006) because their increased short-wavelength content produces improved visual performance at night.
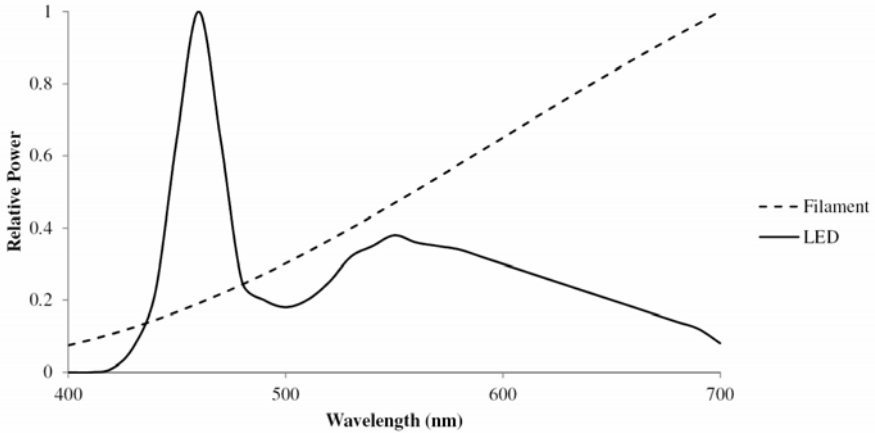


**Fig. 1.** Relative spectral power distributions of filament and LED light sources

The increased short-wavelength spectral distribution of white LEDs may have some potential drawbacks in automotive lighting applications. When equated in terms of conventional photometric quantities, disability glare (the reduction in visibility caused by scattered light in the eyes from a bright light in the field of view) from oncoming headlamps is independent of the short-wavelength spectral content of the headlamps (Schreuder 1969). However, the same cannot be said for discomfort glare, which is the annoying or even painful sensation that accompanies a bright light in the field of view. This response exhibits greater short-wavelength sensitivity (Bullough 2009). The safety implications of potentially increased discomfort glare are not fully understood, but there is evidence linking discomfort glare from oncoming headlamps to behaviors such as increased head movement and throttle variability that in turn are associated with increased crash risk (Bullough *et al.* 2008).

## 4   Discussion

Solid-state lighting technologies have evolved rapidly and continue to do so. LEDs, once relegated to indicator applications, have luminous efficacies and lumen packages that are practical for automotive exterior lighting applications. Indeed, LED sources are attractive for automotive lighting because they offer the potential for lighting energy use reductions, increasing the overall sustainability of automotive transport. In addition, under many circumstances, the performance

characteristics of LEDs support driver visual performance. Issues such as the potential for increase discomfort glare from oncoming vehicles headlamps must be investigated further, but a growing understanding of the spectral mechanisms underlying driver vision may offer guidance in spectrally "tuning" LED sources to optimize energy, visibility and glare concerns.

# References

Bullough, J.D.: Lighting Answers: LED Lighting Systems. Rensselaer, Troy (2003)

Bullough, J.D.: Onset Times and the Detection of Colored Signal Lights. Transportation Research Record 1918, 123–127 (2005)

Bullough, J.D.: Spectral Sensitivity for Extrafoveal Discomfort Glare. Journal of Modern Optics 56(13), 1518–1522 (2009)

Bullough, J.D., Yan, H., Van Derlofske, J.: Effects of Sweeping, Color and Luminance Distribution on Response to Automotive Stop Lamps. SAE Technical Paper 2002-01-0911 (2002)

Bullough, J.D., Skinner, N.P., Pysar, R.P., et al.: Nighttime Glare and Driving Performance: Research Findings. National Highway Traffic Safety Administration, Washington, USA (2008)

Buonarosa, M.L., Sayer, J.R., Flannagan, M.J.: Real-World Frequency of Use of Lighting Equipment. UMTRI, Ann Arbor (2008)

Commission Internationale de l'Éclairage, Recommended System for Mesopic Photometry Based on Visual Performance. Commission Internationale de l'Éclairage, Vienna, Austria (2010)

Hamm, M.: Green Lighting: Analysing the Potential for Reduction of $CO_2$ Emissions in Full-LED Headlamps (2009) SAE Technical Paper 2009-01-0058

Lim, S.R., Kang, D., Ogunseitan, O.A., et al.: Potential Environmental Impacts of LEDs. Environmental Science and Technology 45(1), 320–327 (2011)

Rea, M.S., Bullough, J.D., Freyssinier, J.P., et al.: A Proposed Unified System of Photometry. Lighting Research and Technology 36(2), 85–111 (2004)

Schoettle, B., Sivak, M., Fujiyama, Y.: LEDs and Power Consumption of Exterior Automotive Lighting: Implications for Gasoline and Electric Vehicles. In: Proceedings of ISAL, Darmstadt, Germany, pp. 11–20 (2009)

Schreuder, D.A.: White or Yellow Lights for Vehicle Head-Lamps? Institute for Road Safety Research, Voorburg (1976)

Sivak, M., Flannagan, M., Sato, T., et al.: Reaction Times to Neon, LED, and Fast Incandescent Brake Lamps. Ergonomics 37(6), 989–994 (1994)

Teshima, T., Kouichi, T., Takahashi, K., et al.: Development of LED High Mounted Stop Lamp. SAE Technical Paper 870061 (1987)

Van Derlofske, J., Bullough, J.D.: Spectral Effects of LED Forward Lighting: Visibility and Glare. SAE Technical Paper 2006-01-0102 (2006)

# Model-Based Soil Trip Rollover Prediction Using Driving Dynamics

Rudolf Ertlmeier[1], Holger Faisst[2], Paul Spannaus[3], and Thomas Brandmeier[3]

[1] Institute for Applied Research, University of Applied Sciences Ingolstadt;
Esplanade 10, 85049 Ingolstadt, Germany
phone: +49 (0) 841 – 9348 – 648; fax: +49 (0) 841 – 9348 – 644
`rudolf.ertlmeier@haw-ingolstadt.de`
[2] Continental, Chassis & Safety, Passive Safety and Advanced Driver Assistance Systems;
Osterhofener Str. 19, 93055 Regensburg, Germany
[3] Institute for Applied Research, University of Applied Sciences Ingolstadt;
Esplanade 10, 85049 Ingolstadt, Germany

**Abstract.** This paper presents a new physical model-based approach for improved rollover detection. Using vehicle dynamics information allows the prediction of the future roll motion of a vehicle. The severity of a crash can be forecasted in a very early phase of the accident. Thus, a much faster rollover decision can be made, which is necessary in order to deploy nonreversible restraints, like pyrotechnical belt and curtain airbags in soil trip rollover scenarios in time. The performance of this new approach is validated by a comprehensive database recorded with a scaled rollover test vehicle. Furthermore, the performance and robustness is compared to state-of-the-art model-based rollover detection methods. It can be shown that in most soil trip rollover crashes the roll angle at airbag deployment times can be reduced by up to 52 % compared to standard rollover crash detection methods. In addition, the usage of a scaled test vehicle for the development and validation of soil trip rollover detection methods is discussed. On the one hand, the similarities between a scaled model and its original are described with the help of the dimensional analysis. On the other hand, recorded data from the scaled rollover test vehicle is compared to rollover data of a real vehicle.

## 1  Introduction

According to statistical analyses by the US administration National Highway Traffic Safety Administration (NHTSA), about 12,000 occupants were thrown out of their vehicles in the United States of America in 2009. This usually occurs during a rollover crash situation. Roughly 6,700 of them are fatally injured [6]. To reduce this figure, a new ejection mitigation rule, FMVSS no. 226, was proposed by NHTSA. This rule came into force by the beginning of 2011, while the phase-in is scheduled for 2013. In order to fulfill the requirements of FMVSS no. 226, the vehicle manufacturers rely on the usage of curtain airbags. While it is allowed to perform the test procedure with the curtain bags being deployed, there is a need

for a fast and robust rollover detection system to ensure the positive effect of the airbags in real rollover crash situations. Especially for so-called "soil trip" rollover situations, where the vehicle moves laterally into a sand bed, it is important to improve today's rollover detection algorithms [7].

## 2   State-of-the-Art Model-Based Rollover Algorithms

Current mass-produced rollover detection systems usually observe the vehicle rolling movement around its longitudinal axis. A typically used rollover model can be derived by the principle of conservation of energy [2]. If the kinetic energy of rotation of the vehicle is sufficient to reach the static tilt angle $\kappa$, the system becomes unstable and the vehicle will roll over. The energy-based rollover criterion is based on the comparison of the vehicle's kinetic rotational energy $E_{rot}$ about the vehicle's longitudinal axis and the required change in potential energy $E_{pot}$.

$$E_{rot} > E_{pot}$$

The required change in potential energy for a rollover equals the necessary energy that is needed in order to lift the center of gravity (CoG) by the height $\Delta h$ (Figure 1a).
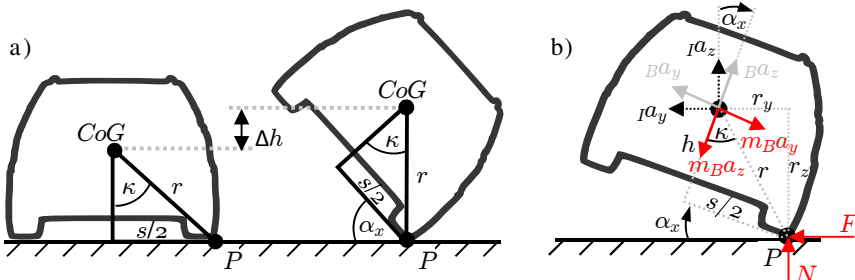


**Fig. 1.** Sketches for planar vehicle roll models a) based on conservation of energy, b) based on conservation of momentum.

Using the physical relations $E_{rot}(t)=1/2\ J_x\omega_x{}^2(t)$ and $E_{pot}(t)=mg\Delta h(t)$ with the earth gravity $g$, the vehicle mass $m$, the inertia $J_x$, the roll rate $\omega_x$, leads to the energy-based rollover stability criterion in the roll rate – roll angle $(\omega_x$-$\alpha_x)$ state space notation.

$$\omega_{crit,1}\big(\alpha_x(t)\big) = \sqrt{\frac{2mgr\big(1-\cos\big(\kappa-\alpha_x(t)\big)\big)}{J_x+mr^2}} \tag{1}$$

An alternative approach to derive a rollover model is the application of Newton's second law of conservation of momentum. [2] proposes to split the rollover sequence into two time intervals. In the first interval, the angular momentum is build

up by the acting forces and generating a potential rollover. In the second interval it is assumed that only the normal force acts, which slows down the roll motion. Solving the differential equation for the first interval leads to exactly the same result eq. (1) shown above. Whereas the solution of the differential equation of the second interval differs slightly giving a less aggressive criterion than eq. (1).

$$\omega_{crit,2}\left(\alpha_x(t)\right)=\sqrt{\frac{2mgr\left(1-\cos\left(\kappa-\alpha_x(t)\right)\right)}{J_x+mr^2\sin^2\left(\kappa-\alpha_x(t)\right)}} \tag{2}$$

Figure 2 shows the principle trajectories of a rollover and a non-rollover scenario in $\omega_x$-$\alpha_x$ state space. While criterion (1) can detect a rollover situation very early, a critical near roll may lead to an inadvertent deployment. However, the stability boundary (2) clearly discriminates between rollover and non-rollover situations, but also leads to a delay in the algorithm decision. For that reason, nowadays a compromise must be found.
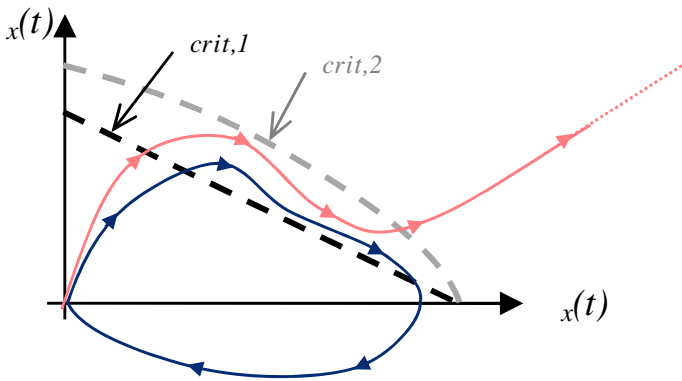


**Fig. 2.** Rollover criteria in $\omega_x$-$\alpha_x$ state space according to eq. (1) and eq. (2) and the principle trajectory of a rollover and non-rollover situation.

## 2 Roll Motion Prediction – A New Approach for a Model Based Rollover Detection Algorithm

Today's model-based rollover detection algorithms consider only the vehicle's roll motion. In most cases, however, a rollover scenario begins with a critical driving situation. According to US statistics [3] about 70% of all rollover accidents are tripped events in which the vehicle is first skidding sideways and then decelerated by hitting an obstacle (e.g. a curb) or because the tires dig into loose soil. In these

situations the knowledge about the vehicle translational movement can help to detect a rollover much faster by predicting the vehicle's roll movement.

## 2.1 Roll Movement Prediction

Assuming a planar vehicle model, see Fig. 1b, the vehicle's angular momentum changes according to

$$L(t_1) = L(t_0) + \int_{t_0}^{t_1} T(t)dt \tag{3}$$

with the angular momentum $L = J_x \omega_x$ and the acting torque $T$, which can be measured by body fixed accelerometers $_B a_{y/z}$ in the center of gravity if a rotation around the pivot point P is assumed

$$T(t) = m\left(_B a_y(t)h - _B a_z(t)\tfrac{s}{2}\right).$$

By defining the current algorithm evaluation step as $t_0$ and the considered predicted time $t_1$ as $t_0+\tau$, eq. (3) can be solved if the accelerations are considered constant $_B a_{y/z}(t) = _B a_{y/z}(t_0)$ in the interval $[t_0, t_1]$:

$$J_x \omega_x(t_0 + \tau) = J_x \omega_x(t_0) + m\left(_B a_y(t_0)h - _B a_z(t_0)\tfrac{s}{2}\right)[t]_{t_0}^{t_0+\tau}$$

The period $\tau$ can be estimated by the duration of deceleration of the vehicle's translational horizontal lateral movement $_I v_y$

$$\tau = -\frac{_I v_y(t_0)}{_I a_y(t_0)} = -\frac{_B v_y(t_0) + _B v_z(t_0)\tan(\alpha_x(t_0))}{_B a_y(t_0) + _B a_z(t_0)\tan(\alpha_x(t_0))} .$$

Altogether this gives for the predicted roll rate $\omega_{prd}(t_0) = \omega_x(t_0 + \tau)$

$$\omega_{prd}(t_0) = \omega_x(t_0) + \frac{m\left(_B a_z(t_0)\tfrac{s}{2} - _B a_y(t_0)h\right)}{J_x} \frac{_B v_y(t_0) + _B v_z(t_0)\tan(\alpha_x(t_0))}{_B a_y(t_0) + _B a_z(t_0)\tan(\alpha_x(t_0))} \tag{4}$$

Furthermore the roll angle $\alpha_x$ can be predicted by vehicle roll rate integration

$$\alpha_x(t_0 + \tau) = \alpha_x(t_0) + \int_{t_0}^{t_0+\tau} \omega_x(t)dt$$

Using the same assumption as for the roll rate prediction leads to a predicted roll angle $\alpha_{prd}(t_0)=\alpha_x(t_0+\tau)$

$$\alpha_{prd}\left(t_0\right)=\alpha_x\left(t_0\right)+\frac{\omega_x\left(t_0\right)+\omega_{prd}\left(t_0\right)}{2}\tau \qquad (5)$$

By comparing the predicted roll rate $\omega_{prd}(t_0)$ with the predicted critical roll rate $\omega_{crit,2}(\alpha_{prd}(t_0))$, see eq. (2) with $\alpha_x(t)=\alpha_{prd}(t_0)$, we get a model based rollover detection algorithm (hereinafter called Roll Motion Prediction - RMP), which is much faster compared to-state-of-the-art model-based approaches.
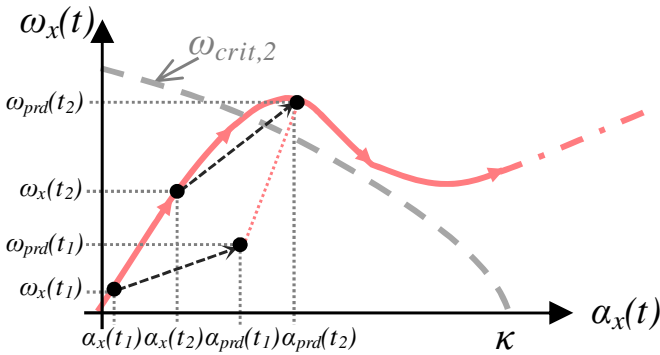


**Fig. 3.** Principle effect of the Roll Motion Prediction – RMP

Figure 3 shows the principle effect of the Roll Motion Prediction part. At a very early rollover stage, where the vehicle has a low roll angle and minor roll rate, the predicted roll angle and roll rate can be very high; an upcoming rollover can be detected at that stage already.

## 2.2 Validation and Comparison of the New Approach

The Roll Motion Prediction is validated by "soil trip" test data. In these tests, the vehicle is accelerated laterally with a sled to a constant speed $v_{sled}$. Then the sled is suddenly decelerated. Due to inertia the vehicle is moving ahead and is sliding into a soil area, where the tires dig into the soil. There are two reasons for using this test scenario for validation: First, according to [9] the "soil trip" test is the most field relevant of all rollover tests. Second, this test is the most challenging scenario to detect a rollover in time [5, 7]. To get a comprehensive data set, we performed 66 soil trip tests with a scaled rollover test vehicle (see Figure 4), where the sled velocity, the side slip angle (SSA) and the friction of the front axle were varied. In 30 cases the vehicle rolled at least *90°*, whereas in 36 cases the vehicle

did not roll over. To show the potential of the new approach, the vehicle's roll angle $\alpha_x$ at detection time TTF (Time-To-Fire) of the Roll Motion Prediction is compared to the state-of-the-art model-based rollover detection methods.
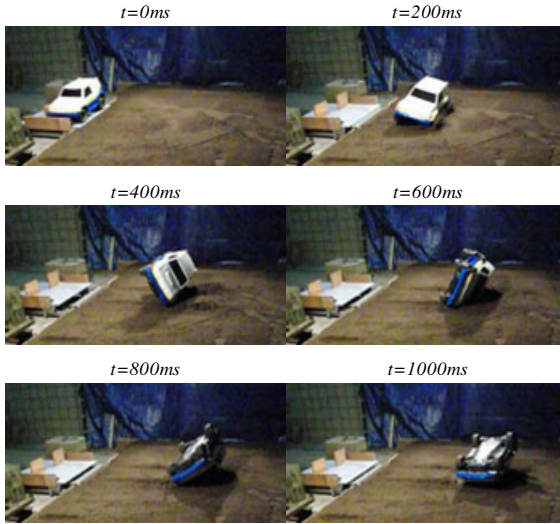


**Fig. 4.** Picture sequence of soil trip test with the scaled vehicle (test # 010)

Table 1 shows the first test series with a SSA of $90°$ and low friction at both vehicle axes, which represents the current state-of-the-art rollover testing method. The column "Requirement" indicates if the vehicle rolled over ("Fire") or not ("NoFire"). It can be seen, that the RMP almost always can detect a rollover at a lower roll angle than both state of the art model based approaches. Furthermore, table 1 and 2 show, that the conservation of energy model-based algorithm according to eq. (1) detects the tests #007 and #008 as a rollover, which in fact are no-roll situations. Whereas the RMP and the conservation of momentum-based algorithm according to eq. (2) do not have any false positive detection in the first test series. Moreover, within the first test series the mean roll angle at time-to-fire of all detected rollovers of the RMP is 52% lower compared to the criterion eq. (2) and 38% lower than the approach according to eq. (1).

Taking also a second test series into consideration (see table 3), where in addition to the variation of the sled velocity the initial SSA and the friction factor at the front axis are changed, the improvement of the mean roll angle at TTF by the RMP is still 34% compared to the critical roll rate eq. (2) and still 12% to eq. (1) methods. In addition, the overall test results show that in four situations eq. (1) leads to inadvertent deployments. Whereas with the RMP and the method according to eq. (2) no test is detected incorrectly. For the sake of completeness, it should be stated that all three considered methods detected all "fire" situation, so there are no false negatives.

**Table 1.** Comparison of RMP (Roll Motion Prediction) algorithm to state-of-the-art model-based rollover detection methods of the first test series with a vehicle side slip angle SSA of 90° and low friction on both vehicle axes.

| Test # | Requirement (Fire/NoFire) | Sled velocity [km/h] | Roll angle at TTF in [°] | | |
|---|---|---|---|---|---|
| | | | $_{crit,1}$/ eq.(1) | $_{crit,2}$/ eq.(2) | RMP |
| 001 | NoFire | 12.1 | - | - | - |
| 002 | NoFire | 14.0 | - | - | - |
| 003 | NoFire | 14.9 | - | - | - |
| 004 | NoFire | 15.9 | - | - | - |
| 005 | NoFire | 15.9 | - | - | - |
| 006 | NoFire | 15.9 | - | - | - |
| 007 | NoFire | 16.9 | 24.0 | - | - |
| 008 | NoFire | 17.0 | 25.0 | - | - |
| 009 | Fire | 17.5 | 23.4 | 44.8 | 23.4 |
| 010 | Fire | 18.0 | 22.8 | 28.1 | 20.8 |
| 011 | Fire | 19.1 | 21.2 | 26.7 | 9.0 |
| 012 | Fire | 19.1 | 21.5 | 25.8 | 15.0 |
| 013 | Fire | 20.1 | 19.9 | 24.0 | 10.5 |
| 014 | Fire | 21.8 | 19.0 | 24.7 | 8.9 |
| 015 | Fire | 22.9 | 17.2 | 21.8 | 8.7 |
| 016 | Fire | 24.6 | 16.8 | 21.3 | 8.9 |

**Table 2.** Result Overview of first test series

| Result Overview | $_{crit,1}$/ eq.(1) | $_{crit,2}$/ eq.(2) | RMP |
|---|---|---|---|
| Number of false positives | 2 | 0 | 0 |
| Number of false negatives | 0 | 0 | 0 |
| Number of detected rollovers | 10 | 8 | 8 |
| Mean angle at Time To Fire [°] | 21.1 | 27.2 | 13.1 |

**Table 3.** Result Overview of all 66 tests

| Result Overview | $_{crit,1}$/ eq.(1) | $_{crit,2}$/ eq.(2) | RMP |
|---|---|---|---|
| Number of false positives | 4 | 0 | 0 |
| Number of false negatives | 0 | 0 | 0 |
| Number of detected rollovers | 34 | 30 | 30 |
| Mean angle at Time To Fire [°] | 23.8 | 31.7 | 21.0 |

## 3  Dimensional Analysis

As a scaled test vehicle was used for the investigation shown above, it is necessary to proof that the findings can be applied to a full scaled vehicle.

**full scale vehicle**                           **scaled test vehicle**

$m = 2200$    kg        $m = 16.4$    kg
$J_x = 1150$  kgm²      $J_x = 0.38$  kgm²
$h = 0.695$   m         $h = 0.136$   m
$s = 1.946$   m         $s = 0.435$   m

a)                                              b)

**Fig. 5.** Parameter comparison between real and scaled vehicle

For this purpose the model car data has to be scaled considering the essential physical parameters of the rollover situation in order to compare them to the signals of a real vehicle.

If the influences of the parameters of a physical model are known in principle, the system can be described by dimensionless constants which can be determined by Buckingham $\Pi$-theorem [1]. This allows the comparison of models ranging in size. For this reason the variables characterizing the system have to be identified. According to the $\Pi$-theorem, the general function $f$ of a physical system $f(x_1, x_2, \ldots, x_n)$ with the system parameters of $i=1\ldots n$ is described, so we get [10]:

$$f\left(x_1, x_2, \ldots, x_n\right) = 0$$

The quantities $x_n$ can be split according to their dimensions or units into two different types of values: linear independent $x_i$ and dependent values $x_j$, with $i+j=n$. Those $j$ dimensionless parameters ($\Pi_j$ numbers) can be found for an arbitrary physical system which enables scalability of different model sizes. Applied to all system-related metrics the following must apply:

$$F\left(\Pi_1, \Pi_2, \ldots, \Pi_j\right) = 0 .$$

The $\Pi_j$ numbers can be determined according to Pawlowski [8] by

$$\Pi_j = x_j \prod_i x_i^{-p_{ij}} .$$

The dimensional analysis is mainly applied in the mathematics of fluid dynamics and their applications. Applied to the scalability of a model-car driving dynamics

in the use of observers, the ratio has been successfully shown by Hilgert in [4], who was able to show the feasibility for dynamic vehicle models.

The system characterizing variables for the presented rollover investigation can be found in eq. (1). Written in the matrix scheme as proposed by Zlokarnik [10] we get table 4, where $\tau'$ is a characteristic time interval.

In order to make a comparison between model and a real vehicle all $\Pi_j$ numbers must be identical $\Pi_{j,1} = \Pi_{j,2}$ if 1 corresponds to the real test car and 2 to the scaled model vehicle. For example, the following must be fulfilled:

$$g\frac{\tau_1'^2}{h_1} = g\frac{\tau_2'^2}{h_2} \Rightarrow \frac{\tau_1'^2}{\tau_2'^2} = \frac{h_1}{h_2}, \quad \omega_{x,1}\tau_1' = \omega_{x,2}\tau_2' \Rightarrow \frac{\omega_{x,1}}{\omega_{x,2}} = \frac{\tau_2'}{\tau_1'} = \sqrt{\frac{h_2}{h_1}} \text{ and } \frac{a_{y/z,1}}{a_{y/z,2}} = 1$$

**Table 4.** Matrix scheme of the systems characterizing variables

| eq. | SI | $m$ | $h$ | $\tau$ | $r$ | $s$ | $a_{y/z}$ | $\omega_x$ | $\Theta$ | $g$ |
|-----|-----|-----|-----|-----|-----|-----|-----|-----|-----|-----|
| I | mass [kg] | 1 | 0 | 0 | 0 | 0 | 0 | 0 | 1 | 0 |
| II | length [m] | 0 | 1 | 0 | 1 | 1 | 1 | 0 | 2 | 1 |
| III | time [s] | 0 | 0 | 1 | 0 | 0 | -2 | -1 | 0 | -2 |
| | $\Pi_j$ | | | | $\dfrac{r}{h}$ | $\dfrac{s}{h}$ | $\dfrac{a_{y/z}}{h}\tau'^2$ | $\omega_x\tau'$ | $\dfrac{\Theta}{mh^2}$ | $\dfrac{g}{h}\tau'^2$ |
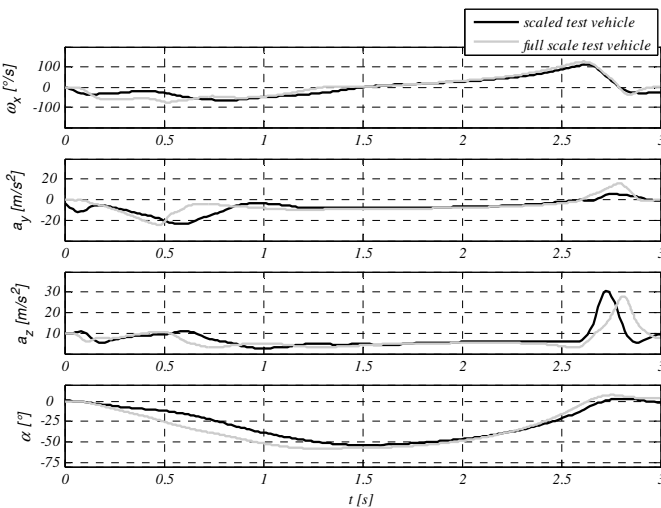


**Fig. 6.** Comparison between full scale car and scaled test vehicle

The dynamics of the model vehicle corresponds to the root of the length ratios in relation to the real test vehicle. The accelerations $a_{y/z}$, however, do not have to be adapted in contrast to the angular velocity $\omega_x$. Fig. 6 shows the signal comparison of a real car to the scaled test vehicle in a soil trip scenario. Therefore, all signals of the scaled vehicle are stretched in time by a time laps factor of $\sqrt{h_1/h_2} = 2.25$. Furthermore, the amplitude of the roll rate $\omega_x$ is adapted with the inverse factor $\sqrt{h_2/h_1}$. It can be seen that there are many similarities in the signal behaviors of the two compared vehicles, which means that our findings about the Roll Movement Prediction can also be transferred to real "full size" vehicles.

## 4 Conclusion

The presented Roll Motion Prediction algorithm improves today's model based rollover detection methods. The roll angle at airbag deployment time can be reduced by an average of 52% without any risks of inadvertent airbag deployment. Using the presented approach, there is no more need for a compromise between performance and robustness in soil trip detection, which enables to meet the challenging requirements and deploy the important restraints in time.

## References

[1] Buckingham, E.: On physically similar systems; illustrations of the use of dimensional equations. Physical Review 4, 345–376 (1914)
[2] Eger, R., Kiencke, U.: Modeling of rollover sequences. Control Eng. Practice 11 (2003)
[3] Eigen, A.: Examination of rollover crash mechanisms and occupant outcomes. In: National Center for Statistics and Analysis, Washington, D.C (2003)
[4] Hilgert, J.: Anwendung der Ähnlichkeitstheorie zur experimentellen Eigenschaftsabsicherung eines Bahnplanungsverfahrens für Fahrzeugführungssysteme. Uni. Duisburg-Essen (2005)
[5] Linstromberg, M., Scherf, O., Scholpp, G.: Test and simulation tools in a rollover protection development process. In: ESV: 19th International Technical Conference ESV (2005)
[6] NHTSA: Traffic Safety Facts 2009 Early Edition. Washington DC (2010)
[7] Paggel, J.: Active and Passive Safety Integration for Advanced Rollover Protection. In: Airbag 2006 - International Symposium and Exhibition on Sophisticated Car Occupant Safety Systems, Vol. 8, pp. V13-1–V13-17 (2006)
[8] Pawlowski, J.: Die Ähnlichkeitstheorie in der physikalisch-technischen Forschung – Grundlagen und Anwendungen. Springer, Berlin (1971)
[9] Viano, D., Parenteau, C.: Rollover crash sensing and safety overview. In: Warrendale, SAE 2004, pp. 85–108 (2004)
[10] Zlokarnik, M.: Modellübertragung in der Verfahrenstechnik. Chem. Ing. Tech. 55 (5) (1983)

# Reliability of Driver Interactions with Road Vehicles

Mirko Novak and Petr Bouchner

Faculty of Transportation Sciences, Czech Technical University in Prague
Konviktska 20, 110 00 Prague 1, Czech Republic
Tel.: +420 224 359 548
{mirko,bouchner}@lss.fd.cvut.cz

**Abstract.** In this contribution are discussed the main problems appearing in development of tools for decreasing the negative impacts of human faults when driving the road vehicle. The interest is given especially to analysis of causes of these faults, to finding of suitable indicators for attention level measurements and to possibilities of improving the driver resistance to attention decreases.

## 1  Introduction

Human society suffers from various systems failures, accidents and catastrophes. Transportation systems, especially the road transportation belong to those, in which the accidents and faults cause extremely high every-year losses, both economic and social. In the EU the level of these losses can be estimated to about 200 billion Euro per year and to about 40,000 people killed. In other countries of the world this situation can be even worse.

A dominant part of these losses is caused by faults of drivers appeared in their interaction with vehicles.

This is the reason why in some research facilities and university laboratories a high attention is given to understanding of the mechanisms of appearance of driver failures and also of traffic operators mistakes and to development of ways for their reduction.

The Joint Laboratory of System Reliability of the Institute of Control and Telematics of the Faculty of Transportation, Czech Technical University in Prague and of the Institute of Computer Science of the Czech Academy of Sciences, Prague belongs to those not too many places, where the systematic research in this area is done for more than 15 years and where a good level of knowledge was reached.

Without respect to the reached results many problems in this area remain still open. Because their complexity is very high no single research group or team is able to solve them alone completely. Therefore the intensive international cooperation is necessary.

## 2  Open Problems

The negative influences of driver caused faults on transportation reliability and safety was recognizable through all the road transportation history; however their significance increases with the size of human population in general and with traffic density, which is different in particular parts of the world.

A large part of these losses is caused by general irregularities in the interaction of human subjects with the artificial systems.

## 3  Problem Formulation

Each activity of systems or systems alliance is realized in some space of its systems functions $F_k$, $k = 1...K$. Systems functions being the input / output manifestation of the processes within the systems.

The size of the space F and the maximum values of the partial systems functions $F_k$ on the relevant boundaries characterize the significance of the particular system. Generally there exist some mutual dependence $f_{n-s} = d(|F|)$ between the average frequency $f_{n-s}$ of non-standard situations of operation or interactions with considered system (or systems alliance), and the size $|F|$ of this space F.

This dependence $f_{n-s}$ is often of the inversely proportional nature. In such case it could be modeled in various ways, but hyperbolic model seems to be of specific interest:

$$\mathbf{f}_{n-s} = c_0 + \frac{c_1}{\left(\left|F\right| + c_2\right)^{c_3}}$$

Where $c_0$, $c_1$, $c_2$ and $c_3$ are real, empirically determined constants, which influence the shape and the position of the hyperbole (Figure 1).
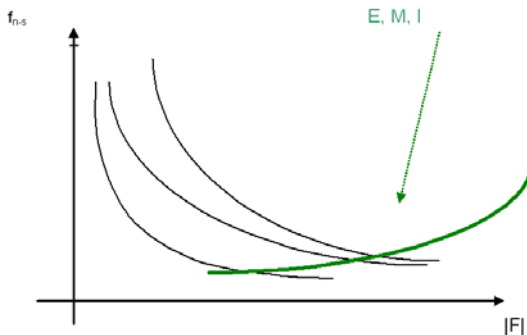


**Fig. 1.** Hyperbolic model of the dependence d between the average frequency of non-standard situations fn-s and size |F| of the space F. The green line represents here the size of energy E, mass M and information I with which deals respective system or alliance.

The black lines demonstrate some typical dependence between frequency of nonstandard situations and size and complexity of the respective system. This means, that the non-standard situations appearing in operation of really complex systems occur much more rarely, than in the case of a simple, in many copies existing systems.

Of course, the hyperbolic model is only the one of many other inversely proportional models, which can be constructed. Even that it is very simple, the estimation of the constants $c_{0,1,2,3}$ could be quite laborious.

For to be able to find realistic values of $c_{0,1,2,3}$, the analysis of the frequency of appearance of non-standard situations has to be made in considerably long history of operation of the considered system. This is evidently a hard requirement, because usually the respective data are not fully at disposal and if so, they can be disturbed by various sources of imperfections. For newly constructed systems or systems alliances such historical data are not at disposal at all and need to be replaced by data sets coming from investigation of other similar cases.

Moreover, the two-valued classification of the systems operation ability which was considered above (system operates well – it is in standard situation and system does not operate well - it is in non-standard situation) does not often represent realistic characteristics of the actual situation. Nevertheless, in any case it is extremely important the systematic recording of all relevant data representing the systems parameters, in which or among which the information on non-standard event in the system operation can be hidden. The creation of the respective database is therefore necessary both for dealing with all systems, for which the size of |F| reaches certain limit or which exist in high enough number M of its copies. As the figure of merit of such necessity, the product M * |F| could be proposed.

One has also to take into account, that all such the parameters $c_{0,1,2,3}$ of all non-standard situation frequency appearance models are usually influenced by the vector of independent variables

$$P = \{p_j\}, j = 1\ldots J, \text{ especially by the time } P = t$$

Therefore, the validity of some particular model is limited to certain region $R_P$ of independent variables P.

The analysis of system operation failures and resulting accidental and catastrophic events hints that only *very rarely they appear absolutely without any preceding markers*.

Such markers can be of course very weak and hardly recognizable, nevertheless, careful and systematic use of sophisticated analysis of data (mainly in the form of time-series) reached from various sensors gives the hope that the *advent of particular non-standard situation can be detected*.

Though there is often very difficult to predict the advent of system operation failures and eventual resulting accidents, our *present knowledge of*:

- Systems theory
- System reliability
- signal analysis.

together with:

- modern computers
- communication technology
- brain science
- modern sensors / actuators.

Open the possibility that reasonable results can be reached.

## 4 Prediction Diagnostic as the Main Methodical Tool

The main tool for such preventive activity of systems operation failures is the wide and deep working out and use of the methods of *predictive diagnostics*, which allow – if well used – not only to indicate the danger of particular system or the whole system alliance failure, but also:

- to estimate the probability of such event,
- to predict the time in which this could happen
- to discover coincidence of concurrent events.

And to find the optimal ways for such event prevention or, if this is not possible, for optimal restitution of the systems and compensation of appearing losses.

Though the principles of prediction diagnostic are known and used for many years, the respective theory and application methodology has to be significantly improved, especially if it concerns the very complex and heterogeneous systems and system alliances with many components, in that also the human interaction play not negligible role.

Such improvement, in which novel approaches to dealing with:

- multidimensional quasi-periodic and quasi-stationary signals
- systems involving uncertain parameters
- time-series prediction for longer prediction horizons respecting the parameters correlations
- methods and tools for analysis of hidden correlations in measured large data sets
- methods for effective and in-time providing of necessary numerical multidimensional analyses and estimations
- progressive approximation methods.

Can be considered as necessary research tools enabling accomplishment of the goal.

For to be able to recognize that there exists an increase of the probability that certain driver will in some prediction horizon loose his/her ability to interact well with by him/her driving car we need:

- to classify the main reasons of such driving failures
- to have at disposal a set of reliable and practically applicable indicators of driver attention decreases

- enough fast and accurate tools for respective measurements applicable either in laboratory or in real vehicle
- enough fast and accurate methods and tools for analysis of respective signals
- the knowledge of acceptable limits of respective signals deviations
- the methods and tools for creation of recognizable and understandable warning signals.

## 5 Discussion

The driver faults can arise from the following three main reasons:

**a) Natural decrease of particular person attention level**

There is well known that no human subject is able to keep his/her attention, understand as vigilance oriented to certain observed object or activity, on high level without any breaks. Usually one is able to be in the state of full attention for 1-2 hours, but often the process of natural decreasing of attention level start already in several decades minutes after start of respective activity, i.e. car driving. In the process of natural attention decrease is possible to recognize the main phases, shown in Fig. 2:

- Phase of the full attention
- Phase of relaxation - the driver is still fully able to control his/her driving activities, but he/she feels to be a bit tired and he/she slightly relaxes
- Phase of somnolence - the driver level of attention is going to fall below the level of reliable and safe driving. Here he/she feels to be really tired, and reliability of his/her driving is limited, reaction time is prolonged significantly (sometimes 3-5 times) and the probability of his/her non-correct response on external stimuli increases.
- Phase of micro-sleep - the driver attention level falls rapidly down till zero or to some very small residual level. In happy cases, this phase lasts considerably shortly (few seconds).
- After that, the driver often awakes to some previous phase, in which his/her ability to drive reliable and safe refreshes. This phase, we can call as the phase of awaking. However, the awaking procedure can be so fast, that the driver reacts in the panic form, with significantly increased probability of wrong decision and reaction.

Such model is made under assumption that:

i)   level of attention $L_{AT}$ can be expressed by real values,
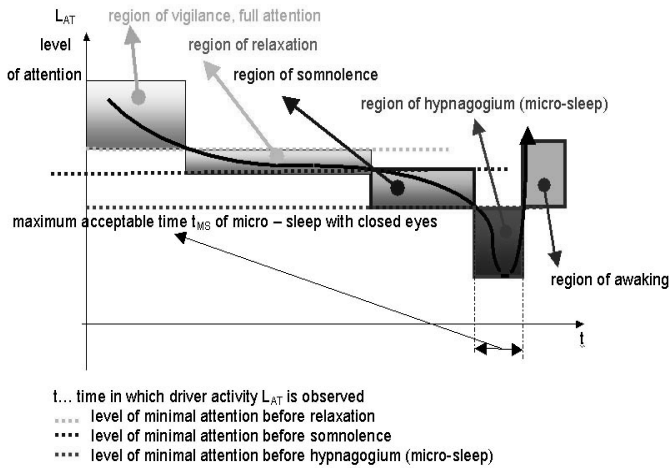ii)  the changes of $L_{AT}$ are smooth.

**Fig. 2.** Five typical phases.

**b) Influence of consumption of alcohol**

Besides natural decreases of driver attention, which causes about 50% of accidents, also the influence of consumption of alcohol (and other drugs) short before and in the course of driving cause a lot of accidents. We estimate this to about 25%. In some countries exist certain legal limits for allowed alcohol concentration in driver blood, but actually it depends very much on driver individuality, if he/she is influenced by alcohol so that he/she cannot drive safely. As concerns drugs, such limits are not known till now.

**c) Conversions of driver behavior**

The last about 25% of driver caused accidents comes from sudden and unexpected conversions of driver behavior from rational and tolerant to non-tolerant and aggressive. Till now it is only hardly predicable. There is urgently necessary to understand more to neuropsychological reasons of such behavior conversions. One can see the hope that by the use of some special training methods based on the so called bio-feedback could be possible to modify the driver behavior for lower tendency to such behavior conversions.

## 5.1  Reliable and Practically Applicable Indicators of Driver Attention Decreases

The indication and measurement of the driver attention level can be based on various indicators. One has to say, that at moment none of known is universal. Relatively well can attention level and its decreases measured on driving simulators, either by reaction delays, or by changes of visual observation field or by probability of correct responses on impacting stimuli. Sometime is used a combination of them.

Another approach can be based on face grimaces changes recognition, on eye blinking changes etc. A common drawback of all these approaches lays in their low specificity and time delay. This can be replaced by analysis of the immediate brain signals, either electric or magnetic. The respective methods of EEG and MEG analysis are considerably accurate and fast, however they are applicable only in laboratory.

One expects therefore, that the solution if the attention indicator problem will be in the use of combination of several practical applicable indicators calibrated in laboratory by EEG (or MEG) methods under respecting of driver individuality.

## 5.2  Signal Analysis

In the course of almost all these measurements and analyses one has to face to necessity of dealing with various biological signals. In contrary to signals appearing usually in artificial systems, these are dominantly of the quasi-periodic and quasi-stationary nature. Therefore the old good methods of harmonic analysis are not direct applicable on them and if this is done (as often happens) the results can be inaccurate and non reproducible. Therefore exists a need to develop other approaches for dealing with such signals. Some hope can be seen e.g. in Gabor filtration by special transfer functions, or on the use of chaos indexes or on the use of approximation by Zolotarev functions. Though the up to now reached results seems to be promising, there are still many white places here.

## 5.3  Regions of Acceptability

For to have reason to start the respective warning, one needs to know, that the respective significant function, expressing the driver ability for safe and reliable activity is approaching or breaks its acceptable limits. These can be expressed by the so called regions of acceptability $R_A$. Some methods for $R_A$ analyses are known and used when dealing with various artificial systems however their investigation is usually very laborious. When one has to deal with interaction of biological and artificial systems, i.e. human subject and vehicle, the situation is much worse because of the parameters uncertainty variability and fuzziness. Another problem of driver regions of acceptable ability and behavior $R_{D\ AB}$ analysis consists in extreme high human individuality. Human brain consisting of about $10^{11}$ neurons and about 10 time more glia cells, connected mutually with about $10^4$ synapses per one neuron in a time variable and individually differing network is so complicated, that one can not expect any brain clones. They are (and newer had been) no two exactly identical brains.  Therefore for each driver the $R_A$ should be investigated individually. This is of course practically impossible. However, the enough systematical analyses can give us a basis for finding some typical forms, which could be used for necessary driver behavior limits investigation.

This is of course a very large challenge for further systematic research for wide research consortia.

# References

Faber, J., Pěkný, J., Piekník, R., Tichý, T.: Bouchner P. et al.: Simultaneous recording of electric and metabolic brain activity. Neural Network World 20(4), 539–557 (2010) ISSN 1210-0552

Votruba, Z., Novák, M., Brandejský, T., Fábera, V., Bouchner, P., et al.: Theory of System Alliances in Transportation Science, p. 162. Institute of Computer Sciences of the Academy of Sciences of Czech Republic, Prague (2009) SBN 978-80-87136-08-9

Bouchner, P., Novotný, S., Piekník, R.: Objective Methods for Assessments of Influence of IVIS (In-Vehicle Information Systems) on Safe Driving. In: Proceedings of the 4th International Driving Symposium on Human Factors, pp. 153–159. Iowa State University, Iowa (2007) ISBN 978-0-87414-158-0

Fábera, V., Bouchner, P.: Car Cockpit Optimization Using Genetic Algorithms Driver Car Interaction & Interface, vol. 1, pp. 42–48. Academy of Sciences of the Czech Republic, Institute of Computer Science, Prague (2008) ISBN 978-80-87136-04-1

Moos, P., Novák, M., Votruba, Z., Bouchner, P.: Estimation of failures probability in alliances of transportation systems. In: IMETI 2008: Proceedings of International Multi-Conference on Engineering and Technological Innovation, vol. I, pp. 163–167. International Institute of Informatics and Systemics, Orlando (2008) ISBN 978-1-934272-43-5

Novák, M., Faber, J., Votruba, Z., Bouchner, P., Tichý, T.: Possibilities for Improving of Resistance to Attention Decrease and other Disturbing factors Driver Car Interaction & Interface, vol. 1, pp. 83–89. Academy of Sciences of the Czech Republic, Institute of Computer Science, Prague (2008) ISBN 978-80-87136-04-1

Novák, M., Votruba, Z., Svítek, M., Bouchner, P.: Improvement of Bus and Truck Driving Safety. In: 2006 IEEE International Conference on Systems, Man, and Cybernetics, IEEE - Systems, Man, and Cybernetics Society, New York (2006); CD-ROM; ISBN 1-4244-0100-3

Novotný, S., Bouchner, P.: Advanced methodology for evaluation of driver's actual state with use of technical driving data. In: Proceedings of the 8th WSEAS International Conference on Systems Theory and Scientific Computation (ISTAC 2008) - New Aspects of Systems Theory and Scientific Computation, pp. 160–165. World Scientific and Engineering Society Press, Athens (2008) ISBN 978-960-6766-96-1

Novotný, S., Bouchner, P., Jiřina, M.: Identification of Driver's Drowsiness Using Driving Information and EEG. In: Driver-Car Interaction & Interface - Book of Proceedings, pp. 11–19. Institute of Computer Sciences, Academy of Science of the Czech Republic, Prague (2009) ISBN 978-80-87136-05-8

# Investigation of Chain Meshwork: Protective Effects and Applications

E. Wilhelm[1], U. Burger[2], and J. Wellnitz[3]

[1] Institute for Technology and Artistic Design GmbH (ITD), Marie-Curie-Str. 6,
   85055 Ingolstadt, Germany
[2] MBDA Deutschland, Landshuter Str. 26, 85716 Unterschleißheim, Germany
[3] University of Applied Sciences Ingolstadt, Esplanade 10, 85055 Ingolstadt, Germany

**Abstract.** The protection of human life and the reduction of harm caused by terrorist attacks or natural catastrophe has a high priority in the design of buildings and means of transportation, for example armoured vehicles. In addition to these safety and security aspects, are considerations of sustainability.

   This paper contains two different protection types based on the usage of chain meshwork, the pure and the hybrid type. The pure metallic chain meshwork was compared in different experimental tests regarding impact detonation loads. For example, if the application of chain meshwork is used as an ordinary curtain combined with a regular window, two major effects are obtained. The first effect is the **reduction of the blasting wave** and the second more important effect is the **shiver protection**. In this case, the chain meshwork avoids the loosening and the following burst of the window glass, resulting in an **increase in the protection level**. On the other hand, a newly developed hybrid composite shows outstanding impact results, as proven by several tests by the German Federal Armed Forces. According to the testing results, an **increase of impact strength up to ~60%** can be achieved by reinforcing common carbon fibre reinforced plastics (CFRP) with a metallic chain mesh. The fibre composite is made out of carbon fibres, unidirectional with polyetheretherketone matrix or woven with epoxy matrix. The scope of this work is the general investigation of the impact behaviour of pure meshwork and fibre composites reinforced with metallic chain mesh, especially in the field of low and high velocity impact. Besides the first production of samples of the new material combination, experimental investigations are carried out on coupon testing level. These include 3-point-bending tests, Charpy-Impact tests and ice impact tests at high velocity on a custom designed gas gun as well as comparison of blast and sliver behaviour. Testing should be accompanied and should work as the validation basement by looking at the possibilities of numerical simulation of the general and hybrid material, so further complex scenarios can be realized and the forecast of effects are visible.

## 1   Introduction

By default, buildings are traditionally made from solid concrete or concrete composites, respectively. This suggests that structural reinforcements regarding the

safety aspect are also made primarily from these materials, which results in massive and sometimes non-decorative structures. Furthermore, the concrete has a negative factor in terms of its environmental record, because it has to be separated completely by material types for recycling, which creates additional energy consumption. Another example regarding massive manufacturing is the armouring of vehicles, because the typical method for this modification is the usage of steel, resulting in an increase in weight and therefore higher fuel consumption.

In terms of sustainability, this work investigates two main versions of an environmentally friendly and lightweight material, which has a wide range of protective effects and can be employed as a replacement to the above mentioned materials. Thematically, it deals with a metallic ring mesh, which can be used for different applications in building security and safety as well as for a variety of other areas, including:

- public authorities
- military installations
- general transport
- sports and leisure.

The following section refers to building protection from various impact loads:

- Blast and window protection
- distance barrier and
- energy absorption of high velocity impact.

## 2   Basic Flex Metal Mesh information

Chain mails are well-known from historical documentations including European knights in the Middle Ages, where chain mail was used for the prevention of stabbing and cutting injuries. Today it is known that chain meshwork shows much more potential than the traditional protection.

The chain meshwork which is used in this work is called Flex Metal Mesh (FMM) and consists of a large number of welded metal rings with a well-defined geometry. There are two different manufacturing methods of the ring closure: laser beam and resistance stud welding.

The arrangement of the rings is known as the European or king version - named 4 in 1 - that means that every single ring is connected with four neighbouring rings (Fig.1).

The technical description of the meshwork includes two main parameters: the outer diameter and the wire gauge. The outer diameter can vary from 3.6 to 12 mm, the outcome of this is a feasible wire gauge, i.e RG12x1.3mm. The pure mesh can be made of different kinds of metal, e.g. titanium, copper or stainless steel. This application of various materials results in tensile strength up to 1000
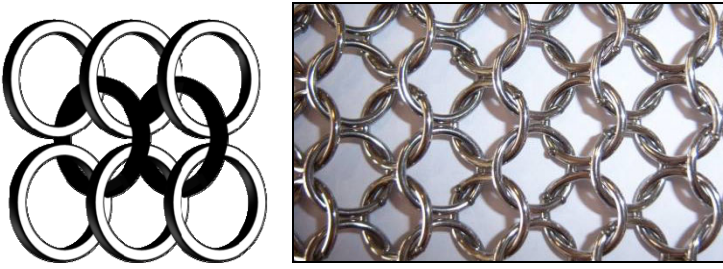
**Fig. 1.** Schematic and realistic arrangement of the rings within a meshwork, 4 in 1

N/per ring. Of course, there is the option of using titanium or aluminium for aerospace applications in order to reduce weight. Some outstanding characteristics of FMM, validated by tests, are:

- macroscopic values:
    - high tensile strength and tensile strain (> 44%)
    - high possible deformation
    - high energy absorption due to plastic deformation
- very good impact behaviour especially at low speed impact,
- low weight of 1,21 – 4,65 kg/m²,
- readily accommodates free-form shapes with negligible shear-stiffness.

## 3   Experimental Investigations

The aims of the following experimental tests relate to the improvement of the steadfastness of buildings and special subcomponents, and the structural protection of general constructions such as ammunition dumps. The focus is on minimizing the damage and increasing the protective effects and advantages of FMM during a detonation or impact caused by terrorist attacks or other disasters.

There have been three main test series regarding blast and the protective effect of the pure and hinged chain meshwork. The test conditions were always a controlled blasting of an ammunition dump or a shock tube respectively with central positioning of the burst charge.

### 3.1   *Experimental Investigation Regarding the Pure Mesh*

The first test series included the general protective effect of the meshwork with and without using a curtain made of FMM with regard to a blast only. Nitropenta (PETN - Pentaerythrityltetranitrat) was used as an explosive in this test series.
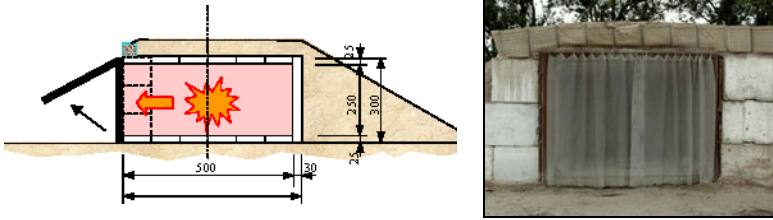
**Fig. 2.** Test condition for the first and second test series in schematic and realistic manner

The used type of FMM was RG12x1.1 mm. The meshwork was fastened to its upper end at the head of the exemplary ammunition dump, so a "free swing" of the lower end of the meshwork was possible as a reaction and energy absorption of the blast. A representation of the first and second test conditions are shown in Figure 2. Reference tests with and without the usage of FMM have been carried out including an explosive amount in the range of 1.0 to 4.0 kg PETN 1.5.

Concerning the point pressure, a reduction is obvious in each test configuration of the first test series. Predominant a reduction of the first peek is visible. The representative test results of the 3.0 kg PETN blast indicated that a reduction of the blasting waves up to 30 per cent can be achieved.

The third test condition was different to the first ones. It was about the usage of FMM as an ordinary curtain in front of a regular window. The study has been carried out with regard to the effects of the blasting wave and the sliver protection.
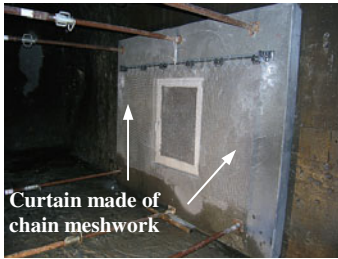


**Fig. 3.** Test condition for the third test series in reality (left); a schematically gridded room in front of the window, the numbers represent the quantity of slivers after the burst (right)

The window was made of synthetic material to represent a typical household window and was placed in the middle of an armoured concrete slab. The here used type of FMM was RG12x1.1 mm and RG12x1.3 mm. The fastening of the meshwork varied between fixations only at the upper end, at the upper and lower end and two additional fixings of the meshwork at both ends.

As a result a clear reduction of the blasting wave was visible. The FMM caused a downsizing of the broken glass parts up to 12 mm and a controlled distance flow. The FMM resisted the blast wave and the blast fragments without any damage. The chain meshwork avoids the loosening as well as the burst and spread of the window glass including dangerous parts and fulfills on of the highest GSA standard classes, here 3a.

## 3.2 Experimental Investigation Regarding the Hybrid Version

The main idea behind the hybrid configuration is to combine FMM out of high strength material as the core together with a resin system with high strain absorption potential such like epoxy resin.

The epoxy system for instance is in parallel stabilizing the geometrical shape of the chain patch and allows the patch to expand in the impacted direction in order to absorb a high rate of kinetic energy. The chain meshwork is able to take a high amount of energy due to debris impact, whereas the debris itself should be contained. The geometrical size of one to four chain rings in order to allow the system to react together with the shape forming material the composite of that structure will give a sandwich construction of lightweight size with even higher energy absorption rates.
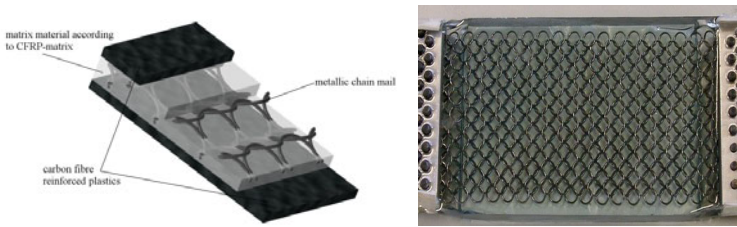


**Fig. 4.** Principle lay-up of the hybrid material (left); FMM (1:4) bonded in an epoxy resin (right)

The material of the matrix system can be epoxy or aluminium foam melted around a layer of patches, and stabilizing the crash and impact characteristics of the chain system.

Several tests were performed in order to characterize the impact behavior and to get analyses sources of FMM or a hybrid containing FMM at ballistic velocities with standard munitions.

Static test results are validated with electronic speckle interferometry in order to develop a Finite Element approach with representative material and deflection behavior. Dynamic test results show the behavior of the sandwich construction in action with collision examples recorded with a digital high speed camera system with up to 10,000 pps. One of these dynamic tests includes the ballistic impact to a hybrid of FMM as core with epoxy resin matrix.

Within the test results a stop effect of the hybrid to the projectile could be obtained, the projectile does not penetrate the hybrid. The analysis of the impact behaviour shows the following:

- destroying of the epoxy resin matrix at the point of impact, the FMM is not deformed in any way and leads to cohesion of the hybrid material
- fragmentation of the epoxy resin matrix in the surrounding area of the impact point, the FMM backing leads to debris containment

- little delamination is observed between FMM and epoxy matrix at impact point
- large deformations of the projectile are observed.

## 4 Conclusion

A few applications of the many-sided repertoire of chain meshwork have been treated in this work, but the general usage of chain meshwork verifies the potential of Flex Metal Mesh concerning protective effects, substantial potentials for the debris containment as well as for protection devices within several speed and impactor mass regimes. Within this potential the FMM will supply its strength in the hinged version and in the hybrid version wherever special material properties and characteristics are demanded.

Of course further investigations regarding the surface treatment for increased strength will be made. And there should be a special focus on the suspension method, which is important to the behaviour and success of the meshwork application. These issues are part of the holistic consideration and are currently underway.

The final goal of the work is to create a realistic simulation model, verified on wide-ranging testing results, that is able to simulate further complex situations and scenarios and which is able to realistic forecast the FMM response.

These proceedings would be cost and time effective and as mentioned before all the advantages named above are highly important for the safety of humans and their survivability during an explosion or an external impact.

## References

[1] TROI Steyerer: Investigation of Flex-Metal-Mesh. Progress report, WTD52-210, Germany (2007)
[2] TROI Steyerer, TROI Stange: Investigation of Flex-Metal-Mesh. Final report, WTD52-210, Germany (2007)

# Sustainable Design of a Side Door Reinforcing Assembly – Optimisation and Material Selection

Mladenko Kajtaz

School of Aerospace, Mechanical and Manufacturing Engineering, RMIT University,
P.O. Box 71 Bundoora VIC 3083, Melbourne Australia
mladenko.kajtaz@rmit.edu.au

**Abstract.** As an extension of the author's previous work, an optimization study of a door reinforcing assembly was presented. It was found that by a careful selection of the cross-sectional shape and usage of "smart" materials, the crash resistance is possible to improve by a factor of 3 while reducing the mass by up to 45%.

## 1 Introduction

A factor analysis study was conducted on a side door reinforcing assembly (Kajtaz, 2011) to provide an insight into the simultaneous effects of multiple input parameters on the optimisation objective. A total of 83 parameters were surveyed and an effects matrix was produced, which is shown in Table 1.

**Table 1.** Summary of Effects of Input Parameters (Kajtaz, 2011)

| Parameter | Max (Mat. Util.) | Max (Crush R.) | min(Vol.) |
|---|---|---|---|
| **Location of upper hinge** | – | Close to CL | – |
| **Location of lower hinge** | Away from CL | Close to CL | Close to CL |
| **Elastic Modulus** | – | Bracket | – |
| **Elastic Limit** | Cross-Bars | – | Cross-Bars |
| **Dimensions perpendicular to loading** | Bracket, Cross-Bars | Bracket, Cross-Bars | Bracket, Cross-Bars |
| **Dim. parallel to loading** | – | Post | – |
| **Thickness** | Yes | Yes | Yes |

The study showed that not all parameters were of equal significance and the most influential parameters were identified. Therefore, by eliminating the less significant parameters the dimensionality of the optimisation is reduced and the search domain is more focused, resulting in an improved optimisation efficiency.

Furthermore, the study showed that improvements in the crash resistance require a higher presence of material and indicated that more detailed material selection process is required to resolve this observation that may perceivably conflict with the weight reduction objective.

This paper presents a natural continuation of the study presented in Kajtaz (2011) with the primary focus on optimisation and material selection process for the sustainability.

## 2  FEA Model

The FEA model presented in Kajtaz (2011), where the side door reinforcing assembly was modelled in the isolation, was extended to include the door panel as well. The assembly components formerly identified as *Bracket* and *Post* were built into the door frame. Point masses were used to model the weight of an average passenger car and they were attached to the door frame. The FEA model used in this investigation is shown in Fig. 1.

### 2.1  *Requirements and Specifications*

The strength and stiffness requirements for side doors of passenger cars are specified by the Australian Design Rule (ADR) 29/00 – Side Door Strength (ADR, 2006). This standard is applicable to all passenger vehicles in Australia. In this particular study the initial crash resistance is considered only and it is defined as the average force required to deform the door over the initial 155mm of crash. The average force is obtained via an integral of the applied load with respect to the crash distance and follows the formulation:

$$CR = \frac{\int F(x)dx}{x}$$

Where: $CR$ – crash resistance; $F(x)$ – force-displacement function, and $x$ - displacement. The test procedure guidelines for establishing the crash resistance, described in the standards, were used to create a representative FEA model. The model was created in ABAQUS (SIMULIA, 2010) and the optimisation was completed using modeFrontier (ESTECO, 2009).



**Fig. 1.** Side door reinforcement assembly – Representative FEA Model as per ADR 29/00.

# 3 Optimisation

The optimised rectangular cross section design from Wu *et al.* (2006) was considered as the baseline model in this study. The gauge lengths are shown in Table 2.

**Table 2.** The gauge lengths of the baseline model (Wu *et al.*, 2006).

| Parameter | Value [mm] | Upper Bar [mm] | Lower Bar [mm] |
|---|---|---|---|
| **Cross-sectional width** | – | 12.45 | 11.25 |
| **Cross-sectional height** | – | 19.57 | 23.47 |
| **Thickness** | – | 1.37 | 2.4 |
| **Left mount thickness** | 1.9 | – | – |
| **Right mount thickness** | 2.22 | – | – |

Although the material properties were not specified, high strength structural steel with yield stress of 600MPa and the density of 7800kg/m$^3$ was assumed.

The optimisation specifications including input parameters, optimisation scheduler, constraints and objective functions were as specified in Kajtaz (2011). The only difference being the number of input parameters due to the removal of insignificant parameters after the factor analysis. The components with the most influential input parameters were the cross members, thus all of their inputs were retained. Due to the FEA model change to include the door frame, all input parameters associated with *Bracket* and *Post*, except for the thickness, became less influential and thus, removed from the optimisation.

## 3.1 Optimal Design

After 4,000 iterations, the optimisation produced a set of solutions that dominated the baseline model and the Pareto frontier is shown in Figure 2. The graph shows the mass minimisation objective on y-axis and the crash resistance maximisation objective on the x-axis. In order to assess the trade-offs and the benefits in comparison to the baseline model, the baseline model was plotted in the top left corner indicating the worst scenario. All other models present in the graph performed better in at least one of the objective, and thus, dominating the baseline solution.

Three designs from the Pareto frontier were deemed as potentially optimal solutions and were assessed further. A more detail insight in the comparison of the chosen designs with the respect to the objectives is shown in Figure 3. The graph shows the performance measures and material properties of the best candidates in a parallel plot. The performance measures were defines as a crash resistance normalised by the performance of the baseline model and a percentage of weight reduction. The graph shows that the crash resistance of the candidates is 2-3 times

**Fig. 2.** Dominating solutions and the Pareto frontier.



**Fig. 3.** Comparison against the baseline model.

a)  b)
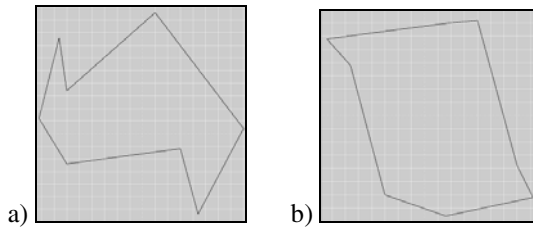
**Fig. 4.** Cross-sectional shapes of the selected design: a) lower cross-member, b) upper cross-member.

better, while the mass can further be reduced by up to 45%. The explanation for such improvements is in the facts that the cross-sectional shapes of the candidates improved the mechanical efficiency of the materials and presence of materials with more favourable properties.

Although the selected designs were equally good, the compromising solution was selected as the best option as the result of this parallel comparison.

The cross-sectional shapes of the cross-members are presented in Figure 4. The cross-members are loaded in bending and the bending is about the vertical axis of the cross-section. As it can be seen, the optimisation favours shapes that increase their bending stiffness. Both of the shown sections tend to distribute more material away from the bending axis and they are oriented in such way that a corner edge is impacted first

### 3.3 Material Selection

A material choice was one of the unconstrained design parameters of this study and as a consequence materials with unrealistic properties may be preferred. This section looks into feasibility of the design from the aspect of the material choice. For that purpose, Granta's CES Material Selector (GRANTA, 2009) was used. Since the objective of the study was to minimise the weight and maximise the stiffness, the most suitable material chart is a plot of Young's Modulus versus Density (GRANTA, 2009).

The material properties of the selected design require relatively high Young's Modulus and relatively low density, both being in the range of aluminium and its alloys. Cost of aluminium per kilogram is higher than that of steel and a separate cost study would be needed to determine full feasibility of replacing steel with aluminium or any other "smart" material.

## 4 Future Work and Conclusion

As an extension of the author's previous work, an optimization study of a door re-inforcing assembly was presented. It was found that by a careful selection of the cross-sectional shape and usage of "smart" materials, the crash resistance is possi-

ble to improve by a factor of 3 while reducing the mass by up to 45%. As the future work structure efficiency as seen in the nature will be considered to compensate for limitations of the traditional materials.

## References

ADR, Vehicle Standard (Australian Design Rule 29/00 – Side Door Strength) (2006),
   `http://www.comlaw.gov.au`
ESTECO. ESTECO Products: modeFrontier (2010),
   `http://www.esteco.com/products.jsp`
GRANTA. Granta Products – CES Selector (2009),
   `http://www.grantadesign.com/products/ces/`
Kajtaz, M.: Sustainable design of a side door reinforcing assembly – exploratory optimisation. In: Conference ICSAT 2011, Greenville SC, USA (2011)
SIMULIA. Simulia Products - Abaqus FEA (2010),
   `http://www.simulia.com/products/abaqus_fea.html`
Wu, C.-H., Liang, C.-P., Lee, J.-H.: Optimization of Side Impact Bar for Crashworthiness. Society of Automotive Engineers (SAE) 2006-01-0245 (2006)

# Development of Automatic Overtaking between Vehicles Using Model Predictive Control

Xi Chen and Harutoshi Ogai

Graduate School of Information, Production and Systems, Waseda University,
Kitakyushu, Fukuoka, Japan
{chenxi,ogai}@waseda.jp

**Abstract.** In the past few years, there has been a variety of research on the automatic driving system. However, research on overtaking between vehicles, especially implementation for the real condition seems to be somewhat neglected. In this study, an overtaking method using the model predictive control (MPC) has been introduced. A combination of continuation and generalized minimum residual method has been presented to optimize the system which is required to keep the minimal safe distance and choose the best time to make overtaking action. Also, the performance of the control system is verified by experiment using robot cars.

## 1   Introduction

In the past years, great development of automobile technology has been made to improve the movement of human beings; however, problems caused by vehicles have been becoming more and more severe. Traffic accidents and traffic jams are a major problem, which cannot be avoided by only improving automobile itself. Besides, some negative issues come, such as environment problems by exhaust emissions and automobile fuel problem [1].

Obviously, these problems cannot be solved only by drivers' qualification, since there are many uncertainties on the road that drivers cannot deal with. Therefore, an intelligent vehicle control system is needed.

In this paper, a brief look of the model predictive control (MPC) using continuation and generalized minimum residual method (C/GMRES) is presented [2]. Then the construction of the control system is introduced, followed by the simulation of the whole overtaking control system. Finally, the performance of the control system is verified by experiment using robot cars.

## 2   Algorithm of the Model Predictive Control

In general, we assume that the state equation and constrains are as follows, respectively [3]:

$$\dot{x} = f(x(t), u(t)) \tag{1}$$

$$C(x(t), u(t)) = 0 \tag{2}$$

In the receding horizon (RH) control, the performance is evaluated by

$$J(u(\tau)) = \int_{t}^{t+T} \left[ L(x(\tau), u(\tau), \tau) \right] d\tau \tag{3}$$

Here, $\tau$ is the virtual time, $T$ is the length of the horizon time; $x$ is a state variable vector of host vehicle and surrounding vehicles $u$ is the control input vector.

Equation (3) is the evaluation equation of the whole control system. In order to get the optimal control input, $J(u(t))$ should be minimized. The requirements are listed as follows [5]:

$$\dot{x} = H_{\lambda} \tag{4}$$

$$\dot{\lambda} = H_{x}, \lambda(t+T) = 0 \tag{5}$$

$$H_{u} = 0 \tag{6}$$

Here, $\lambda$ is the co-state vector of the same size with $x$. $H_{\lambda}$, $H_{u}$ and $H_{x}$ refers to the partial differential equation for $\lambda$, $u$ and $x$. $H$ refers to the Hamiltonian equation defined as:

$$H(x, u, \lambda, t) = L(x, u, t) + \lambda^{T} * f(x, u) \tag{7}$$

To make the discretization of control input, we divide the prediction horizon $[t, t+T]$ into N sampling period:

$$U(t) = (u(\tau_{0}), u(\tau_{1}), ... u(\tau_{N-1})) \tag{8}$$

$$\tau_{i} = t + \frac{i}{N} T, (i = 1, 2, ..., N-1) \tag{9}$$

And, $x(\tau_{i})$, $\lambda(\tau_{i})$ can be calculated by the eq. (4) and (5), respectively.

At each period, an optimal control problem results in nonlinear simultaneous equations:

$$F(U, x, t) = 0 \tag{10}$$

With differentiation for the both side of eq. (10), we obtain:

$$F_{U}\dot{U}(t) + F_{x}\dot{x}(t) + F_{t} = 0 \tag{11}$$

After a complete calculation for one time period, the optimal control input $u$ can be updated:

$$U(t + \Delta t) = U(t) + U(t)\Delta t \tag{12}$$

# 3   Model of Vehicle Driving Control

## 3.1   State Equations

As the first step of this research, a situation of surrounding vehicles driving on a straight motorway is considered. Only the host car can change the lane.

Thus, the state equation of the host vehicle can be explained as longitudinal and lateral directions.

$$\dot{x}_0 = v_0$$
$$\dot{v}_0 = u_x \tag{13}$$

$$\dot{y}_0 = -\omega y_0 + \omega u_y \tag{14}$$

Where: $x_0$, $v_0$, $u$ are the position, velocity and acceleration respectively. $y_0$ is lateral position status, where $y_0 = 1$, refers to the left lane, $y_0 = -1$, for the right lane, and $\omega$ is an overtaking parameter.

On the other hand, the state of surrounding cars can be described in the longitudinal direction:

$$\dot{x}_i = v_i$$
$$\dot{v}_i = k_1^i e_r^i + k_2^i e_{rv}^i + k_v^i e_v^i \tag{15}$$

Where,

$$e_r^i = x_{p_i} - x_i - h_i v_i$$
$$e_{rv}^i = v_{p_i} - v_i \tag{16}$$
$$e_v^i = v_i^d - v_i$$

$$k_1^i = K_1 \cdot sgm(-e_r^i, \lambda_1) \cdot sgm(-e_v^i, \lambda_v) \cdot sgm(-e_{rv}^i, \lambda_2)$$
$$k_2^i = K_2 \cdot sgm(-e_r^i, \lambda_1) \cdot sgm(-e_v^i, \lambda_v) \tag{17}$$
$$k_v^i = K_v \cdot sgm(e_r^i, \lambda_1) \cdot sgm(e_v^i, \lambda_v)$$

Here, $x_i$, $v_i$ and $v_i^d$ stand for the position velocity and ideal velocity of the $i$-th vehicle, $x_p$ and $v_p$ for preceding vehicle. sgm function can be describes as:

$$sgm\lambda x = \frac{1}{1+\exp(-\lambda x)} \tag{18}$$

## 3.2 Evaluation Function

The vehicle performance is evaluated with the following criteria:
1. Acceleration is small

$$L_x = \frac{1}{2}u_x^2 \tag{19}$$

2. Lane changes do not occur frequently

$$L_y = \frac{(u_y - y_0)^2}{2} \tag{20}$$

3. The desired velocity of the host vehicle is maintained as much as possible

$$L_v = \frac{(v_0 - v_0^d)^2}{2} \tag{21}$$

4. Keep certain distance away from surrounding vehicles

$$L_s = c(y_0)(l_{Lf} + l_{Lb}) + c(-y_0)(l_{Rf} + l_{Rb}) \tag{22}$$

Here, $c(y_0)$ stands for the lane status: $c(y_0) = \dfrac{1 + y_0}{2}$

Therefore, the evaluation function is expressed as

$$L = w_x L_x + w_y L_y + w_v L_v + w_s L_s \tag{23}$$

Here, $w_x, w_y, w_v, w_s$ are their weights.

## 3.3 Overtaking Model

In the overtaking model, we focus on the $u_y$ in eq. (14). We set it as:

$$u_y = 1 - 2sgm\lambda(l_i^* - l_i) \tag{24}$$

In this equation, $l_i$ stands for overtake decision parameter (ODP):

$$l_i = \max(l(x_i, v_i, x_b, v_b), l(x_f, v_f, x_i, v_i)) \qquad (25)$$

Here, $l_i^*$ is the reference ODP, and $l_i$ is the actual ODP:

$$l(x_f, v_f, x_b, v_b) = \alpha \frac{v_B^2}{(\frac{x_F - x_B}{\beta})^2 + 1} + (\frac{1-\alpha}{1 + e^{-\lambda_s(v_B - v_0)}}) \frac{(v_B - v_F)^2}{(\frac{x_F - x_B}{\beta})^2 + 1} \qquad (26)$$

Additionally, $\beta$ is standardized coefficient, $\alpha$ is a constant coefficient.

## 4  Control System Simulation

### 4.1  Simulation Condition

As we can see in Figure 1 above, the whole simulation process is set as following conditions:

1. vehicle A is set as the host car
2. total simulation time is set to 50s
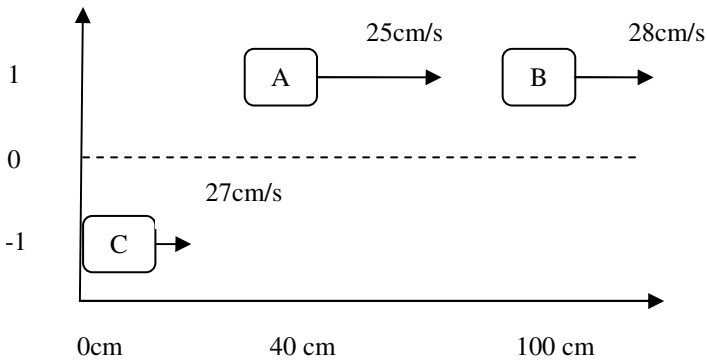


**Fig. 1.** Simulation initial condition 2.
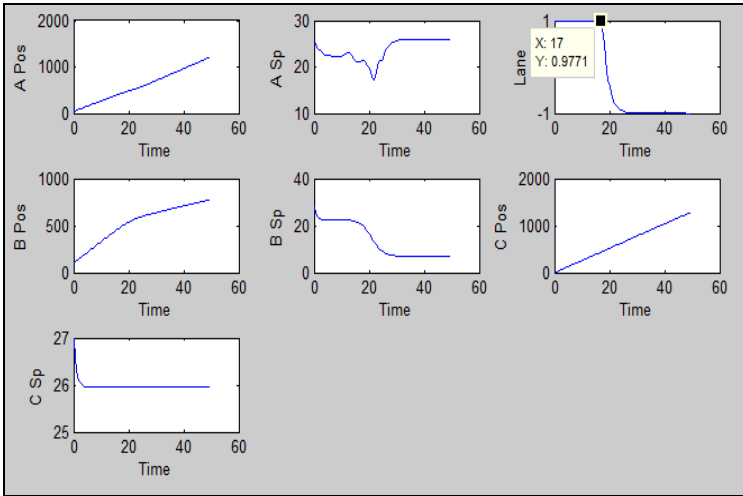
**Fig. 2.** Simulation process.
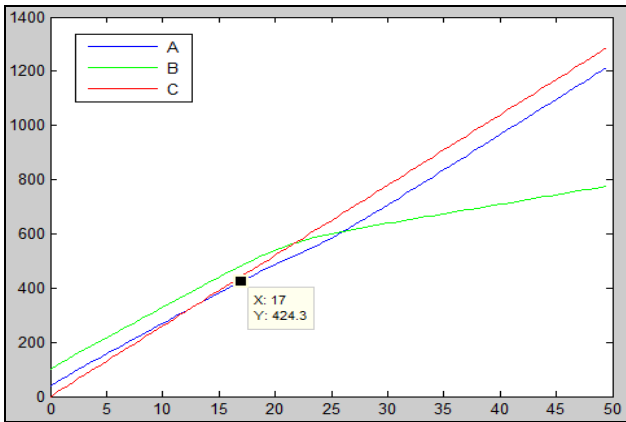


**Fig. 3.** Vehicles' position.

Figure 2 and 3 shows the whole process of the simulation, from which we can see the host car start to change lane at 17.0s to overtake vehicle B, and follows the vehicle C.

## 5   Implementation

We implement the C/GMRES algorithm of MPC method into robot cars.
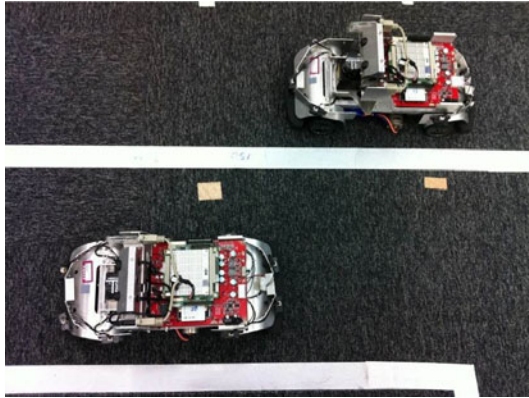
**Fig. 4.** Experimental robot car's overtaking moment.

In order to fit our experiment conditions, a two vehicles' overtaking model was made:
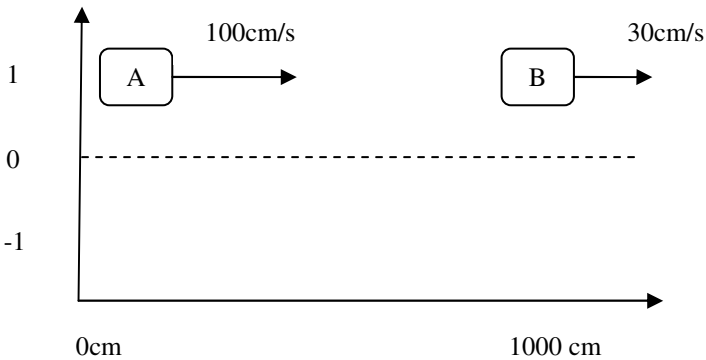


**Fig. 5.** Simulation initial condition 1.

As we can see in the Fig. 5 above, the whole simulation process is set as following conditions:

1. set the vehicle A as the host car
2. total simulation time is set to be 100s
3. the preceeding vehicle B is set to move in constant speed
4. the right lane is set to be the fast track, which the ideal speed is 100cm/s

There's one thing that should be concerned: how to avoid the data overflow when the two cars are getting too close. As we can obtain in the eq. (26), the actual ODP

will become very large as with the denominator decreases. Consequently, this work modifies the ODP equation by $(\dfrac{x_F - x_B}{\beta})^2 + 1$ rather than $(x_F - x_B)^2$.

The programing code is C, and data recorded in the robot car is plotted with MATLAB (Figure 6).
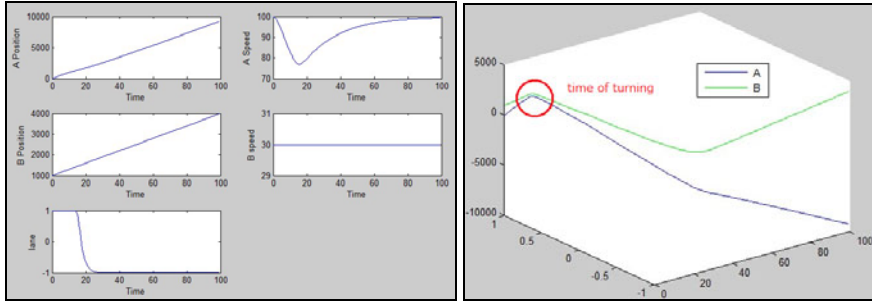


**Fig. 6.** Simulation process.

According to the Figure 6, we obtain that the host car A decelerate and get close to preceding car B at first; when the real ODP was larger than the reference ODP, A changed the lane to overtake B. Here, we set turning angel to be maximum, so that a quick overtaking action can be obtained. After host car switch into the fast track, is start to accelerate until reaching the ideal speed 100cm/s.

## 6 Conclusions

In order to make driving to faster and safer, an optimal driving control assist system is required. In this paper, a nonlinear model predictive control method is introduced. And the overtake model is designed and two vehicle overtake model is confirmed by experiment. Moreover, we plan to apply the model into the electronics vehicles, which is for the elders to make the vehicle accessible for more people.

However, our work is far from complete. Many other aspects such as fuel economy, road recognition, etc. should be added into the automobile control system, to make it contribute for realizing sustainable and environmental friendly intelligent transportation.

## References

1. Furukawa, Y.: Status and Future Direction of Intelligent Drive Assist Technology. In: 2000 Proceedings of IEEE Intelligent Transportation Systems Conference, USA, October 1-3 (2000)
2. Ohtsuka, T.: A continuation/GMRES method for fast computation of nonlinear receding horizon control. Automatica 40-4, 563–574 (2004)

3. Xia, Y.: Automobile Optimal Driving Control based on Model Prediction Control Master thesis, Waseda University (2009)
4. Kawabe, T., Nishira, H., Ohtsuka, T.: An Optimal Path Generator Using a Receding Horizon Control Scheme for Intelligent Automo-biles. In: Proceedings of the 2004 IEEE lntemational Conference on Control Applications Taipei, Taiwan (2004)
5. Wu, D., et al.: Automobile Optimal Driving Control Using Information of Traffic Jam and Signal based on Model Prediction Control. In: ICROS-SICE International Joint Conference (2009)

# Author Index